Investigating Novel Acyclic Lanthanide Complexes Suitable For Magnetic Resonance Imaging

By

Kamentheren Padayachy

Thesis submitted to the Faculty of Science, University of the Witwatersrand, South Africa, for the degree of Doctor of Philosophy.

Supervised by:

Prof. A. S. de Sousa

Prof. H. M. Marques

SCHOOL OF CHEMISTRY

UNIVERSITY OF THE WIWATERSRAND

JOHANNESBURG

SOUTH AFRICA

February 2014

Declaration

I hereby declare that this thesis is my own work. It is submitted for the fulfilment of the degree of Doctor of Philosophy in the Faculty of Science of the University of the Witwatersrand. This thesis has never been submitted before for any degree or examination in any other university.

.....

K. Padayachy

12th of February 2014

Abstract

The ligands 2-(bis(2-(octahydro-2-oxobenzo[b][1,4]oxazin-4-yl)ethyl)amino)acetic acid trihydrochloride and bis(2-(octahydro-2-oxobenzo[b][1,4]oxazin-4-yl)ethyl)amine trihydrochloride are synthesized for the formation of Gd(III) complexes, potentially useful as MRI contrast agents. Speciation and hydration numbers of the Gd(III) complexes of 1,7-bis(2-hydroxycyclohexyl)-1,4,7-tris(carboxymethyl)-1,4,7-triazaheptane (Cy_2DETA.3A) and 1,7-bis(2-hydroxycyclohexyl)-1,7-bis(carboxymethyl)-1,4,7-triazaheptane (Cy_2DETA.2A) can be inferred from spectroscopic studies of the analogous Eu(III) complexes, due to their similar ionic radii, charge and coordination geometry. The phosphorescence emission spectra for the Eu(III) complexes are recorded as function of pH, in buffered and aqueous media. Modulation of the relative intensities of the emission bands is observed for both Eu(III) complexes. Spectroscopically determined pK_a values are used to determine potential solution speciation. Ligand pK_a values were determined potentiometrically. Attempts were made to correlate results from potentiometric titrations with that of lanthanide luminescent titrations of these complexes. Hydration states (q) were determined for the Eu(III) complexes at spectroscopically significant pH values, in buffered and aqueous media. The results confirm the formation of a octadentate complex between Eu(III) and Cy_2DETA.3A, with the inclusion of one H_2O molecule in the inner sphere. The complex has high stability and is responsive towards changes in pH and analyte concentration (*o*-phthalate); potentially suitable as a luminescent sensor. The heptadentate complex formed between Cy_2DETA.2A and Eu(III) is substantially weaker, with precipitation of $Eu(OH)_3$ observed at neutral pH, that limits its potential application as a luminescent sensor.

Acknowledgements

I would like to extend my gratitude to my supervisors Prof. Alvaro de Sousa and Prof. Helder Marques for their guidance. I would also like to thank the members of the Bioinorganic laboratory for their support and friendship.

I thank the Department of Chemistry's NMR and MS services for sample analysis and Dr Manuel Fernandes for XRD data collection. I would also like to thank Piero Benincasa from the Department of Chemistry of the University of Cape Town (UCT) for CHN analysis.

I thank the University of the Witwatersrand (Wits), the National Research Foundation (NRF), and the Council for Scientific and Industrial Research (CSIR) for funding my research.

Finally, I thank my family and friends for their belief, support and encouragement.

Table of Contents

Chapter 1: Introduction 1

1.1 Magnetic Resonance Imaging 2

1.1.1 Behaviour of Nuclei in a Magnetic Field 2

1.1.2 The MRI Experiment 4

1.1.3 Contrast Agents 7

1.1.4 Gadolinium-based Contrast Agents 8

1.1.5 Contrast Agent Development 11

1.2 Lanthanide Luminescence 21

1.2.1 Origin of Luminescence 21

1.2.2 The Luminescence Experiment 25

1.2.3 Luminescent Lanthanide Sensors 27

1.3 Project Aims 32

1.4 References 34

Chapter 2: Materials and Methods 38

2.1 Materials 38

2.2 Characterization Techniques 41

2.2.1 Mass Spectrometry (MS) 41

2.2.2 Nuclear Magnetic Resonance Spectroscopy (NMR) 41

2.2.3 Infrared Spectroscopy (IR) 42

2.2.4 Elemental Analysis 42

2.2.5 Single Crystal X-Ray Diffraction (XRD) 42

2.2.6 Melting Points 43

2.3 Distillation of Solvents 44

2.3.1 Acetonitrile 44

2.3.2 Diethyl ether 44

2.3.3 Ethanol 44

2.3.4 Tetrahydrofuran 44

2.4 Synthetic Procedure 45

2.4.1 Synthesis of 1,7-Bis(2-hydroxycyclohexyl)-1,4,7-triazaheptane (Cy_2DETA) 45

2.4.2 Attempted synthesis of 1,7-Bis(2-hydroxycyclohexyl)-1,4,7-tris(ethylacetate)-1,4,7-triazaheptane (Ac_3Cy_2DETA) 49

2.4.3 Synthesis of 1,7-Bis(2-hydroxycyclohexyl)-1,4,7-tris(t-butylcarboxymethyl)-1,4,7-triazaheptane (Cy_2DETA.3E) 54

2.4.4 Synthesis of 1,7-Bis(2-hydroxycyclohexyl)-1,4,7-tris(carboxymethyl)-1,4,7-triazaheptane (Cy_2DETA.3A) 57

2.4.4.1 Synthesis of Sodium-1,7-Bis(2-hydroxycyclohexyl)-1,4,7-triacetate triazaheptane (Na_3Cy_2DETA.3A) 57

2.4.4.2 Synthesis of 2-(Bis(2-(octahydro-2-oxobenzo[b][1,4]oxazin-4-yl)ethyl) amino)acetic acid trihydrochloride (Cy_2DETA.3A.3HCl) 59

2.4.5 Synthesis of Bis(2-(octahydro-2-oxobenzo[b][1,4]oxazin-4-yl)ethyl)amine trihydrochloride (Cy_2DETA.2A.3HCl) 61

2.4.6 Attempted Synthesis of 1,7-Bis(2-hydroxycyclopentyl)-1,4,7-triazaheptane (Cyp_2DETA) 63

2.5 Lanthanide Complexation 70

2.5.1 Attempted Synthesis of Europium(III)-1,7-Bis(2-hydroxycyclohexyl)-1,4,7-tris(carboxymethyl)-1,4,7-triazaheptane ([Eu(Cy_2DETA.3A)]) 70

2.5.2 Attempted Synthesis of Gadolinium(III)-1,7-Bis(2-hydroxycyclohexyl)-1,4,7-tris(carboxymethyl)-1,4,7-triazaheptane ([Gd(Cy_2DETA.3A)]) 71

2.5.3 Attempted Synthesis of Gadolinium(III)-1,7-Bis(2-hydroxycyclohexyl)-1,7-bis(carboxymethyl)-1,4,7-triazaheptane ([Gd(Cy_2DETA.2A)]) 72

2.6 Potentiometry 73

2.6.1 Preparation of the Standard Solutions 73

2.6.2 Determination of pK_a values 73

2.7 Luminescence Studies 74

2.8 Determination of q 75

2.9 References 76

Chapter 3: Single Crystal Structures 78

3.1 Cy_2DETA 78

3.2 Cy_2DETA.3HClO_4 86

3.3 Ts_2DETA 92

3.4 [NaCy_2DETA.3E]Br 95

3.5 Bis(2-bromoethyl)ammonium bromide 104

3.6 Morpholinium bromide 107

3.7 References 110

Chapter 4: Results and Discussion 111

4.1 Synthetic Procedure 111

4.1.1 Synthesis of 1,7-Bis(2-hydroxycyclohexyl)-1,4,7-triazaheptane (Cy_2DETA) 111

4.1.2 Synthesis of 1,7-Bis(2-hydroxycyclohexyl)-1,7-bis(carboxymethyl)-1,4,7-triazaheptane trihydrochloride (Cy_2DETA.2A.3HCl) 113

4.1.3 Synthesis of 1,7-Bis(2-hydroxycyclohexyl)-1,4,7-tris(t-butylcarboxymethyl)-1,4,7-triazaheptane (Cy_2DETA.3E) 117

4.1.4 Synthesis of 1,7-Bis(2-hydroxycyclohexyl)-1,4,7-tris(carboxymethyl)-1,4,7-triazaheptane (Cy_2DETA.3A) salts 119

4.1.5 Attempted Synthesis of 1,7-Bis(2-hydroxycyclopentyl)-1,4,7-triazaheptane (Cyp_2DETA) 122

4.1.6 Attempted Synthesis of Lanthanide(III)-1,7-Bis(2-hydroxycyclohexyl)-1,4,7-tris(carboxymethyl)-1,4,7-triazaheptane ([Eu(Cy_2DETA.3A)] and [Gd(Cy_2DETA.3A)]) 124

4.1.7 Attempted Synthesis of Gadolinium(III)-1,7-Bis(2-hydroxycyclohexyl)-1,7-bis(carboxymethyl)-1,4,7-triazaheptane ([Gd.(Cy_2DETA.2A)]) 125

4.2 Potentiometric Titrations 126

4.2.1 Cy_2DETA.3A.3HCl pK_a determination 126

4.2.2 Cy_2DETA.2A.3HCl pK_a determination 128

4.3 Luminescence Data 130

4.3.1 Cy_2DETA.3A.3HCl / Eu(III) 130

4.3.1.1 Cy_2DETA.3A.3HCl / Eu(III), aqueous solution 130

4.3.1.2 Cy_2DETA.3A.3HCl / Eu(III), multi-component buffered system, upon initial preparation 137

4.3.1.3 Cy_2DETA.3A.3HCl / Eu(III), multi-component buffered system, upon reaching equilibrium 143

4.3.2 Cy_2DETA.2A.3HCl / Eu(III) 150

4.3.2.1 Cy_2DETA.2A.3HCl / Eu(III), aqueous solution 150

4.3.2.2 Cy_2DETA.2A.3HCl / Eu(III), multi-component buffered system, upon initial preparation 156

4.4 Determination of q 164

4.4.1 Determination of the solution hydration state of $[Eu(Cy_2DETA.3A)]^{3+}$ 165

4.4.1.1 Cy_2DETA.3A.3HCl / Eu(III), aqueous solution 165

4.4.1.2 Cy_2DETA.3A.3HCl / Eu(III), multi-component buffered system 170

4.4.2 Determination of the solution hydration state of $[Eu(Cy_2DETA.2A)]^{3+}$ 181

4.4.2.1 Cy_2DETA.2A.3HCl / Eu(III), aqueous solution 181

4.4.2.2 Cy_2DETA.2A.3HCl / Eu(III), multi-component buffered system 187

4.5 References 194

Chapter 5: Summary, Conclusions and Future Work 199

5.1 Summary and Conclusions 199

5.2 Future work 205

5.3 References 206

Appendices 208

Appendix A – MS Data 208

Appendix B – NMR Data 225

Appendix C – IR Data 242

Appendix D – Single Crystal X-Ray Diffraction Data 252

Appendix E – Potentiometry Data 304

Appendix F – Luminescence Data 320

Appendix G – Determination of q 342

List of Publications 370

TurnItIn Report 371

List of Figures

Figure 1.1:	MRI longitudinal-section of the human head before (left) and after (right) the administration of a gadolinium-based contrast agent	1
Figure 1.2:	Diagrammatic representation of the precession of a nucleus in an external magnetic field	3
Figure 1.3:	Schematic of an MRI scanner	5
Figure 1.4:	Gd-DTPA dimeglumine	8
Figure 1.5:	Schematic representation of a Gd(III)-chelate with one innersphere water molecule	9
Figure 1.6:	Commercially available Gd-DTPA diamide contrast agents	13
Figure 1.7:	The aryl-modified Gd-DTPA complex, Gd-EOB-DTPA	15
Figure 1.8:	The aryl-modified Gd-DTPA complex, Gd-BOPTA	15
Figure 1.9:	Azepane (AZEP-DTPA, (i)) and piperidine (PIP-DTPA, (ii)) backboned DTPA derivatives	16
Figure 1.10:	Temperature-sensitive liposomal MRI contrast agent	18
Figure 1.11:	Derivative of DTPA which responds to endogenous Zn(II)	19
Figure 1.12:	The phosphodiester-based contrast agent MS-325	20
Figure 1.13:	Promotion of an electron from the ground state to an excited state	22
Figure 1.14:	Summary of the relaxation processes following excitation of a molecular species	23
Figure 1.15:	Schematic representation of a spectrofluorimeter	25
Figure 1.16:	The effect of an antenna in sensitizing luminescence emission from the complexed lanthanide(III) ion.	28
Figure 1.17:	Diagram of cyclen	29
Figure 1.18:	Modified octadentate polyaminocarboxylates, the target compounds of this research	32
Figure 1.19:	Modified heptadentate polyaminocarboxylates, the target compounds of this research	33

Figure 2.1:	XRD structure of Cy_2DETA	48
Figure 2.2:	XRD structure of Cy_2DETA.3HClO$_4$	49
Figure 2.3:	XRD structure of Ts_2DETA	53
Figure 2.4:	XRD structure of [NaCy$_2$DETA.3E]Br	57
Figure 2.5:	XRD structure of bis(2-bromoethyl)ammonium bromide	66
Figure 2.6:	XRD structure of morpholinium bromide	67
Figure 3.1:	The molecular structure of Cy_2DETA, showing the atom-labelling scheme and 50% probability displacement ellipsoids	78
Figure 3.2:	Unit cell of Cy_2DETA viewed along the *a*-axis	79
Figure 3.3:	The plane defined by the diethylenetriamine backbone and a cyclohexyl ring in Cy_2DETA	79
Figure 3.4:	Hydrogen-bonding array of Cy_2DETA viewed along the *c*-axis (H atoms omitted for clarity)	80
Figure 3.5:	Hydrogen-bonding array of Cy_2DETA viewed along the *a*-axis	80
Figure 3.6:	Hydrogen-bonding array of Cy_2DETA viewed along the *b*-axis (H atoms omitted for clarity)	80
Figure 3.7:	Close contact interactions within a sheet of Cy_2DETA viewed along the *a*-axis	81
Figure 3.8:	Hydrogen-bonding array between sheets of Cy_2DETA	81
Figure 3.9:	Hydrogen-bonding array between sheets of Cy_2DETA (H atoms omitted for clarity)	82
Figure 3.10:	The C15-H15B···N3 close contact interactions between sheets of Cy_2DETA	82
Figure 3.11:	Spacefill diagram showing the ‘sandwich-like’ appearance of Cy_2DETA	83
Figure 3.12:	Interactions between ‘sandwiches’ of Cy_2DETA viewed along the *a*-axis	83
Figure 3.13:	Interactions between ‘sandwiches’ of Cy_2DETA	84
Figure 3.14:	Spacefill diagram showing the stacking of ‘sandwiches’ of Cy_2DETA	84

Figure 3.15: Close contact interactions between the terminal amine and alcohol moieties of Cy_2DETA, resulting in H-H repulsions between the cyclohexyl ring and triazaheptane backbone 85

Figure 3.16: Bond angles around the terminal amines of Cy_2DETA (H atoms omitted for clarity) 85

Figure 3.17: The molecular structure of $Cy_2DETA.3HClO_4$, showing the atom-labelling scheme and 50% probability displacement ellipsoids 86

Figure 3.18: The plane defined by the diethylenetriamine backbone and a cyclohexyl ring in $Cy_2DETA.3HClO_4$ (H atoms omitted for clarity) 87

Figure 3.19: Unit cell of $Cy_2DETA.3HClO_4$ viewed along the *b*-axis (ClO_4^- ions omitted for clarity) 87

Figure 3.20: Hydrogen-bonding array of $Cy_2DETA.3HClO_4$ viewed along the *b*-axis 88

Figure 3.21: Bond angles around the terminal amines of $Cy_2DETA.3HClO_4$ (H atoms and ClO_4^- ions omitted for clarity) 88

Figure 3.22: Close contact interactions within a sheet of $Cy_2DETA.3HClO_4$ viewed along the *b*-axis 89

Figure 3.23: Hydrogen-bonding array between sheets of $Cy_2DETA.3HClO_4$ viewed along the *a*-axis 90

Figure 3.24: Stacking of sheets of $Cy_2DETA.3HClO_4$ viewed along the *c*-axis (H atoms omitted for clarity) 91

Figure 3.25: Spacefill diagram showing the 'sandwich-like' appearance of $Cy_2DETA.3HClO_4$ 91

Figure 3.26: The molecular structure of Ts_2DETA, showing the atom-labelling scheme and 50% probability displacement ellipsoids 92

Figure 3.27: Interactions between dichloromethane and Ts_2DETA viewed along the *b*-axis 93

Figure 3.28: N1-H1H$\cdots$N2^{i}, N1-H1H$\cdots$N3^{i}, N3-H3H$\cdots$O2^{j}, and C8-H8A$\cdots$O1^{i} hydrogen bonds between molecules of Ts_2DETA ($i = {}^{3}/_{2}$-x, y, ${}^{1}/_{2}$+z, $j = {}^{3}/_{2}$-x, y, -${}^{1}/_{2}$+z) 94

Figure 3.29: Close contact interactions responsible for aromatic ring puckering of Ts_2DETA 94

Figure 3.30: The molecular structure of [$NaCy_2$DETA.3E]Br, showing the atom-labelling scheme and 50% probability displacement ellipsoids 95

Figure 3.31: Unit cell of [$NaCy_2$DETA.3E]Br viewed along the *b*-axis (H atoms omitted for clarity) 96

Figure 3.32: Orthogonal relationship between donor atom planes in [$NaCy_2$DETA.3E]Br (H atoms omitted for clarity) 97

Figure 3.33: Selected close contacts and torsional angles for (a) Cy_2DETA and (b) [$NaCy_2$DETA.3E]Br (H atoms omitted for clarity, Br^- ion not shown) 98

Figure 3.34: Hydrogen bonding between alcohol groups and bromine ion of [$NaCy_2$DETA.3E]Br 99

Figure 3.35: Close contacts of [$NaCy_2$DETA.3E]Br, viewed along the *a*-axis 99

Figure 3.36: Hydrogen bonding of [$NaCy_2$DETA.3E]Br, viewed along the *b*-axis (H atoms omitted for clarity) 100

Figure 3.37: C41-H(41C) $\cdots C411^{i}$ interactions between chains of [$NaCy_2$DETA.3E]Br, viewed along the *b*-axis (H atoms omitted for clarity, i = 1-x, 1-y, -z) 101

Figure 3.38: Close contacts of [$NaCy_2$DETA.3E]Br, viewed along the *c*-axis (H atoms omitted for clarity) 102

Figure 3.39: Three dimensional packing of [$NaCy_2$DETA.3E]Br (H atoms omitted for clarity) 102

Figure 3.40: The molecular structure of bis(2-bromoethyl)ammonium bromide, showing the atom-labelling scheme and 50% probability displacement ellipsoids 104

Figure 3.41: Torsional angles of bis(2-bromoethyl)ammonium bromide (H atoms omitted for clarity) 105

Figure 3.42: Close contact interactions of bis(2-bromoethyl)ammonium bromide, viewed along the *b*-axis 105

Figure 3.43: Intermolecular N-H$\cdots$Br chains of bis(2-bromoethyl)ammonium bromide 106

Figure 3.44: The molecular structure of morpholinium bromide, showing the atom-labelling scheme and 50% probability displacement ellipsoids 107

Figure 3.45: Intermolecular N-H···Br hydrogen bonding of morpholinium bromide, viewed along the *b*-axis 108

Figure 3.46: Hydrogen bonding between ladders of morpholinium bromide, viewed along the *b*-axis 108

Figure 3.47: The C1-H1C···O1 interaction of morpholinium bromide, viewed along the *b*-axis 109

Figure 3.48: The C1-H1C···O1 interaction of morpholinium bromide, viewed along the *a*-axis 109

Figure 4.1: Titration curve of 1,7-bis(2-hydroxycyclohexyl)-1,4,7-tris(carboxymethyl)-1,4,7-triazaheptane, in aqueous solution 127

Figure 4.2: Titration curve for 1,7-bis(2-hydroxycyclohexyl)-1,7-bis(carboxymethyl)-1,4,7-triazaheptane trihydrochloride, in aqueous solution 129

Figure 4.3: Phosphorescence emission spectrum of europium(III)-1,7-bis(2-hydroxycyclohexyl-1,4,7-tris(carboxymethyl)-1,4,7-triazaheptane, as a function of time (λ_{ex} = 223 nm) 131

Figure 4.4: Phosphorescence emission intensity of europium(III)-1,7-bis(2-hydroxycyclohexyl)-1,4,7-tris(carboxymethyl)-1,4,7-triazaheptane, as a function of time (λ_{ex} = 223 nm) 132

Figure 4.5: Phosphorescence emission spectrum of europium(III)-1,7-bis(2-hydroxycyclohexyl)-1,4,7-tris(carboxymethyl)-1,4,7-triazaheptane, as a function of pH (λ_{ex} = 223 nm) 133

Figure 4.6: Phosphorescence emission intensity at 592 nm ($\Delta J = 1$), as a function of pH (λ_{ex} = 223 nm) 134

Figure 4.7: Phosphorescence emission intensity at 617 nm ($\Delta J = 2$), as a function of pH (λ_{ex} = 223 nm) 134

Figure 4.8: Phosphorescence emission intensity at 693 nm ($\Delta J = 4$), as a function of pH (λ_{ex} = 223 nm) 135

Figure 4.9: Proposed speciation and reaction mechanism of europium(III)-1,7-bis(2-hydroxycyclohexyl)-1,4,7-tris(carboxymethyl)-1,4,7-triazaheptane 136

Figure 4.10: Relationship between $\Delta J = 2$ and $\Delta J = 1$ of europium(III)-1,7-bis(2-hydroxycyclohexyl)-1,4,7-tris(carboxymethyl)-1,4,7-triazaheptane, as a function of pH 136

Figure 4.11: Phosphorescence emission spectrum of europium(III)-1,7-bis(2-hydroxycyclohexyl)-1,4,7-tris(carboxymethyl)-1,4,7-triazaheptane, as a function of pH (λ_{ex} = 229 nm) 138

Figure 4.12: Phosphorescence emission spectrum of europium(III)-1,7-bis(2-hydroxycyclohexyl)-1,4,7-tris(carboxymethyl)-1,4,7-triazaheptane, as a function of pH (λ_{ex} = 279 nm) 138

Figure 4.13: Phosphorescence emission intensity at 592 nm ($\Delta J = 1$), as a function of pH (λ_{ex} = 279 nm) 139

Figure 4.14: Phosphorescence emission intensity at 617 nm ($\Delta J = 2$), as a function of pH (λ_{ex} = 279 nm) 140

Figure 4.15: Phosphorescence emission intensity at 697 nm ($\Delta J = 4$), as a function of pH (λ_{ex} = 279 nm) 140

Figure 4.16: Relationship between $\Delta J = 2$ and $\Delta J = 1$ of europium(III)-1,7-bis(2-hydroxycyclohexyl)-1,4,7-tris(carboxymethyl)-1,4,7-triazaheptane, as a function of pH, in a multi-component buffered system 141

Figure 4.17: Phosphorescence emission spectrum of europium(III)-1,7-bis(2-hydroxycyclohexyl)-1,4,7-tris(carboxymethyl)-1,4,7-triazaheptane, as a function of pH (after 3 days, λ_{ex} = 240 nm) 144

Figure 4.18: Phosphorescence emission spectrum of europium(III)-1,7-bis(2-hydroxycyclohexyl)-1,4,7-tris(carboxymethyl)-1,4,7-triazaheptane, as a function of pH (after 3 days, λ_{ex} = 266 nm) 145

Figure 4.19: Phosphorescence emission spectrum of europium(III)-1,7-bis(2-hydroxycyclohexyl)-1,4,7-tris(carboxymethyl)-1,4,7-triazaheptane, as a function of pH (after 14 days, λ_{ex} = 240 nm) 145

Figure 4.20: Phosphorescence emission spectrum of europium(III)-1,7-bis(2-hydroxycyclohexyl)-1,4,7-tris(carboxymethyl)-1,4,7-triazaheptane, as a function of pH (after 14 days, λ_{ex} = 266 nm) 146

Figure 4.21: Phosphorescence emission intensity at 617 nm ($\Delta J = 2$), as a function of pH (after 3 days, λ_{ex} = 266 nm) 147

Figure 4.22: Phosphorescence emission intensity at 617 nm ($\Delta J = 2$), as a function of pH (after 14 days, λ_{ex} = 266 nm) 147

Figure 4.23: Comparison of the $\Delta J_2/\Delta J_1$ ratio for europium(III)-1,7-bis(2-hydroxycyclohexyl)-1,4,7-tris(carboxymethyl)-1,4,7-triazaheptane, as a function of pH, in a multi-component buffered system 148

Figure 4.24: Comparison of the $\Delta J_2/\Delta J_1$ relationship of europium(III)-1,7-bis (2-hydroxycyclohexyl)-1,4,7-tris(carboxymethyl)-1,4,7-triazaheptane, in a buffered and non-buffered system upon equilibration, as a function of pH 149

Figure 4.25: Phosphorescence emission spectrum of europium(III)-1,7-bis(2-hydroxycyclohexyl)-1,7-bis(carboxymethyl)-1,4,7-triazaheptane, as a function of time (λ_{ex} = 252 nm) 151

Figure 4.26: Phosphorescence emission intensity of europium(III)-1,7-bis(2-hydroxycyclohexyl)-1,7-bis(carboxymethyl)-1,4,7-triazaheptane, as a function of time (λ_{ex} = 252 nm) 151

Figure 4.27: Phosphorescence emission spectrum of europium(III)-1,7-bis(2-hydroxycyclohexyl)-1,7-bis(carboxymethyl)-1,4,7-triazaheptane, as a function of pH (λ_{ex} = 252 nm) 152

Figure 4.28: Phosphorescence emission intensity at 592 nm ($\Delta J = 1$), as a function of pH (λ_{ex} = 252 nm) 153

Figure 4.29: Phosphorescence emission intensity at 616 nm ($\Delta J = 2$), as a function of pH (λ_{ex} = 252 nm) 153

Figure 4.30: Phosphorescence emission intensity at 697 nm ($\Delta J = 4$), as a function of pH (λ_{ex} = 252 nm) 154

Figure 4.31: Proposed structures and reaction mechanisms of europium(III)-1,7-bis(2-hydroxycyclohexyl)-1,7-bis(carboxymethyl)-1,4,7-triazaheptane 155

Figure 4.32: Relationship between $\Delta J = 2$ and $\Delta J = 1$ of europium(III)-1,7-bis (2-hydroxycyclohexyl)-1,7-bis(carboxymethyl)-1,4,7-triazaheptane, as a function of pH 156

Figure 4.33: Phosphorescence emission spectrum of europium(III)-1,7-bis(2-hydroxycyclohexyl)-1,7-bis(carboxymethyl)-1,4,7-triazaheptane, as a function of pH (λ_{ex} = 233 nm) 157

Figure 4.34: Phosphorescence emission spectrum of europium(III)-1,7-bis(2-hydroxycyclohexyl)-1,7-bis(carboxymethyl)-1,4,7-triazaheptane, as a function of pH (λ_{ex} = 276 nm) 157

Figure 4.35: Phosphorescence emission intensity at 592 nm ($\Delta J = 1$), as a function of pH (λ_{ex} = 233 nm) 158

Figure 4.36: Phosphorescence emission intensity at 616 nm ($\Delta J = 2$), as a function of pH (λ_{ex} = 233 nm) 159

Figure 4.37: Phosphorescence emission intensity at 697 nm ($\Delta J = 4$), as a function of pH (λ_{ex} = 233 nm) 159

Figure 4.38: Phosphorescence emission intensity at 592 nm ($\Delta J = 1$), as a function of pH (λ_{ex} = 276 nm) 160

Figure 4.39: Phosphorescence emission intensity at 616 nm ($\Delta J = 2$), as a function of pH (λ_{ex} = 276 nm) 160

Figure 4.40: Phosphorescence emission intensity at 697 nm ($\Delta J = 4$), as a function of pH (λ_{ex} = 276 nm) 161

Figure 4.41: Comparison of the $\Delta J_2/\Delta J_1$ relationship of europium(III)-1,7-bis(2-hydroxycyclohexyl)-1,7-bis(carboxymethyl)-1,4,7-triazaheptane, as a function of pH, in a buffered vs. non-buffered system 162

Figure 4.42: Comparison of phosphorescence emission spectra of (i) stock solution, (ii) sample 1, and (iii) sample 2 of europium(III)-1,7-bis(2-hydroxycyclohexyl)-1,4,7-tris(carboxymethyl)-1,4,7-triazaheptane, as a function of pH, in H_2O (λ_{ex} = 223 nm). *Inset*: Emission profile at 617 nm (cyan lines indicate selected pH values for the phosphorescence decay experiment) 167

Figure 4.43: Comparison of phosphorescence emission spectra of (i) stock solution, (ii) sample 1, and (iii) sample 2 of europium(III)-1,7-bis(2-hydroxycyclohexyl)-1,4,7-tris(carboxymethyl)-1,4,7-triazaheptane, as a function of pD, in D_2O (λ_{ex} = 223 nm) 168

Figure 4.44: The proposed equilibrium between the heptadentate and octadentate species of europium(III)-1,7-bis(2-hydroxycyclohexyl)-1,4,7-tris(carboxymethyl)-1,4,7-triazaheptane, upon initial preparation at low pH 169

Figure 4.45: The proposed equilibrium between the octadentate species of europium(III)-1,7-bis(2-hydroxycyclohexyl)-1,4,7-tris(carboxymethyl)-1,4,7-triazaheptane, upon reaching equilibrium at neutral to high pH 170

Figure 4.46: Comparison of phosphorescence emission spectra of (i) stock solution, (ii) sample 1, (iii) sample 2, (iv) sample 3, and (v) sample 4 of europium(III)-1,7-bis(2-hydroxycyclohexyl)-1,4,7-tris (carboxymethyl)-1,4,7-triazaheptane, as a function of pH, in H_2O, in a multi-component buffered system (λ_{ex} = 276 nm). *Inset*: Emission profile at 617 nm (cyan lines indicate selected pH values for the phosphorescence decay experiment) 175

Figure 4.47: Comparison of phosphorescence emission spectra of (i) stock solution, (ii) sample 1, (iii) sample 2, (iv) sample 3, and (v) sample 4 of europium(III)-1,7-bis(2-hydroxycyclohexyl)-1,4,7-tris (carboxymethyl)-1,4,7-triazaheptane, as a function of pD, in D_2O, in a multi-component buffered system (λ_{ex} = 276 nm) 176

Figure 4.48: Proposed speciation of europium(III)-1,7-bis(2-hydroxycyclohexyl)-1,4,7-tris(carboxymethyl)-1,4,7-triazaheptane, in a multi-component buffered system, upon initial preparation 177

Figure 4.49: Proposed speciation of europium(III)-1,7-bis(2-hydroxycyclohexyl)-1,4,7-tris(carboxymethyl)-1,4,7-triazaheptane, in a multi-component buffered system, upon reaching equilibrium (3 days) 179

Figure 4.50: Proposed speciation of europium(III)-1,7-bis(2-hydroxycyclohexyl)-1,4,7-tris(carboxymethyl)-1,4,7-triazaheptane, in a multi-component buffered system, upon reaching equilibrium (14 days) 180

Figure 4.51: Comparison of phosphorescence emission spectra of (i) stock solution, (ii) sample 1, and (iii) sample 2 of europium(III)-1,7-bis (2-hydroxycyclohexyl)-1,7-bis(carboxymethyl)-1,4,7-triazaheptane, as a function of pH, in H_2O (λ_{ex} = 252 nm). *Inset*: Emission profile at

616 nm (cyan lines indicate selected pH values for the phosphorescence decay experiment) 183

Figure 4.52: Comparison of phosphorescence emission spectra of (i) stock solution, (ii) sample 1, and (iii) sample 2 of europium(III)-1,7-bis (2-hydroxycyclohexyl)-1,7-bis(carboxymethyl)-1,4,7-triazaheptane, as a function of pH, in D_2O (λ_{ex} = 252 nm) 184

Figure 4.53: Proposed speciation of europium(III)-1,7-bis(2-hydroxycyclohexyl)-1,7-bis(carboxymethyl)-1,4,7-triazaheptane, in aqueous solution, upon initial preparation 185

Figure 4.54: Proposed speciation of europium(III)-1,7-bis(2-hydroxycyclohexyl)-1,7-bis(carboxymethyl)-1,4,7-triazaheptane, in aqueous solution, upon reaching equilibrium (48 hours) 186

Figure 4.55: Proposed speciation of europium(III)-1,7-bis(2-hydroxycyclohexyl)-1,7-bis(carboxymethyl)-1,4,7-triazaheptane, in aqueous solution, upon reaching equilibrium (7 days) 187

Figure 4.56: Comparison of phosphorescence emission spectra of (i) stock solution, (ii) sample 1, and (iii) sample 2 of europium(III)-1,7-bis (2-hydroxycyclohexyl)-1,7-bis(carboxymethyl)-1,4,7-triazaheptane, as a function of pH, in H_2O (λ_{ex} = 276 nm). *Inset*: Emission profile at 616 nm (cyan lines indicate selected pH values for the phosphorescence decay experiment) 189

Figure 4.57: Comparison of phosphorescence emission spectra of (i) stock solution, (ii) sample 1, and (iii) sample 2 of europium(III)-1,7-bis (2-hydroxycyclohexyl)-1,7-bis(carboxymethyl)-1,4,7-triazaheptane, as a function of pD, in D_2O (λ_{ex} = 276 nm) 190

Figure 4.58: Proposed speciation of europium(III)-1,7-bis(2-hydroxycyclohexyl)-1,7-bis(carboxymethyl)-1,4,7-triazaheptane, in a multi-component buffered system, upon initial preparation 192

Figure 4.59: Proposed speciation of europium(III)-1,7-bis(2-hydroxycyclohexyl)-1,7-bis(carboxymethyl)-1,4,7-triazaheptane, in a multi-component buffered system, upon reaching equilibrium 193

Figure A.1: FAB-MS spectrum of Cy_2DETA 208

Figure A.2: FAB-MS spectrum of residue from the recrystallization of Cy_2DETA 209

Figure A.3: FAB-MS spectrum of Ac_3Cy_2DETA 209

Figure A.4: FAB-MS spectrum of Fraction 1 from chromatographic separation of Ac_3Cy_2DETA 210

Figure A.5: FAB-MS spectrum of Fractions 2 - 4 from chromatographic separation of Ac_3Cy_2DETA 210

Figure A.6: FAB-MS spectrum of Fractions 5 - 14 from chromatographic separation of Ac_3Cy_2DETA 211

Figure A.7: FAB-MS spectrum of Fractions 15 - 17 from chromatographic separation of Ac_3Cy_2DETA 211

Figure A.8: FAB-MS spectrum of Fractions 18 - 21 from chromatographic separation of Ac_3Cy_2DETA 212

Figure A.9: FAB-MS spectrum of Fractions 22 - 62 from chromatographic separation of Ac_3Cy_2DETA 212

Figure A.10: FAB-MS spectrum of TsEDA 213

Figure A.11: FAB-MS spectrum of Ts_2DETA 213

Figure A.12: FAB-MS spectrum of Ts_2DETA.3E 214

Figure A.13: ESI-MS spectrum of Cy_2DETA.3E, attempted synthesis in DCM 214

Figure A.14: ESI-MS spectrum of Cy_2DETA.3E, attempted synthesis in THF 215

Figure A.15: ESI-MS spectrum of Cy_2DETA.3E, attempted synthesis in DMF 215

Figure A.16: ESI-MS spectrum of Cy_2DETA.3E 216

Figure A.17: ESI-MS spectrum of Cy_2DETA.3E after TFA hydrolysis 216

Figure A.18: ESI-MS spectrum of the TFA hydrolysis product of Cy_2DETA.3E, refluxed in H_2O for 7 days 217

Figure A.19: FAB-MS spectrum of Na_3Cy_2DETA.3A 217

Figure A.20: ESI-MS spectrum of Cy_2DETA.3E after HCl hydrolysis 218

Figure A.21: ESI-MS spectrum of the HCl hydrolysis product of Cy_2DETA.3E, after continuous extraction for 10 days and lyophilisation 218

Figure A.22: FAB-MS spectrum of the crude product obtained from the reaction of glyoxal with Cy_2DETA 219

Figure A.23: ESI-MS spectrum of Cy_2DETA.2A.3HCl 219
Figure A.24: FAB-MS spectrum of Cyp_2DETA 220
Figure A.25: ESI-MS spectrum of bis(2-bromoethyl)ammonium bromide 220
Figure A.26: ESI-MS spectrum of bis(2-chloroethyl)ammonium chloride 221
Figure A.27: ESI-MS spectrum of the crude product from the two-step synthesis of Cyp_2DETA 221
Figure A.28: ESI-MS spectrum of the aqueous extract from the two-step synthesis of Cyp_2DETA 222
Figure A.29: ESI-MS spectrum of the organic extract from the two-step synthesis of Cyp_2DETA 222
Figure A.30: ESI-MS spectrum of the [Eu(Cy_2DETA.3A)] synthesis in acetonitrile 223
Figure A.31: FAB-MS spectrum of the [Eu(Cy_2DETA.3A)] synthesis in deionised water 223
Figure A.32: ESI-MS spectrum of the [Gd(Cy_2DETA.3A)] synthesis in acetonitrile 224
Figure A.33: ESI-MS spectrum of the [Gd(Cy_2DETA.2A)] synthesis in acetonitrile 224
Figure B.1: ^{1}H-NMR spectrum of Cy_2DETA 225
Figure B.2: ^{13}C-NMR spectrum of Cy_2DETA 226
Figure B.3: ^{1}H-NMR spectrum of TsEDA 227
Figure B.4: ^{13}C-NMR spectrum of TsEDA 228
Figure B.5: ^{1}H-NMR spectrum of Ts_2DETA 229
Figure B.6: ^{13}C-NMR spectrum of Ts_2DETA 230
Figure B.7: ^{1}H-NMR spectrum of Cy_2DETA.3E 231
Figure B.8: ^{13}C-NMR spectrum of Cy_2DETA.3E 232
Figure B.9: ^{1}H-NMR spectrum of Na_3Cy_2DETA.3A 233
Figure B.10: ^{1}H-NMR spectrum of Cy_2DETA.3A.3HCl 234
Figure B.11: ^{13}C-NMR spectrum of Cy_2DETA.3A.3HCl 235
Figure B.12: ^{1}H-NMR spectrum of Cy_2DETA.2A.3HCl 236
Figure B.13: ^{13}C-NMR spectrum of Cy_2DETA.2A.3HCl 237

Figure B.14: ^{1}H-NMR spectrum of bis(2-bromoethyl)ammonium bromide and morpholinium bromide 238
Figure B.15: ^{1}H-NMR spectrum of bis(2-chloroethyl)ammonium chloride 239
Figure B.16: ^{1}H-NMR spectrum of 2-Aminocyclopentanol 240
Figure B.17: ^{13}C-NMR spectrum of 2-Aminocyclopentanol 241
Figure C.1: IR spectrum of Cy_2DETA 242
Figure C.2: IR spectrum of $Cy_2DETA.3HClO_4$ 243
Figure C.3: IR spectrum of TsEDA 244
Figure C.4: IR spectrum of Ts_2DETA 245
Figure C.5: IR spectrum of $Cy_2DETA.3E$ 246
Figure C.6: IR spectrum of $Na_3Cy_2DETA.3A$ 247
Figure C.7: IR spectrum of $Cy_2DETA.3A.3HCl$ 248
Figure C.8: IR spectrum of $Cy_2DETA.2A.3HCl$ 249
Figure C.9: IR spectrum of bis(2-bromoethyl)ammonium bromide 250
Figure C.10: IR spectrum of bis(2-chloroethyl)ammonium chloride 251
Figure D.1: XRD structure of Cy_2DETA 252
Figure D.2: XRD structure of $Cy_2DETA.3HClO_4$ 260
Figure D.3: XRD structure of Ts_2DETA 266
Figure D.4: XRD structure of $[NaCy_2DETA.3E]Br$ 274
Figure D.5: XRD structure of bis(2-bromoethyl)ammonium bromide 291
Figure D.6: XRD structure of morpholinium bromide 300
Figure F.1: Absorbance spectrum of europium(III)-1,7-bis(2-hydroxycyclohexyl)-1,4,7-tris(carboxymethyl)-1,4,7 triazaheptane, as a function of pH 321
Figure F.2: Absorbance spectrum of europium(III)-1,7-bis(2-hydroxycyclohexyl)-1,4,7-tris(carboxymethyl)-1,4,7 triazaheptane, in a buffered solution, as a function of pH 324
Figure F.3: Absorbance spectrum of europium(III)-1,7-bis(2-hydroxycyclohexyl)-1,4,7-tris(carboxymethyl)-1,4,7 triazaheptane, in a buffered solution, as a function of pH 329

Figure F.4: Absorbance spectrum of europium(III)-1,7-bis(2-hydroxycyclohexyl)-1,7-bis(carboxymethyl)-1,4,7 triazaheptane, as a function of pH 335

Figure F.5: Absorbance spectrum of europium(III)-1,7-bis(2-hydroxycyclohexyl)-1,7-bis(carboxymethyl)-1,4,7 triazaheptane, in a buffered solution, as a function of pH 337

Figure G.1: Absorbance spectrum of europium(III)-1,7-bis(2-hydroxycyclohexyl)-1,4,7-tris(carboxymethyl)-1,4,7 triazaheptane in H_2O, as a function of pH, upon initial preparation 343

Figure G.2: Absorbance spectrum of europium(III)-1,7-bis(2-hydroxycyclohexyl)-1,4,7-tris(carboxymethyl)-1,4,7 triazaheptane in D_2O, as a function of pD, measured upon initial preparation 345

Figure G.3: Absorbance spectrum of europium(III)-1,7-bis(2-hydroxycyclohexyl)-1,4,7-tris(carboxymethyl)-1,4,7 triazaheptane in H_2O, as a function of pH, in a multi-component buffered system 348

Figure G.4: Absorbance spectrum of europium(III)-1,7-bis(2-hydroxycyclohexyl)-1,4,7-tris(carboxymethyl)-1,4,7 triazaheptane in D_2O, as a function of pD, in a multi-component buffered system 354

Figure G.5: Absorbance spectrum of europium(III)-1,7-bis(2-hydroxycyclohexyl)-1,7-bis(carboxymethyl)-1,4,7 triazaheptane in H_2O, as a function of pH 358

Figure G.6: Absorbance spectrum of europium(III)-1,7-bis(2-hydroxycyclohexyl)-1,7-bis(carboxymethyl)-1,4,7 triazaheptane in D_2O, as a function of pD 361

Figure G.7: Absorbance spectrum of europium(III)-1,7-bis(2-hydroxycyclohexyl)-1,7-bis(carboxymethyl)-1,4,7 triazaheptane in H_2O, as a function of pH, in a multi-component buffered system 363

Figure G.8: Absorbance spectrum of europium(III)-1,7-bis(2-hydroxycyclohexyl)-1,7-bis(carboxymethyl)-1,4,7 triazaheptane in D_2O, as a function of pD, in a multi-component buffered system 367

List of Tables

Table 1.1:	Relaxation time constants for non-pathological human tissues (main field of 1.5T)	7
Table 1.2:	Cost per application of contrast agents, assuming body weight = 70 kg (as of 2005)	32
Table 2.1:	List of reagents used	38
Table 2.2:	Optimization conditions for the synthesis of Cy_2DETA	45
Table 2.3:	Crystal data and structure refinement of Cy_2DETA	47
Table 2.4:	Crystal data and structure refinement for Cy_2DETA.3$HClO_4$	48
Table 2.5:	Crystal data and structure refinement for Ts_2DETA	52
Table 2.6:	Crystal data and structure refinement for [NaCy_2DETA.3E]Br	56
Table 2.7:	Optimization conditions for the synthesis of Cyp_2DETA	64
Table 2.8:	Crystal data and structure refinement for bis(2-bromoethyl)ammonium bromide	65
Table 2.9:	Crystal data and structure refinement for morpholinium bromide	66
Table 4.1:	Comparison of pK_a values from the potentiometric titration of 1,7-bis(2-hydroxycyclohexyl)-1,4,7-tris(carboxymethyl)-1,4,7-triazaheptane (Cy_2DETA.3A) with DTPA	127
Table 4.2:	Comparison of pK_a values from the potentiometric titration of 1,7-bis(2-hydroxycyclohexyl)-1,7-bis(carboxymethyl)-1,4,7-triazaheptane (Cy_2DETA.2A) with Cy2DETA.3A and DTPA	128
Table 4.3:	Phosphorescence decay constants for europium(III)-1,7-bis (2-hydroxycyclohexyl)-1,4,7-tris(carboxymethyl)-1,4,7-triazaheptane, as a function of pH, upon initial preparation (0 hours, λ_{ex} = 223 nm, λ_{em} = 616 nm)	165
Table 4.4:	Phosphorescence decay constants for europium(III)-1,7-bis (2-hydroxycyclohexyl)-1,4,7-tris(carboxymethyl)-1,4,7-triazaheptane, as a function of pH, at equilibrium (24 hours, λ_{ex} = 223 nm, λ_{em} = 616 nm)	166

Table 4.5: Phosphorescence decay constants for europium(III)-1,7-bis (2-hydroxycyclohexyl)-1,4,7-tris(carboxymethyl)-1,4,7-triazaheptane, as a function of pH, at equilibrium (6 days, λ_{ex} = 223 nm, λ_{em} = 616 nm) 166

Table 4.6: Phosphorescence decay constants for europium(III)-1,7-bis (2-hydroxycyclohexyl)-1,4,7-tris(carboxymethyl)-1,4,7-triazaheptane, as a function of pH, multi-component buffered system , upon initial preparation (0 hours, λ_{ex} = 276 nm, λ_{em} = 616 nm) 171

Table 4.7: Phosphorescence decay constants for europium(III)-1,7-bis (2-hydroxycyclohexyl)-1,4,7-tris(carboxymethyl)-1,4,7-triazaheptane, as a function of pH, multi-component buffered system, (3 days, λ_{ex} = 276 nm, λ_{em} = 616 nm) 171

Table 4.8: Phosphorescence decay constants for europium(III)-1,7-bis (2-hydroxycyclohexyl)-1,4,7-tris(carboxymethyl)-1,4,7-triazaheptane, as a function of pH, multi-component buffered system, (14 days, λ_{ex} = 276 nm, λ_{em} = 616 nm) 172

Table 4.9: Phosphorescence decay constants for europium(III)-1,7-bis (2-hydroxycyclohexyl)-1,7-bis(carboxymethyl)-1,4,7-triazaheptane, as a function of pH, aqueous solution, upon initial preparation (0 hours, λ_{ex} = 252 nm, λ_{em} = 616 nm) 181

Table 4.10: Phosphorescence decay constants for europium(III)-1,7-bis (2-hydroxycyclohexyl)-1,7-bis(carboxymethyl)-1,4,7-triazaheptane, as a function of pH, aqueous solution, at equilibrium (48 hours, λ_{ex} = 252 nm, λ_{em} = 616 nm) 182

Table 4.11: Phosphorescence decay constants for europium(III)-1,7-bis (2-hydroxycyclohexyl)-1,7-bis(carboxymethyl)-1,4,7-triazaheptane, as a function of pH, aqueous solution, at equilibrium (7 days, λ_{ex} = 252 nm, λ_{em} = 616 nm) 182

Table 4.12: Phosphorescence decay constants for europium(III)-1,7-bis (2-hydroxycyclohexyl)-1,7-bis(carboxymethyl)-1,4,7-triazaheptane, as a function of pH, multi-component buffered system, upon initial preparation (0 hours, λ_{ex} = 276 nm, λ_{em} = 616 nm) 188

Table 4.13: Phosphorescence decay constants for europium(III)-1,7-bis (2-hydroxycyclohexyl)-1,7-bis(carboxymethyl)-1,4,7-triazaheptane, as a function of pH, multi-component buffered system, at equilibrium (7 days, λ_{ex} = 276 nm, λ_{em} = 616 nm) 188

Table D.1: Crystal data and structure refinement for Cy_2DETA 252

Table D.2: Atomic coordinates ($\times 10^4$) and equivalent isotropic displacement parameters ($Å^2 \times 10^3$) for Cy_2DETA. U(eq) is defined as one third of the trace of the orthogonalized U^{ij} tensor 253

Table D.3: Bond lengths (Å) for Cy_2DETA 254

Table D.4: Bond angles (°) for Cy_2DETA 255

Table D.5: Anisotropic displacement parameters ($Å^2 \times 10^3$) for Cy_2DETA. Anisotropic displacement factor exponent: $-2p^2[h^2a^{*2}U^{11} + ... + 2\ h\ k\ a^*\ b^*\ U^{12}]$ 257

Table D.6: Torsion angles (°) for Cy_2DETA 258

Table D.7: Hydrogen bonds for Cy_2DETA (Å and °) 259

Table D.8: Crystal data and structure refinement for $Cy_2DETA.3HClO_4$ 260

Table D.9: Atomic coordinates ($\times 10^4$) and equivalent isotropic displacement parameters ($Å^2 \times 10^3$) for $Cy_2DETA.3HClO_4$. U(eq) is defined as one third of the trace of the orthogonalized U^{ij} tensor 261

Table D.10: Bond lengths (Å) for $Cy_2DETA.3HClO_4$ 262

Table D.11: Bond angles (°) for $Cy_2DETA.3HClO_4$ 262

Table D.12: Anisotropic displacement parameters ($Å^2 \times 10^3$) for $Cy_2DETA.3HClO_4$. Anisotropic displacement factor exponent: $-2p^2[h^2a^{*2}U^{11} + ... + 2\ h\ k\ a^*\ b^*\ U^{12}]$ 264

Table D.13: Torsion angles (°) for $Cy_2DETA.3HClO_4$ 264

Table D.14: Hydrogen bonds for $Cy_2DETA.3HClO_4$ (Å and °) 265

Table D.15: Crystal data and structure refinement for Ts_2DETA 266

Table D.16: Atomic coordinates ($\times 10^4$) and equivalent isotropic displacement parameters ($Å^2 \times 10^3$) for Ts_2DETA. U(eq) is defined as one third of the trace of the orthogonalized U^{ij} tensor 267

Table D.17: Bond lengths (Å) for Ts_2DETA 268

Table D.18: Bond angles (°) for Ts_2DETA 269

Table D.19: Anisotropic displacement parameters ($Å^2 \times 10^3$) for Ts_2DETA. Anisotropic displacement factor exponent: $-2p^2[h^2a^{*2}U^{11} + ... + 2\ h\ k\ a^*\ b^*\ U^{12}]$ 271

Table D.20: Torsion angles (°) for Ts_2DETA 272

Table D.21: Hydrogen bonds for Ts_2DETA (Å and °) 273

Table D.22: Crystal data and structure refinement for [$NaCy_2$DETA.3E]Br 274

Table D.23: Atomic coordinates ($\times 10^4$) and equivalent isotropic displacement parameters ($Å^2 \times 10^3$) for [$NaCy_2$DETA.3E]Br. U(eq) is defined as one third of the trace of the orthogonalized U^{ij} tensor 275

Table D.24: Bond lengths (Å) for [$NaCy_2$DETA.3E]Br 277

Table D.25: Bond angles (°) for [$NaCy_2$DETA.3E]Br 279

Table D.26: Anisotropic displacement parameters ($Å^2 \times 10^3$) for [$NaCy_2$DETA.3E]Br. Anisotropic displacement factor exponent: $-2p^2[h^2a^{*2}U^{11} + ... + 2\ h\ k\ a^*\ b^*\ U^{12}]$ 283

Table D.27: Torsion angles (°) for [$NaCy_2$DETA.3E]Br 284

Table D.28: Hydrogen bonds for [$NaCy_2$DETA.3E]Br (Å and °) 290

Table D.29: Crystal data and structure refinement for bis(2-bromoethyl)ammonium bromide 291

Table D.30: Atomic coordinates ($\times 10^4$) and equivalent isotropic displacement parameters ($Å^2 \times 10^3$) for bis(2-bromoethyl)ammonium bromide. U(eq) is defined as one third of the trace of the orthogonalized U^{ij} tensor 292

Table D.31: Bond lengths (Å) for bis(2-bromoethyl)ammonium bromide 293

Table D.32: Bond angles (°) for bis(2-bromoethyl)ammonium bromide 295

Table D.33: Anisotropic displacement parameters ($Å^2 \times 10^3$) for bis(2-bromoethyl)ammonium bromide. Anisotropic displacement factor exponent: $-2p^2[h^2a^{*2}U^{11} + ... + 2\ h\ k\ a^*\ b^*\ U^{12}]$ 297

Table D.34: Torsion angles (°) for bis(2-bromoethyl)ammonium bromide 298

Table D.35: Hydrogen bonds for bis(2-bromoethyl)ammonium bromide (Å and °) 299

Table D.36:	Crystal data and structure refinement for morpholinium bromide	300
Table D.37:	Atomic coordinates ($\times 10^4$) and equivalent isotropic displacement parameters ($Å^2 \times 10^3$) for morpholinium bromide. U(eq) is defined as one third of the trace of the orthogonalized U^{ij} tensor	301
Table D.38:	Bond lengths (Å) for morpholinium bromide	301
Table D.39:	Bond angles (°) for morpholinium bromide	302
Table D.40:	Anisotropic displacement parameters ($Å^2 \times 10^3$) for morpholinium bromide. Anisotropic displacement factor exponent: $-2p^2[h^2a^{*2}U^{11} + ... + 2\ h\ k\ a^*\ b^*\ U^{12}]$	302
Table D.41:	Torsion angles (°) for morpholinium bromide	303
Table D.42:	Hydrogen bonds for morpholinium bromide (Å and °)	303
Table E.1:	Results from titration of 0.0100 M KHP with 0.0500 M NaOH / 0.0500 M $NaNO_3$	305
Table E.2:	Results from titration of 0.0100 M KHP with 0.0100 M NaOH / 0.0900 M $NaNO_3$	306
Table E.3:	Results from titration of 0.0500 M HNO_3 / 0.0500 M $NaNO_3$ with 0.0495 M NaOH / 0.0500 M $NaNO_3$	307
Table E.4:	Electrode standardization raw data	311
Table E.5:	Cy_2DETA.3A.3HCl pK_a determination raw data	312
Table E.6:	Electrode standardization raw data	316
Table E.7:	Cy_2DETA.2A.3HCl pK_a determination raw data	316
Table F.1:	Cy_2DETA.3A.3HCl / Eu(III) phosphorescence emission raw data, λ_{ex} = 223 nm	322
Table F.2:	Cy_2DETA.3A.3HCl / Eu(III) phosphorescence emission raw data, λ_{ex} = 279 nm (multi-component buffered system, no equilibration)	324
Table F.3:	Cy_2DETA.3A.3HCl / Eu(III) phosphorescence emission raw data, λ_{ex} = 229 nm (multi-component buffered system, no equilibration)	326
Table F.4:	Cy_2DETA.3A.3HCl / Eu(III) phosphorescence emission raw data, λ_{ex} = 240 nm (multi-component buffered system, upon reaching equilibrium)	330

Table F.5: Cy_2DETA.3A.3HCl / Eu(III) phosphorescence emission raw data, λ_{ex} = 266 nm (multi-component buffered system, upon reaching equilibrium) 332

Table F.6: Cy_2DETA.2A.3HCl / Eu(III) phosphorescence emission raw data, λ_{ex} = 252 nm 335

Table F.7: Cy_2DETA.2A.3HCl / Eu(III) phosphorescence emission raw data, λ_{ex} = 276 nm (multi-component buffered system, no equilibration) 338

Table F.8: Cy_2DETA.2A.3HCl / Eu(III) phosphorescence emission raw data, λ_{ex} = 233 nm (multi-component buffered system, no equilibration) 340

Table G.1: Cy_2DETA.3A.3HCl / Eu(III) phosphorescence emission decay data (in H_2O, aqueous solution, λ_{ex} = 223 nm) 343

Table G.2: Cy_2DETA.3A.3HCl / Eu(III) phosphorescence emission decay data (in D_2O, aqueous solution, λ_{ex} = 223 nm) 346

Table G.3: Cy_2DETA.3A.3HCl / Eu(III) phosphorescence emission decay data (in H_2O, multi-component buffered system, λ_{ex} = 276 nm) 349

Table G.4: Cy_2DETA.3A.3HCl / Eu(III) phosphorescence emission decay data (in H_2O, multi-component buffered system, λ_{ex} = 227 nm) 351

Table G.5: Cy_2DETA.3A.3HCl / Eu(III) phosphorescence emission decay data (in D_2O, multi-component buffered system, λ_{ex} = 276 nm) 355

Table G.6: Cy_2DETA.3A.3HCl / Eu(III) phosphorescence emission decay data (in D_2O, multi-component buffered system, λ_{ex} = 227 nm) 356

Table G.7: Cy_2DETA.2A.3HCl / Eu(III) phosphorescence emission decay data (in H_2O, aqueous solution, λ_{ex} = 252 nm) 359

Table G.8: Cy_2DETA.2A.3HCl / Eu(III) phosphorescence emission decay data (in D_2O, aqueous solution, λ_{ex} = 252 nm) 362

Table G.9: Cy_2DETA.2A.3HCl / Eu(III) phosphorescence emission decay data (in H_2O, multi-component buffered system, λ_{ex} = 276 nm) 364

Table G.10: Cy_2DETA.2A.3HCl / Eu(III) phosphorescence emission decay data (in H_2O, multi-component buffers present, λ_{ex} = 233 nm) 365

Table G.11: Cy_2DETA.2A.3HCl / Eu(III) phosphorescence emission decay data (in D_2O, multi-component buffered system, λ_{ex} = 276 nm) 368

Table G.12: $Cy_2DETA.2A.3HCl$ / Eu(III) phosphorescence emission decay data (in D_2O, multi-component buffered system, λ_{ex} = 233 nm) 369

Abbreviations

MRI	Magnetic Resonance Imaging
NMR	Nuclear Magnetic Resonance
RF	radio frequency
DTPA	diethylenetriaminepentaacetic acid
NSF	nephrogenic systemic fibrosis
DTPA-BMA	diethylenetriaminepentaacetic acid-bis(methylamide)
DTPA-BMEA	diethylenetriaminepentaacetic acid-bis(methoxyethylamide)
EOB-DTPA	ethoxybenzyl diethylenetriaminepentaacetic acid
BOPTA	benzyloxypropionictetraacetate
HSA	human serum albumin
HTf	human serum transferrin
UV-vis	UV-visible
Ln	lanthanide
Cyclen	1, 4, 7, 10-tetraazacyclododecane
MS	mass spectrometry
ESI	electrospray ionization
FAB	fast atom bombardment
NBA	3-nitrobenzyl alcohol
IR	infrared
XRD	X-ray diffraction
Cy_2DETA	1,7-Bis(2-hydroxycyclohexyl)-1,4,7-triazaheptane
Ac_3Cy_2DETA	1,7-Bis(2-hydroxycyclohexyl)-1,4,7-tris(ethylacetate)-1,4,7-triazaheptane
EtOH	ethanol
TsEDA	N-*p*-tolylsulfonylethylenediamine
Ts_2DETA	N, N”-Bis(*p*-tolylsulfonyl) diethylenetriamine

NaOEt	sodium ethoxide
THF	tetrahydrofuran
Cy_2DETA.3E	1,7-Bis(2-hydroxycyclohexyl)-1,4,7-tris(t-butylcarboxymethyl)-1,4,7-triazaheptane
DCM	dichloromethane
DMF	dimethylformamide
Cy_2DETA.3A	1,7-Bis(2-hydroxycyclohexyl)-1,4,7-tris(carboxymethyl)-1,4,7-triazaheptane
Cy_2DETA.3A.3HCl	2-(Bis(2-(octahydro-2-oxobenzo[b][1,4]oxazin-4-yl)ethyl)amino)acetic acid trihydrochloride
TFA	trifluoroacetic acid
Cy_2DETA.2A	1,7-Bis(2-hydroxycyclohexyl)-1,7-bis(carboxymethyl)-1,4,7-triazaheptane
Cy_2DETA.2A.3HCl	Bis(2-(octahydro-2-oxobenzo[b][1,4]oxazin-4-yl)ethyl)amine trihydrochloride
Cyp_2DETA	1,7-Bis(2-hydroxycyclopentyl)-1,4,7-triazaheptane
KHP	potassium hydrogen phthalate
MES	2-(*N*-Morpholino)-ethanesulfonic acid
MOPS	3-(*N*-Morpholino)-propanesulfonic acid
CHES	2-(*N*-Cyclohexylamino)-ethanesulfonic acid
Tris	Tris-(hydroxymethyl)aminoethane
λ_{ex}	excitation wavelength
λ_{em}	emission wavelength
PET	photo-induced electron transfer
CN	coordination number

Chapter 1

Introduction

Magnetic Resonance Imaging (MRI) is an important non-invasive diagnostic technique for obtaining high-resolution images of body tissues, and is the modality of choice for the investigation of the central nervous system and the spine. One of the main advantages of this technique is that it uses no ionizing radiation, thus making MRI completely harmless. The three-dimensional images obtained from this technique provide detailed information with regard to the location of tissue abnormalities such as the growth of cancerous cells. These images can be further enhanced by the administration of a contrast agent.

The images obtained by MRI are due to the localized NMR signals of water protons in the tissue under study. Administering an MRI contrast agent alters the relaxivity of the water protons, thus achieving enhancement of the image.

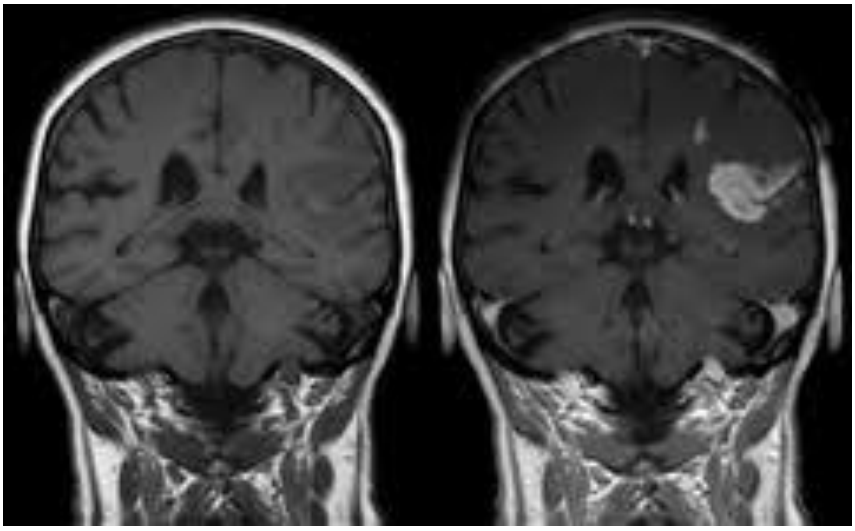


Figure 1.1: MRI longitudinal-section of the human head before (left) and after (right) the administration of a gadolinium-based contrast agent[1].

In South Africa, the capital needs for the acquisition of MRI units is compounded by the additional costs of the required contrast agents, both of which are manufactured overseas. Hence, this imaging modality is generally more readily available in private hospitals and

clinics, thereby limiting its access to most South Africans due to the exorbitant financial implications. It is therefore in the country's interest that efforts towards the local development of contrast agents be encouraged.

The functioning of contrast agents is strongly dependent on its structure. Contrast agents can be developed and their *in vivo* chemistry determined from luminescent molecular analogues.

1.1 Magnetic Resonance Imaging

1.1.1 Behaviour of Nuclei in a Magnetic Field

Magnetic Resonance Imaging is based upon the same principles that govern Nuclear Magnetic Resonance (NMR). According to the laws of quantum mechanics, every nucleus has an associated quantity known as spin. This quantity is attributed to the subatomic particles which make up the nucleus, namely protons and neutrons. Both have spin, but protons also have a charge. Since pairs of spins tend to cancel each other, only nuclei with an odd number of protons and neutrons will have spin, such as ^{1}H (one proton) and ^{13}C (six protons, seven neutrons)[2-9].

There is a fundamental law of physics which states that a spinning mass will induce a magnetic field about itself. If the spinning mass is charged, the induced magnetic field is greater. Since the nucleus is a spinning, charged mass, it has a magnetic field associated with it. This magnetic field has a magnetic dipole moment (μ), which has its axis oriented parallel to the spin axis. The nucleus also has an angular momentum (ρ) associated with it, which is also oriented in the same direction as the magnetic moment (Figure 1.2)[2-9].

If the nucleus is placed in an external magnetic field, the magnetic field exerts a force upon the magnetic moment, causing μ to align itself with the field (a low energy conformation). The angular momentum, however, prevents this immediate alignment. The result is that the spin axis of the nucleus precesses around the field axis instead of aligning with it. The

frequency of this precession, υ_0, is the resonant frequency of nuclear magnetic resonance. This is also known as the Larmor frequency, and is given by the following equation:

$$\upsilon_0 = \gamma B_0$$

where B_0 is the strength of the external magnetic field and γ is a constant called the gyromagnetic ratio, which is different for each nucleus[2-9].

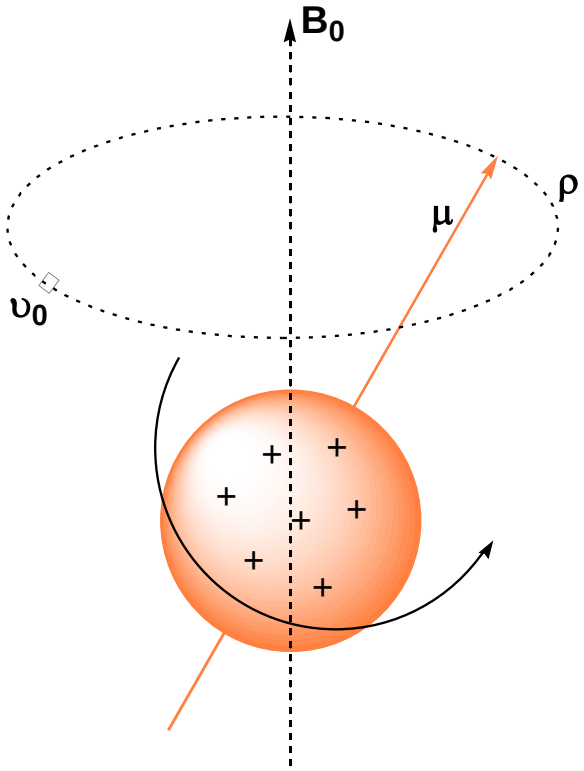


Figure 1.2: Diagrammatic representation of the precession of a nucleus in an external magnetic field[5].

The process following the orientation of the magnetic moment in the external field in addition to precession is known as relaxation. This is essentially a time-mediated energy equilibration, in which the magnetic moment becomes completely aligned with the external field. A magnetic dipole moment in an external magnetic field adopts a low energy configuration when it is completely aligned with the external field and has a high energy configuration when aligned opposite to the field. Thus, a precessing nucleus must release energy in order to adopt a low energy configuration. This process usually occurs in the form of random thermal

motions of the molecules in solution. The time required for this equilibration to occur is dependent on how tightly coupled the thermal motions are to the orientation of the dipole moment[2-9].

As it is impossible to measure the action of an individual nucleus in the presence of an external magnetic field, the signals obtained in an NMR experiment are the result of a bulk phenomenon from many nuclei, as many as 10^{26} nuclei. For MRI, the hydrogen (^1H) nucleus is the atom of choice, for a number of reasons. The proton, the hydrogen (^1H) nucleus, has the largest magnetic moment of all naturally occurring nuclei. It also has the largest gyromagnetic ratio of all NMR-active nuclei, thus resulting in a much stronger signal which can be obtained from other nuclei. Most importantly, hydrogen is abundant in the human body, mainly in the form of water (H_2O), constituting 80% of all atoms. This large abundance makes it extremely useful for MRI[2-9].

1.1.2 The MRI Experiment

In Magnetic Resonance Imaging, the magnetization of an object placed in a static magnetic field is detected and processed to form an image. This is achieved via the utilization of several pieces of hardware and signal processing devices.

Under normal conditions, the nuclear magnetic dipoles in the body (the hydrogen nuclei in a water molecule) are randomly distributed, resulting in a zero net magnetization. When a patient is placed in the presence of a strong external magnetic field, the individual nuclear magnetic moments align with the external field, creating a weak equilibrium magnetization M_0. The magnitude of M_0 is directly proportional to the local proton density. With net magnetization in the direction of B_0 (designated as the z-axis of a Cartesian coordinate system), not only are the magnetic moments aligned, but each individual nucleus is precessing at the Larmor frequency[2-5, 8-12].

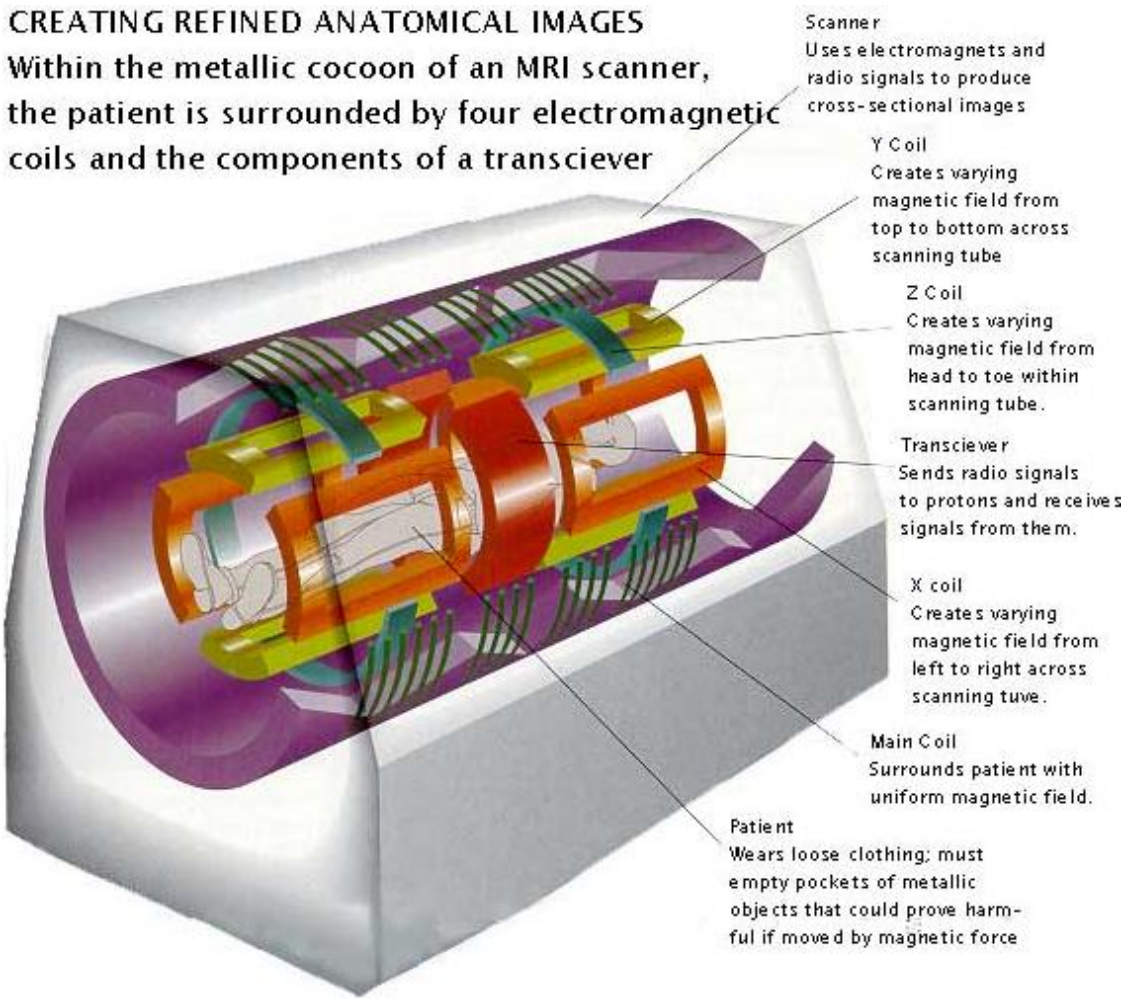


Figure 1.3: Schematic of an MRI scanner[13].

The local equilibrium magnetization M_0 is not directly observable as it is several orders of magnitude weaker than B_0. However, if all the dipoles that contribute to M_0 could be tipped away from B_0, they would precess around the field at the same rate. The result is that M_0 would also tip away by the same amount (the flip angle α) and begin to precess around the main field. Tipping of the magnetization produces a measurable, transient signal, and is accomplished by a radio frequency (RF) pulse. The source of this RF pulse is an RF coil, located perpendicular to B_0, creating another weaker magnetic field B_1, perpendicular to B_0. The RF pulse transmitted into the body must be at the same resonant frequency of the precessing nuclei, i.e. the Larmor frequency, in order for energy to be absorbed[2-5, 8-12].

The precessing magnetization induces a current in a nearby RF coil, resulting in a measurable signal. In order to generate images, spatial information must be encoded into the measured

signal. This is accomplished by using time-varying magnetic gradients, these gradients are produced by three orthogonal coils placed inside the magnet and surrounding the RF coil and the patient (Figure 1.3)[2-5, 8-13].

Once the RF pulse is turned off, relaxation processes take place. There are two processes which occur simultaneously:

- Longitudinal (T_1) Relaxation

This process is the return of the M_z component to its equilibrium position and occurs either via a spontaneous emission or stimulated emission of energy (in the case of MRI, the emission is stimulated). This stimulation occurs in the form of a fluctuating magnetic field at the Larmor frequency, which is formed by the random motion of the molecules in the surrounding medium. As the molecules move, the magnetic moments are altered, resulting in a magnetic 'noise' at the site of each nucleus that covers the υ_0 of the nuclei and stimulates the transition back to the lower energy level (i.e. alignment with B_0)[2-5, 8-12].

- Transverse (T_2) Relaxation

Consider a 90° RF pulse. Immediately after the pulse, the individual spins rotate coherently around the B_0 field at the Larmor frequency, thus creating a macroscopic magnetization in the xy-plane. In an ideal system, all the nuclei in a given chemical environment in a magnetic field would spin at the same frequency. However, in real systems, minor differences in the chemical environment results in a fluctuating magnetic field. The fluctuating magnetic field caused by the random motion of the molecules will produce random fluctuations in the angular momentum of the individual spins, resulting in a loss of phase coherence or 'dephasing' of the spins. As dephasing of the spins increases, M_{xy} will decrease to zero[2-5, 8-12].

In biological tissues, T_1 increases with increasing magnetic field strength B_0, while T_2 is relatively independent of B_0. Different tissues also exhibit different relaxation times, and

these differences can be used to generate image contrast. Table 1.1 lists the relaxation times of different tissues[14].

Table 1.1: Relaxation time constants for non-pathological human tissues (B_0 = 1.5 T)[14].

Tissue Type	T_1 (ms)	T_2 (ms)
Adipose	240 – 250	60 – 80
Whole blood	1350	50 (deoxygenated) – 200 (oxygenated)
Cerebrospinal fluid	4200 – 4500	2100 – 2300
Grey matter (cerebrum)	920	100
White matter (cerebrum)	780	90
Liver	490	40
Kidneys	650	60 – 75
Muscles	860 – 900	50

1.1.3 Contrast Agents

The use of contrast-enhancing agents has become an integral part of MRI, as these can be used to discriminate between certain tissues when producing an image. In particular, contrast agents have been used to investigate brain pathology associated with altered blood volume, such as stroke or tumours. Currently available MR contrast agents can be categorized according to their magnetic behaviour, biodistribution, and effect on the image[3, 12, 15].

The aim of using a contrast agent in MRI is to accelerate the relaxation of H_2O protons in the surrounding tissue. This effect is best described in terms of its effect on the relaxation rate constant R, the inverse of the relaxation time.

For brain tissues, the transverse relaxation rate R_2 (= 1 / T_2) is approximately ten times larger than the longitudinal relaxation rate R_1 (= 1 / T_1). The effect of the contrast agent is to add to each of these rates a change ΔR, which is proportional to the concentration of the contrast

agent. This effect, as well as the implications for the design of new contrast agents, will be discussed for gadolinium-based contrast agents[3, 12, 15].

1.1.4 Gadolinium-based Contrast Agents

The most commonly used contrast agents involve metal ions that have one or more unpaired electrons, resulting in a permanent magnetic dipole. Paramagnetic metals cannot be used as contrast agents in their ionic form due to an undesirable biodistribution and high toxicity of the metal ions. By binding the metal to a ligand, a more desirable safety profile can be achieved[3, 12, 15].

The most commonly used acyclic paramagnetic contrast agent is Gd-DTPA (gadolinium(III) diethylenetriaminepentaacetic acid, Figure 1.4). It has become the benchmark by which all modern contrast agents are judged, due to its low toxicity and good contrast enhancement. Gadolinium (Gd(III)) is the active part of the agent and DTPA is the chelating agent. Gd(III) is a lanthanide metal ion that has seven unpaired electrons and the interaction of the large magnetic dipole moments of these electrons with the smaller magnetic moments of the water molecule protons leads to a decrease in the local relaxation times[3, 12, 15].

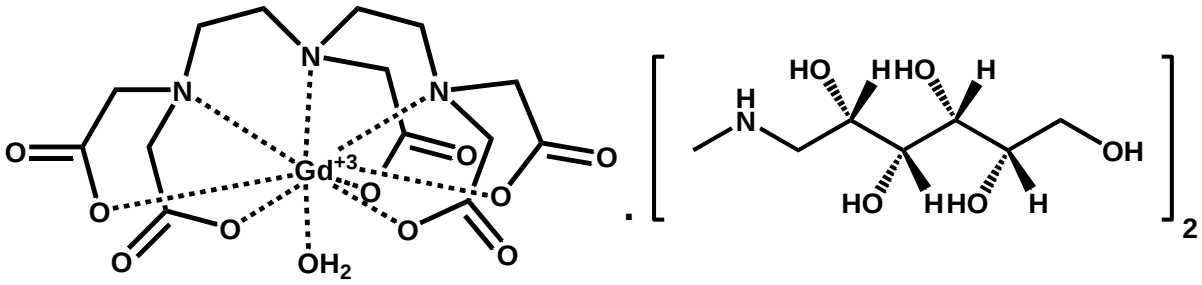


Figure 1.4: Gd-DTPA dimeglumine[16].

Gd(III) acts primarily as a T_1-agent, altering the T_1 spins that come into contact with it. Due to the large effect that Gd(III) has on T_1, the contrast agent is only required in moderate concentrations (generally 0.2 mL/kg of body weight). When Gd-DTPA is injected into the patient, the blood-brain barrier in the healthy portions of the brain prevents the contrast agent from leaving the vasculature. However, if there is a tumour with a leaky blood-brain barrier,

the contrast agent then enters the tissue, reducing the local T_1 and thus increasing the signal from the tumour in a T_1-weighted image[3, 12].

The relaxivity enhancement afforded by the Gd(III) complex is distance-dependent, decreasing rapidly with increased distance from the Gd(III) ion. Therefore, the chemical interactions that bring the water protons into the immediate vicinity of the metal ion play an important role in the propagation of the paramagnetic effect in the bulk solution. For Gd(III), this corresponds to the binding of a water molecule(s) in the first coordination sphere and the subsequent exchange of these innersphere water protons with the bulk, as seen in Figure 1.5. Therefore, the rate of exchange of the innersphere water protons with the bulk k_{ex} (= 1 / τ_M), where τ_M is the residence time of the water protons on the paramagnetic centre, is important. The relaxivity is also dependent on the long range interactions of the paramagnetic centre with the bulk solvent. These interactions make up the outersphere contribution to the overall relaxivity[3, 12, 17].

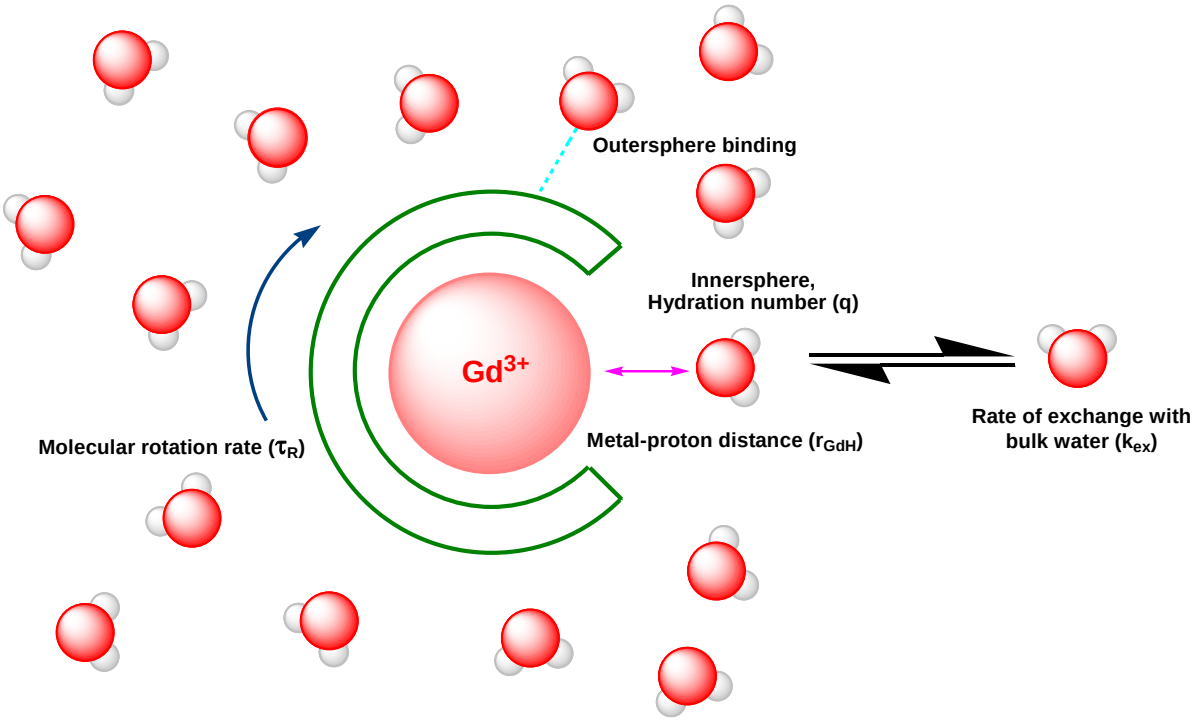


Figure 1.5: Schematic representation of a Gd(III)-chelate with one innersphere water molecule[17].

There are a number of properties to be considered when attempting to maximize the efficacy of a contrast agent:

- Complex stability

The contrast agent must show stability *in vivo*. There must be a high affinity of the chelate for the metal ion, reflected by the thermodynamic binding constant of the complex. If the agent is not sufficiently stable, precipitation of the gadolinium ion can occur, with potential toxicity. The chelate must have high selectivity for the Gd(III) ion itself so that metal exchange with endogenous ions does not occur. The compound must also exhibit slow kinetics in regard to the release of the Gd(III) ion, making possible near complete excretion of the complex[3, 12, 18, 19].

- The hydration number (q)

The hydration number is linearly proportional to the innersphere proton relaxivity. Due to the high toxicity of the aqua ion, in this case $[Gd(OH_2)_9]^{3+}$, the metal ion is incorporated into a multidentate ligand to protect it. All approved Gd(III) contrast agents are polyaminocarboxylates, where the ligand occupies eight coordination sites, leaving only one site available for the coordination of H_2O. There has been much interest in developing Gd(III) complexes with higher q values (e.g. heptadentate ligands) that will possess higher relaxivities. However, increases in the hydration number have resulted in a corresponding increase in the toxicity of the contrast agent, due to the complexes not being kinetically inert *in vivo*[20].

- Gd – H Distance (r_{GdH})

Relaxivity is dependent on the distance between the coordinated water proton and the Gd(III) electron spin (r_{GdH}). A decrease of 0.1 Å in the Gd – H distance corresponds to a 20% increase in relaxivity, while a decrease of 0.2 Å results in as much as a 50% increase[3, 12].

- Water residence time (τ_M)

τ_M modulates the efficiency of chemical exchange from the innersphere of the metal to the bulk. The exchange rates may depend on the pH of the bulk solution. The exchange mechanism of the water protons also has consequences on contrast agent design, in terms of steric crowding of the ligand around the site of proton exchange[3, 12].

- Rotational correlation time (τ_R)

The rotational correlation time (i.e. molecular tumbling) is important for small molecular weight Gd(III) chelates, as it effectively determines the overall correlation time for proton relaxation. The fact that the relaxivity of small Gd(III) chelates is limited by rapid tumbling has led to a variety of ways to slow down rotation by increasing the molecular weight of the complex. This is the most obvious approach to increase proton relaxivity[3, 12].

1.1.5 Contrast Agent Development

The design of efficient, non-toxic and target-specific gadolinium complexes has become the focus of attention in the development of MRI contrast agents. The target-specific contrast agent can accumulate in the specific organ or tissue, increasing the concentration, thus producing the required change in signal intensity and greater contrast of MR images[3, 18].

There are a number of criteria that must be met in the design of an MRI contrast agent[18, 19]:

- The first and most important criterion is the ability of the contrast agent to alter the parameters responsible for image contrast in clinical MRI. The efficiency of the contrast agent in increasing the relaxation rates of the target tissue is the most notable parameter.
- The contrast agent should possess tissue specificity *in vivo* so that it is delivered to a tissue or organ in a higher concentration than to other areas in the body. The contrast agent must remain localized for a reasonable period of time so that

imaging can be performed; i.e. the residence time of the contrast agent must be of the same order as the signal acquisition time.

- To minimize the potential toxicity effects, the contrast agent must be substantially cleared from the target tissue or organ in a reasonable period of time, usually several hours after imaging. The contrast agent must also be excreted from the body, usually via the renal or hepatobiliary routes.
- Contrast agents must have low toxicity and must be stable *in vivo* while being administered in doses that can affect the MR relaxation parameters sufficiently to result in a visible contrast enhancement on the MR image.
- The target tissue or organ to be imaged will dictate the desired characteristics of the metal complex. For example, it is known that negatively charged complexes accumulate in the heart; and an overall neutral complex is required for crossing the blood-brain barrier. Lipophilic complexes will generally have greater uptake in the liver and fatty tissues.
- The contrast agent must possess a suitable shelf-life for storage.

Gadopentate dimeglumine (Gd-DTPA bis (N-methylglucammonium) salt) or Magnevist® (Figure 1.4) was the first gadolinium complex to be developed for clinical use, mainly in the characterization of lesions in the central nervous system. DTPA (diethylenetriaminepentaacetic acid) is an octadentate ligand that coordinates Gd^{3+} by using all three nitrogen and five carboxylate oxygen donor atoms. The ninth position is occupied by a molecule of water. The resulting complex is very stable ($\log K_{ML} = 22.46$), but displays poor selectivity of Gd(III) over Zn(II), resulting in a large amount of Gd(III) *in vivo*. However, the residence time of Gd-DTPA in the body is so short that the poor selectivity is not of significant concern. Gd-DTPA, although desirable because of biological acceptability, suffers in that it lacks tissue specificity for organs other than the kidneys, its route of excretion[12, 15, 16].

The success of Gd-DTPA dimeglumine has led to extensive studies aimed at the modification of DTPA by the introduction of suitable residues into either the acetic acid side-arms or the diethylenetriamine backbone. The purpose of these modifications is to obtain, after

complexation of Gd(III), complexes featuring improved properties in terms of selectivity and/or tolerability[12].

Besides Gd-DTPA, the gadolinium complexes of DTPA-diamides have probably been the most studied class of MRI contrast agents, because of the facile synthesis of these ligands. Bisamide derivatives of DTPA, in which two carboxylates of DTPA are replaced by amide functionalities, form neutral complexes with lanthanide metals. These neutral complexes offer a significant advantage to their ionic counterparts. There have been concerns of nephrogenic systemic fibrosis (NSF, a hardening of kidney tissue leading to renal failure) due to contrast agents. Neutral contrast agents have reduced osmolarity and viscosity (as compared to their ionic counterparts), thus reducing the amount of contrast agent required for administration for an MRI scan. Gd(III) complexes of DTPA diamides, namely Gd-DTPA-BMA (gadodiamide or Omniscan®) and Gd-DTPA-BMEA (gadoversetamide or OptiMARK®) are now available commercially as contrast agents (Figure 1.6)[12, 15, 16, 21-24].

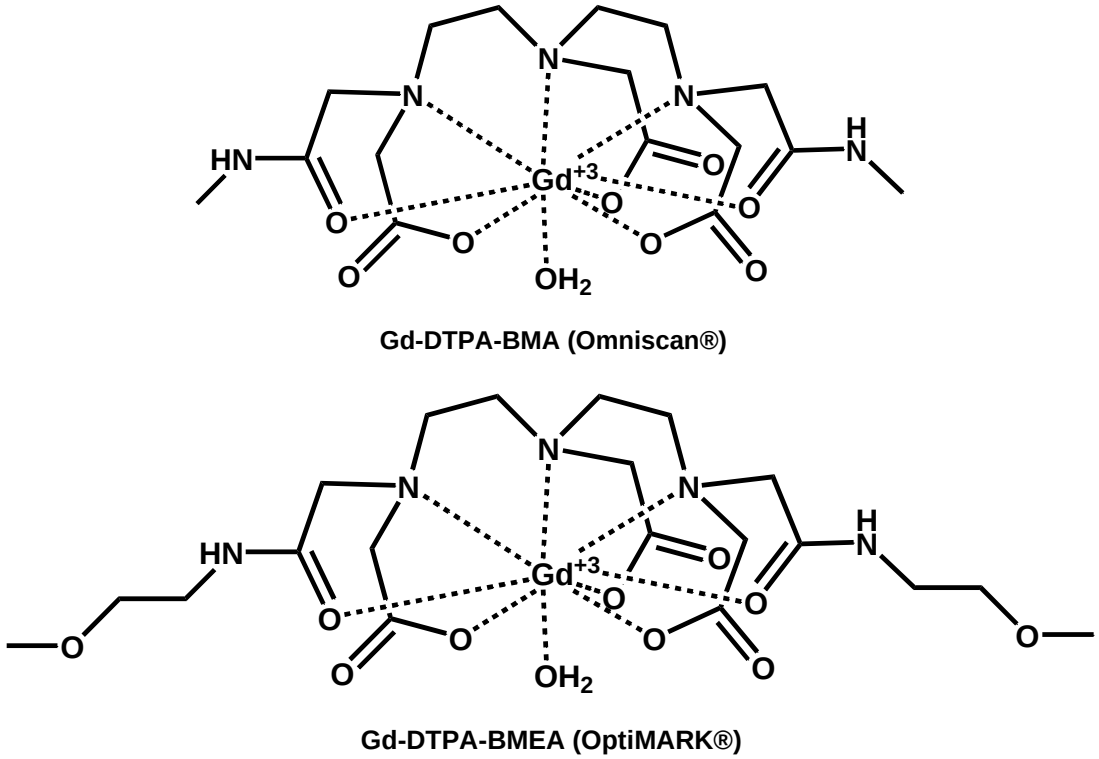
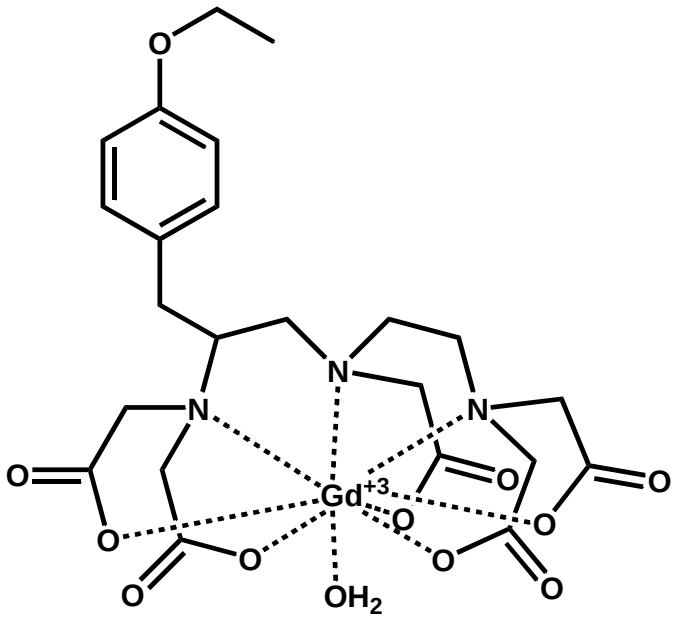


Figure 1.6: Commercially available Gd-DTPA diamide contrast agents[24].

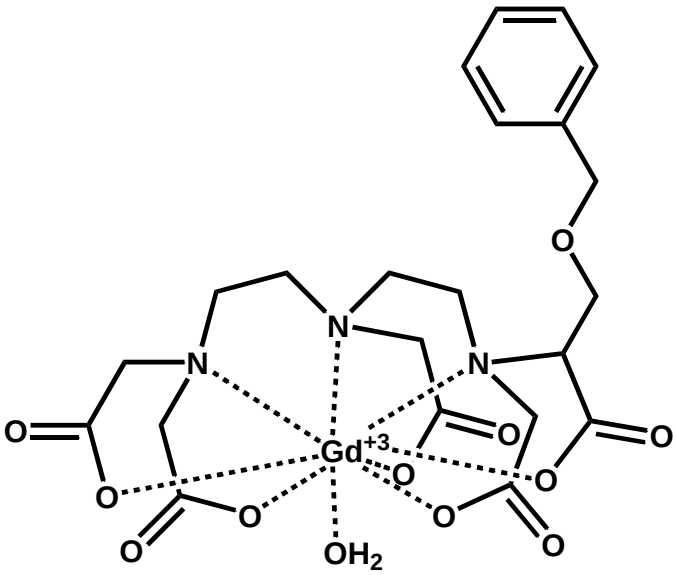
The thermodynamic stability of Gd(III) complexes of DTPA diamides is a few orders of magnitude smaller than Gd-DTPA. Conversion of one carboxylate group to an amide still yields an octadentate ligand, but the removal of one anionic donor atom and replacement by a non-ionic functional group results in a decrease in stability of the resulting Gd(III) complex (log K_{ML} = 16.85 for Gd-DTPA-BMA, and log K_{ML} = 16.84 for Gd-DTPA-BMEA). This demonstrates that the charge on the ligand side-chain and the basicity of that donor group are important determinants of complex stability. However, the drop in overall thermodynamic stability is not as important as the increase in selectivity for Gd(III) over other endogenous ions, such as Ca(II), Zn(II), and Cu(II), thus resulting in an *in vivo* toxicity three times lower than that of Gd-DTPA[12, 15, 16, 24].

The introduction of a lipophilic group into the structure of DTPA can be used to tune the specificity of the complex. Selective delivery of small molecule contrast agents to normal liver tissue was achieved using aryl-modified Gd(III) complexes, namely Gd-EOB-DTPA (Figure 1.7) and Gd-BOPTA (MultiHance®, Figure 1.8). Gd-EOB-DTPA comprises a Gd-DTPA core with a *para*-ethoxybenzyl side-chain linked through the carbon backbone of the chelate. In the BOPTA ligand, the terminal acetate methylene was used as a site for the introduction of the pendant aryl functionality. The ligands BOPTA and EOB-DTPA possess the same number and type of donor atoms as DTPA, resulting in similar stability constants (log K_{ML} = 22.59 for Gd-BOPTA, and log K_{ML} = 23.46 for Gd-EOB-DTPA)[12, 15, 24-28].



Gd-EOB-DTPA (Eovist®/Primovist®)

Figure 1.7: The aryl-modified Gd-DTPA complex, Gd-EOB-DTPA[24].



Gd-BOPTA (MultiHance®)

Figure 1.8: The aryl-modified Gd-DTPA complex, Gd-BOPTA[24].

Conformationally constrained ligands have been synthesized in order to achieve metal complexes whose *in vivo* dissociation is depressed. There are two main factors to substantiate this synthetic route: (i) a certain degree of pre-organization should favour the complexation process, and (ii) dissociation should be disfavoured due to the presence of steric barriers. This

has been achieved by incorporating cyclohexene into the diethylenetriamine backbone, as well as (more recently) using piperidine and azepane moieties, resulting in higher lipophilicity and greater hepatobiliary uptake of these complexes (Figure 1.9). This increase in the rigidity of the chelate system allows for some control of the geometry of the donor groups, and thus has a substantial effect on the stability of the metal complex. The addition of these lipophilic groups would also impact upon τ_M and τ_R, as these would decrease molecular tumbling and impart a greater electronic effect upon the metal centre, both leading to an increase in relaxivity[12, 15, 29].

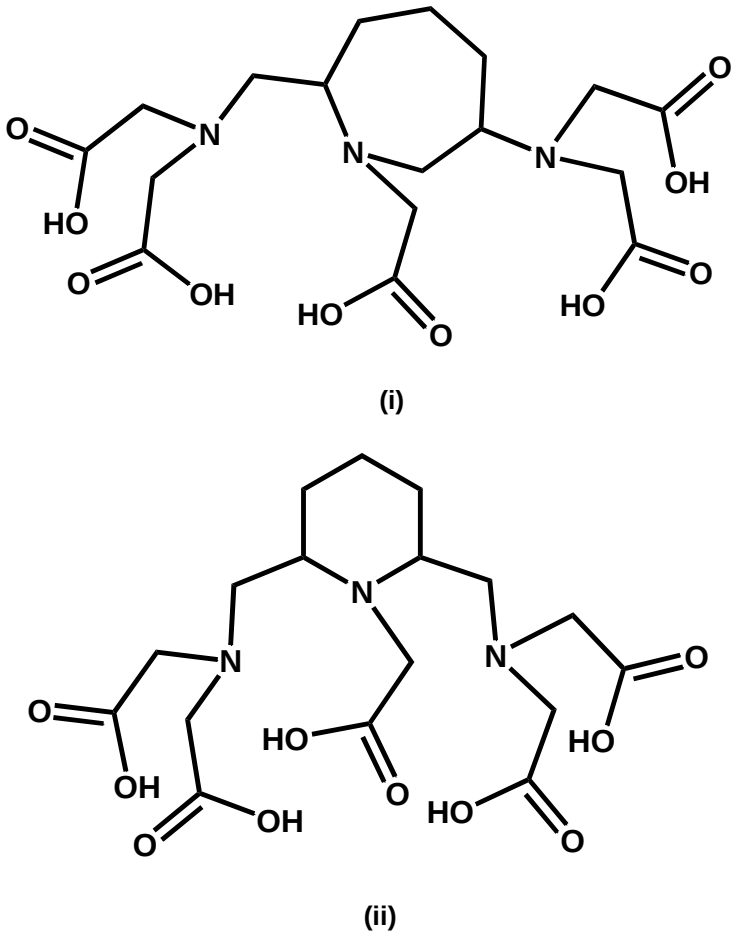


Figure 1.9: Azepane (AZEP-DTPA, (i)) and piperidine (PIP-DTPA, (ii)) backboned DTPA derivatives[29].

Another area of contrast agent research is the development of responsive or 'smart' contrast agents. The relaxivity and corresponding signal intensity of these agents respond to changes in the physiological environment[24]:

- The development of pH-responsive contrast agents has been stimulated by the observation that the extracellular pH of tumours (~ 6.8 – 6.9) is more acidic than tumour intracellular (7.2) and normal extracellular tissue pH (~ 7.4). Contrast agents that can respond to small changes in pH can be used to highlight tumours.
- The hypothermia treatment of tumours has been made possible due to the development of thermosensitive contrast agents. Temperature-sensitive liposome-encapsulated Gd-DTPA-BMA has already been designed in this respect (Figure 1.10). The liposomal composition was chosen to control the gel-to-liquid crystalline phase-transition temperature (T_m) of the liposomes. Below this threshold temperature, the water exchange rate between the interior and exterior is slow, and T_1 is reduced. As the temperature increases and exceeds T_m, the water permeability of the liposomal membrane increases, allowing for faster water exchange.
- Contrast agents have also been designed to respond to different *in vivo* concentrations of certain ions, e.g. Zn(II), thus altering the relaxivity. Figure 1.11 illustrates an example whereby relaxivity is decreased upon the binding of endogenous Zn(II). In this case, chelation of Zn(II) greatly decreases the accessibility of the Gd(III) complex to the bulk solvent, resulting in high τ_M and thus reduced relaxivity.

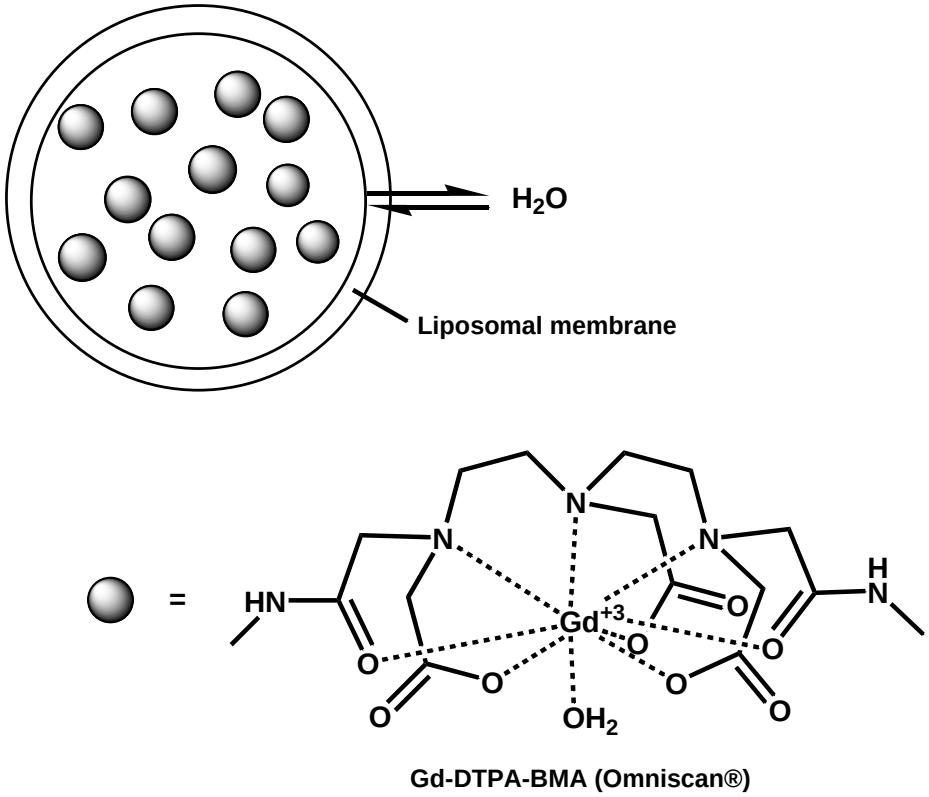


Figure 1.10: Temperature-sensitive liposomal MRI contrast agent[24].

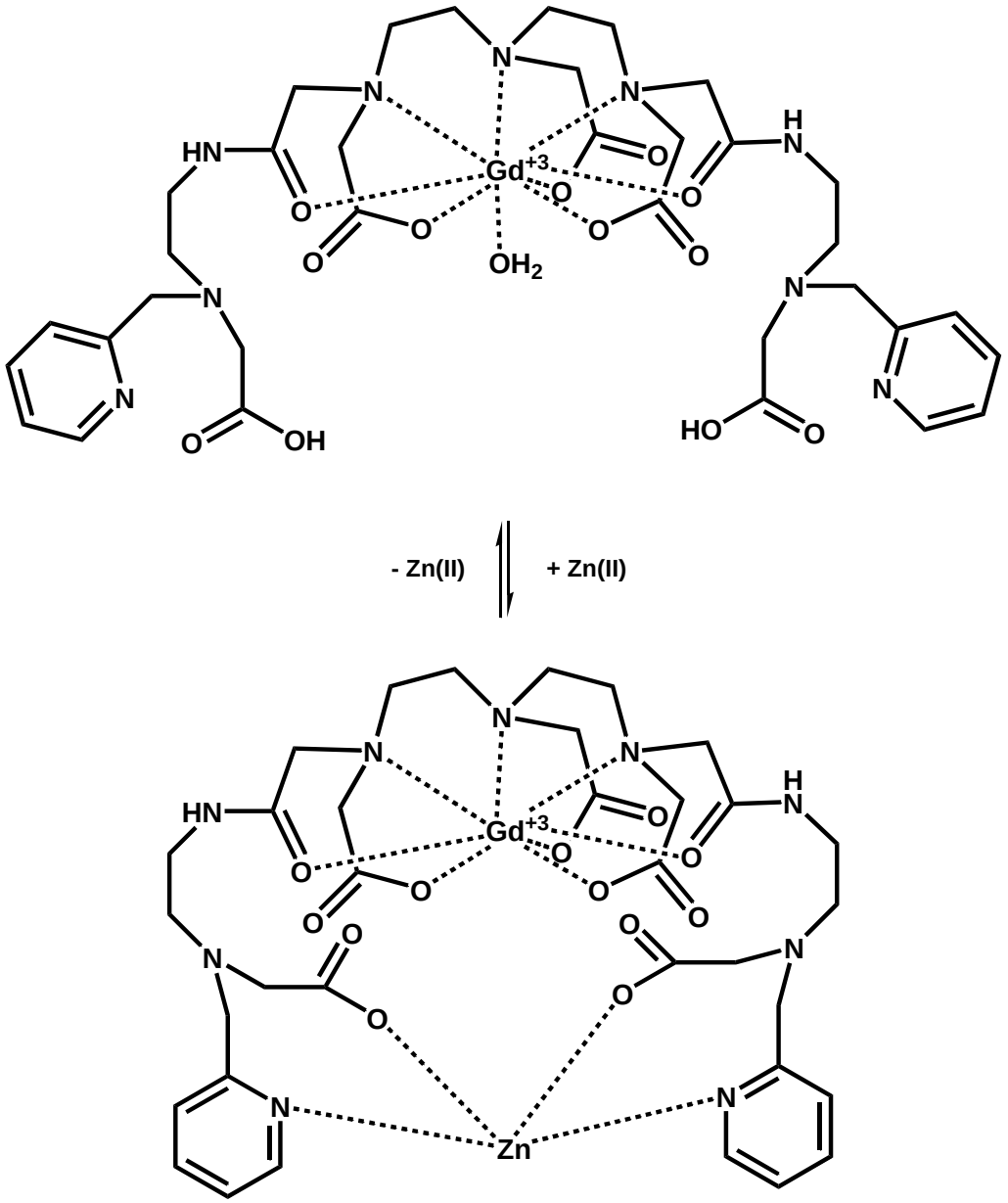


Figure 1.11: Derivative of DTPA which responds to endogenous Zn(II)[24].

Applications involving protein/Gd(III) chelate conjugates have been exploited due to their prolonged intravascular retention time as opposed to smaller molecules such as Gd-DTPA. In the circulatory system, human serum albumin (HSA) is the most common protein capable of binding metal ions and their chelates and human serum transferrin (HTf) is the most important binding protein of lanthanide complexes. Both proteins play an important role in the uptake and transportation of contrast agents in the body. Two mechanisms have been exploited to achieve vascular retention: increased molecular weight (achieved by the attachment of polymers or dendrimers to the contrast agent, to slow down molecular tumbling) and non-covalent binding to endogenous plasma proteins. One such example of

this second mechanism is the albumin-bound ligand MS-325, which has been proposed as a candidate contrast agent for MR angiography (Figure 1.12). The introduction of the phosphodiester group is critical for protein binding and increasing the residence time of the compound. The latter is achieved due to a shift from liver uptake to the renal excretion path, presumably due to the glomerular filtration process being slower than excretion by the liver[12, 24].

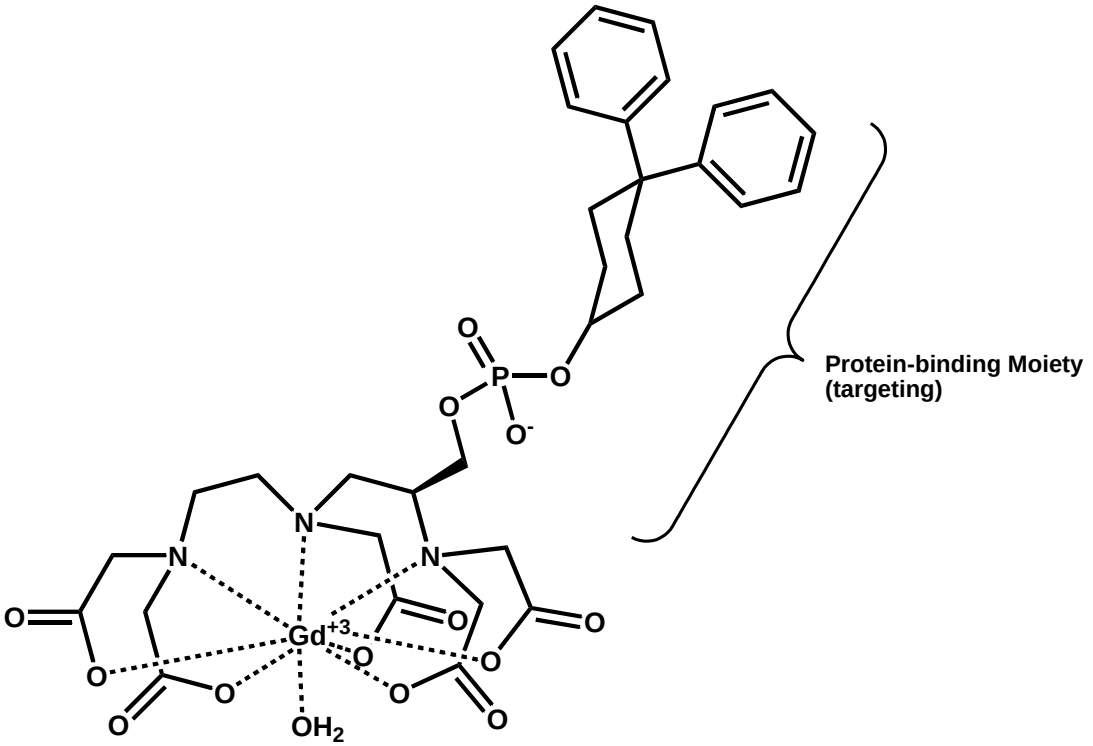


Figure 1.12: The phosphodiester-based contrast agent MS-325[24].

1.2 Lanthanide Luminescence

Europium(III) is a poor contrast agent compared to Gd(III), but it is an efficient luminescent species, and can therefore be used as a structural probe for corresponding Gd(III) analogues (due to its similar charge and ionic radius (Gd(III) = 1.107 Å and Eu(III) = 1.12 Å))[30]. Luminescence spectra aid the determination of complex speciation, structure and symmetry, as well as hydration states, and have thus aided the development of new contrast agents[3, 12, 31, 32].

1.2.1 Origin of Luminescence

Luminescence is the emission of light by a substance. This process first involves the promotion of an electron from the lowest vibrational level of the electronic ground state of the molecule (i.e. the lowest lying electronic state, corresponding to the state having the configuration in which all electrons are in the lowest energy orbitals available) to one of the many vibrational levels in the electronically excited state of the molecule (which is normally a higher energy, unoccupied orbital in the ground state). Electron promotion from a ground singlet state (an electronic state of the molecule in which there are no unpaired electrons) to an excited state occurs as the result of the absorption of electromagnetic radiation (usually in the UV-visible region of the spectrum) by a molecule. This electron promotion can occur in one of two ways[33-37]:

- If the promotion of an electron occurs from the ground singlet state with the retention of the original spin, then the electron is excited to an excited singlet state.
- If the promotion of the electron results in a change of spin, there will be two unpaired electrons in the molecule (the promoted electron and the residual electron), and the molecule is in an excited triplet state (Figure 1.13).

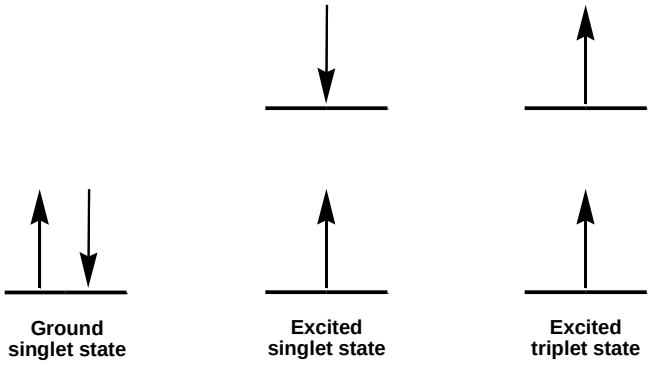


Figure 1.13: Promotion of an electron from the ground state to an excited state[35].

The absorption process is followed by an emission process (also known as a relaxation process). During the relaxation process, the excited electron returns to the ground state, thus resulting in the emission of energy (in the form of a photon) without generating heat. The wavelength of the re-emitted radiation is usually longer than the wavelength of the radiation absorbed because the initial relaxation process involves a radiationless transition from the higher vibrational levels of the electronically excited state to the lowest vibrational level of the electronically excited state. The molecule loses its excitation energy only by going to a lower electronic energy level, and this can be accomplished in one of three ways[33-37]:

- If the higher vibrational levels of the ground state overlap with the lower vibrational levels of the electronically excited state, then vibrational relaxation of the excited state follows and the excess vibrational energy is lost as kinetic energy to other molecules with which it collides.
- If the energy separations of the upper and lower electronic states are relatively large, a radiative transition occurs from the lowest vibrational level of the upper electronic state to a vibrational level in the lower electronic state. The excess energy is released as a photon of visible or UV-light. This radiative form of relaxation is known as fluorescence, and denotes luminescence which occurs when a molecule makes an allowed optical transition (i.e. from an excited singlet state to a ground singlet state).
- If there is sufficient overlap between the lower vibrational levels of the excited singlet state and the upper vibrational levels of a triplet state, there is a finite probability that the triplet state can be populated from the excited singlet state.

The mechanism by which this occurs is known as singlet-triplet intersystem crossing. This process is accompanied by a change of spin. Relaxation from the excited triplet state to the ground singlet state then occurs by the release of energy in the form of a photon. This mode of relaxation is known as phosphorescence. Phosphorescence is not as common as fluorescence since the probability that a change of spin can occur is much lower than for the corresponding process with no change of spin.

The relaxation processes are summarised in Figure 1.14.

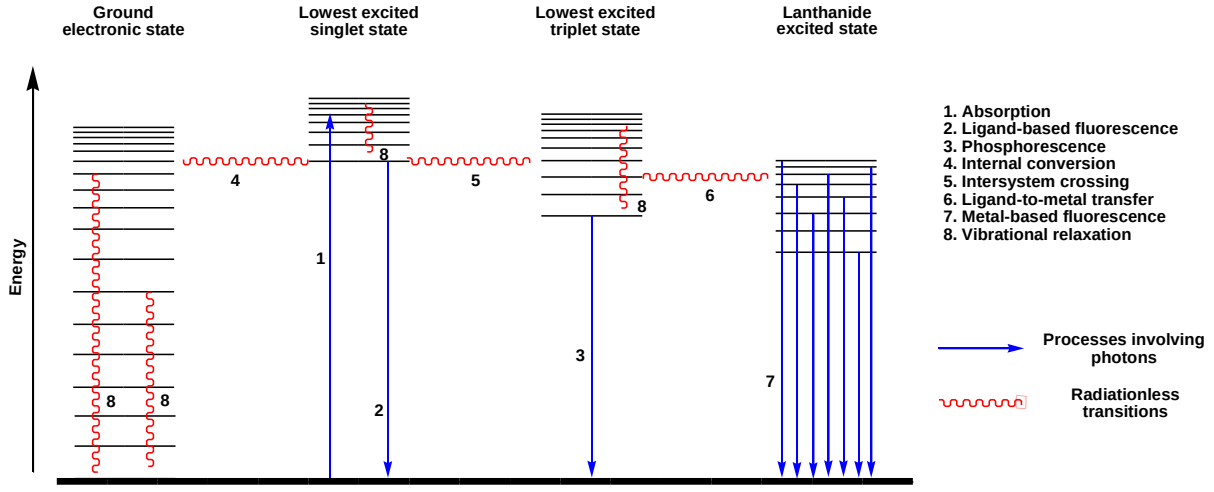


Figure 1.14: Summary of the relaxation processes following excitation of a molecular species[35].

The structure of the molecule impacts greatly on luminescence. Aliphatic molecules and others which do not have rigid molecular structures rarely exhibit luminescence. This is due to the greater number of vibrational levels that the molecule possesses, thus allowing for a favourable vibrational dissipation of energy. A luminescent lanthanide (Ln) complex is a system in which light is absorbed by the organic ligand, transferred to the metal centre (in the +3 oxidation state), and emitted by the cation (Figure 1.14). Luminescent Ln complexes have a rich history as unique lumophores. Their uniqueness lies in their line-like emission (at long wavelengths) in their frequency domain and their delayed emission in the time domain, thus permitting sensitive signal detection. These complexes have many useful applications, including replacements for radioimmunoassay (owing to their low detection limits and that the problems associated with the handling and disposal of radiolabelled substances are

avoided); alternatives to standard luminescent dyes; donors in energy transfer experiments to measure both static and time-varying distances; and uses as 'tags' to monitor the fate of ions or molecules within cells[20, 38-42].

Though several Ln(III) ions exhibit luminescence, the majority of luminescent Ln labels use the trivalent cations of terbium (Tb) and europium (Eu). The excitation of Ln(III) ions is locked away in their inner f orbitals, thus restricting the impact of environmental processes upon excitation. This is critical for their function as luminescent labels, since a label must remain constant in all its parameters in whatever environment it is placed into. However, hydration of these cations results in loss of luminescence (i.e. quenching), since an alternative relaxation pathway (vibrational relaxation, in this case) is available. This problem can be overcome by replacing the hydration sphere with hard ligating atoms devoid of O-H bonds[43-48].

Ln(III) ions are poor absorbers of excitation energy, due to the difficulty of the f-f electronic transition. However, the advantage of these disallowed transitions is that once the excited state of the Ln(III) ion has been populated, the difficulty in the de-excitation process (i.e. the emission of luminescence) forces a longer excited state lifetime. In other words, the luminescence lifetimes of the Ln(III) ions are of the order of milliseconds, compared to typical luminescence lifetimes in the nanosecond to microsecond range. However, the formation of complexes of these Ln(III) ions allow for faster and more efficient population of the lowest excited state, as a result of ligand-to-metal charge transfer. Encapsulation of the Ln(III) ion within a ligand structure also reduces its toxicity within a biological environment. This makes the use of luminescent lanthanide complexes in biological media highly advantageous, as it allows for time-resolved detection procedures, thus allowing for discrimination of luminescence emission from the Ln sensor from the short-lived background luminescence of biological materials. This enables extremely low levels of detection of analyte concentration[20, 42-48].

1.2.2 The Luminescence Experiment

The instrument that is used for the measurement of luminescence in a sample is called a spectrofluorimeter. It consists essentially of a light source, an excitation monochromator, an emission monochromator, and a photodetector. The light source is required to electronically excite the molecule, and must therefore have an intense output containing all the wavelengths in the near UV-visible range. The excitation monochromator separates the light of desired wavelength for the excitation process from the source (using gratings), with the required wavelength for excitation being determined via UV-visible spectrophotometry. The purpose of the emission monochromator is to separate the excited light from the luminescence emission falling on the photodetector. The photodetector is responsible for translating the luminescent light into an electrical signal that can be measured[33].

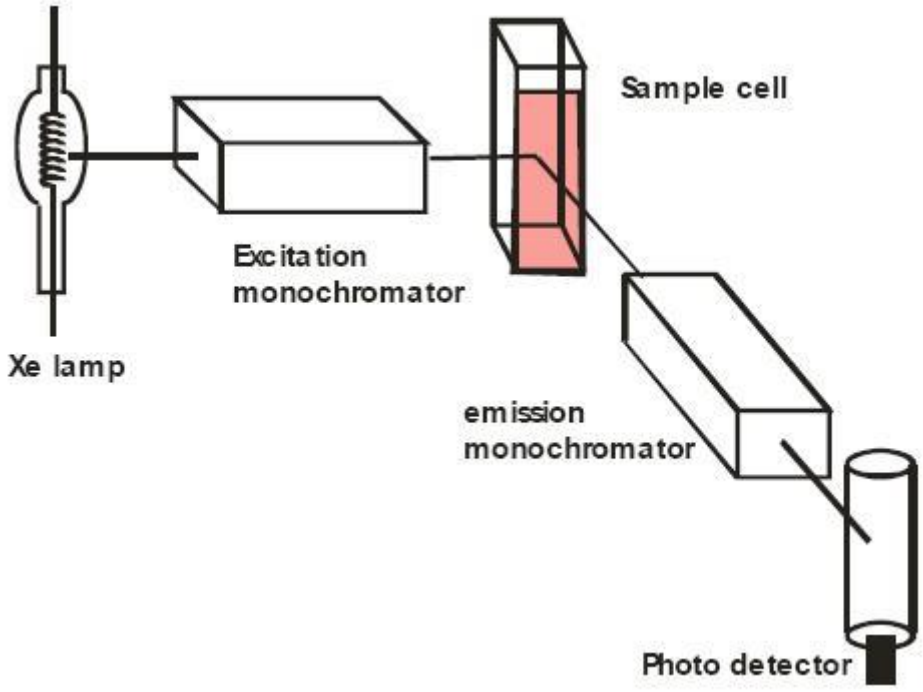


Figure 1.15: Schematic representation of a spectrofluorimeter[49].

The intensity of luminescence spectra is extremely sensitive to solvent polarity and hydrogen bonding properties, due to the change in dipole moment accompanying the excitation process of the luminescent molecules and the effect of the non-bonding and lone electron pairs of the

solvent on the excited molecules. Molecules which are more polar in the excited state usually show longer wavelengths of luminescence in increasingly polar solvents[33].

The excitation process is usually more affected by the hydrogen bond donor properties of the solvent than solvent polarity. If a non-bonding electron pair on a luminescent molecule is bound by a hydrogen atom of the solvent, the hydrogen bond stabilises both the ground and excited states of the molecule. The result is a shift in the spectra to shorter wavelengths with increasing hydrogen bond donor capacity of the solvent. A similar effect on the luminescence spectrum is observed with increasing hydrogen bond donor capacity of the solvent, when interacting with lone pairs on functional groups such as –OH and $–NH_2$ on the luminescent molecule. Hydrogen bond acceptor solvents produce shifts to longer wavelengths when interacting with lone pairs on functional groups such as –OH and $–NH_2$. However, in most cases, increases in solvent hydrogen bonding or polarity produce decreases in luminescence efficiency. The reason for this is that the hydrogen bonding and/or dipole-dipole interaction in the excited state increases the rate of vibrational relaxation[33].

The addition of acids or bases to the solvent containing the luminescent molecule can affect the spectrum obtained in one of two ways. If the addition of the acid or base to the solvent is insufficient to either protonate lone electron pairs or abstract a proton from a functional group, then the added acid or base can hydrogen-bond to the basic or acidic functional groups, thus affecting the wavelength of the emission in the same way as for a hydrogen bond donor or acceptor solvent. If the acidity of the medium after the addition of acid or base is able to promote the protonation or the abstraction of a proton from a functional group, then the result is a chemical species whose electronic structure and reactivity differ from that of the original molecule. Protonation of non-bonded pairs on functional groups which are charge-transfer acceptors in the excited state (e.g. carboxyl or carbonyl groups) stabilise the excited state relative to the ground state, and result in a shift of the spectra to higher wavelengths. Protonation of lone pairs on functional groups which are charge-transfer donors in the excited state (e.g. –OH and $–NH_2$) result in an inhibition of the donor properties of these groups and cause a shifting of the spectra to shorter wavelengths[33].

The spectrofluorimeter is used in several applications such as the determination of the luminescence lifetime of a luminescent species; measuring the concentration of analytes in solution (determined from the intensity of the luminescence); and qualitative immunoluminescent identification of pathogens and in the identification of cellular structures by luminescent staining techniques. This technique lends itself particularly well to the determination of pK_a values associated with hydrolysis of metal complexes and the removal of dissociable protons in ligating systems. The experiment involves the preparation of a series of buffered solutions containing equal amounts of analyte at varying pH values. Fluorimetric titrations of this nature afford information from the recorded spectra, such as maxima of recorded bands and their relative shifts, allowing for an accurate estimation of pK_a values associated with deprotonation equilibria[33].

1.2.3 Luminescent Lanthanide Sensors

Luminescent sensors provide information about the chemical nature of its environment by means of the emission of luminescence. Molecular luminescence is a useful biosensing technique due to the ease and sensitivity of its detection. Thus, low concentrations of luminescent molecules can be measured, and even the single molecule level can be approached. Luminescent sensors also provide a technique with which the presence of cations or anions in solution can be determined[50, 51].

Lanthanide metal complexes (most commonly Tb(III) and Eu(III)) have found use as biological sensors, due to their long-lived excited state lifetimes, despite the difficulty of the Laporte forbidden f-f transitions. A solution to overcoming the inefficient direct excitation of the Ln(III) ion is to incorporate a sensitising chromophore into the structure of the lanthanide-binding ligand, thus allowing for indirect excitation of the complexed lanthanide ion. This absorbing chromophore is often referred to as an antenna, and is an organic π-electron system. The principle is that the antenna absorbs light strongly at a suitable wavelength to excite the Ln(III) ion. The antenna must then be able to efficiently transfer its excitation energy (via an electronic energy transfer process) to the metal ion, thus exciting the metal ion to an emissive state (Figure 1.16). An antenna is therefore essential for the widespread exploitation of lanthanide(III) luminescence[20, 40, 43, 52].

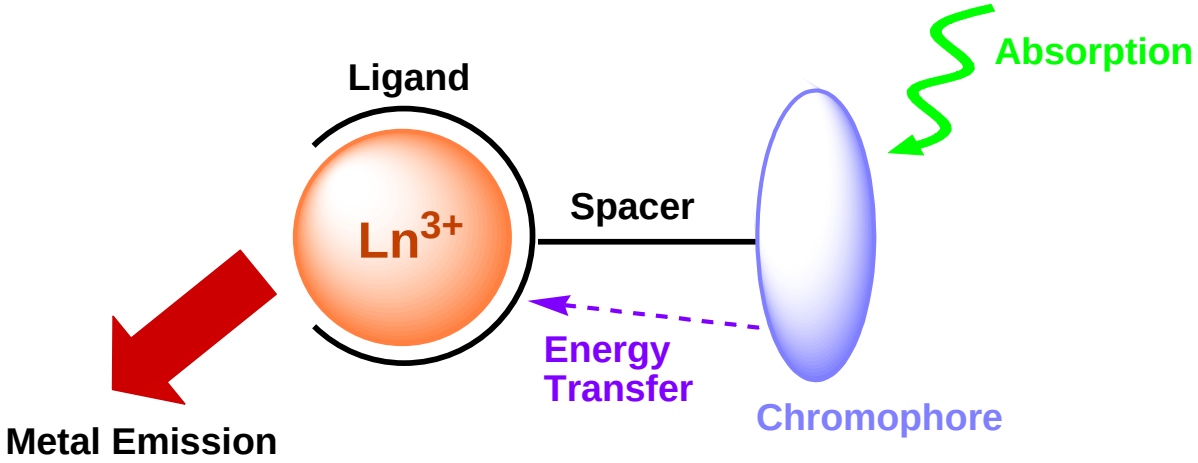


Figure 1.16: The effect of an antenna in sensitizing luminescence emission from the complexed lanthanide(III) ion[51].

The Ln(III) complexes must show high kinetic stability in the pH range 3-10, in order to prevent significant metal dissociation at high dilution. In other words, suitable complexes should display very low dissociation constants. This is extremely important for applications concerned with the detection of molecules at low concentration, otherwise qualitative measurements would not be possible[20, 52].

The most common co-ordination numbers of the Ln(III) ions are eight and nine. To form stable complexes in aqueous solutions, the ligand should possess donor atoms with which to complex the hard Ln(III) ion. Among neutral donors, the more polarisable amine nitrogens are preferred over less polar substituents, such as alcohols. Hard anionic donors bind well to the trication, thus making groups such as carboxylates an attractive choice. Therefore, polyaminocarboxylates are good candidates for use as ligands in the formation of luminescent Ln complexes[20].

Ln complexes should be efficiently shielded from the competitive, non-radiative deactivation pathways which are likely to arise in solution. The deactivation of the emissive metal states occurs via vibrational relaxation, and often involves solvent water molecules. This effect arises through an energy transfer process from the metal excited state to the O–H stretching vibrations of coordinated or closely diffusing water molecules. Deactivation may also occur by means of vibrational relaxation to N–H, C–H, or C=O oscillators of the bound ligand or of

the solvent. This results in a decrease in both the lifetime and intensity of the emission, with reductions of lifetime from the millisecond range to less than 2.5μs. In fact, luminescence lifetimes are inversely related to the number of water molecules coordinated to the Ln(III) ion[20, 42, 53].

Therefore, to reduce the quenching effect of solvent molecules on the luminescent metal centre, octa- or nonadentate ligands are suggested for the complexation of Ln(III) ions. For heptadentate lanthanide complexes in aqueous media, up to two water molecules may be coordinated. The quenching H_2O molecules can be efficiently displaced by anionic species, resulting in significant emission enhancement[52].

Two other criteria that should be met in the design of suitable ligands for the complexation of the Ln(III) ion are the solubility of the complex and the overall charge of the complex. The solubility becomes important because of potential precipitation problems and the overall charge is important for solubility and for avoiding non-specific labelling of cellular components, which are usually negatively charged[38].

The majority of luminescent Ln complexes employ cyclic ligands to chelate the Ln(III) ion. Of these cyclic ligands, the derivatives of 1, 4, 7, 10-tetraazacyclododecane (cyclen, Figure 1.17) are the most commonly used, owing to their very low dissociation constants. There are, however, a number of luminescent Ln species comprised of acyclic ligands. Most acyclic ligands are derived from DTPA, owing to its excellent solubility; relatively high coordination numbers; efficient energy transfer to the complexed Ln(III) ion, and low dissociation constants[38].

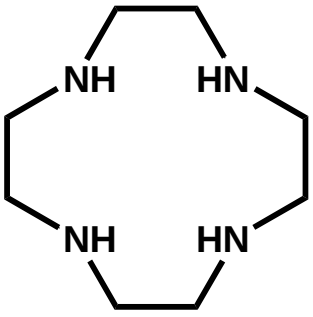


Figure 1.17: Diagram of cyclen.

Lanthanide luminescent sensors function as a result of the interaction between the substrate and the lanthanide complex (usually an electrostatic interaction). Substrate recognition is communicated by the enhancement or decrease of the light emission[50]. These recognition events can be monitored from the modulation of the emission bands. Observation of the 'hypersensitive' emission band (Eu(III) = 615 nm and Tb(III) = 540 nm) is essential as the modulation of this band is particularly sensitive to changes in metal ion environment[48]. The response of the hypersensitive band has been developed to monitor ionic species such as citrate and lactate in solution, thus allowing for determination at low concentration[54].

The accuracy of the luminescence experiment can be further increased by calibrating two emission bands at different wavelengths, thus reducing the effect of background noise[55-58]. This ratiometric response is often observed by employing a bis-lanthanide ensemble, comprised of a mixture of Eu(III) and Tb(III) complexes. Such ratiometric probes have been employed as pH sensors[56, 57] and for the detection of $^{\cdot}OH$ and ClO^{-}[58]. The ratiometric ratio has also been observed for a single lanthanide system, as a pH sensor in alkaline media[59].

The design of responsive lanthanide sensors for the detection of biomolecules in aqueous media is significant for several industrial, environmental and medicinal applications. Detection of carboxylate anions is of particular importance. Enzymes, antibodies, amino acids and metabolic intermediates contain a variety of carboxylate moieties that, in some cases, account for characteristic biochemical behaviour. Coordinatively unsaturated lanthanide probes (i.e. Ln(III) complexes bearing ligand heptadenticity) are often utilised to detect these molecules, with successive displacement of coordinated aqua ligands, resulting in the formation of carboxylate ternary complexes bearing bidentate chelation. Sensing of aromatic and aliphatic carboxylate biomolecules have been successfully demonstrated for several Eu(III), Tb(III), and Yb(III) complexes[60-64].

The recognition of dicarboxylate anions is of medicinal and biological significance, as many metabolic and energy storage processes involve the participation of these dianions. The detection of phthalates (a class of aromatic dicarboxylate species) and their metabolites in biological media is particularly crucial. Phthalates are widespread micro-pollutants

commonly used as softeners in the manufacture of plastics, such as PVC. Human exposure to phthalates occurs through food (meat, fish and milk products commonly packaged in PVC material) and plastic medical devices (such as intravenous tubing and blood transfusion bags). Human exposure to phthalates has revealed their function as endocrine disruptors (resulting in obesity and possible insulin resistance) and results in disorders of the genital tract (observed in infant males)[65-70]. The detection of terephthalic acid has been observed for dinuclear Tb(III) complexes (comprised of two, heptadentate Tb(III) complexes linked via a p-xylyl spacer)[62]. An alternative strategy for the detection of phthalates involves the use of photophysically-silent Ln(III) complexes (i.e. a luminescent sensor in which a covalently-appended chromophore is absent), with the aromatic phthalate dianion serving as the antenna. Thus, upon the formation of a phthalate ternary complex, lanthanide ion emission would be enhanced (via antenna excitation). This strategy has been successfully employed in the detection of several aromatic carboxylates, using cyclic Eu(III) and Tb(III) complexes[63].

1.3 Project Aims

The high cost of gadolinium-based contrast agents can be highlighted in terms of the cost per treatment. Prices range from US $90 and US $236 (2009 figures). Additional costs include the manufacturing and importation duties, consumables and labour[23].

Table 1.2: Cost per application of contrast agents, assuming body weight = 70 kg (as of 2005)[71].

Name	Dosage Regimen	Cost Per Treatment
Magnevist®	0.2 mL/kg	US $94.91
Omniscan®	0.2 mL/kg	US $98.00
MultiHance®	0.2 mL/kg	US $98.98
OptiMARK®	0.2 mL/kg	US $81.95

Several administrations of the contrast agent are often required for an imaging protocol, thus making this process very expensive. This high cost, as well as the need for improved contrast agents, is the general motivation behind this research project. The specific aim of this project is to synthesize new polyaminocarboxylate ligands from relatively cheap starting materials with improved efficiency as contrast agents in the MRI experiment. The target compounds are illustrated below.

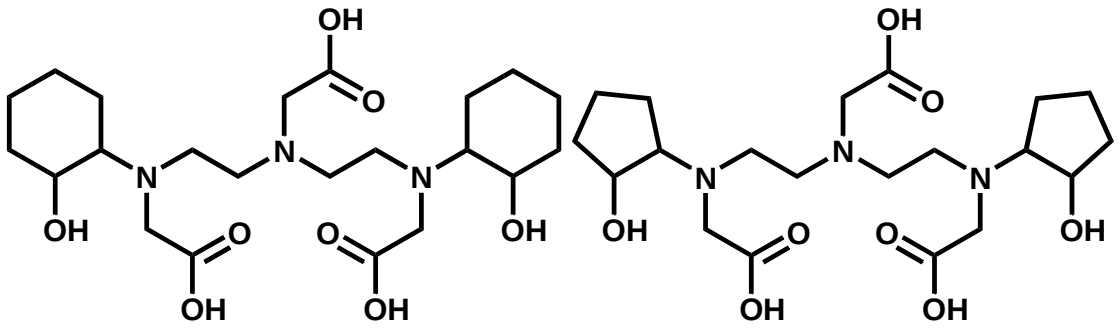


Figure 1.18: Modified octadentate polyaminocarboxylates, the target compounds of this research.

The target compounds shown in Figure 1.18 are DTPA derivatives, where two of the terminal acetic acid side-arms have been replaced by cyclohexanol and cyclopentanol moieties. Fusing

the bulkier alkyl groups on pendant moieties is expected to affect the relaxivity of the metal complex by modulation of the rotational correlation time (τ_R) in solution due to the bulkier alkyl substituents, and the rate of exchange of coordinated water molecules at the metal centre (i.e. a decrease in τ_M). Additionally, the incorporation of the weaker chelating alcohol moieties may facilitate fluxional ligand denticity of the lanthanide complex in the presence of biomolecules in aqueous solution. The responsive nature of the Ln(III) complex towards ions in solution may lead to improved relaxivity in the MRI experiment (using Gd^{3+}) or modulation of the photophysical properties (using Eu^{3+} or Tb^{3+}) upon analyte recognition[24].

Heptadentate ligands (Figure 1.19) permit more coordinated water molecules in the coordination polyhedron. Greater hydration and improved exchange with the bulk solvent is essential in improving the *in vivo* performance of contrast agents.

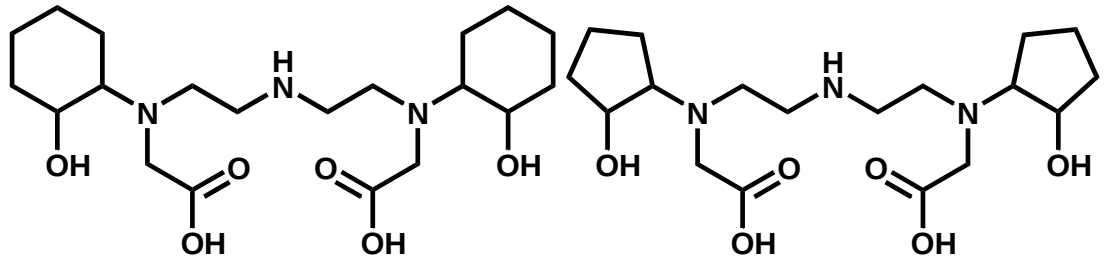


Figure 1.19: Modified heptadentate polyaminocarboxylates, the target compounds of this research.

The structure, speciation, and hydration sphere of the Gd(III) complexes were to be elucidated by studying the luminescent Eu(III) analogues using fluorescence spectroscopy.

The pK_a values for the ligands were determined.

1.4 References

1. MRI contrast agent. http://pediaview.com/openpedia/MRI_contrast_agent (2013-03-31),
2. Hannel, J. W., Kryst-Widzgowska, T., Klinowski, J., *A Primer Of Magnetic Resonance Imaging*. Imperial College Press: London, 1997.
3. Jones, C. J., and Thornback, J. R., *Medical Applications Of Coordination Chemistry*. The Royal Society Of Chemistry: Cambridge, 2007.
4. Bushong, S. C., *Magnetic Resonance Imaging: Physical And Biological Properties*. The C. V. Mosby Company: Missouri, 1988.
5. Buxton, R. B., *Introduction To Functional Magnetic Resonance Imaging: Principles And Techniques*. Cambridge University Press: 2002.
6. MRI Tutor. http://www.mritutor.org/mritutor/index.html (2013-03-31),
7. Faulkner, W. Basic Principles Of MRI. http://www.e-radiography.net/mrict/Basic_MR.pdf (2013-03-31),
8. Hornak, J. P. The Basics Of MRI. http://www.cis.rit.edu/htbooks/mri/ (2013-03-31),
9. Lacoste-Julien, S. Nuclear Magnetic Resonance Imaging. http://msdl.cs.mcgill.ca/people/slacoste/school/electromagnetic_theory/MRIpdf.pdf (2013-03-31),
10. Magnetic resonance imaging. http://en.wikipedia.org/wiki/Magnetic_resonance_imaging (2013-03-31),
11. Kean, D., and Smith, M., *Magnetic Resonance Imaging: Principles And Applications*. William Heinemann Medical Books: London, 1986.
12. Merbach, A. E., and Tóth, É., *The Chemistry Of Contrast Agents In Medical Magnetic Resonance Imaging*. John Wiley & Sons, Ltd.: 2001.
13. Magnetic Resonance Imaging (MRI). http://www.ebme.co.uk/arts/mri (2013-03-31),
14. Relaxation (NMR). http://en.wikipedia.org/wiki/Relaxation_(NMR) (2013-03-31),
15. Sherry, A. D., Caravan, P., and Lenkinski, R. E., *J. Magn. Reson. Imaging* **2009,** 30, (6), 1240-1248.
16. Choppin, G. R., and Schaab, K. M., *Inorg. Chim. Acta* **1996,** 252, (1-2), 299-310.
17. Mishra, A., *Design, Synthesis and characterization of smart MR contrast agents sensitive to pH/calcium changes during neural activity.* University of Tübingen, 2004.

18. Stark, D. D. a. B. J., W. G., *Magnetic Resonance Imaging Volume I*. 3rd. ed.; Mosby: 1999.
19. Edelman, R. R., Hesselink, J. R., and Zlatkin, M. B., *Clinical Magnetic Resonance Imaging Volume I*. 2nd ed.; W. B. Saunders Company: 1996.
20. Parker, D., and Williams, J. A. G., *J. Chem. Soc., Dalton Trans.* **1996,** 1996, (18), 3613-3628.
21. Nonionic Intravenous Contrast Agents. http://www.mr-tip.com/serv1.php?type=db1&dbs=Nonionic%20Intravenous%20Contrast%20Agents (2013-03-31),
22. Ionic Intravenous Contrast Agents. http://www.mr-tip.com/serv1.php?type=db1&dbs=Ionic%20Intravenous%20Contrast%20Agents (2013-03-31),
23. Laskaris, J. X., *Issues That Matter* **2009,** 2, (6).
24. Zhang, Z., Nair, S. A., and McMurry, T. J., *Curr. Med. Chem.* **2005,** 12, (7), 751-778.
25. Pálinkás, Z., Baranyai, Z., Brücher, E., and Rózsa, B., *Inorg. Chem.* **2011,** 50, (8), 3471-3478.
26. Schmitt-Willich, H., Brehm, M., Ewers, Ch. L. J., Michl, G., Müller-Fahrnow, A., Petrov, O., Platzek, J., Radüchel, B., and Sülzle, D., *Inorg. Chem.* **1999,** 38, (6), 1134-1144.
27. Reichert, D. E., Lewis, J. S., and Anderson, C. J., *Coord. Chem. Rev.* **1999,** 184, (1), 3-66.
28. Lorusso, V., Pascolo, L., Fernetti, C., Anelli, P. L., Uggeri, F., and Tiribelli, C., *Curr. Pharm. Design* **2005,** 11, (31), 4079-4098.
29. Choong, H., Garmestani, K., Bryant Jr., L. H., Milenic, D. E., Overstreet, T., Birch, N., Le, T., Brady, E. D., and Brechbiel, M. W., *J. Med. Chem.* **2006,** 49, (6), 2055-2062.
30. Shannon, R. D., *Acta Cryst. A* **1976,** 32, (5), 751-767.
31. Bottrill, M., Kwok, L., and Long, N. J., *Chem. Soc. Rev.* **2006,** 35, (6), 557-571.
32. Urbanczyk-Pearson, L. M., Femia, F. J., Smith, J., Parigi, G., Duimstra, J. A., Eckermann, A. L., Luchinat, C., and Meade, T. J., *Inorg. Chem.* **2008,** 47, (1), 56-68.
33. Schulman, S. G., *Fluorescence and Phosphorescence Spectroscopy: Physicochemical Principles and Practice*. Pergamon Press: Exeter, U. K., 1977.
34. Luminescence and Fluorescence. http://www.uvminerals.org/luminese.htm (2013-03-31),

35. UV-Vis Luminescence Spectroscopy. http://teaching.shu.ac.uk/hwb/chemistry/tutorials/molspec/lumin1.htm (2013-03-31),
36. Luminescence. http://www.answers.com/topic/luminescence?cat=health (2013-03-31),
37. Fluorescence. http://www.answers.com/topic/fluorescence?cat=health (2013-03-31),
38. Li, M., and Selvin, P. R., *J. Am. Chem. Soc.* **1995,** 117, (31), 8132-8138.
39. Remuiñán, M. J., Román, H., Alonso, M. T., and Rodríguez-Ubis, J. C., *J. Chem. Soc., Perkin Trans. 2* **1993,** 1993, (6), 1099-1102.
40. de Silva, A. P., Fox, D. B., Huxley, A. J. M., McClenagham, N. D., and Roiron, J., *Coord. Chem. Rev.* **1999,** 185-186, 297-306.
41. Parker, D., *Chem. Soc. Rev.* **2004,** 33, (3), 156 - 165.
42. Parker, D., and Williams, J. A. G., *J. Chem. Soc., Dalton Trans.* **1996,** 1996, (18), 3613 - 3628.
43. de Silva, A. S., Gunaratne, H. Q. N., Gunnlaugsson, T., Huxley, A. J. M., McCoy, C. P., Rademacher, J. T., and Rice, T. E., *Chem. Rev.* **1997,** 97, (5), 1515-1566.
44. Richardson, F. S., *Chem. Rev.* **1982,** 82, (5), 541-552.
45. Balzani, V., and Ballardini, R., *Photochem. and Photobiol.* **1990,** 52, (2), 409-416.
46. Sabbatini, N., Guardigli, M., and Lehn, J., *Coord. Chem. Rev.* **1993,** 123, (1-2), 201-228.
47. Bünzli, J., *Nature Chem.* **2010,** 2, (8), 696.
48. Bünzli, J. G., *Chem. Rev.* **2010,** 110, (5), 2729-2755.
49. Spectrofluorometer: Wikis. http://www.thefullwiki.org/Spectrofluorometer (2013-03-31),
50. Fabbrizzi, L., Licchelli, M., Rabaioli G., and Taglietti, A., *Coord. Chem. Rev.* **2000,** 205, (1), 85-108.
51. Bryan, A. J., de Silva, A. P., de Silva, S. A., Rupasinghe, R. A. D. D., and Sandanayake, K. R. A. S., *Biosensors* **1989,** 4, (3), 169-179.
52. Parker, D., *Coord. Chem. Rev.* **2000,** 205, (1), 109-130.
53. Canfi, A., Bailey, M. P., and Rocks, B. F., *Analyst* **1989,** 114, (11), 1405-1406.
54. Pal, R., Parker, D., and Costello, L. C., *Org. Biomol. Chem.* **2009,** 7, (8), 1525-1528.
55. Tremblay, M. S., Halim, M., and Sames, D., *J. Am. Chem. Soc.* **2007,** 129, (24), 7570-7577.
56. Liu, M., Ye, Z., Xin, C., and Yuan, J., *Anal. Chim. Acta* **2013,** 761, 149-156.

57. Smith, D. G., McMahon, B. K., Pal, R., and Parker, D., *Chem. Commun.* **2012,** 48, (68), 8520-8522.
58. Xiao, Y., Ye, Z., Wang, G., and Yuan, J., *Inorg. Chem.* **2012,** 51, (5), 2940-2946.
59. Plush, S. E., and Gunnlaugsson, T., *Dalton Trans.* **2008**, (29), 3801-3804.
60. Arbuse, A., Anda, C., Martinez, M. A., Perez-Miron, J., Jaime, C., Parella, T., and Llobet, A., *Inorg. Chem.* **2007,** 46, (25), 10632-10638.
61. Dickins, R. S., Aime, S., Batsanov, A. S., Beeby, A., Botta, M., Bruce, J. I., Howard, J. A. K., Love, C. S., Parker, D., Peacock, R. D., and Puschmann, H., *J. Am. Chem. Soc.* **2002,** 124, (43), 12697-12705.
62. Harte, A. J., Jensen, P., Plush, S. E., Kruger, P. E., and Gunnlaugsson, T., *Inorg. Chem.* **2006,** 45, (23), 9465-9474.
63. Gunnlaugsson, T., Harte, A. J., Leonard, J. P., and Nieuwenhuyzen, M., *Supramol. Chem.* **2003,** 15, (7-8), 505-519.
64. Plush, S. E., and Gunnlaugsson, T., *Org. Lett.* **2007,** 9, (10), 1919-1922.
65. Eveillard, A., Lasserre, F., de Tayrac, M., Polizzi, A., Claus, S., Canlet, C., Mselli-Lakhal, L., Gotardi, G., Paris, A., Guillon, H., Martin, P. G. P., and Pineau, T., *Toxicol. Appl. Pharmacol.* **2009,** 236, (3), 282-292.
66. Desvergne, B., Feige, J. N., and Casal-Casas, C., *Mol. Cell. Endocrinol.* **2009,** 304, (1-2), 43-48.
67. Casal-Casas, C., and Desvergne, B., *Annu. Rev. Physiol.* **2011,** 73, 135-162.
68. Fukuwatari, T., Ohsaki, S., Kukuoka. S., Sasaki, R., and Shibata, K., *Toxicol. Sci.* **2004,** 81, (2), 302-308.
69. Hatch, E. E., Nelson, J. W., Stahlhut, R. W., and Webster, T. F., *Int. J. Androl.* **2010,** 33, (2), 324-332.
70. Feige, J. N., Gelman, L., Rossi, D., Goete, V., Metivier, R., Tudor, C., Anghel, S. I., Grosdidier, A., Lathion, C., Engelborghs, Y., Michielin, O., Wahli, W., and Desvergne, B., *J. Biol. Chem.* **2007,** 282, (26), 19152-19166.
71. Multihance. http://www.pmprb-cepmb.gc.ca/english/View.asp?x=483&mp=572 (2013-03-31),

Chapter 2

Materials and Methods

2.1 Materials

The ligands in this study were synthesized from commercially available materials. The metal salts and solvents were purchased directly from suppliers (Table 2.1). The grades of each chemical are also listed.

Table 2.1: List of reagents used.

Reagent	Grade / Purity	Supplier
Diethylenetriamine	Synthetic grade	MERCK-Schuchardt
Cyclohexene oxide	98%	Aldrich
Tert-Butyl bromoacetate	98%	Aldrich
Sodium carbonate anhydrous	uniLAB	SaarChem
Trifluoroacetic acid	ReagentPlus® 99%	Sigma-Aldrich
Hydrochloric acid, 32%		ACE
Glyoxal (40% in H_2O)		Aldrich
Sodium hydroxide pellets	uniLAB	MERCK
Diethanolamine	uniLAB	SaarChem
Ethyl bromoacetate	95%	Fluka
Toluene-4-sulphonyl chloride	uniLAB	SaarChem
Ethylenediamine	99%	Aldrich
Paraformaldehyde, powder	95%	Sigma-Aldrich
Hexadecyltrimethylammonium bromide	$\geq$ 98%	Sigma
Anthracene	Reagent grade, 97%	Aldrich

Acetic acid (glacial)	Chemically pure	N.T. Laboratory Supplies
Hydrobromic acid, 48%		Sigma-Aldrich
Perchloric acid, 70%		Sigma-Aldrich
Europium(III) trifluoromethanesulfonate	98%	Aldrich
Calcium nitrate hydrate		Aldrich
Zinc nitrate hexahydrate	Reagent grade, 98%	Sigma-Aldrich
Sodium nitrate	99.995% metals basis	Aldrich
Potassium hydrogen phthalate	univAR	SaarChem
CHES (2-[*N*-Cyclohexylamino]-ethanesulfonic acid)	99%	Sigma
MOPS (3-[*N*-Morpholino]-propanesulfonic acid)	99.5%	Sigma
MES hydrate (2-[*N*-Morpholino]-ethanesulfonic acid hydrate)	99.5%	Sigma
Tris (hydroxymethyl)-aminoethane	Reagent grade	MERCK
Nitric acid 0.1mol/0.1N	ConvoL NORMADOSE	VWR Prolabo®
Sodium hydroxide 0.1mol/0.1N	ConvoL	VWR Prolabo®
Diphosphorus pentoxide		MERCK
Benzophenone	99% (GC)	Aldrich
Sodium metal lumps	univAR	SaarChem
Iodine, chips	99+%	Aldrich
Magnesium turnings	≥99.5% Mg basis	Ziedel-de Haën
Calcium chloride anhydrous	univAR	SaarChem
Potassium iodide	Analytical grade	ACE

Cesium carbonate	99.9% trace metals basis	Aldrich
Magnesium sulphate anhydrous	uniLAB	SaarChem
Thionyl chloride	Synthetic grade	MERCK-Schuchardt
trans-2-Aminocyclopentanol hydrochloride	97%	Aldrich
Gadolinium(III) trifluoromethanesulfonate	98%	Aldrich
Tosyl aziridine	Synthetic grade	Aldrich
Deuterium oxide	99.9 atom% D	Aldrich
Deuterium chloride	32 wt.% in D_2O, 99 atom% D	Aldrich
Deuterated sodium hydroxide	40 wt.% in D_2O, 99.5 atom% D	Aldrich
Chloroform-d, contains 1% v/v tetramethylsilane	99.8 atom% D	Aldrich
Acetone	Analytical grade	MERCK
Acetonitrile	HPLC grade	MERCK
Chloroform	LC grade	MERCK
Dichloromethane	LC grade	MERCK
Diethyl ether	Chemical grade	SaarChem
N,N-Dimethylformamide	univAR	SaarChem
Ethanol Absolut puriss. p.a.		Sigma-Aldrich
n-Hexane		Sigma-Aldrich
Tetrahydrofuran	uniLAB	SaarChem
Toluene	uniLAB	SaarChem

Deionised water used in this study was decanted from a Millipore Direct-Q 3 Water Purification System, with a resistivity reading of 18.2 MΩ.cm at 25 °C.

2.2 Characterization Techniques

2.2.1 Mass Spectrometry (MS)

Low-resolution mass spectra were recorded on a Thermo Finnigan LXQ Mass Spectrometer. The polarity used was positive. The ionisation method used was electrospray ionization (ESI). Samples were prepared in deionised water, methanol or dichlorometheane. Elution was performed using either methanol in 0.1% formic acid or a 50:50 methanol:water mixture in 0.1% formic acid. The data obtained were processed using the Xcalibur software[1], and are quoted as: m/z value.

Fast atom bombardment (FAB) mass spectra were recorded on a VG 70SE Magnetic Sector Mass Spectrometer at 8 kV, with xenon atom gas. Samples were prepared in an NBA (3-nitrobenzyl alcohol) matrix. The data obtained were processed using the MASPEC II Data System[2].

All MS data are found in Appendix A.

2.2.2 Nuclear Magnetic Resonance Spectroscopy (NMR)

Hydrogen (^{1}H) and carbon (^{13}C) NMR spectra were recorded on a Bruker Avance-300 instrument, at a frequency of 300 MHz. The probe temperature for all experiments was 300 ± 1 K. All spectra were recorded in either deuterium oxide (D_2O) or deuterated chloroform ($CDCl_3$) in 5 mm NMR tubes unless otherwise stated. Chemical shifts are reported in parts per million (ppm) relative to tetramethylsilane as internal standard in the case of ^{1}H-NMR, and relative to the central signal of deuterated chloroform taken at δ 77.00 for the ^{13}C-NMR. ^{13}C-NMR obtained from D_2O were referenced externally to 3-(trimethylsilyl)-propanesulfonic acid sodium salt. The ^{1}H-NMR chemical shifts are reported as: value

(splitting pattern, assignment, number of hydrogens). ^{13}C-NMR chemical shifts are reported as: value (assignment). Abbreviations used: s = singlet, d = doublet, t = triplet, q = quartet, m = multiplet.

All NMR data are found in Appendix B.

2.2.3 Infrared Spectroscopy (IR)

Infrared spectra were recorded on a Bruker TENSOR27 Standard System FT-IR spectrometer, using a diamond anvil cell. The data was collected and processed using the OPUS software[3], with scan range of 4000 cm^{-1} to 400 cm^{-1}, and a resolution setting of 4 cm^{-1}. The signals are reported as: wavenumber (cm^{-1}), assignment[4].

All IR data are found in Appendix C.

2.2.4 Elemental Analysis

Elemental analysis was performed on a Thermo Flash EA1112 CHNS-O Combustion Analyzer.

2.2.5 Single Crystal X-Ray Diffraction (XRD)

Intensity data were collected on a Bruker APEX II CCD area detector diffractometer with graphite monochromated Mo K_α radiation (50 kV, 30 mA) using the APEX 2 [5] data collection software. The collection method involved ω-scans of width 0.5° and 512 × 512 bit data frames. Data reduction was carried out using the program SAINT+[6] and face indexed absorption corrections were made using the program XPREP[6].

The crystal structure was solved by direct methods using SHELXT[7]. Non-hydrogen atoms were first refined isotropically, followed by anisotropic refinement by full matrix least-

squares calculations based on F^2 using SHELXTL. Hydrogen atoms were first located in the difference map then positioned geometrically and allowed to ride on their respective parent atoms. Diagrams as well as publication material were generated using SHELXTL, PLATON[8] and ORTEP-3 [9].

All XRD data are found in Appendix D.

2.2.6 Melting Points

Melting points were determined on an X4 Melting-Point apparatus with microscope, using a JM628 digital thermometer. The reported melting points are uncorrected.

2.3 Distillation of Solvents

A number of solvents required distillation before being used in synthetic procedures.

2.3.1 Acetonitrile

The exclusion of water from acetonitrile was achieved by refluxing over diphosphorus pentoxide, in an argon atmosphere. The dried solvent was stored with molecular sieves (4 Å)[10].

2.3.2 Diethyl ether

The exclusion of water from diethyl ether was achieved by refluxing over sodium (containing benzophenone), in an argon atmosphere. The dried solvent was stored with molecular sieves (4 Å)[10].

2.3.3 Ethanol

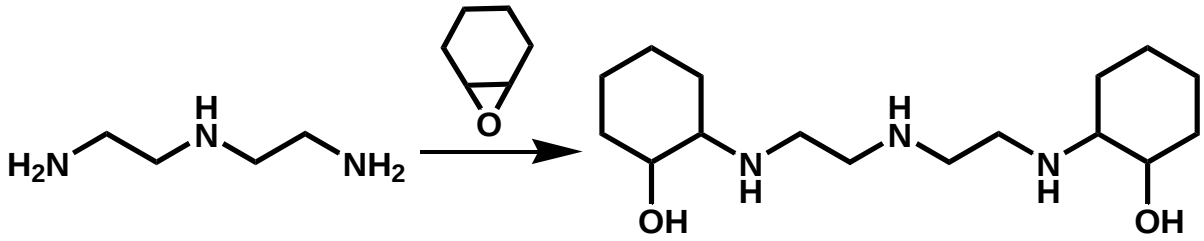
5 g of magnesium turnings and 0.5 g of iodine was placed in a distillation flask, followed by 100 mL of ethanol. The mixture is heated until a vigorous reaction occurred. Up to 1 L of ethanol was then added to the flask, and the mixture refluxed for an hour (under an argon atmosphere), before the dried ethanol was distilled off[10].

2.3.4 Tetrahydrofuran

The method used for the removal of water from tetrahydrofuran is identical to that used for diethyl ether, i.e. refluxing over sodium (containing benzophenone), in an argon atmosphere. The dried solvent was stored with molecular sieves (4 Å)[10].

2.4 Synthetic Procedure

2.4.1 Synthesis of 1,7-Bis(2-hydroxycyclohexyl)-1,4,7-triazaheptane (Cy_2DETA)



Diethylenetriamine (4.00 g, 38.8 mmol) was dissolved in 120 mL of dry ethanol. To this solution, cyclohexene oxide (9.50 g, 96.9 mmol) was added. The solution was allowed to reflux for 24 hours, with a calcium chloride drying tube attached. Upon completion, the solvent was removed under reduced pressure to yield viscous yellow oil, which solidifies over a few days. Trituration with ice-cold acetone affords a white solid (7.08 g, 61%), which was filtered off and dried.

The synthetic procedure was optimised by modifying either the number of equivalents of epoxide added or altering the duration of the reaction. These are tabulated below (Table 2.2).

Table 2.2: Optimization conditions for the synthesis of Cy_2DETA.

	1	**2**	**3**	**4**
Mass of DETA (g)	1.9991	2.0030	2.0032	2.0041
Moles of DETA (mmol)	19.377	19.415	19.417	19.425
Mass of Epoxide (g)	9.4949	9.5069	9.5047	4.7654
Moles of Epoxide (mmol)	96.739	96.861	96.839	48.552
Epoxide	5	5	5	2.5

Equivalents				
Time (hr)	24	48	6	24
Product Mass (g)	2.4478	0.9191	3.0511	3.5284
Product Yield (%)	42	16	53	61

The reaction was performed several times, and the product obtained was characterized by NMR, MS, IR, and elemental analysis.

^{1}H-NMR (D_2O): 1.314 (m, cyclohexyl CH_2, 8H); 1.730 (m, cyclohexyl C$\underline{H_2}$CHNH, 4H); 2.009 (m, cyclohexyl C$\underline{H_2}$CHOH, 4H); 2.427 (dt, cyclohexyl C$\underline{H}$NH, 2H); 2.761 (m, backbone CH_2, 8H); 3.390 (m, cyclohexyl C$\underline{H}$OH, 2H).

^{13}C-NMR ($CDCl_3$): 24.481 (cyclohexyl NHCH$_2\underline{C}$H$_2$); 25.202 (cyclohexyl OHCH$_2\underline{C}$H$_2$); 31.068 (cyclohexyl NH$\underline{C}$H$_2$CH$_2$); 33.498 (cyclohexyl OH$\underline{C}$H$_2$CH$_2$); 45.983 (backbone NCH$_2\underline{C}$H$_2$N$\underline{C}$H$_2$CH$_2$N); 49.438 (backbone N$\underline{C}$H$_2$CH$_2$NCH$_2\underline{C}$H$_2$N); 63.573 (cyclohexyl CHNH); 73.936 (cyclohexyl CHOH).

FAB-MS (m/z): 300.1 (Cy_2DETA^+ + 1).

IR, free ligand (cm^{-1}):

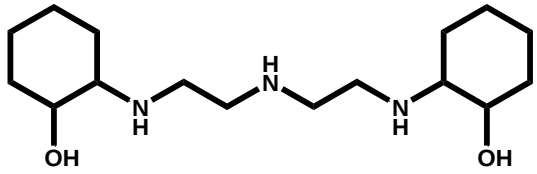
3248 (N-H stretch), 3070 (O-H stretch), 2919 (C-H stretch, asymmetric), 2852 (C-H stretch, symmetric), 1498 (CH_2 bending), 1447 (C-H bending), 1359 (O-H deformation), 1261 (C-N stretch), 1201 (C-O stretch), 1036 (C-N stretch), 910 (C-C stretch), 843 (N-H bending), 821 (C-H bending).

IR, $Cy_2DETA.3HClO_4$ salt (cm^{-1}):

3441 (N-H stretch), 3080 (O-H stretch), 2941 (C-H stretch, asymmetric), 2861 (C-H stretch, symmetric), 1560 (N-H deformation), 1498 (CH_2 bending), 1446 (C-H bending), 1421 (O-H deformation), 1292 (C-N stretch), 1065 (Cl-O stretch),

1047 (C-N stretch), 921 (C-C stretch), 884 (N-H bending), 614 (Cl-O bending).

Elemental Analysis:



Calculated elemental composition: $C_{16}H_{33}N_3O_2$

Calculated: 64.18% C, 11.11% H, 14.03% N.

Calculated molar C:N ratio: 5.33:1

Found: 63.47% C, 9.93% H, 14.68% N.

Found molar C:N ratio: 5.04:1

Melting point: 126 – 127 °C (free ligand).

196 – 198 °C $Cy_2DETA.3HClO_4$.

Solid state structures for the free ligand and the protonated ligand were also obtained and solved. The free ligand crystals were obtained from acetonitrile and the perchloric acid salt was obtained from water. The solid state structure data of the free ligand is tabulated in Table 2.3 and that of the protonated ligand is tabulated in Table 2.4.

Table 2.3: Crystal data and structure refinement of Cy_2DETA.

Temperature	173 K
Crystal System	Triclinic
Space Group	P-1
Unit Cell Dimensions	a = 5.5150(1) Å α = 82.471(1)° b = 12.2025(3) Å β = 79.679(1)° c = 12.9514(3)Å γ = 84.284(1)°
Volume	847.50(3) $Å^3$
Z	2
Density (calculated)	1.173 g/cm^3
R-factor (%)	4.77

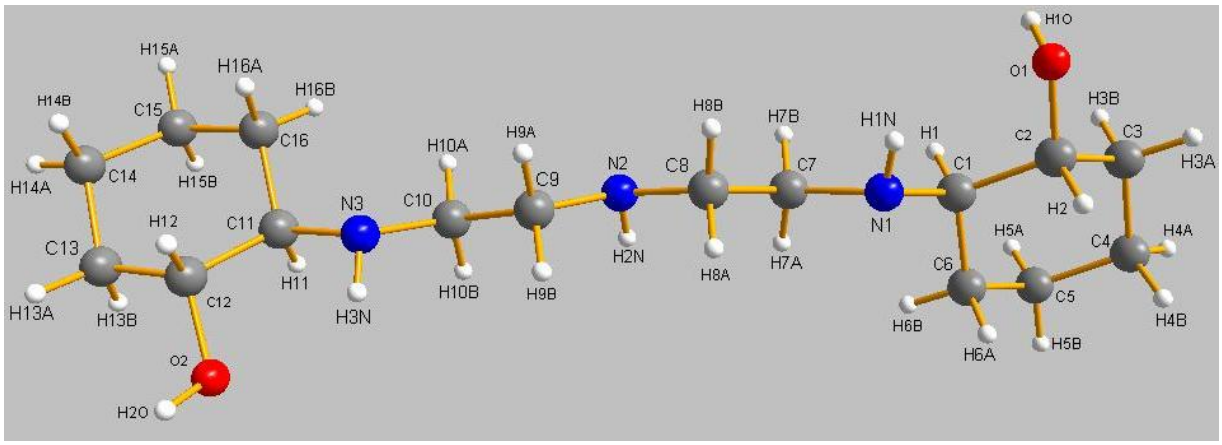


Figure 2.1: XRD structure of Cy_2DETA.

Table 2.4: Crystal data and structure refinement for $Cy_2DETA.3HClO_4$.

Temperature	173 K
Crystal System	Monoclinic
Space Group	C2/c
Unit Cell Dimensions	a = 30.0985(5) Å α = 90.00(0)° b = 8.4256(1) Å β = 99.798(1)° c = 9.6679(2)Å γ = 90.00(0)°
Volume	2416.00(7) $Å^3$
Z	4
Density (calculated)	1.652 g/cm^3
R-factor (%)	3.17

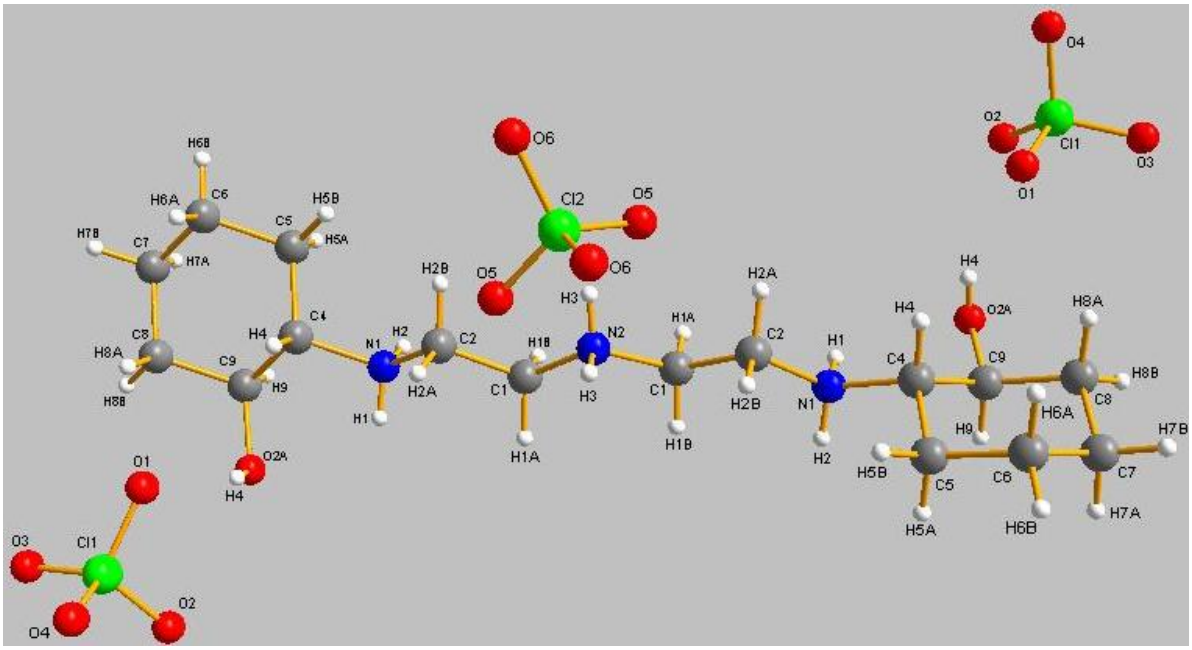
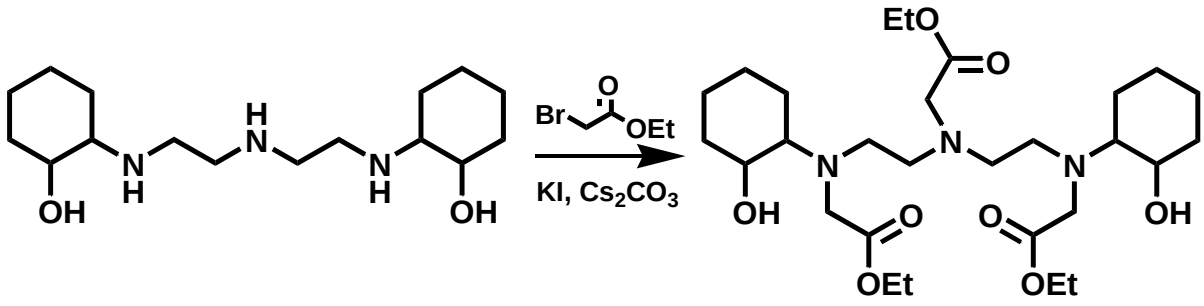


Figure 2.2: XRD structure of $Cy_2DETA.3HClO_4$.

2.4.2 Attempted synthesis of 1,7-Bis(2-hydroxycyclohexyl)-1,4,7-tris(ethylacetate)-1,4,7-triazaheptane (Ac_3Cy_2DETA)

This synthetic procedure was attempted using two different methods.

a) Direct esterification of Cy_2DETA



Cy_2DETA (0.4996 g, 1.67 mmol) was dissolved in 30 mL of absolute ethanol. To this solution, KI (0.9685 g, 5.83 mmol) and Cs_2CO_3 (0.8140 g, 2.50 mmol) was added. Ethyl bromoacetate (1.0043 g, 6.01 mmol) was dissolved in 10 mL of absolute alcohol and added to the solution via a dropping funnel over one hour. The solution was heated at 80 °C for 4 days.

Upon cooling, the solvent was removed to dryness. The remaining oil was dissolved in 50 mL of chloroform and washed three times with deionised water. The organic layer was dried with anhydrous $MgSO_4$, filtered, and the solvent removed to dryness, to yield an orange oil.

The product was characterized by MS.

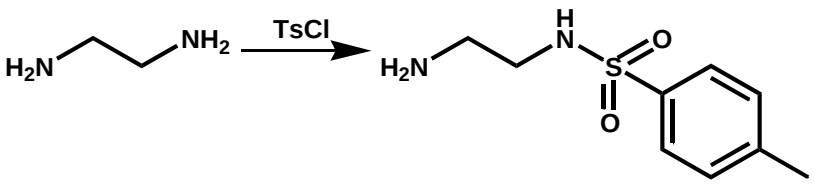
FAB-MS (m/z): 558.1 ($Ac_3Cy_2DETA^+$ + 1), 619.2 ($Ac_4Cy_2DETA^+$ + 1).

Column chromatography was used in an attempt to separate the desired product from the synthetic by-products. This was performed on normal silica, using a mobile phase of 10% methanol in chloroform (column length = 40 cm, diameter = 2 cm). The fractions were monitored on TLC plates and combined accordingly. These various fractions were dried and analysed by mass spectrometry. Spectra of these fractions indicated no recognisable products had been successfully separated and that the starting material had degraded during the separation.

b) Esterification of protected diethylenetriamine

This synthetic approach was approached in three steps. The first two steps involved the synthesis of a terminally-protected diethylenetriamine derivative, while the final step in the procedure consists of the esterification of this protected amine:

Step 1:

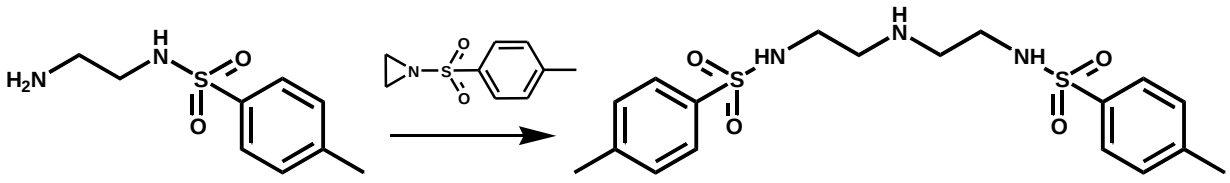


N-*p*-tolylsulfonylethylenediamine (TsEDA) was prepared according to the procedure reported by Dijksman[11]. A mixture of *p*-toluenesulfonyl chloride (1.91 g, 10 mmol) in

dichloromethane (25 mL) was slowly added to a stirred solution of ethylenediamine (6.0 g, 100 mmol) in dichloromethane (25 mL). The resulting mixture was stirred for an additional 15 minutes, washed with distilled water (2 × 25 mL) and dried over $MgSO_4$. The solvent was removed *in vacuo* to give a fine white powder (1.62 g, 76%). The product obtained was characterized by NMR and MS.

^{1}H-NMR ($CDCl_3$):	2.347 (s, CH_3, 3H); 2,702 (t, Ts-NHC<u>H</u>$_2$, 2H); 2.880 (t, C<u>H</u>$_2$NH$_2$, 2H); 7.241 (d, CH_3C<u>H</u> Ar, 2H); 7.689 (d, CHC-SO_2 Ar, 2H).
^{13}C-NMR ($CDCl_3$):	21.433 (CH_3); 40.918 (CH_2NH_2); 45.399 (Ts-$NHCH_2$); 126.980 (aromatic <u>C</u>H-C-CH_3), 129.645 (aromatic <u>C</u>H-C-SO_2), 136.945 (aromatic <u>C</u>-CH_3), 143.249 (aromatic C-SO_2).
FAB-MS (m/z):	215.1 (Ts-EDA$^+$ + 1).
IR (cm^{-1}):	3364 and 3303 (N-H stretch), 2944 (aliphatic C-H stretch, asymmetric), 1597 and 1093 (C-N stretch), 1316 and 1147 (R-SO_2-NH stretch), 814 and 763 (*p*-substituted aromatic), 657 and 577 (aromatic C-H stretch).
Melting Point:	113 – 114 °C.

Step 2:



N, N"-Bis(*p*-tolylsulfonyl) diethylenetriamine (Ts_2DETA) was prepared according to the procedure reported by Martin[12]. N-*p*-tolylsulfonylethylenediamine (1.0 g, 4.67 mmol) was dissolved in 22 mL of dry acetonitrile and heated to reflux under argon. An acetonitrile solution (11 mL) of N-*p*-tolylsulfonylaziridine (0.92 g, 4.67 mmol) was added via a dropping funnel over a period of 3 hours, and the mixture was allowed to reflux for a further 12 hours. This solution was allowed to cool to room temperature. Removal of the solvent under

reduced pressure yielded a pale yellow oil. The target compound was crystallized from dichloromethane and diethyl ether (50:50) to give a crystalline solid. Product yield: 70%.

The product obtained was characterized by NMR and MS.

^{1}H-NMR ($CDCl_3$):	2.411 (s, CH_3, 6H); 2,599 (t, $C\underline{H}_2NHC\underline{H}_2$, 4H); 2.942 (t, Ts-$NHC\underline{H}_2$, 4H); 7.305 (d, $CH_3C\underline{H}$ Ar, 4H); 7.755 (d, CHC-SO_2 Ar, 4H).
^{13}C-NMR ($CDCl_3$):	21.484 (CH_3); 42.525 ($\underline{C}H_2NH\underline{C}H_2$); 47.715 (Ts-$NHCH_2$); 127.177 (aromatic $\underline{C}$H-C-CH_3), 129.637 (aromatic $\underline{C}$H-C-SO_2), 136.708 (aromatic $\underline{C}$-CH_3), 143.375 (aromatic C-SO_2).
FAB-MS (m/z):	412.1 (Ts_2DETA^+ + 1).
IR (cm^{-1}):	3299 (N-H stretch), 2926, (aliphatic C-H stretch, asymmetric), 2867 (aliphatic C-H stretch, symmetric), 1597 and 1071 (C-N stretch), 1319 and 1152 (R-SO_2-NH stretch), 812 and 766 (*p*-substituted aromatic) 659 and 575 (aromatic C-H stretch).
Melting Point:	60 – 61 °C.

The solid state structure for the protected triamine was obtained and solved (Table 2.5). The solvent (dichloromethane) was included in the crystal structure.

Table 2.5: Crystal data and structure refinement for Ts_2DETA.

Temperature	173 K
Crystal System	Orthorhombic
Space Group	$Pca2_1$
Unit Cell Dimensions	a = 25.4644(4) Å α = 90.00(0)° b = 11.2639(2) Å β = 90.00(0)° c = 8.10410(1)Å γ = 90.00(0)°
Volume	2324.49(6) $Å^3$

Z	4
Density (calculated)	1.419 g/cm^3
R-factor (%)	4.71

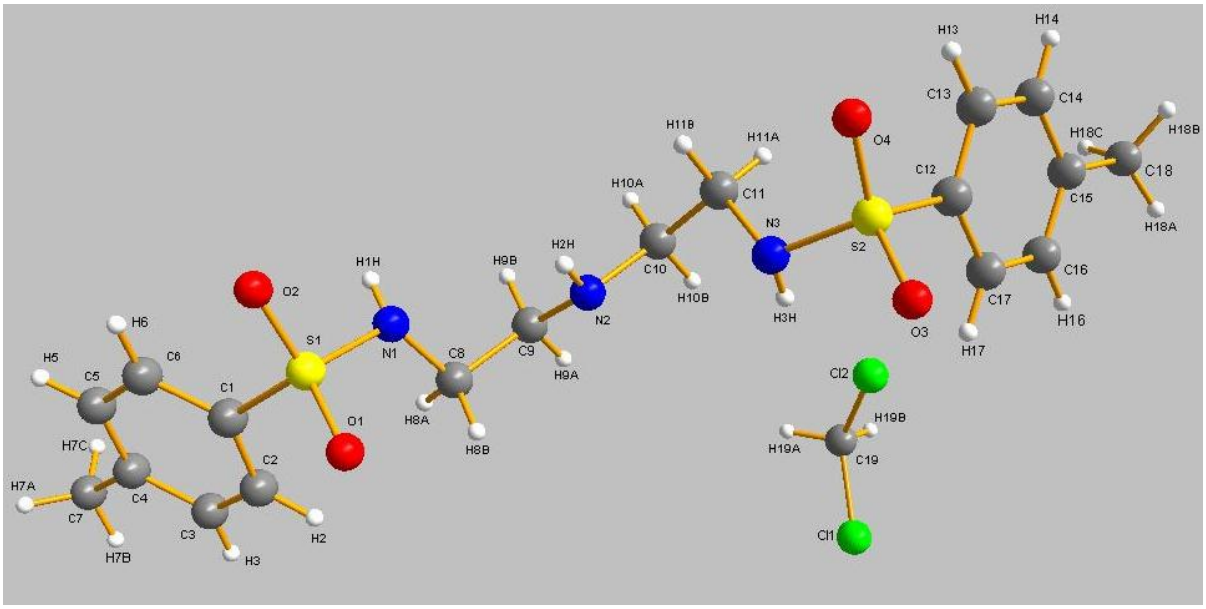
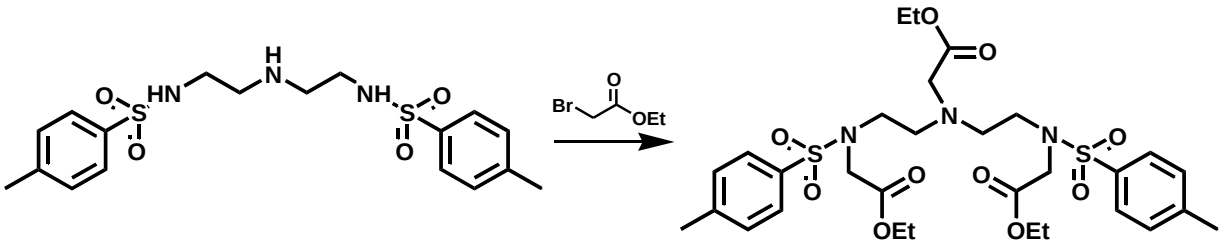


Figure 2.3: XRD structure of Ts_2DETA[13].

Step 3:



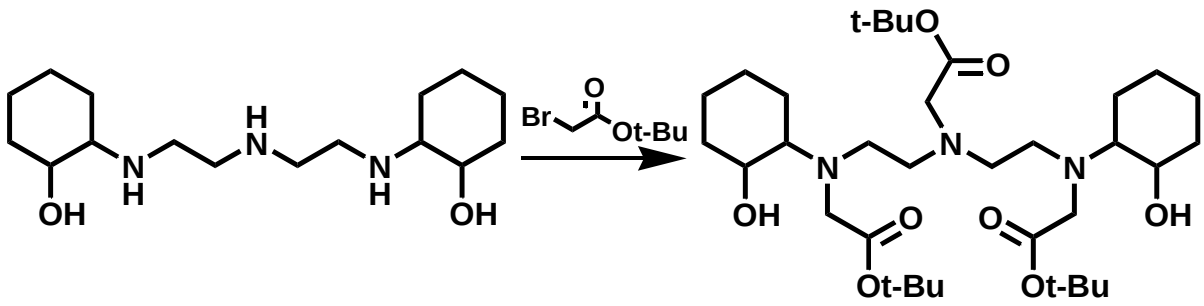
Sodium metal (0.11 g, 4.86 mmol) was added to dry absolute ethanol (15 mL) in order to form NaOEt. To this solution was added Ts_2DETA (0.49 g, 1.21 mmol), followed by ethyl bromoacetate (0.82 g, 4.87 mmol). This solution was then allowed to reflux for 24 hours, under an argon atmosphere. Upon completion, the solution was allowed to cool to room temperature, filtered (to remove the NaBr by-product), and then evaporated to yield a white solid (0.58 g).

The solid (Ts_2DETA.3E) was characterized by MS.

FAB-MS (m/z): 498.3 (mono-substituted Ts_2DETA^+ + 1), 520.3 (mono-substituted Ts_2DETA + Na^+), 584.4 (di-substituted Ts_2DETA^+ + 1), 606.4 (di-substituted Ts_2DETA + Na^+), 670.3 (tri-substituted Ts_2DETA^+ + 1), 692.4 (tri-substituted Ts_2DETA + Na^+).

This reaction was also attempted by synthesizing and isolating NaOEt, and performing the addition of the ester in THF and chloroform. Similar results were obtained. Attempts at separating the products using chromatography proved unsuccessful, due to the poor separation of the bands on the column. This synthetic approach was therefore abandoned.

2.4.3 Synthesis of 1,7-Bis(2-hydroxycyclohexyl)-1,4,7-tris(t-butylcarboxymethyl)-1,4,7-triazaheptane (Cy_2DETA.3E)



A further attempt was made at the direct esterification of the aminoalcohol Cy_2DETA. The ester of choice was the more robust tert-butyl bromoacetate. After consulting the literature[14-20], a qualitative approach was adopted to optimize the reaction conditions before scaling up. The first method used was to evaluate the effect of solvent in the reaction procedure. The solvents evaluated were dichloromethane (DCM), tetrahydrofuran (THF) and dimethylformamide (DMF). One equivalent of Cy_2DETA was dissolved in the solvent of choice, followed by the addition of 3.5 equivalents of Na_2CO_3 and 3.5 equivalents of the ester. The reaction vessel was sealed and allowed to stir at room temperature for a period of

24 hours. The solution was filtered and the solvent removed to dryness. The product obtained was characterized by MS.

ESI-MS (m/z, DCM): 528.44 (di-substituted Cy_2DETA^+ + 1), 550.42 (di-substituted $Cy_2DETA + Na^+$), 642.48 (tri-substituted Cy_2DETA^+ + 1), 664.50 (tri-substituted $Cy_2DETA + Na^+$), 756.40 (tetra-substituted Cy_2DETA^+ + 1).

ESI-MS (m/z, THF): 528.44 (di-substituted Cy_2DETA^+ + 1), 550.42 (di-substituted $Cy_2DETA + Na^+$), 642.48 (tri-substituted Cy_2DETA^+ + 1), 664.50 (tri-substituted $Cy_2DETA + Na^+$), 756.40 (tetra-substituted Cy_2DETA^+ + 1).

ESI-MS (m/z, DMF): 642.48 (tri-substituted Cy_2DETA^+ + 1), 664.50 (tri-substituted $Cy_2DETA + Na^+$).

The reaction was scaled up, using DMF as the solvent. Cy_2DETA (1.00 g, 3.34 mmol) was dissolved in dry DMF to make a 0.06M solution. Na_2CO_3 (1.08 g, 10.2 mmol) was then added to the solution, with stirring. Tert-butyl bromoacetate (1.99 g, 10.2 mmol) was introduced to the solution drop-wise. The solution was sealed and allowed to stir at room temperature for a period of 24 hours. The solid material was allowed to settle and the solution filtered. The solvent was removed under reduced pressure. Traces of DMF were washed off using DCM. After drying the oil on a high-vacuum line, the sample was re-dissolved in chloroform and extracted 3 times with deionised water. The organic layer was then dried, to leave a yellow oil (2.01 g, 94%). Upon standing, the oil began to crystallize.

The oil was characterized using NMR, IR, and MS.

^{1}H-NMR ($CDCl_3$): 1.181 (m, cyclohexyl CH_2, 8H); 1.446 (s, ester CH_3, 27H); 1.748 (m, cyclohexyl C<u>H</u>$_2$CHNH and cyclohexyl C<u>H</u>$_2$CHOH, 6H); 2.066 (m, cyclohexyl C<u>H</u>$_2$CHOH, 2H); 2.250 (m, cyclohexyl C<u>H</u>NH, 2H); 2.687 (m, backbone CH_2, 8H); 3.273 (m, ester CH_2 and cyclohexyl C<u>H</u>OH, 8H).

^{13}C-NMR ($CDCl_3$):	24.188 (cyclohexyl $NHCH_2\underline{C}H_2$); 24.557 (cyclohexyl $OHCH_2\underline{C}H_2$); 25.495 (cyclohexyl $NH\underline{C}H_2CH_2$); 28.055 (ester CH_3, closest to ring); 28.176 (ester CH_3, central); 33.309 (cyclohexyl $OH\underline{C}H_2CH_2$); 49.773 (backbone CH_2); 53.292 (backbone CH_2); 53.992 (ester arms CH_2, closest to ring); 56.116 (ester arms CH_2, central); 68.831 (cyclohexyl CHNH); 69.982 (cyclohexyl CHOH); 81.071 (ester $C(CH_3)_3$)); 170.546 (C=O, central); 172.289 (C=O, closest to ring).
IR (cm^{-1}):	3458 (N-H stretch), 2976 (O-H stretch), 2930 (C-H stretch, asymmetric), 2857 (C-H stretch, symmetric), 1727 (C=O stretch), 1451 (CH_2 bending), 1412 (C-H bending), 1366 (O-H deformation), 1261 (C-N stretch), 1148 (C-O stretch), 1081 (C-N stretch), 947 (C-C stretch), 846 (N-H bending), 750 (C-H bending).
ESI-MS (m/z):	642.46 (tri-substituted Cy_2DETA^+ + 1), 664.47 (tri-substituted $Cy_2DETA + Na^+$).
Melting Point:	107 – 121 °C.

The solid state structure for the ester was obtained and solved (Table 2.6). The structure was obtained as a sodium complex, with a bromide counter-ion.

Table 2.6: Crystal data and structure refinement for [$NaCy_2DETA.3E$]Br.

Temperature	173 K
Crystal System	Triclinic
Space Group	P-1
Unit Cell Dimensions	a = 10.7723(2) Å α = 79.0030(10)° b = 10.7883(2) Å β = 80.1240(10)° c = 19.5647(4)Å γ = 66.0520(10)°
Volume	2028.57(7) $Å^3$
Z	2

Density (calculated)	1.219 g/cm^3
R-factor (%)	7.80

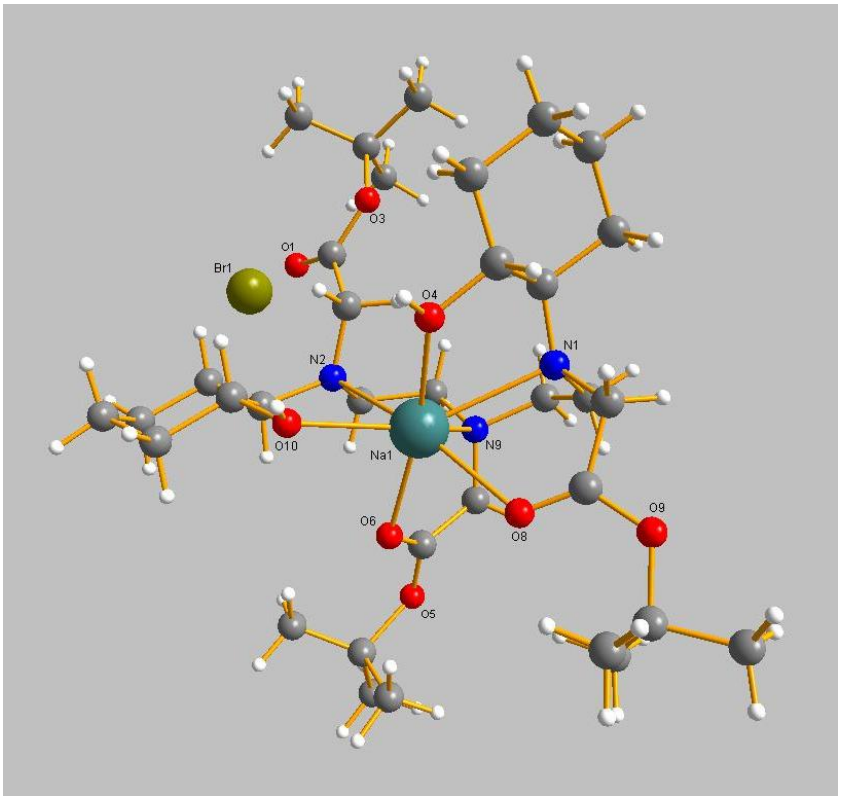
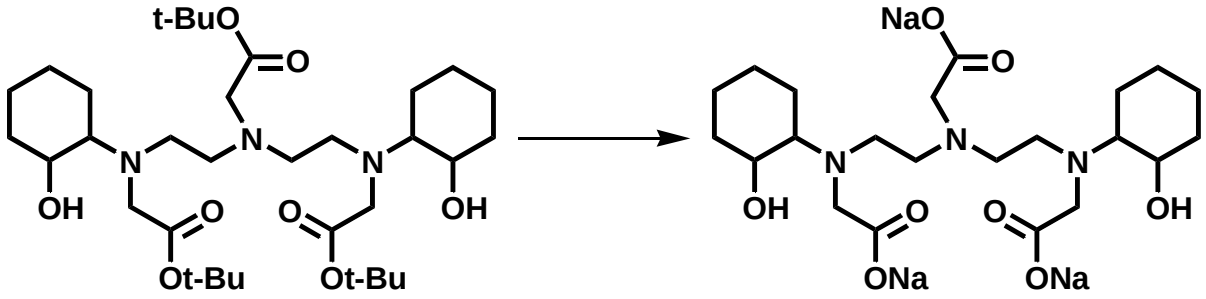


Figure 2.4: XRD structure of [NaCy$_2$DETA.3E]Br.

2.4.4 Synthesis of 1,7-Bis(2-hydroxycyclohexyl)-1,4,7-tris(carboxymethyl)-1,4,7-triazaheptane (Cy$_2$DETA.3A)

2.4.4.1 Synthesis of Sodium-1,7-Bis(2-hydroxycyclohexyl)-1,4,7-triacetate triazaheptane (Na$_3$Cy$_2$DETA.3A)



The conversion of Cy_2DETA.3E (2.00 g) to the tri-carboxylate was initially achieved using trifluoroacetic acid (TFA, 20 mL) in dichloromethane (DCM, 40 mL) in a 1:2 ratio (to make a 60 mL solution)[14-20]. The solution was stirred at room temperature, for a period of 24 hours. The solvent was removed under reduced pressure, to yield a viscous oil. This oil was re-dissolved in deionised water and allowed to reflux for a period of 7 days, to reverse dehydration across the alcohol and terminal carboxylic acid moieties. The resulting solution was continuously extracted with chloroform, for 10 days, to remove any organic by-products. The aqueous layer was then retrieved, frozen, and lyophilized, to yield a brown solid. The solid material was re-dissolved in deionised water, yielding a highly acidic solution (pH = 1). The pH of the solution was adjusted to 9 using 6M NaOH and refluxed for 24 hours. After cooling, the solution was neutralized (using HCl) and the solvent evaporated. The NaCl by-product was removed by re-dissolving the obtained solid material in dry EtOH. Removal of the solvent yielded a resinous mass, which was then triturated with acetonitrile. The resulting suspension was then filtered and the solid material dried *in vacuo*, to yield a deliquescent off-white powder (1.44 g, 85%).

The product (Na_3Cy_2DETA.3A) was characterized by NMR and MS.

^{1}H-NMR (D_2O): 1.264 (m, cyclohexyl CH_2, 8H); 1.715 (m, cyclohexyl C<u>H</u>$_2$CHNH and cyclohexyl C<u>H</u>$_2$CHOH, 6H); 2.028 (m, cyclohexyl CH_2C<u>H</u>OH, 2H); 2.461 (m, cyclohexyl C<u>H</u>NH, 2H); 2.997 (m, backbone CH_2, 8H); 3.121 (s, central carboxylate arm CH_2, 1H); 3.177 (s, central carboxylate arm CH_2, 1H); 3.447 (m, cyclohexyl C<u>H</u>OH and terminal carboxylate arms CH_2, 6H).

ESI-MS (m/z, crude product, prior to refluxing in H_2O):

438 (Cy_2DETA.3A$^+$ - di-morpholone), 456 (Cy_2DETA.3A$^+$ - mono-morpholone), 478 (Cy_2DETA.3A.Na$^+$ - mono-morpholone).

ESI-MS (m/z, after refluxing for 7 days in H_2O):

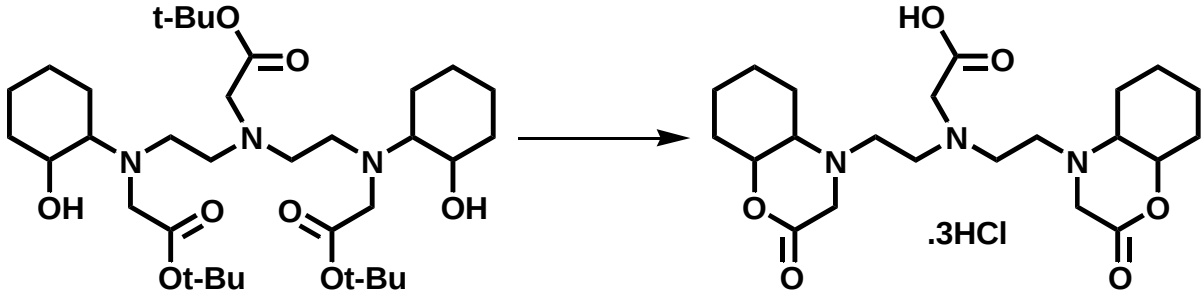
456 ($Cy_2DETA.3A^+$ - mono-morpholone), 474 ($Cy_2DETA.3A^+$ - tri-acetate).

FAB-MS (m/z, $Na_3Cy_2DETA.3A$):

494 ($Cy_2DETA.3A.Na^+$), 518 ($Cy_2DETA.3A.2Na^+$), 540 ($Cy_2DETA.3A.3Na^+$), 562 ($Cy_2DETA.3A.4Na^+$).

IR (cm^{-1}): 3350 (O-H stretch), 2934 (C-H stretch, asymmetric), 2859 (C-H stretch, symmetric), 1683 (C=O stretch), 1583 (CO_2^- stretch, asymmetric), 1408 (CO_2^- stretch, symmetric), 1412 (C-H bending), 1326 (O-H deformation), 1205 (C-N stretch), 1130 (C-O stretch), 1081 (C-N stretch), 839 (N-H bending), 722 (-$(CH_2)_n$- stretch).

2.4.4.2 Synthesis of 2-(Bis(2-(octahydro-2-oxobenzo[b][1,4]oxazin-4-yl)ethyl)amino)acetic acid trihydrochloride ($Cy_2DETA.3A.3HCl$)



The ester cleavage procedure was further refined, by using concentrated HCl[21]. $Cy_2DETA.3E$ (2.02 g) was dissolved in 30 mL of concentrated HCl (32%). The solution was allowed to reflux for 4 hours, over a base trap. Upon cooling, the solvent was removed to dryness, to yield an off-white solid. This was re-dissolved in deionised water and then continuously extracted with chloroform, for 10 days, to remove any organic by-products. The aqueous layer was then retrieved, frozen, and lyophilized, to yield a deliquescent white solid (1.78 g, 89%).

This trihydrochloride salt was characterized by NMR, MS, IR, and elemental analysis.

^{1}H-NMR (D_2O): 1.295 (m, cyclohexyl CH_2, 8H); 1.799 (m, cyclohexyl C<u>H$_2$</u>CHN, 4H); 2.052 (m, cyclohexyl C<u>H$_2$</u>CHO, 4H); 2.656 (m, central amino acid CH_2, 2H); 3.108 (m, NCH$_2$C<u>H$_2$</u>NC<u>H$_2$</u>CH$_2$N, 4H); 3.283 (m, terminal amino acid CH_2, 4H); 3.511 (m, NC<u>H$_2$</u>CH$_2$NCH$_2$C<u>H$_2$</u>N, 4H); 3.746 (m, cyclohexyl C<u>H</u>NH, 2H); 4.150 (m, cyclohexyl C<u>H</u>OH, 2H).

^{13}C-NMR (D_2O): 25.88 (cyclohexyl NHCH$_2$<u>C</u>H$_2$); 26.23 (cyclohexyl OHCH$_2$<u>C</u>H$_2$); 36.17 (cyclohexyl NH<u>C</u>H$_2$CH$_2$); 37.12 (cyclohexyl OH<u>C</u>H$_2$CH$_2$); 51.29 (backbone CH_2); 55.36 (carboxylate arm CH_2, central); 65.52 (cyclohexyl CHNH); 70.12 (carboxylate arms CH_2, closest to ring); 81.14 (cyclohexyl CHOH); 171.74 (C=O, central); 176.68 (C=O, closest to ring).

ESI-MS (m/z, crude product):

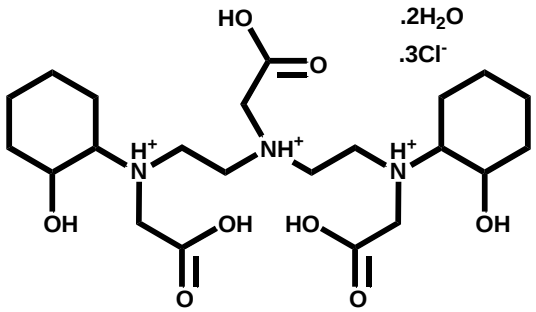
456 (mono-morpholone of $Cy_2DETA.3A^+$ + 1), 474 ($Cy_2DETA.3A^+$ + 1), 496 ($Cy_2DETA.3A.Na^+$).

ESI-MS (m/z, after continuous extraction for 10 days, followed by lyophilization):

438 ($Cy_2DETA.3A^+$ - di-morpholone), 456 ($Cy_2DETA.3A^+$ - mono-morpholone), 460 ($Cy_2DETA.3A.Na^+$ - di-morpholone), 478 ($Cy_2DETA.3A.Na^+$ - mono-morpholone).

IR (cm^{-1}): 2944 (C-H stretch, asymmetric), 2869 (C-H stretch, symmetric), 1741(C=O stretch), 1451 (CH_2 bending), 1397 (C-H bending), 1253 (O-H deformation), 1212 (C-N stretch), 1057 (C-O stretch), 953 (C-C stretch).

Elemental Analysis:



Calculated elemental composition: $C_{22}H_{46}N_3O_{10}Cl_3$

Calculated: 42.69% C, 7.49% H, 6.79% N.

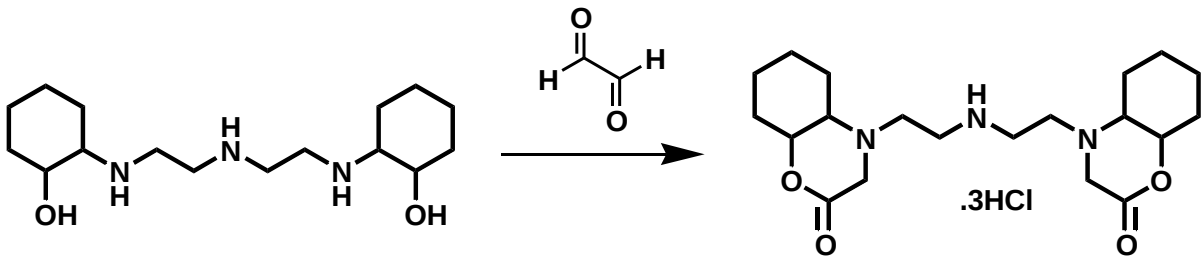
Calculated molar C:N ratio: 7.33:1

Found: 41.96% C, 6.54% H, 7.52% N.

Found molar C:N ratio: 6.51:1

Melting Point: 136 – 138 °C.

2.4.5 Synthesis of Bis(2-(octahydro-2-oxobenzo[b][1,4]oxazin-4-yl)ethyl)amine trihydrochloride (Cy_2DETA.2A.3HCl)



The selective addition of the acetic acid arms to the terminal amines was achieved using the method reported by Farfán[22]. Glyoxal solution (0.84 mL, 7.35 mmol) was added to Cy_2DETA (1.00 g, 3.32 mmol), followed by 3 mL of deionised water. The reaction vessel was sealed and allowed to stir at 70 °C for 16 hours. Upon cooling, the solvent was removed to dryness. The product was re-dissolved in a small quantity of deionised water and the pH raised to 10 using a concentrated NaOH solution. This solution was continuously extracted with $CHCl_3$ for 2 days. The aqueous layer was then acidified with concentrated HCl to a pH of 1, and extracted continuously for a further day. After retrieving the aqueous phase, the solvent was removed to dryness. The solid material was washed with dry methanol and filtered. The methanol solution obtained was then dried. The solid obtained from the methanol solution was then re-dissolved in deionised water, frozen, and lyophilized, to yield a light brown solid. This solid was re-dissolved in deionised water and the solution passed through a Sep-pak® column. The filtrate was collected, frozen and lyophilized to yield the deliquescent final product (0.39 g, 24%).

The product obtained was characterized by NMR, MS, IR and elemental analysis.

^{1}H-NMR (D_2O): 1.316 (m, cyclohexyl CH_2, 8H); 1.846 (m, cyclohexyl C$\underline{H_2}$CHN, 4H); 2.067 (m, cyclohexyl C$\underline{H_2}$CHO, 4H); 3.310 (m, NCH$_2$C$\underline{H_2}$NC$\underline{H_2}$CH$_2$N, 3H); 3.621 (m, amino acid CH_2, 3H); 3.779 (m, NC$\underline{H_2}$CH$_2$NCH$_2$C$\underline{H_2}$N, 6H); 4.069 (m, cyclohexyl C$\underline{H}$NH and cyclohexyl C$\underline{H}$OH, 4H).

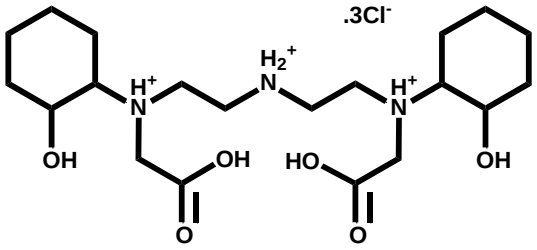
^{13}C-NMR (D_2O): 25.23 (cyclohexyl NHCH$_2$C$\underline{H_2}$); 26.65 (cyclohexyl OHCH$_2$C$\underline{H_2}$); 25.79 (cyclohexyl NHC$\underline{H_2}$CH$_2$); 26.26 (cyclohexyl OHC$\underline{H_2}$CH$_2$); 44.97 (backbone NCH$_2$C$\underline{H_2}$NC$\underline{H_2}$CH$_2$N); 46.14 (backbone NC$\underline{H_2}$CH$_2$NCH$_2$C$\underline{H_2}$N); 61.88 (cyclohexyl CHNH); 65.13 (cyclohexyl CHOH); 70.06 (carboxylate arm CH_2); 72.95 (carboxylate arm CH_2); 178.88 (C=O).

FAB-MS (m/z): 322.1 (bisoxazolidine of Cy2DETA), 380.1 (di-morpholone of $Cy_2DETA.2A^+$ + 1), 398.1 (mono-morpholone of $Cy_2DETA.2A^+$ + 1), 420.1 (mono-morpholone of $Cy_2DETA.2A.Na^+$ + 1).

ESI-MS (m/z): 398 (mono-morpholone of $Cy_2DETA.2A^+$ + 1), 420 (mono-morpholone of $Cy_2DETA.2A.Na^+$).

IR (cm^{-1}): 3336 (N-H stretch), 2942 (C-H stretch, asymmetric), 2866 (C-H stretch, symmetric), 1739 (carboxylate C=O stretch), 1652 (morpholone C=O stretch), 1451 (CH_2 bending), 1398 (C-H bending), 1264 (O-H deformation), 1213 (C-N stretch), 1071 (C-O stretch), 924 (C-C stretch), 851 (N-H bending).

Elemental Analysis:



Calculated elemental composition: $C_{20}H_{40}N_3O_6Cl_3$

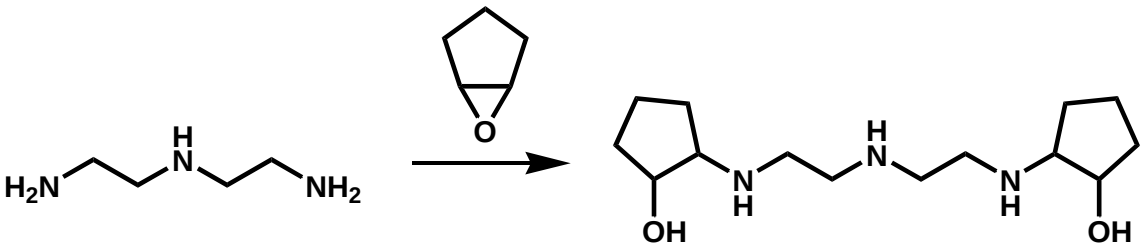
Calculated: 45.76% C, 7.68% H, 8.01% N.

Calculated molar C:N ratio: 6.66:1

Found: 45.37% C, 7.38% H, 6.93% N.

Found molar C:N ratio: 7.64:1

2.4.6 Attempted Synthesis of 1,7-Bis(2-hydroxycyclopentyl)-1,4,7-triazaheptane (Cyp_2DETA)



Diethylenetriamine was dissolved in 20mL of dry ethanol. To this solution, cyclopentene oxide was added. The solution was allowed to reflux, with a calcium chloride drying tube attached. Upon completion, the solvent was removed under reduced pressure. The oil obtained was dissolved in deionised water and washed with $CHCl_3$. The aqueous layer was then collected and dried to yield a viscous brown oil.

Attempts to optimize the synthetic procedure included manipulating the number of epoxide equivalents added or altering reaction times. These are tabulated below (Table 2.7).

Following each attempt, the product obtained was characterized by MS.

FAB-MS (m/z): 188.1 ($CypDETA^+$ + 1), 272.2 (Cyp_2DETA^+ + 1), 356.2 (Cyp_3DETA^+ + 1).

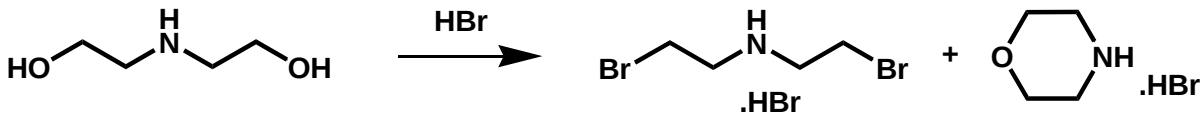
Further attempts of separating the target compound from the crude product were made. Continuous extraction was performed on the crude sample using chloroform, however the target compound was also extracted into the organic phase. Column chromatography was also attempted using normal silica, reverse-phase silica and alumina, but in all cases, poor separation was observed.

Table 2.7: Optimization conditions for the synthesis of Cyp_2DETA.

	1	2	3	4	5
Mass of DETA (g)	0.5036	0.5023	0.5031	0.5012	0.5046
Moles of DETA (mmol)	4.881	4.869	4.876	4.858	4.891
Mass of Epoxide (g)	2.0397	2.0377	2.0419	2.0405	1.0202
Moles of Epoxide (mmol)	24.248	24.224	24.274	24.257	12.128
Epoxide Equivalents	5	5	5	5	2.5
Time (hr)	24	2	48	6	24

An alternative two-step approach was adopted to attempt the synthesis of the target compound.

Step 1:



Bis(2-bromoethyl)ammonium bromide was prepared according to the procedure reported by Pettit[23]. Diethanolamine (12 g, 0.114 mol) was added, with cooling, to 100 mL of 48% HBr. The reaction vessel was then fitted with a Vigreaux column and a Dean-Stark apparatus. The solution was then heated and water was removed via azeotropic distillation until an approximate volume of 70 mL had been decanted. The remaining HBr was then removed by means of a rotary evaporator, to yield a viscous orange oil which crystallized upon cooling. The product was recrystallized from an ethanol – diethyl ether solution to yield white needles (13.061 g, 37%).

The product obtained was characterized by NMR, MS and IR.

^{1}H-NMR (D_2O):	3.342 (t, bromoethylamine C<u>H$_2$</u>NH, 4H); 3.667 (t, morpholine C<u>H$_2$</u>NH, 4H); 3.779 (t, morpholine C<u>H$_2$</u>O, 4H); 3.992 (t, bromoethylamine C<u>H$_2$</u>Br, 4H).
ESI-MS (m/z):	232 ($C_4H_9NBr_2^+$ + 1).
IR (cm^{-1}):	2925 (C-H stretch, asymmetric), 2769 (C-H stretch, symmetric), 1580 (N-H deformation), 1424 (C-H bending), 1273 (C-N stretch), 1096 (C-O stretch), 925 (C-C stretch), 868 (N-H bending), 811 (C-H bending), 666 (C-Br stretch, axial).

Two different solid state structures were obtained and solved (Table 2.8 and Table 2.9). In both cases, the compounds were isolated as HBr salts.

<u>Table 2.8:</u> Crystal data and structure refinement for bis(2-bromoethyl)ammonium bromide.

Temperature	173 K
Crystal System	Monoclinic
Space Group	$P2_1$
Unit Cell Dimensions	a = 15.8861(13) Å α = 90.00(0)° b = 7.4891(6) Å β = 117.450(0)° c = 17.1018(18)Å γ = 90.00(0)°
Volume	1805.6(3) $Å^3$
Z	8
Density (calculated)	2.294 g/cm^3
R-factor (%)	10.73

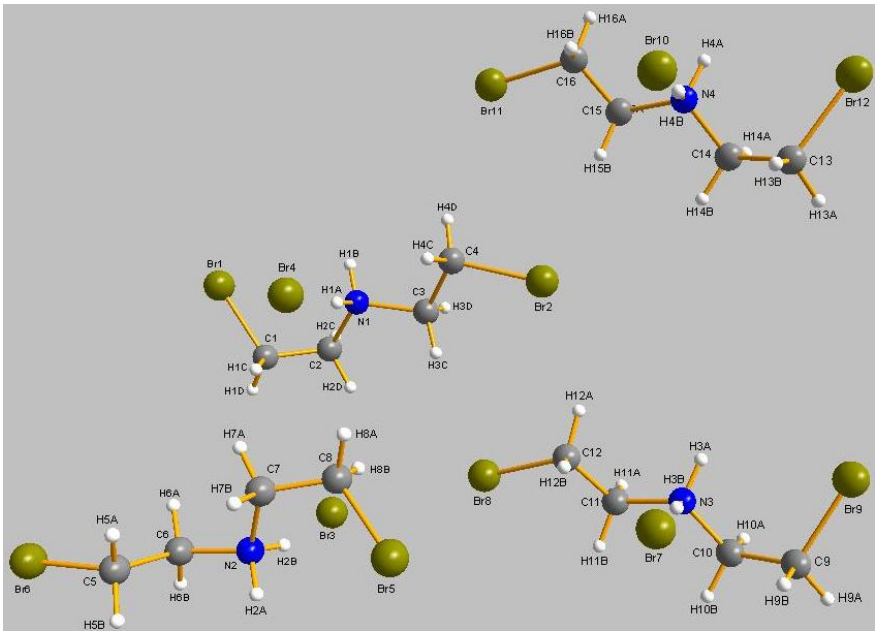


Figure 2.5: XRD structure of bis(2-bromoethyl)ammonium bromide[24].

Table 2.9: Crystal data and structure refinement for morpholinium bromide.

Temperature	173 K
Crystal System	Monoclinic
Space Group	P21/c
Unit Cell Dimensions	a = 6.1247(2) Å α = 90.00(0)° b = 10.3063(3) Å β = 100.312(0)° c = 10.1141(3)Å γ = 90.00(0)°
Volume	628.12(3) $Å^3$
Z	4
Density (calculated)	1.777 g/cm^3
R-factor (%)	3.88

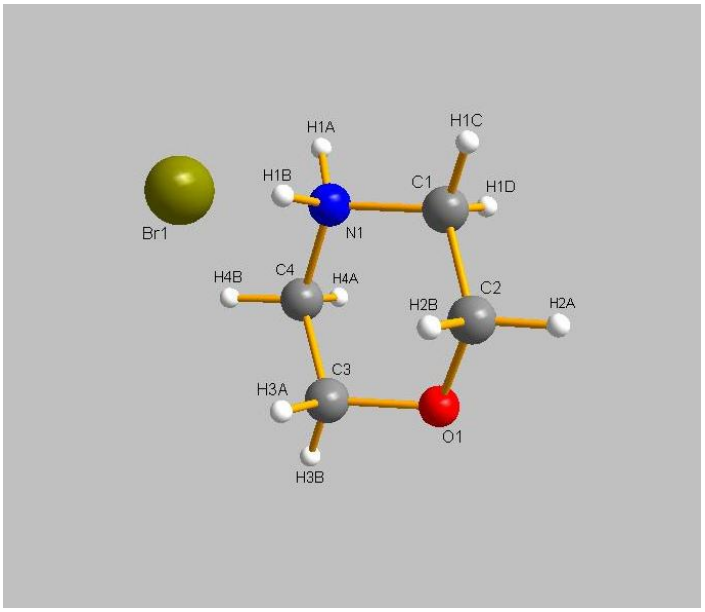
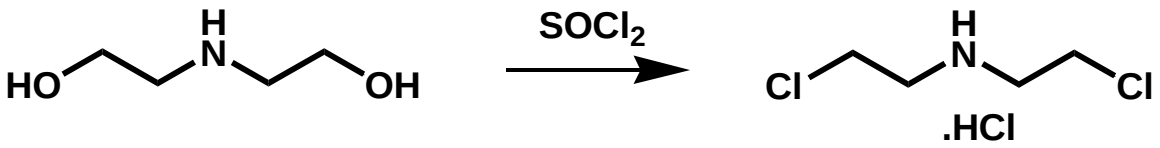


Figure 2.6: XRD structure of morpholinium bromide[25].

Due to the difficulty in isolating the target compound and the lack of reproducible results with this particular reaction, this synthetic route was abandoned. The synthesis of the analogous bis(2-chloroethyl)ammonium chloride was pursued instead.

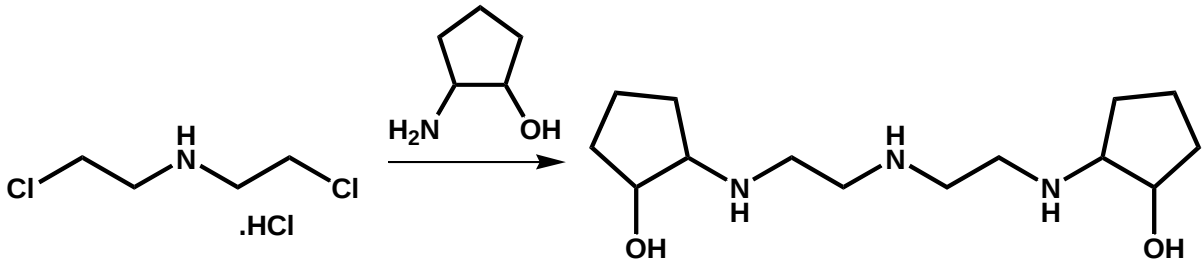


Bis(2-chloroethyl)ammonium chloride was prepared according to the procedure reported by Yin[26]. Diethanolamine (15.8 g, 150 mmol) was dissolved in 21 mL of chloroform. This was introduced drop-wise to a solution of thionyl chloride (132 mL, 1.80 mol) in chloroform (35 mL) over a period of 1 hour, keeping the reaction vessel at 0 °C. After the addition was complete, the contents were allowed to stir at room temperature for 3 hours. Upon completion, the solvent was removed under vacuum. The solid obtained was re-crystallised three times from ethanol and hexane (50:50). The white, needle-like crystals obtained were finally washed with hexane and dried (12.7084 g, 47%).

The product obtained was characterized by NMR, IR and MS.

^{1}H-NMR (D_2O):	3.572 (t, C$\underline{H}_2$NH, 4H), 3.944 (t, CH_2Cl, 4H).
ESI-MS (m/z):	143.50 ($C_4H_9NCl_2^+$ + 1).
IR (cm^{-1}):	2988 (C-H stretch, asymmetric), 2722 (C-H stretch, symmetric), 1592 (N-H deformation), 1429 (C-H bending), 1288 (C-N stretch), 955 (C-C stretch), 883 (N-H bending), 790 (C-H bending), 667 (C-Cl stretch).
Melting Point:	216 – 217 °C.

Step 2:



The *trans*-2-aminocyclopentanol used in this reaction was the neutral form. This was obtained from the purchased hydrochloride salt by means of neutralizing the acid with K_2CO_3, followed by an extraction into chloroform. Removal of the chloroform yielded a yellow oil, which was characterized by NMR.

^{1}H-NMR ($CDCl_3$):	1.273 (m, CH_2, 1H), 1.512 (m, CH_2, 1H), 1.636 (m, C$\underline{H}_2$CHNH_2, 2H), 1.960 (m, C$\underline{H}_2$CHOH, 2H), 2.480 (s, NH_2 and OH, 3H), 2.988 (q, C$\underline{H}$NH_2, 1H), 3.688 (q, C$\underline{H}$OH, 1H).
^{13}C-NMR ($CDCl_3$):	19.673 (CH_2), 31.957 ($\underline{C}H_2$CHNH_2), 32.328 ($\underline{C}H_2$CHOH), 59.976 (CHNH_2), 79.722 (CHOH).

Bis(2-chloroethyl)ammonium chloride (1.00 g, 5.61 mmol) was added drop-wise (in 25 mL of dry acetonitrile) to 2-aminocyclopentanol (1.54 g, 15.28 mmol), K_2CO_3 (3.10 g, 22.49 mmol) and KI (3.73 g, 22.47 mmol) in 40 mL of CH_3CN. The reaction mixture is then allowed to reflux for 48 hours. Upon cooling, the solvent is removed to dryness, followed by

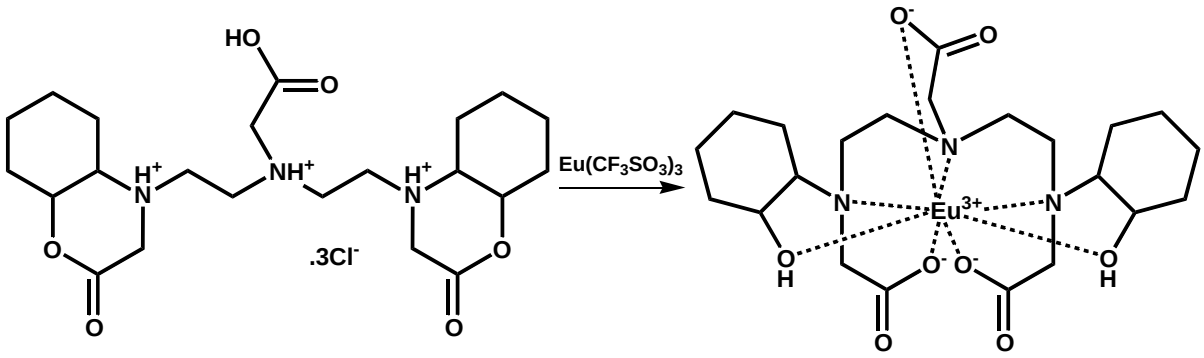
an aqueous/organic extraction using deionised water and chloroform. Both extracts were dried and analysed by MS. However, in both extracts, no recognisable products were found.

The synthetic procedure was repeated, using ethanol as the solvent. Upon cooling, the solvent was removed and the product obtained was extracted. Both the aqueous and organic extracts were isolated, dried and analysed by MS; again no products could be identified from either extract in the spectra.

2.5 Lanthanide Complexation

The following section details the attempts made to synthesize and isolate the europium(III) and gadolinium(III) complexes of our synthetic ligands.

2.5.1 Attempted Synthesis of Europium(III)-1,7-Bis(2-hydroxycyclohexyl)-1,4,7-tris(carboxymethyl)-1,4,7-triazaheptane ([Eu(Cy_2DETA.3A)])



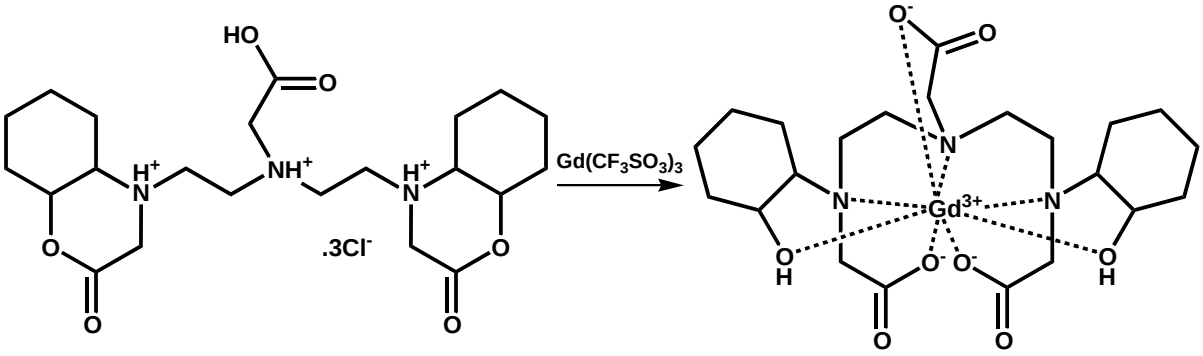
Cy_2DETA.3A.3HCl (0.29 g, 0.52 mmol) and europium(III) triflate powder (0.35 g, 0.58 mmol) were dissolved in 40 mL of dry acetonitrile. The reaction vessel was sealed with a condenser and flushed with argon gas continuously. The mixture was allowed to reflux for 4 days. Upon cooling, the solvent was removed to dryness, to yield a powder (0.48 g). This sample was analyzed by MS, however, no recognizable products or by-products could be identified from the spectrum.

An alternative synthetic approach involved using deionised water as the solvent for the complexation. In this attempt, Cy_2DETA.3A.3HCl (0.31 g, 0.56 mmol) and europium(III) triflate powder (0.37 g, 0.62 mmol) were dissolved in 20 mL of deionised water. The reaction vessel was sealed with a condenser and this mixture was allowed to reflux for 4 days. Upon cooling, the solvent was removed to dryness, to yield a powder (0.56 g). This sample was characterized by MS.

FAB-MS (m/z): 625 (Cy_2DETA.3A.Eu^+ + 1).

Attempts were made at crystallizing the desired product, by either slow evaporation, or by freezing a sample dissolved in acetonitrile and diethyl ether. Both attempts proved unsuccessful.

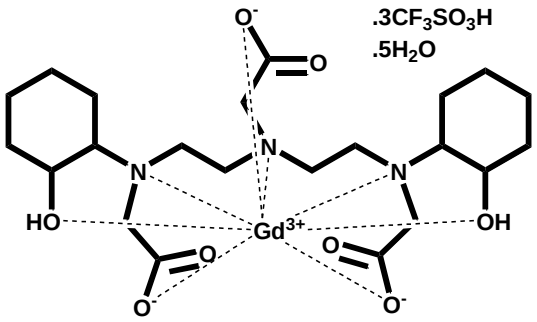
2.5.2 Attempted Synthesis of Gadolinium(III)-1,7-Bis(2-hydroxycyclohexyl)-1,4,7-tris(carboxymethyl)-1,4,7-triazaheptane ([Gd(Cy_2DETA.3A)])



Cy_2DETA.3A.3HCl (1.59 g, 2.91 mmol) and gadolinium(III) triflate powder (1.76 g, 2.91 mmol) were dissolved in 30 mL of dry acetonitrile. The reaction vessel was sealed with a condenser and flushed with argon gas continuously. This mixture was allowed to reflux for 4 days. Upon cooling, the solvent was removed to dryness, to yield a powder (3.22 g, 96%). This sample was characterized by MS and elemental analysis.

ESI-MS (m/z): 626 (Cy_2DETA.3A.Gd^+ + 1).

Elemental Analysis:



Calculated elemental composition: $C_{25}H_{49}N_3O_{22}GdF_9S_3$

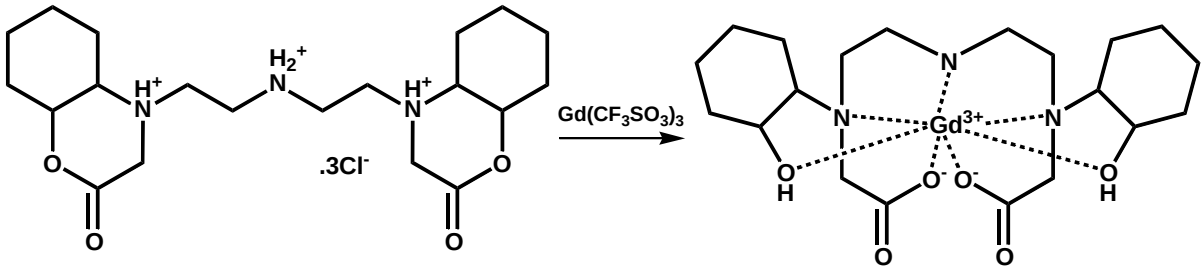
Calculated: 25.71% C, 4.23% H, 3.60% N, 8.24% S.

Calculated molar C:N ratio: 8.33:1

Found: 25.83% C, 4.10% H, 3.38% N, 8.57% S.

Found molar C:N ratio: 8.91:1

2.5.3 Attempted Synthesis of Gadolinium(III)-1,7-Bis(2-hydroxycyclohexyl)-1,7-bis(carboxymethyl)-1,4,7-triazaheptane ([Gd(Cy_2DETA.2A)])



Cy_2DETA.2A.3HCl (0.30 g, 0.61 mmol) and gadolinium(III) triflate powder (0.38 g, 0.63 mmol) were dissolved in 30 mL of dry acetonitrile. The reaction vessel was sealed with a condenser and flushed with argon gas continuously. This mixture was allowed to reflux for 4 days. Upon cooling, the solvent was removed to dryness, to yield a powder (0.59 g). This sample was characterized by MS.

ESI-MS (m/z): 398 (mono-morpholone of Cy_2DETA.2A^+ + 1).

2.6 Potentiometry

Potentiometric studies were conducted on a Metrohm 809 Titrando instrument. A Metrohm 602 Combined Metrosensor glass electrode was initially calibrated using pH 4, pH 7 and pH 10 standard solutions. The electrode was later standardized by titrating a prepared standard solution of HNO_3 with NaOH, in order to determine the Nernstian slope and standard electrode potential (E°) values prior to each study. Each potentiometric study was carried out using the Tiamo software[27].

2.6.1 Preparation of the Standard Solutions

Each standard solution used in this study was prepared such that the ionic strength was 0.1 M, with the exception of potassium hydrogen phthalate (KHP). The KHP solution was used to determine the concentrations of other standard solutions (where indicated) by means of an acid-base titration, using phenolphthalein as an indicator.

The 0.1 M HNO_3 and 0.1 M NaOH standard solutions were prepared using purchased ampoules.

The preparation of each standard solution is detailed in Appendix E.

2.6.2 Determination of pK_a Values

The pK_a determinations for Cy_2DETA.3A and Cy_2DETA.2A were conducted on a Metrohm 809 Titrando instrument, using a calibrated glass electrode. The electrode was standardized before each determination, in order to determine the Nernstian slope and standard electrode potential (E°) values. Each titration was performed in a jacketed cell at 25 °C, with stirring. N_2 gas was bubbled gently through the solution to expel dissolved CO_2.

The data for the electrode standardization and pK_a determination for each ligand are found in Appendix E.

2.7 Luminescence Studies

The luminescence properties of the Eu(III)-ligand systems were investigated. The excitation wavelength (λ_{ex}) used for the luminescence study was determined from UV-visible absorbance spectra, obtained using a Cary 3E UV-visible Spectrophotometer, using Hellma quartz SUPRASIL® cells (type: 110-QS, path length = 10 mm). The phosphorescence emission spectra were then recorded, as a function of pH, on a Cary Eclipse Fluorescence Spectrophotometer, using Hellma quartz SUPRASIL® cells (type: 111-QS, path length = 10 mm).

All pH measurements were made using a Metrohm 713 pH meter, using a Metrohm 602 Combined Metrosensor glass electrode which was calibrated against pH 4, pH 7 and pH 10 standard commercial buffers.

The Eu(III)-ligand system was maintained at a temperature of 25 °C by means of a jacketed-cell and a water-circulating bath. Adjustments in pH were made by drop-wise addition of either concentrated HCl or NaOH solutions. UV-visible absorbance spectra and phosphorescence emission spectra were recorded at 25 °C.

For each Eu(III) complex, buffered solutions (using a multi-component buffer system comprised of MES, MOPS, CHES, Tris and KHP) were compared to solutions containing no buffers. Samples of these solutions were prepared in pH intervals from 2 to 10. The pH of the solutions were measured before and after each experiment.

The solution preparation procedure and the raw data for each experiment are detailed in Appendix F.

2.8 Determination of q

The number of O-H oscillators (q) of the Eu(III)-ligand systems were determined from the measurement of the luminescence emission decay rate constants in H_2O (k_{H_2O}) and D_2O (k_{D_2O}). The excitation wavelength (λ_{ex}) to be used for this study was determined from UV-visible absorbance spectra, obtained using a Cary 3E UV-visible Spectrophotometer, using Hellma quartz SUPRASIL® cells (type: 110-QS, path length = 10 mm).

Phosphorescence emission spectra were recorded, as a function of pH, on a Cary Eclipse Fluorescence Spectrophotometer, using Hellma quartz SUPRASIL® cells (type: 111-QS, path length = 10 mm). The samples were excited by using the $\Delta J = 1$, $\Delta J = 2$ and $\Delta J = 4$ wavelength values from the emission spectra, and phosphorescence emission decay spectra were recorded over 100 ms.

All pH measurements were conducted with a Metrohm 713 pH meter, using a Metrohm 602 Combined Metrosensor glass electrode which was calibrated against pH 4, pH 7 and pH 10 standard commercial buffers. Adjustments in pH were made by drop-wise addition of either concentrated HCl or NaOH solutions for the H_2O solutions. For the D_2O solutions, concentrated DCl and NaOD were used for the pH adjustments.

The Eu(III)-ligand system was maintained at a temperature of 25 °C by means of a jacketed-cell and a water-circulating bath. UV-visible absorbance spectra and phosphorescence emission spectra were recorded at 25 °C.

For each Eu(III) complex, buffered solutions were prepared using a multi-component buffer system (comprised of MES, CHES, MOPS, Tris and KHP) and compared to solutions containing no buffers. Samples of these solutions were prepared according to their pK_a values, as observed from the luminescence study of each system.

The solution preparation procedure and the raw data for each experiment are detailed in Appendix G.

2.9 References

1. *Xcalibur*, 2.0.7; Thermo Fisher Scientific Inc.: U. S. A., 2006.
2. Blaymire, S. *MASPEC II Data System*, 2.0c; Mass Spectrometry Services Ltd: Manchester, U. K., 1994.
3. *OPUS*, 4.2; Bruker Optik GmbH: Ettlingen, Germany, 1997-2002.
4. Furniss, B. S., Hannaford, A. J., Smith, P. W. G., and Tatchell, A. R., *Vogel's Textbook Of Practical Organic Chemistry*. 5th. ed.; Pearson Prentice Hall: London, U. K., 1989.
5. Bruker *APEX2*, Bruker AXS Inc.: Madison, Wisconsin, U.S.A., 2005.
6. Bruker *SAINT-NT*, Bruker AXS Inc.: Madison, Wisconsin, U.S.A., 2005.
7. Bruker *SHELXTL*, Bruker AXS Inc.: Madison, Wisconsin, U.S.A., 1999.
8. Spek, A. L., *J. Appl. Cryst.* **2003,** 36, 7-13.
9. Farrugia, L. J., *J. Appl. Cryst.* **1997,** 30, 565.
10. Armarego, W. L. F., and Chai, C. L. L., *Purification Of Laboratory Chemicals*. Butterworth-Heinemann: Cornwall, Great Britain, 2003.
11. Dijksman, A., Elzinga, J. M., Li, Y-X., Arends, I. W. C. E., and Sheldon, R. A., *Tetrahedron: Asymmetry* **2002,** 13, (8), 879-884.
12. Martin, A. E., Ford, T. M., Bulkowski, J. E., *J. Org. Chem.* **1982,** 47, (3), 412-415.
13. Padayachy, K., Fernandes, M. A., Marques, H. M., and de Sousa, A. S., *J. Chem. Crystallogr.* **2008,** 38, (8), 577-582.
14. Caravan, P., Amedio Jr., J. C., Dunham, S. U., Greenfield, M. T., Cloutier, N. J., McDermid, S. A., Spiller, M., Zech, S. G., Looby, R. J., Raitsimring, A. M., McMurry, T. J., and Lauffer, R. B., *Chem. Eur. J.* **2005,** 11, (20), 5866-5874.
15. Fedi, V., Altamura, M., Balacco, C., Canfarini, F., Criscuoli, M., Giannotti, D., Giolitti, A., Giuliani, S., Guidi, A., Harmat, N. J. S., Nannicini, R., Pasqui, F., Patacchini, R., Perrotta, E., Tramontana, M., Tirolo, A., and Maggi, C. A., *J. Med. Chem.* **2004,** 47, (27), 6935-6947.
16. Bräuner-Osborne, H., Bunch, L., Chopin, N., Couty, F., Evano, G., Jensen, A. A., Kusk, M., Nielsen, B., and Rabasso, N., *Org. Biomol. Chem.* **2005,** 3, (21), 3926-3936.
17. Herberich, B., Scott, J. D., and Williams, R. M., *Bioorg. Med. Chem.* **2000,** 8, (3), 523-532.

18. Tan, T. H. S., Hickman, D. T., Morral, J., Beadham, I. G., and Micklefield, J., *Chem. Commun.* **2004**, (5), 516-517.
19. Greenwald, R. B., Zhao, H., Yang, K., Reddy, P., and Martinez, A., *J. Med. Chem.* **2004,** 47, (3), 726-734.
20. Smith, G., Mikkelsen, G., Eskildsen, J., and Bundgaard, C., *Bioorg. Med. Chem. Lett.* **2006,** 16, (15), 3981-3984.
21. Aime, S., Cravotto, G., Crich, S. G., Giovenzana, G. B., Ferrari, M., Palmisano, G., and Sisti, M., *Tet. Lett.* **2002,** 43, (5), 783-786.
22. Farfán, N., Cuéllar, L., Aceves, J. M., and Contreras, R., *Synthesis* **1987**, (10), 927-929.
23. Pettit, G. R., Chamberland, M. R., and Blonda, D. S., *Can. J. Chem.* **1964,** 42, (7), 1699-1706.
24. Padayachy, K., Fernandes, M. A., Marques, H. M., and de Sousa, A. S., *Acta Cryst. E* **2012,** E68, (8), o2570 - o2571.
25. Padayachy, K., Mgcima, Z., Fernandes, M. A., Marques, H. M., and de Sousa, A. S., *Acta Cryst. E* **2011,** E67, (10), o2594.
26. Yin, H., Xu, Y., and Qian, X., *Bioorg. Med. Chem.* **2007,** 15, (3), 1356-1362.
27. *Tiamo*, 1.2; Metrohm AG: Herisau, Switzerland, 2006.

Chapter 3

Single Crystal Structures

3.1 Cy_2DETA

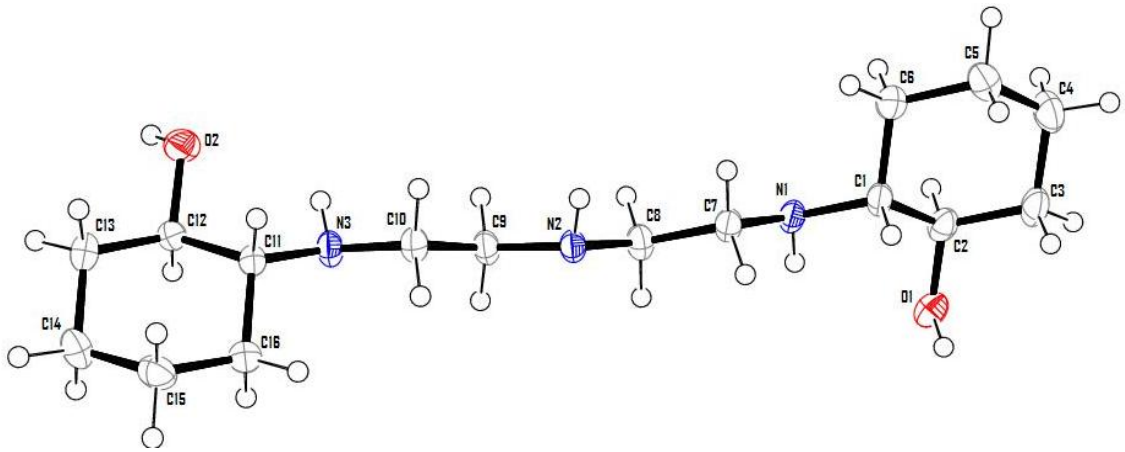


Figure 3.1: The molecular structure of Cy_2DETA, showing the atom-labelling scheme and 50% probability displacement ellipsoids.

Cy_2DETA crystallizes in the P-1 space group, with equivalent molecules symmetrically related by a centre of inversion. The unit cell (Figure 3.2) consists of the *R*,*R* and *S*,*S* enantiomeric pairs. Both cyclohexyl rings adopt the chair conformation, the rings are not coplanar. A plane through the diethylenetriamine backbone and one of the cyclohexyl rings indicates that the second ring is almost orthogonal to the plane (Figure 3.3).

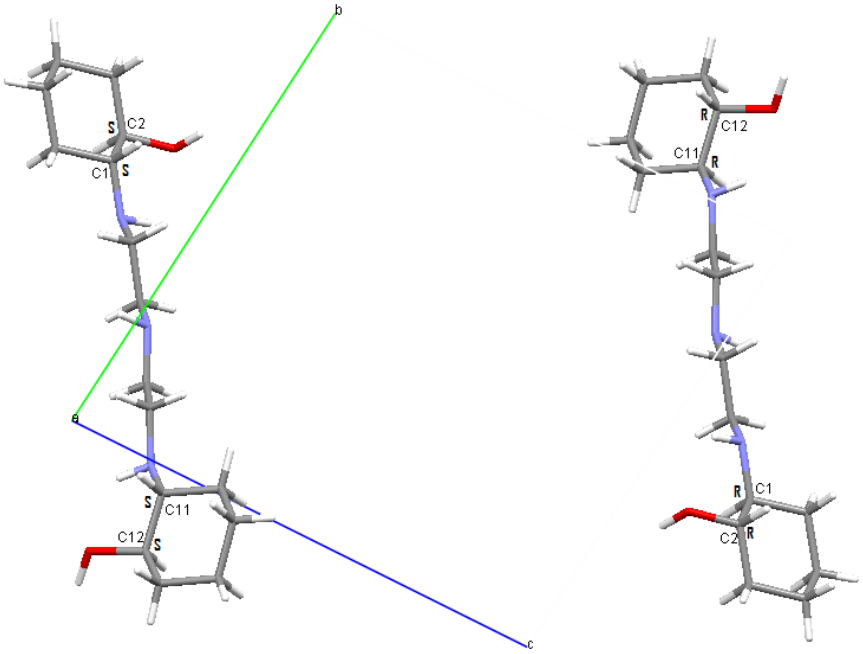


Figure 3.2: Unit cell of Cy_2DETA viewed along the *a*-axis.

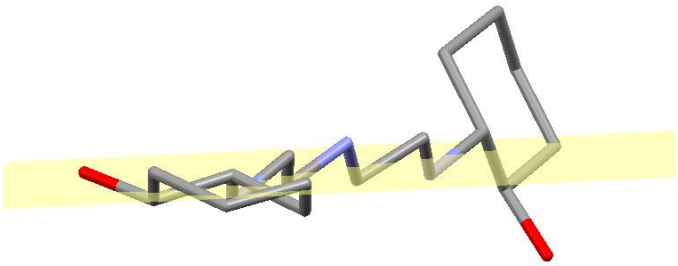


Figure 3.3: The plane defined by the diethylenetriamine backbone and a cyclohexyl ring in Cy_2DETA (H atoms omitted for clarity).

The crystal forms a sheet-like packing arrangement, with a hydrogen bonding array between molecules in the same sheet (Figure 3.4). The hydrogen-bonding pattern is largely determined by O1-H1O···N2 and N2-H2N···O2 interactions. Both hydrogen bonds result in unitary $R_2^2(16)$ ring motifs and a binary $C_2^2(16)$ motif between both enantiomers[1]. This pattern occurs throughout the sheet (Figure 3.5). Molecules within the sheet are related to each other by means of an inversion centre (Figure 3.6). This orientation facilitates favourable hydrogen-bonding, as D-H···A angles, O1-H1O···N2 and N2-H2N···O2, are both over 170°.

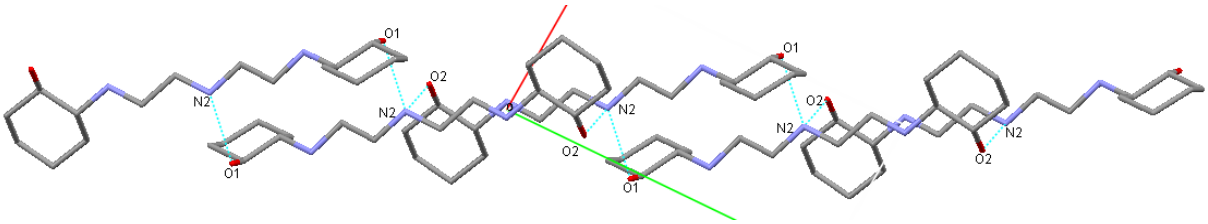


Figure 3.4: Hydrogen-bonding array of Cy_2DETA viewed along the *c*-axis (H atoms omitted for clarity).

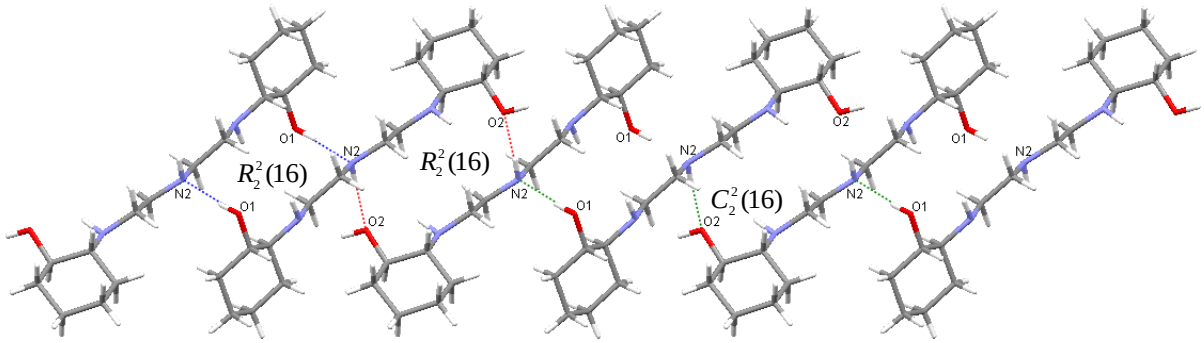


Figure 3.5: Hydrogen-bonding array of Cy_2DETA viewed along the *a*-axis.

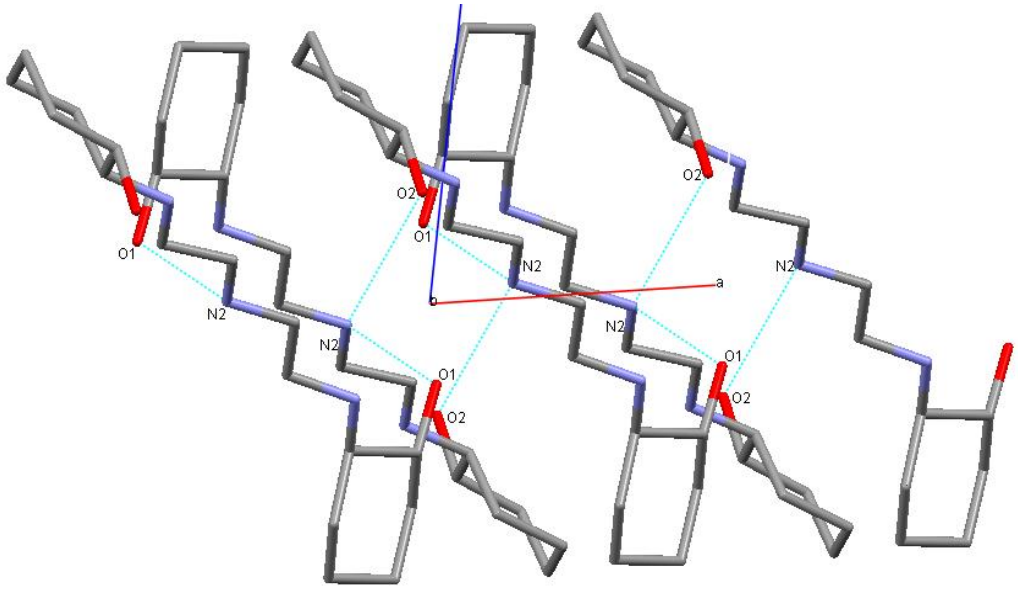


Figure 3.6: Hydrogen-bonding array of Cy_2DETA viewed along the *b*-axis (H atoms omitted for clarity).

The hydrogen bonds within each sheet are reinforced by the close contact interaction of C8-H8A···O2 (Figure 3.7). This interaction is shown to occur between the centrosymmetrically-related Cy_2DETA molecules, resulting in a $R_2^2(18)$ motif between enantiomers.

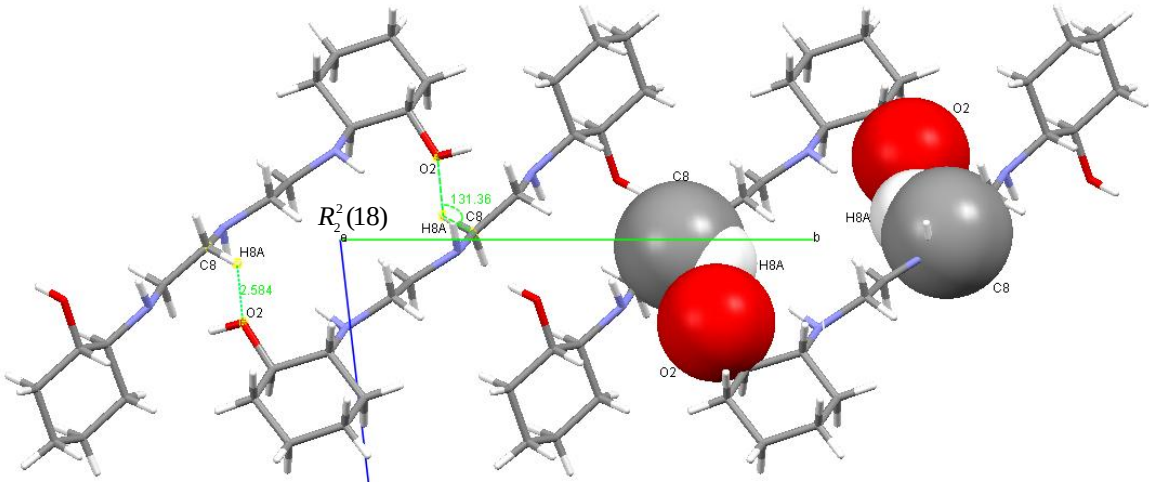


Figure 3.7: Close contact interactions within a sheet of Cy_2DETA viewed along the *a*-axis.

Each sheet is hydrogen-bonded to the next via the O2-H2O···N1 interaction (Figures 3.8 and 3.9), forming a $R_2^2(22)$ motif. The sheet stacking is reinforced by the close contact interaction of C15-H15B···N3 (Figure 3.10).

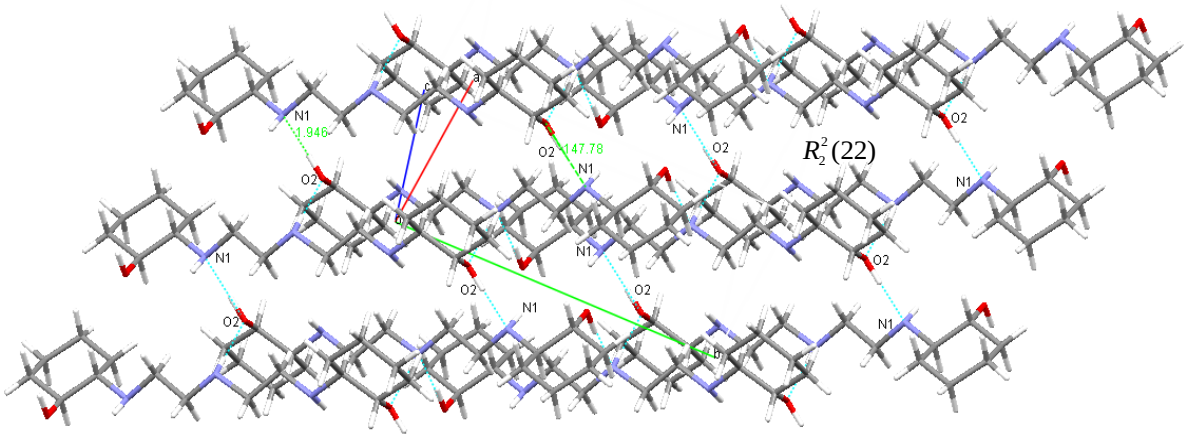


Figure 3.8: Hydrogen-bonding array between sheets of Cy_2DETA.

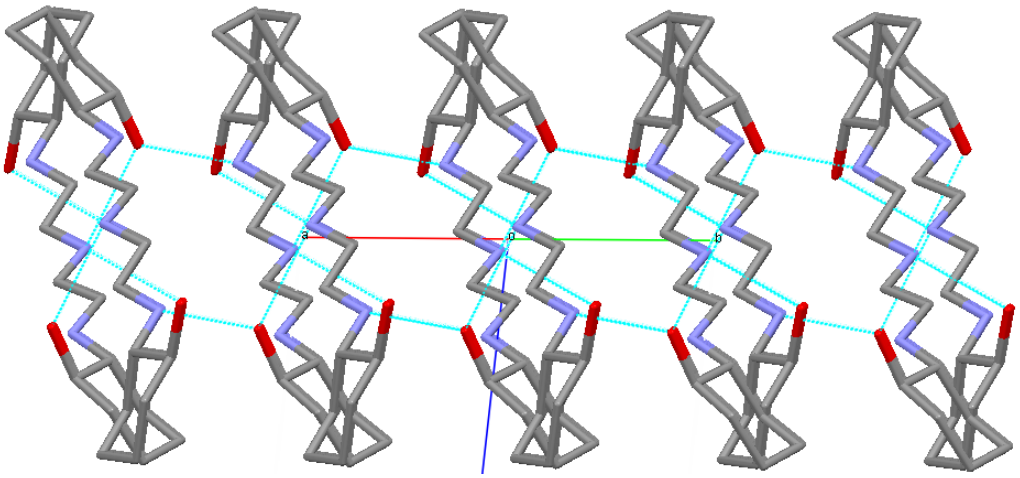


Figure 3.9: Hydrogen-bonding array between sheets of Cy_2DETA (H atoms omitted for clarity).

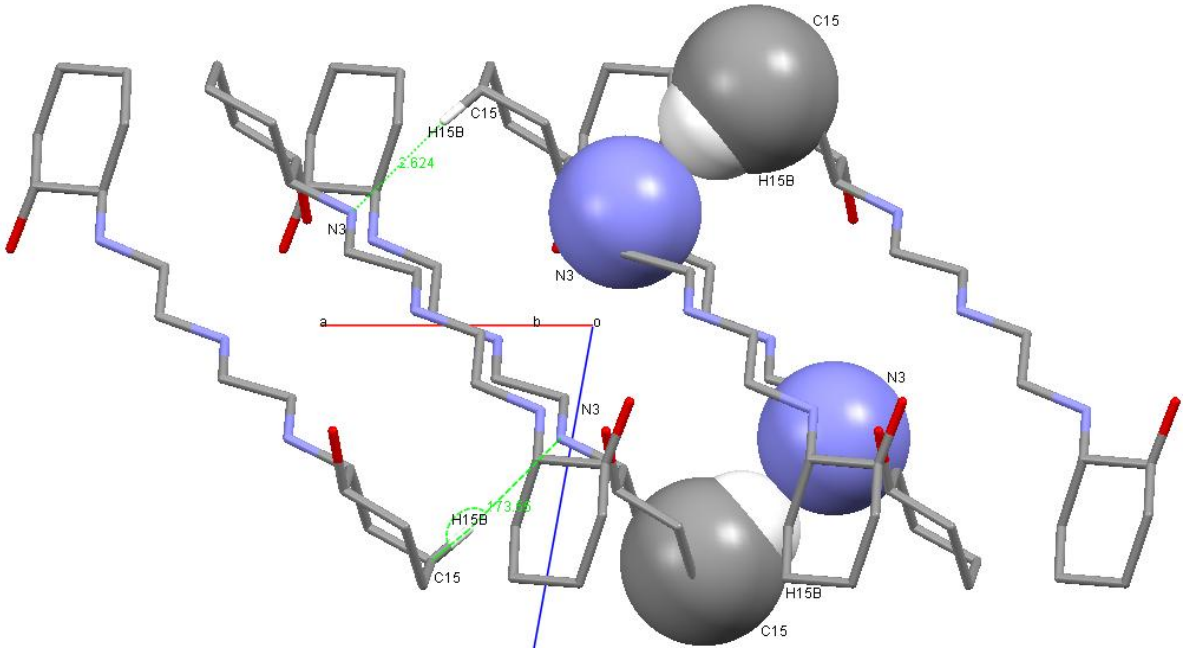


Figure 3.10: The C15-H15B···N3 close contact interactions between sheets of Cy_2DETA.

The hydrogen-bonding array observed between stacked Cy_2DETA sheets is such that the cyclohexyl rings are situated on the outer surface of the stacked sheets, while the hydrogen bonding takes place in the centre of the stack, yielding a hydrophilic inner core. Figure 3.11 illustrates this 'sandwich-like' appearance.

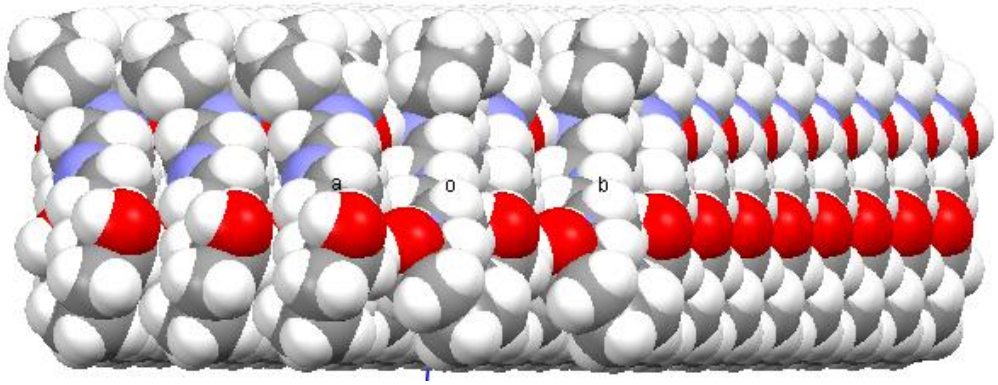


Figure 3.11: Spacefill diagram showing the 'sandwich-like' appearance of Cy_2DETA.

It is further observed that these 'sandwiches' stack on top of each other. Figure 3.12 shows interactions between the H15A atoms between 'sandwich-layers.' The distance between these hydrogen atoms is shorter than the sum of their van der Waals radii (2.335 Å)[2]. The C15-H15A···C15^{i} (i = -1-x, -y, 1-z) is not a typical hydrogen bond, but the distance between the carbon C15 and hydrogen H15A between layers is shorter than the sum of their van der Waals radii. This interaction results in a *C*(5) motif between equivalent enantiomers.

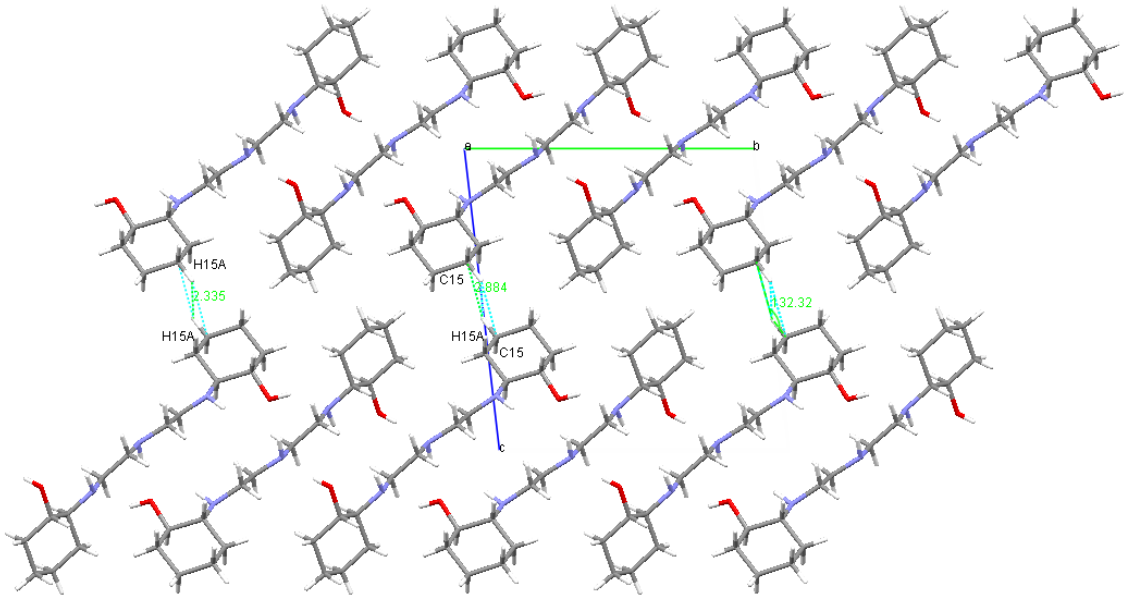


Figure 3.12: Interactions between 'sandwiches' of Cy_2DETA viewed along the *a*-axis.

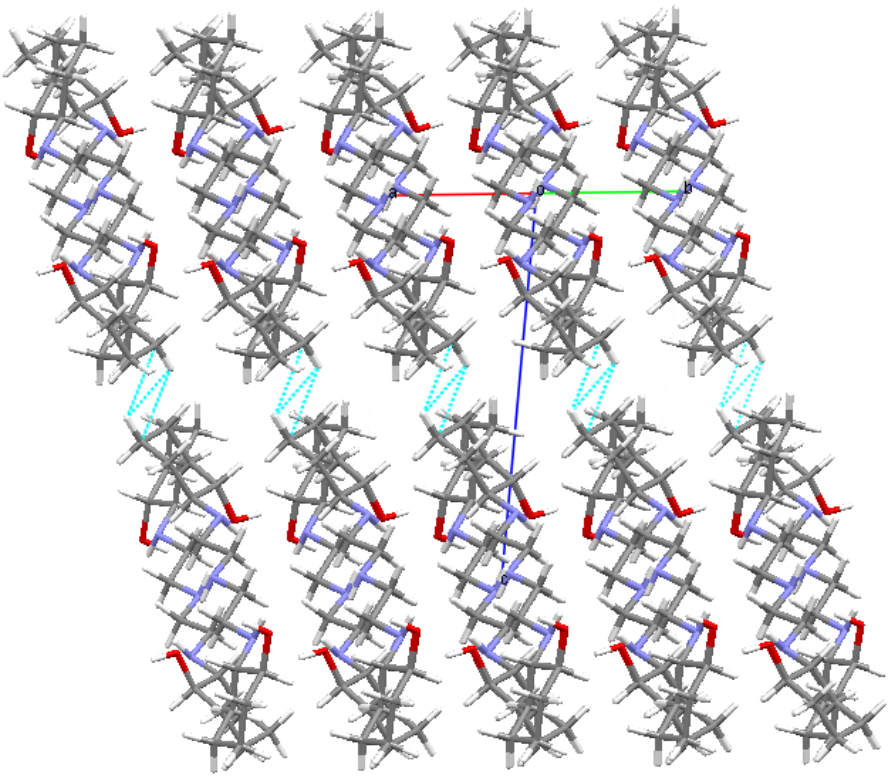


Figure 3.13: Interactions between 'sandwiches' of Cy_2DETA.

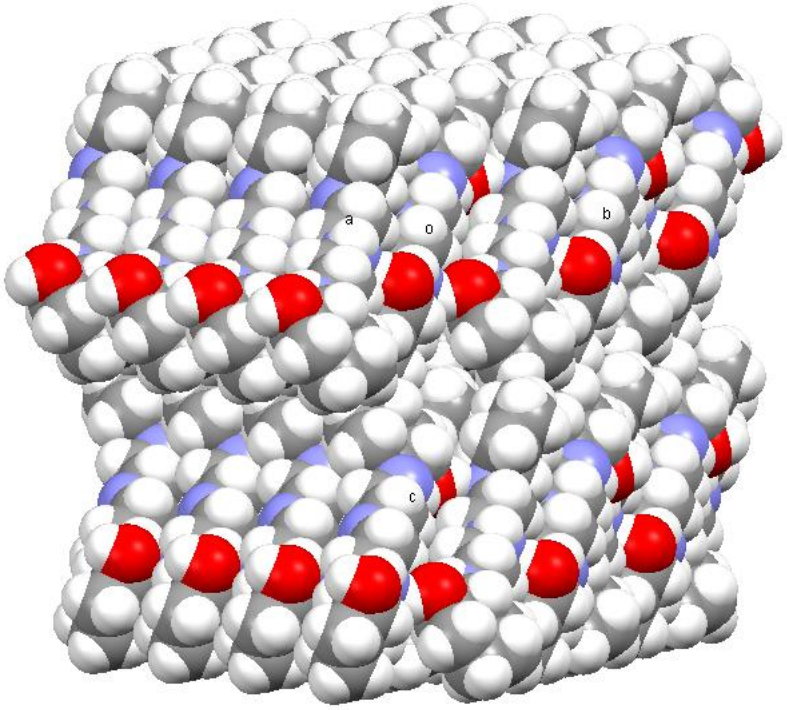


Figure 3.14: Spacefill diagram showing the stacking of 'sandwiches' of Cy_2DETA.

Close contacts occur between the hydrogen on the terminal amine moieties and their alcohol substituent, N1-H1N···O1 and N3-H3N···O2 (Figure 3.15), both adopting *S*(5) motifs. In both instances, the distance between the hydrogen and oxygen atoms is well below the sum of the van der Waals radii (hydrogen has a van der Waals radius of 1.20 Å and oxygen 1.52 Å)[2]. The angle between the donor and acceptor atoms is below the optimal 120° angle for a hydrogen bond, resulting in a weak interaction. The short distances observed are possibly a result of a minimization of the close contact interactions of hydrogen atoms in the cyclohexyl ring and diethylenetriamine backbone (red arrows). Figure 3.16 demonstrates the deviation from ideal tetrahedral geometry about the terminal amine as a result of the minimization of these van der Waals repulsions.

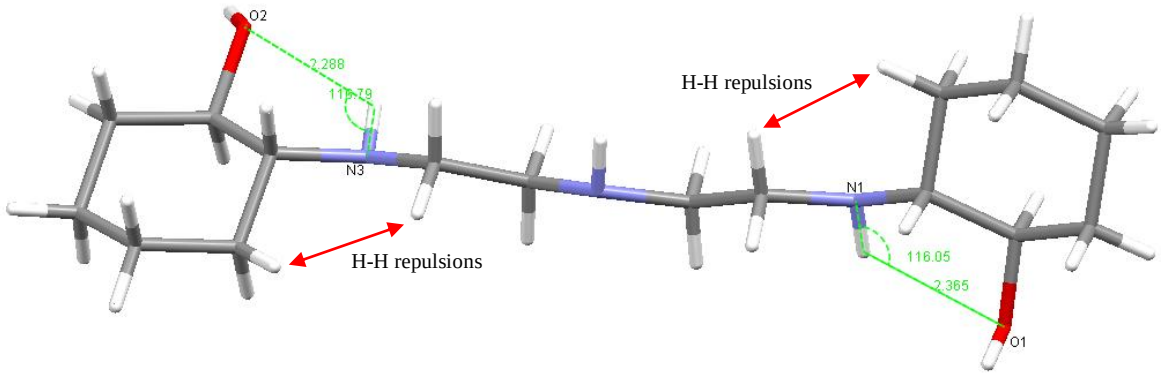


Figure 3.15: Close contact interactions between the terminal amine and alcohol moieties of Cy_2DETA, resulting in H-H repulsions between the cyclohexyl ring and triazaheptane backbone (red arrows).

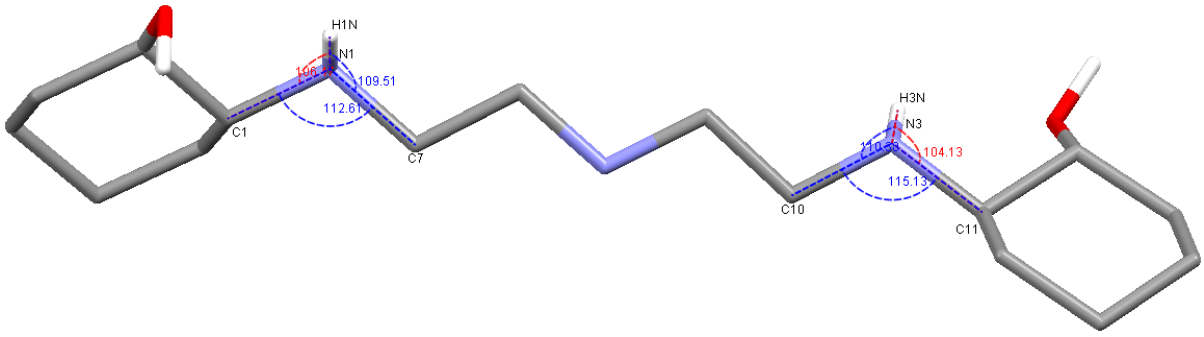


Figure 3.16: Bond angles around the terminal amines of Cy_2DETA (H atoms omitted for clarity).

3.2 $Cy_2DETA.3HClO_4$

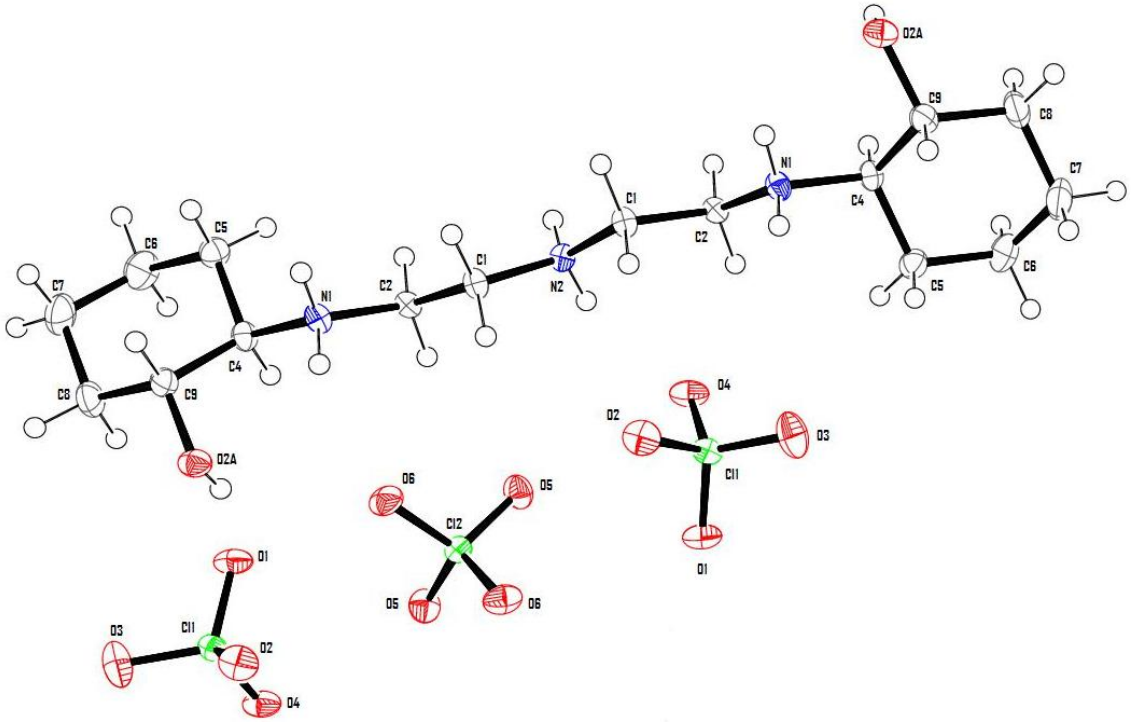


Figure 3.17: The molecular structure of $Cy_2DETA.3HClO_4$, showing the atom-labelling scheme and 50% probability displacement ellipsoids.

$Cy_2DETA.3HClO_4$ crystallizes in the C2/c space group. Equivalent molecules are generated via a two-fold screw axis. The cyclohexyl rings have adopted the chair conformation and are not coplanar (Figure 3.18). Figure 3.19 illustrates the unit cell consisting of *R*,*R* and *S*,*S* enantiomeric pairs.

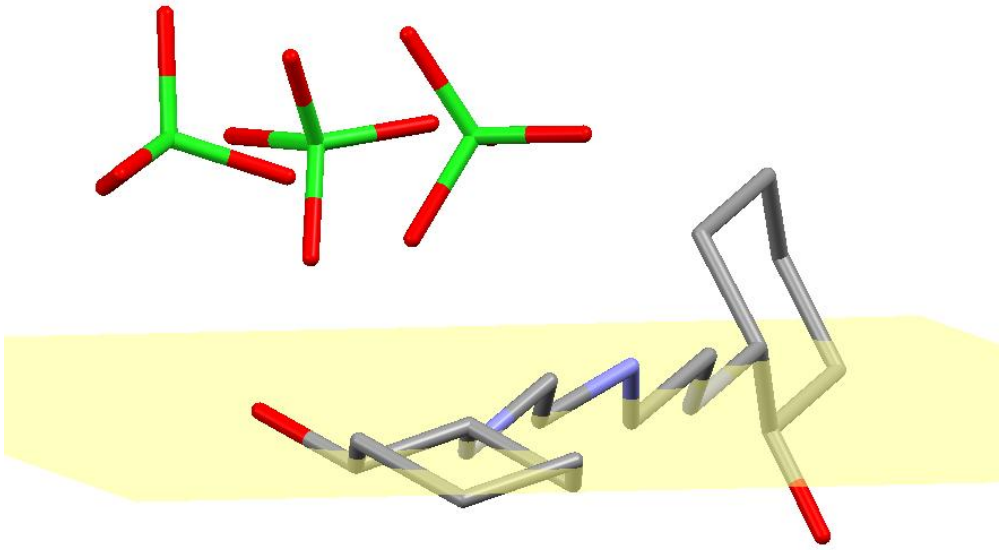


Figure 3.18: The plane defined by the diethylenetriamine backbone and a cyclohexyl ring in $Cy_2DETA.3HClO_4$ (H atoms omitted for clarity).

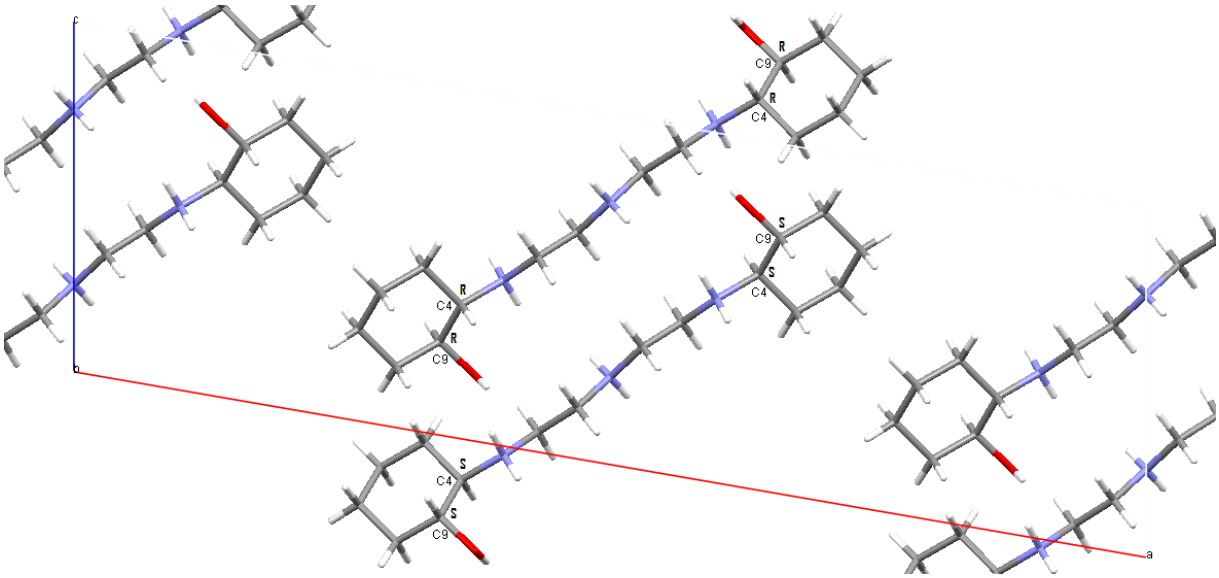


Figure 3.19: Unit cell of $Cy_2DETA.3HClO_4$ viewed along the *b*-axis (ClO_4^- ions omitted for clarity).

Molecules of Cy_2DETA within a sheet are separated by perchlorate ions that define the observed hydrogen bonding (Figure 3.20). The N1-H1···O6, O2A-H4···O1, and N2-H3···O4 hydrogen bonds exhibit bond lengths and bond angles within the acceptable limits (Table D.14, Appendix D). The O2A-H4···O6 hydrogen bond has a bond angle of 113.47°, below the acceptable 120° for a hydrogen bond. As for the N1-H1N···O1 and N3-H3N···O2 close contacts in Cy_2DETA, these interactions possibly arises as a consequence of minimizing the van der Waals repulsions between hydrogen atoms on the triazaheptane backbone and

cyclohexyl ring (Figure 3.21). The C4-N1-H1 bond angle deviates quite markedly from the 109° expected for the protonated sp^3-hybridized nitrogen atom, while the large C2-N1-C4 bond angle demonstrates the conformation adopted by the backbone and ring in order to minimise H-H repulsions between them.

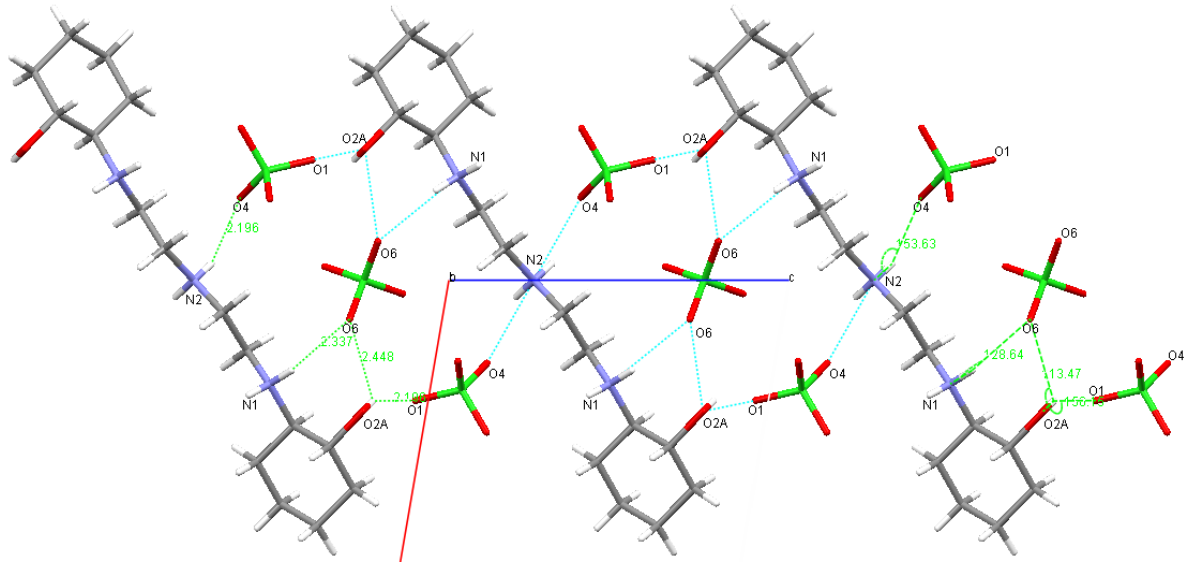


Figure 3.20: Hydrogen-bonding array of $Cy_2DETA.3HClO_4$ viewed along the *b*-axis.

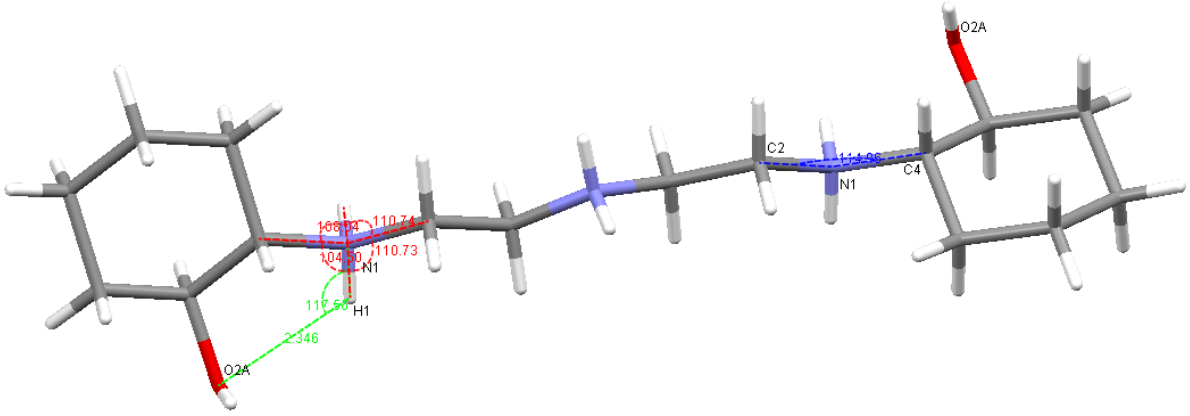


Figure 3.21: Bond angles around the terminal amines of $Cy_2DETA.3HClO_4$ (H atoms and ClO_4^- ions omitted for clarity).

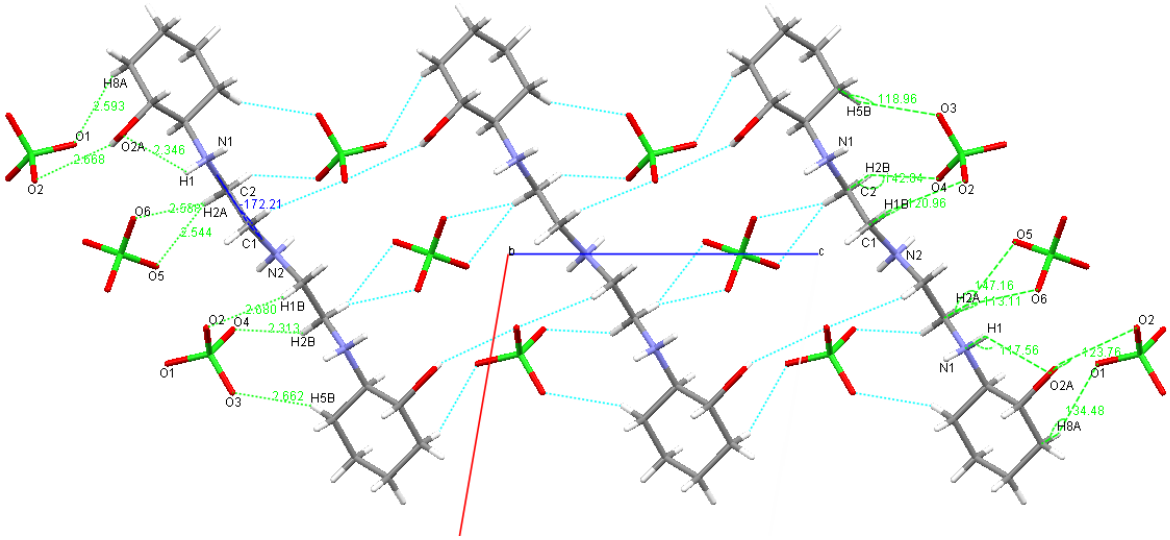


Figure 3.22: Close contact interactions within a sheet of $Cy_2DETA.3HClO_4$ viewed along the *b*-axis.

Figure 3.22 illustrates close contact interactions occurring within a sheet. A change in the N2-C1-C2-N1 torsion angle (i.e. the triazaheptane backbone) of almost 6° is observed when compared to the free base (Cy_2DETA). The interactions between C8-H8A···O1, C2-H2A···O5 and C2-H2B···O4 are typical hydrogen bonds, due to the bond lengths and bond angles exhibited for these close contacts. An interesting feature is the close contact between the terminal amine and alcohol groups, i.e. N1-H1···O2A. Protonation of the terminal amine is shown to alter the N1-C4-C9-O2A torsional angle, but has minimal effect on the bond angle or bond length when compared to Cy_2DETA.

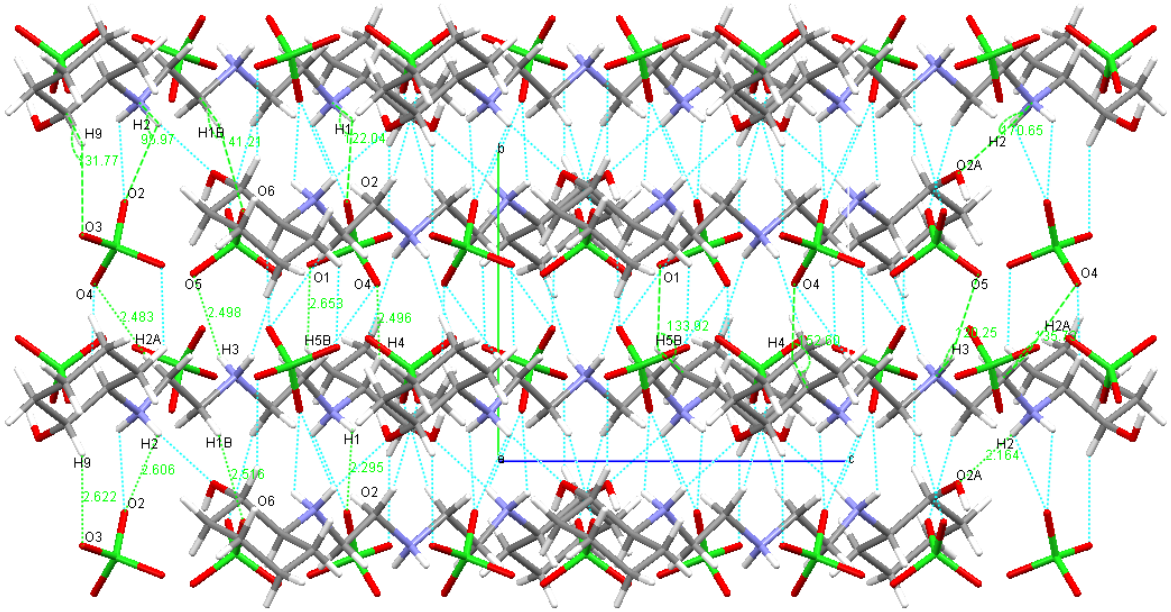


Figure 3.23: Hydrogen-bonding array between sheets of $Cy_2DETA.3HClO_4$ viewed along the *a*-axis.

The sheets are linked to each other by an extensive array of hydrogen-bonding and van der Waals interactions (Figure 3.23). There is a slight puckering of the cyclohexyl rings due to a minimal increase in the torsional angles of the ring. This is a result of the increased interactions of the cycloalkyl ring and alcohol moeity with the perchlorate ions and the protonated amines between sheets.

The arrangement of the sheet stacking for $Cy_2DETA.3HClO_4$ adopts a similar 'sandwich-like' appearance to that of the free base (Figures 3.24 and 3.25). The inclusion of the perchlorate ions in the inner hydrophilic core results in an expanded 'sandwich.' However, there appears to be no hydrogen bonding or close contact interactions that support the stacking of 'sandwiches' observed for Cy_2DETA.

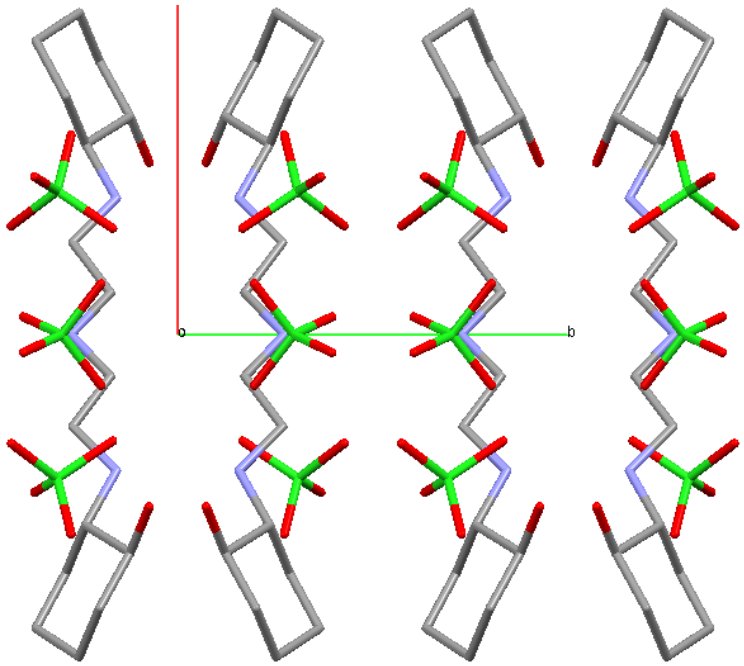


Figure 3.24: Stacking of sheets of $Cy_2DETA.3HClO_4$ viewed along the *c*-axis (H atoms omitted for clarity).

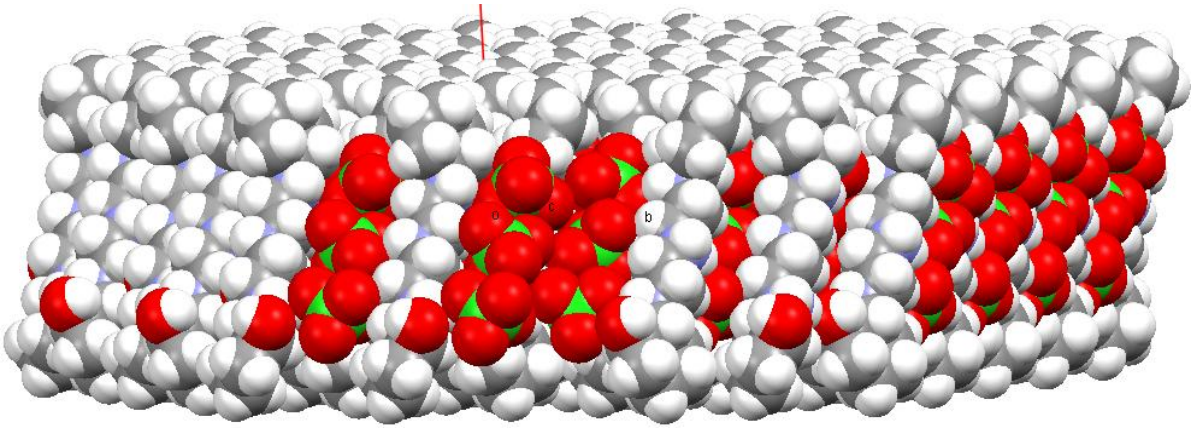


Figure 3.25: Spacefill diagram showing the 'sandwich-like' appearance of $Cy_2DETA.3HClO_4$.

3.3 Ts_2DETA

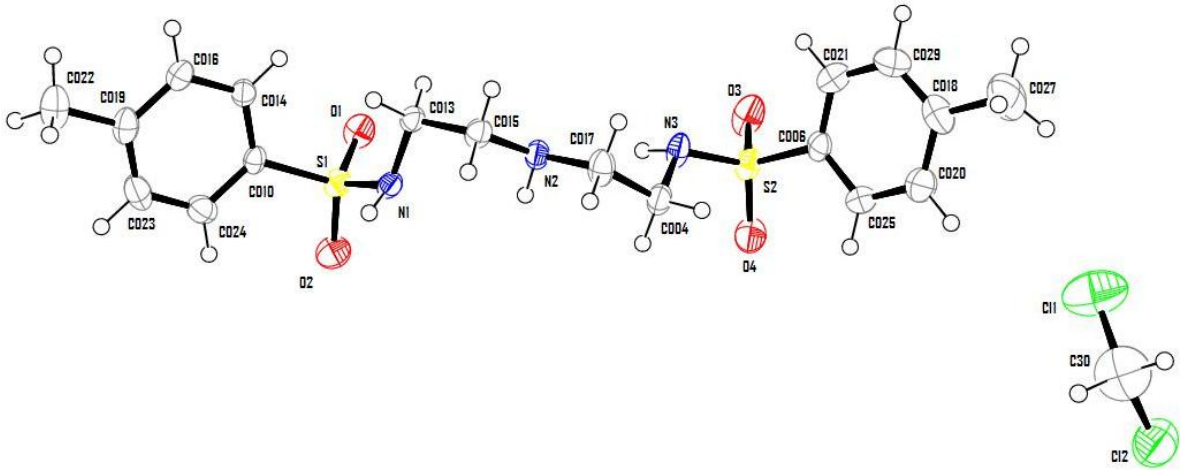


Figure 3.26: The molecular structure of Ts_2DETA, showing the atom-labelling scheme and 50% probability displacement ellipsoids.

The crystal structure of Ts_2DETA has been reported[3]. Ts_2DETA crystallizes in the $Pca2_1$ space group. The crystal structure is stabilized by the inclusion of the solvent dichloromethane. The dichloromethane molecules occupy the gaps between the Ts_2DETA layers, and are related via a two-fold screw axis (Figure 3.27). The bond angle and bond length of the C19-H19B···O1 interaction has the characteristics of a hydrogen bond, and is important in stabilizing the crystal packing of the tosylated amine. There also appears to be an interaction between the solvent molecules, the distance between the H19A and Cl1 atoms between dichloromethane molecules suggests that this interaction is significant (2.864 Å < 1.20 Å + 1.80 Å).

The hydrogen bonding that takes place between molecules of Ts_2DETA gives rise to a molecular chain (Figure 3.27). Figure 3.28 demonstrates the N1-H1H···$N2^i$ (i = $^3/_2$-x, y, $^1/_2$+z), N1-H1H···$N3^i$, N3-H3H···$O2^j$ (j = $^3/_2$-x, y, -$^1/_2$+z), and C8-H8A···$O1^i$ hydrogen bonds between Ts_2DETA molecules. The unitary graph set includes a C(5) chain motif, defined by the intermolecular N1-H1H···N2 hydrogen bond, and a C(10) motif, defined by the N3-H3H···O2 intermolecular hydrogen bond. A combination of the N1-H1H···N2 and N3-H3H···O2 hydrogen bonds results in a binary graph set that includes a $C_2^2(15)$ chain

motif and a $R_2^2(9)$ ring motif. The N2-H2H···O3^{i} interaction has a length (2.756 Å) and angle (165.59°) that is similar to a hydrogen bond.

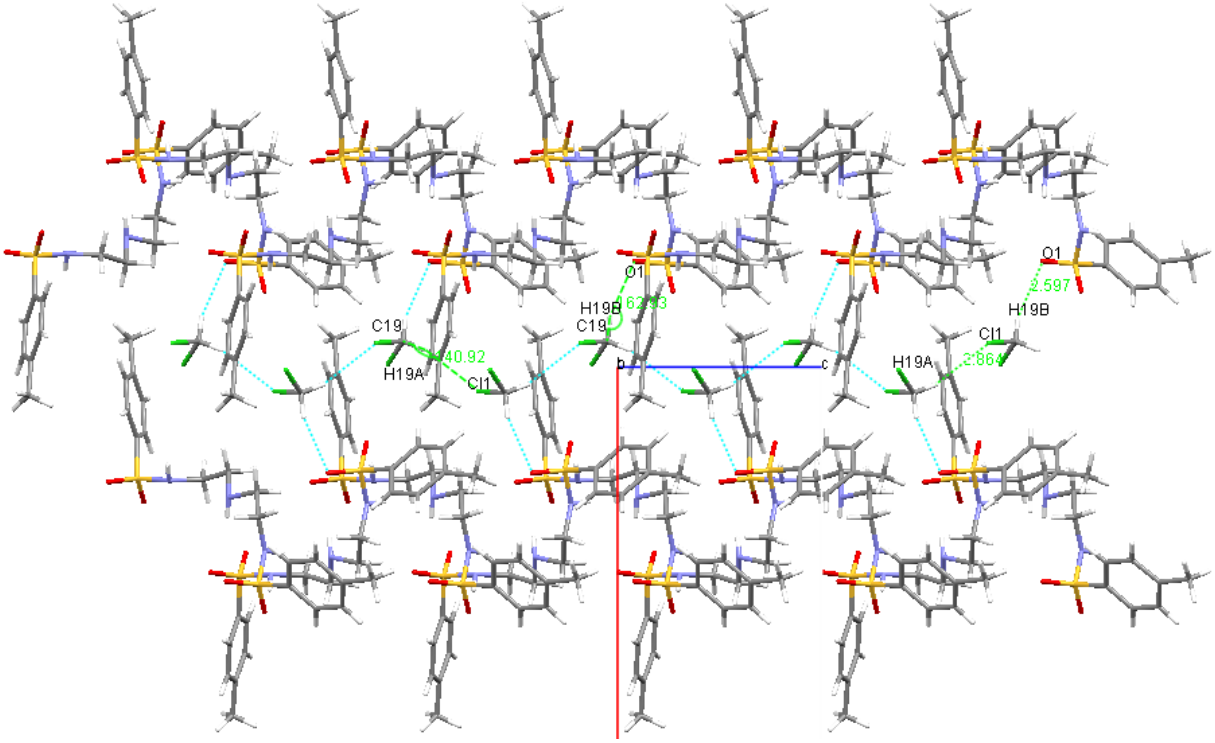


Figure 3.27: Interactions between dichloromethane and Ts_2DETA viewed along the *b*-axis.

A slight puckering of the aromatic ring consisting of atoms C1-C2-C3-C4-C5-C6 is observed, deviating from the ideally flat conformation expected for an aromatic ring. The C2-C3-C4-C5 (-1.74°), C3-C4-C5-C6 (2.57°), C5-C6-C1-C2 (-1.80°) and C6-C1-C2-C3 (2.61°) torsional angles provide evidence of this deviation. This is a result of the close contact interactions of C3-H3···O4 (distance = 2.592 Å) and C7-H7B···O4 (2.634 Å, Figure 3.29).

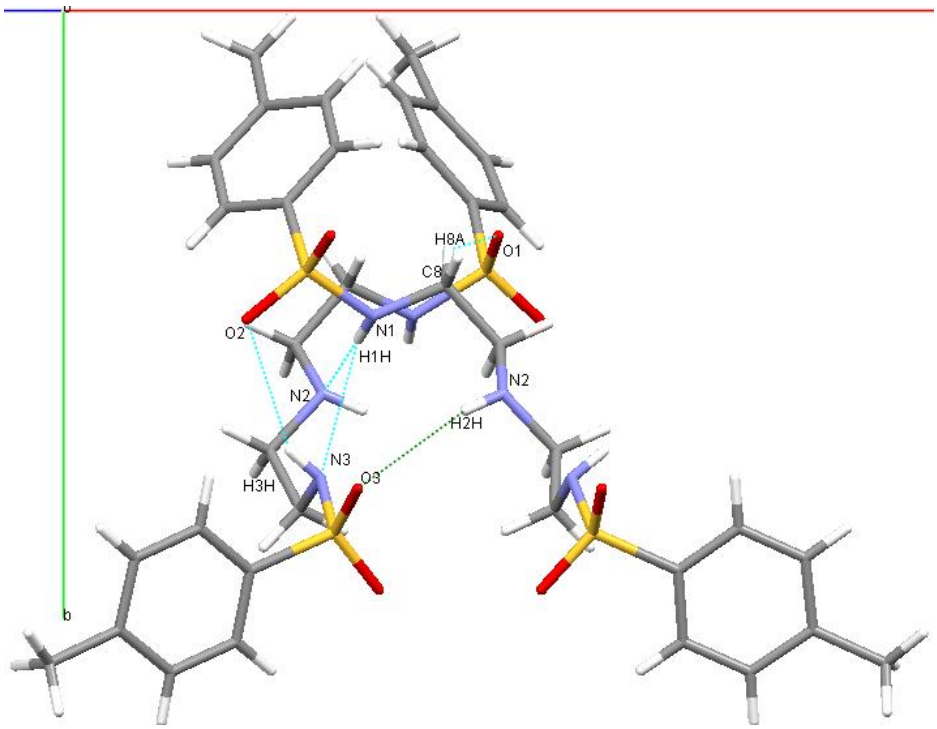


Figure 3.28: N1-H1H···N2^{i}, N1-H1H···N3^{i}, N3-H3H···O2^{j}, and C8-H8A···O1^{i} hydrogen bonds between molecules of Ts_2DETA (i = $^{3}/_{2}$-x, y, $^{1}/_{2}$+z, j = $^{3}/_{2}$-x, y, -$^{1}/_{2}$+z).

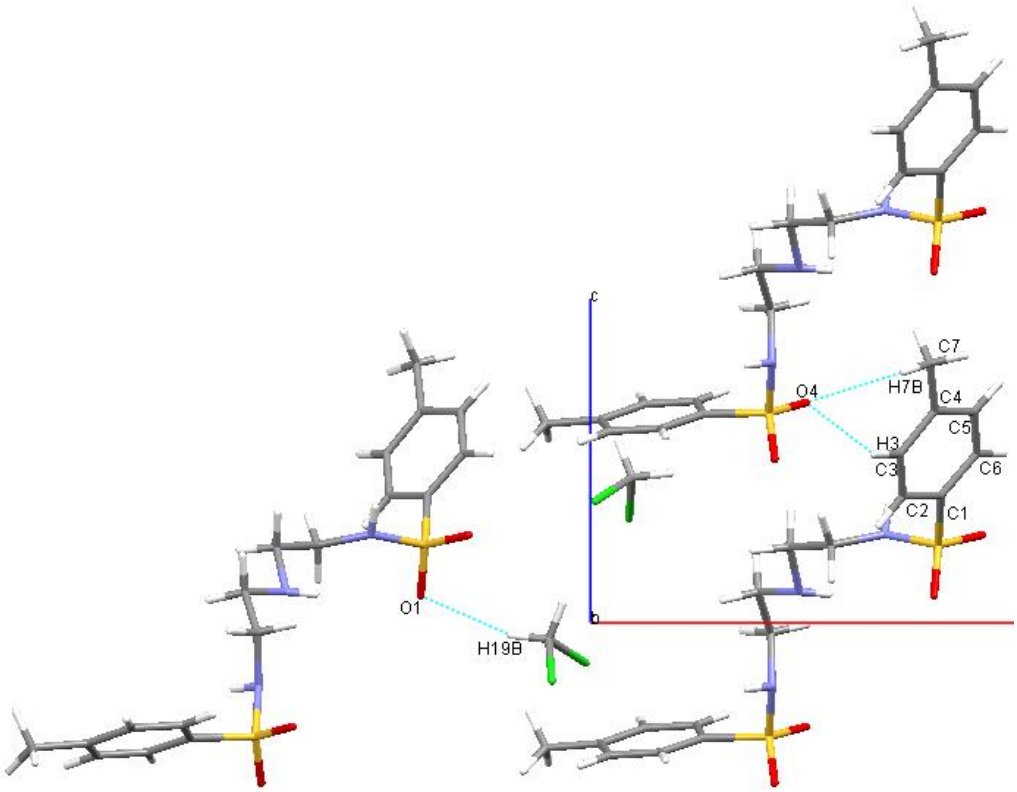


Figure 3.29: Close contact interactions responsible for aromatic ring puckering of Ts_2DETA.

3.4 [NaCy$_2$DETA.3E]Br

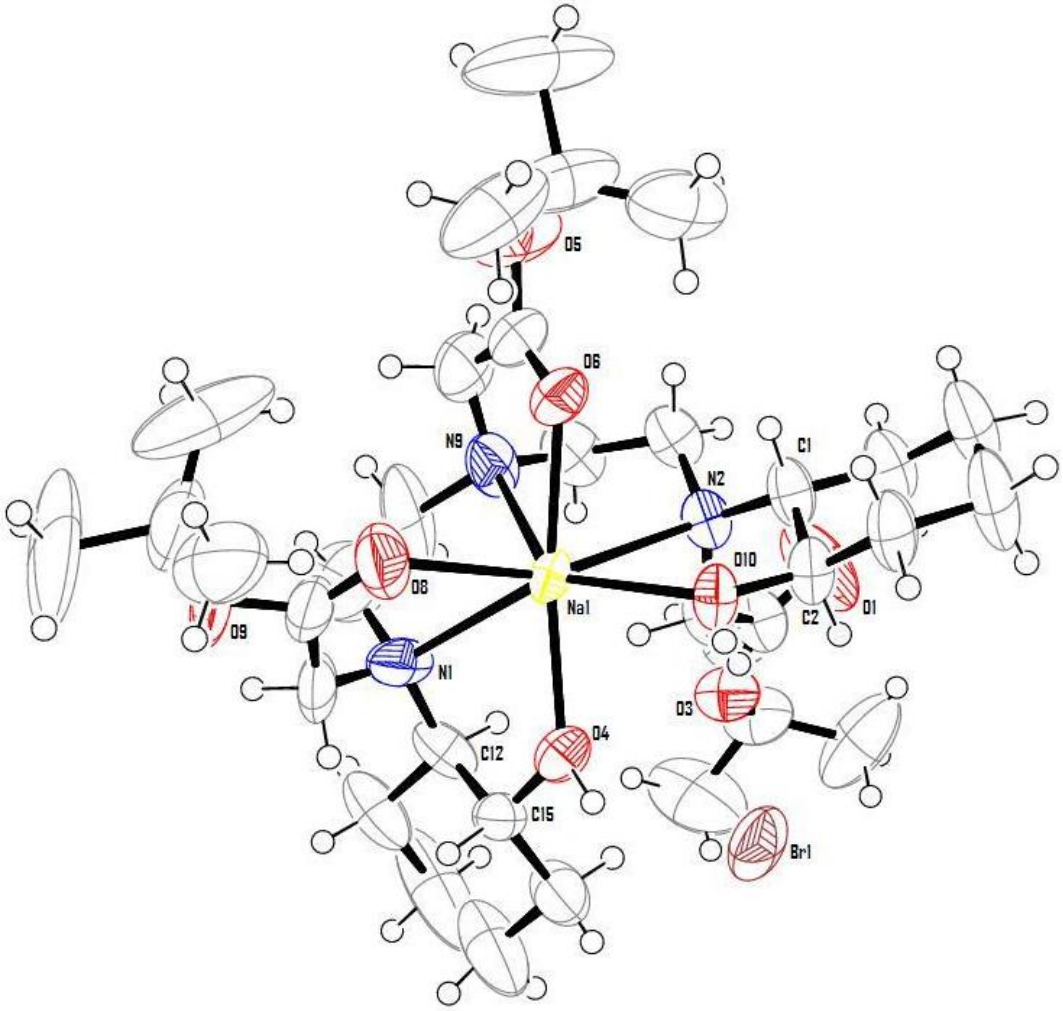


Figure 3.30: The molecular structure of [NaCy$_2$DETA.3E]Br, showing the atom-labelling scheme and 50% probability displacement ellipsoids.

The sodium complex of Cy$_2$DETA.3E crystallizes in the P-1 space group. The structure includes a bromide ion to balance the charge of the complex. The cyclohexyl rings maintain a chair conformation. The unit cell consists of the *R*,*R* and *S*,*S* enantiomeric pairs (Figure 3.31).

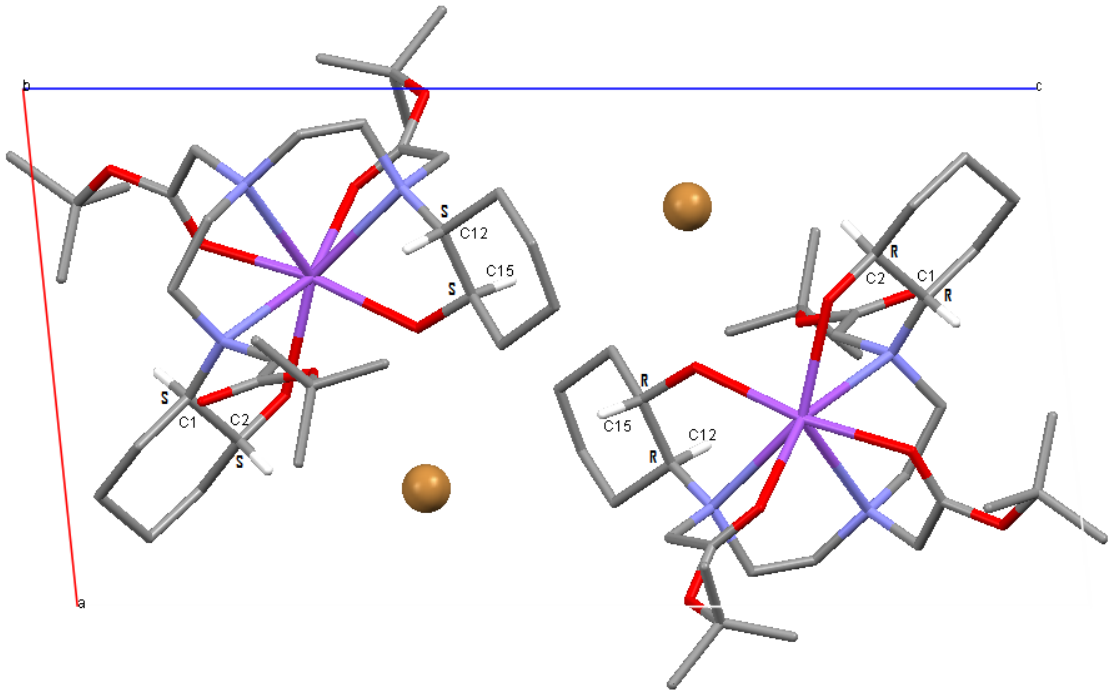


Figure 3.31: Unit cell of [$NaCy_2DETA.3E$]Br viewed along the *b*-axis (H atoms omitted for clarity).

Coordination of the sodium cation occurs via the three tertiary nitrogen atoms of the diethylenetriamine backbone; two hydroxycyclohexyl oxygen atoms and two carbonyl oxygen atoms of the pendent ester functionalities, yielding a heptadentate complex. Figure 3.32 indicates that donor atoms O10, N2, N9 and O8 coordinate to Na1 equatorially (defined by the calculated plane), while O4, N1 and O6 donors atoms chelating Na1 define a plane approximately orthogonal (80.71°) to the equatorial plane (where Na1 is coplanar with O4, N1 and O6).

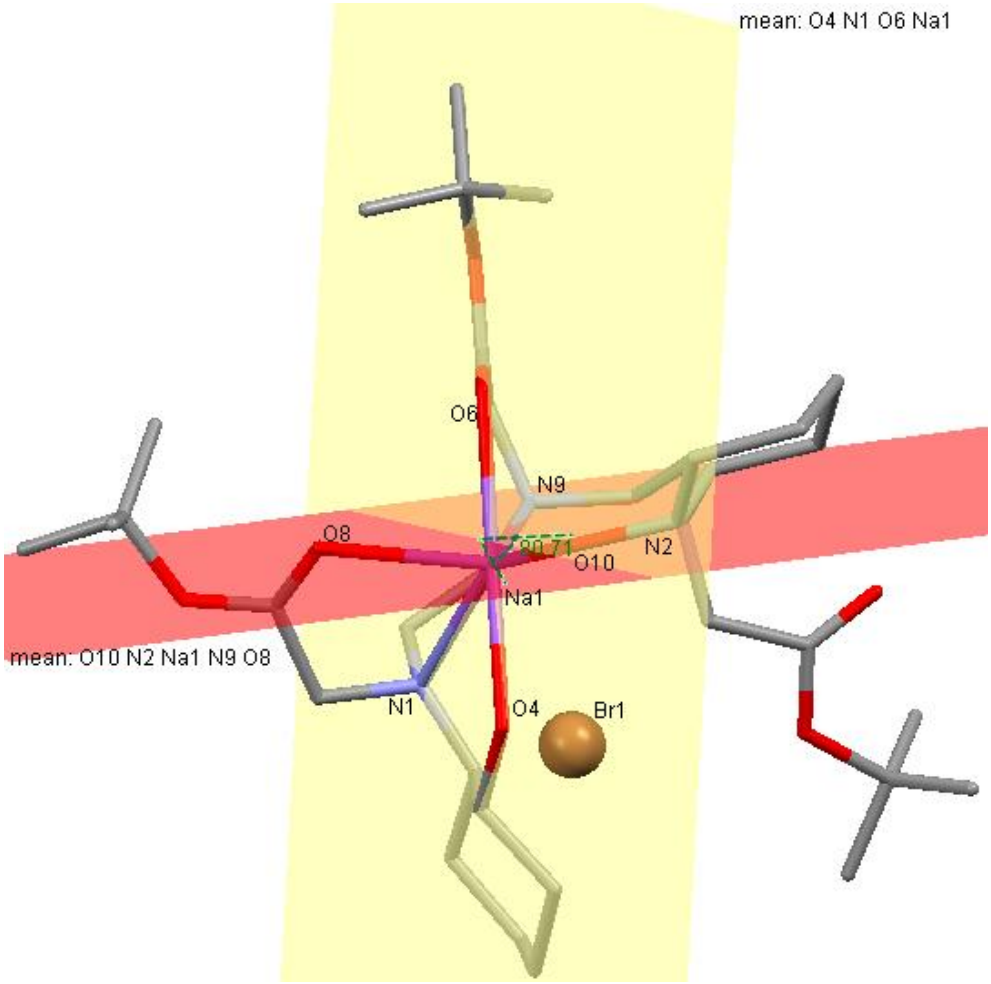
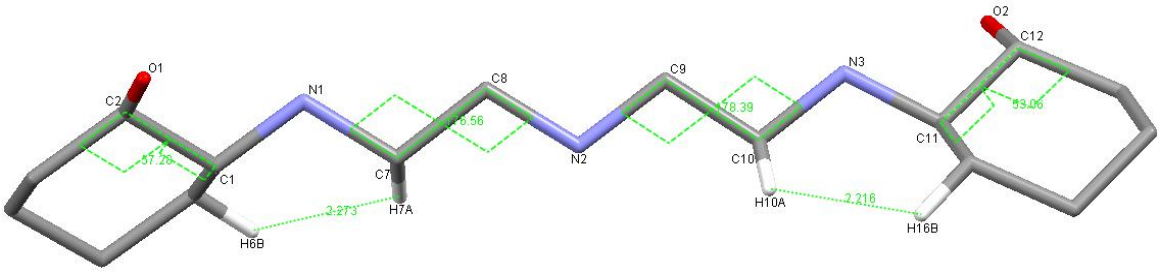


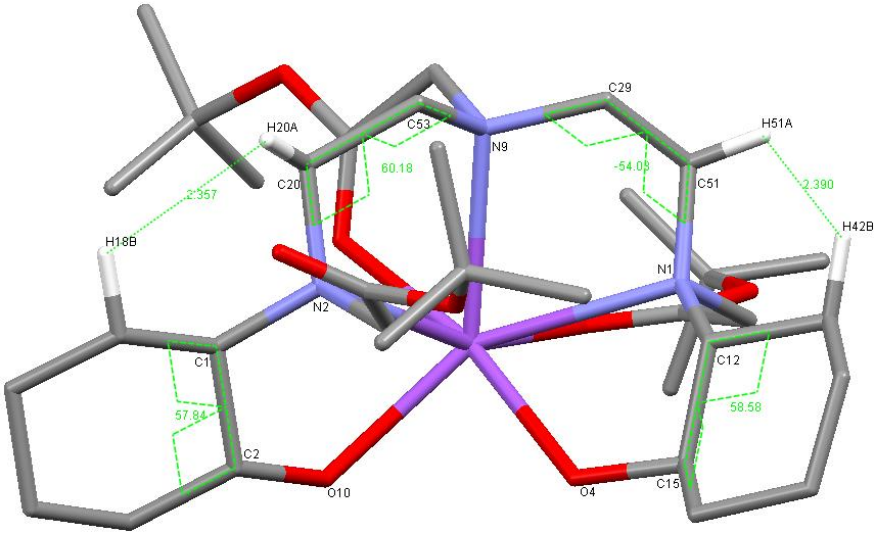
Figure 3.32: Orthogonal relationship between donor atom planes in [NaCy$_2$DETA.3E]Br (H atoms omitted for clarity).

A comparison of the torsional angles of [NaCy$_2$DETA.3E]Br with Cy$_2$DETA offers useful information with respect to the level of preorganization offered by the inclusion of the cyclohexanol moiety into the ligand architecture (Figure 3.33 (a) and (b)). The torsional angles of O1-C2-C1-N1 and N3-C11-C12-O2 for Cy$_2$DETA, compared to O10-C2-C1-N2 and N1-C12-C15-O4 for [NaCy$_2$DETA.3E]Br, have not changed significantly upon complexation of the sodium ion. This indicates that the nitrogen and oxygen donor atoms across the cyclohexenyl bridge were in an energetically-efficient conformation prior to complexation. There is a necessarily significant change in the torsional angles of the backbone as all three nitrogen donors are complexed with the sodium ion. However, the nitrogen donors do not complex the metal within the same plane, thus reducing the van der Waals interactions between hydrogen atoms in the diethylenetriamine backbone (H20A and H51A) and those in the cyclohexyl rings (H18B and H42B). Figure 3.33 (b) shows that the

H18B-H20A and H51A-H42B interactions are approximately equal to the sum of their van der Waals radii.



(a)



(b)

Figure 3.33: Selected close contacts and torsional angles for (a) Cy_2DETA and (b) [$NaCy_2DETA.3E$]Br (H atoms omitted for clarity, Br^- ion not shown).

The bromide counter-ion is hydrogen bonded to alcohol moieties of the complex, as a result of the O10-H1O···Br1 and O4-H2O···Br1 interactions (Figure 3.34), forming a binary $R_2^1(6)$ ring motif.

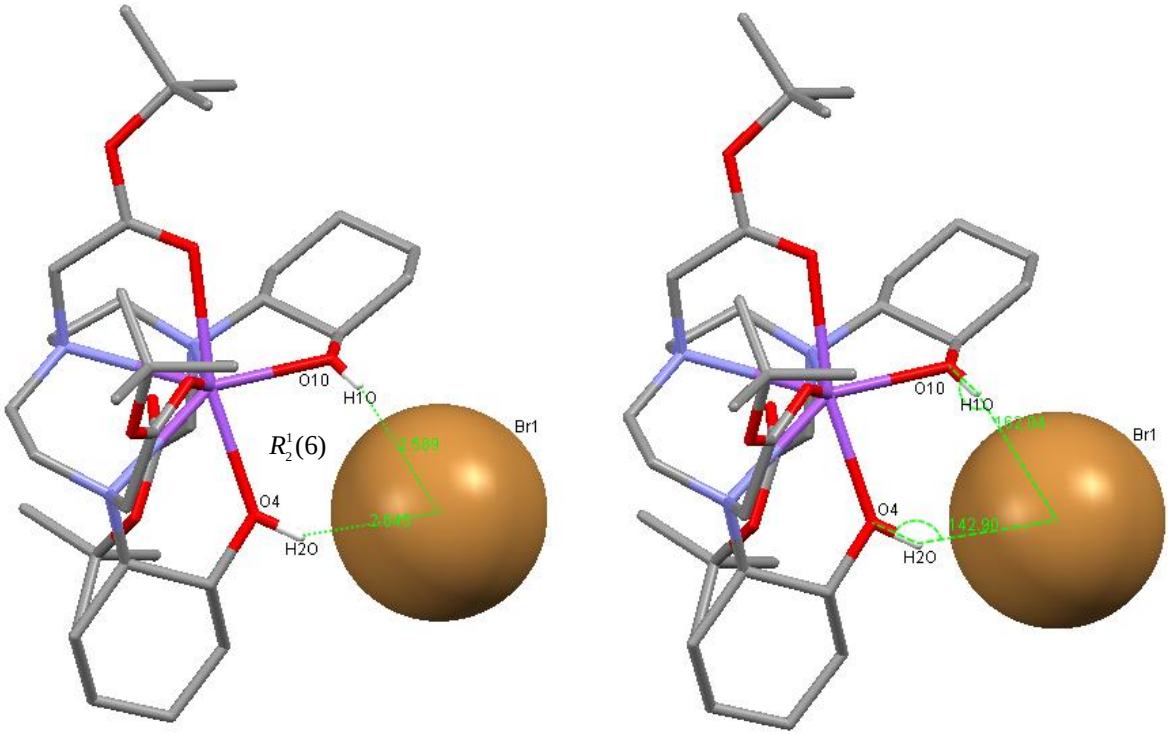


Figure 3.34: Hydrogen bonding between alcohol groups and bromine ion of [NaCy$_2$DETA.3E]Br.

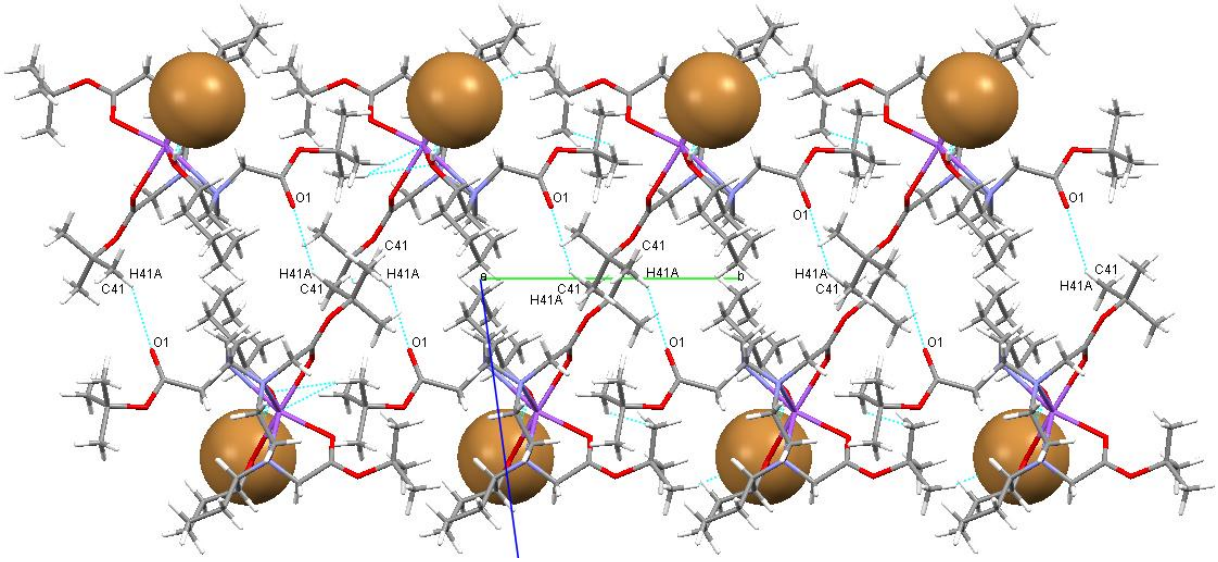


Figure 3.35: Close contacts of [NaCy$_2$DETA.3E]Br, viewed along the *a*-axis.

The crystal packing for [NaCy$_2$DETA.3E]Br occurs in the form of sheets that are linked to form a three-dimensional array (Figure 3.35). When viewed along the *a*-axis, the complexes of [NaCy$_2$DETA.3E]Br in adjacent layers are related by a centre of inversion. Complexes in adjacent sheets are linked by C41-H41A···O1 hydrogen bonds between pairs of enantiomers

(Figure 3.36), resulting in the formation of a $R_2^2(22)$ ring motif. There are also close contact interactions between the H41C atoms of the complex systems in adjacent sheets (Figure 3.37).

The bromide ion is largely responsible for the packing observed within a [NaCy$_2$DETA.3E]Br sheet. Figure 3.36 shows the C51-H51A···Br1 close contact between adjacent enantiomerically equivalent complexes. Inspection of [NaCy$_2$DETA.3E]Br along the *c*-axis (Figure 3.36) indicates that a binary $C_2^1(7)$ chain motif is obtained when the O10-H1O···Br1 or O4-H2O···Br1 hydrogen bonds are combined with the C51-H51A···Br1 interaction.

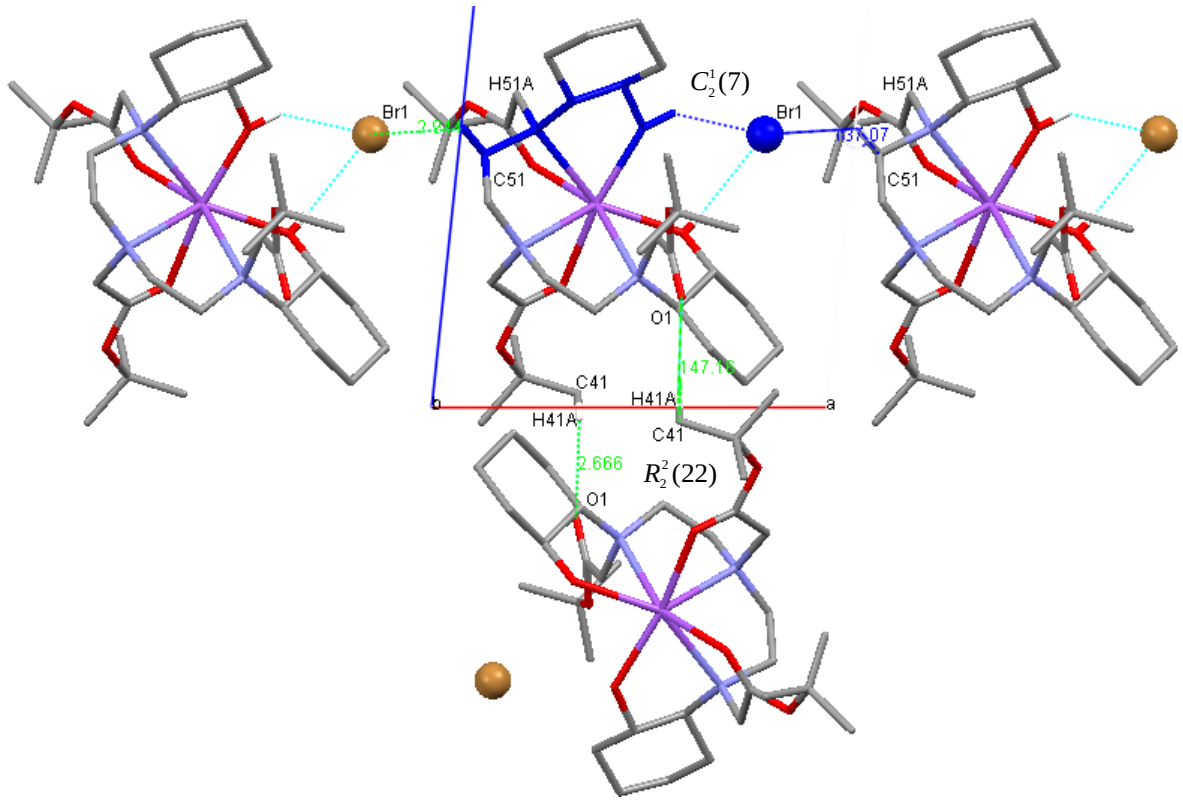


Figure 3.36: Hydrogen bonding of [NaCy$_2$DETA.3E]Br, viewed along the *b*-axis (H atoms omitted for clarity).

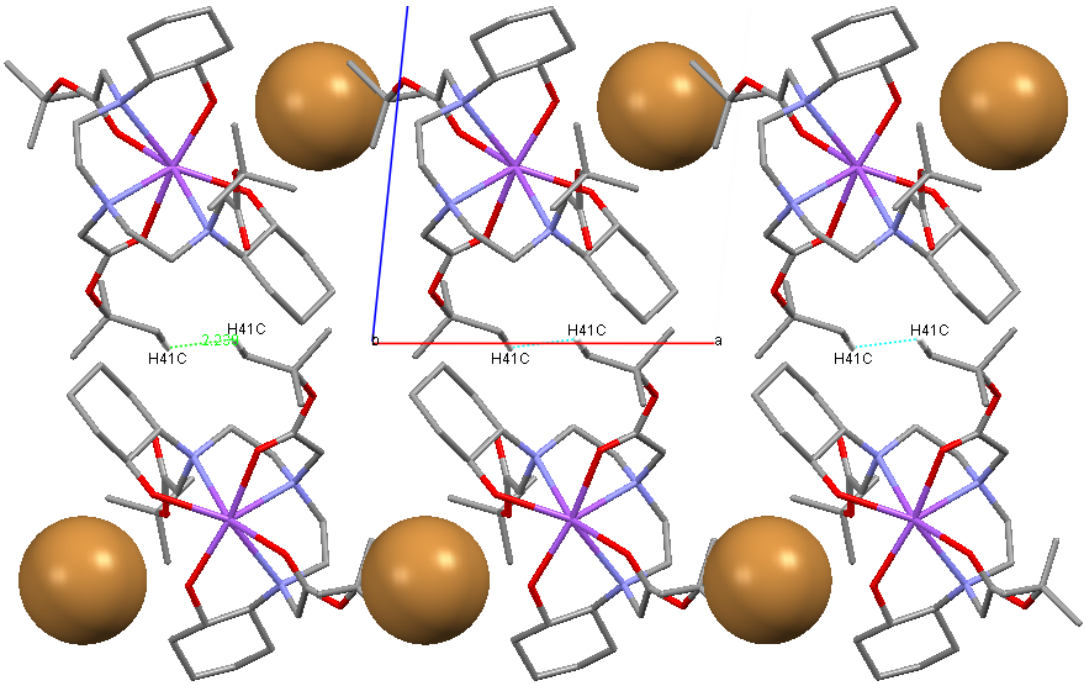


Figure 3.37: C41-H(41C) ···C411^{i} interactions between chains of [NaCy$_2$DETA.3E]Br, viewed along the *b*-axis (H atoms omitted for clarity, i = 1-x, 1-y, -z).

The interaction of C55-H55B···Br1^{i} (i = -1+x, 1+y, z) results in the observed interactions between H39A and H47A of adjacent complexes (Figure 3.38). A binary $C_2^1(10)$ chain motif is obtained when the O10-H1O···Br1 hydrogen bond is combined with the C55-H55B···Br1 interaction. Figure 3.39 also highlights the C38-H38C···O10^{j} (j = x, -1+y, z) hydrogen bond. The observed interaction between H38C and Na1 does not exist, as the distance between the two (3.38 Å) is larger than the sum of their van der Waals radii (Na = 1.86 Å and H = 1.20 Å).

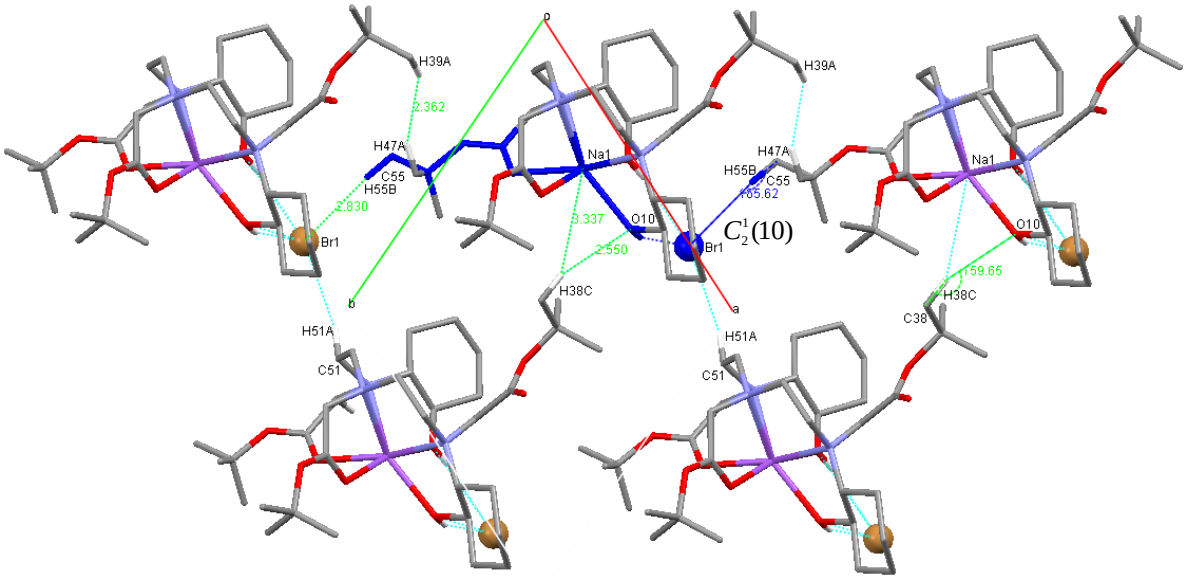


Figure 3.38: Close contacts of [$NaCy_2DETA.3E$]Br, viewed along the *c*-axis (H atoms omitted for clarity).

Figure 3.39 indicates the three dimensional packing of [$NaCy_2DETA.3E$]Br.

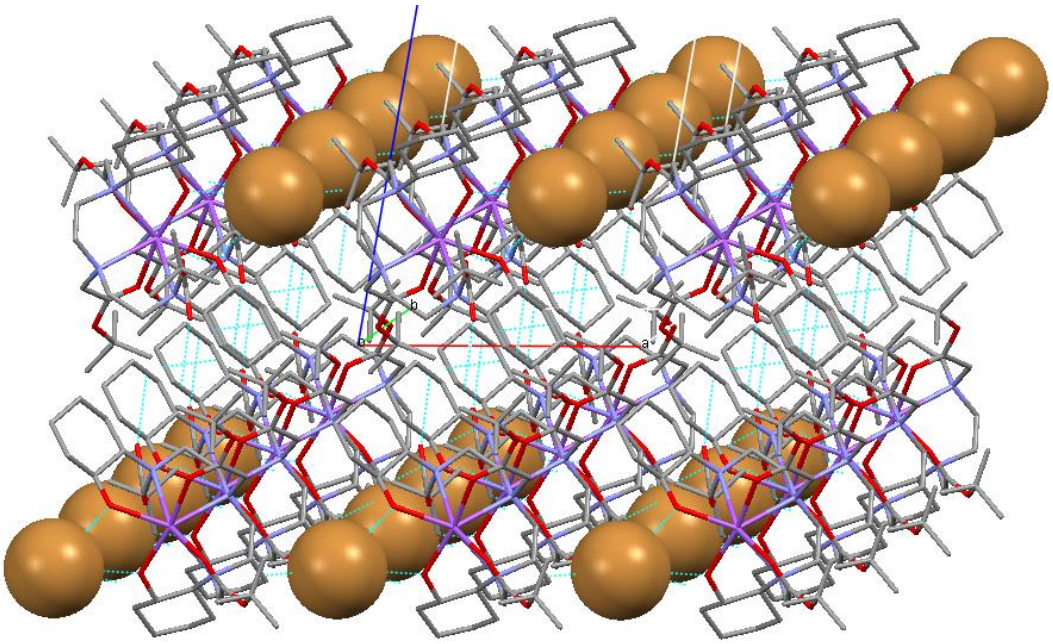


Figure 3.39: Three dimensional packing of [$NaCy_2DETA.3E$]Br (H atoms omitted for clarity).

The isolation of the Na^+ structure offers useful insight into the possible coordination environment of the target lanthanide complex, as the coordination geometry and ionic radius are similar to many lanthanide ions[4-6]. Coordination of the sodium ion occurs via three amine, two alcoholic and two ester (C=O) donors, resulting in a 7-coordinate incomplete square anti-

prism geometry. Coordination of the third ester arm is prevented to minimise steric repulsion between the tertiary butyl and hydroxycyclohexyl groups. It could therefore be assumed that upon hydrolysis of the ester groups, the coordination of the Na^+ ion (and by extension, the coordination of a lanthanide ion) would include each of the eight available coordination sites present in the ligand structure (i.e. three amine, three carboxylate and two alcoholic donors).

As most lanthanide ions adopt a nine-coordinate geometry, complexation by the present hydrolysed ligand system would leave the cation coordinatively unsaturated. The final coordination site would therefore be occupied by a single solvent molecule. The complex is expected to be neutral and should therefore not include any counterions. The preferred geometries around the lanthanide centre are monocapped square antiprismatic and tricapped trigonal prismatic, with Gd(III)-DTPA and some of its derivatives adopting a tricapped trigonal prismatic geometry[7-9]. The adopted geometry would depend on which conformation optimally minimizes the H-H interactions between the triazaheptane backbone and the hydroxycyclohexyl subtituents.

3.5 Bis(2-bromoethyl)ammonium bromide

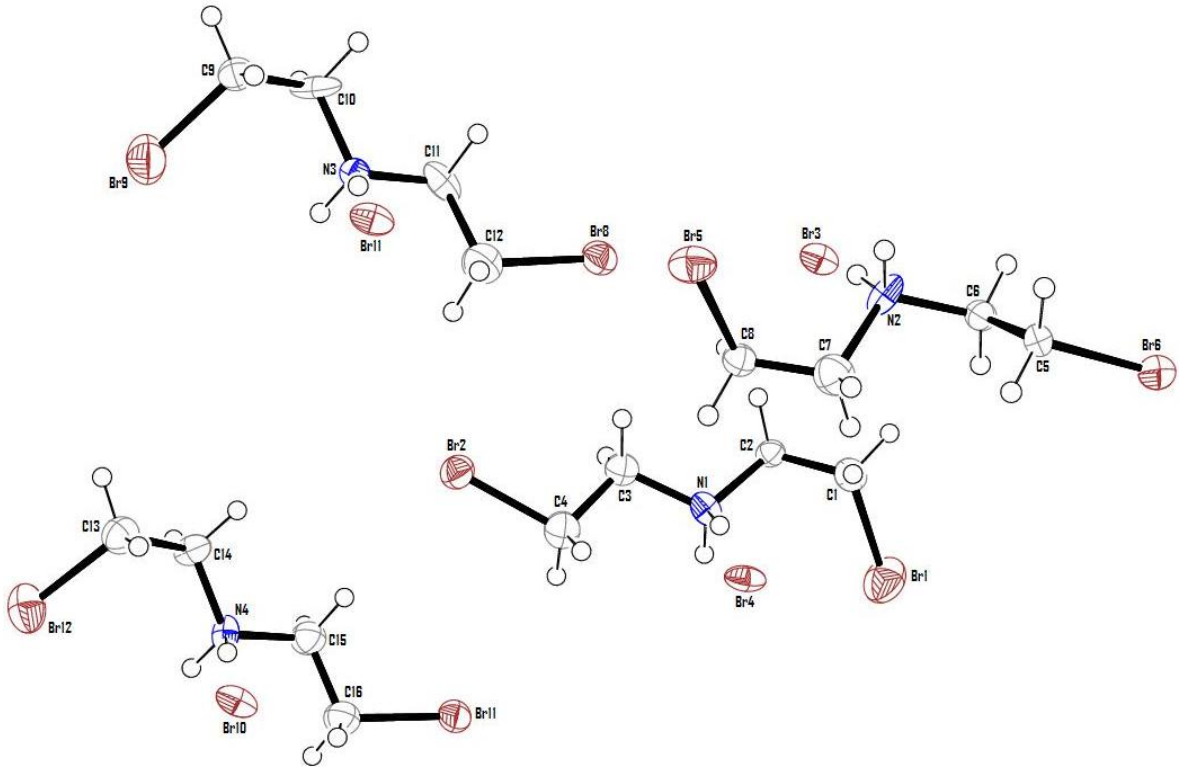


Figure 3.40: The molecular structure of bis(2-bromoethyl)ammonium bromide, showing the atom-labelling scheme and 50% probability displacement ellipsoids.

The crystal structure of bis(2-bromoethyl)ammonium bromide has been reported[10]. Bis-(2-bromoethyl)ammonium bromide crystallizes in the $P2_1$ space group. The unit cell contains four of these ion pairs. The ammonium cations differ from one another due to differences in the N-C-C-Br torsional angles (Figure 3.41) and adopt the less preferred *anti*-conformation in the solid state in order to reduce intramolecular Br-Br interactions.

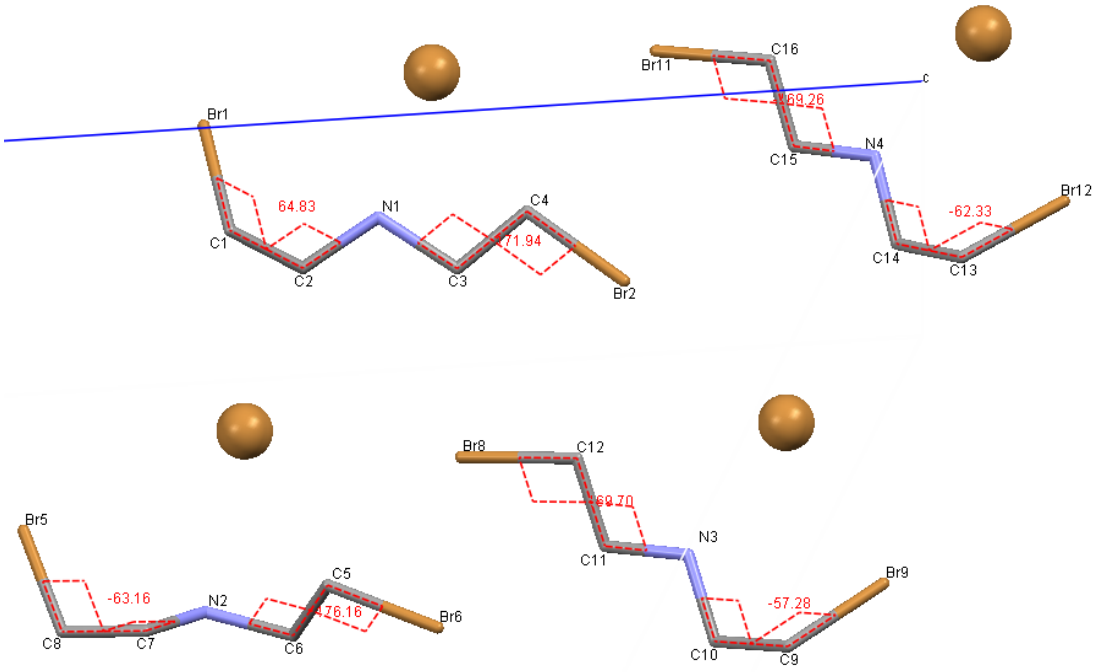


Figure 3.41: Torsional angles of bis(2-bromoethyl)ammonium bromide (H atoms omitted for clarity).

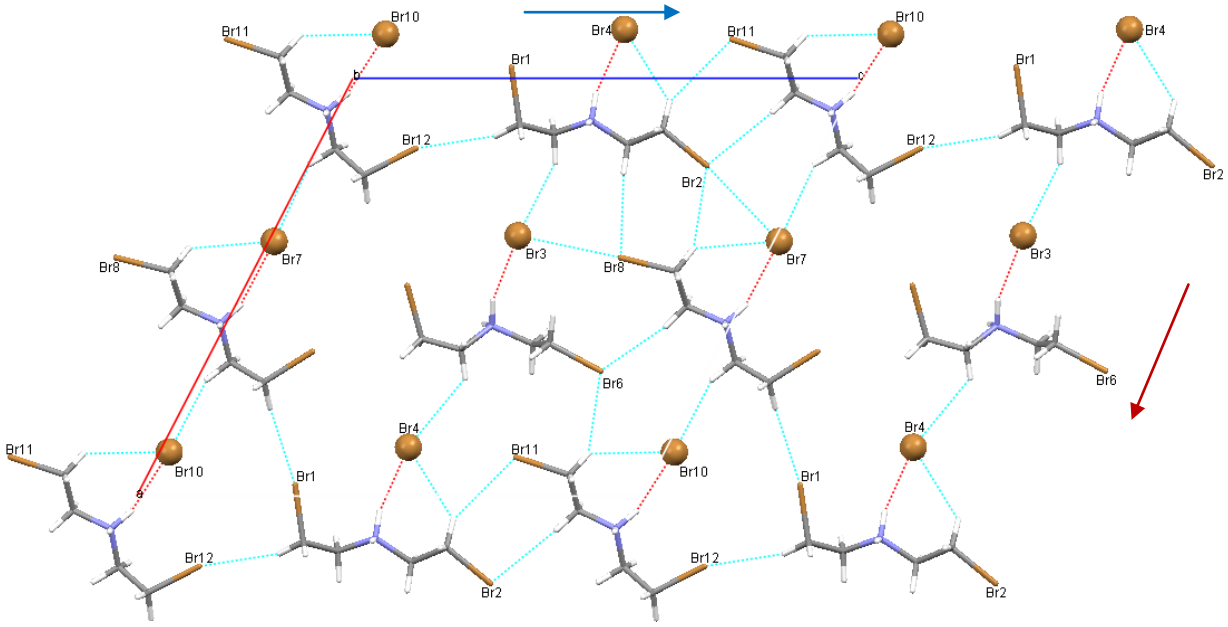


Figure 3.42: Close contact interactions of bis(2-bromoethyl)ammonium bromide, viewed along the *b*-axis.

The close contact interactions of this crystal system are shown in Figure 3.42. When viewed along the *c*-axis (blue arrow), it can be seen that the ammonium ions are arranged in alternating rows of ammonium ions and bromide ions, with the rows linked by N-H···Br and C-H···Br hydrogen bonds. The Br2-Br7 and Br8-Br3 close contact interactions also aid in

stabilizing this crystal packing arrangement. The arrangement of the ammonium ions differs from row to row, in that one row contains the N1 and N4 ammonium ions while the next ammonium ion row consists of the N2 and N4 ions. Viewing along the *a*-axis (red arrow) shows that within each row the ammonium ion alternates with a bromide ion. Again, the ammonium ions differ in each row, with a row containing the N4 and N3 ammonium ions alternating with a row containing the N2 and N1 ions.

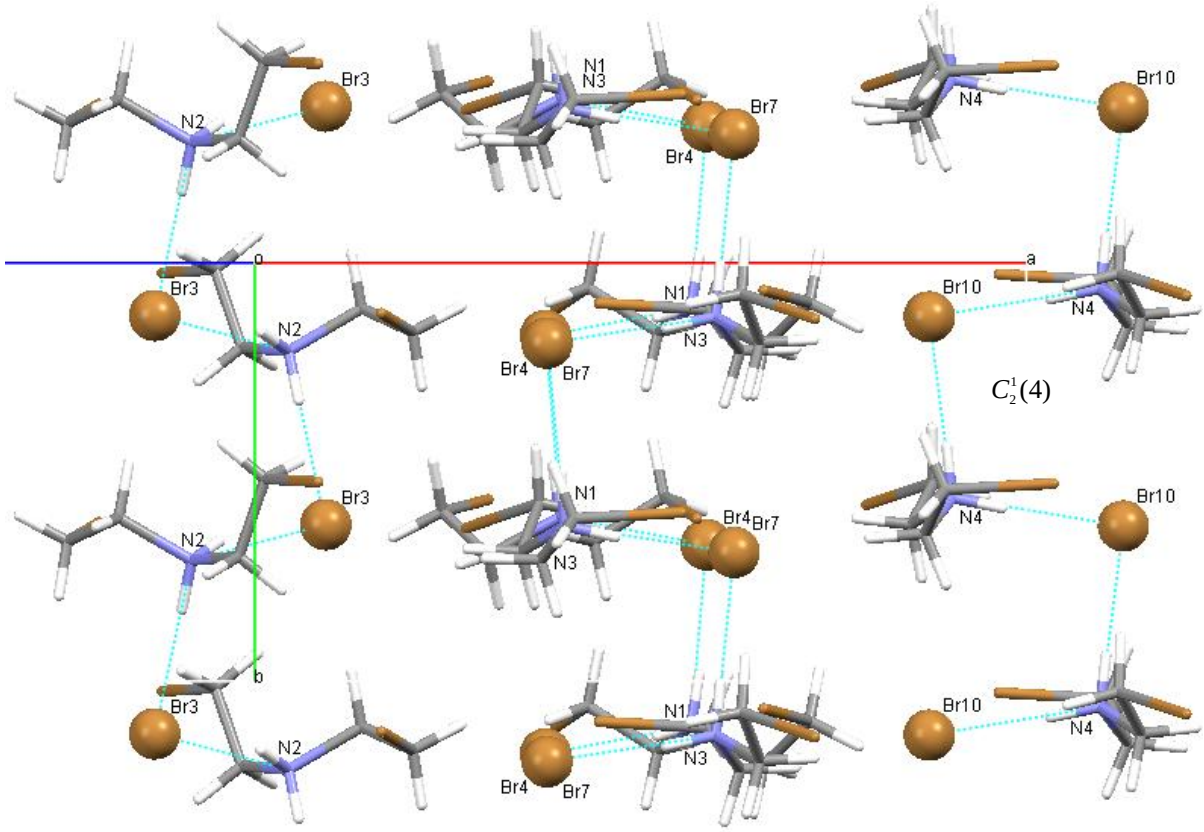


Figure 3.43: Intermolecular N-H···Br chains of bis(2-bromoethyl)ammonium bromide.

The intermolecular hydrogen bonding between the ammonium and bromide ions results in the formation of staggered chains along the *b*-axis, defining a binary $C_2^1(4)$ chain motif (Figure 3.43). As a result, a three dimensional network is obtained.

3.6 Morpholinium bromide

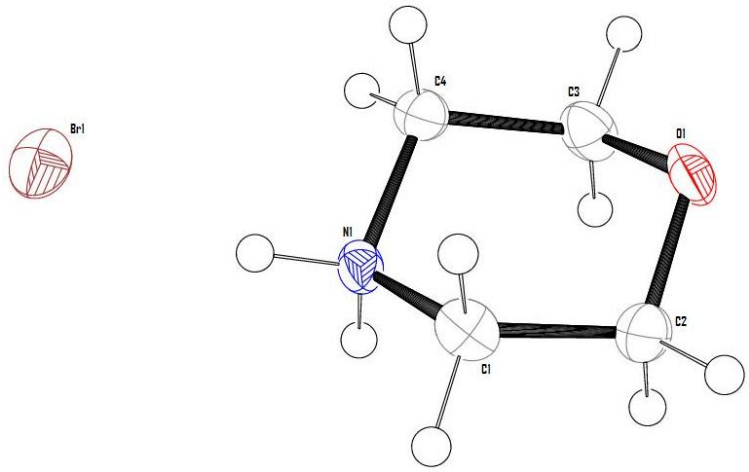


Figure 3.44: The molecular structure of morpholinium bromide, showing the atom-labelling scheme and 50% probability displacement ellipsoids.

The crystal structure of morpholinium bromide has been reported[11]. This compound crystallizes in the P21/c space group. The morpholinium ion adopts a chair configuration, as shown in Figure 3.45. The hydrogen bonding viewed along the *b*-axis adopts a ladder-like appearance. The 'edges' of the ladder are due to the N1-H1A···Br1 and N1-H1B···Br1^{i} (i = x-1, y, z) hydrogen bonds, while the ladder's 'rungs' are a result of a second N1-H1A···Br1^{j} (j = -x+1, -y, -z) interaction between the two ladder 'edges.' These N-H···Br hydrogen bonds define the unitary $C_2^1(4)$ chain motif along the *a*-axis and binary $R_2^2(4)$ and $R_4^2(8)$ ring motifs for the ladders. The ladder demonstrates two of the symmetry operations observed for this crystal. Equivalent molecules are generated via a two-fold screw axis that exists along the *a*-axis (along the length of the ladder), while an inversion centre is observed along the *b*-axis (between the 'edges' of the ladder).

The morpholinium bromide ladders are linked to adjacent ladders along the *c*-axis (Figure 3.46). This is a result of the C4-H4A···O1^{k} (k = -x+1, -y, -z+1) hydrogen bonds between the 'edges' of adjacent ladders, defining a $R_2^2(8)$ ring motif. The crystal packing therefore takes on a sheet-like appearance, as a result of cross-linking of ladders.

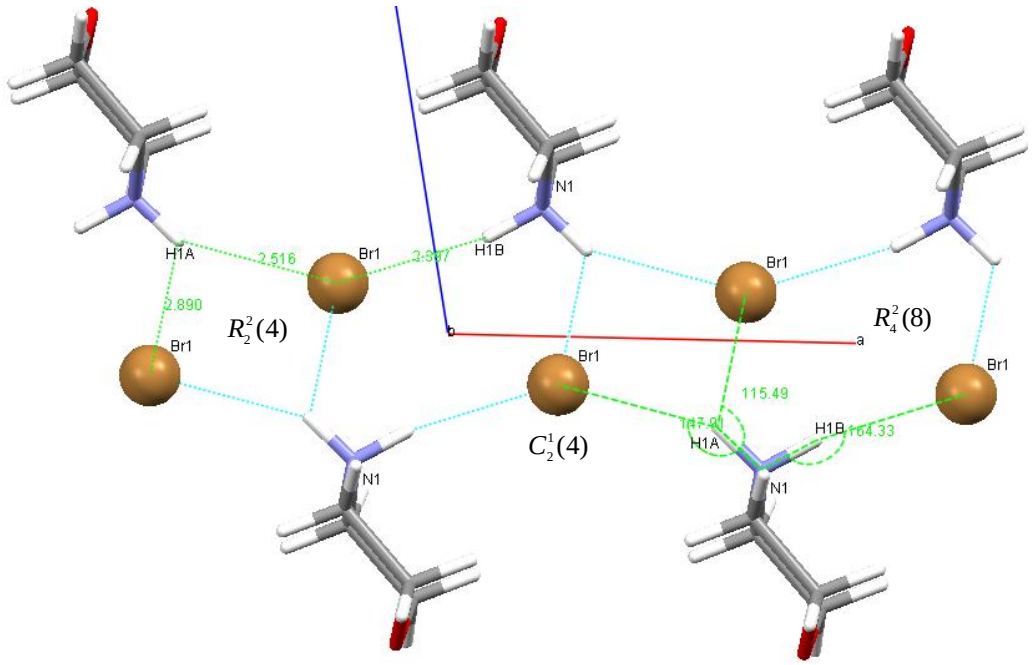


Figure 3.45: Intermolecular N-H···Br hydrogen bonding of morpholinium bromide, viewed along the *b*-axis.

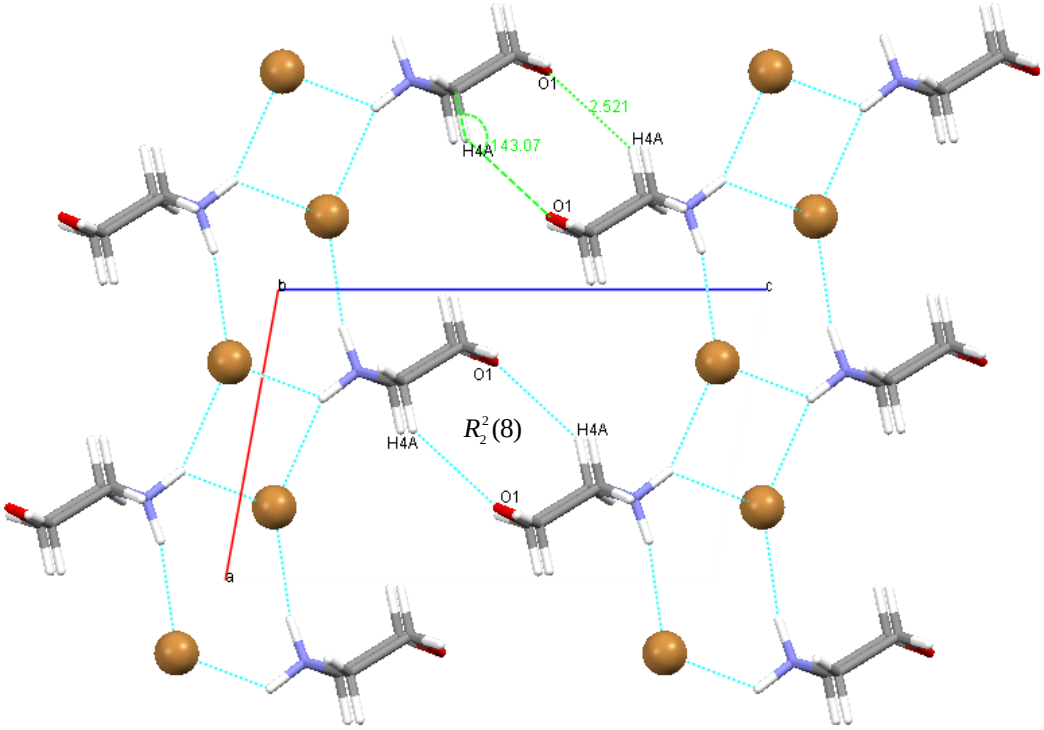


Figure 3.46: Hydrogen bonding between ladders of morpholinium bromide, viewed along the *b*-axis.

The sheets of morpholinium bromide are further linked, due to the C1-H1C···O1^{i} (i = x, -y+$^{1}/_{2}$, z-$^{1}/_{2}$) hydrogen bonds (Figures 3.47 and 3.48), resulting in a three dimensional network.

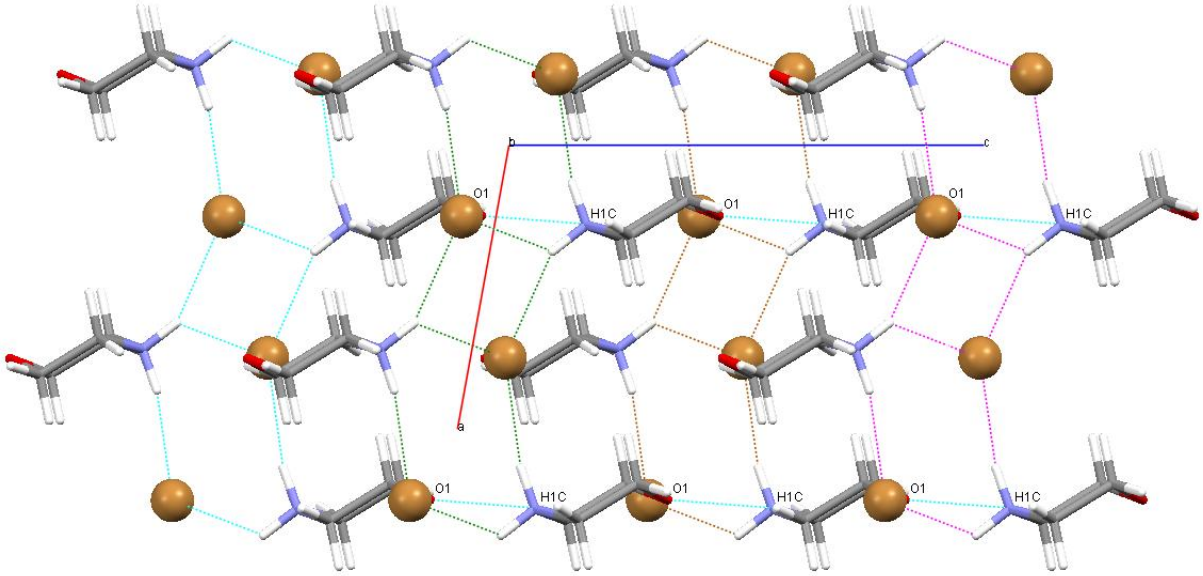


Figure 3.47: The C1-H1C···O1 interaction of morpholinium bromide, viewed along the *b*-axis.

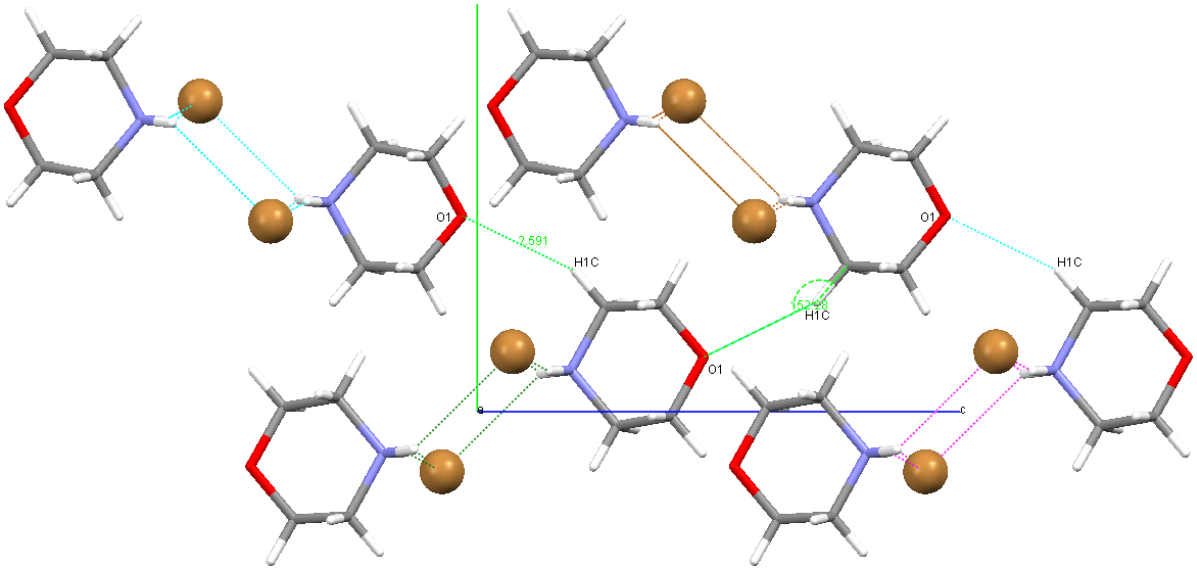


Figure 3.48: The C1-H1C···O1 interaction of morpholinium bromide, viewed along the *a*-axis.

3.7 References

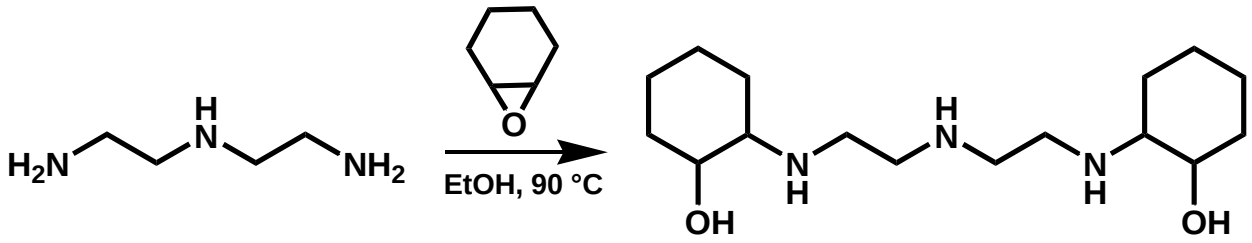
1. Bernstein, J., Davis, R. E., Shimoni, L., and Chang, N.L., *Angew. Chem. Int. Ed. Engl.* **1995,** 34, (15), 1555-1573.
2. Shannon, R. D., *Acta Cryst. A* **1976,** 32, (5), 751-767.
3. Padayachy, K., Fernandes, M. A., Marques, H. M., and de Sousa, A. S., *J. Chem. Crystallogr.* **2008,** 38, (8), 577-582.
4. Harte, A. J., Jensen, P., Plush, S. E., Kruger, P. E., and Gunnlaugsson. T., *Inorg. Chem.* **2006,** 45, (23), 9465-9474.
5. Gunnlaugsson, T., Brougham, D. F., Fanning, A., Nieuwenhuyzen, M., O'Brian, J. E., and Viguier, R., *Org. Lett.* **2004,** 6, (26), 4805-4808.
6. Govenlock, L. J., Howard, J. A. K., Moloney, J. M., Parker, D., Peacock, R. D., and Siligardi, G., *J. Chem. Soc. Perkin Trans. 2* **1999**, (11), 2415-2418.
7. Bénazeth, S., Purans, J., Chalbot, M., Nguyen-van-Duong, M. K., Nicolas, L., Keller, F., and Gaudemer, A., *Inorg. Chem.* **1998,** 37, (15), 3667-3674.
8. Dutta, S., Kim, S., Lee, E. J., Kim, T., Kang, D., Chang, Y., Kang, S. O., and Han, W., *Bull. Korean Chem. Soc.* **2006,** 27, (7), 1038-1042.
9. Hsieh, W., and Liu, S., *Inorg. Chem.* **2004,** 43, (19), 6006-6014.
10. Padayachy, K., Fernandes, M. A., Marques, H. M., and de Sousa, A. S., *Acta Cryst. E* **2012,** E68, (8), o2570-o2571.
11. Padayachy, K., Mgcima, Z., Fernandes, M. A., Marques, H. M., and de Sousa, A. S., *Acta Cryst. E* **2011,** E67, (10), o2594.

Chapter 4

Results and Discussion

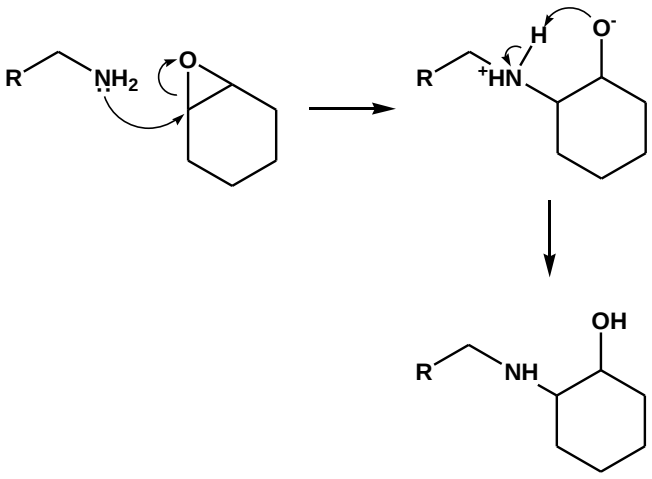
4.1 Synthetic Procedure

4.1.1 Synthesis of 1,7-Bis(2-hydroxycyclohexyl)-1,4,7-triazaheptane (Cy_2DETA)



Scheme 1

Cyclohexene oxide is a suitable reagent for terminal N-alkylation of diethylenetriamine, permitting facile synthesis of corresponding β-aminoalcohol derivatives (Scheme 1). In terms of 'green chemistry,' this is a very atom efficient procedure for the introduction of β-alcohol functional groups. The mechanism for this addition is shown below (Scheme 2):



Scheme 2

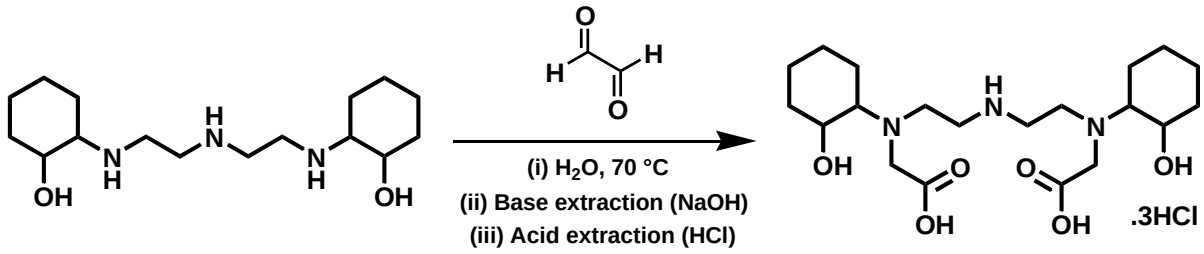
The addition of the second cyclohexenyl group is likely to occur as a result of internal hydrogen bonding of the hydroxyl group with the second addition site[1]. Further substitution is however possible and tri- and tetra-substituted products are seen in the mass spectrum for the residue from the recrystallized product (Appendix A, Figure A.2, m/z = 398 and m/z = 496)[1-4].

Replacing the ethylene bridge between the N- and O-donors with a cyclohexylene moiety has been shown to lead to an increase in complex stability[1, 5-7]. The reinforcement of the bridges between the donor atoms results in an increased 'preorganization' of the ligand, as the rigid cyclohexyl ring constrains the donor atoms spatially into positions that are energetically favourable for metal complexation. The bridged N- and O-donor atoms adopt a *trans*-configuration, which is a more energetically efficient conformation for complexation of metal ions. This arrangement of the donor atoms would result in the formation of a five-membered chelate ring, generally favouring complexation of larger metal ions. However, it has been shown that when the donor atoms are linked by a cyclohexenyl bridge, there is a greater selectivity for smaller metal ions[5-7]. The complexation of smaller metal ions increases the curvature of the ligand, reducing the steric interactions between the cyclohexyl moiety and the diethylenetriamine backbone and increasing complex stability[1, 5, 7].

The increase in steric bulk would also prove useful when complexing lanthanides such as Eu(III) or Tb(III) as the energy transfer between ligand and metal would be more efficient. The greater rigidity of the ligand system results in fewer vibrational levels in the excited state of the ligand, thus allowing for efficient ligand-to-metal energy transfer and longer luminescence emission[5, 8-10].

The denticity of this compound can be further increased by the addition of pendant arms to the secondary amines. In this study, we chose to focus on the heptadentate and octadentate ligands that could be made from Cy_2DETA.

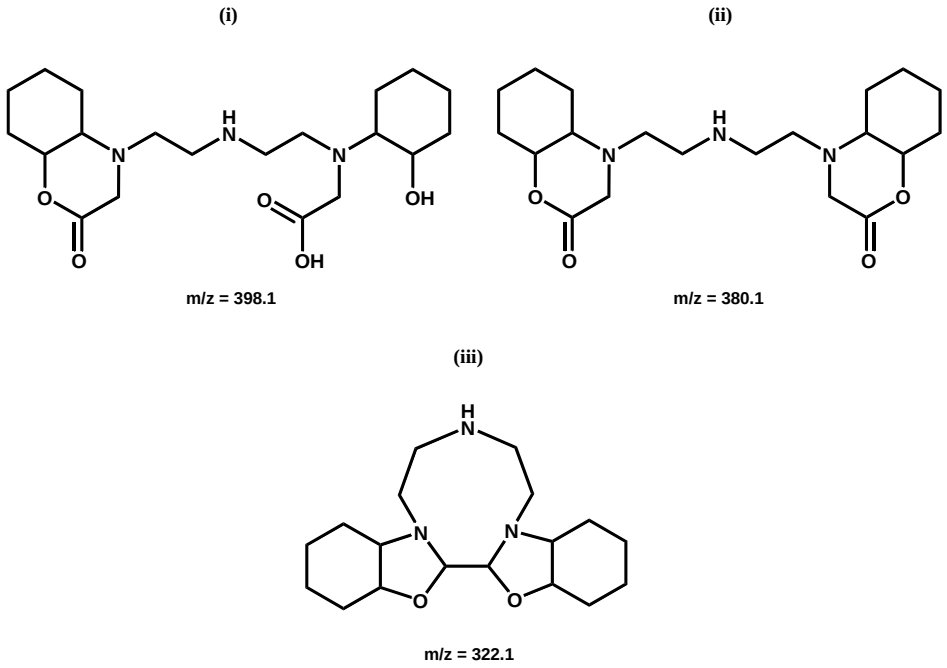
4.1.2 Synthesis of 1,7-Bis(2-hydroxycyclohexyl)-1,7-bis(carboxymethyl)-1,4,7-triazaheptane trihydrochloride (Cy_2DETA.2A.3HCl)



Scheme 3

A single step procedure for the addition of acetic acid pendant arms to β-aminoalcohols was discovered in the literature[11]. The procedure is specific for N-alkylation of secondary amines bearing alcohol substituents. Applying the synthetic protocol to Cy_2DETA would afford a heptadentate chelate.

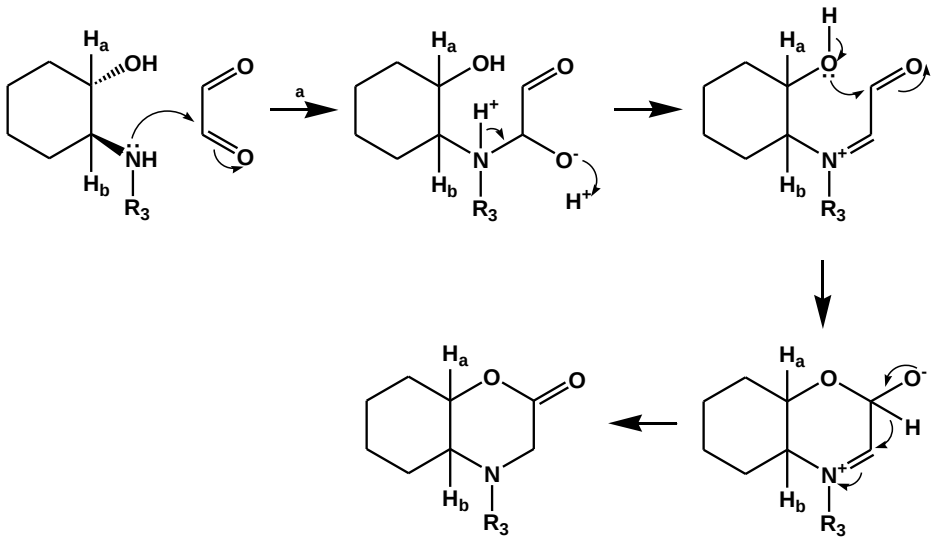
The target compound (Scheme 3) could not be readily identified in the crude product using mass spectrometry FAB-MS (Appendix A, Figure A.22). However, there were three structures that could be identified:



Scheme 4

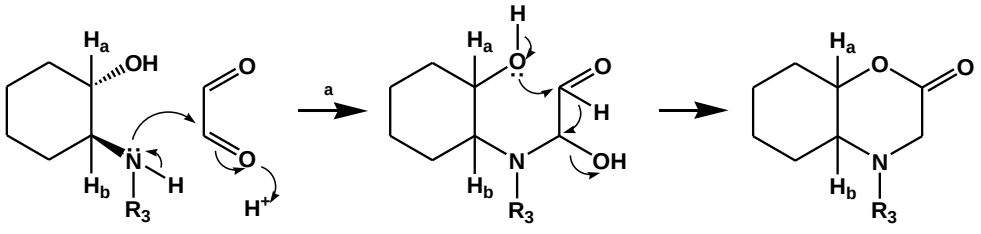
Structures (i) and (ii) are related to the desired product. In each product (structures (i) and (ii), Scheme 4), 2 molecules of glyoxal have been added to the starting material. Internal cyclization results in the formation of a morpholone ring. Two mechanisms afford an explanation for morpholone ring formation (Scheme 5 and Scheme 6)[12-18]:

(1) Imine formation, followed by a Cannizzaro rearrangement[12-18]:



Scheme 5

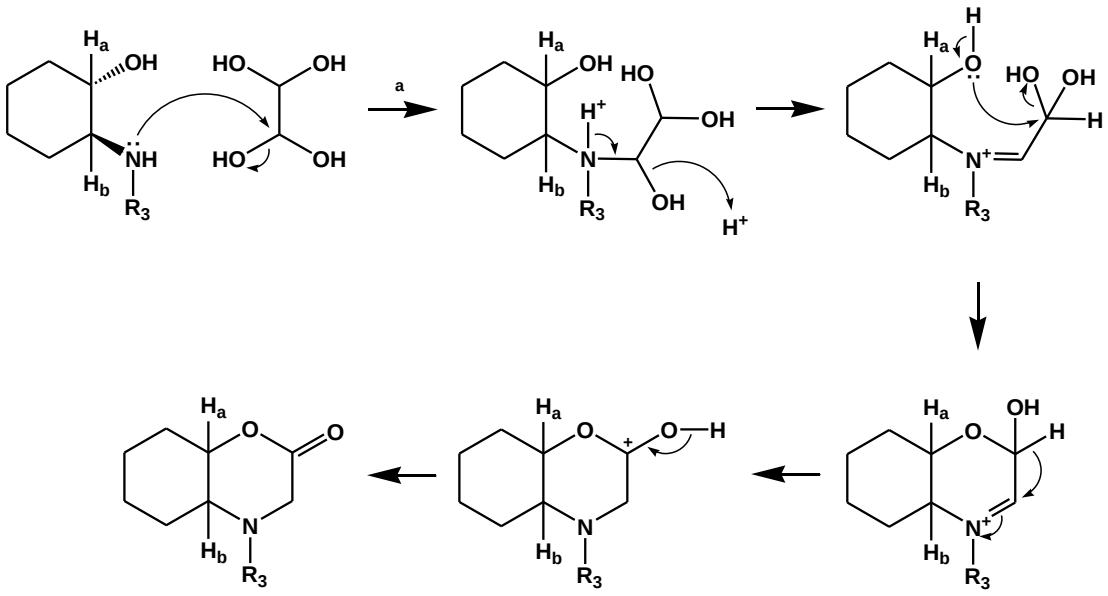
(2) Direct nucleophilic attack, followed by a Cannizzaro rearrangement:



Scheme 6

However, NMR evidence suggests glyoxal exists in the dihydrate and not di-aldehyde form[19-21]. Thus, the proposed reaction mechanisms have been modified to reflect this (Scheme 7 and Scheme 8):

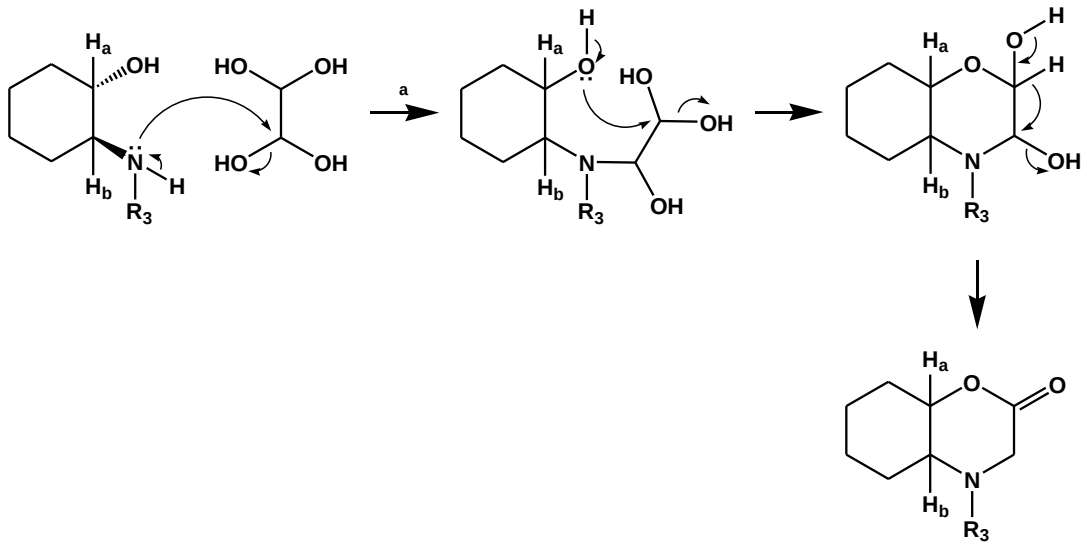
(1)



Conditions: (a) H_2O, 70 °C, 16 h

Scheme 7

(2)



Conditions: (a) H_2O, 70 °C, 16 h

Scheme 8

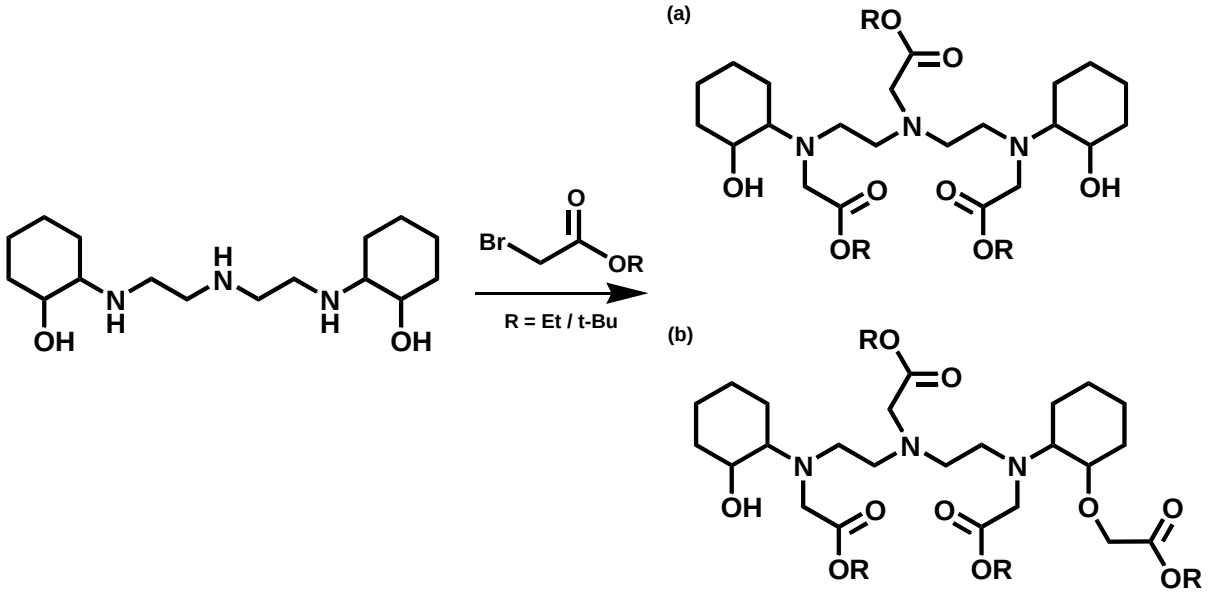
The presence of the morpholone system is supported by the NMR and IR spectra. The ^{1}H-NMR for Cy_2DETA.2A.3HCl (Appendix B, Figure B.12, δ_H H_a and H_b = 4.069) shows an expected downfield shift of the signals for protons H_a and H_b when compared to the spectrum for the starting material (Appendix B, Figure B.1, δ_H H_a = 3.390 and δ_H H_b = 2.427). The IR spectrum (Appendix C, Figure C.8) shows the difference between the carbonyl C=O stretches for structure (i) above. The signal at 1739 cm^{-1} corresponds to the C=O stretch for a carboxylate pendant arm, while the signal at 1652 cm^{-1} corresponds to the morpholone C=O stretch[22]. Santes et al., report morpholone formation is favoured by fused bulky cyclohexyl rings that stabilize the morpholone structure[22].

It should be emphasised that the formation of the morpholone ring from glyoxal is not catalyzed by acidic conditions. Although the product is isolated as a trihydrochloride salt, it can be seen that the morpholone system is already present in the crude product (Appendix A, Figure A.22, m/z = 380 and 398).

Structure (iii) in scheme 4 shows a proposed intramolecular bridging of a single glyoxal molecule across both β-aminoalcohol moieties of a single Cy_2DETA molecule. The formation of this bisoxazolidine system is a viable by-product of a reaction with glyoxal[22-24]. We were, however, unable to isolate this compound.

Therefore, while the target dicarboxylic acid ligand (Scheme 3) could not be isolated using the applied procedure, the synthesized trihydrochloride morpholone derivatives undergo hydrolysis in aqueous solution to afford the desired dicarboxylate compound, which is sequestered by a metal ion.

4.1.3 Synthesis of 1,7-Bis(2-hydroxycyclohexyl)-1,4,7-tris(t-butylcarboxymethyl)-1,4,7-triazaheptane (Cy_2DETA.3E)



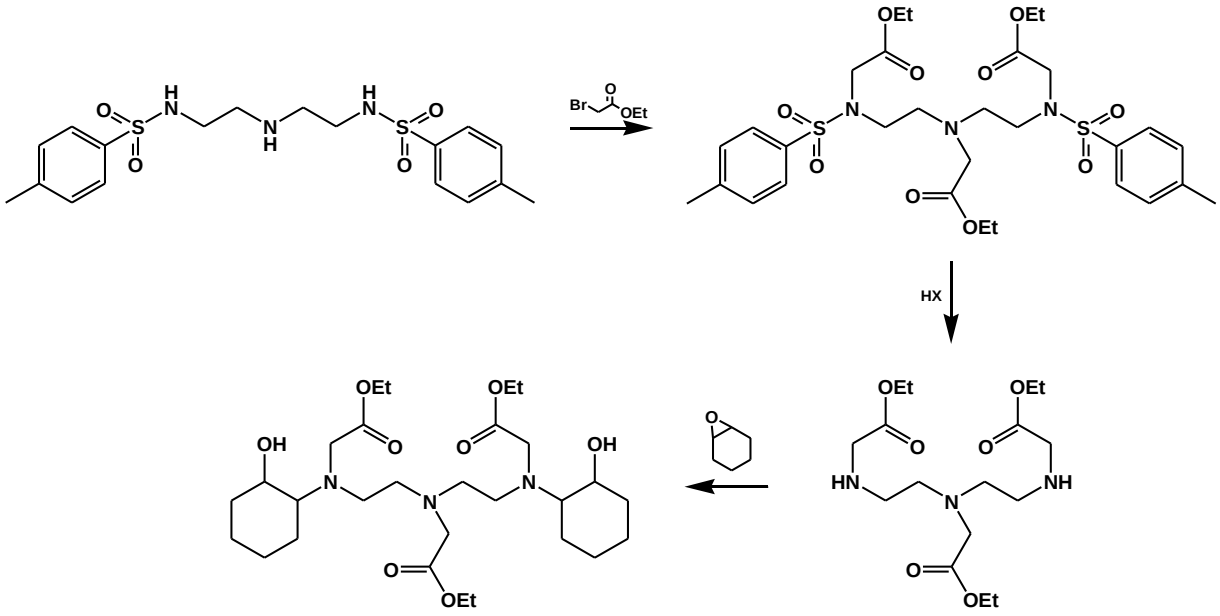
Scheme 9

The addition of acetate pendant arms to Cy_2DETA was attempted by the introduction of the ester functional group, as the addition of an ester followed by acid hydrolysis would yield the desired product.

The choice of ethyl bromoacetate (Scheme 9, R = Et) as the ester of choice allowed for milder deprotection conditions. However, the product spectrum consisted of the desired tri-substituted derivative (Scheme 9, product (a); Appendix A, Figure A.3, m/z = 558) and the tetra-substituted product (Scheme 9, product (b); Appendix A, Figure A.3, m/z = 619). Isolation of the desired product using column chromatography proved difficult since hydrolysis occurred during elution from the column.

To prevent the formation of a tetra-substituted product, terminal amines of diethylenetriamine were protected, using *p*-toluenesulfonyl chloride[25-27], prior to esterification. Deprotection of the tri-ester was followed by further reaction with cyclohexene oxide to yield the desired product (Scheme 10). However, the product spectrum included mono-, di-, and tri-substituted

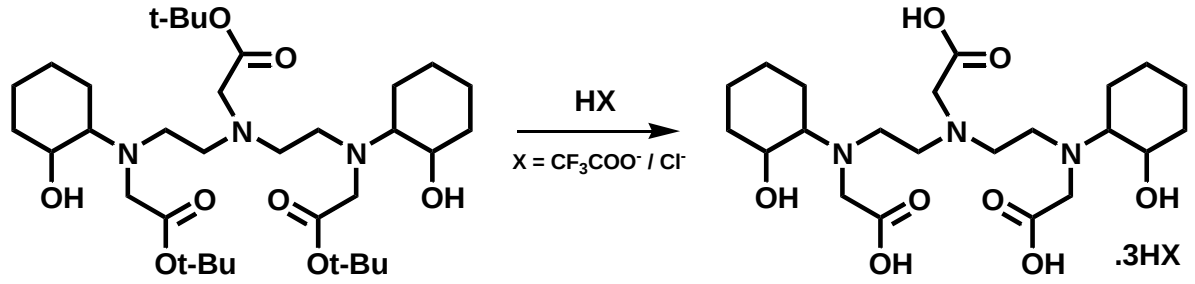
derivatives (Appendix A, Figure A.12, m/z = 498, 584, and 670) rendering this synthetic route impractical.



Scheme 10

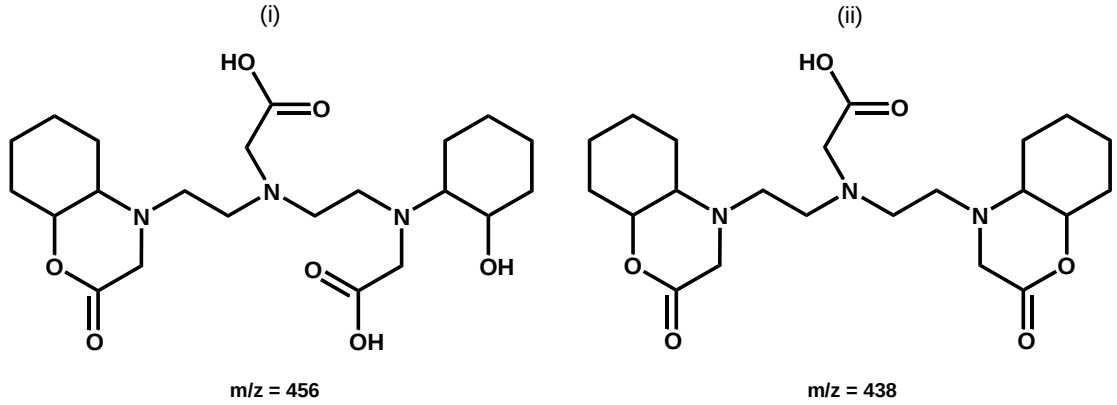
Esterification of Cy_2DETA using tert-butyl bromoacetate (Scheme 9, R = t-Bu) was attempted. Literature reports a variety of reaction conditions, using this compound, for alkylating amines[28-35]. The effect of the solvent, in the presence of Na_2CO_3 (to neutralize the HBr produced in the reaction) at room temperature, was additionally scrutinized. Results indicate DMF to be the most effective solvent, consistently affording high yields of the target compound. The absence of any side-products (Appendix A, Figure A.16) required no further optimization of this synthetic procedure.

4.1.4 Synthesis of 1,7-Bis(2-hydroxycyclohexyl)-1,4,7-tris(carboxymethyl)-1,4,7-triazaheptane (Cy_2DETA.3A) salts



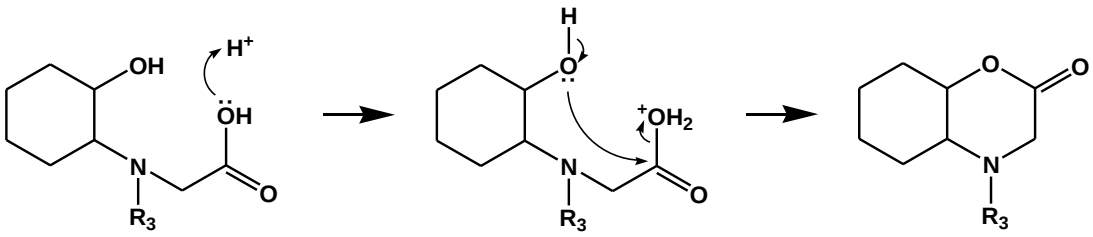
Scheme 11

The desired carboxylate pendant arms were obtained by acid hydrolysis of the ester moieties (Scheme 11). In the case of the tert-butyl ester, a strong acid is required to promote the hydrolysis. Fedi[30] and Greenwald[33] make use of trifluoroacetic acid (TFA) in DCM (1:2 ratio) at room temperature. Hydrolysis is complete after 24 hours. However, the mass spectrum of the crude product (Appendix A, Figure A.17) identifies two products (Scheme 12):



Scheme 12

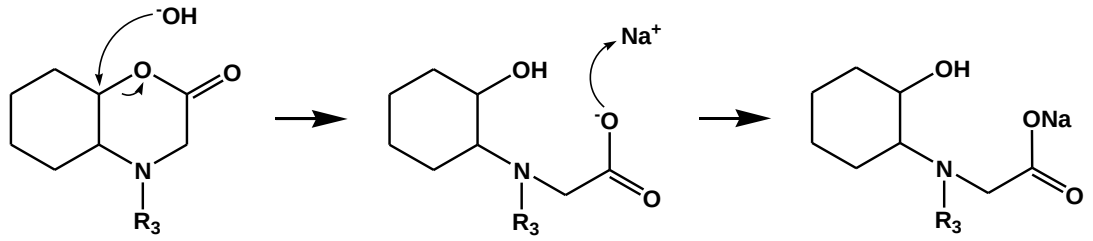
A morpholone system is being formed, but the cyclization mechanism differs from that of Cy_2DETA.2A.3HCl in the reaction with glyoxal. TFA is proposed to promote cyclization via dehydration across alcohol and carboxylic acid moieties (Scheme 13).



Scheme 13

It is likely that the presence of the bulky cyclohexyl group stabilises this formation. Refluxing the morpholone products in water reverses the mechanism (Appendix A, Figure A.18, m/z = 474), but the long reaction time (~7 days) suggests hydrolysis of the morpholone system is kinetically slow.

A sodium triacetate salt of the target ligand (i.e. $Na_3Cy_2DETA.3A$) was isolated by raising the pH of a solution containing the morpholone products. The reaction time was considerably shorter (24 hours), indicating that the opening of the morpholone ring system is base-catalyzed (Scheme 14).



Scheme 14

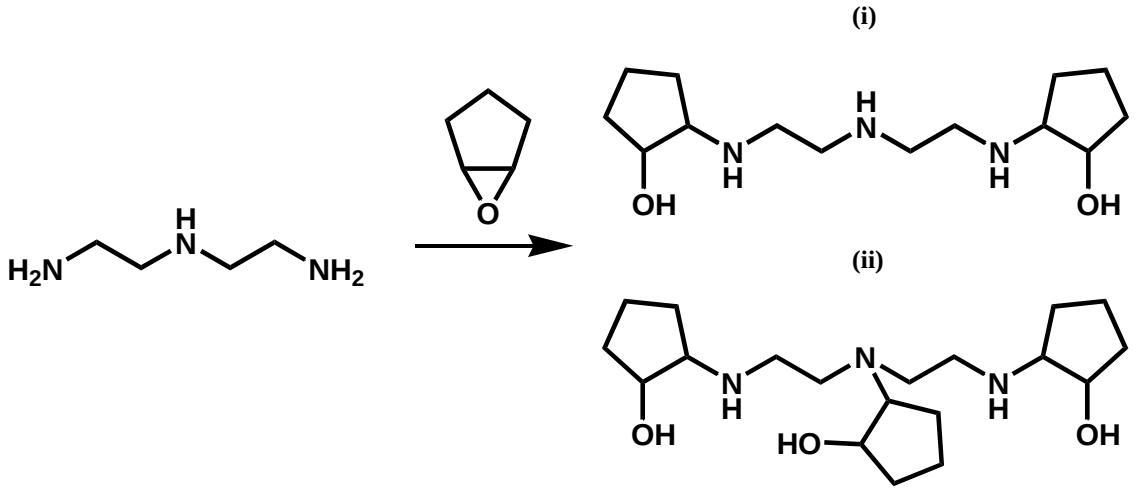
The structure was confirmed by the mass spectrum (Appendix A, Figure A.19, m/z = 540) and IR spectrum (Appendix C, Figure C.6, CO_2^- asymmetric stretch at 1583 cm^{-1}). The tri-sodium salt is, however, hygroscopic. The use of the ligand as a tri-sodium salt in complexation reactions would result in competition between the sodium and target metal cations for the donor sites. A cation-exchange resin would therefore be required to isolate the ligand in a metal-free form before attempting any complexation reactions.

Removal of the tert-butyl ester groups can also be accomplished by refluxing in concentrated HCl[35]. The procedure proved effective, as confirmed from the mass spectrum of the crude product (Appendix A, Figure A.20). The predicted masses for the mono-morpholone product (m/z = 456) and morpholone-free product (m/z = 474) are present. Morpholone formation is not as prevalent due to hydrolysis occurring in aqueous HCl, resulting in an equilibrium between the morpholone and carboxylate forms. The decreasing acid concentration (due to the evolution of HCl gas) during hydrolysis slows the dehydration.

Lyophilization of the extracted product provides us with the morpholone derivatives (Appendix A, Figure A.21, m/z = 438 and 456). The tri-hydrochloride salt is hygroscopic. The presence of the chloride ion for our intended solution studies is tolerable, as the chloride ion is spectroscopically silent.

Overall, hydrolysis of the tert-butyl ester using HCl was more efficient compared to the procedure requiring TFA, as experimental yields were generally greater using HCl. Isolation of the morpholone derivatives are suitable for complexation of metal ions, as hydrolysis in aqueous solution yields the target tricarboxylic acid form of the ligand. Sequestering of metal ions in aqueous solution is more efficient using the trihydrochloride salt, as use of the tri-sodium derivative of the ligand would introduce unwanted metal ion competition.

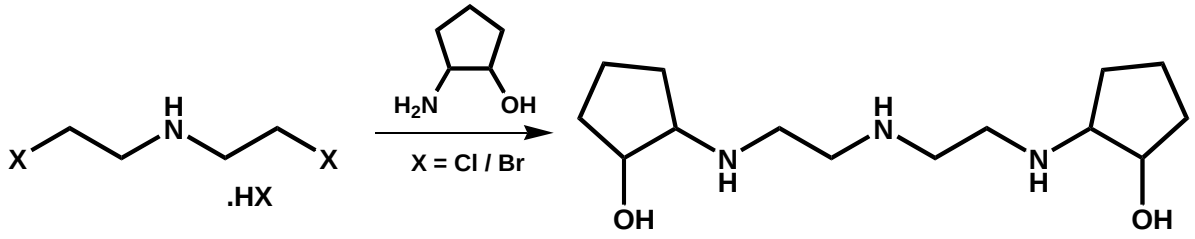
4.1.5 Attempted Synthesis of 1,7-Bis(2-hydroxycyclopentyl)-1,4,7-triazaheptane (Cyp_2DETA)



Scheme 15

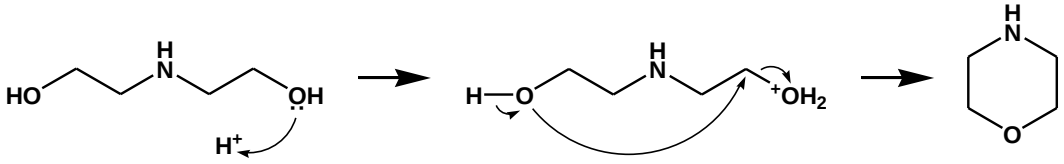
The synthesis of an aminoalcohol analogous to Cy_2DETA was attempted, where the cyclohexyl bridge has been substituted with a cyclopentyl bridge (Scheme 15). The choice of a smaller cycloalkane bridge would relieve van der Waals repulsion between the ring and the diethylenetriamine backbone, thus promoting complexation of larger metal ions.

The synthesis of Cyp_2DETA was approached using the same synthetic method employed for Cy_2DETA. Two products were obtained from this procedure (Appendix A, Figure A.24): the desired di-substituted product (Scheme 15 (i); Appendix A, Figure A.24, m/z = 272) and a tri-substituted product (Scheme 15 (ii); Appendix A, Figure A.24, m/z = 356). All attempts at separating the two products proved futile. Thus, an alternate approach was required (Scheme 16).



Scheme 16

The starting material was synthesized in the bromide form first, as the bromide is a better leaving group compared to chloride. The synthesis of bis(2-bromoethyl)ammonium bromide is achieved by heating diethanolamine in a concentrated aqueous solution of HBr and relies on azeotropic distillation to drive the substitution reaction. If there is not enough acid present, the substitution does not occur on both ends of the diethanolamine molecule, resulting in the formation of a morpholinium species (Scheme 17)[36].



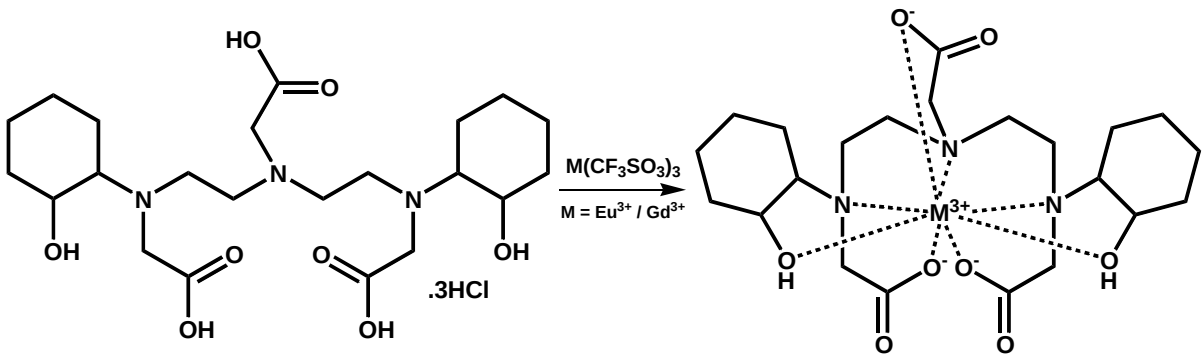
Scheme 17

Bis(2-bromoethy)ammonium bromide[37] and morpholinium hydrobromide[38] were both formed in this reaction. Several recrystallizations from ethanol and diethyl ether failed to completely separate these products. Therefore, the synthesis of bis(2-chloroethyl)ammonium chloride was pursued. Bis(2-chloroethyl)ammonium chloride was synthesized in an excess of thionyl chloride and recrystallized from ethanol and hexane[39].

The reaction of bis(2-chloroethyl)ammonium chloride with *trans*-2-aminocyclopentanol was attempted in the presence of base, using two different solvent systems, but this procedure proved to be unsuccessful as no recognisable products could be distinguished from the mass spectra (Appendix A, Figure A.27, A.28, and A.29).

The synthesis of Cyp_2DETA was later abandoned on the basis that complexation via the N- and O-donor atoms across the cyclopentyl bridge would result in increased torsional strain of the ring, as interconversion between the strain-relieving puckered conformations would be prevented, thus resulting in the formation of weak metal complexes[40].

4.1.6 Attempted Synthesis of Lanthanide(III)-1,7-Bis(2-hydroxycyclohexyl)-1,4,7-tris(carboxymethyl)-1,4,7-triazaheptane ([Eu(Cy_2DETA.3A)] and [Gd(Cy_2DETA.3A)])

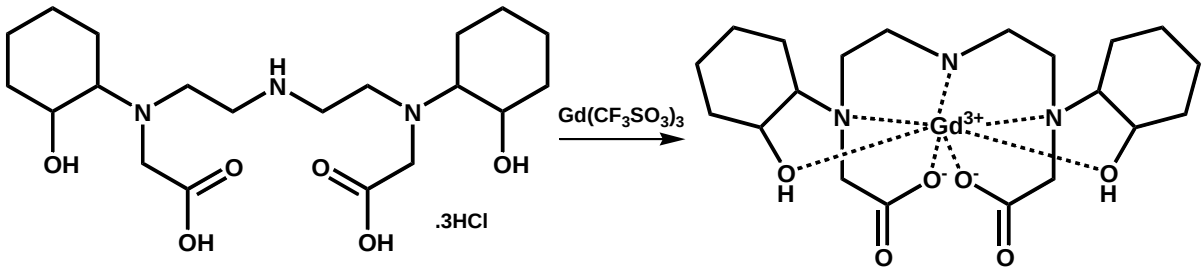


Scheme 18

The formation of the Eu(III) complex of Cy_2DETA.3A (Scheme 18, M = Eu^{3+}) was shown to occur in water (Appendix A, Figure A.31, m/z = 625). Using the tri-hydrochloride form of the ligand is advantageous as the low pH of the solution prevents precipitation of $Eu(OH)_3$. Although the acidified solution also favours the formation of the morpholone ring system, the Lewis acidity of the trivalent Eu cation favours complexation. Attempts were made at crystallizing the complex, but isolation of the Eu(III) complex was not possible.

Synthesis of the Gd(III) complex of Cy_2DETA.3A (Scheme 18, M = Gd^{3+}) was successful in acetonitrile, with monomeric and dimeric forms of the complex observable from mass spectrometry (Appendix A, Figure A.32, m/z = 626 (monomer), 1252 (dimer)). The Lewis acidity of the trivalent Gd cation favours complexation over morpholone ring formation under acidic conditions. Isolation of the Gd(III) complex by crystallization was unsuccessful.

4.1.7 Attempted Synthesis of Gadolinium(III)-1,7-Bis(2-hydroxycyclohexyl)-1,7-bis(carboxymethyl)-1,4,7-triazaheptane ([Gd.(Cy_2DETA.2A)])



Scheme 19

The complexation of Gd(III) using Cy_2DETA.2A (Scheme 19) was attempted in acetonitrile. Mass spectrometry provided no evidence for complexation products $[Gd(Cy_2DETA.2A)]^{n+}(CF_3SO_3)_n$ (Appendix A, Figure A.33, m/z = 398, starting material). Thermodynamic stability of the seven-coordinate complex may not permit the formation of this species under the employed reaction conditions.

4.2 Potentiometric Titrations

Ligand pK_a values were determined potentiometrically. The results correlated to spectroscopically determined pK_a values, allow for elucidation of species present in solution, as a function of pH[41, 42].

Titrations were conducted using solutions of ionic strength (I) = 0.1 M. Sample preparation procedures and acquired experimental data are detailed in Appendix E. Titrations were conducted at ambient temperature (25 °C). The solutions were degassed with N_2 to prevent the build-up of dissolved CO_2. Calculation of stability constants were conducted using the modelling program ESTA[43-46].

4.2.1 Cy_2DETA.3A.3HCl pK_a determination

A potentiometric titration of 0.0167 M 1,7-bis(2-hydroxycyclohexyl)-1,4,7-tris(carboxymethyl)-1,4,7-triazaheptane trihydrochloride was conducted to determine the pK_a values for the ligand. The titration curve for the protonated ligand is shown in Figure 4.1. The ligand was protonated with a 0.0491 M HNO_3 / 0.0500 M $NaNO_3$ standard solution and titrated against a 0.00966 M NaOH / 0.0900 M $NaNO_3$ standard solution, with ionic strength of 0.1 M maintained using a 0.1 M $NaNO_3$ standard solution. The conditions for the titration are represented in Appendix E (Section E.2.1).

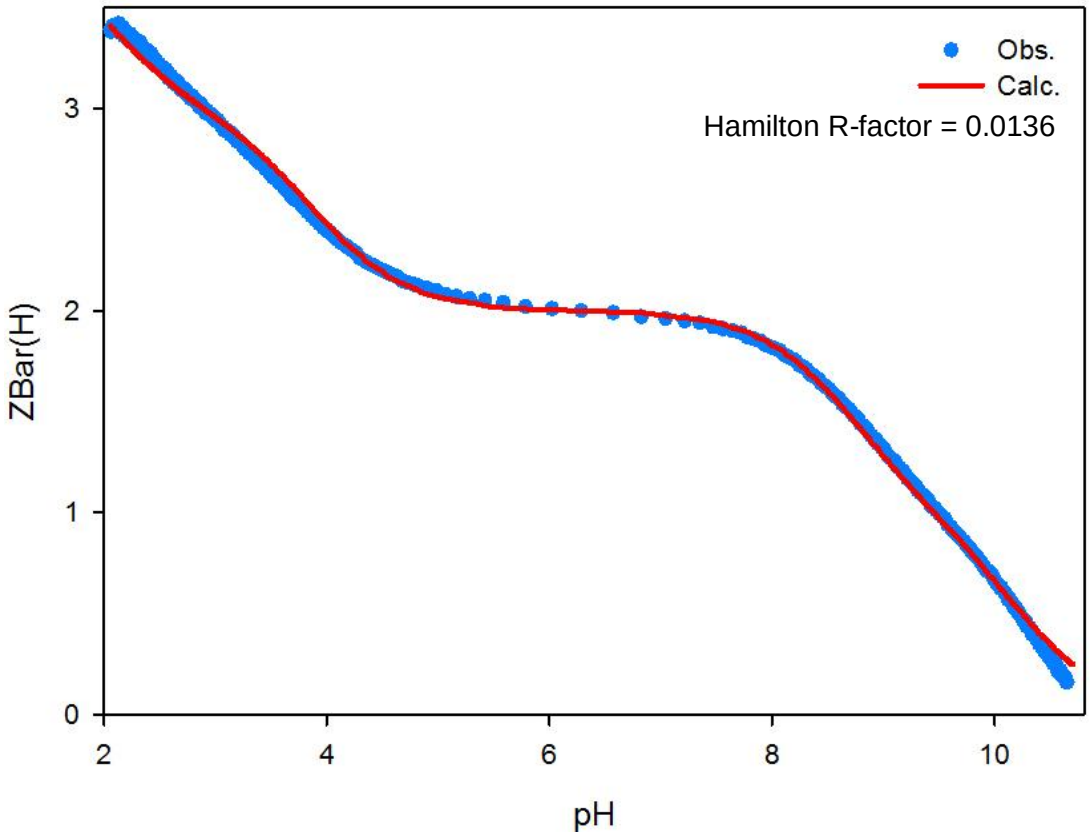


Figure 4.1: Titration curve of 1,7-bis(2-hydroxycyclohexyl)-1,4,7-tris(carboxymethyl)-1,4,7-triazaheptane, in aqueous solution.

Table 4.1: Comparison of pK_a values from the potentiometric titration of 1,7-bis(2-hydroxycyclohexyl)-1,4,7-tris(carboxymethyl)-1,4,7-triazaheptane (Cy_2DETA.3A) with DTPA[47].

	pK_a (Cy_2DETA.3A)	**pK_a (DTPA)**
pK_a1	10.21 ± 0.01	10.54 ± 0.03
pK_a2	8.70 ± 0.01	8.56 ± 0.01
pK_a3	3.87 ± 0.01	4.30 ± 0.03
pK_a4	1.92 ± 0.02	2.77 ± 0.05

Four pK_a values were determined from regression analysis of potentiometric titration data (Table 4.1). pK_a1, pK_a2 and pK_a3 are assigned to subsequent protonation of the amine donors present on the diethylenetriamine backbone, while the fourth protonation constant (pK_a4) accounts for a carboxymethyl pendant arm. The protonation constants determined for amine donors present on the diethylenetriamine backbone involves initial deprotonation of the central amine moiety (pK_a3). Subsequent deprotonation of a terminal amine donor (pK_a2)

results in migration of the final amine proton to the central position resulting in the observed value for pK_a1, as proposed by Kotek[48].

The calculated pK_a1 and pK_a2 values for Cy_2DETA.3A are comparable with the protonation constants observed for amine donors of DTPA (Table 4.1, DTPA, pK_a1 and pK_a2). However, the pK_a3 and pK_a4 values for Cy_2DETA.3A are more acidic than DTPA (Table 4.1, DTPA, pK_a3 and pK_a4). It is proposed that the presence of the bulky hydroxycyclohexyl pendants is responsible for the observed decrease in the pK_a3 and pK_a4 protonation constants, as a consequence of induction.

4.2.2 Cy_2DETA.2A.3HCl pK_a determination

The pK_a values for 1,7-bis(2-hydroxycyclohexyl)-1,7-bis(carboxymethyl)-1,4,7-triazaheptane trihydrochloride were determined by potentiometric titration of a 0.0167 M solution of the ligand. The titration curve for the protonated ligand is illustrated in Figure 4.2. The ligand was protonated with a 0.0491 M HNO_3 / 0.0500 M $NaNO_3$ standard solution and titrated against a 0.00959 M NaOH / 0.0900 M $NaNO_3$ standard solution, with ionic strength of 0.1 M maintained using a 0.1 M $NaNO_3$ standard solution. The conditions for the titration are described in Appendix E (Section E.2.2).

Table 4.2: Comparison of pK_a values from the potentiometric titration of 1,7-bis(2-hydroxycyclohexyl)-1,7-bis(carboxymethyl)-1,4,7-triazaheptane (Cy_2DETA.2A) with Cy2DETA.3A and DTPA[47].

	pK_a (Cy_2DETA.2A)	**pK_a (Cy_2DETA.3A)**	**pK_a (DTPA)**
pK_a1	10.91 ± 0.01	10.21 ± 0.01	10.54 ± 0.03
pK_a2	8.41 ± 0.01	8.70 ± 0.01	8.56 ± 0.01
pK_a3	5.47 ± 0.01	3.87 ± 0.01	4.30 ± 0.03
pK_a4	3.11 ± 0.02	1.92 ± 0.01	2.77 ± 0.05

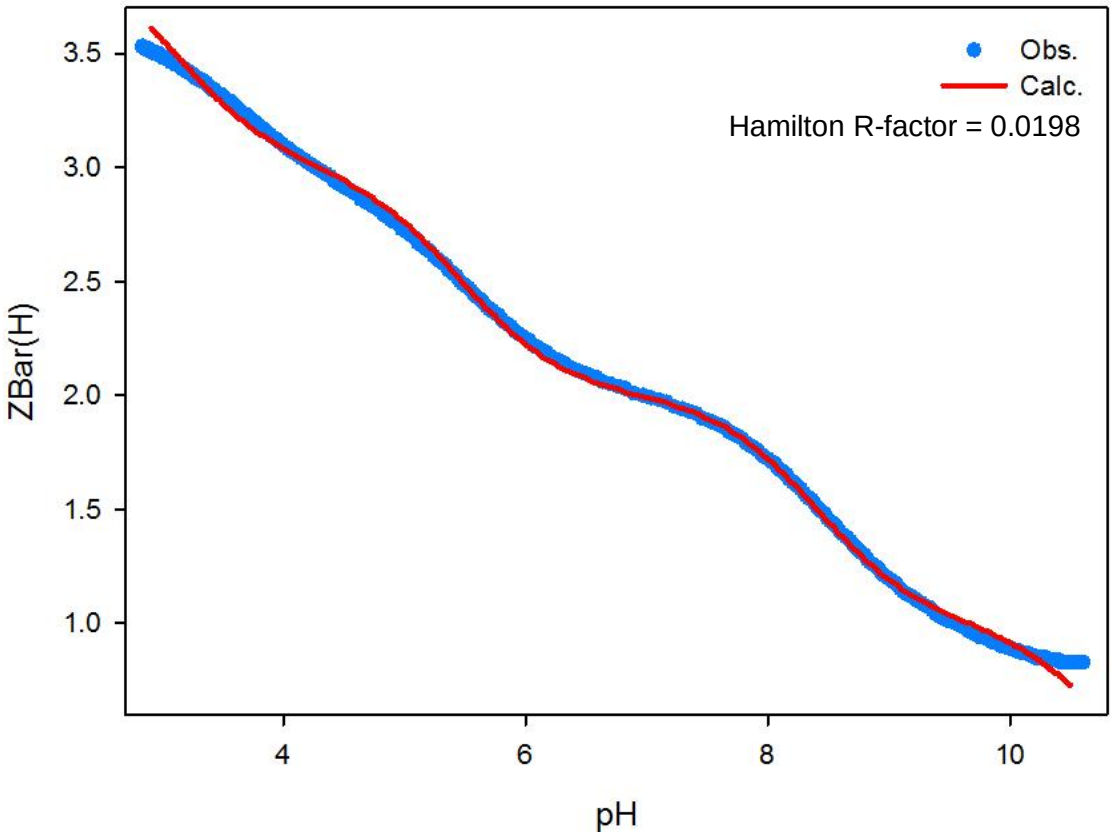


Figure 4.2: Titration curve for 1,7-bis(2-hydroxycyclohexyl)-1,7-bis(carboxymethyl)-1,4,7-triazaheptane trihydrochloride, in aqueous solution.

Four pK_a values were determined from the potentiometric titration data for Cy_2DETA.2A (Table 4.2). pK_a1, pK_a2 and pK_a3 are assigned to protonation of the amine donors, while pK_a4 represents protonation of a pendant carboxymethyl moiety. Amine protonation constants for the diethylenetriamine backbone involves initial deprotonation of the central amine moiety (pK_a3). Subsequent terminal amine deprotonation (pK_a2) results in migration of the final amine proton to the central position (pK_a1), as proposed by Kotek[48].

The calculated pK_a1, pK_a2 and pK_a4 values for Cy_2DETA.2A compare favourably with protonation constants observed for the amine groups of DTPA (Table 4.2)[47, 49]. The pK_a3 value is higher than that observed for DTPA, as Cy_2DETA.2A possesses a secondary amine in the central position of the diethylenetriamine backbone. Comparison of the protonation constants for Cy_2DETA.2A with those determined for Cy_2DETA.3A (Table 4.2) reveals greater basicity for the pK_a3 and pK_a4 values for Cy_2DETA.2A, as the lack of a central pendant carboxymethyl arm removes the inductive effect afforded by its presence.

4.3 Luminescence Data

In solution, the hydrated Eu(III) ion is nine-coordinate, i.e. $[Eu(H_2O)_9]^{3+}$. Complexation of the Eu^{3+} ion by a suitable ligating species results in the displacement of water molecules from the inner coordination sphere (as a function of the denticity of the ligand), whilst maintaining the coordination number of nine. In luminescence spectroscopy, the number of coordinated water molecules in a Eu(III) complex has a strong influence on the observed luminescence emission intensity, due to the quenching effect of O-H oscillators[50].

Luminescence emission spectra were obtained for the synthesized Eu(III) complexes as a function of pH. Experiments were conducted in varied multi-component buffer systems (consisting of MES, MOPS, CHES, Tris and KHP) at room temperature (25°C). The sample preparation procedures and emission data are detailed in Appendix F. Excitation wavelengths for each experiment were determined from UV-visible spectroscopy (Appendix F).

The emission intensities obtained from the luminescence data allowed for the crude determination of spectroscopic pK_a values of the Eu-complexes. Modelling of luminescent data was done using SigmaPlot[51] and the weighted averages of the calculated pK_a values are reported. Complex speciation, as a function of pH, was evaluated by monitoring the ratio of the $\Delta J = 2$ and $\Delta J = 1$ emission bands, due to the sensitivity of the $\Delta J = 2$ emission band to changes within the coordination environment of the Eu(III) complex[50, 52].

4.3.1 Cy_2DETA.3A.3HCl / Eu(III)

4.3.1.1 Cy_2DETA.3A.3HCl / Eu(III), aqueous solution

The minimum period required for europium(III)-1,7-bis(2-hydroxycyclohexyl)-1,4,7-tris(carboxymethyl)-1,4,7-triazaheptane to reach equilibrium was determined by monitoring the emission spectrum of a single sample at fixed pH (5.82) over a period of six days (Figure 4.3). The selected excitation wavelength of 223 nm was determined from UV-visible spectroscopy.

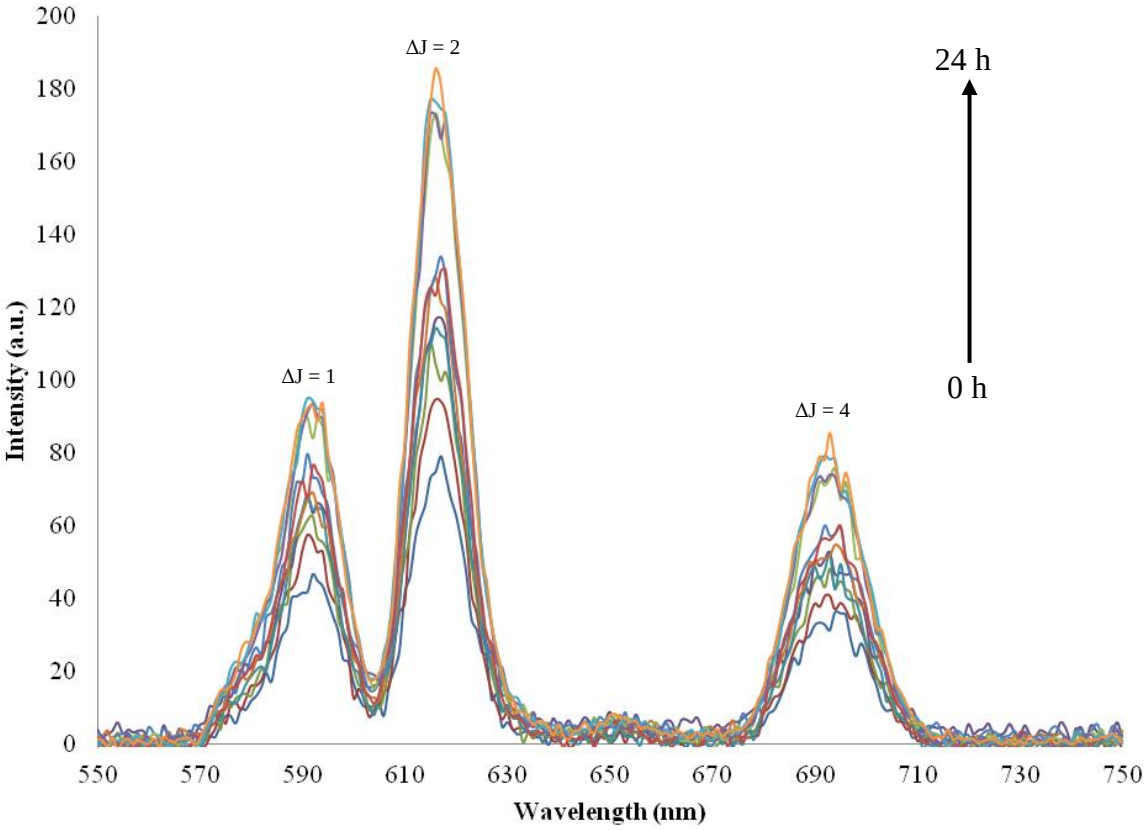


Figure 4.3: Phosphorescence emission spectrum of europium(III)-1,7-bis(2-hydroxycyclohexyl)-1,4,7-tris(carboxymethyl)-1,4,7-triazaheptane, as a function of time (λ_{ex} = 223 nm).

Emission intensities of emission bands (J-bands; ΔJ = 1 (592 nm), ΔJ = 2 (616 nm), and ΔJ = 4 (696 nm)) were plotted against time (Figure 4.4). Each emission band displayed a stabilization of emission intensity, corresponding to the completion of complex formation, after approximately 24 hours.

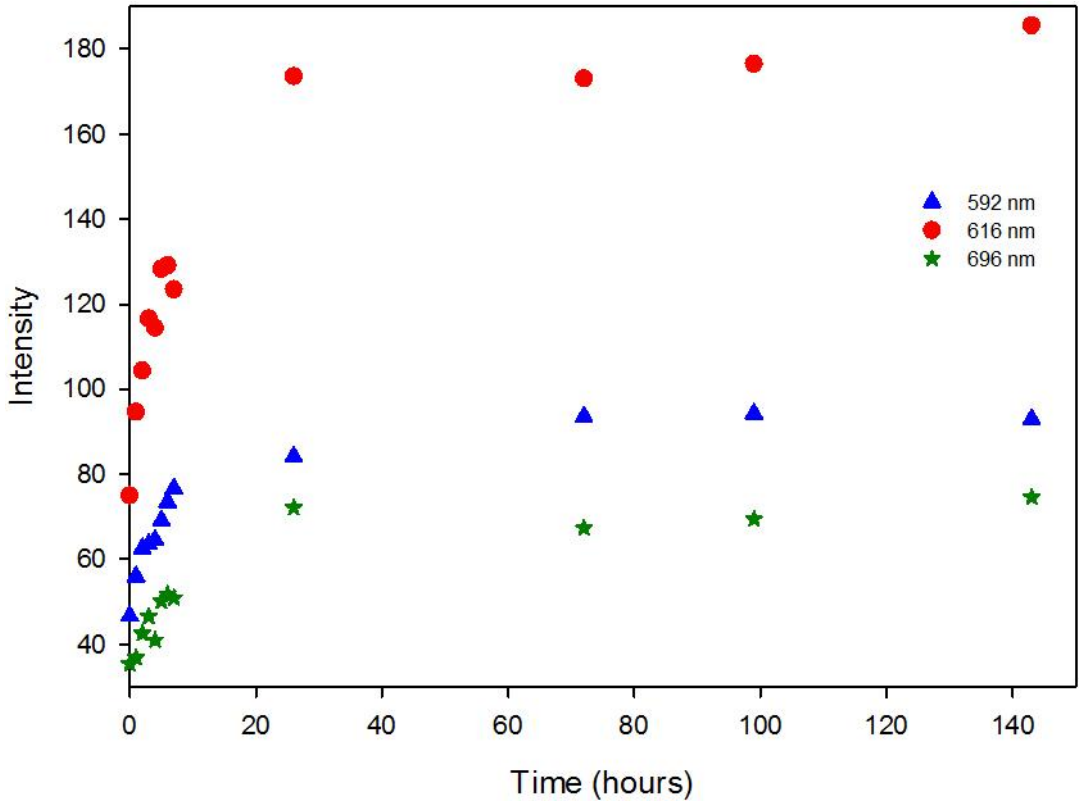


Figure 4.4: Phosphorescence emission intensity of europium(III)-1,7-bis(2-hydroxycyclohexyl)-1,4,7-tris(carboxymethyl)-1,4,7-triazaheptane, as a function of time (λ_{ex} = 223 nm).

The phosphorescence emission spectrum of a 0.3 mM aqueous solution of europium(III)-1,7-bis(2-hydroxycyclohexyl)-1,4,7-tris(carboxymethyl)-1,4,7-triazaheptane was recorded over a pH range of 2 and 11 (Figure 4.5). The spectrum of each prepared sample was recorded upon reaching equilibrium (after 24 hours), using an excitation wavelength of 223 nm, determined from UV-visible spectroscopy (Appendix F, Figure F.1).

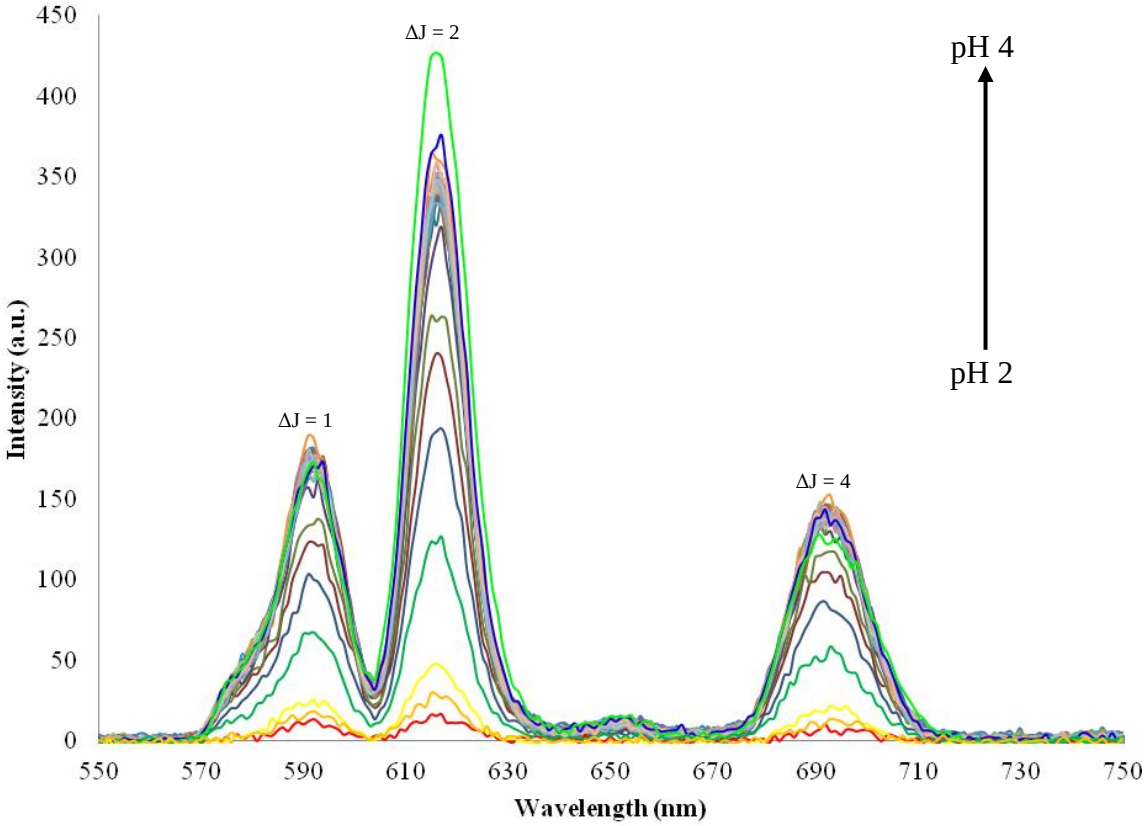


Figure 4.5: Phosphorescence emission spectrum of europium(III)-1,7-bis(2-hydroxycyclohexyl)-1,4,7-tris(carboxymethyl)-1,4,7-triazaheptane, as a function of pH (λ_{ex} = 223 nm).

Emission intensity varied as a function of pH, increasing from pH 2 to pH 4. Between pH 4 and pH 10, the emission intensity remained constant. Precipitation was not observed across the experimental pH range.

The emission intensities for each of the emission bands were tabulated (Appendix F, Table F.1). The emission intensities for the ΔJ = 1 (592 nm), ΔJ = 2 (617 nm), and ΔJ = 4 (693 nm) bands were plotted against their equilibrium pH values. A model for a single pK_a was employed to obtain a non-linear least squares fit for the ΔJ = 1 and ΔJ = 4 emission bands (Figures 4.6 and 4.8), while a two pK_a model was used to fit the ΔJ = 2 emission data (Figure 4.7).

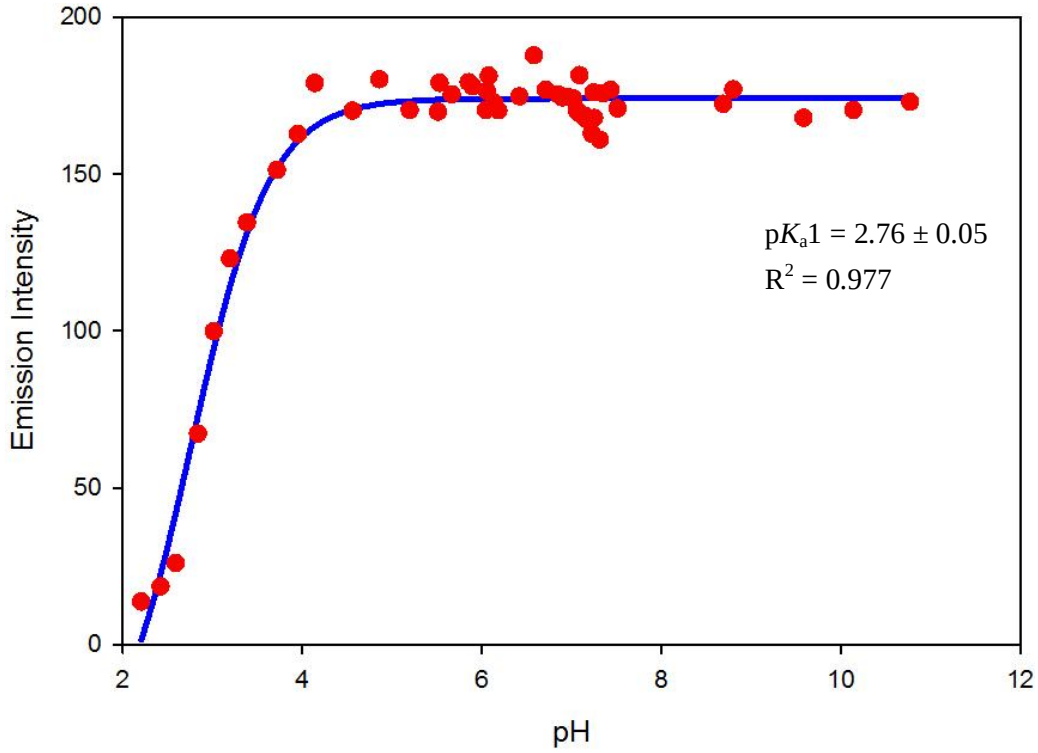


Figure 4.6: Phosphorescence emission intensity at 592 nm (ΔJ = 1), as a function of pH (λ_{ex} = 223 nm).

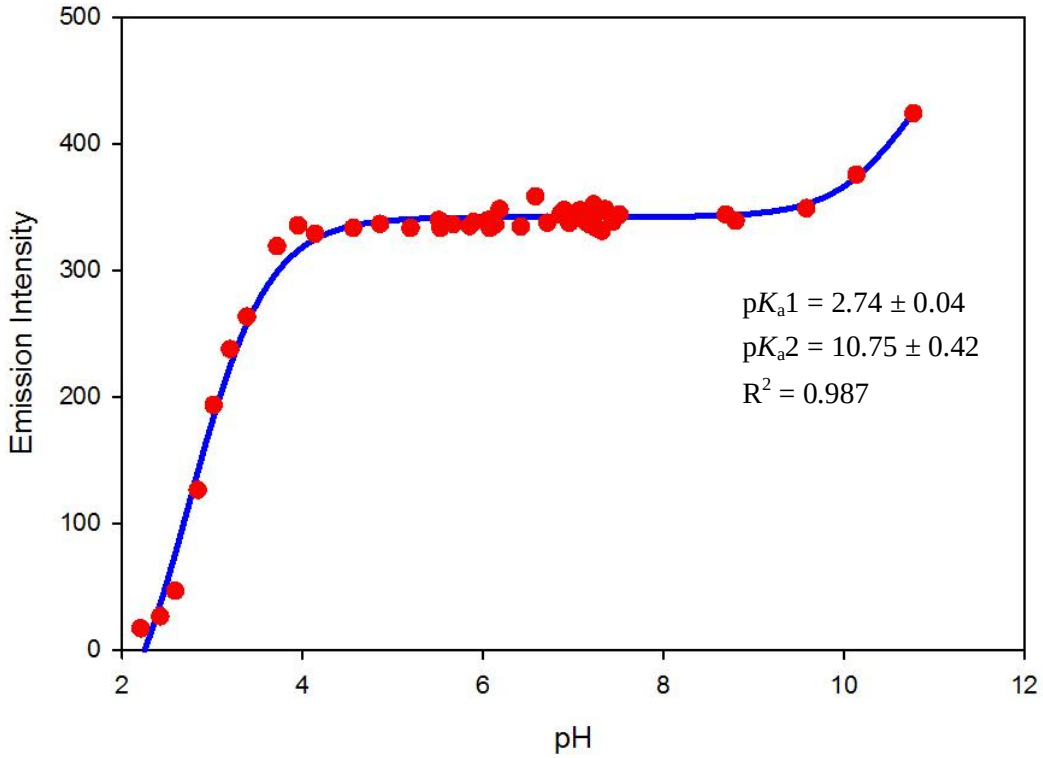


Figure 4.7: Phosphorescence emission intensity at 617 nm (ΔJ = 2), as a function of pH (λ_{ex} = 223 nm).

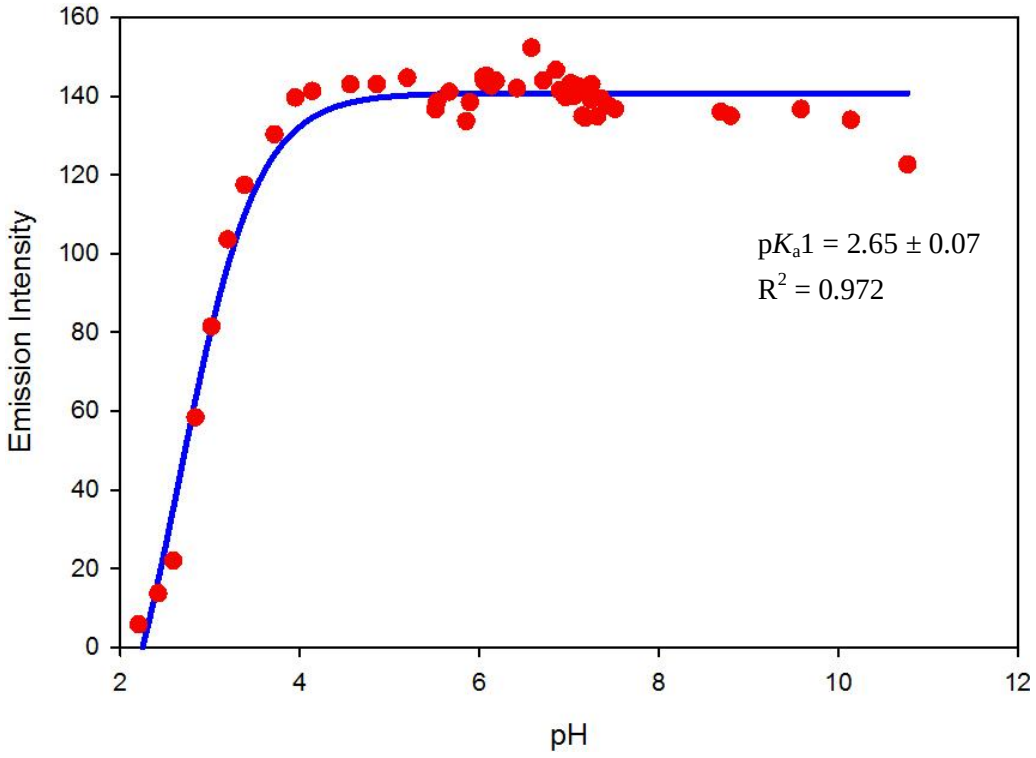


Figure 4.8: Phosphorescence emission intensity at 693 nm (ΔJ = 4), as a function of pH (λ_{ex} = 223 nm).

Typical pK_a values for protonated amines range between 8 and 10 [53], whilst carboxylic acids range between 2 and 4 [54]. However, pK_a values are significantly lowered by several orders of magnitude due to the electron-withdrawing properties accompanied upon complexation of a tri-valent lanthanide cation[42]. The weighted average pK_a1 value obtained for the three J-bands is 2.71 ± 0.07 and can be attributed to the deprotonation of the central amine moiety, as deprotonation of the terminal amines is expected to occur more readily due to the additional steric bulk of the hydroxycyclohexyl substituent. Carboxylate moieties are deprotonated at lower pH upon lanthanide complexation and do not correspond to the calculated pK_a. An increase in the emission intensity for the ΔJ = 2 band was observed at high pH, however, insufficient data points results in greater uncertainty for the calculated pK_a2 value. Comparison of the spectroscopically observed pK_a1 value with the potentiometrically determined protonation constant for the central amine moiety (Section 4.2.1, Table 4.1, pK_a1 = 10.21 ± 0.01) reveals an eight-order magnitude decrease in the pK_a value upon chelation of the Eu^{3+} cation.

The reaction mechanism and solution species proposed for pK_a1 are illustrated in Figure 4.9. The figure demonstrates a change in the coordination environment around the Eu(III) ion

(due to an increase in coordination number for the ligand, i.e. an increase from CN = 7 to CN = 8), while still maintaining an overall coordination number of nine.

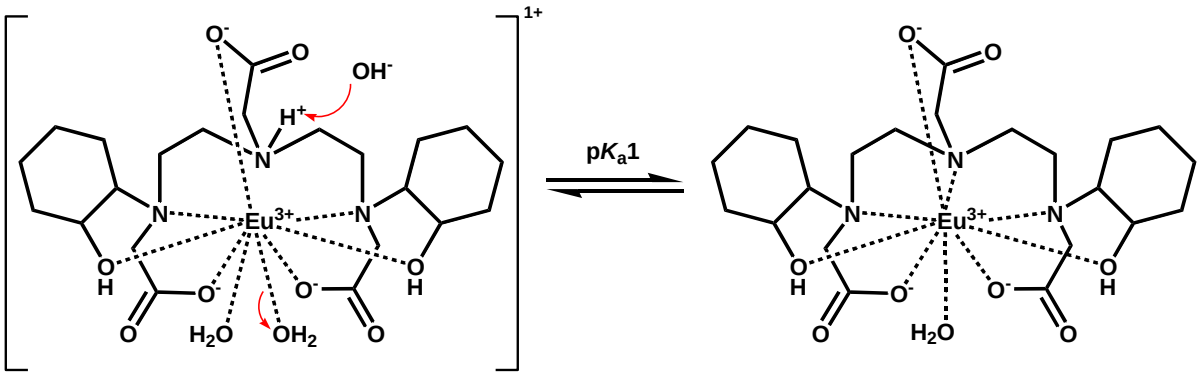


Figure 4.9: Proposed speciation and reaction mechanism of europium(III)-1,7-bis(2-hydroxycyclohexyl)-1,4,7-tris(carboxymethyl)-1,4,7-triazaheptane.

The $\Delta J_2/\Delta J_1$ relationship was evaluated as a function of pH to observe changes in speciation of the complex (Figure 4.10). A 2pK_a fit was attempted on the data.

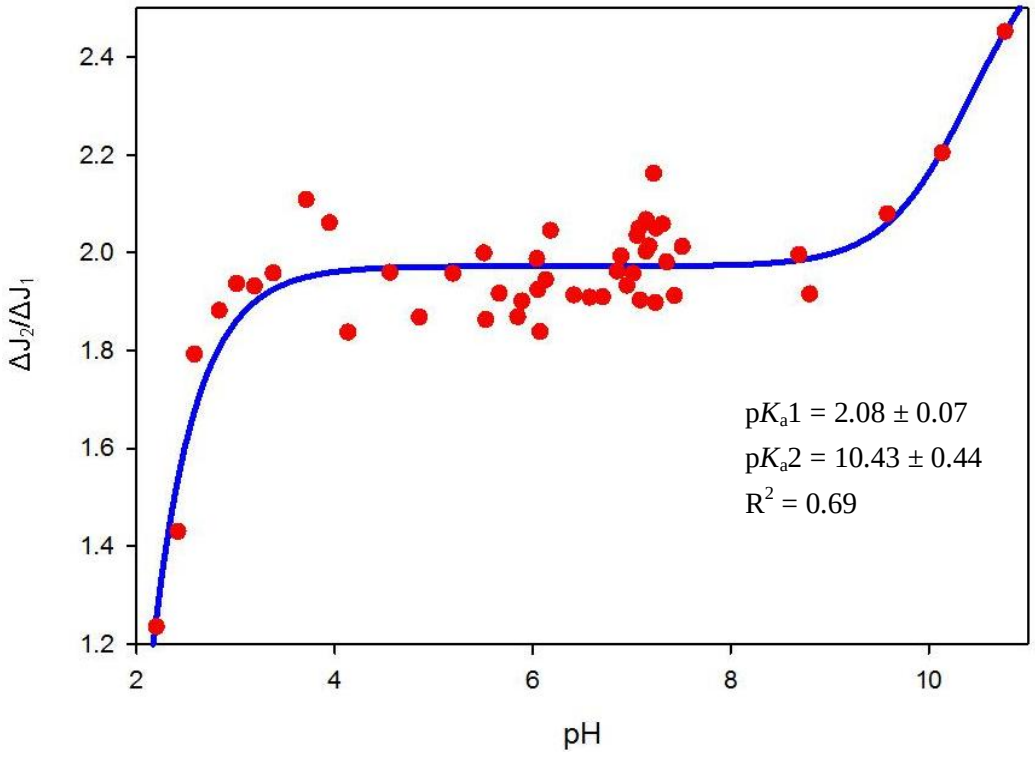


Figure 4.10: Relationship between $\Delta J = 2$ and $\Delta J = 1$ of europium(III)-1,7-bis(2-hydroxycyclohexyl)-1,4,7-tris(carboxymethyl)-1,4,7-triazaheptane, as a function of pH.

The pH 2 to 4 interval depicted in Figure 4.10 (corresponding to pK_a1) signals the shift from heptadentate to octadentate coordination of the metal ion by the ligand, due to the deprotonation of the central amine moiety (Figure 4.9), which would be accompanied by an increase in emission intensity. The proposed reconfiguration in the coordination environment would also be accompanied by a change in the overall charge of the complex, from a cationic $[Eu(HCy_2DETA.3A)(H_2O)_2]^+$ to a neutral $[Eu(Cy_2DETA.3A)(H_2O)]$. Between pH 4 and 9, the relative stability of the $\Delta J_2/\Delta J_1$ ratio would suggest that one complex species exists, i.e. $[Eu(Cy_2DETA.3A)(H_2O)]$. The complex would be expected to adopt a coordination geometry similar to that of Gd-DTPA and its acyclic analogues, i.e. a tricapped trigonal prismatic geometry[50].

The increase in emission intensity observed beyond pH 9 (Figures 4.7 and 4.10) could be attributed to the deprotonation of the coordinated water molecule; the removal of an inner-sphere O-H oscillator would contribute towards increased emission intensity. However, this observed increase in luminescent intensity after pH 9 may arise from the formation of a pendant alkoxide, as deprotonation of coordinated hydroxycyclohexyl moieties decreases the number of quenching innersphere O-H oscillators, resulting in enhanced luminescence. These results suggest the synthesized Eu(III) complex is potentially useful as a ratiometric pH sensor in both highly acidic and highly alkaline media[41, 55-57].

4.3.1.2 Cy_2DETA.3A.3HCl / Eu(III), multi-component buffered system, upon initial preparation

The emission spectra of a 0.15 mM solution of europium(III)-1,7-bis(2-hydroxycyclohexyl)-1,4,7-tris(carboxymethyl)-1,4,7-triazaheptane were recorded as a function of pH, in the presence of a 0.015 mM multi-component buffer system. The phosphorescence emission spectrum of each sample was measured upon initial preparation (i.e. at time = 0 hours), once a steady pH value was recorded. The selected excitation wavelengths of 229 nm and 279 nm were determined from UV-visible spectroscopy (Appendix F, Figure F.2). Two sets of emission patterns were obtained for each sample (Figures 4.11 and 4.12).

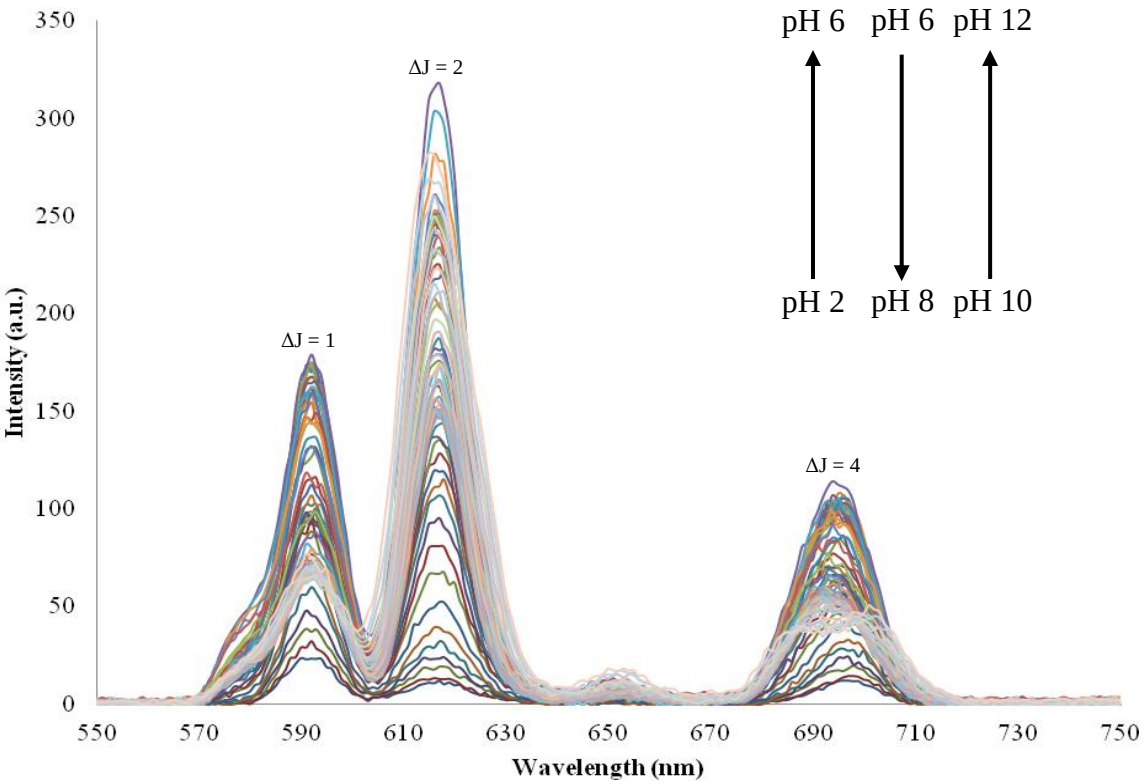


Figure 4.11: Phosphorescence emission spectrum of europium(III)-1,7-bis(2-hydroxycyclohexyl)-1,4,7-tris(carboxymethyl)-1,4,7-triazaheptane, as a function of pH (λ_{ex} = 229 nm).

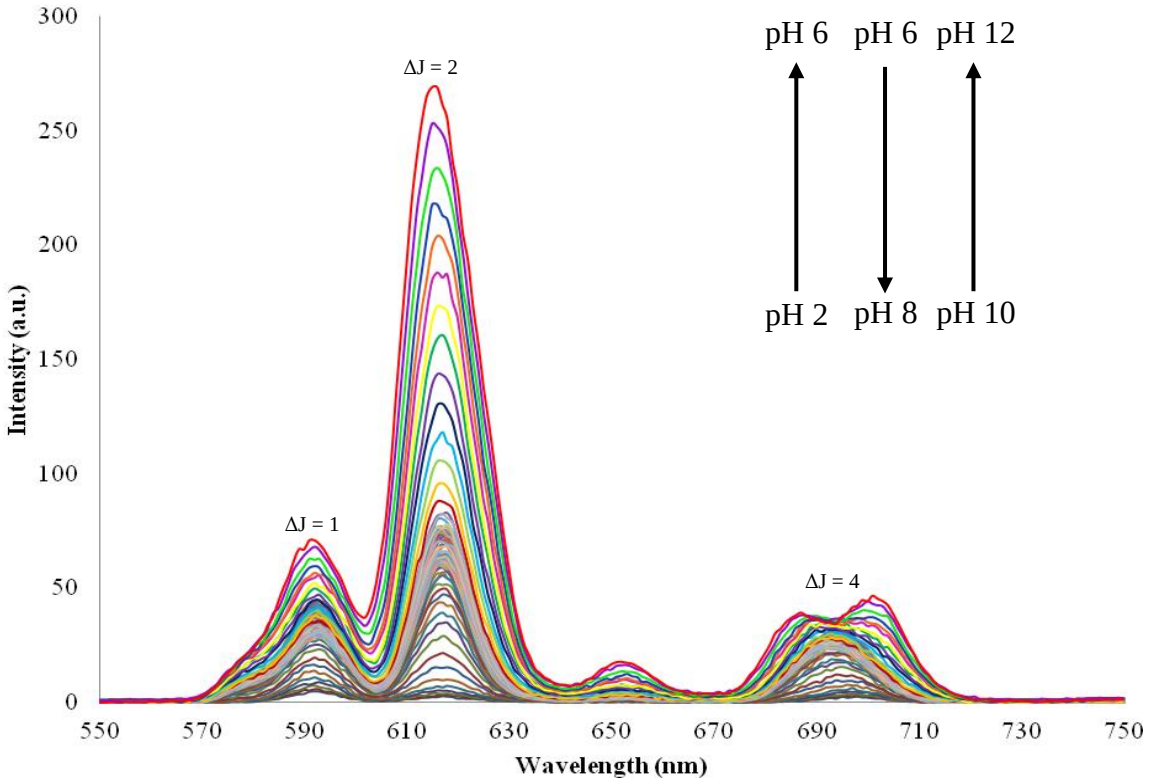


Figure 4.12: Phosphorescence emission spectrum of europium(III)-1,7-bis(2-hydroxycyclohexyl)-1,4,7-tris(carboxymethyl)-1,4,7-triazaheptane, as a function of pH (λ_{ex} = 279 nm).

The observed emission spectra (Figures 4.11 and 4.12) displayed an increase in intensity between pH 2 and pH 6, followed by a slight decrease between pH 6 and pH 8. The intensity remained constant between pH 8 and pH 10, and was followed by a sharp increase in intensity between pH 10 and pH 12. Precipitation was not observed over the experimental pH range. The $\Delta J = 2$ emission band showed the greatest modulation as a function of pH. Under basic conditions, a splitting of the $\Delta J = 4$ band was observed.

The emission intensities for each J-band were tabulated (Appendix F, Tables F.2 and F.3). The emission intensities for the $\Delta J = 1$ (592 nm), $\Delta J = 2$ (617 nm), and $\Delta J = 4$ (697 nm) bands for Figure 4.10 were plotted against the measured pH values. A four pK_a model was employed to obtain a non-linear least squares fit for $\Delta J = 1$, $\Delta J = 2$ and $\Delta J = 4$ emission bands (Figures 4.13, 4.14, and 4.15).

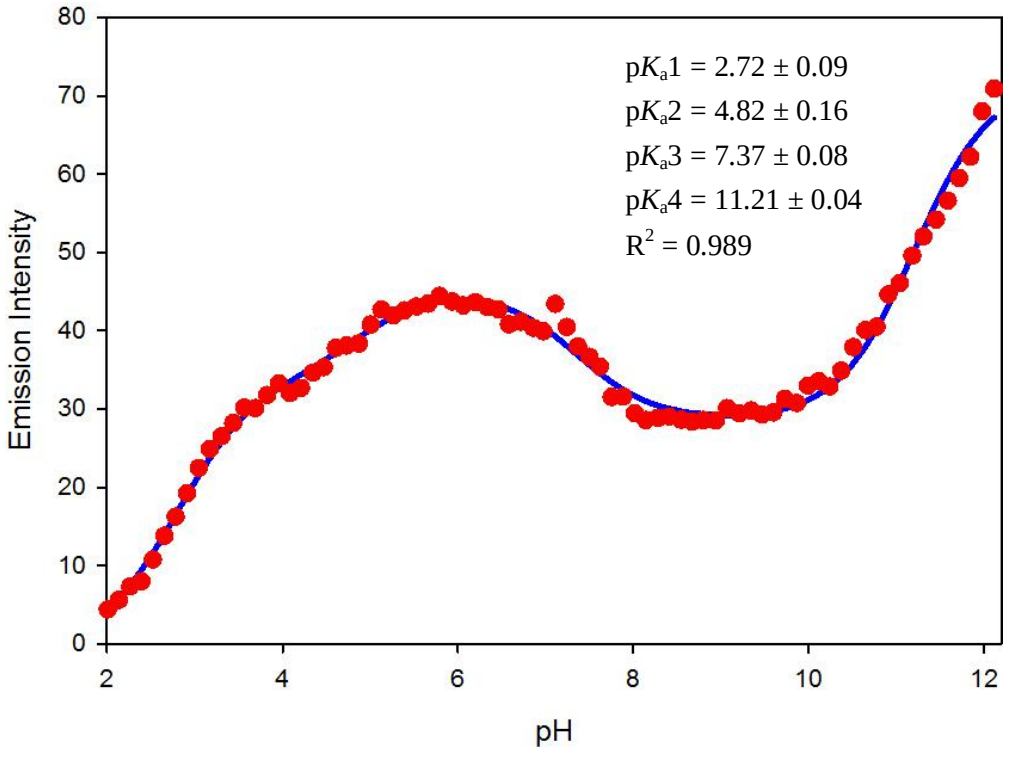


Figure 4.13: Phosphorescence emission intensity at 592 nm ($\Delta J = 1$), as a function of pH (λ_{ex} = 279 nm).

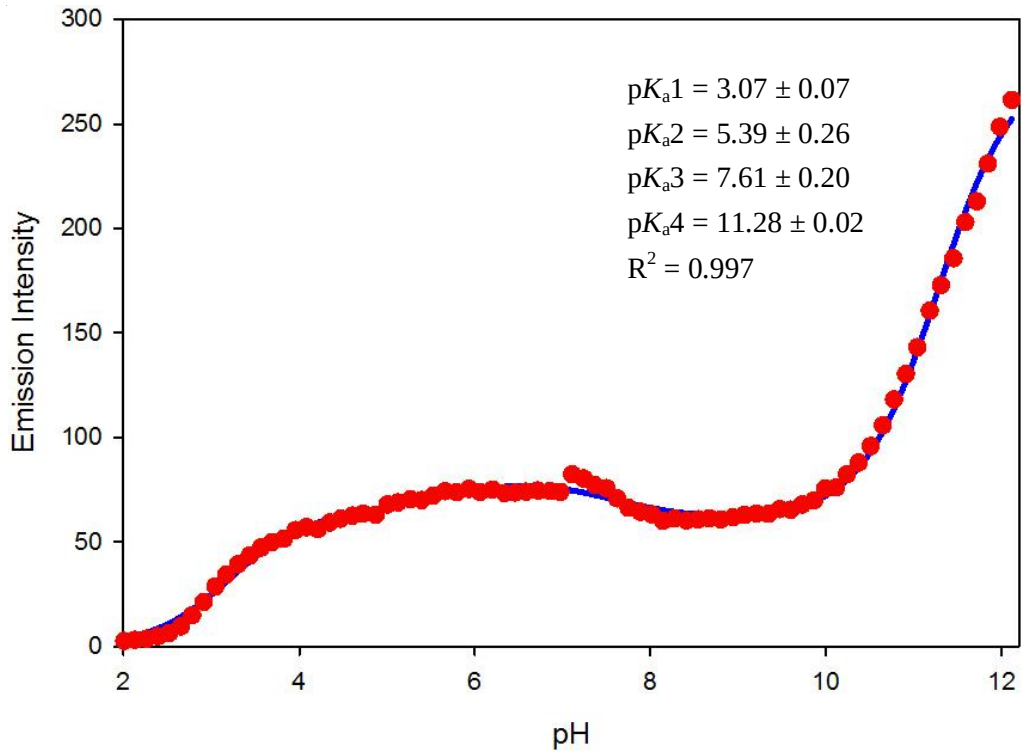


Figure 4.14: Phosphorescence emission intensity at 617 nm (ΔJ = 2), as a function of pH (λ_{ex} = 279 nm).

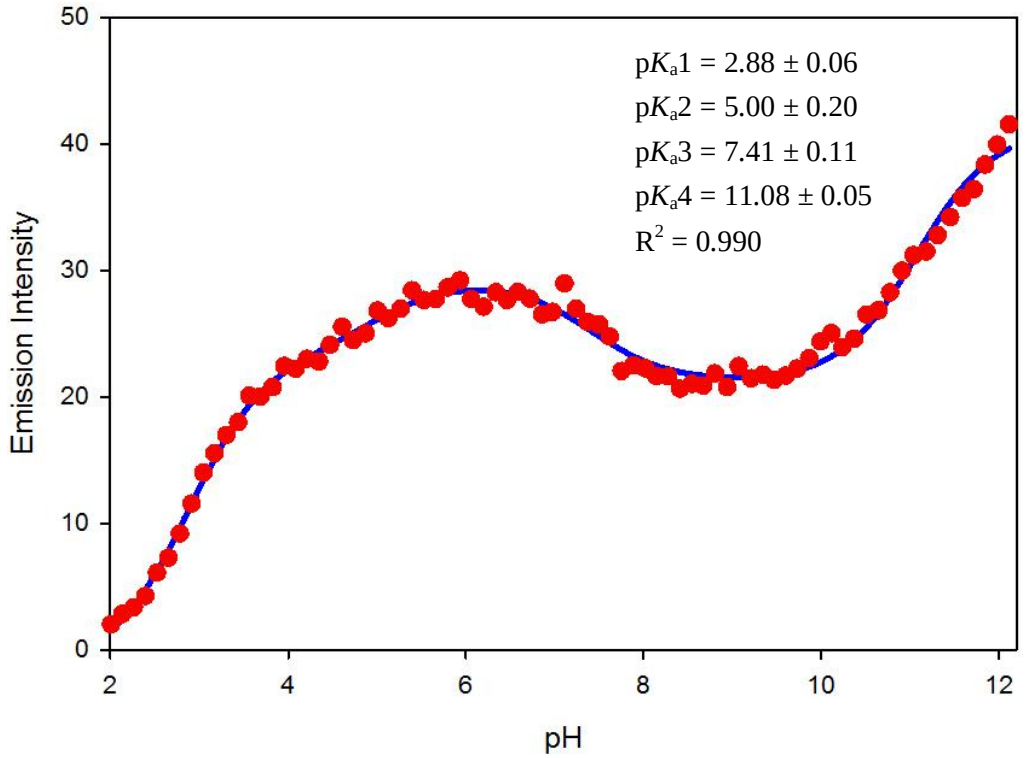


Figure 4.15: Phosphorescence emission intensity at 697 nm (ΔJ = 4), as a function of pH (λ_{ex} = 279 nm).

Before attempting to assign the calculated pK_a values, it may be useful to observe the $\Delta J_2/\Delta J_1$ relationship in the presence of a multi-component buffer system (Figure 4.16). A 3 pK_a model was fitted to the data. A 4 pK_a model was attempted on the data set, but this resulted in a poor R^2 value.

It should be noted that, while Figure 4.16 compares pH emission profiles of buffered and non-buffered media, the speciation of these profiles is different. The comparison illustrates buffer addition results in formation of ternary complexes. The choice of KHP as a component of the buffer system is significant, as there are examples where lanthanide complexes have displayed enhancement in luminescent intensity upon the formation of a ternary complex between the lanthanide complex and the carboxylate ion[58-62]. The Tris buffer has also been shown to coordinate to various bi- and tri-valent transition metals[63-66], and, owing to the oxophilic nature of the Eu(III) ion, it is therefore possible that the formation of a ternary complex with Tris may be favoured.

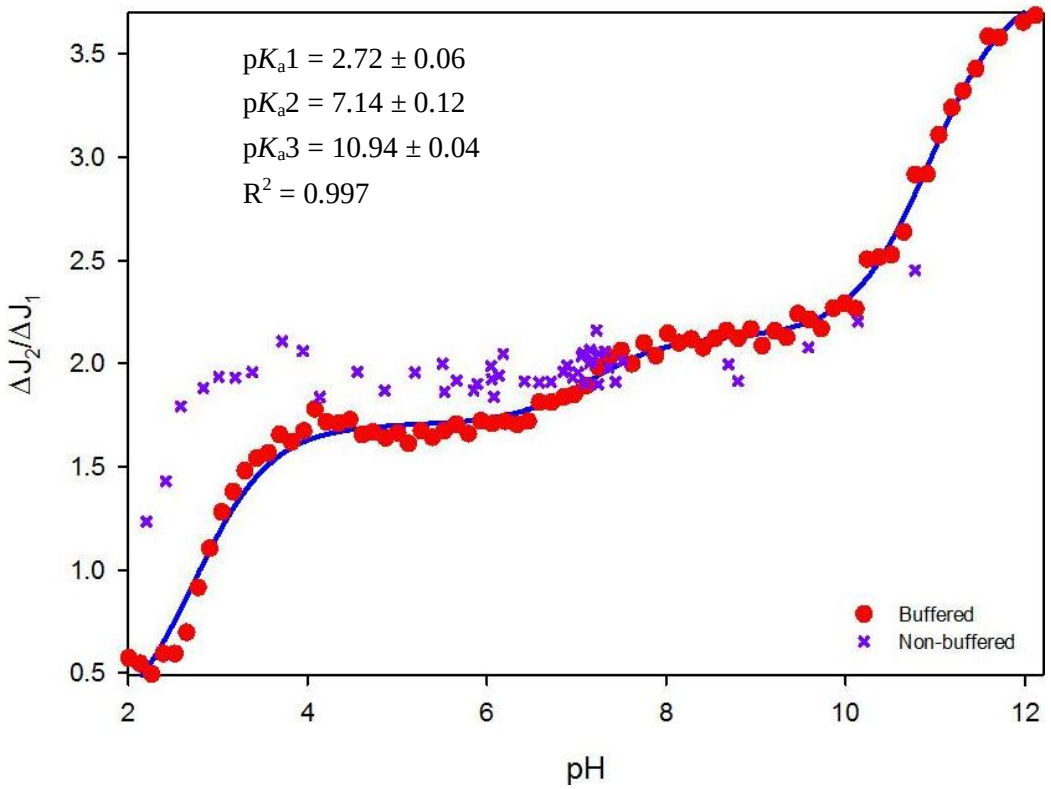


Figure 4.16: Relationship between $\Delta J = 2$ and $\Delta J = 1$ of europium(III)-1,7-bis(2-hydroxycyclohexyl)-1,4,7-tris(carboxymethyl)-1,4,7-triazaheptane, as a function of pH, in a multi-component buffered system.

Regarding Figures 4.13, 4.14, and 4.15, the weighted average pK_a1 value for the three J-bands yields a result of 2.87 ± 0.21, proposed to correspond to the deprotonation of the central amine moiety that coincides with the phthalate pK_a (phthalate pK_a1 = 2.75)[67]. The weighted average pK_a2 value of 5.01 ± 0.37 is in agreement with the formation of the phthalate dianion (phthalate pK_a2 = 4.93)[67]. The pK_a3 average value of 7.45 ± 0.14 is attributed to the deprotonation of an innersphere H_2O. The weighted average pK_a4 value of 11.18 ± 0.12 may originate from: the formation of an alkoxide (due to the deprotonation of a coordinated alcohol pendant arm); the formation of a ternary complex involving the Tris buffer. The pK_a1, pK_a2, and pK_a4 values, correlate favourably with the 3 pK_a model of $\Delta J_2/\Delta J_1$ ratiometric data (Figure 4.16).

The speciation associated with the observed equilibria requires the consideration of the present buffer system. Although the increase observed for the ratiometric data at pH 3 (Figure 4.16) corresponds with the deprotonation of the central amine (pK_a1), the species may not necessarily be identical to that observed for the non-buffered system at the same pH. The presence of the hydroxycyclohexyl pendants in the ligand structure could facilitate formation of a ternary complex involving the phthalate ion, resulting in a hydrogen bond array formed between the carboxylate group on the phthalate ion and the alcohol moieties of the ligand and coordinated (innersphere) water molecules. The interaction of outersphere anions with Eu(III)-complexes has been shown to modulate emission intensity, as demonstrated for phosphate diesters[68].

The $\Delta J_2/\Delta J_1$ ratio remains constant between pH 4 and 6, however the $\Delta J_2/\Delta J_1$ ratio is lower when compared to that of the non-buffered solution (Figure 4.16). This pH range would therefore account for the formation of the ternary complex involving the phthalate ion, where pK_a2 is the second deprotonation of the phthalate ion. Coordination of carboxylates to a lanthanide metal centre has been commonly shown to occur in a bidentate manner[58, 59, 61], and this could be expected for the present system. Binding of the phthalate anion directly to the metal centre facilitates photo-induced electron transfer (PET), resulting in enhancement of emission intensity compared to the non-buffered system (as a result of efficient population of the electronic excited state of the metal)[69-71]. As the ligand system employed in this study is octadentate and the Eu(III) ion has a coordination number of nine, it follows that binding of the phthalate ion requires the replacement of a ligand pendant moiety. The

hydroxycyclohexyl moiety is most likely not accommodated by the metal. Conformation of the coordination polyhedron requires determination of the hydration state within the pH range under scrutiny. The slight increase in the ratio observed at pH 7 (Figure 4.16) demonstrates a further change to the coordination polyhedron of the complex, proposed to correspond with deprotonation of an innersphere water molecule (pK_a3). The change in speciation may reflect displacement of the phthalate ion by OH^- at elevated pH.

The $\Delta J_2/\Delta J_1$ ratio remains constant between pH 8 and 10 and increases dramatically beyond pH 10, suggesting a significant change in the coordination geometry about the Eu(III) ion (Figure 4.16). The increased emission intensity could be attributed to the presence of the Tris buffer in solution. Tris has been shown to coordinate to transition metals via its amine and alcohol moieties[63-66]. It is proposed that at high pH, the deprotonation of the alcohol groups on Tris would occur, and could coordinate directly to the metal centre. As there are three alcohol groups present in Tris, it could further be proposed that a Tris molecule may form a ternary complex involving multiple $[Eu(Cy_2DETA.3A)]^{3+}$ complexes leading to cluster formation, accounting for the observed emission enhancement. As proposed for phthalate binding, the formation of a ternary complex with Tris would result in the substitution of a coordinated water molecule or ligand pendant arm. Therefore, elucidation of the hydration state of the complex at this pH is imperative for determining the speciation of the complex. However, enhanced emission intensity at elevated pH was similarly observed in aqueous solution (Figure 4.10), indicating that the observed increase in emission intensity at high pH for the buffered system is due to possible alkoxide formation (the result of deprotonation of a coordinated hydroxycyclohexyl pendant arm) or the formation of a hydroxo-complex.

This result is promising as the Eu(III) complex could be used as a ratiometric sensor for the detection of phthalate (and possibly other anionic species) under appropriate pH conditions[41].

4.3.1.3 Cy_2DETA.3A.3HCl / Eu(III), multi-component buffered system, upon reaching equilibrium

Phosphorescence emission spectra of a 0.15 mM solution of europium(III)-1,7-bis(2-hydroxycyclohexyl)-1,4,7-tris(carboxymethyl)-1,4,7-triazaheptane were measured as a

function of pH, in the presence of a 0.015 mM multi-component buffer system. The solutions were allowed to reach equilibrium over 3 days (25 °C). Excitation wavelengths for the emission spectra were selected upon measurement of the UV-visible spectra of the prepared samples (Appendix F, Figure F.3). The pH and emission spectrum of each sample were recorded (Figures 4.17 and 4.18). The samples were resealed and the pH and emission spectra remeasured after 14 days (Figures 4.19 and 4.20).

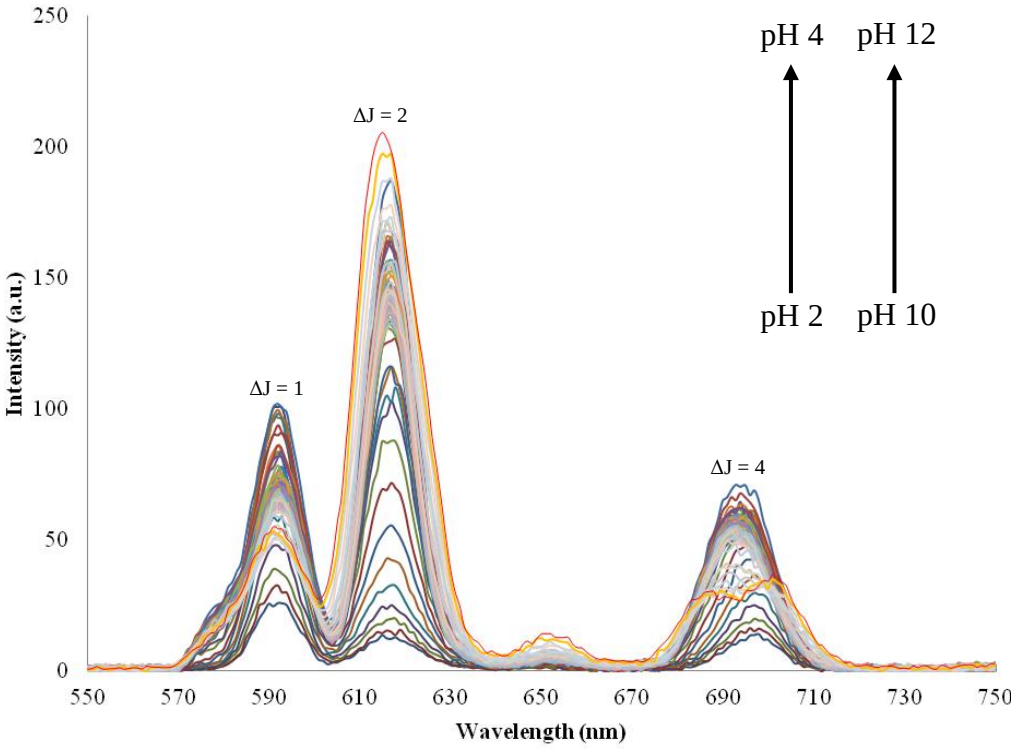


Figure 4.17: Phosphorescence emission spectrum of europium(III)-1,7-bis(2-hydroxycyclohexyl)-1,4,7-tris(carboxymethyl)-1,4,7-triazaheptane, as a function of pH (after 3 days, λ_{ex} = 240 nm).

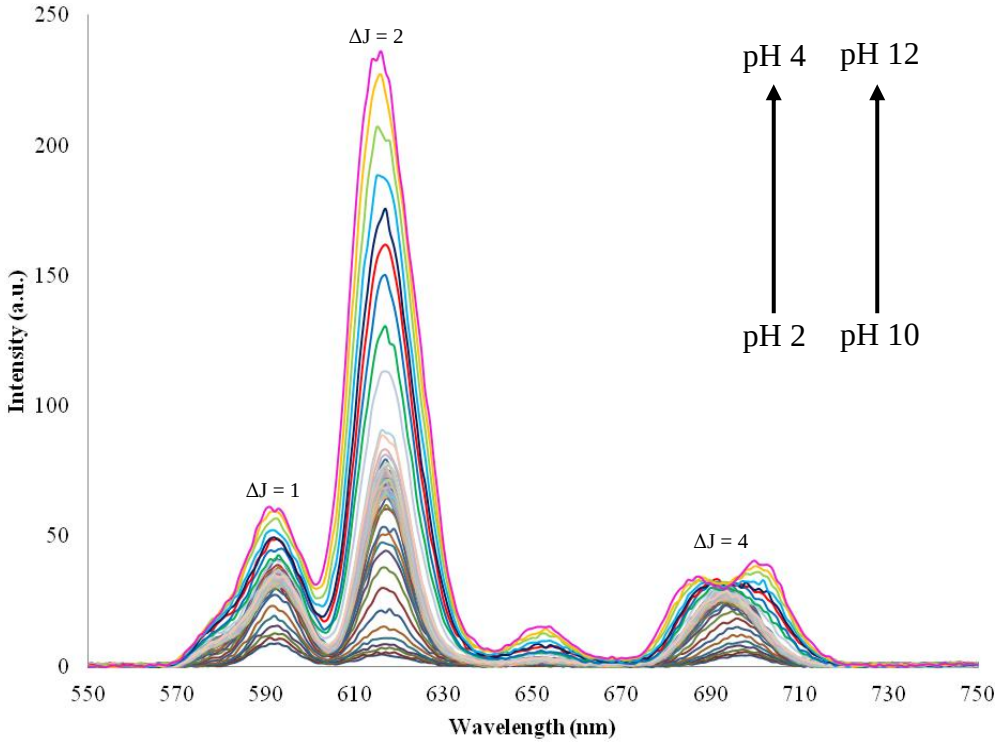


Figure 4.18: Phosphorescence emission spectrum of europium(III)-1,7-bis(2-hydroxycyclohexyl)-1,4,7-tris(carboxymethyl)-1,4,7-triazaheptane, as a function of pH (after 3 days, λ_{ex} = 266 nm).

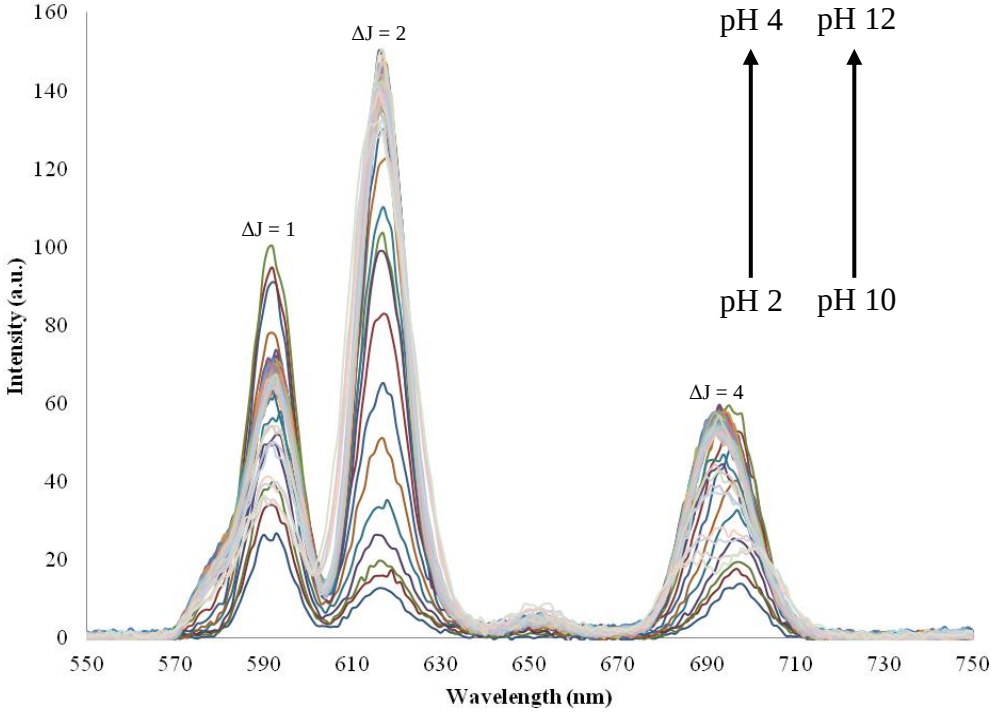


Figure 4.19: Phosphorescence emission spectrum of europium(III)-1,7-bis(2-hydroxycyclohexyl)-1,4,7-tris(carboxymethyl)-1,4,7-triazaheptane, as a function of pH (after 14 days, λ_{ex} = 240 nm).

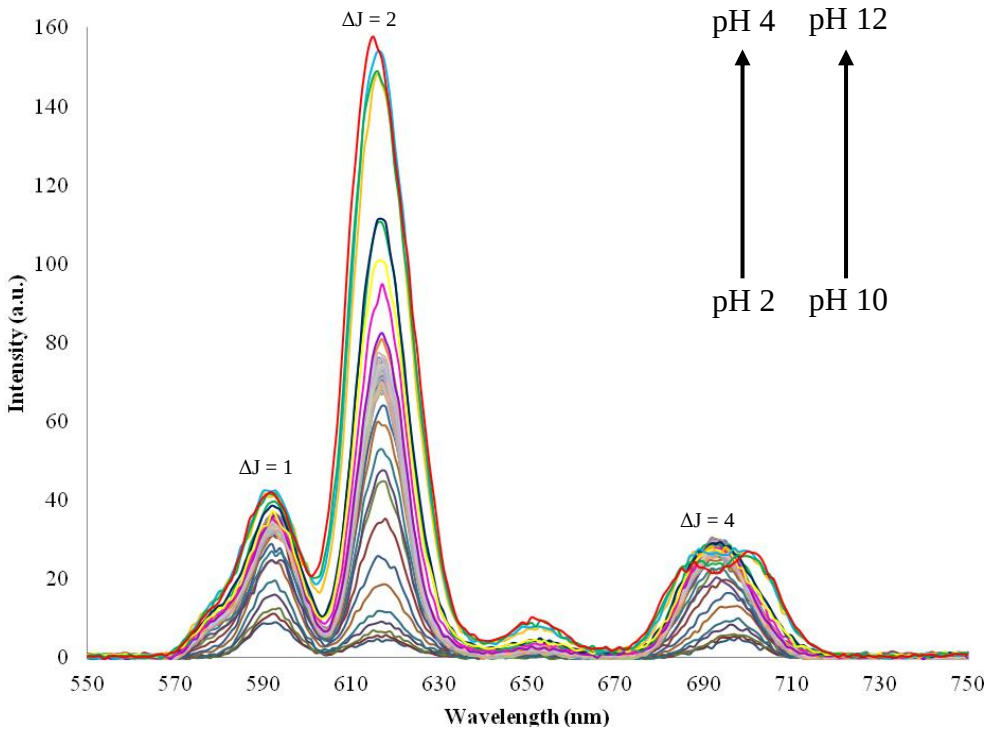


Figure 4.20: Phosphorescence emission spectrum of europium(III)-1,7-bis(2-hydroxycyclohexyl)-1,4,7-tris(carboxymethyl)-1,4,7 triazaheptane, as a function of pH (after 14 days, λ_{ex} = 266 nm).

Observation of the modulation of emission intensity for both 3 day and 14 day measurements indicated an increase in intensity between pH 2 and pH 4. Emission intensity remained seemingly constant between pH 4 and pH 10, and increased significantly between pH 10 and pH 12. Precipitation was not observed across the experimental pH range. The ΔJ = 2 emission band showed the greatest modulation as a function of pH, while splitting of the ΔJ = 4 band was observed at high pH.

The emission intensities for each J-band were tabulated (Appendix F, Tables F.4 and F.5). The emission intensities for the ΔJ = 2 (617 nm) band for excitation at 266 nm (Figures 4.18 and 4.20) were plotted against the measured pH values. A two pK_a model rendered the best non-linear regression analysis for ΔJ = 2 emission bands (Figures 4.21 and 4.22).

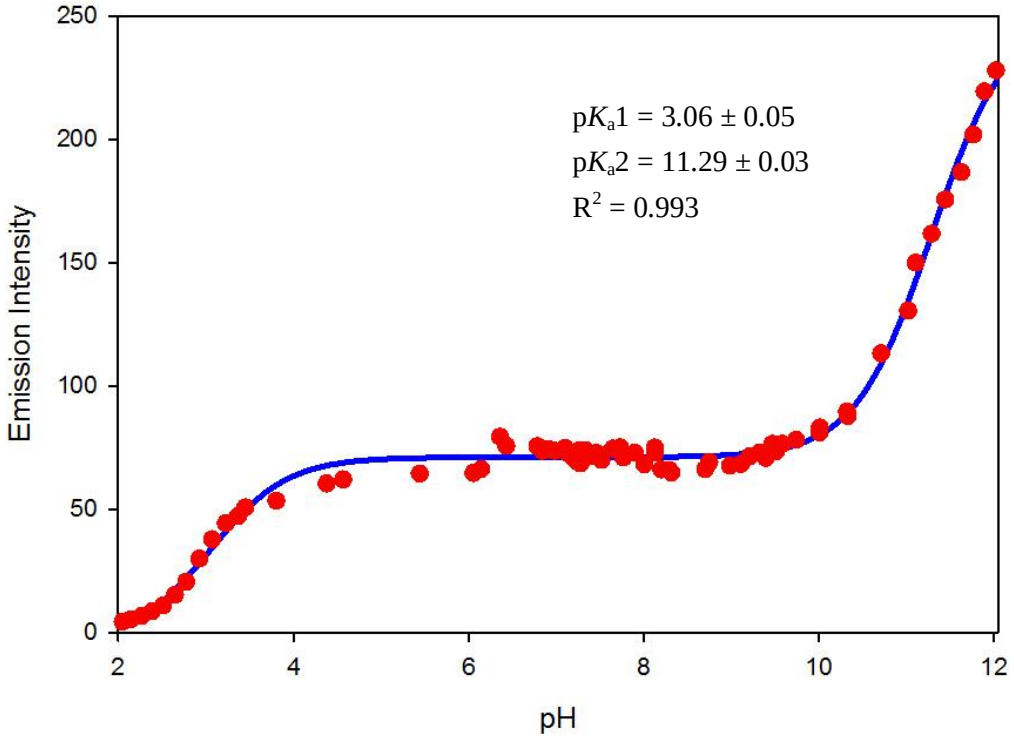


Figure 4.21: Phosphorescence emission intensity at 617 nm (ΔJ = 2), as a function of pH (after 3 days, λ_{ex} = 266 nm).

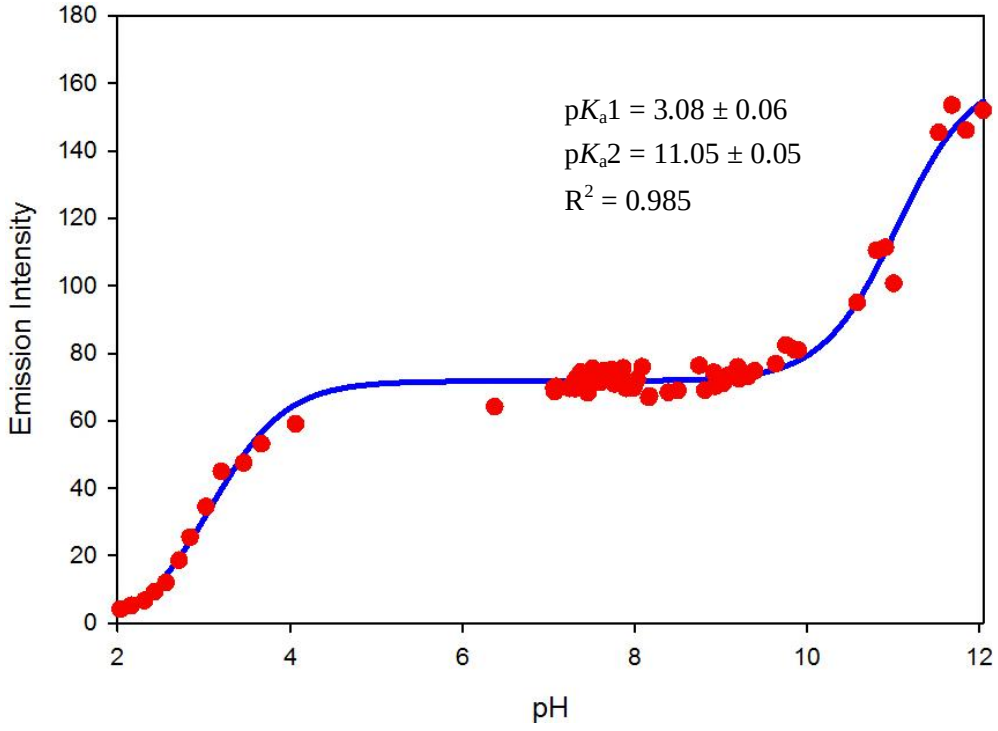


Figure 4.22: Phosphorescence emission intensity at 617 nm (ΔJ = 2), as a function of pH (after 14 days, λ_{ex} = 266 nm).

Analysis of the ΔJ = 2 emission intensities for the buffered system before reaching equilibrium (Figure 4.14, 0 hours) and after reaching equilibrium (Figure 4.21, 3 days, and Figure 4.22, 14 days) accommodate 4 pK_a and 2 pK_a models respectively. Further commentary on speciation requires comparison of the $\Delta J_2/\Delta J_1$ relationship for the buffered systems before (0 hours) and after (3 days and 14 days) reaching equilibrium, illustrated in Figure 4.23.

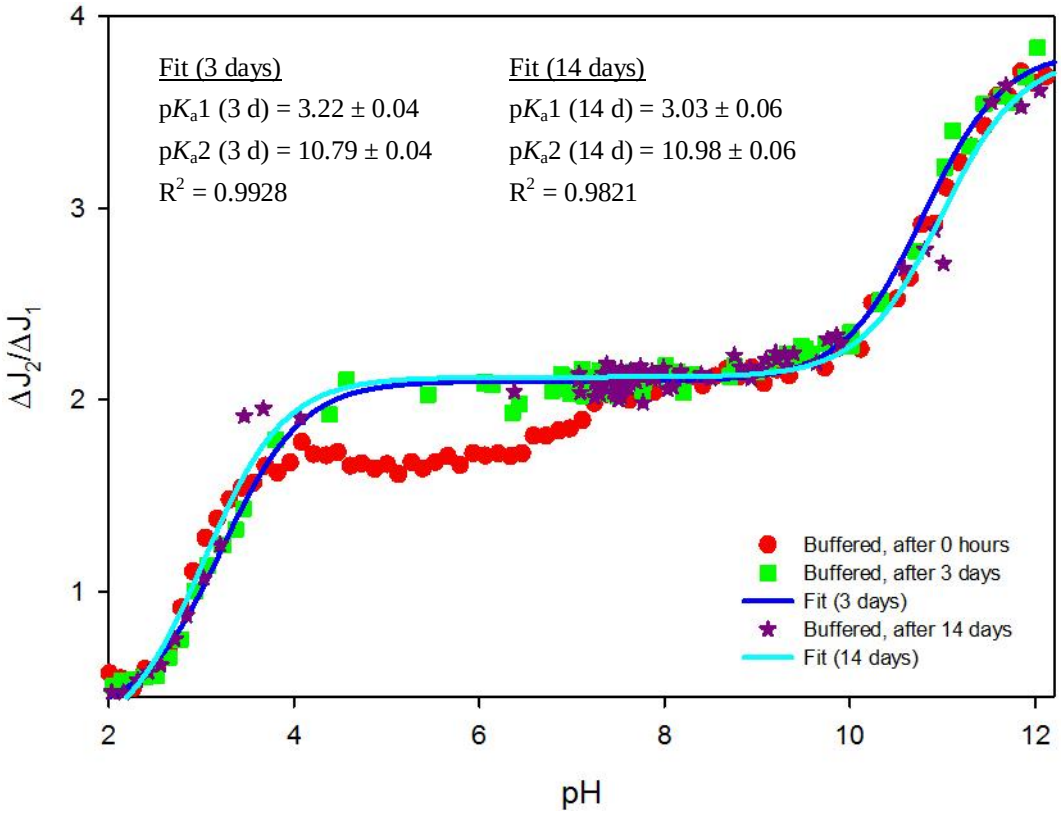


Figure 4.23: Comparison of the $\Delta J_2/\Delta J_1$ ratio for europium(III)-1,7-bis(2-hydroxycyclohexyl)-1,4,7-tris(carboxymethyl)-1,4,7-triazaheptane, as a function of pH, in a multi-component buffered system.

The pK_a1 value (Figures 4.21, 4.22 and 4.23) is congruent with amine deprotonation (central nitrogen donor of the triazaheptane backbone), while pK_a2 value may be attributed to the formation of an alkoxide (due to the deprotonation of a coordinated hydroxycyclohexyl pendant moiety).

The pH of solutions prepared between pH 4 and pH 7 (Figures 4.21 and 4.22) showed marked variation in pH upon reaching equilibrium (compared to Figure 4.14). This phenomenon is associated with phthalate ternary complex formation. Binding of the phthalate anion depletes

the buffering capacity in the pH 4 to pH 7 range (the functional pH range for KHP), due to the low concentration of the buffer system (0.015 mM) employed in this study (the Eu(III) complex to buffer ratio is 10:1). This is also accompanied by the disappearance of pK_a2 (Figure 4.14, pK_a2 = 5.39 ± 0.26, associated with the formation of the phthalate dianion), which suggests that the outersphere phthalate ion is fully deprotonated. The good correlation observed for the 3 sets of ratiometric data at high pH (Figure 4.23) illustrates that the complexes at elevated pH are stable over time. However, comparison of Figures 4.21 and 4.22 reveal decreasing emission intensity of the individual samples prepared between the pH 11 and pH 12 over time. Dissociation of the proposed ternary complex clusters with Tris may be responsible for the decrease in emission intensity. The reduction in emission intensity at high pH over time could be the result of dissociation of the Eu(III) complex, resulting in the precipitation of $Eu(OH)_3$ from solution. However, no evidence of a precipitate was found for the high pH samples.

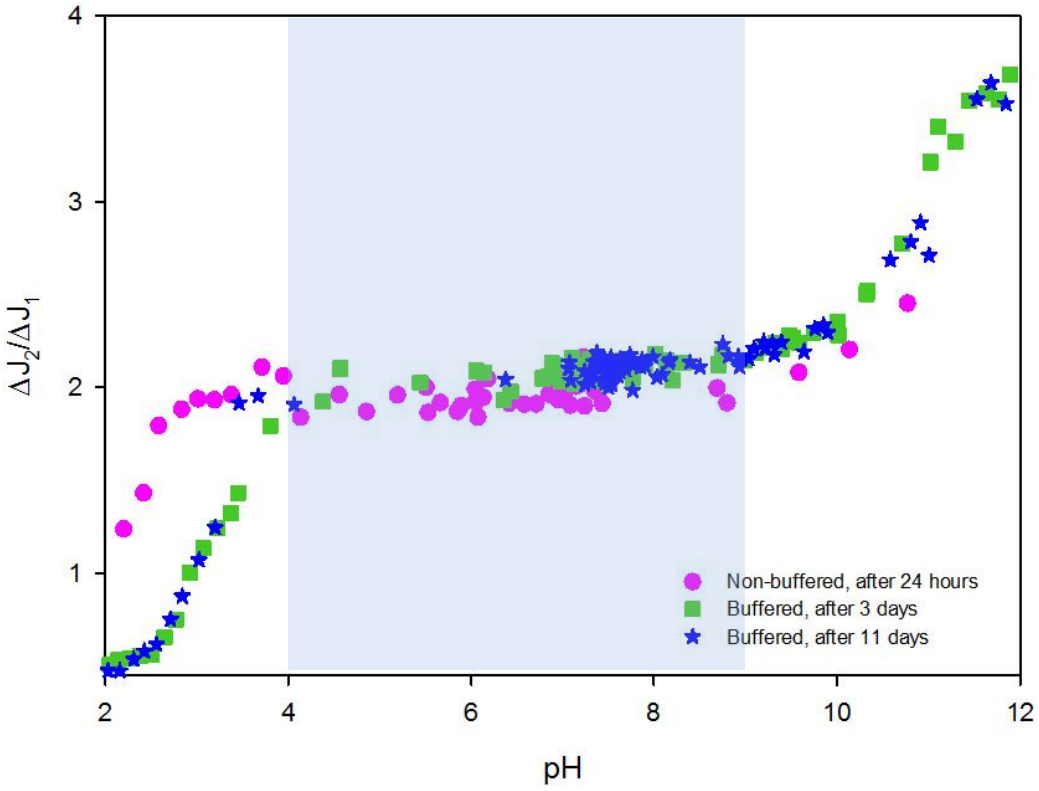


Figure 4.24: Comparison of the $\Delta J_2/\Delta J_1$ relationship of europium(III)-1,7-bis(2-hydroxycyclohexyl)-1,4,7-tris(carboxymethyl)-1,4,7-triazaheptane, in a buffered and non-buffered system upon equilibration, as a function of pH.

A comparison of pH profiles for buffered and non-buffered systems upon reaching equilibrium (Figure 4.24) reveals the strikingly similar responsive nature of $[Eu(Cy_2DETA.3A)]^{3+}$ towards variation in pH. Both buffered and non-buffered solutions also display the formation of a species with a coordination environment that is fairly constant between pH 4 and pH 9 (highlighted in Figure 4.24). As speciation in aqueous solution between pH 4 and pH 9 indicates the presence of the monoaqua $[Eu(Cy_2DETA.3A)]^{3+}$ (Figure 4.10), the similar $\Delta J_2/\Delta J_1$ ratio observed for the buffered system indicates dissociation of ternary complex formed with phthalate upon reaching equilibrium, thus yielding the monoaqua Eu(III) complex.

4.3.2 Cy_2DETA.2A.3HCl / Eu(III)

4.3.2.1 Cy_2DETA.2A.3HCl / Eu(III), aqueous solution

The minimum period required for europium(III)-1,7-bis(2-hydroxycyclohexyl)-1,7-bis(carboxymethyl)-1,4,7-triazaheptane to reach equilibrium was determined by monitoring the emission spectrum of a single sample at fixed pH (5.51) over a period of four days (Figure 4.25). The selected excitation wavelength of 252 nm was determined from UV-visible spectroscopy.

Emission intensities for each J-band were plotted as a function of time (Figure 4.26). Each emission band displayed maximum intensity, corresponding to complexation equilibrium, after approximately 48 hours. The long equilibration time is possibly due to the required morpholone hydrolysis (Scheme 3) prior to metal complexation.

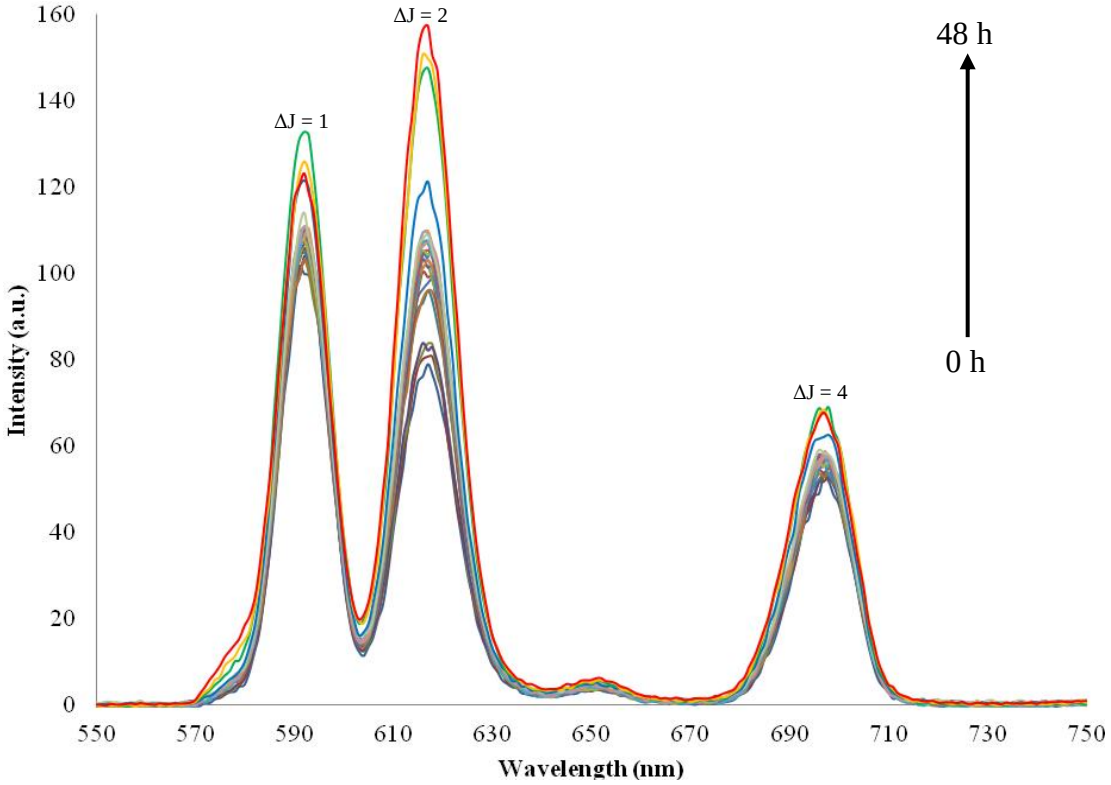


Figure 4.25: Phosphorescence emission spectrum of europium(III)-1,7-bis(2-hydroxycyclohexyl)-1,7-bis(carboxymethyl)-1,4,7-triazaheptane, as a function of time (λ_{ex} = 252 nm).

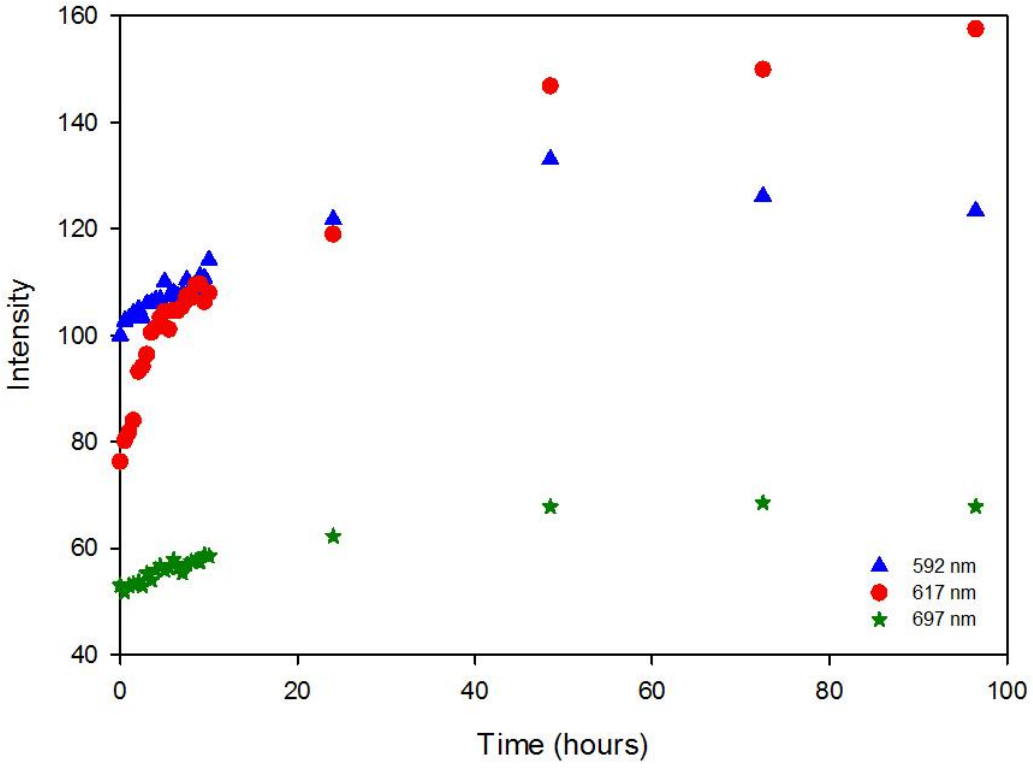


Figure 4.26: Phosphorescence emission intensity of europium(III)-1,7-bis(2-hydroxycyclohexyl)-1,7-bis(carboxymethyl)-1,4,7-triazaheptane, as a function of time (λ_{ex} = 252 nm).

The emission spectrum of a 0.3 mM aqueous solution of europium(III)-1,7-bis(2-hydroxycyclohexyl)-1,7-bis(carboxymethyl)-1,4,7-triazaheptane was recorded as a function of pH, upon reaching equilibrium (Figure 4.27). The excitation wavelength of 252 nm was determined from UV-visible spectroscopy (Appendix F, Figure F.4).

A steady increase in emission intensity was observed between pH 2 and pH 6. This was followed by a sharp decline in intensity between pH 6 and pH 8, as a result of precipitation.

The emission intensities for the ΔJ = 1 (592 nm), ΔJ = 2 (616 nm), and ΔJ = 4 (697 nm) bands were plotted against pH. Non-linear regression analysis of this spectroscopic data was best accommodated by a two pK_a model considering data acquired prior to precipitation (Figures 4.28, 4.29, and 4.30).

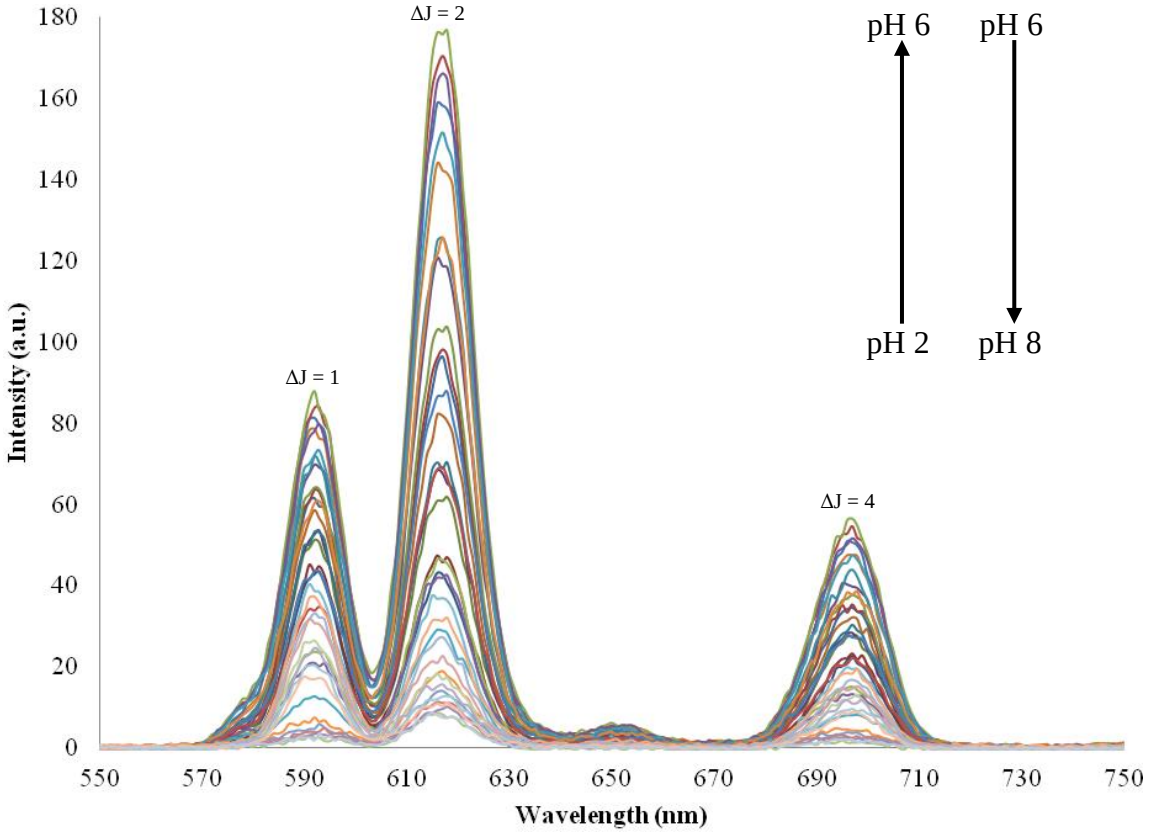


Figure 4.27: Phosphorescence emission spectrum of europium(III)-1,7-bis(2-hydroxycyclohexyl)-1,7-bis(carboxymethyl)-1,4,7-triazaheptane, as a function of pH (λ_{ex} = 252 nm).

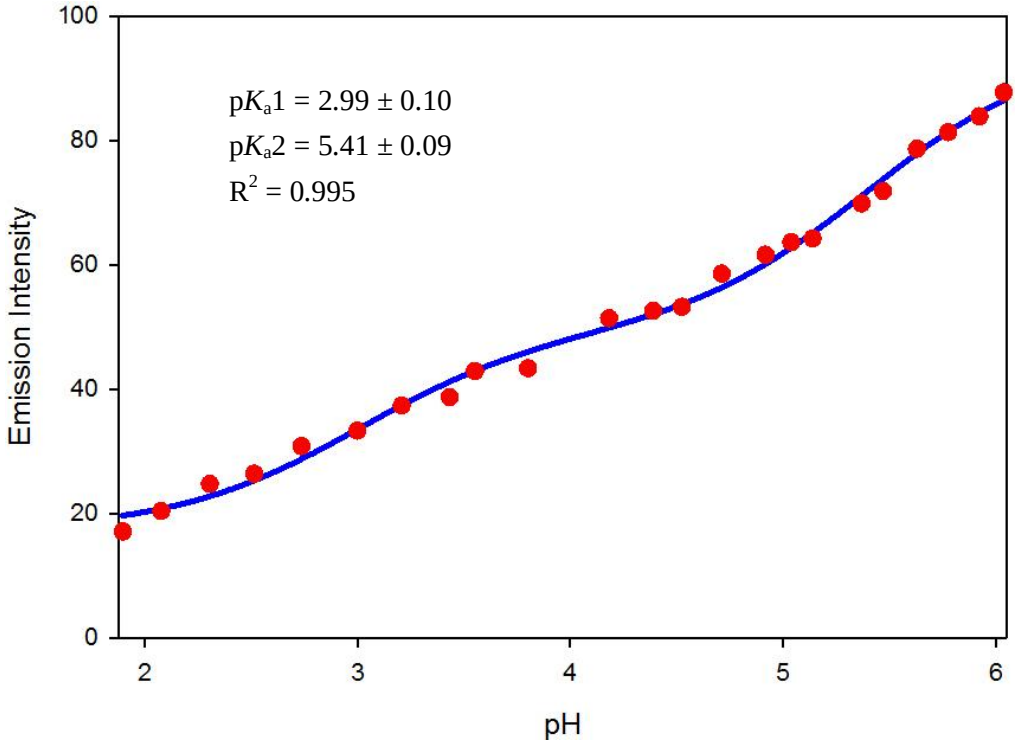


Figure 4.28: Phosphorescence emission intensity at 592 nm (ΔJ = 1), as a function of pH (λ_{ex} = 252 nm).

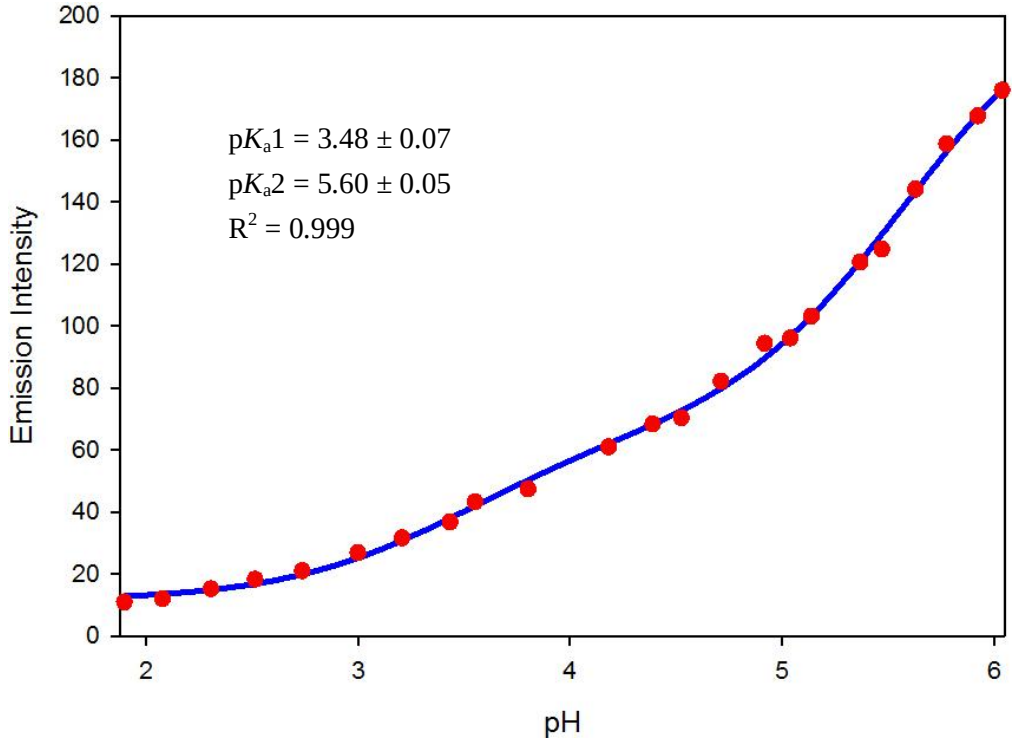


Figure 4.29: Phosphorescence emission intensity at 616 nm (ΔJ = 2), as a function of pH (λ_{ex} = 252 nm).

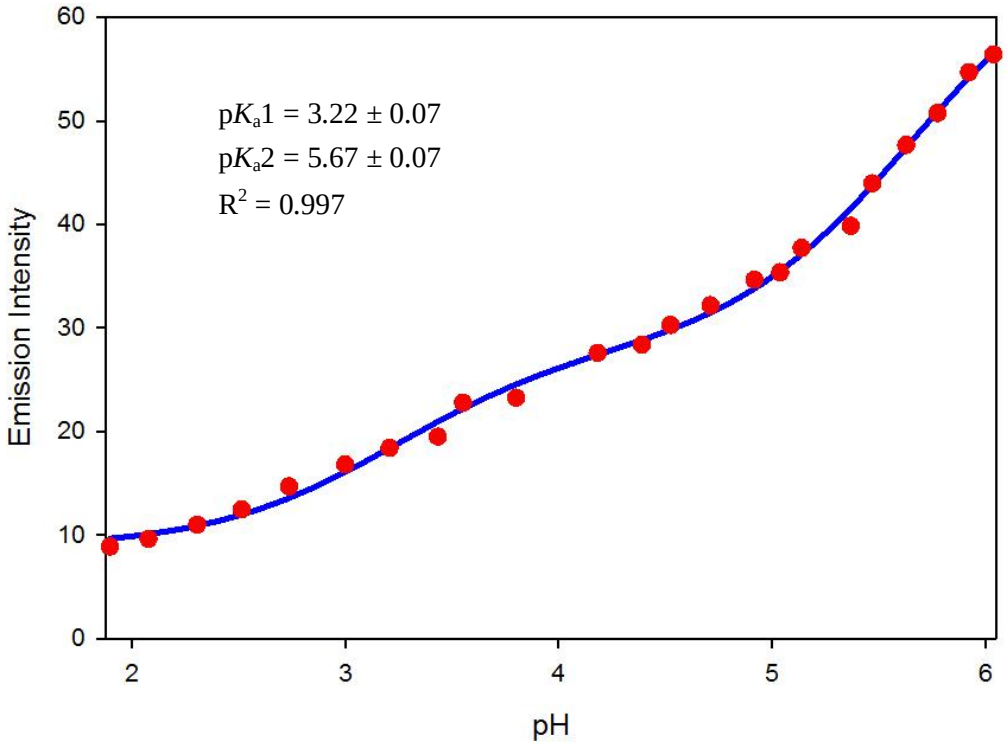


Figure 4.30: Phosphorescence emission intensity at 697 nm ($\Delta J = 4$), as a function of pH (λ_{ex} = 252 nm).

The first protonation of the amine moieties on the diethylenetriamine backbone is observed to occur for the central nitrogen donor. The second protonation results in migration of the H^+ ion from the central amine to the outer nitrogen donor (i.e. both terminal amines are protonated), thus minimising electrostatic repulsions between the two incoming protons[48]. The weighted average pK_a1 value (3.19 ± 0.33), coincides with amine deprotonation at either terminal position, while pK_a2 (5.55 ± 0.17) can be attributed to subsequent amine deprotonation of the central, unsubstituted secondary amine on the triazaheptane backbone. The comparison of the spectroscopic pK_a values with protonation constants determined potentiometrically (Section 4.2.2, Table 4.2, pK_a2 = 8.41 ± 0.01 and pK_a1 = 10.91 ± 0.01) demonstrates a five-order magnitude decrease in the pK_a values upon coordination of the Eu(III) ion. The proposed structures and reaction mechanisms responsible for the observed pK_a values are illustrated in Figure 4.31.

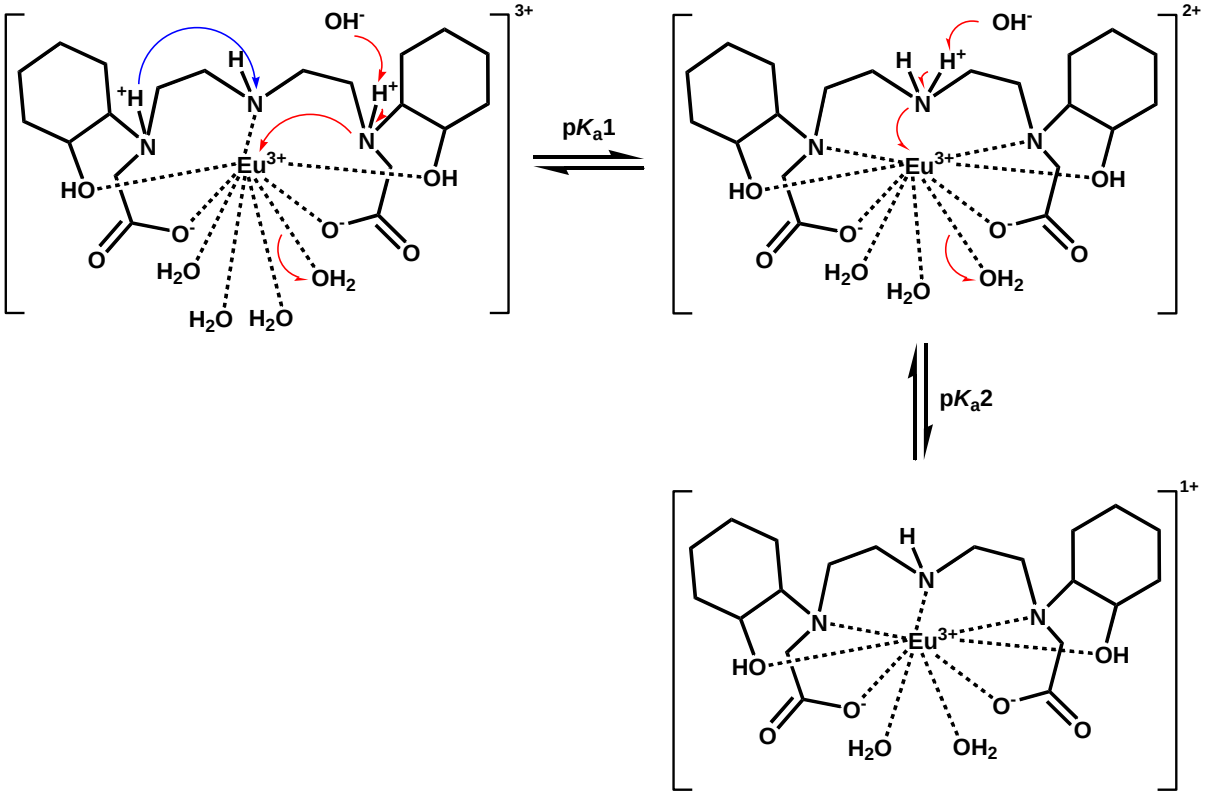


Figure 4.31: Proposed structures and reaction mechanisms of europium(III)-1,7-bis(2-hydroxycyclohexyl)-1,7-bis(carboxymethyl)-1,4,7-triazaheptane.

The $\Delta J_2/\Delta J_1$ relationship for $[Eu(Cy_2DETA.2A)]^{3+}$ as a function of pH is illustrated (Figure 4.32). Data points acquired prior to precipitation (indicated by the red dots) endorse a 2 pK_a model, and displayed good correlation with the pK_a values determined from pH profiles of individual J-bands (Figures 4.28, 4.29 and 4.30). The steady increase in the ratio between pH 3 and pH 6 demonstrates the change in coordination polyhedron across this pH range. Deprotonation of amine nitrogen donors result in increased encapsulation of the Eu(III) ion with consequent decrease in the number of water molecules coordinated directly to the metal centre, followed by enhanced emission.

The randomness of the $\Delta J_2/\Delta J_1$ ratio observed above pH 6.8 (Figure 4.32, green stars) coincides with precipitation of $Eu(OH)_3$ from solution, thus indicating poor stability of this heptadentate complex at high pH. The decreased denticity of $Cy_2DETA.2A$ (compared to $Cy_2DETA.3A$) translates into lower complex stability. At higher OH^- concentration, formation of $Eu(OH)_3$ is favoured, resulting in the observed precipitation.

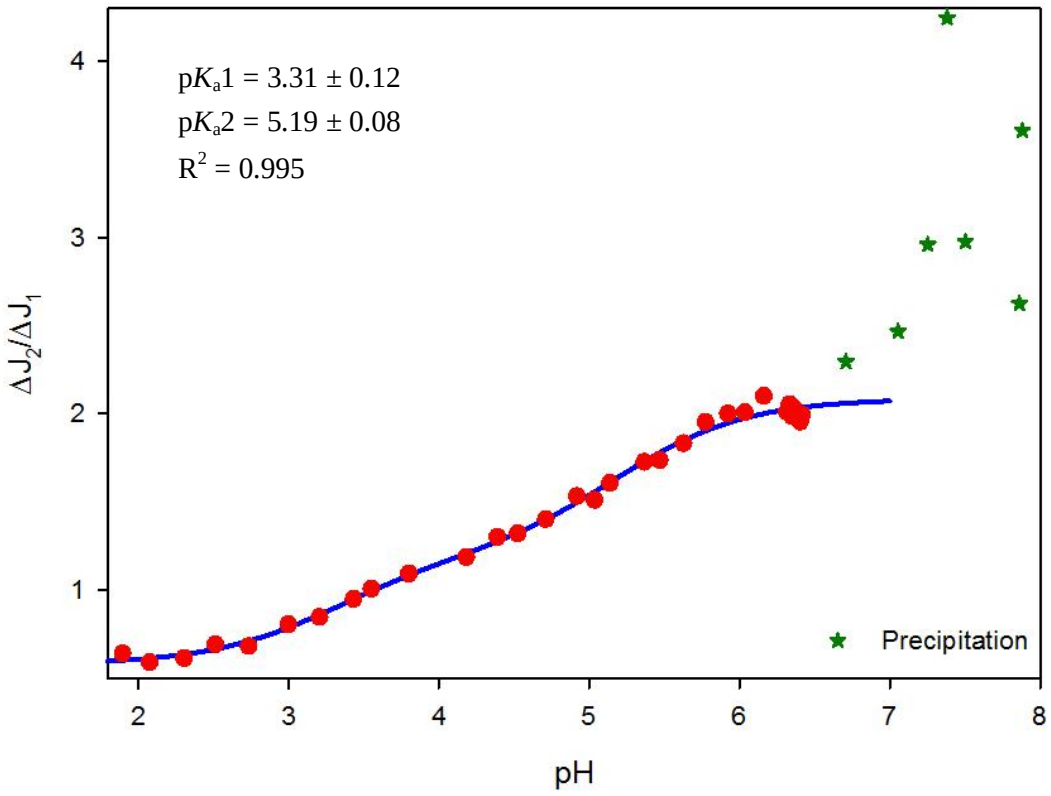


Figure 4.32: Relationship between ΔJ = 2 and ΔJ = 1 of europium(III)-1,7-bis(2-hydroxycyclohexyl)-1,7-bis(carboxymethyl)-1,4,7 triazaheptane, as a function of pH.

4.3.2.2 Cy_2DETA.2A.3HCl / Eu(III), multi-component buffered system, upon initial preparation

Emission spectra of a 0.15 mM solution of europium(III)-1,7-bis(2-hydroxycyclohexyl)-1, 7-bis(carboxymethyl)-1,4,7-triazaheptane were recorded as a function of pH, in the presence of a 0.015 mM multi-component buffer system. Excitation wavelengths of 233 nm and 276 nm were determined from UV-visible spectroscopy (Appendix F, Figure F.5). The emission spectrum of each sample was measured upon initial preparation, once a steady pH value was recorded (Figures 4.33 and 4.34).

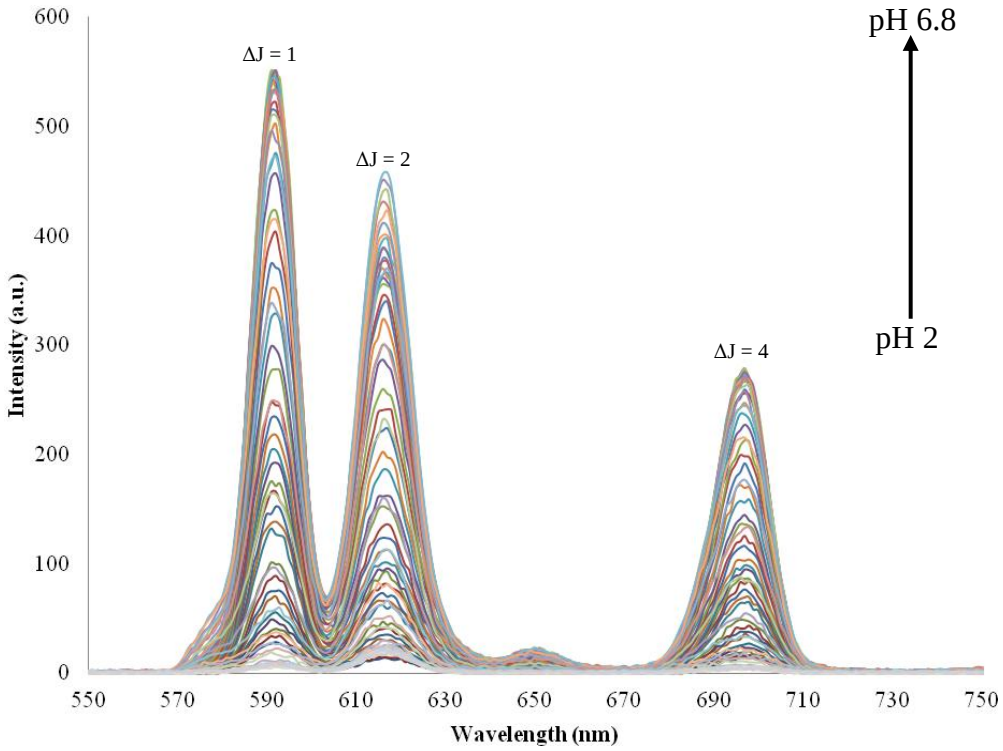


Figure 4.33: Phosphorescence emission spectrum of europium(III)-1,7-bis(2-hydroxycyclohexyl)-1,7-bis(carboxymethyl)-1,4,7-triazaheptane, as a function of pH (λ_{ex} = 233 nm).

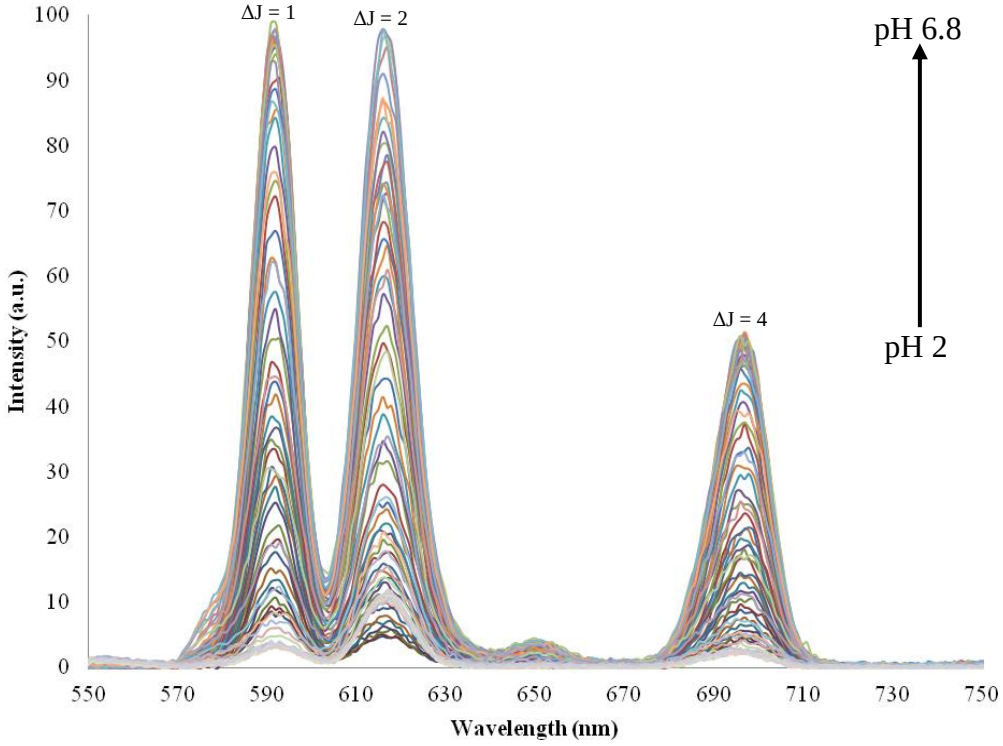


Figure 4.34: Phosphorescence emission spectrum of europium(III)-1,7-bis(2-hydroxycyclohexyl)-1,7-bis(carboxymethyl)-1,4,7-triazaheptane, as a function of pH (λ_{ex} = 276 nm).

The emission spectra displayed an increase in intensity between pH 2 and pH 6.8, followed by a sharp decrease in intensity between pH 6.8 and pH 9.5, as precipitation is observed.

The J-band emission intensities ($\Delta J = 1$ (592 nm), $\Delta J = 2$ (616 nm), and $\Delta J = 4$ (697 nm)) were tabulated (Appendix F, Tables F.7 and F.8) and plotted against the measured pH values (Figures 4.35 to 4.40). A two pK_a model was employed to obtain a non-linear least squares fit for the $\Delta J = 2$ emission band (Figure 4.33, λ_{ex} = 233 nm), and the $\Delta J = 1$ and $\Delta J = 4$ (λ_{ex} = 276 nm) emission bands in Figure 4.34, using data acquired prior to precipitation. For the $\Delta J = 2$ (λ_{ex} = 276 nm) emission band in Figure 4.34, and the $\Delta J = 1$, and $\Delta J = 4$ (λ_{ex} = 233 nm) emission bands for Figure 4.33, a three pK_a model afforded the analysis with optimal correlation coefficient (R^2).

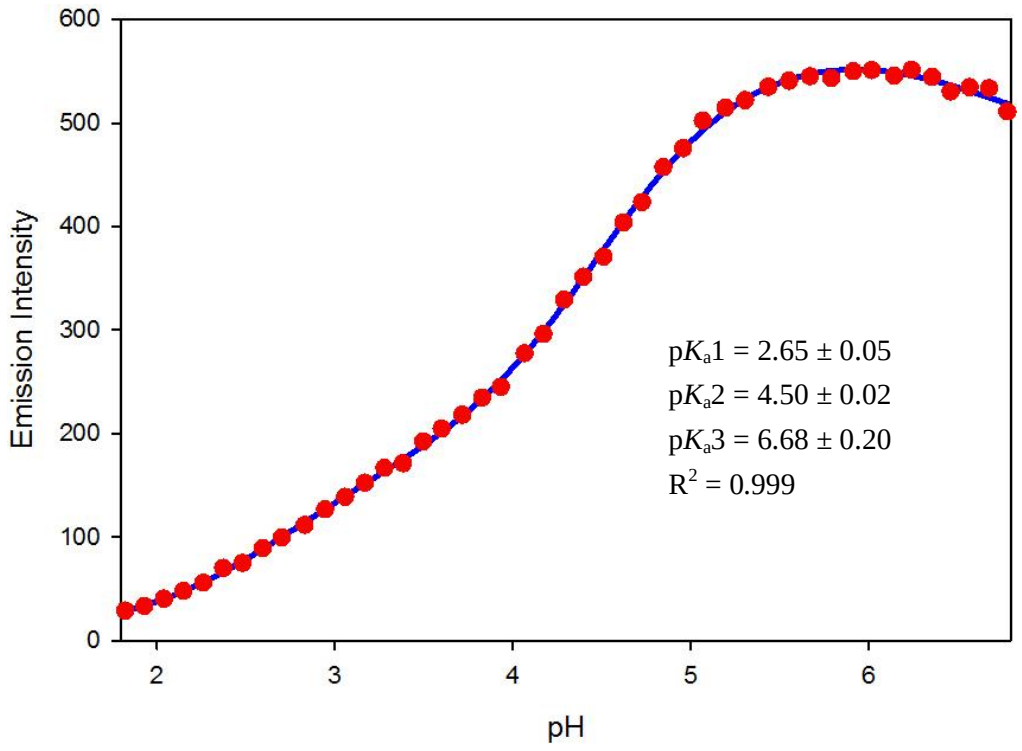


Figure 4.35: Phosphorescence emission intensity at 592 nm ($\Delta J = 1$), as a function of pH (λ_{ex} = 233 nm).

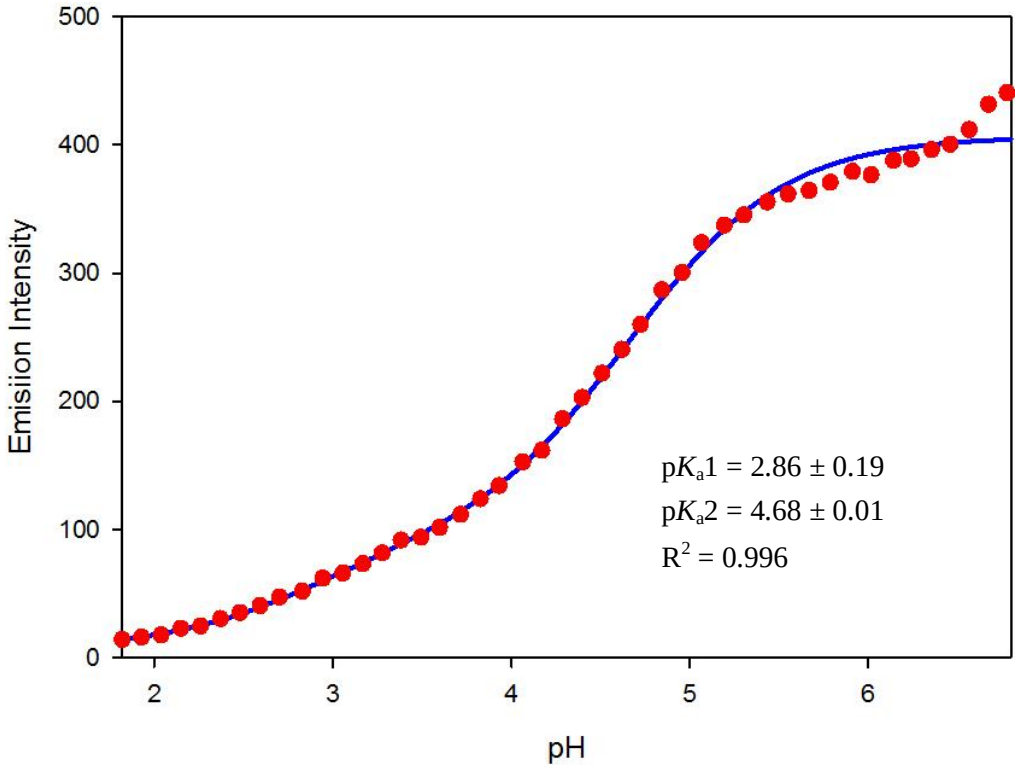


Figure 4.36: Phosphorescence emission intensity at 616 nm (ΔJ = 2), as a function of pH (λ_{ex} = 233 nm).

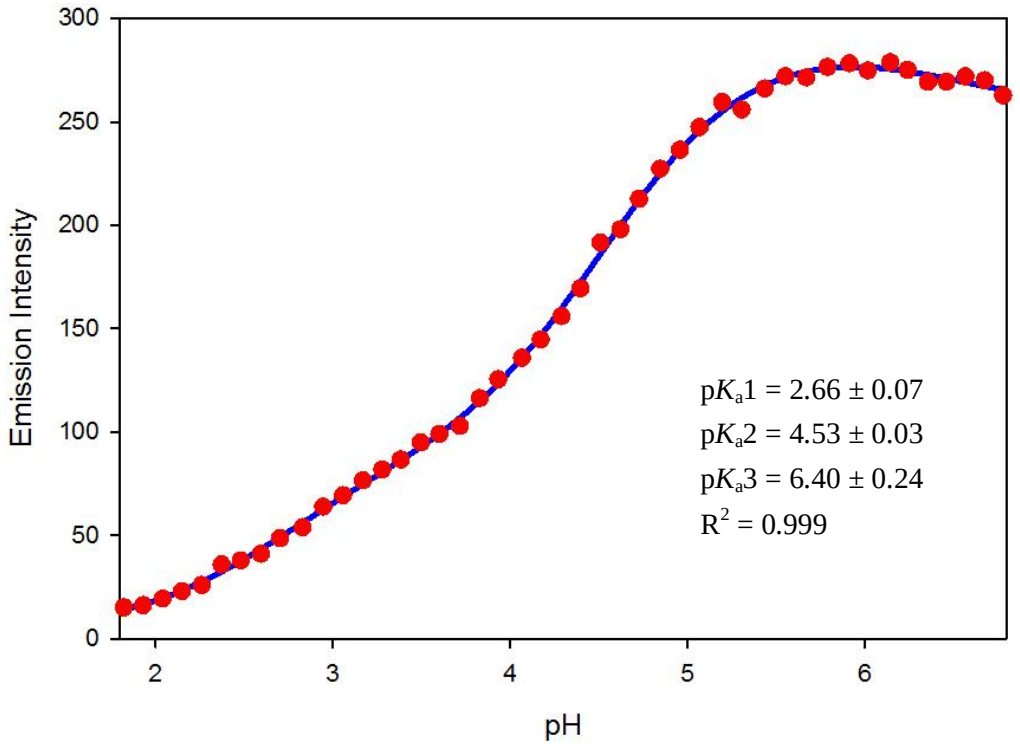


Figure 4.37: Phosphorescence emission intensity at 697 nm (ΔJ = 4), as a function of pH (λ_{ex} = 233 nm).

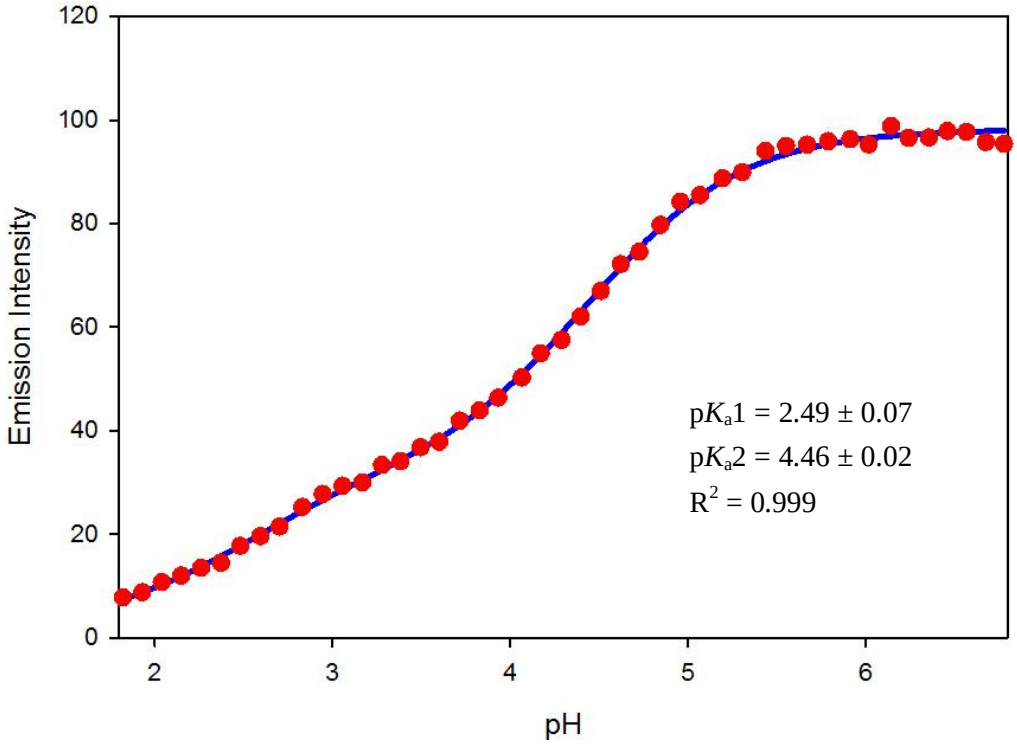


Figure 4.38: Phosphorescence emission intensity at 592 nm (ΔJ = 1), as a function of pH (λ_{ex} = 276 nm).

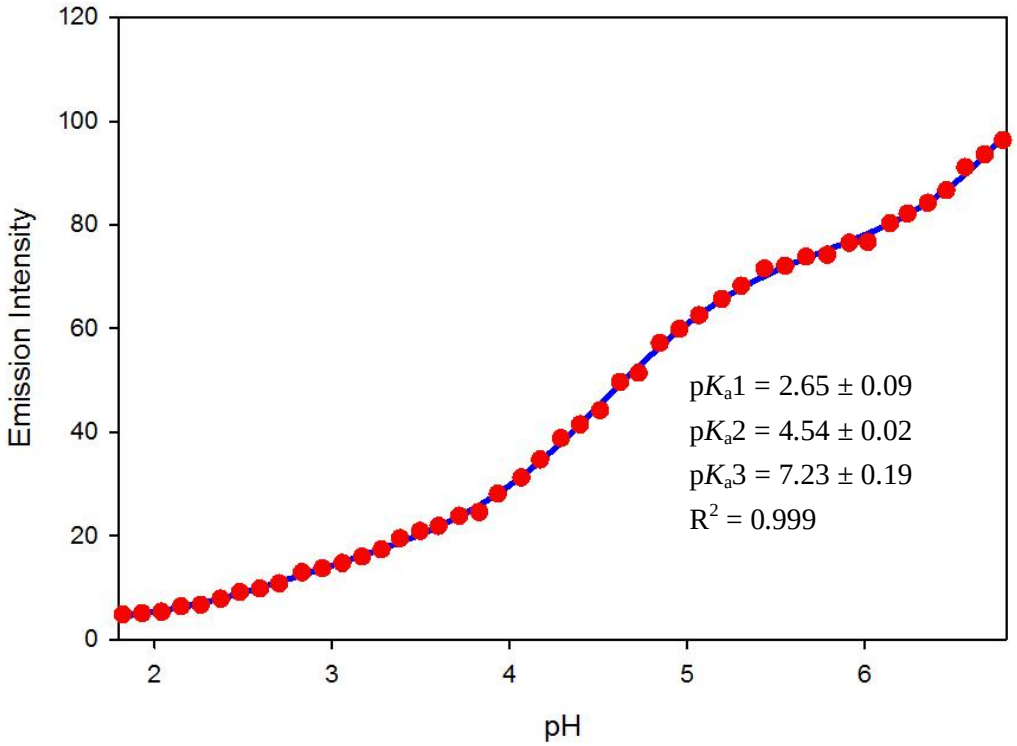


Figure 4.39: Phosphorescence emission intensity at 616 nm (ΔJ = 2), as a function of pH (λ_{ex} = 276 nm).

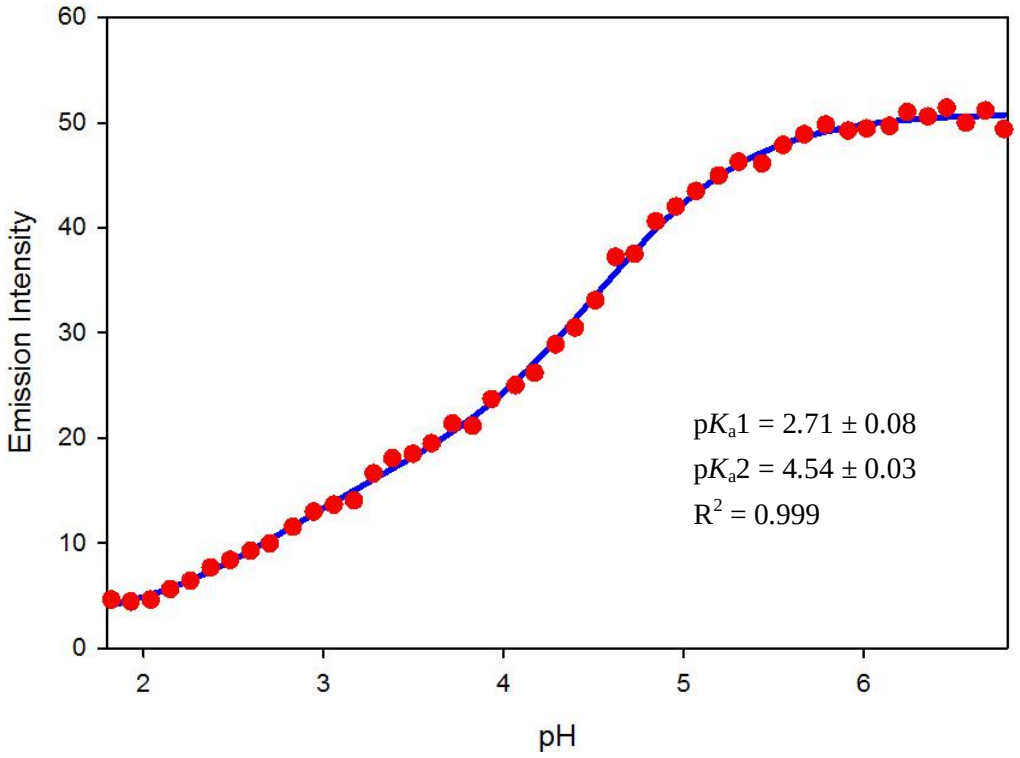


Figure 4.40: Phosphorescence emission intensity at 697 nm ($\Delta J = 4$), as a function of pH (λ_{ex} = 276 nm).

The average pK_a1 value for all data (Figures 4.35 to 4.40) yielded a result of 2.66 ± 0.09. The first pK_a is assigned to the deprotonation of the terminal amine moiety, while the average pK_a2 value (4.54 ± 0.02) accounts for subsequent deprotonation (the central amine) of the triazaheptane backbone, or conversion of the phthalate ion to the phthalate dianion. It should be noted that the calculated pK_a values are significantly lower than the values obtained for the non-buffered solution. The pK_a3 values (Figures 4.35, 4.37 and 4.39) are tenuously linked to deprotonation of a coordinated water molecule, since precipitation was observed in this pH range. Precipitation contributes to greater uncertainty (higher standard deviation) of pK_a3 values, compared to pK_a1 and pK_a2 values at lower pH.

The $\Delta J_2/\Delta J_1$ ratio is plotted using data prior to precipitation. The ratios obtained for buffered and non-buffered solutions are illustrated in Figure 4.41. Regression analysis of ratiometric data, using a 3 pK_a model, affords pK_a values with larger standard deviations, when compared to counterparts determined from analysis of J-band modulation (Figures 4.35 to 4.40). This is largely a consequence of the complex:substrate ratio (10:1).

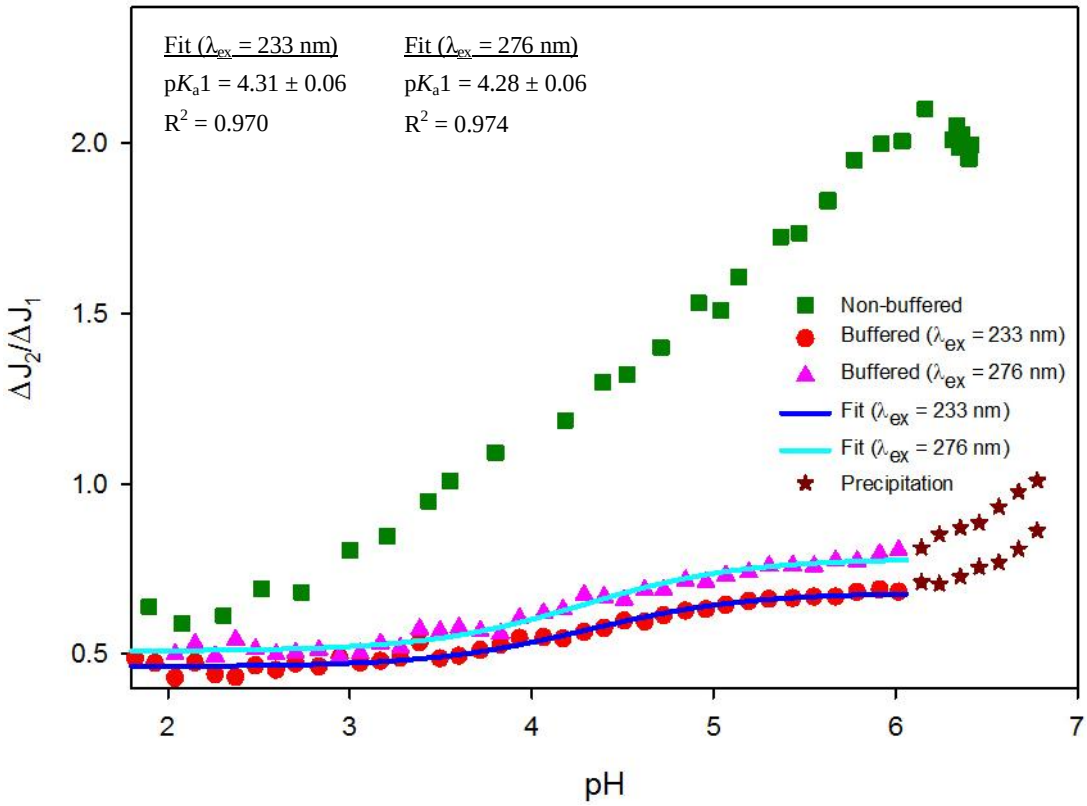


Figure 4.41: Comparison of the $\Delta J_2/\Delta J_1$ relationship of europium(III)-1,7-bis(2-hydroxycyclohexyl)-1,7-bis(carboxymethyl)-1,4,7 triazaheptane, as a function of pH, in a buffered vs. non-buffered system.

The $\Delta J_2/\Delta J_1$ ratio for the buffered system (Figure 4.41) remains constant between pH 1.8 and pH 3.5, implying that a single ternary species exists at low pH. The low emission intensity observed for the samples within this pH range (Figures 4.35 to 4.40) suggests quenching of the lanthanide-based emission by coordinated water molecules is prevalent. An increase in the number of O-H oscillators coordinated directly to the metal centre would be responsible for quenching the observed emission intensity. The hydration state is a consequence of protonation of nitrogen donors on the ligand backbone, preventing full encapsulation of the Eu(III) ion. The ratiometric profiles for the buffered and non-buffered solutions vary significantly, indicative of the effect of the added buffer – the phthalate ion in particular. It is proposed that, between pH 1.8 and 3.5, an outersphere interaction between the phthalate ion and the complex is observed. However, the nature of this interaction cannot be established without knowledge of the complex hydration state.

The steady increase in the $\Delta J_2/\Delta J_1$ ratio of the buffered solution between pH 3.5 and pH 5 (Figure 4.41) is proposed to represent the introduction of the phthalate ion from the

outersphere to the innersphere of the complex. The coordination of the phthalate ion to the metal is expected to occur in a bidentate manner[58, 59]. However, bidentate coordination of the phthalate ion would result in the substitution of two donor groups in the inner coordination sphere. Because the denticity of the ligand has been reduced (the heptadentate Cy_2DETA.2A ligand possess two carboxymethyl pendant arms, compared to the three arms found for the octadentate Cy_2DETA.3A ligand), it is possible that a bifurcated binding of the phthalate ion to the metal centre may be accommodated without the substitution of the ligand donor groups. The formation of this proposed ternary complex would result in the observed increase in emission intensity, as bidentate coordination of the phthalate ion would substitute two water molecules from the innersphere of the complex. Direct binding of the phthalate ion to the Eu(III) ion would promote photo-induced electron transfer, resulting in enhanced emission intensity. Precipitation of $Eu(OH)_3$ was again observed above pH 7, as was encountered for the non-buffered solution (Figure 4.32), thus confirming the poor stability of the heptadentate complex at high pH.

Determination of the solution hydration state will aid in confirming the phthalate binding mode and its dependence upon solution pH.

4.4 Determination of q

The hydration number (q) was determined for each Eu(III)-complex. The number of water molecules bound to the metal ion was calculated using a mathematical expression, derived and developed, by Horrocks and Supkowski[72-75]:

$$q = A(k_{H_2O} - k_{D_2O} - \alpha - \beta n_{OH} - \gamma n_{NH} - \delta n_{O=CNH}) \qquad [1]$$

The initial model was developed to determine hydration states of aqueous lanthanide complexes based on relationships observed in hydration numbers of known crystalline structures[72]. Equation [1] accounts for quenching oscillator effects for amide, amine and alcohol pendants in the inner coordination sphere[73] and outersphere water molecules of Ln(III) complexes[75]. The *A* term is a constant of 1.11 (water molecules.ms). The k_{H_2O} and k_{D_2O} terms are the phosphorescence decay rate constants for the Eu(III) complex determined in H_2O and D_2O respectively. The α term accounts for the effect of outersphere water molecules in shortening luminescence lifetimes, with $\alpha = 0.31$ ms^{-1}. β (0.44 ms^{-1}), γ (0.99 ms^{-1}), and δ (0.075 ms^{-1}) terms account for quenching effects from alcoholic O-H, amine N-H and amide N-H oscillators in the inner coordination sphere, while n_{OH}, n_{NH} and $n_{O=CNH}$ refer to the numbers of each type of oscillator[72-77].

Solution preparation and sample measurement procedures are detailed in Appendix G. Solutions were prepared in both H_2O and D_2O at similar concentrations, in aqueous and buffered (consisting of MES, CHES, MOPS, Tris, and KHP) media. Hydration states are determined for samples at different pH, to be correlated to spectroscopically determined pK_a values. pH values of the prepared samples were recorded upon initial preparation of the samples and upon reaching equilibrium. Phosphorescence emission spectra were measured upon initial preparation and upon reaching equilibrium at room temperature (25 °C), using excitation wavelengths determined from UV-visible spectroscopy. Phosphorescence decay experiments were conducted at room temperature (25 °C), using measured ΔJ = 1, ΔJ = 2, and ΔJ = 4 emission wavelengths. The k_{H_2O} and k_{D_2O} values were calculated for the $^5D_0 \rightarrow {}^7F_2$ (ΔJ = 2) emissive transition as this band displays the greatest modulation to changes in the coordination polyhedron of the Eu(III) complex.

4.4.1 Determination of the solution hydration state of $[Eu(Cy_2DETA.3A)]^{3+}$

4.4.1.1 $Cy_2DETA.3A.3HCl$ / Eu(III), aqueous solution

Phosphorescence decay spectra of 0.15 mM solutions of europium(III)-1,7-bis(2-hydroxycyclohexyl)-1,4,7-tris(carboxymethyl)-1,4,7-triazaheptane were recorded as a function of pH. The phosphorescence emission and decay spectra of each sample were measured upon initial preparation (0 hours) and reaching equilibrium (after 1 and 6 days), using an excitation wavelength of 223 nm. The q values were calculated using the k_{H_2O} and k_{D_2O} values determined for the $\Delta J = 2$ emission band (616nm), and are reported in Tables 4.3, 4.4 and 4.5.

Table 4.3: Phosphorescence decay constants for europium(III)-1,7-bis(2-hydroxycyclohexyl)-1,4,7-tris(carboxymethyl)-1,4,7-triazaheptane, as a function of pH, upon initial preparation (0 hours, λ_{ex} = 223 nm, λ_{em} = 616 nm).

Sample	pH (0 h)	pD (0 h)	k_{H_2O} (ms^{-1})	k_{D_2O} (ms^{-1})	Δk (ms^{-1})	q‡
Stock[a]	3.38	3.77	2.92	0.37	2.55	1.5
Sample 1[b]	4.05	4.09	2.94	0.43	2.51	1.5
Sample 2[b]	7.75	7.73	2.67	0.53	2.14	1.1

‡ $q = \{\Delta k - [0.31 + (0.44 \times 2) + (0.99 \times 0) + (0.075 \times 0)]\} \times 1.11$

[a] contains 0.15mM Eu(III) complex, pH unadjusted

[b] contains 0.15mM Eu(III) complex, pH adjusted

The selection of experimental pH values was considered using the luminescence emission profile for the $\Delta J = 2$ emission band (Figure 4.7). Calculation of hydration states (q values) in Tables 4.3, 4.4 and 4.5 assumed nine-coordinate polyhedra involving metal ion coordination by all pendant hydroxycyclohexyl and carboxymethyl moieties and amine donors of the ligand backbone. Therefore, two alcoholic O-H oscillators are contributed by the ligand. Due to the presence of tertiary amines and the lack of amide functionalities in the ligand structure, the number of amine N-H oscillators and amide N-H oscillators are both taken to be zero.

Table 4.4: Phosphorescence decay constants for europium(III)-1,7-bis(2-hydroxycyclohexyl)-1,4,7-tris(carboxymethyl)-1,4,7-triazaheptane, as a function of pH, at equilibrium (24 hours, λ_{ex} = 223 nm, λ_{em} = 616 nm).

Sample	pH (24 h)	pD (24 h)	k_{H_2O} (ms^{-1})	k_{D_2O} (ms^{-1})	Δk (ms^{-1})	q‡
Stock[a]	3.43	3.59	2.51	0.41	2.10	1.0
Sample 1[b]	3.86	3.82	2.51	0.45	2.06	0.98
Sample 2[b]	7.08	7.10	2.47	0.52	1.95	0.85

‡ $q = \{\Delta k - [0.31 + (0.44 \times 2) + (0.99 \times 0) + (0.075 \times 0)]\} \times 1.11$

[a] contains 0.15mM Eu(III) complex, pH unadjusted

[b] contains 0.15mM Eu(III) complex, pH adjusted

Table 4.5: Phosphorescence decay constants for europium(III)-1,7-bis(2-hydroxycyclohexyl)-1,4,7-tris(carboxymethyl)-1,4,7-triazaheptane, as a function of pH, at equilibrium (6 days, λ_{ex} = 223 nm, λ_{em} = 616 nm).

Sample	pH (6 d)	pD (6 d)	k_{H_2O} (ms^{-1})	k_{D_2O} (ms^{-1})	Δk (ms^{-1})	q‡
Stock[a]	3.48	3.46	2.44	0.45	1.99	0.89
Sample 1[b]	4.04	3.60	2.46	0.46	2.00	0.90
Sample 2[b]	7.10	6.88	2.44	0.50	1.94	0.84

‡ $q = \{\Delta k - [0.31 + (0.44 \times 2) + (0.99 \times 0) + (0.075 \times 0)]\} \times 1.11$

[a] contains 0.15mM Eu(III) complex, pH unadjusted

[b] contains 0.15mM Eu(III) complex, pH adjusted

The differences observed in the calculated q values for both sets of measurements can be more easily understood when the phosphorescence emission spectra are compared (Figures 4.42 and 4.43). The emission intensity for the samples prepared in D_2O is substantially larger compared to those observed for the H_2O samples. This is due to the poor efficiency of O-D oscillators in quenching luminescence[72-75]. Both sets of samples prepared in H_2O and D_2O display significant increases in the intensity of the $\Delta J = 2$ band upon reaching equilibrium (after 24 hours), accompanied by a decrease in the calculated q values for these samples over the same time period (Tables 4.3 and 4.4). The samples prepared at low pD in D_2O (Figure

4.43, (i) and (ii)) display significant variation in the relative intensities of the $\Delta J = 1$ and $\Delta J = 2$ emission bands upon initial preparation and after reaching equilibrium. There is significant modulation in the pH of the samples prepared at neutral pH in H_2O and D_2O (see pH and pD values for sample 2, Tables 4.3, 4.4 and 4.5).

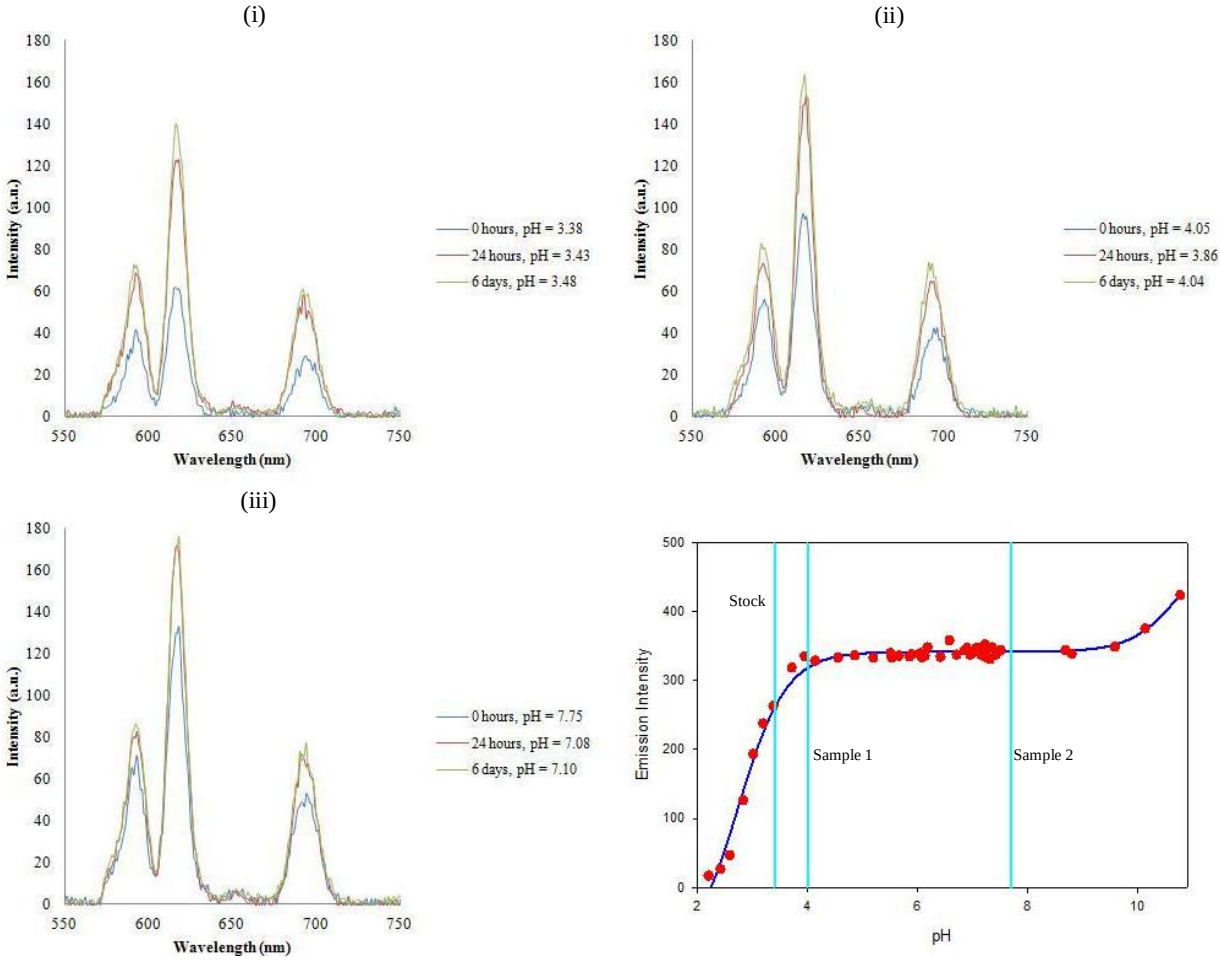


Figure 4.42: Comparison of phosphorescence emission spectra of (i) stock solution, (ii) sample 1, and (iii) sample 2 of europium(III)-1,7-bis(2-hydroxycyclohexyl)-1,4,7-tris(carboxymethyl)-1,4,7-triazaheptane, as a function of pH, in H_2O (λ_{ex} = 223 nm). *Inset*: Emission profile at 617 nm (cyan lines indicate selected pH values for the phosphorescence decay experiment).

The q value of 1.5 observed for the low pH samples upon initial preparation (Table 4.3, stock solution and sample 1) suggest an incomplete encapsulation of the Eu(III) ion by the ligand. As the pH of these samples lie in the range for the spectroscopically determined pK_a1 value for this complex system (Section 4.3.1.1), this would suggest that an equilibrium between a di- and monoaqua species is observed. A proposed shift in ligand denticity from heptadentate to octadentate, due to the deprotonation of the central amine moiety on the ligand backbone,

agrees with the observed q values (Figure 4.44, pK_a1). The sample prepared at neutral pH (Table 4.3, sample 2) has a q value of approximately 1, indicating an octadentate Eu(III) complex with a single, coordinated water molecule (Figure 4.44, species (ii)). Enhancement in emission intensity (with increasing pH) results from a decrease in the number of innersphere O-H oscillators (i.e. a decrease in q).

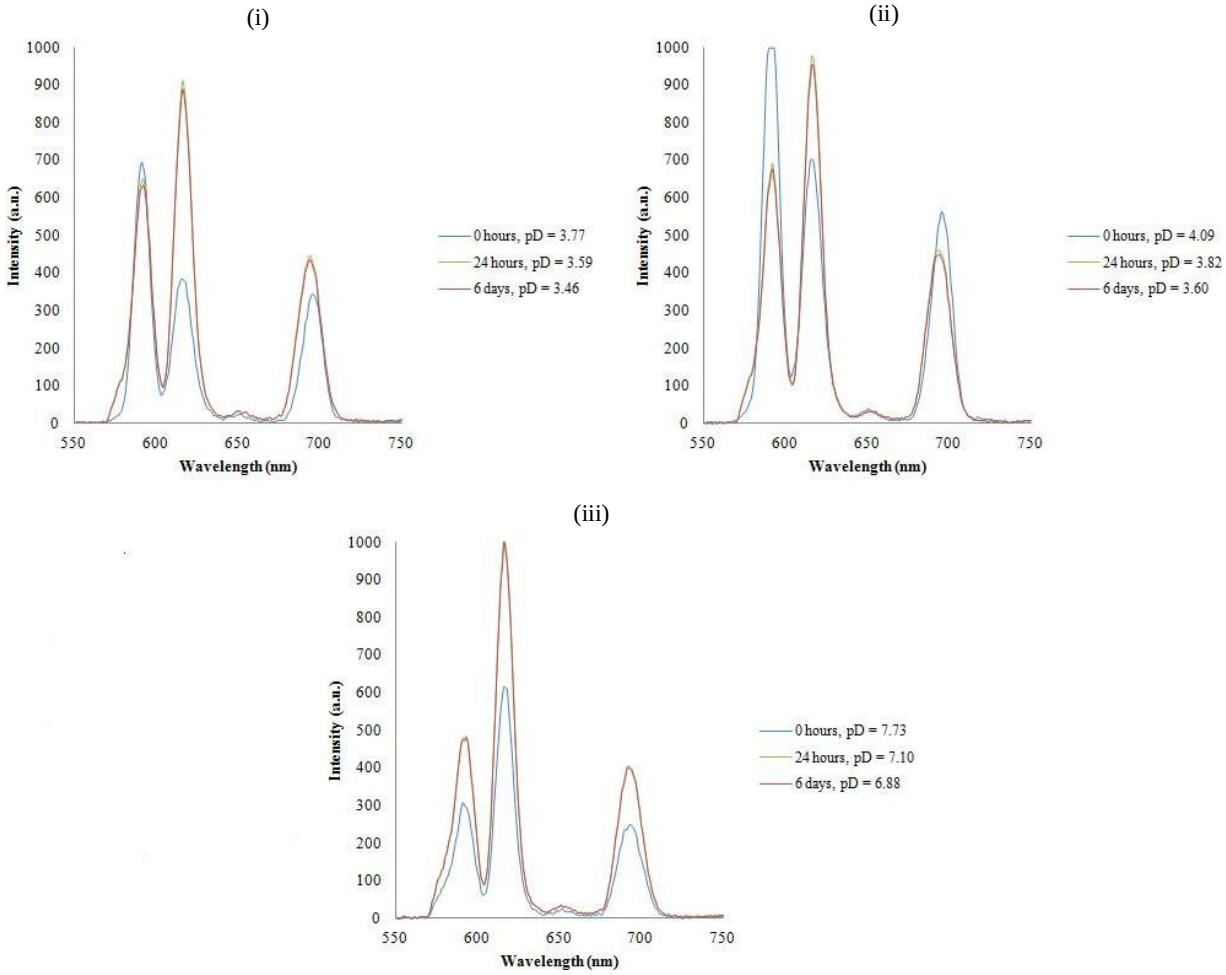


Figure 4.43: Comparison of phosphorescence emission spectra of (i) stock solution, (ii) sample 1, and (iii) sample 2 of europium(III)-1,7-bis(2-hydroxycyclohexyl)-1,4,7-tris(carboxymethyl)-1,4,7-triazaheptane, as a function of pD, in D_2O (λ_{ex} = 223 nm).

The reduction in the value of q upon reaching equilibrium is readily reconciled with enhancement of phosphorescence emission intensity for the low pH samples (Tables 4.4 and 4.5, stock solution and sample 1). The decrease in q value, from 1.5 to 0.9, strongly suggests the complexation equilibrium favours a monoaqua species at low pH. It is therefore correct to assume ligand octadenticity upon reaching equilibrium, at low pH (i.e. for Figure 4.44, the equilibrium lies to the right, favouring species (ii)). This result would account for the

observed decrease in pH of the samples, due to the release of H^+ from the inner coordination sphere.

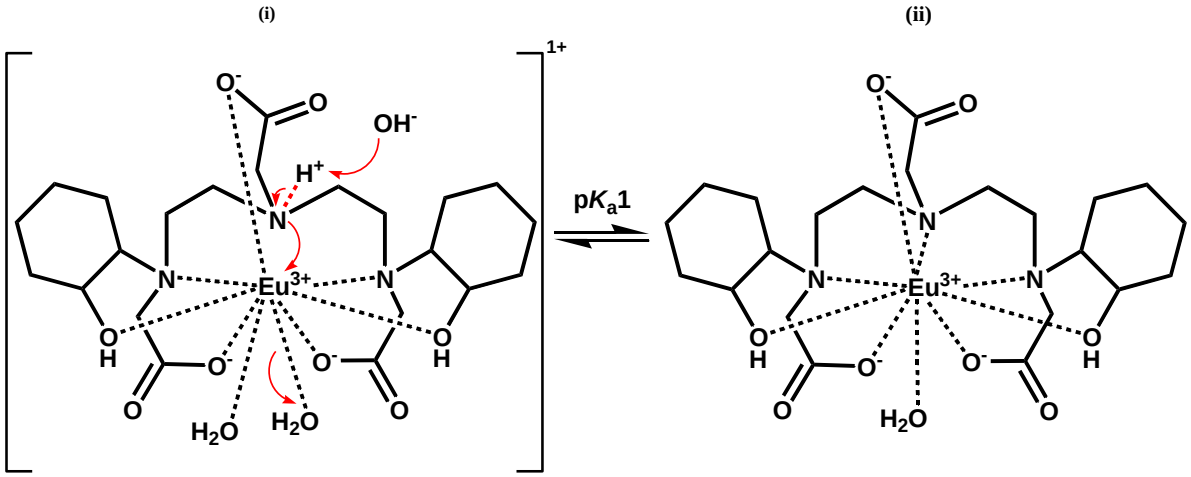


Figure 4.44: The proposed equilibrium between the heptadentate and octadentate species of europium(III)-1,7-bis(2-hydroxycyclohexyl)-1,4,7-tris(carboxymethyl)-1,4,7-triazaheptane, upon initial preparation at low pH.

Upon reaching equilibrium, the sample prepared at neutral pH (sample 2, Tables 4.4 and 4.5) displayed a slight decrease in q (from 1.1 to 0.84). An increase in phosphorescence emission was observed, together with a substantial decrease in pH (from 7.75 to 7.10). A second protonation equilibrium is proposed at elevated pH, between an octadentate, monoaqua species [Eu(Cy_2DETA.3A)(H_2O)] and octadentate, monohydroxo-species [Eu(Cy_2DETA.3A)(OH)]$^-$, as depicted in Figure 4.45. The formation of this hydroxide species would certainly account for the decrease in pH observed for the prepared solution, and would agree with the pK_a2 value observed for the $\Delta J = 2$ emission data (Section 4.3.1.1, Figure 4.7).

It should be noted that the equilibrium pH values of samples 1 and 2 in D_2O and H_2O (Tables 4.4 and 4.5) differ from their pH values upon initial preparation (Table 4.3). Samples were prepared at comparable pH values, with no further alteration to the sample. Therefore, for the remainder of this discussion, it is proposed that for the prepared H_2O and D_2O samples, differences in the equilibrium pH from the values measured upon initial preparation should be compared with the relevant emission profiles (Section 4.3). In this instance, the sample prepared at neutral pH displayed a decrease of 0.6 pH units, between the initial preparation value (Table 4.3, sample 2) and the equilibrium value (Table 4.5, sample 2). Although this is

a large decrease, both pH values occur within the same region of the emission profile obtained from the luminescence data (Figure 4.7, plateau region of the titration curve). The same equilibrium is therefore being observed for the sample at different pH values, allowing for some degree of comparison. The argument can be advanced for the sample prepared at neutral pD in D_2O (Tables 4.3 and 4.5, sample 2, $\Delta pD = 0.9$). For the sample prepared at low pD (Tables 4.3 and 4.5, sample 1, $\Delta pD = 0.4$), the pD values both occur on the increasing gradient of the emission profile, which therefore allows for comparison of the calculated q values.

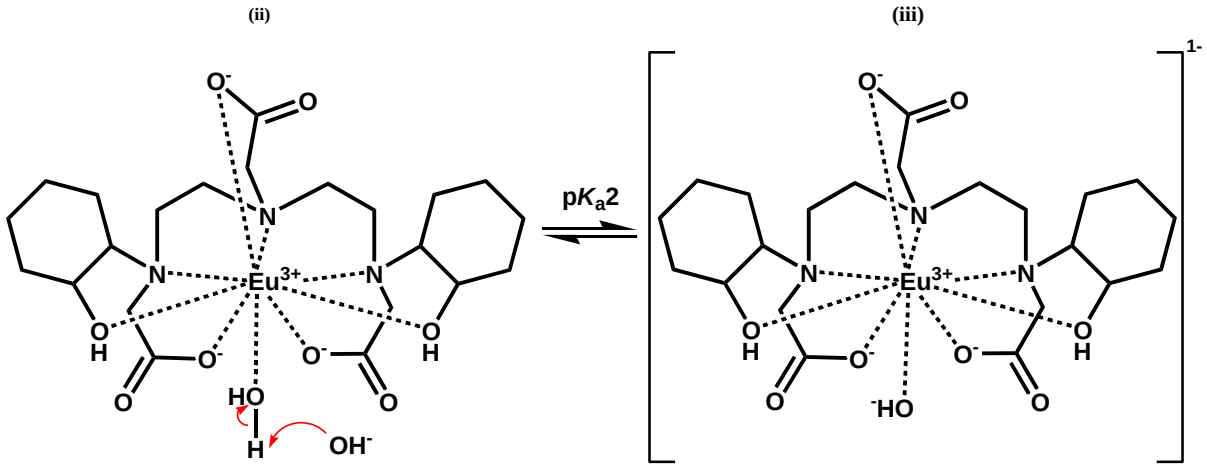


Figure 4.45: The proposed equilibrium between the octadentate species of europium(III)-1,7-bis(2-hydroxycyclohexyl)-1,4,7-tris(carboxymethyl)-1,4,7-triazaheptane, upon reaching equilibrium at neutral to high pH.

4.4.1.2 Cy_2DETA.3A.3HCl / Eu(III), multi-component buffered system

Phosphorescence decay spectra of 0.15 mM europium(III)-1,7-bis(2-hydroxycyclohexyl)-1,4,7-tris(carboxymethyl)-1,4,7-triazaheptane, in the presence of a 0.015 mM multi-component buffer system, prepared in H_2O and D_2O, were recorded as a function of pH. The pH, phosphorescence emission and decay spectra of each sample were measured upon initial preparation and reaching equilibrium (after 3 days and 14 days). Excitation wavelengths of 227 nm and 276 nm were determined from UV-visible spectroscopy (Appendix G, Figures G.3 and G.4). The $^5D_0 \rightarrow {}^7F_2$ ($\Delta J = 2$) transition at 616 nm was monitored in H_2O and D_2O for the lifetime determination. The q values were determined for the $\Delta J = 2$ emission bands, excited at 276 nm, and are reported in Tables 4.6, 4.7 and 4.8.

Table 4.6: Phosphorescence decay constants for europium(III)-1,7-bis(2-hydroxycyclohexyl)-1,4,7-tris(carboxymethyl)-1,4,7-triazaheptane, as a function of pH, multi-component buffered system , upon initial preparation (0 hours, λ_{ex} = 276 nm, λ_{em} = 616 nm).

Sample	pH (0 h)	pD (0 h)	k_{H_2O} (ms^{-1})	k_{D_2O} (ms^{-1})	Δk (ms^{-1})	$q^{\ddagger}$	$q^{\dagger}$	$q^{\spadesuit}$
Stock[a]	3.45	4.36	4.80	0.85	3.95	3.1	3.6	**4.0**
Sample 1[b]	3.07	3.06	4.19	0.44	3.75	2.9	3.3	**3.8**
Sample 2[b]	5.42	5.46	4.26	0.84	3.42	2.5	3.0	**3.5**
Sample 3[b]	7.59	7.62	3.37	0.50	2.87	1.9	2.4	**2.8**
Sample 4[b]	11.28	11.28	2.40	0.55	1.85	**0.73**	1.2	1.7

‡ $q = \{\Delta k - [0.31 + (0.44 \times 2) + (0.99 \times 0) + (0.075 \times 0)]\} \times 1.11$

† $q = \{\Delta k - [0.31 + (0.44 \times 1) + (0.99 \times 0) + (0.075 \times 0)]\} \times 1.11$

$^{\spadesuit}$ $q = \{\Delta k - [0.31 + (0.44 \times 0) + (0.99 \times 0) + (0.075 \times 0)]\} \times 1.11$

[a] contains 0.15mM Eu(III) complex and 0.015 mM multi-component buffer system, pH unadjusted

[b] contains 0.15mM Eu(III) complex and 0.015 mM multi-component buffer system, pH adjusted

Table 4.7: Phosphorescence decay constants for europium(III)-1,7-bis(2-hydroxycyclohexyl)-1,4,7-tris(carboxymethyl)-1,4,7-triazaheptane, as a function of pH, multi-component buffered system, at equilibrium (3 days, λ_{ex} = 276 nm, λ_{em} = 616 nm).

Sample	pH (3 d)	pD (3 d)	k_{H_2O} (ms^{-1})	k_{D_2O} (ms^{-1})	Δk (ms^{-1})	$q^{\ddagger}$	$q^{\dagger}$	$q^{\spadesuit}$
Stock[a]	3.46	3.74	2.74	0.48	2.26	1.2	**1.7**	2.2
Sample 1[b]	3.19	3.13	2.85	0.48	2.37	1.3	**1.8**	2.3
Sample 2[b]	4.70	4.12	3.12	0.49	2.63	1.6	**2.1**	2.6
Sample 3[b]	6.61	7.10	2.92	0.50	2.42	**1.4**	1.9	2.3
Sample 4[b]	11.22	11.15	2.39	0.49	1.90	**0.79**	1.3	1.8

‡ $q = \{\Delta k - [0.31 + (0.44 \times 2) + (0.99 \times 0) + (0.075 \times 0)]\} \times 1.11$

† $q = \{\Delta k - [0.31 + (0.44 \times 1) + (0.99 \times 0) + (0.075 \times 0)]\} \times 1.11$

$^{\spadesuit}$ $q = \{\Delta k - [0.31 + (0.44 \times 0) + (0.99 \times 0) + (0.075 \times 0)]\} \times 1.11$

[a] contains 0.15mM Eu(III) complex and 0.015 mM multi-component buffer system, pH unadjusted

[b] contains 0.15mM Eu(III) complex and 0.015 mM multi-component buffer system, pH adjusted

Table 4.8: Phosphorescence decay constants for europium(III)-1,7-bis(2-hydroxycyclohexyl)-1,4,7-tris(carboxymethyl)-1,4,7-triazaheptane, as a function of pH, multi-component buffered system, at equilibrium (14 days, λ_{ex} = 276 nm, λ_{em} = 616 nm).

Sample	pH (14 d)	pD (14 d)	k_{H_2O} (ms^{-1})	k_{D_2O} (ms^{-1})	Δk (ms^{-1})	$q^{\ddagger}$	$q^{\dagger}$	$q^{\spadesuit}$
Stock[a]	3.64	3.78	2.44	0.50	1.94	**0.83**	1.3	1.8
Sample 1[b]	3.22	3.16	2.52	0.50	2.02	**0.92**	1.4	1.9
Sample 2[b]	5.83	4.23	2.76	0.49	2.27	**1.2**	1.7	2.2
Sample 3[b]	6.91	6.99	2.65	0.49	2.16	**1.1**	1.6	2.1
Sample 4[b]	11.19	10.27	2.38	0.49	1.89	**0.78**	1.3	1.8

‡ $q = \{\Delta k - [0.31 + (0.44 \times 2) + (0.99 \times 0) + (0.075 \times 0)]\} \times 1.11$

† $q = \{\Delta k - [0.31 + (0.44 \times 1) + (0.99 \times 0) + (0.075 \times 0)]\} \times 1.11$

$^{\spadesuit}$ $q = \{\Delta k - [0.31 + (0.44 \times 0) + (0.99 \times 0) + (0.075 \times 0)]\} \times 1.11$

[a] contains 0.15mM Eu(III) complex and 0.015 mM multi-component buffer system, pH unadjusted

[b] contains 0.15mM Eu(III) complex and 0.015 mM multi-component buffer system, pH adjusted

Experimental pH values were selected using the luminescence emission profile for the $\Delta J = 2$ emission band upon initial preparation (Figure 4.14). The addition of the multi-component buffer (specifically KHP) resulted in modulation of the emission profile (when compared to the emission profile recorded in aqueous solution, Figure 4.7). It is feasible for outersphere anions to alter hydration states of lanthanide complexes via hydrogen bonding that includes the hydroxycyclohexyl pendant arms[68].

Calculation of the q values[75] in Tables 4.6, 4.7 and 4.8 were initially conducted under the assumption that the formation of the Eu(III) complex would occur by coordination of the metal ion by the hydroxycyclohexyl and carboxymethyl pendant arms present in the ligand structure and the amine functionalities along the ligand backbone. Due to the presence of tertiary amines and the lack of amide functionalities in the ligand structure, the number of amine N-H oscillators and amide N-H oscillators are both taken to be zero. The number of alcohol O-H oscillators was varied (n_{OH} = 0, 1 or 2) to account for interactions between the outersphere phthalate anion and the hydroxycyclohexyl pendant arms, resulting in the 3 sets of q values (Tables 4.6, 4.7, and 4.8, $q^{\ddagger}$ (n_{OH} = 2), $q^{\dagger}$ (n_{OH} = 1), and $q^{\spadesuit}$ (n_{OH} = 0)) for the varied innersphere hydroxyalkyl contributions.

The phosphorescence emission spectra for the samples prepared in H_2O and D_2O are illustrated in Figures 4.46 and 4.47. The samples prepared in H_2O at low pH (Figure 4.46, (i) stock solution (pH 3.45), (ii) sample 1 (pH 3.07), and (iii) sample 2 (pH 5.42)) display significant modulation in the emission intensity ratio of the $\Delta J = 1$ (592 nm) and $\Delta J = 2$ (617 nm) emission bands over time. The modulation of the $\Delta J_2/\Delta J_1$ ratio for the low pH samples indicates a change in the coordination environment of the metal complex. The $\Delta J = 2$ emission band for the low pH samples displayed an overall increase in emission intensity, while the samples prepared at neutral (Figure 4.46, (iv) sample 3 (pH 7.59)) and high pH (Figure 4.46, (v) sample 4, (pH 11.28)) revealed decreased emission intensity over time. The samples prepared in D_2O (Figure 4.47, (i) stock solution (pD 4.36), (ii) sample 1 (pD 3.06), (iii) sample 2 (pD 5.46), (iv) sample 3 (pD 7.62), and (v) sample 4 (pD 11.28)) displayed emission intensity that exceeded the measurement parameters of the instrument, which necessitated the samples be diluted for further measurements (dilution factor of five). The D_2O samples displayed a general increase in emission intensity over time. Each of the prepared samples displayed significant decreases in the determined q values over time, with the exception of sample 4 which remained relatively constant (Tables 4.6, 4.7 and 4.8).

Upon reaching equilibrium, the emission profile for the buffered system reveals a shift from a four pK_a system (Figure 4.14, upon initial preparation) to a two pK_a system (Figures 4.21 and 4.22, after 3 days and 14 days respectively), accompanied by marked variation in the pH of the solutions prepared within the emission enhancement window (Figure 4.14, pH 4 to pH 8). This phenomenon is due to ternary phthalate complex formation. Binding of the phthalate ion depletes the buffering capacity in the pH 4 to pH 8 range (the functional pH window for KHP), as a result of the low concentration of buffer system employed in the study (Eu(III) complex to buffer ratio is 10:1), with concomitant change in pH. Consequently, pK_a2 and pK_a3 values (Figure 4.14, corresponding to formation of the phthalate dianion and deprotonation of a coordinated aqua ligand) can no longer be resolved from the emission profile upon equilibrium.

Differences between the pH and pD values for the prepared samples measured upon initial preparation are small (Table 4.6, $\Delta_{pH/pD} = 0.01$ (sample 1), $\Delta_{pH/pD} = 0.04$ (sample 2), $\Delta_{pH/pD} = 0.03$ (sample 3), $\Delta_{pH/pD} = 0.00$ (sample 4)), with the exception of the stock solution (Table

4.6, $\Delta_{pH/pD}$ = 0.91 (stock solution)). Therefore, the calculated q values upon initial preparation display good accuracy.

There is little variation in the pH and pD values measured for sample 1 upon reaching equilibrium (Figure 4.46, (ii), and Figure 4.47, (ii)). The small difference between the pH and pD values (Table 4.7, $\Delta_{pH/pD}$ = 0.06 (sample 1), and Table 4.8, $\Delta_{pH/pD}$ = 0.06 (sample 1)) reveals high accuracy in the calculated q values for sample 1. This agrees with the observed emission profiles, as there is little variation observed between the initial and equilibrium emission intensities at low pH (Figures 4.14, 4.21, and 4.22, pH 2 to pH 4). Equilibrium pH values for sample 4 displays small variation (Figure 4.46, (v)), while the pD value for the sample varies by approximately 1 pD unit (Figure 4.47, (v)). Although $\Delta_{pH/pD}$ for sample 4 is observed to increase over the duration of the experiment (Table 4.7, $\Delta_{pH/pD}$ = 0.07 (sample 4), and Table 4.8, $\Delta_{pH/pD}$ = 0.92 (sample 4)), the calculated q values are considered accurate as the measured pH and pD values upon reaching equilibrium lie within the pH range of the emission profile corresponding to a constant hydration state (Figure 4.23, pH 10 to pH 12).

Samples prepared within the emission enhancement window (Figure 4.14, pH 4 to pH 8) would be subject to variation in their equilibrium pH and pD values, due to buffer capacity exhaustion (the result of phthalate ternary complex formation). This was observed for the pH and pD values for sample 2 (Figure 4.46, (iii), and Figure 4.47, (iii)) and sample 3 (Figure 4.46, (iv), and Figure 4.47, (iv)). The equilibrium pH and pD values for samples 3 and 4 lie within the pH range of the emission profile where emission intensity is seemingly constant (Figures 4.21 and 4.22, pH 4 to pH 8), however further comment on the accuracy of the calculated q values for these samples cannot be made without consideration of the proposed equilibria.

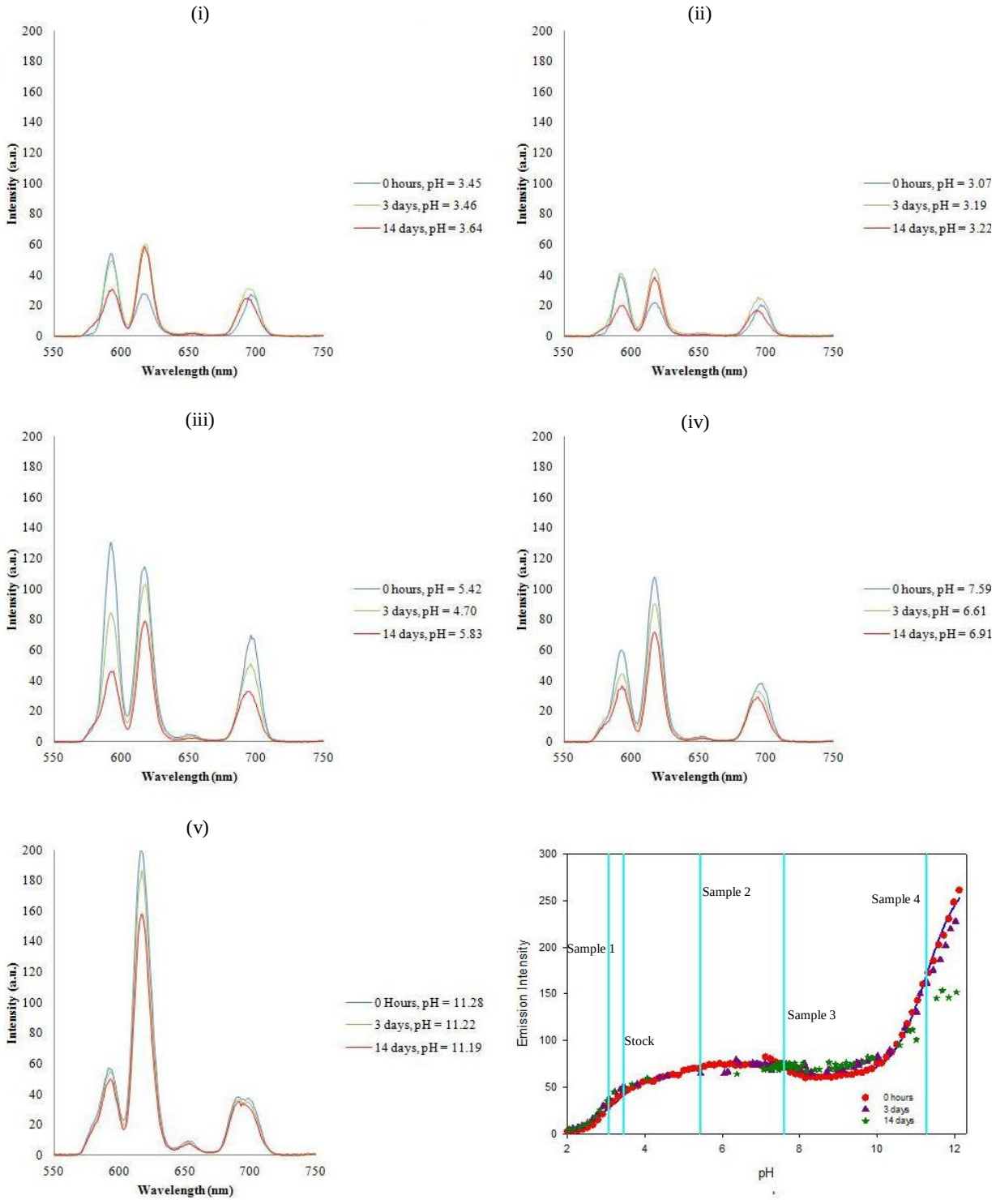


Figure 4.46: Comparison of phosphorescence emission spectra of (i) stock solution, (ii) sample 1, (iii) sample 2, (iv) sample 3, and (v) sample 4 of europium(III)-1,7-bis(2-hydroxycyclohexyl)-1,4,7-tris(carboxymethyl)-1,4,7-triazaheptane, as a function of pH, in H_2O, in a multi-component buffered system (λ_{ex} = 276 nm). *Inset*: Emission profile at 617 nm (cyan lines indicate selected pH values for the phosphorescence decay experiment).

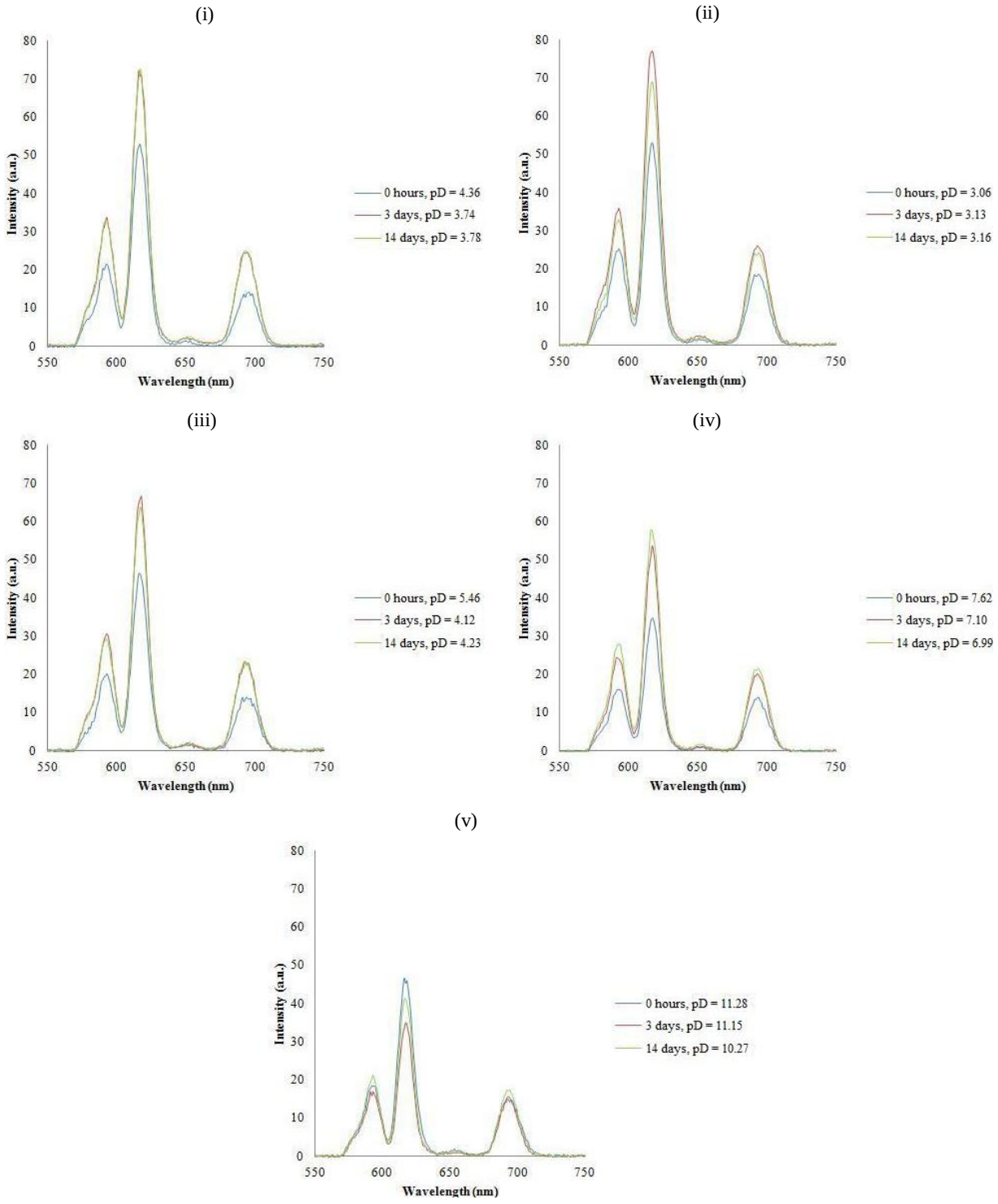


Figure 4.47: Comparison of phosphorescence emission spectra of (i) stock solution, (ii) sample 1, (iii) sample 2, (iv) sample 3, and (v) sample 4 of europium(III)-1,7-bis(2-hydroxycyclohexyl)-1,4,7-tris(carboxymethyl)-1,4,7-triazaheptane, as a function of pD, in D_2O, in a multi-component buffered system (λ_{ex} = 276 nm).

The pH values for the stock solution (Table 4.6, pH 3.45) and sample 1 (Table 4.6, pH 3.07) upon initial preparation coincide with the spectroscopically observed pK_a1 value (Figure 4.14, pK_a1 = 3.07 ± 0.07), for the deprotonation equilibrium of the central amine moiety on

the ligand backbone. Calculated q values for the buffered system (Table 4.6, stock solution and sample 1) are significantly higher than that obtained at corresponding pH in aqueous solution (Table 4.3, stock solution, pH 3.38, q = 1.5), revealing a higher number of coordinated water molecules. It is proposed the phthalate anion (from the added multi-component buffer system) hydrogen bonds, via O-H···O^- or O-H···O interactions to a hydroxycyclohexyl pendant arm and the apical, innersphere water molecule forming an outersphere ternary complex (Figure 4.48, pK_a1, and Table 4.6, $q^{\spadesuit}$ value for stock solution = 4.0, and sample 1 = 3.8). The non-integral values of q arise from proximal contributions by water molecules of the bulk solvent.

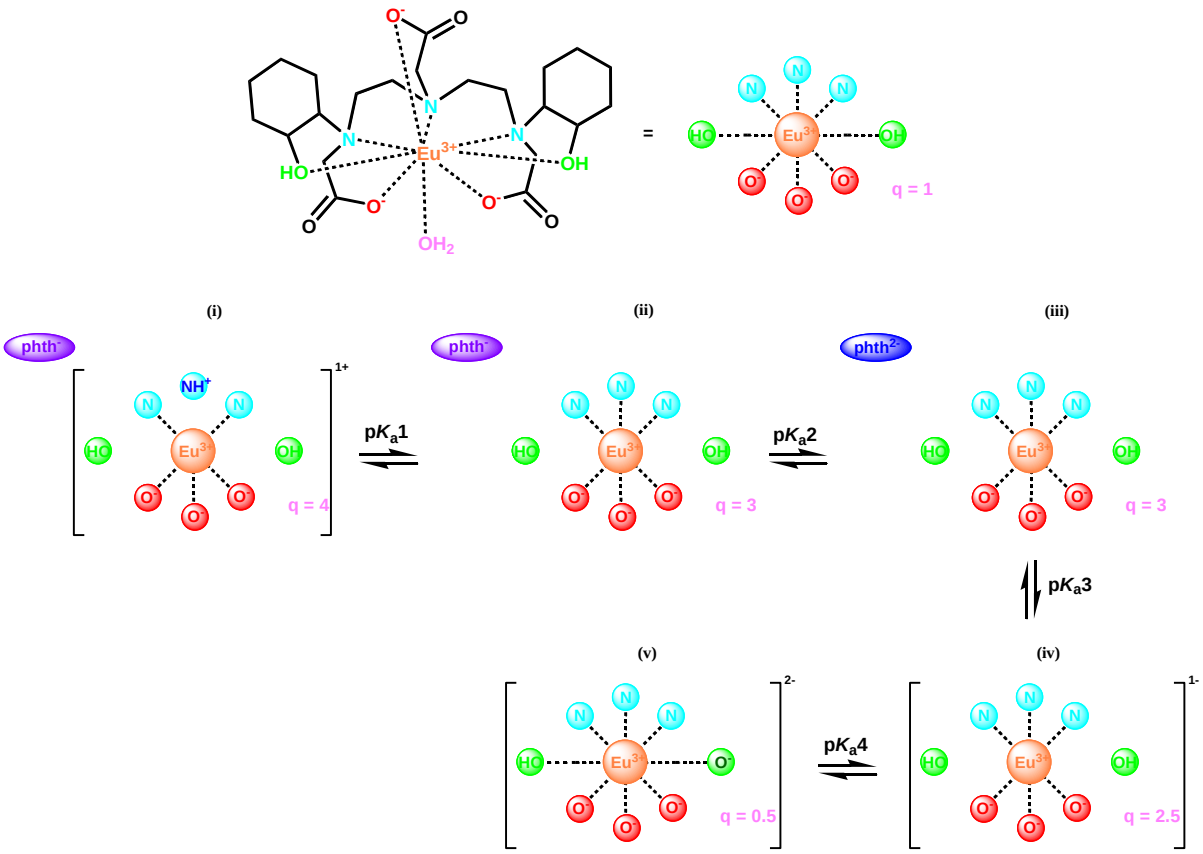


Figure 4.48: Proposed speciation of europium(III)-1,7-bis(2-hydroxycyclohexyl)-1,4,7-tris(carboxymethyl)-1,4,7-triazaheptane, in a multi-component buffered system, upon initial preparation.

The pH value for sample 2 upon initial preparation (Table 4.6, pH 5.42) compares favourably with the spectroscopically determined pK_a2 value (Figure 4.14, pK_a2 = 5.39 ± 0.26). The q value considered here reflects the phthalate deprotonation equilibrium ($phth^{1-} \rightleftharpoons phth^{2-}$) and formation of the ternary complex involving the dianion (Figure 4.48, pK_a2). The high value

of q (Table 4.6, sample 2, $q^{\spadesuit} = 3.5$) suggests the formation of an outersphere ternary complex involving the phthalate dianion is accompanied by an increased number of coordinated water molecules. The latter is possible for an outersphere ternary complex in which pendant hydroxycyclohexyl moieties are uncoordinated. The deprotonation of the carboxylate group on the outersphere phthalate ion does not significantly alter the hydration sphere around the metal centre (Figure 4.48, pK_a2), as observed from the difference in $q^{\spadesuit}$ values for samples 1 and 2 (Table 4.6, $\Delta q^{\spadesuit} = 0.3$). Therefore, emission enhancement observed for the $\Delta J = 2$ band (Figure 4.14, between pH 4 and pH 6) signals the formation of an outersphere ternary complex with the phthalate dianion.

The spectroscopically determined pK_a3 value for the buffered system upon initial preparation (Figure 4.14, pK_a3 = 7.61 ± 0.20) coincides with the pH value for sample 3 (Table 4.6, pH 7.59). The observed q value reflects the hydration state of the complex upon deprotonation of the apical aqua ligand (Figure 4.48, pK_a3). A reduction in the number of innersphere O-H oscillators (due to the deprotonation of a coordinated water molecule) results in the observed decrease in the q value (Table 4.6, sample 2, $q^{\spadesuit} = 2.8$). The high q value suggests that the hydroxycyclohexyl pendant arms remain uncoordinated (as a result of ternary complex formation with an outersphere phthalate dianion). Decreasing emission intensity observed for the $\Delta J = 2$ band (Figure 4.14, between pH 7 and pH 9) reveals dissociation of the phthalate ternary complex with increasing hydroxo-ligand concentration, due to electrostatic repulsion between the anionic species.

The high pH value of sample 4 upon initial preparation (Table 4.6, pH 11.28) is comparable to the pK_a4 value determined from the luminescence emission spectrum for the $\Delta J = 2$ band (Figure 4.14, pK_a4 = 11.28 ± 0.02). The q value determined reflects the alkoxo-species formation equilibrium (Figure 4.48, pK_a4). The substantial decrease in q value with increasing pH, coincides with phthalate displacement from the outersphere. Dissociation of the phthalate ternary complex affords chelation by the pendant hydroxycyclohexyl moieties and the observed decrease in the hydration number (Table 4.6, sample 4, $q^{\ddagger} = 0.73$).

Upon reaching equilibrium (after 3 days), the q values for samples prepared at low pH (Table 4.7, $q^{\dagger} = 1.7$ (stock solution), $q^{\dagger} = 1.8$ (sample 1), $q^{\dagger} = 2.1$ (sample 2)) are consistent with an

Eu(III) complex bearing a ligated hydroxycyclohexyl moiety, with the second uncoordinated alcohol donor available for hydrogen bonding with the outersphere phthalate ion (Figure 4.49, species (i), (ii), and (iii)). The phthalate ion is gradually displaced from the outersphere with increasing pH (Figure 4.47, species (iv)), resulting in complete encapsulation of the metal ion by the ligand at high pH (Figure 4.49, species (v)), with concomitant decrease in the value of q (Table 4.7, $q^{\ddagger}$ = 1.4 (sample 3), $q^{\ddagger}$ = 0.79 (sample 4)).

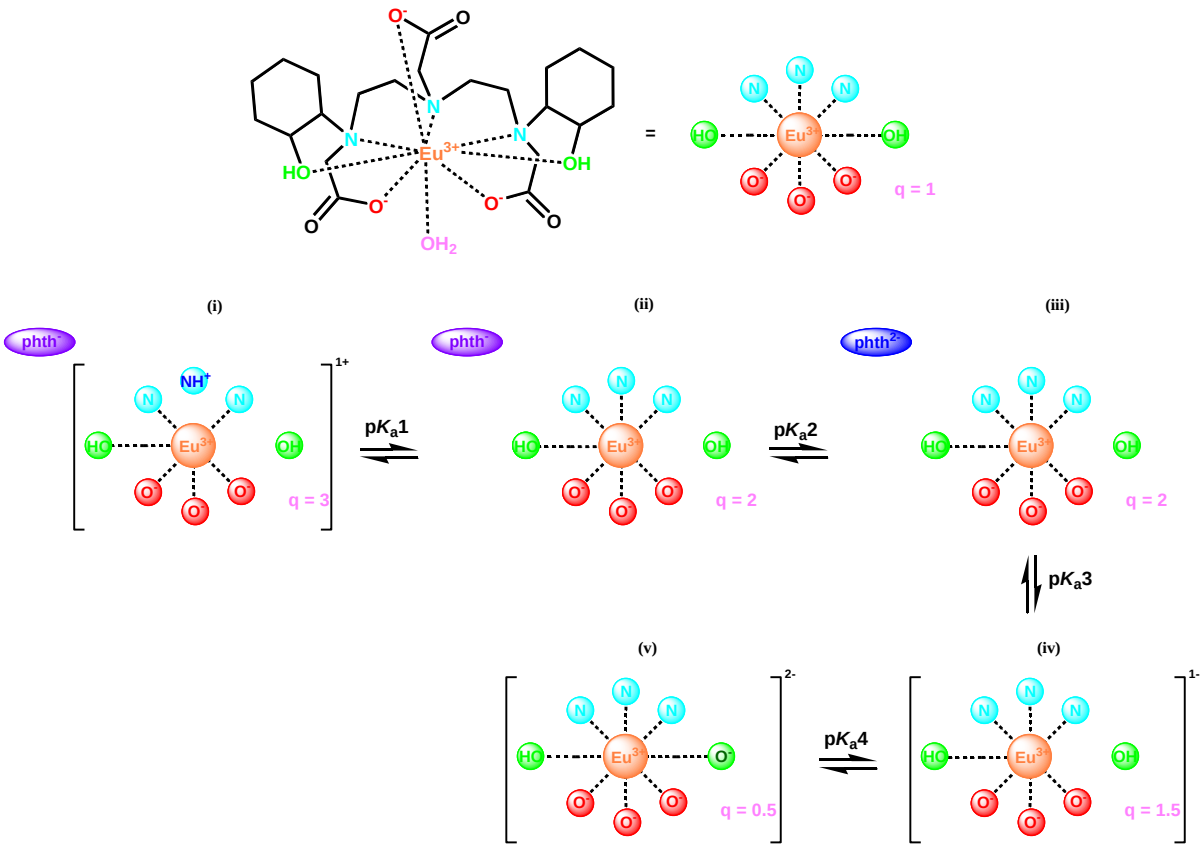


Figure 4.49: Proposed speciation of europium(III)-1,7-bis(2-hydroxycyclohexyl)-1,4,7-tris(carboxymethyl)-1,4,7-triazaheptane, in a multi-component buffered system, upon reaching equilibrium (3 days).

The further decrease observed for q values after 14 days (Table 4.8, $q^{\ddagger}$ values) reveal chelation by both hydroxycyclohexyl pendants across the experimental pH range (Figure 4.50). Coordination by the two alcohol donors at low pH suggest the outersphere phthalate ternary complex may be no longer present, due to loss of resolution in the pH 4 to pH 8 range of the emission profile (Figure 4.22). Emission enhancements between pH 10 and pH 12 are not significantly altered upon reaching equilibrium (comparing Figure 4.14, upon initial preparation, with Figures 4.21 and 4.22, upon reaching equilibrium). The spectroscopically

observed pK_a4 value measured upon initial preparation (Figure 4.14, pK_a4 = 11.28 ± 0.02) is comparable to the pK_a2 value obtained from the emission profile upon reaching equilibrium (Figure 4.21, pK_a2 = 11.29 ± 0.03, and Figure 4.22, pK_a2 = 11.05 ± 0.05). At high pH, the increased concentration of hydroxide ions prevents ternary complex formation as a result of electrostatic repulsion between the hydroxo-ligand and phthalate dianion.

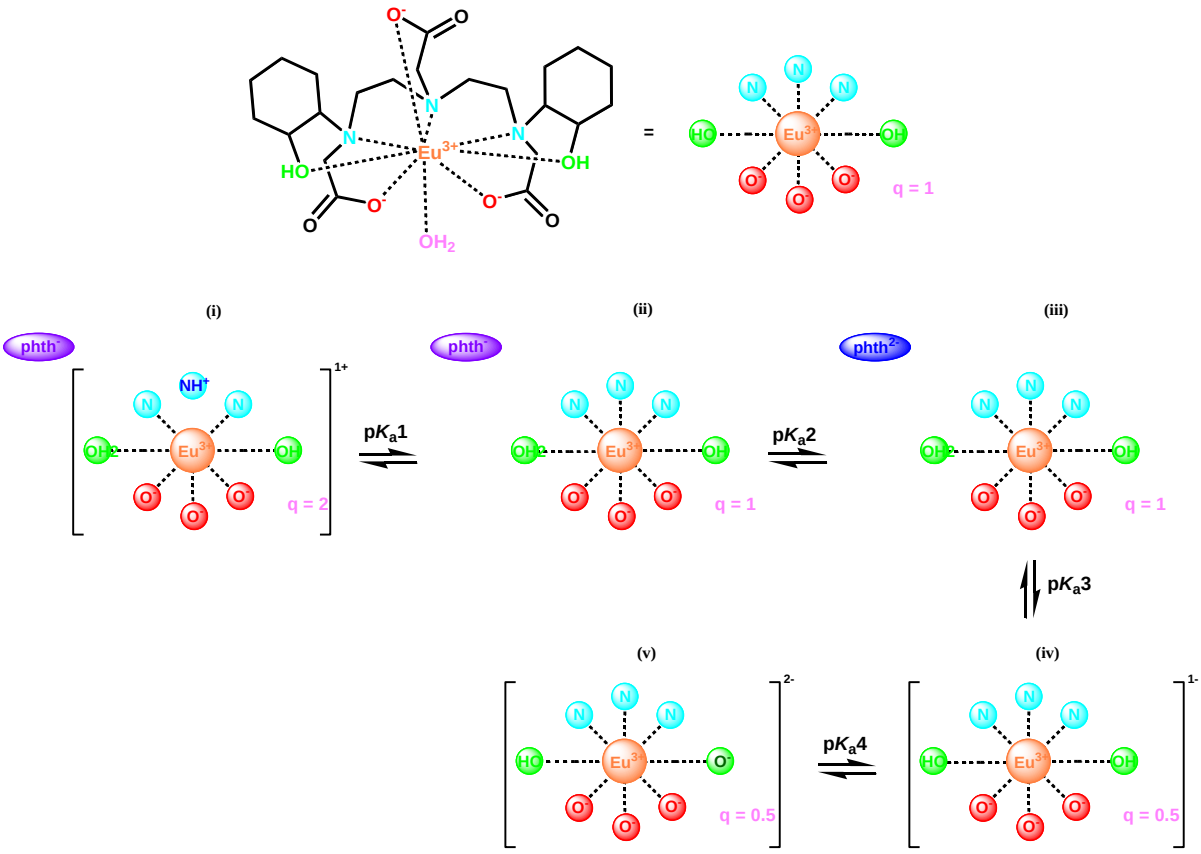


Figure 4.50: Proposed speciation of europium(III)-1,7-bis(2-hydroxycyclohexyl)-1,4,7-tris(carboxymethyl)-1,4,7-triazaheptane, in a multi-component buffered system, upon reaching equilibrium (14 days).

The significance of equilibrium q values for samples 2 and 3 is inferred from the proposed models (Figures 4.48, 4.49 and 4.50). Though differences exist between the equilibrium pH and pD values for samples 3 and 4 (Table 4.7, $\Delta_{pH/pD}$ = 0.58 (sample 2), $\Delta_{pH/pD}$ = 0.49 (sample 3) and Table 4.8, $\Delta_{pH/pD}$ = 1.60 (sample 2), $\Delta_{pH/pD}$ = 0.08 (sample 3)), the calculated q values correspond to comparable hydration states (Figures, 4.48, 4.49 and 4.50, species (ii) and (iii)).

4.4.2 Determination of the solution hydration state of $[Eu(Cy_2DETA.2A)]^{3+}$

4.4.2.1 $Cy_2DETA.2A.3HCl$ / Eu(III), aqueous solution

Emission decay constants of 0.15 mM europium(III)-1,7-bis(2-hydroxycyclohexyl)-1,7-bis(carboxymethyl)-1,4,7-triazaheptane, prepared in H_2O and D_2O, were determined as a function of pH. The pH, phosphorescence emission and decay constant of each sample were measured upon initial preparation (0 hours) and after reaching equilibrium (2 and 7 days). The excitation wavelength of 252 nm was determined from UV-visible spectroscopy (Appendix G, Figures G.5 And G.6). The $^5D_0 \rightarrow {}^7F_2$ ($\Delta J = 2$) emissive transition at 616 nm was monitored in H_2O and D_2O for the lifetime determination and the data tabulated in Tables 4.9, 4.10, and 4.11.

Table 4.9: Phosphorescence decay constants for europium(III)-1,7-bis(2-hydroxycyclohexyl)-1,7-bis(carboxymethyl)-1,4,7-triazaheptane, as a function of pH, aqueous solution, upon initial preparation (0 hours, λ_{ex} = 252 nm, λ_{em} = 616 nm).

Sample	pH (0 h)	pD (0 h)	k_{H_2O} (ms^{-1})	k_{D_2O} (ms^{-1})	Δk (ms^{-1})	$q^{\dagger}$	$q^{\ddagger}$	$q^{\spadesuit}$	$q^{\blacklozenge}$
Stock[a]	3.87	4.69	6.53	1.53	5.00	3.1	4.2	3.6	**4.7**
Sample 1[b]	2.89	2.88	7.72	1.37	6.35	4.6	5.7	5.1	**6.2**
Sample 2[b]	5.43	5.40	4.51	1.32	3.19	1.1	**2.2**	1.6	2.7

† $q = \{\Delta k - [0.31 + (0.44 \times 2) + (0.99 \times 1) + (0.075 \times 0)]\} \times 1.11$

‡ $q = \{\Delta k - [0.31 + (0.44 \times 2) + (0.99 \times 0) + (0.075 \times 0)]\} \times 1.11$

$^{\spadesuit}$ $q = \{\Delta k - [0.31 + (0.44 \times 1) + (0.99 \times 1) + (0.075 \times 0)]\} \times 1.11$

$^{\blacklozenge}$ $q = \{\Delta k - [0.31 + (0.44 \times 1) + (0.99 \times 0) + (0.075 \times 0)]\} \times 1.11$

[a] contains 0.15mM Eu(III) complex, pH unadjusted

[b] contains 0.15mM Eu(III) complex, pH adjusted

Table 4.10: Phosphorescence decay constants for europium(III)-1,7-bis(2-hydroxycyclohexyl)-1,7-bis(carboxymethyl)-1,4,7-triazaheptane, as a function of pH, aqueous solution, at equilibrium (48 hours, λ_{ex} = 252 nm, λ_{em} = 616 nm).

Sample	pH (48 h)	pD (48 h)	k_{H_2O} (ms^{-1})	k_{D_2O} (ms^{-1})	Δk (ms^{-1})	q[†]	q[‡]	q[♠]	q[♦]
Stock[a]	4.19	5.02	4.87	1.32	3.55	1.5	2.6	2.0	**3.1**
Sample 1[b]	2.95	2.89	7.11	1.27	5.84	4.0	5.2	4.6	**5.6**
Sample 2[b]	5.65	5.44	4.22	1.24	2.98	0.89	**2.0**	1.4	2.5

[†] $q = \{\Delta k - [0.31 + (0.44 \times 2) + (0.99 \times 1) + (0.075 \times 0)]\} \times 1.11$
[‡] $q = \{\Delta k - [0.31 + (0.44 \times 2) + (0.99 \times 0) + (0.075 \times 0)]\} \times 1.11$
[♠] $q = \{\Delta k - [0.31 + (0.44 \times 1) + (0.99 \times 1) + (0.075 \times 0)]\} \times 1.11$
[♦] $q = \{\Delta k - [0.31 + (0.44 \times 1) + (0.99 \times 0) + (0.075 \times 0)]\} \times 1.11$
[a] contains 0.15mM Eu(III) complex, pH unadjusted
[b] contains 0.15mM Eu(III) complex, pH adjusted

Table 4.11: Phosphorescence decay constants for europium(III)-1,7-bis(2-hydroxycyclohexyl)-1,7-bis(carboxymethyl)-1,4,7-triazaheptane, as a function of pH, aqueous solution, at equilibrium (7 days, λ_{ex} = 252 nm, λ_{em} = 616 nm).

Sample	pH (7 d)	pD (7 d)	k_{H_2O} (ms^{-1})	k_{D_2O} (ms^{-1})	Δk (ms^{-1})	q[†]	q[‡]	q[♠]	q[♦]
Stock[a]	5.10	4.83	4.41	1.21	3.20	1.1	2.2	1.6	**2.7**
Sample 1[b]	2.98	2.96	6.06	1.27	4.79	2.9	4.0	3.4	**4.5**
Sample 2[b]	6.07	5.48	4.14	1.13	3.01	0.92	**2.0**	1.4	2.0

[†] $q = \{\Delta k - [0.31 + (0.44 \times 2) + (0.99 \times 1) + (0.075 \times 0)]\} \times 1.11$
[‡] $q = \{\Delta k - [0.31 + (0.44 \times 2) + (0.99 \times 0) + (0.075 \times 0)]\} \times 1.11$
[♠] $q = \{\Delta k - [0.31 + (0.44 \times 1) + (0.99 \times 1) + (0.075 \times 0)]\} \times 1.11$
[♦] $q = \{\Delta k - [0.31 + (0.44 \times 1) + (0.99 \times 0) + (0.075 \times 0)]\} \times 1.11$
[a] contains 0.15mM Eu(III) complex, pH unadjusted
[b] contains 0.15mM Eu(III) complex, pH adjusted

Experimental pH values were selected using the luminescence emission profile for the $\Delta J = 2$ emission band (Figure 4.29). Calculated hydration states (Tables 4.9, 4.10, and 4.11) assumed Eu(III) cation chelation by pendant hydroxycyclohexyl and carboxymethyl moieties present in the ligand structure, and amine donors present on the ligand backbone. Chelating modes with varied amine N-H and alcoholic O-H oscillators were considered (n_{NH} = 0 or 1, n_{OH} = 0

or 1), resulting in four hydration state models (Tables 4.9, 4.10, and 4.11, $q^{\dagger}$ (n_{NH} = 1, n_{OH} = 2), $q^{\ddagger}$ (n_{NH} = 0, n_{OH} = 2), $q^{\spadesuit}$ (n_{NH} = 1, n_{OH} = 1), $q^{\blacklozenge}$ (n_{NH} = 0, n_{OH} = 1)).

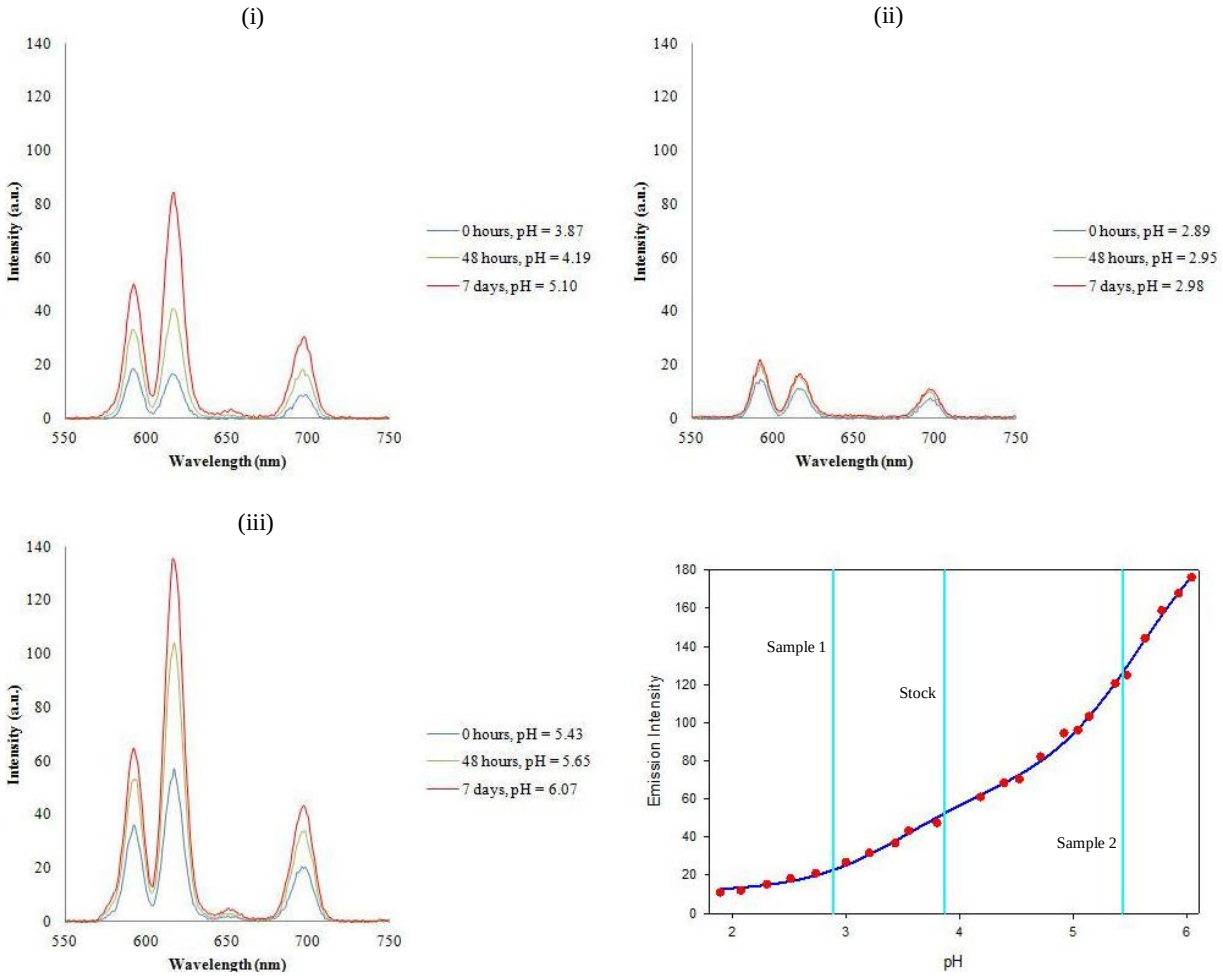


Figure 4.51: Comparison of phosphorescence emission spectra of (i) stock solution, (ii) sample 1, and (iii) sample 2 of europium(III)-1,7-bis(2-hydroxycyclohexyl)-1,7-bis(carboxymethyl)-1,4,7-triazaheptane, as a function of pH, in H_2O (λ_{ex} = 252 nm). *Inset*: Emission profile at 616 nm (cyan lines indicate selected pH values for the phosphorescence decay experiment).

The differences observed in the calculated q values for both sets of measurements can be more easily understood when the phosphorescence emission spectra are compared (Figures 4.51 and 4.52). Samples prepared in D_2O (Figure 4.52) exhibit substantially larger emission intensity compared to that observed for the H_2O samples (Figure 4.51), due to poor efficiency of O-D oscillators in quenching luminescence[72-75]. Both sets of samples prepared in H_2O and D_2O display increasing emission as a function of pH. The D_2O and H_2O emission scans also reveal modulation in the relative intensities of the ΔJ = 1 (592 nm) and ΔJ = 2 (616 nm)

emission bands with increasing pH (Figures 4.51 and 4.52, spectra (ii) and (iii)), thus indicating a change in the coordination geometry around the Eu(III) ion.

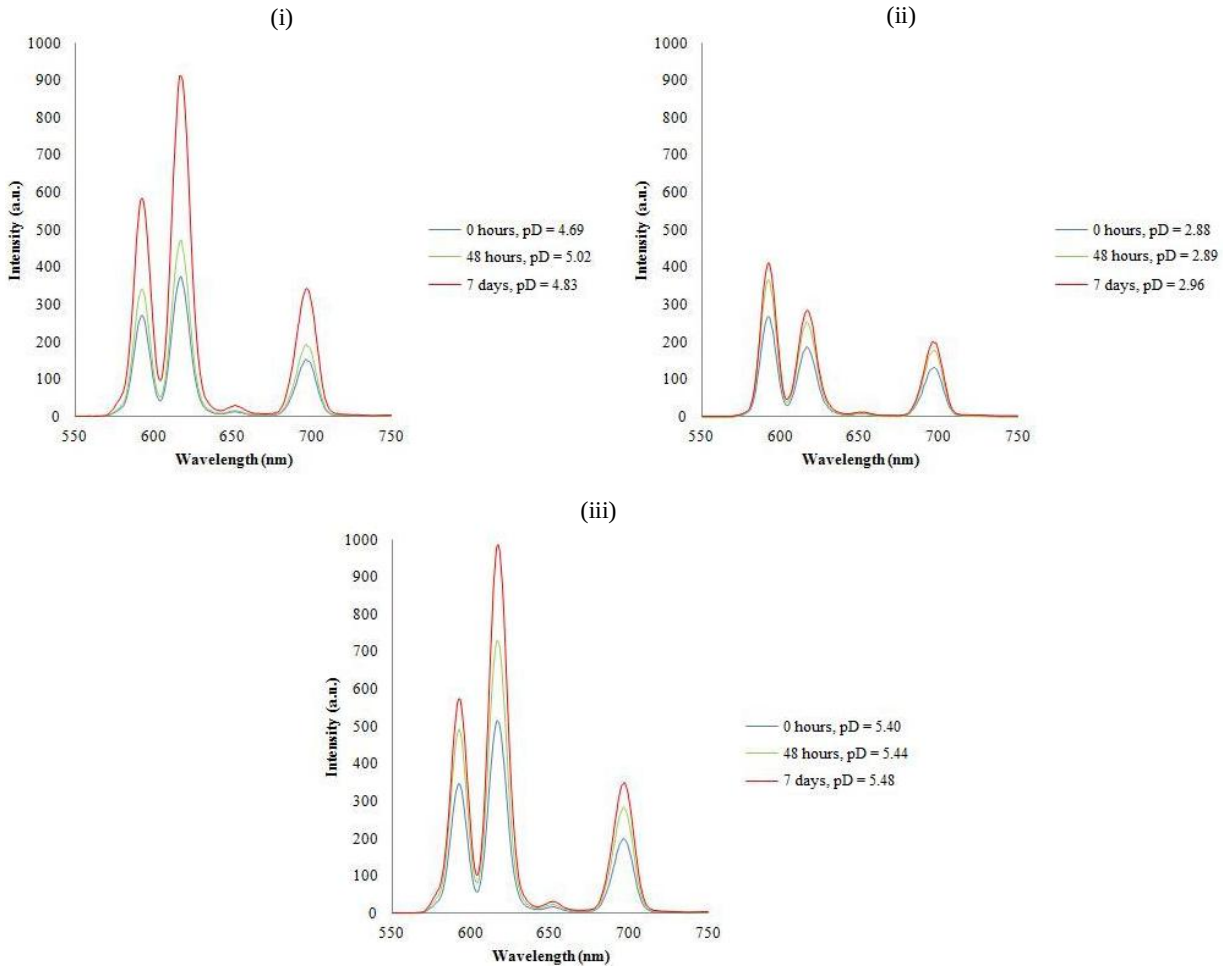


Figure 4.52: Comparison of phosphorescence emission spectra of (i) stock solution, (ii) sample 1, and (iii) sample 2 of europium(III)-1,7-bis(2-hydroxycyclohexyl)-1,7-bis(carboxymethyl)-1,4,7-triazaheptane, as a function of pH, in D_2O (λ_{ex} = 252 nm).

The pH values for the stock solution and sample 2 (Figure 4.51, (i) and (iii)) and pD value for stock solution (Figure 4.52, (i)) were found to fluctuate over time. The small difference between the pH and pD values for sample 1 over the duration of the experiment (Table 4.9, $\Delta_{pH/pD}$ = 0.01 (sample 1), Table 4.10, $\Delta_{pH/pD}$ = 0.06 (sample 1), Table 4.11, $\Delta_{pH/pD}$ = 0.02 (sample 1)) indicate good accuracy for the calculated q values. Although differences between pH and pD values for sample 2 were observed to increase over time (Table 4.9, $\Delta_{pH/pD}$ = 0.03 (sample 2), Table 4.10, $\Delta_{pH/pD}$ = 0.21 (sample 2), Table 4.11, $\Delta_{pH/pD}$ = 0.59 (sample 2)), the calculated q values are considered to represent a comparable hydration state (Figure 4.29, pH 5 to pH 6). The pH and pD differences for the stock solution are large (Table 4.9, $\Delta_{pH/pD}$ =

0.82 (stock), Table 4.10, $\Delta_{pH/pD}$ = 0.83 (stock), Table 4.11, $\Delta_{pH/pD}$ = 0.27 (stock)), due to the fluctuating pH of this solution (Figure 4.51 (i)). The emission profile within this pH range is associated with changes of hydration state and calculated q values are averages of possible hydration states (Figure 4.29, pH 3.8 to pH 5.1).

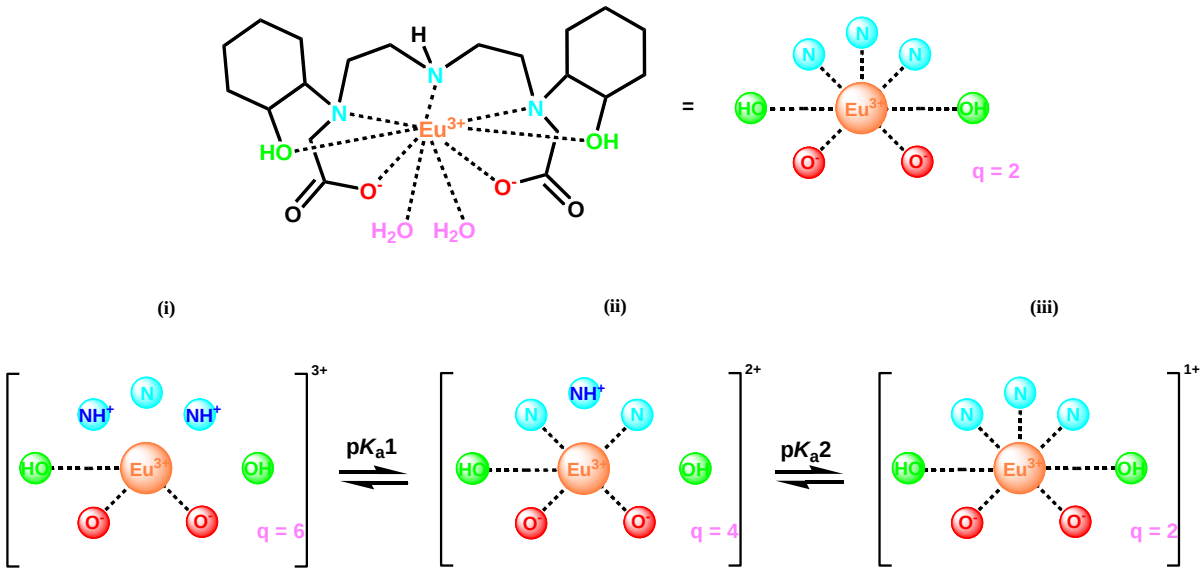


Figure 4.53: Proposed speciation of europium(III)-1,7-bis(2-hydroxycyclohexyl)-1,7-bis(carboxymethyl)-1,4,7-triazaheptane, in aqueous solution, upon initial preparation.

The large q values calculated for the low pH samples upon initial preparation (Table 4.9, sample 1 (pH 2.89), $q^{\blacklozenge}$ = 6.2) indicates incomplete encapsulation of the Eu(III) ion. The pH values of sample 1 lies before the spectroscopically observed pK_a1 value (Figure 4.29, pK_a1 = 3.48 ± 0.07), indicating that the calculated q value corresponds to the first deprotonation equilibrium for the amine donors on the ligand backbone. Protonation of the terminal amines[48] impedes binding by the central nitrogen donor. Therefore, the $q^{\blacklozenge}$ of 6.2 suggests chelation by three pendant oxygen donors, with the amine donors and a pendant hydroxycyclohexyl moiety remaining uncoordinated to the Eu(III) cation at low pH (Figure 4.53, (i)). Proton migration is known to occur upon initial deprotonation of the dipositive diethylenetriamine backbone[48], thus allowing for ligation by the terminal amine donors (Figure 4.53 (ii)), resulting in a decreased q value (Table 4.9, stock (pH 3.87), $q^{\blacklozenge}$ = 4.7). Increasing pH results in the subsequent deprotonation of the central amine donor (Figure 4.29, pK_a2 = 5.60 ± 0.05). Sample 2 (Table 4.9, pH 5.43, $q^{\ddagger}$ = 2.2) displays a decrease in q indicating all donor atoms present in the ligand (four oxygen pendant donors and three amine

moieties) are fully coordinated to the metal ion (Figure 4.53 (iii)). Solutions were not prepared at neutral or high pH, due to precipitation observed in the corresponding fluorescence emission study.

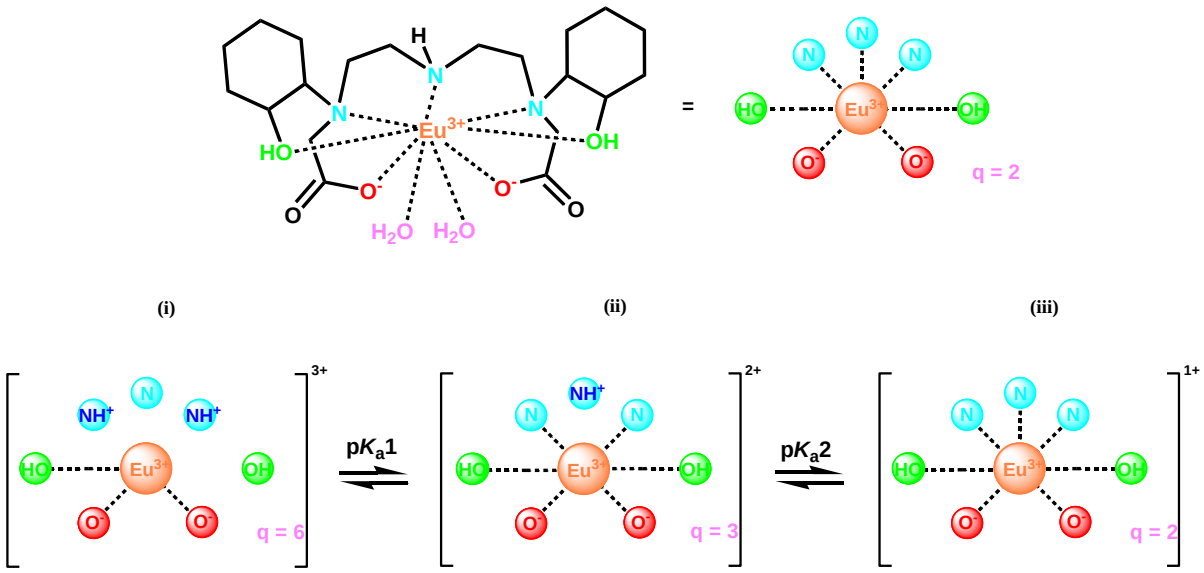


Figure 4.54: Proposed speciation of europium(III)-1,7-bis(2-hydroxycyclohexyl)-1,7-bis(carboxymethyl)-1,4,7-triazaheptane, in aqueous solution, upon reaching equilibrium (48 hours).

Upon reaching equilibrium (48 hours), the large q value for sample 1 (Table 4.10, sample 1 (pH 2.95), $q^{\blacklozenge}$ = 5.6) indicates the amine donors and a hydroxycycloalkyl moiety remain uncoordinated at low pH (Figure 4.54 (i)). The decrease in the q value observed for the stock solution (Table 4.10, pH 4.19, $q^{\blacklozenge}$ = 3.1) suggests possible coordination of both hydroxycyclohexyl pendants at low pH (Figure 4.54 (ii)).

After 7 days, the sharp decline observed in the q value for sample 1 (Table 4.11, sample 1 (pH 2.98), $q^{\blacklozenge}$ = 4.5) demonstrates that the equilibrium for the first amine deprotonation lies to the right (Figure 4.53, pK_a1). The q values determined for the stock solution and sample 2 (Table 4.11, stock (pH 5.10), $q^{\blacklozenge}$ = 2.7, sample 2 (pH 6.07), $q^{\ddagger}$ = 2.0) indicate both hydroxycyclohexyl pendants coordinate the Eu(III) metal ion upon amine deprotonation (Figure 4.29, pK_a2 = 5.60 ± 0.05). The proposed species are illustrated in Figure 4.55.

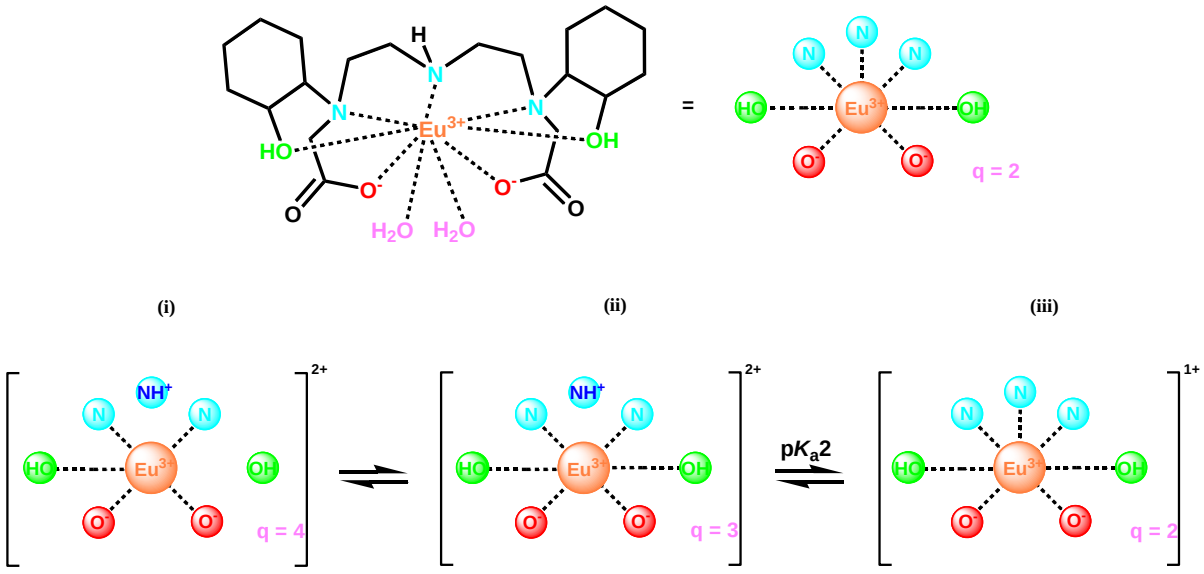


Figure 4.55: Proposed speciation of europium(III)-1,7-bis(2-hydroxycyclohexyl)-1,7-bis(carboxymethyl)-1,4,7-triazaheptane, in aqueous solution, upon reaching equilibrium (7 days).

4.4.2.2 Cy_2DETA.2A.3HCl / Eu(III), multi-component buffered system

Phosphorescence decay constants of 0.15 mM europium(III)-1,7-bis(2-hydroxycyclohexyl)-1,7-bis(carboxymethyl)-1,4,7-triazaheptane, in the presence of a 0.015 mM multi-component buffer system, prepared in H_2O and D_2O, were determined as a function of pH. The pH, phosphorescence emission and decay spectra for each sample were measured upon initial preparation and upon reaching equilibrium (after 7 days). Excitation wavelengths of 227 nm and 276 nm were determined from UV-visible spectroscopy (Appendix G, Figures G.7 and G.8). The $^5D_0 \rightarrow {}^7F_2$ ($\Delta J = 2$) transition at 616 nm was monitored in H_2O and D_2O for lifetime determinations. The q values were determined for the $\Delta J = 2$ emission band, excited at 276 nm, and are reported in Tables 4.12 and 4.13.

Experimental pH values were selected considering the luminescence emission profile for the $\Delta J = 2$ emission band (Figure 4.39). Hydration states (Tables 4.12 and 4.13) were calculated assuming chelation of the Eu(III) metal ion by each nitrogen and oxygen donor present in the ligand structure. The number of amine N-H and alcoholic O-H oscillators were varied (n_{NH} = 0 or 1, n_{OH} = 0 or 1), resulting in four hydration state models (Tables 4.12, and 4.13, $q^{\dagger}$ (n_{NH} = 1, n_{OH} = 2), $q^{\ddagger}$ (n_{NH} = 0, n_{OH} = 2), $q^{\spadesuit}$ (n_{NH} = 1, n_{OH} = 1), $q^{\blacklozenge}$ (n_{NH} = 0, n_{OH} = 1)).

Table 4.12: Phosphorescence decay constants for europium(III)-1,7-bis(2-hydroxycyclohexyl)-1,7-bis(carboxymethyl)-1,4,7-triazaheptane, as a function of pH, multi-component buffered system, upon initial preparation (0 hours, λ_{ex} = 276 nm, λ_{em} = 616 nm).

Sample	pH (48 h)	pD (48 h)	k_{H_2O} (ms^{-1})	k_{D_2O} (ms^{-1})	Δk (ms^{-1})	q†	q‡	q♠	q♦
Stock[a]	3.85	5.41	7.11	0.81	6.30	4.6	5.7	5.1	6.2
Sample 1[b]	2.58	2.56	7.00	0.93	6.07	4.3	5.4	4.8	**5.9**
Sample 2[b]	4.44	4.46	5.80	0.84	4.96	3.1	4.2	**3.6**	4.7

† $q = \{\Delta k - [0.31 + (0.44 \times 2) + (0.99 \times 1) + (0.075 \times 0)]\} \times 1.11$
‡ $q = \{\Delta k - [0.31 + (0.44 \times 2) + (0.99 \times 0) + (0.075 \times 0)]\} \times 1.11$
♠ $q = \{\Delta k - [0.31 + (0.44 \times 1) + (0.99 \times 1) + (0.075 \times 0)]\} \times 1.11$
♦ $q = \{\Delta k - [0.31 + (0.44 \times 1) + (0.99 \times 0) + (0.075 \times 0)]\} \times 1.11$
[a] contains 0.15mM Eu(III) complex, pH unadjusted
[b] contains 0.15mM Eu(III) complex, pH adjusted

Table 4.13: Phosphorescence decay constants for europium(III)-1,7-bis(2-hydroxycyclohexyl)-1,7-bis(carboxymethyl)-1,4,7-triazaheptane, as a function of pH, multi-component buffered system, at equilibrium (7 days, λ_{ex} = 276 nm, λ_{em} = 616 nm).

Sample	pH (48 h)	pD (48 h)	k_{H_2O} (ms^{-1})	k_{D_2O} (ms^{-1})	Δk (ms^{-1})	q†	q‡	q♠	q♦
Stock[a]	5.48	5.66	4.50	0.70	3.80	1.8	2.9	2.3	3.4
Sample 1[b]	2.67	2.65	7.03	0.93	6.10	4.4	5.5	4.8	**5.9**
Sample 2[b]	5.72	4.93	4.82	0.75	4.07	**2.1**	3.2	2.6	3.7

† $q = \{\Delta k - [0.31 + (0.44 \times 2) + (0.99 \times 1) + (0.075 \times 0)]\} \times 1.11$
‡ $q = \{\Delta k - [0.31 + (0.44 \times 2) + (0.99 \times 0) + (0.075 \times 0)]\} \times 1.11$
♠ $q = \{\Delta k - [0.31 + (0.44 \times 1) + (0.99 \times 1) + (0.075 \times 0)]\} \times 1.11$
♦ $q = \{\Delta k - [0.31 + (0.44 \times 1) + (0.99 \times 0) + (0.075 \times 0)]\} \times 1.11$
[a] contains 0.15mM Eu(III) complex, pH unadjusted
[b] contains 0.15mM Eu(III) complex, pH adjusted

The phosphorescence emission spectra for samples prepared in H_2O (Figure 4.56) reveal an increase in emission intensity over time. Emission intensity is also observed to increase with increasing pH, accompanied by modulation of the relative ratio between the $\Delta J = 1$ (592 nm) and $\Delta J = 2$ (616 nm) emission bands. Phosphorescence emission spectra for samples prepared in D_2O are illustrated in Figure 4.57. The emission intensity for sample 1 (Figure 4.57, (ii))

increased over time. The emission intensity recorded for the stock solution (Figure 4.57, (i)) and sample 2 (Figure 4.57, (iii)) exceeded the detection range, for the chosen instrument settings. Therefore, detector sensitivity was reduced for these samples, resulting in the 'apparent' decreased emission intensity over time.

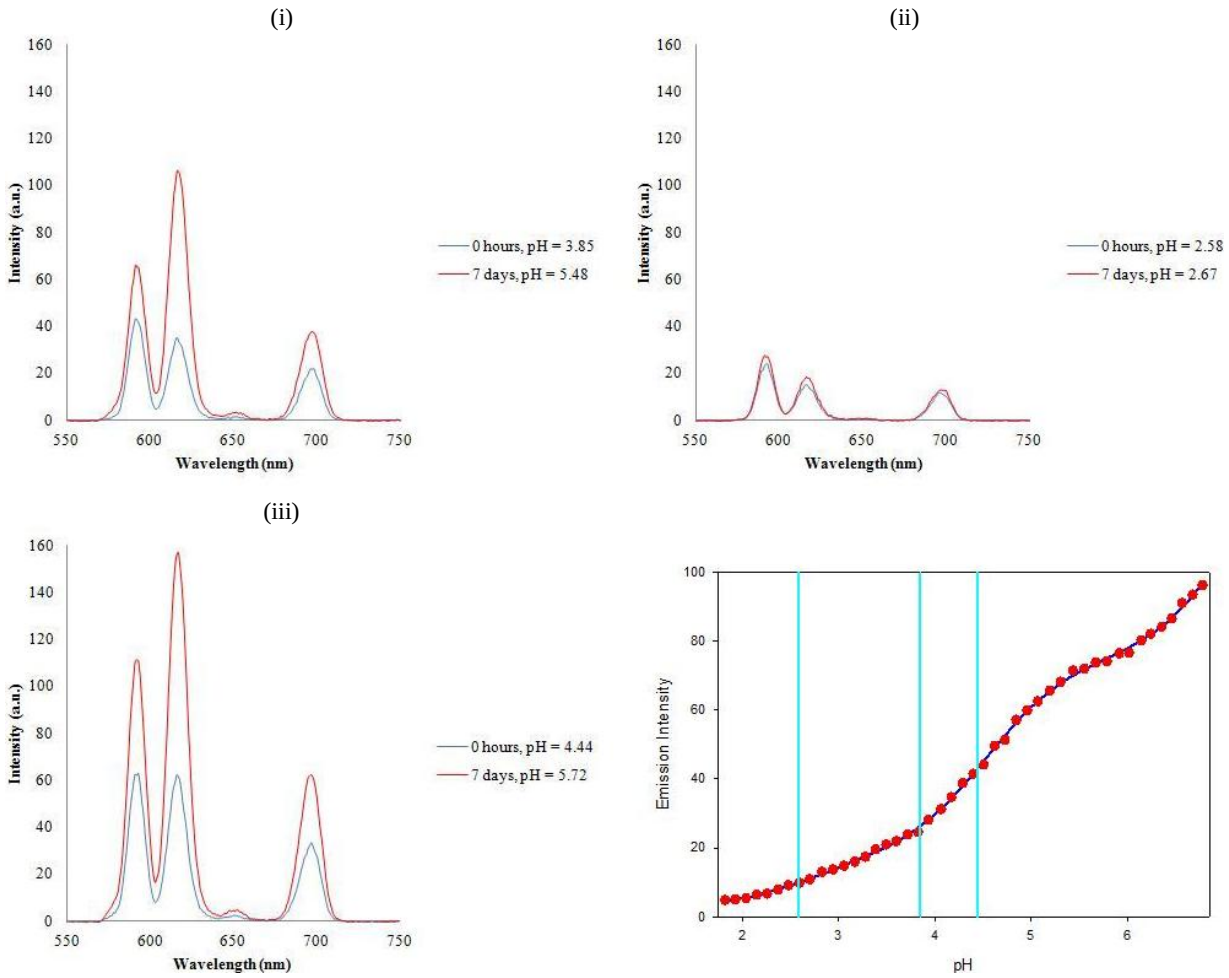


Figure 4.56: Comparison of phosphorescence emission spectra of (i) stock solution, (ii) sample 1, and (iii) sample 2 of europium(III)-1,7-bis(2-hydroxycyclohexyl)-1,7-bis(carboxymethyl)-1,4,7-triazaheptane, as a function of pH, in H_2O (λ_{ex} = 276 nm). *Inset*: Emission profile at 616 nm (cyan lines indicate selected pH values for the phosphorescence decay experiment).

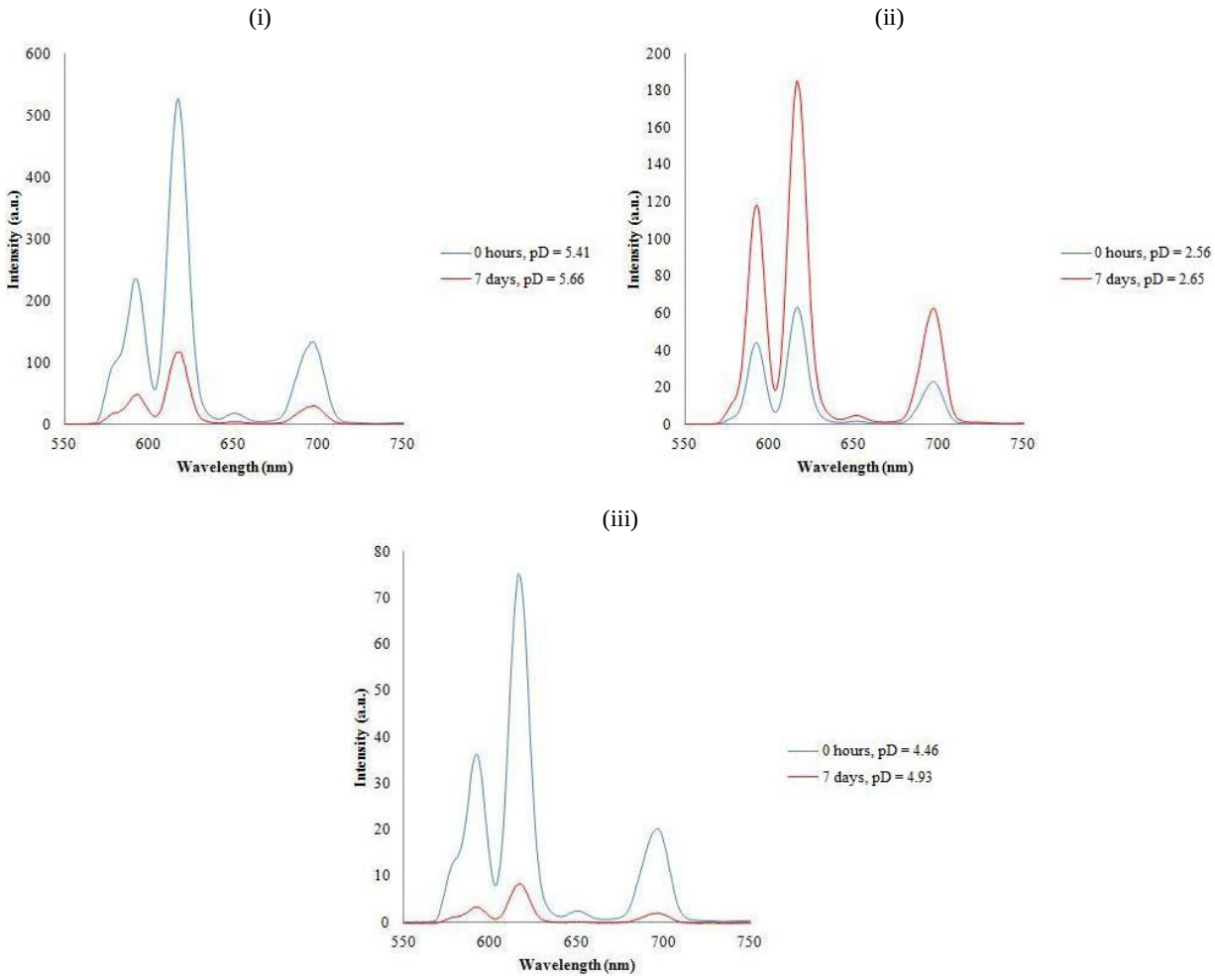


Figure 4.57: Comparison of phosphorescence emission spectra of (i) stock solution, (ii) sample 1, and (iii) sample 2 of europium(III)-1,7-bis(2-hydroxycyclohexyl)-1,7-bis(carboxymethyl)-1,4,7-triazaheptane, as a function of pD, in D_2O (λ_{ex} = 276 nm).

The pH and pD values for sample 1 were observed to fluctuate very little over time (Figure 4.56, (ii), and Figure 4.57, (ii)). The difference between the pH and pD values for sample 1 upon initial preparation (Table 4.12, $\Delta_{pH/pD}$ = 0.02 (sample 1)) and upon reaching equilibrium (Table 4.13, $\Delta_{pH/pD}$ = 0.02 (sample 1)) confirm the accuracy of the calculated q values. The small difference between the pH and pD values for sample 2 upon initial preparation (Table 4.12, $\Delta_{pH/pD}$ = 0.02 (sample 2)) indicate that the calculated q value is accurate. However, upon reaching equilibrium, the difference between pH and pD increases (Table 4.13, $\Delta_{pH/pD}$ = 0.79 (sample 2)). The pH of sample 2 varies significantly over time (Tables 4.12 and 4.13, sample 2, ΔpH = 1.28, ΔpD = 0.47). The possible formation of an outersphere ternary complex with the phthalate ion results in depletion of the buffering capacity (due to the low buffer to complex ratio used, 1:10), and is responsible for the large fluctuation for samples prepared between pH 4 and pH 6 (functional buffering window for KHP). The equilibrium

pH (Table 4.13, sample 2 (pH 5.72)) and pD (Table 4.13, sample 2 (pD 4.93)) values for sample 2 lie within a pH range corresponding to slight variation in the gradient for the emission profile (Figure 4.39, gradient between pH 4.9 and pH 5.7), suggesting measured q values are averages of prevalent hydration states within this pH range. The pH value for the stock solution was also observed to vary over time, due to ternary complex formation (Tables 4.12 and 4.13, stock solution, ΔpH = 1.63, ΔpD = 0.25). pH and pD values for the stock solution upon initial preparation differ (Table 4.12, $\Delta_{pH/pD}$ = 1.83 (stock)), indicating poor accuracy for the calculated q value. However, the equilibrium pH and pD values are comparable (Table 4.13, $\Delta_{pH/pD}$ = 0.18 (stock)), suggesting better accuracy for the equilibrium q values.

Sample 1 exhibits large q values upon initial preparation at low pH (Table 4.12, sample 1 (pH 2.58), $q^{\blacklozenge}$ = 5.9), suggesting incomplete chelation of the Eu(III) ion. The pH of sample 1, lower than the spectroscopically determined pK_a1 value (Figure 4.39, pK_a1 = 2.65 ± 0.09), suggests calculated q values for this sample may reflect the hydration state upon initial amine deprotonation of the dipositive diethylenetriamine backbone. However, pK_a1 additionally coincides with the first deprotonation for the added phthalate[67]. Comparison of the $q^{\blacklozenge}$ value for sample 1 in the buffered solution is similar to that observed for sample 1 in aqueous solution (Table 4.9, sample 1 (pH 2.89), $q^{\blacklozenge}$ = 6.2), suggesting the equilibrium observed is the first deprotonation of the amine donors on the diethylenetriamine backbone and that the amine donors and one pendant hydroxycyclohexyl arm are not coordinated to the metal centre (Figure 4.58 (i)). Sample 2 (Table 4.12, sample 2 (pH 4.44), $q^{\spadesuit}$ = 3.6) displays a decrease in the q value indicating increased encapsulation of the metal ion by the ligand donor groups. The hydration state of sample 2 can be associated with the spectroscopically determined pK_a2 (Figure 4.39, pK_a1 = 4.54 ± 0.02) – complete deprotonation of the diethylenetriamine backbone. The q value strongly suggests a hydroxycyclohexyl pendant remains uncoordinated (Figure 4.58 (ii) and (iii)).

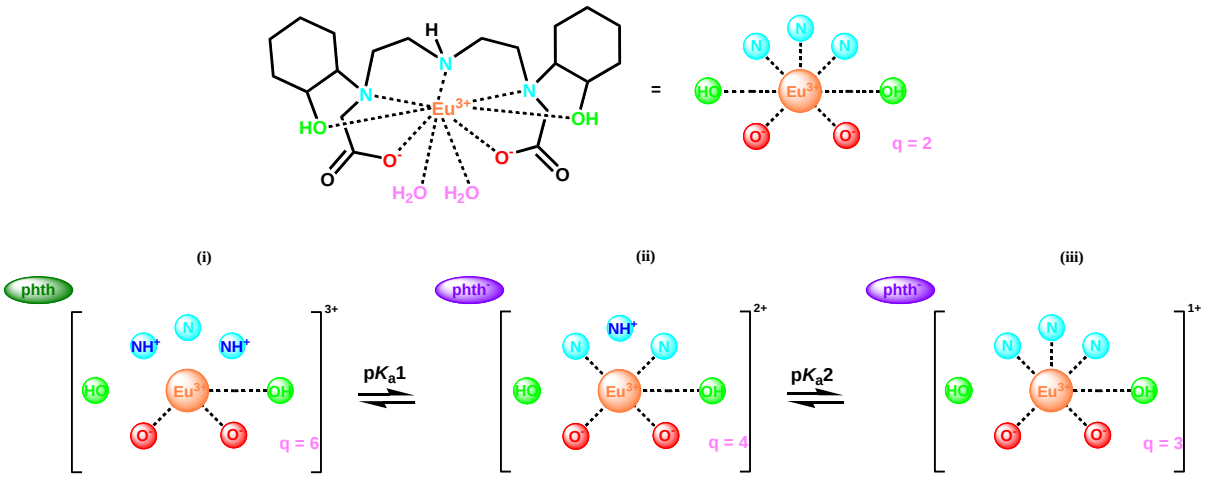


Figure 4.58: Proposed speciation of europium(III)-1,7-bis(2-hydroxycyclohexyl)-1,7-bis(carboxymethyl)-1,4,7-triazaheptane, in a multi-component buffered system, upon initial preparation.

The q value for sample 1 upon reaching equilibrium (Table 4.13, sample 1 (pH 2.67), $q^{\blacklozenge}$ = 5.9) shows little change from the q value determined upon initial preparation (Table 4.12, sample 1, $q^{\blacklozenge}$ = 5.9), affirming incomplete ligation of the Eu(III) metal ion (Figure 4.59, (i)). The equilibria associated with the second deprotonatation of the diethylenetriamine backbone and formation of the phthalate dianion occur concurrently above pH 5. In aqueous media, the sample 2 q value upon reaching equilibrium (Table 4.11, sample 2 (pH 6.07), $q^{\ddagger}$ = 2.0) suggested chelation by the seven available donor groups present in the ligand. The $q^{\dagger}$ value for sample 2 in buffered media (Table 4.13, sample 2 (pH 5.72), $q^{\dagger}$ = 2.1) similarly indicates complexation by the ligand donors, suggesting possible dissociation of the outersphere phthalate ternary complex upon reaching equilibrium (Figure 4.59, (vi)).

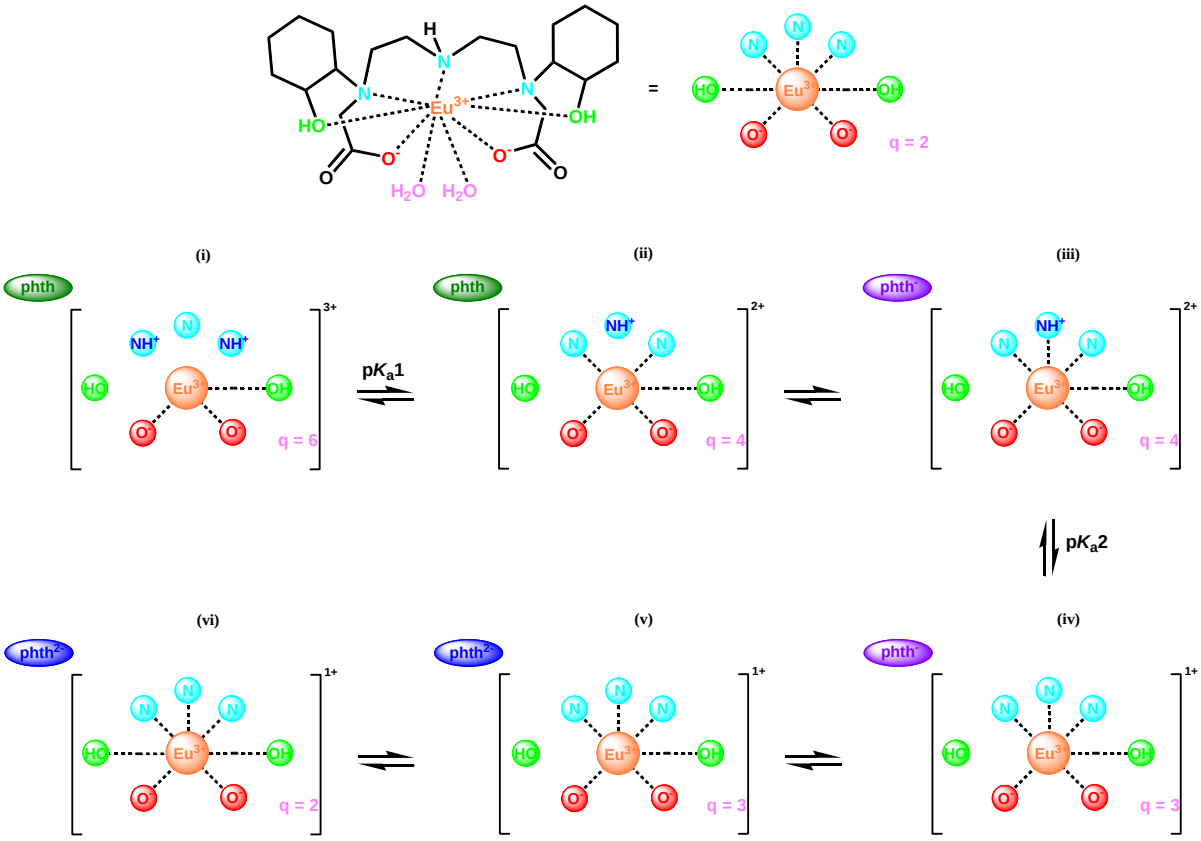


Figure 4.59: Proposed speciation of europium(III)-1,7-bis(2-hydroxycyclohexyl)-1,7-bis(carboxymethyl)-1,4,7-triazaheptane, in a multi-component buffered system, upon reaching equilibrium.

4.5 References

1. de Sousa, A. S., and Hancock, R. D., *J. Chem. Soc., Chem. Commun.* **1995**, (4), 415-416.
2. Gorzynski-Smith, J., *Synthesis* **1984**, (8), 629-656.
3. Saito, S., Yamashita, S., Nishikawa, T., Yokoyama, Y., Inaba, M., and Moriwake, T., *Tet. Lett.* **1989,** 30, (31), 4153-4156.
4. Yamada, J., Yumoto, M., and Yamamoto, Y., *Tet. Lett.* **1989,** 30, (32), 4255-4258.
5. de Sousa, A. S., Hancock, R. D., and Reibenspies, J. H., *J. Chem. Soc., Dalton Trans.* **1997,** 1997, (16), 2831-2835.
6. de Sousa, A. S., Croft, G. J. B., Wagner, C. A., Michael, J. P., and Hancock, R. D., *Inorg. Chem.* **1991,** 30, (18), 3525-3529.
7. de Sousa, A. S., Hancock, R. D., and Reibenspies, J. H., *J. Chem. Soc., Dalton Trans.* **1997,** 1997, (6), 939-944.
8. Li, M., and Selvin, P. R., *J. Am. Chem. Soc.* **1995,** 117, (31), 8132-8138.
9. Parker, D., and Williams, J. A. G., *J. Chem. Soc., Dalton Trans.* **1996,** 1996, (18), 3613-3628.
10. Remuiñán, M. J., Román, H., Alonso, M. A., and Rodríguez-Ubis, J. C., *J. Chem. Soc., Perkin Trans. 2* **1993**, (6), 1099-1102.
11. Farfán, N., Cuéllar, L., Aceves, J. M., and Contreras, R., *Synthesis* **1987**, (10), 927-929.
12. Agami, C., Couty, F., Hamon, L., Prince, B., and Puchot, C., *Tetrahedron* **1990,** 46, (20), 7003-7010.
13. Agami, C., Couty, F., Hamon, L., and Puchot, C., *Tet. Lett.* **1992,** 33, (25), 3645-3646.
14. Agami, C., Couty, F., Prince, B., and Venier, O., *Tet. Lett.* **1993,** 34, (44), 7061-7062.
15. Moulay, S., *Chem. Educ. Res. Pract. Eur.* **2002,** 3, (1), 33-64.
16. Zeng, J., and Davies, M. J., *Chem. Res. Toxicol.* **2005,** 18, (8), 1232-1241.
17. Schramm, C., and Rinderer, B., *Anal. Chem.* **2000,** 72, (23), 5829-5833.
18. Ortiz, A., Farfán, N., Santillan, R., Rosales, M., García-Baéz, E., Daran, J. C., and Halut, S., *Tetrahedron: Asymmetry* **1995,** 6, (11), 2715-2722.
19. Fratzke, A. R., and Reilly, P. J., *Int. J. Chem. Kinet.* **1986,** 18, (7), 757-773.
20. Whipple, E. B., *J. Am. Chem. Soc.* **1970,** 92, (24), 7183-7186.

21. Ohshima, T., Yamamoto, Y., Takaki, U., Inoue, Y., Saeki, T., Itou, K., Maegawa, Y., Iawsaki, T., and Mashima, K., *Chem. Commun.* **2009**, (19), 2688-2690.
22. Santes, V., Ortíz, A., Santillan, R., Gutiérrez, A., and Farfán, N., *Synthetic Commun.* **1999,** 29, (8), 1277-1286.
23. Santes, V., Gómez, E., Zárate, V., Santillan, R., Farfán, N., and Rojas-Lima, S., *Tetrahedron: Asymmetry* **2001,** 12, (2), 241-247.
24. Ortiz, A., Farfán, N., Höpfl, H., Santillan, R., Ochoa, M. E., and Gutiérrez, A., *Tetrahedron: Asymmetry* **1999,** 10, (4), 799-811.
25. Dijksman, A., Elzinga, J. M., Li, Y-X., Arends, I. W. C. E., and Sheldon, R. A., *Tetrahedron: Asymmetry* **2002,** 13, (8), 879-884.
26. Martin, A. E., Ford, T. M., and Bulkowski, J. E., *J. Org. Chem.* **1982,** 47, (3), 412-415.
27. Padayachy, K., Fernandes, M. A., Marques, H. M., and de Sousa, A. S., *J. Chem. Crystallogr.* **2008,** 38, (8), 577-582.
28. Herberich, B., Scott, J. D., and Williams, R. M., *Bioorg. Med. Chem.* **2000,** 8, (3), 523-532.
29. Caravan, P., Amedio Jr., J. C., Dunham, S. U., Greenfield, M. T., Cloutier, N. J., McDermid, S. A., Spiller, M., Zech, S. G., Looby, R. J., Raitsimring, A. M., McMurry, T. J., and Lauffer, R. B., *Chem. Eur. J.* **2005,** 11, (20), 5866-5874.
30. Fedi, V., Altamura, M., Balacco, C., Canfarini, F., Criscuoli, M., Giannotti, D., Giolitti, A., Giuliani, S., Guidi, A., Harmat, N. J. S., Nannicini, R., Pasqui, F., Patacchini, R., Perrotta, E., Tramontana, M., Tirolo, A., and Maggi, C. A., *J. Med. Chem.* **2004,** 47, (27), 6935-6947.
31. Bräuner-Osborne, H., Bunch, L., Chopin, N., Couty, F., Evano, G., Jensen, A. A., Kusk, M., Nielsen, B., and Rabasso, N., *Org. Biomol. Chem.* **2005,** 3, (21), 3926-3936.
32. Tan, T. H. S., Hickman, D. T., Morral, J., Beadham, I. G., and Micklefield, J., *Chem. Commun.* **2004**, (5), 516-517.
33. Greenwald, R. B., Zhao, H., Yang, K., Reddy, P., and Martinez, A., *J. Med. Chem.* **2004,** 47, (3), 726-734.
34. Smith, G., Mikkelsen, G., Eskildsen, J., and Bundgaard, C., *Bioorg. Med. Chem. Lett.* **2006,** 16, (15), 3981-3884.
35. Aime, S., Cravotto, G., Crich, S. G., Giovenzana, G. B., Ferrari, M., Palmisano, G., and Sisti, M., *Tet. Lett.* **2002,** 43, (5), 783-786.

36. Pettit, G. R., Chamberland, M. R., and Blonda, D. S., *Can. J. Chem.* **1964,** 42, (7), 1699-1706.
37. Padayachy, K., Fernandes, M. A., Marques, H. M., and de Sousa, A. S., *Acta Cryst. E* **2012,** E68, (8), o2570-o2571.
38. Padayachy, K., Mgcima, Z., Fernandes, M. A., Marques, H. M., and de Sousa, A. S., *Acta Cryst. E* **2011,** E67, (10), o2594.
39. Yin, H., Xu, Y., and Qian, X., *Bioorg. Med. Chem.* **2007,** 15, (3), 1356-1362.
40. Kemp, D. S., and Vellaccio, F., *Organic Chemistry*. Worth Publishers: London, 1980.
41. Plush, S. E., and Gunnlaugsson, T., *Dalton Trans.* **2008**, (29), 3801-3804.
42. Plush, S. E., Clear, N. A., Leonard, J. P., Fanning, A., and Gunnlaugsson, T., *Dalton Trans.* **2010,** 39, (15), 3644-3652.
43. May, P. M., *Talanta* **1988,** 35, (11), 825-830.
44. May, P. M., *Talanta* **1988,** 35, (12), 933-941.
45. May, P. M., *Talanta* **1998,** 35, (12), 927-932.
46. Filella, M., and May, P. M., *Talanta* **2005,** 65, (5), 1221-1225.
47. Anderegg, G., Arnaud-Neu, F., Delgado, R., Felcman, J., and Popov, K., *Pure Appl. Chem.* **2005,** 77, (8), 1445-1495.
48. Kotek, J., Lebdušoeková, P., Hermann, P., Vander Elst, L., Muller, R. N., Geraldes, C. F. G. C., Maschmeyer, T., Lukeš, I., and Peters, J. A., *Chem. Eur. J.* **2003,** 9, (23), 5899-5915.
49. Moeller, T., and Thompson, L. C., *J. Inorg. Nucl. Chem.* **1962,** 24, (5), 499-510.
50. Parker, D., Dickins, R. S., Puschmann, H., Crossland, C., and Howard, J. A. K., *Chem. Rev.* **2002,** 102, (6), 1977-2010.
51. *SigmaPlot*, 11.0; Systat Software Inc.: 2008.
52. Bünzli, J. G., *Chem. Rev.* **2010,** 110, (5), 2729-2755.
53. Hall, H. K., Jr., *J. Am. Chem. Soc.* **1957,** 79, (20), 5441.
54. Dawson, R. M. C., Elliott, D. C., Elliott, W. H., and Jones, K. M., *Data For Biochemical Research*. Clarendon Press: Oxford, 1959.
55. Lowe, M. P., and Parker, D., *Inorg. Chim. Acta* **2001,** 317, (1-2), 163-173.
56. Gunnlaugsson, T., *Tet. Lett.* **2001,** 42, (50), 8901-8905.
57. Gunnlaugsson, T., Leonard, J. P., Sénéchal, K., and Harte, A. J., *J. Am. Chem. Soc.* **2003,** 125, (40), 12062-12063.

58. Gunnlaugsson, T., Harte, A. J., Leonard, J. P., and Nieuwenhuyzen, M., *Supramol. Chem.* **2003,** 15, (7-8), 505-519.
59. Harte, A. J., Jensen, P., Plush, S. E., Kruger, P. E., and Gunnlaugsson, T., *Inorg. Chem.* **2006,** 45, (23), 9465-9474.
60. Bruce, J. I., Dickins, R. S., Govenlock, L. J., Gunnlaugsson, T., Lopinski, S., Lowe, M. P., Parker, D., Peacock, R. D., Perry, J. J. B., Aime, S., and Botta, M., *J. Am. Chem. Soc.* **2000,** 122, (40), 9674-9684.
61. Plush, S. E., and Gunnlaugsson, T., *Org. Lett.* **2007,** 9, (10), 1919-1922.
62. Dickins, R. S., Aime, S., Batsanov, A. S., Beeby, A., Botta, M., Bruce, J. I., Howard, J. A. K., Love, C. S., Parker, D., Peacock, R. D., and Puschmann, H., *J. Am. Chem. Soc.* **2002,** 124, (43), 12697-12705.
63. Dotson, R. L., *J. Inorg. Nucl. Chem.* **1972,** 34, (10), 3131-3138.
64. Schwartz, M. A., *Bioorg. Chem.* **1982,** 11, (1), 4-18.
65. Tracey, A. S., and Gresser, M. J., *Inorg. Chem.* **1988,** 27, (7), 1269-1275.
66. Bai, K. S., and Hong, K. H., *Bull. Korean Chem. Soc.* **2000,** 21, (6), 650-652.
67. Wang, Z.-M., van de Burgt, L. J., and Choppin, G. R., *Inorg. Chim. Acta* **1999,** 293, (2), 167-177.
68. Huang, C., Hammell, J., Ratnakar, S. J., Sherry, A. D., and Morrow, J. R. , *Inorg. Chem.* **2010,** 49, (13), 5963-5970.
69. Sun, J., Chen, C., and Qin, Z., *J. Lumin.* **1988,** 40-41, 246-247.
70. Yang, L., Zhao, Y., Su, Y., and Wu, J., *Spectrochim. Acta A* **2002,** 58, (13), 2803-2808.
71. Enculescu, M., Preda, N., Matei, E., and Enculescu, I., *Mater. Chem. Phys.* **2012,** 136, (1), 51-58.
72. Horrocks, J., W. DeW., and Sudnick, D. R., *J. Am. Chem. Soc.* **1979,** 101, (2), 334-340.
73. Chappell, L. L., Voss, Jr., D. A., Horrocks, Jr., W. DeW., and Morrow, J. R., *Inorg. Chem.* **1998,** 37, (16), 3989-3998.
74. Supkowski, R. M., and Horrocks, Jr., W. DeW., *Inorg. Chem.* **1999,** 38, (24), 5616-5619.
75. Supkowski, R. M., and Horrocks, Jr., W. DeW., *Inorg. Chim. Acta* **2002,** 340, 44-48.
76. Beeby, A., Clarkson, I. M., Dickins, R. S., Faulkner, S., Parker, D., Royle, L., de Sousa, A. S., Williams, J. A. G., and Woods, M., *J. Chem. Soc. Perkin Trans. 2* **1999**, (3), 499-503.

77. Parker, D., *Coord. Chem. Rev.* **2000,** 205, (1), 109-130.

Chapter 5

Summary, Conclusions and Future Work

5.1 Summary and Conclusions

Phthalates are common additives in the manufacture of plastic materials, such as polyvinylchloride (PVC), imparting flexibility to the products and are also present in toys, pesticides, cosmetics and food wrap. However, phthalates are common air, soil and water contaminants. Human exposure to phthalates could prove toxic, as studies on laboratory animals have demonstrated disruption of metabolic and reproductive processes as a result of phthalate exposure. Therefore, detection of trace amounts of phthalate is of paramount importance[1-8].

Lanthanide luminescence offers an elegant solution for the detection of low level concentrations of biological analytes, due to their long-lived excited states. Direct excitation of a lanthanide ion, such as Eu(III) or Tb(III), is difficult, due to Laporte forbidden f-f transitions. Incorporation of aromatic groups into ligand architecture ensures efficient population of the metal excited state upon chelation, due to energy transfer from the ligand singlet excited state to the lanthanide triplet excited state. However, analyte recognition events could modulate the luminescent response of the lanthanide complex. Detection of phthalates by lanthanide luminescence is particularly attractive as the presence of the aromatic moiety in the phthalate structure would efficiently sensitize the Ln(III) excited state, ensuring emission enhancement upon the formation of a ternary complex[9-14].

There are numerous investigations involving the detection of aliphatic and aromatic dicarboxylates (such as phthalates) by means of ternary complex formation with lanthanide chelates[9-14]. However, ternary complex formation relies on coordinatively unsaturated lanthanide systems, with at least two vacant sites present on the metal centre (i.e. lanthanide complexes bearing ligand heptadenticity). While several literature examples demonstrate the detection of the *m*- and *p*-forms of phthalic acid by ternary complex formation with cyclen-

derived heptadentate lanthanide systems[9-12, 14], little research has been considered for *o*-phthalic acid.

The aim of this project was to develop novel Gd(III) MRI contrasts agents that are responsive to the concentrations of certain biomolecules under physiological conditions. Analyte detection in aqueous solution was scrutinized by monitoring modulations in the spectroscopic signatures of analogous Eu(III) complexes (due to the similarity of the ionic radius, speciation and coordination polyhedra). An acyclic ligand system derived from DTPA was considered, where two terminal carboxymethyl pendant arms have been replaced by neutral OH donors to maximize binding interactions between the substrate molecule and Ln(III)-complex. The [Eu(Cy_2DETA.3A)] complex is investigated as a possible octadentate sensor for phthalic acid, by monitoring changes in the emission profiles and hydration states in aqueous and buffered media, as a function of pH. The performance of the octadentate sensor was compared to [Eu(Cy_2DETA.2A)], a heptadentate sensor proposed to favour phthalate ternary complex formation.

The synthesis of novel acyclic hydroxypolyaminocarboxylate ligands, analogous to DTPA, was attempted by replacing terminal carboxylate pendant arms of DTPA with neutral hydroxycyclohexyl moieties. The synthetic prodecure involved initial alkylation of diethylenetriamine with cyclohexene oxide by refluxing in ethanol. The synthesis was successful, with the target β-aminoalcohol (Cy_2DETA) isolated in moderate yield (60%). Cy_2DETA was fully characterized by NMR, IR, MS and elemental analysis, with single crystal structures obtained for the free base and perchloric acid salt. Esterification of the aminoalcohol with ethyl bromoacetate was unsuccessful due to poor selectivity (resulting in unwanted esterification of the alcohol groups). The synthetic procedure was modified by using the robust tert-butyl bromoacetate, and evaluating esterification at room temperature using different solvents (dichloromethane (DCM), tetrahydrofuran (THF) and dimethylformamide (DMF)), with high selectivity and yield (>90%) of the desired product achieved in DMF. The tri-ester (Cy_2DETA.3E) was analyzed by NMR, IR and MS techniques. A single crystal structure of Cy_2DETA.3E was obtained as a Na-complex (with a Br^- counterion). The isolation of this complex is useful as Na-complexes are isostructural with europium complexes, as the ions are of similar size (Na^+: 1.12 Å (CN = 7), 1.24 Å (CN = 9); Eu^{3+}: 1.12 Å (CN = 9)) and coordination requirement[10, 15, 16]. The structure revealed a

Na-complex adopting an incomplete square antiprism geometry bearing ligand heptadenticity and one uncoordinated ester arm (due to the steric bulk of the tert-butyl group). This observation suggested ligand hydrolysis would favour complete coordination by each of the donor groups, likely resulting in the square antiprism geometry which is commonly observed for DTPA and its derivatives. Ester deprotection was attempted with TFA (trifluoroacetic acid), resulting in formation of unwanted-side products. The hydrolysed ester (Cy_2DETA.3A) was efficiently synthesized by refluxing Cy_2DETA.3E in concentrated HCl[17], and isolated in good yield (85%) upon work-up. NMR, IR and MS analysis of Cy_2DETA.3A revealed the formation of a di-morpholone (due to dehydration across the terminal carboxymethyl and hydroxycyclohexyl pendants, characterized by the morpholone C=O stretch at 1650 cm^{-1} from IR spectroscopy).

The synthesis of the heptadentate analogue of Cy_2DETA.3A (i.e. Cy_2DETA.2A) was achieved via a one-pot procedure involving the aminoalcohol (Cy_2DETA) and glyoxal, exploiting the preferred reaction of glyoxal with β-substituted aminoalcohols[18]. The product was isolated in moderate yield (70%) upon work-up, with NMR, IR, and MS characterizations revealing the formation of the di-morpholone. The proposed synthesis of the hydroxycyclopentyl analogue of DTPA was abandoned, as metal complexes formed with this ligand are expected to be weak due to high torsional strain of the ring upon chelation[19].

Potentiometrically determined pK_a values for both heptadentate (Cy_2DETA.2A) and octadentate (Cy_2DETA.3A) ligands demonstrated favourable comparison with protonation constants determined for DTPA[20].

Luminescence emission spectra recorded for the octadentate [Eu(Cy_2DETA.3A)] complex in aqueous solution aided in determination of a spectroscopic pK_a value (2.71 ± 0.07, assigned to deprotonation of the central amine moiety on the ligand backbone) for the metal complex. Comparison with the potentiometrically determined ligand protonation constant for the equivalent process (10.21 ± 0.01) reveals an eight order magnitude decrease upon chelation of the Eu^{3+} cation, demonstrating the effect of the trivalent Lewis acid in decreasing ligand pK_a values upon complexation. Measurement of luminescence decay constants for [Eu(Cy_2DETA.3A)] assisted elucidation of the hydration sphere (q values) around the Eu^{3+}

cation. Therefore, in the absence of solid-state data, correlation between the luminescence emission and lifetime decay spectra offers a valuable means of determining solution speciation. A ratiometric response at low pH was revealed for the complex, with a corresponding q value of 1.5 (a result of the protonation equilibrium involving the central amine donor present on the diethylenetriamine backbone of the ligand), suggesting this Eu-system could be potentially useful as a low pH sensor[21-24]. At physiological pH and in the absence of other analytes, the ligand donor groups are fully coordinated to the cation (ligand octadenticity), with a single water molecule capping the coordination polyhedron, indicated by a q value of 1.0.

Correlation of the emission profiles with the q values for the [Eu(Cy_2DETA.3A)] complex in a multi-component buffered solution revealed a pH-dependant response of the complex towards phthalate, as a function of time. The formation of a phthalate ternary complex results in better resolution of the emission profile between pH 4 and pH 8, coinciding with complete deprotonation of the phthalate ion (5.01 ± 0.37). The improved resolution allows for the detection of the pK_a corresponding to deprotonation of the apical water molecule (7.45 ± 0.14). Observation of the pK_a assigned to alkoxide formation (11.18 ± 0.12) further illustrates the decrease in ligand pK_a values upon coordination of a Lewis acid. The large hydration numbers observed for the buffered solution upon initial preparation suggests possible phthalate ternary complex formation is due to outersphere hydrogen-bonding of the hydroxycyclohexyl pendant arm and apical water molecule present in the complex with the carboxylate moieties of the analyte. The hydrogen bonding of the outersphere is accompanied by dissociation of a single hydroxycyclohexyl moiety, reflected in larger q values. Emission enhancement decreases upon reaching equilibrium (buffer capacity exhaustion), with concomitant decrease in q values that signify dissociation of the ternary complex and renewed coordination of the hydroxcyclohexyl pendant arm. Therefore, the functioning of the complex as a biological sensor relies upon the ‘on/off’ chelation of a neutral hydroxycyclohexyl pendant arm.

Regression analysis on the luminescence emission profile for the heptadentate [Eu(Cy_2DETA.2A)] complex in aqueous solution revealed two spectroscopic pK_a values, assigned to subsequent deprotonation of amine donors on the diethylenetriamine backbone (3.19 ± 0.33 and 5.55 ± 0.17). Comparison with potentiometrically determined ligand pK_as

(8.41 ± 0.01 and 10.91 ± 0.01) reveal a five-order magnitude decrease in the protonation constants upon Eu(III) complexation. Luminescence decay spectra for samples prepared at spectroscopically observed pK_a values reveal large q values (q = 4.5) prior to initial deprotonation of the diethylenetriamine backbone at low pH. Protonation of the terminal amine moieties prevent coordination of the diethylenetriamine N-donors with the metal ion, resulting in large q values. Increasing pH promotes chelation by the amine groups upon deprotonation (q = 2). Precipitation of $Eu(OH)_3$ was observed at neutral pH, demonstrating weak coordination for the [Eu(Cy_2DETA.2A)] heptadentate complex.

Phthalic acid detection was attempted for the [Eu(Cy_2DETA.2A)] complex, as decreased ligand denticity (compared to Cy_2DETA.3A) would prompt innersphere ternary complex formation by displacement of the coordinated water molecules. Two spectroscopic pK_a values were determined from regression analysis of the luminescence emission profile for [Eu(Cy_2DETA.2A)] in buffered media. Though the pK_a values (2.66 ± 0.09 and 4.54 ± 0.02) are assigned to deprotonation of the diethylenetriamine N-donors, these protonation constants may coincide with subsequent deprotonation of phthalate (2.75 and 4.93)[13]. Significantly large q values were determined from the luminescence decay spectra for [Eu(Cy_2DETA.2A)] upon initial preparation, contrary to formation of an innersphere phthalate ternary complex. The large q values (pH 2.58: q = 5.9, and pH 4.44, q = 3.6) suggest outersphere phthalate detection as a result of hydrogen-bonding of the hydroxycyclohexyl pendant arm and apical water molecule of the complex with the carboxylate groups of the phthalate dianion, accompanied by weakened chelation of the brachial arm. Upon reaching equilibrium, decreases in the q values are observed with increasing pH, signifying dissociation of the phthalate ternary complex. The weak coordination of the [Eu(Cy_2DETA.2A)] heptadentate complex was exposed upon observing precipitation of $Eu(OH)_3$ at neutral pH.

The response of the [Eu(Cy_2DETA.3A)] and [Eu(Cy_2DETA.2A)] complexes towards phthalic acid in aqueous solution was successfully demonstrated due to observed modulation of the photophysical properties of the novel lanthanide complexes upon analyte recognition, resulting in the formation of ternary outersphere complexes. The biomolecule sensing event is reliant upon the on/off chelation of the neutral hydroxycyclohexyl pendant arm. Substituting Eu(III) with the magnetically-susceptible Gd(III) ion would therefore result in the synthesis of novel MRI contrast agents, capable of varied hydration states in response to

in vivo concentrations of specific biomolecules. The fluxional ligand denticity is advantageous for the MRI experiment as detection of the target substrate molecule would result in an increased hydration state (q) of the complex. Additionally, the formation of a ternary complex upon analyte recognition would result in an increase in the molecular weight of the Gd(III) chelate, thus reducing molecular tumbling. Therefore, ternary complex formation (upon recognition of a target substrate molecule) would result in increased relaxivity of the Gd(III)-complex[25], leading to improved contrast enhancement of MR images. An increased relaxivity of the MRI contrast agent may permit use of lower concentrations of the Gd(III)-complex, thus reducing possible bio-accumulation of unsequestered Gd^{3+} ions *in vivo*.

5.2 Future Work

Elucidation of formation constants of the [Eu(Cy_2DETA.3A)] and [Eu(Cy_2DETA.2A)] is of importance to confirm the suitability of these complexes for use in biological media. Formation constants for other biologically active metal cations (such as Ca^{2+} and Zn^{2+}) should be investigated to determine the competitive nature of these ions in relation to Eu^{3+}.

The response of the [Eu(Cy_2DETA.3A)] complex to changing concentrations of *o*-pthalic acid could be further investigated to tailor detection of the analyte. The response of [Eu(Cy_2DETA.3A)] towards *m*- and *p*-phthalic acid could be investigated to offer comparison with the results observed for *o*-phthalic acid. Other biological important substrates bearing carboxylate groups (such as citrates, malonates, succinates and glutarates) could be evaluated, to observe modulation of the emission spectrum due to ternary complex formation[9-12, 26]. The synthesis of [Tb(Cy_2DETA.3A)] would be a worthy endeavour, as several ratiometric lanthanide probes involve the use of structurally related europium and terbium complexes. The differing emission profiles for the Tb(III)- and Eu(III)-complexes can therefore be used as an optical probe, in response to a particular analyte[27-31].

The q values determined from the luminescence decay studies for [Eu(Cy_2DETA.3A)] can be used to estimate the hydration of the corresponding Gd(III) derivative, due to similarity in charge and ionic radius[32]. The [Eu(Cy_2DETA.3A)] q value of ~1.0 suggests [Gd(Cy_2DETA.3A)] would possess a similar hydration state. A water molecule present in the inner coordination sphere of the Gd-complex is magnetically susceptible, resulting in an altered relaxation rate of the coordinated H_2O protons in comparison to the H_2O present in the bulk solution. Therefore, synthesis and relaxometric studies of [Gd(Cy_2DETA.3A)] is encouraged to determine the suitability of the complex as a responsive MRI contrast agent.

5.3 References

1. Casal-Casas, C., and Desvergne, B., *Annu. Rev. Physiol.* **2011,** 73, 135-162.
2. Suzuki, T., Yaguchi, K., and Suzuki, S., *Environ. Sci. Technol.* **2001,** 35, (18), 3757-3763.
3. Guo, Y., Alomirah, H., Cho, H-S., Minh, T. B., Mohd, M. A., Nakata, H., and Kannan, K., *Environ. Sci. Technol.* **2011,** 45, (7), 3138-3144.
4. Desvergne, B., Feige, J. N., and Casal-Casas, C., *Mol. Cell. Endocrinol.* **2009,** 304, (1-2), 43-48.
5. Eveillard, A., Lasserre, F., de Tayrac, M., Polizzi, A., Claus, S., Canlet, C., Mselli-Lakhal, L., Gotardi, G., Paris, A., Guillon, H., Martin, P. G. P., and Pineau, T., *Toxicol. Appl. Pharmacol.* **2009,** 236, (3), 282-292.
6. Fukuwatari, T., Ohsaki, S., Kukuoka. S., Sasaki, R., and Shibata, K., *Toxicol. Sci.* **2004,** 81, (2), 302-308.
7. Hatch, E. E., Nelson, J. W., Stahlhut, R. W., and Webster, T. F., *Int. J. Androl.* **2010,** 33, (2), 324-332.
8. Feige, J. N., Gelman, L., Rossi, D., Goete, V., Metivier, R., Tudor, C., Anghel, S. I., Grosdidier, A., Lathion, C., Engelborghs, Y., Michielin, O., Wahli, W., and Desvergne, B., *J. Biol. Chem.* **2007,** 282, (26), 19152-19166.
9. Gunnlaugsson, T., Harte, A. J., Leonard, J. P., and Nieuwenhuyzen, M., *Supramol. Chem.* **2003,** 15, (7-8), 505-519.
10. Harte, A. J., Jensen, P., Plush, S. E., Kruger, P. E., and Gunnlaugsson, T., *Inorg. Chem.* **2006,** 45, (23), 9465-9474.
11. Plush, S. E., and Gunnlaugsson, T., *Org. Lett.* **2007,** 9, (10), 1919-1922.
12. Tilney, J. A., Sørensen, T. J., Burton-Pye, B. P., and Faulkner, S., *Dalton Trans.* **2011,** 40, (45), 12063-12066.
13. Wang, Z.-M., van de Burgt, L. J., and Choppin, G. R., *Inorg. Chim. Acta* **1999,** 293, (2), 167-177.
14. Dickins, R. S., Aime, S., Batsanov, A. S., Beeby, A., Botta, M., Bruce, J. I., Howard, J. A. K., Love, C. S., Parker, D., Peacock, R. D., and Puschmann, H., *J. Am. Chem. Soc.* **2002,** 124, (43), 12697-12705.
15. Gunnlaugsson, T., Brougham, D. F., Fanning, A.-M., Nieuwenhuyzen, M., O'Brien, J. E., and Viguier, R., *Org. Lett.* **2004,** 6, (26), 4805-4808.

16. Shannon, R. D., *Acta Cryst. A.* **1976,** 32, (5), 751-767.
17. Aime, S., Cravotto, G., Crich, S. G., Giovenzana, G. B., Ferrari, M., Palmisano, G., and Sisti, M., *Tet. Lett.* **2002,** 43, (5), 783-786.
18. Farfán, N., Cuéllar, L., Aceves, J. M., and Contreras, R., *Synthesis* **1987**, (10), 927-929.
19. Kemp, D. S., and Vellaccio, F., *Organic Chemistry*. Worth Publishers: London, 1980.
20. Anderegg, G., Arnaud-Neu, F., Delgado, R., Felcman, J., and Popov, K., *Pure Appl. Chem.* **2005,** 77, (8), 1445-1495.
21. Plush, S. E., and Gunnlaugsson, T., *Dalton Trans.* **2008**, (29), 3801-3804.
22. Gunnlaugsson, T., *Tet. Lett.* **2001,** 42, (50), 8901-8905.
23. Gunnlaugsson, T., Leonard, J. P., Sénéchal, K., and Harte, A. J., *J. Am. Chem. Soc.* **2003,** 125, (40), 12062-12063.
24. Lowe, M. P., and Parker, D., *Inorg. Chim. Acta* **2001,** 317, (1-2), 163-173.
25. Parker, D., and Williams, J. A. G., *J. Chem. Soc., Dalton Trans.* **1996,** 1996, (18), 3613-3628.
26. Pal, R., Parker, D., and Costello, L. C., *Org. Biomol. Chem.* **2009,** 7, (8), 1525-1528.
27. Liu, M., Ye, Z., Xin, C., and Yuan, J., *Anal. Chim. Acta* **2013,** 761, 149-156.
28. Ma, B., Wu, S., and Zeng, F., *Sensor Actuat. B-Chem.* **2010,** 145, (1), 451-456.
29. Smith, D. G., McMahon, B. K., Pal, R., and Parker, D., *Chem. Commun.* **2012,** 48, (68), 8520-8522.
30. Tremblay, M. S., Halim, M., and Sames, D., *J. Am. Chem. Soc.* **2007,** 129, (24), 7570-7577.
31. Xiao, Y., Ye, Z., Wang, G., and Yuan, J., *Inorg. Chem.* **2012,** 51, (5), 2940-2946.
32. Urbanczyk-Pearson, L. M., Femia, F. J., Smith, J., Parigi, G., Duimstra, J. A., Eckermann, A. L., Luchinat, C., and Meade, T. J., *Inorg. Chem.* **2008,** 47, (1), 56-68.

Appendix A – MS Data

All MS data was generated in the manner described in Chapter 2.

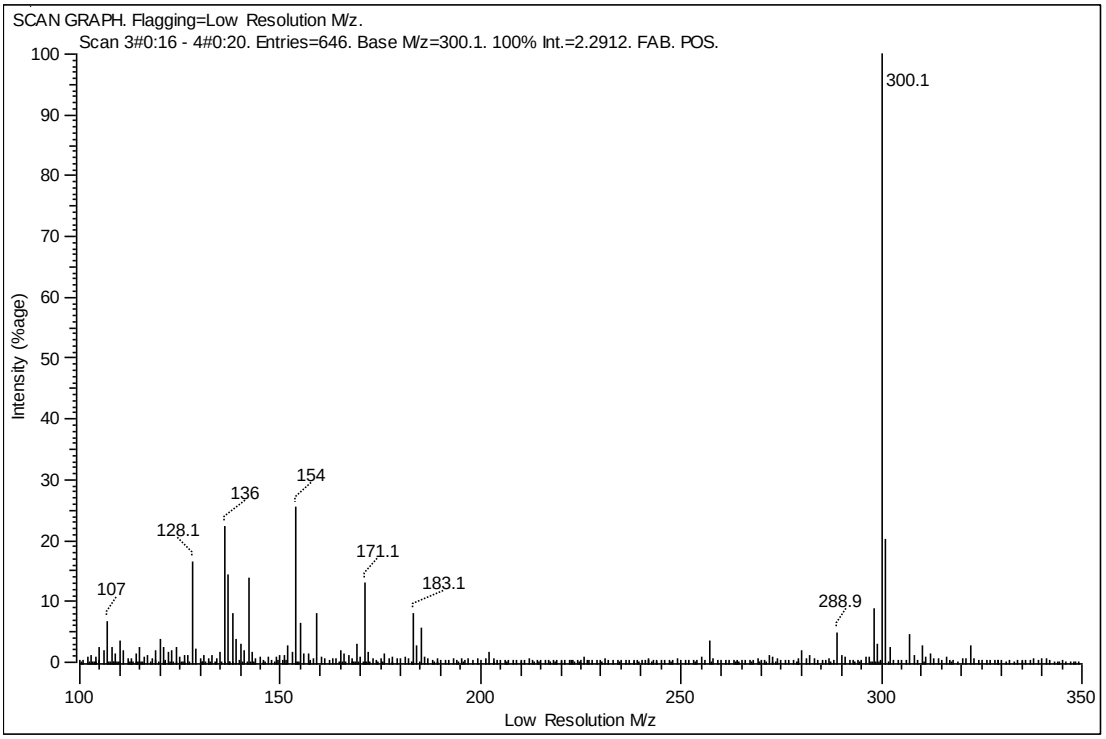


Figure A.1: FAB-MS spectrum of Cy_2DETA.

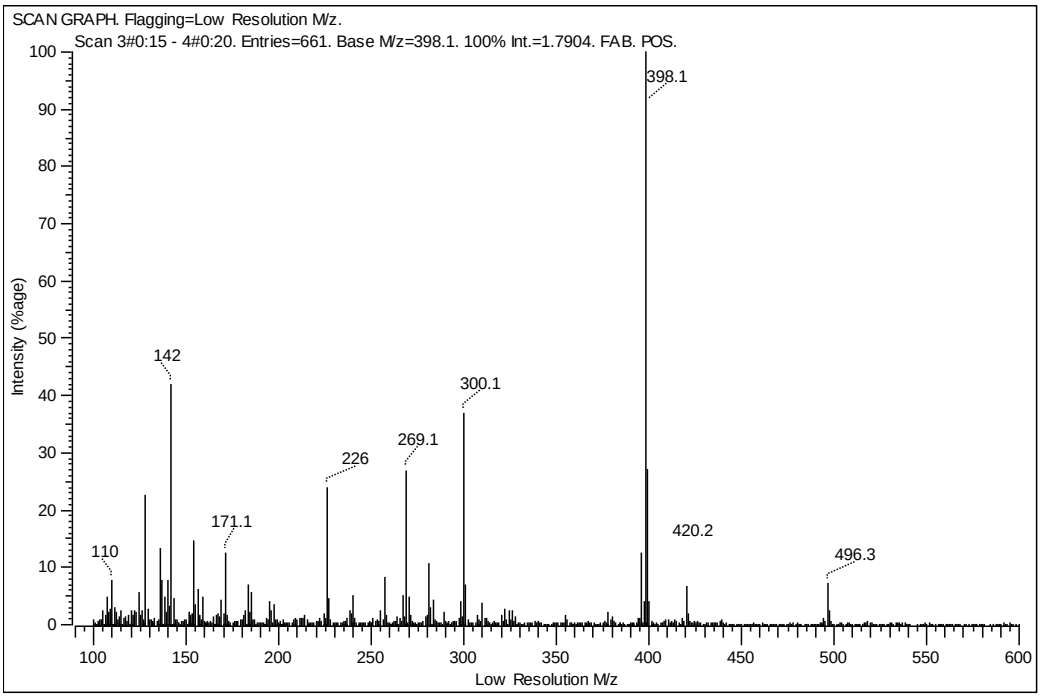


Figure A.2: FAB-MS spectrum of residue from the recrystallization of Cy_2DETA.

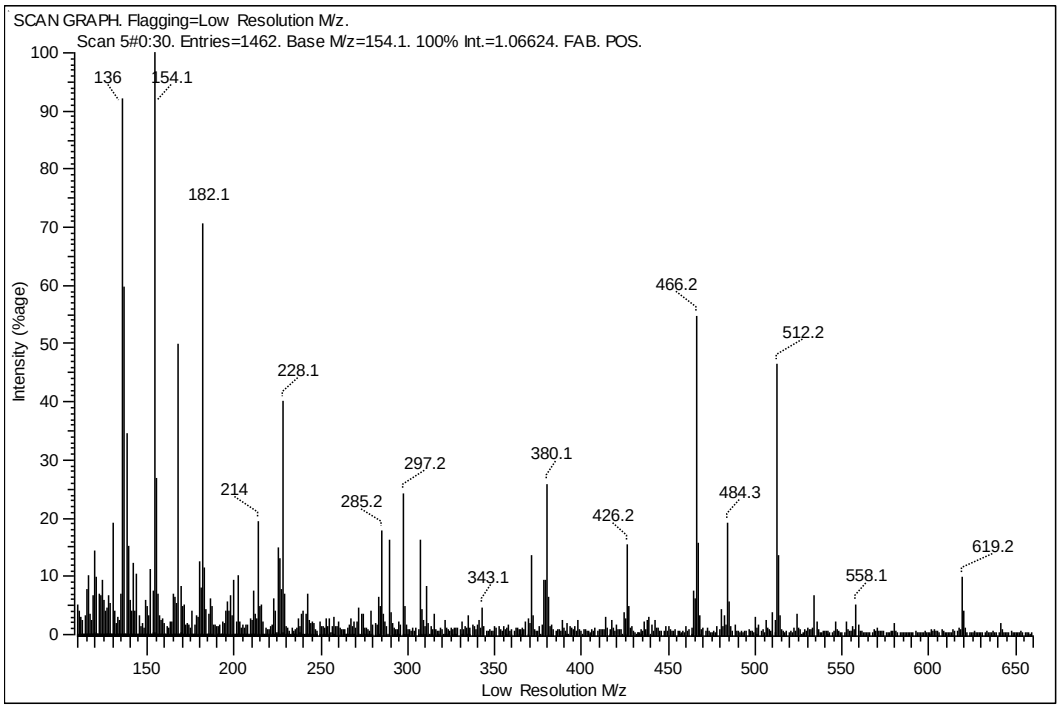


Figure A.3: FAB-MS spectrum of Ac_3Cy_2DETA.

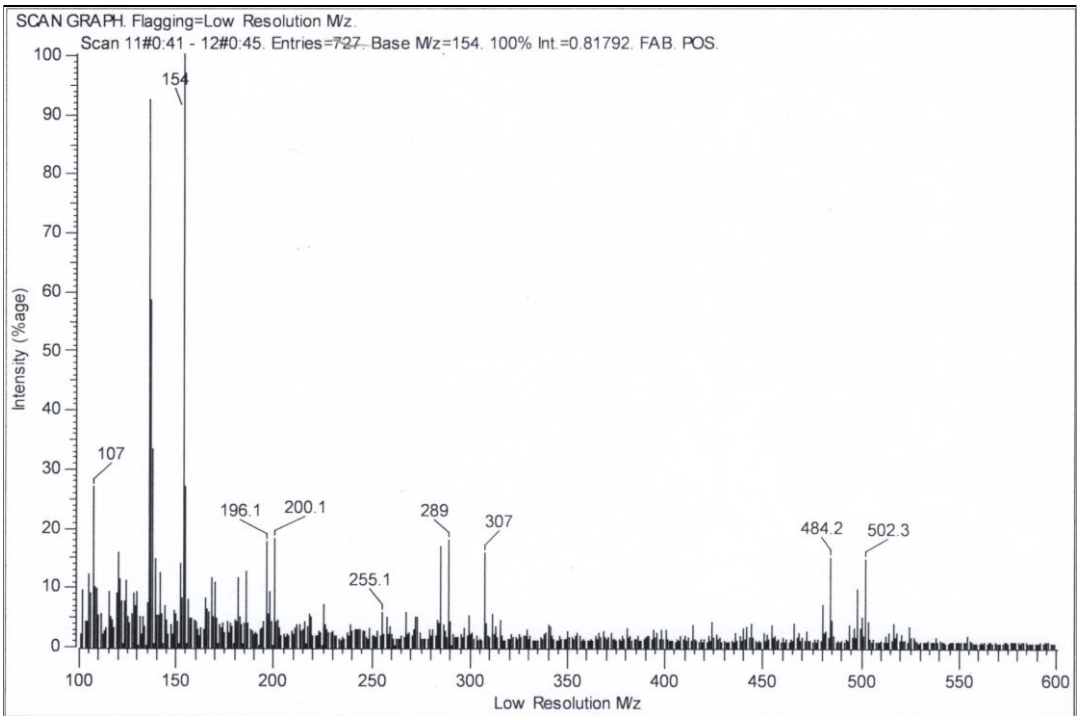


Figure A.4: FAB-MS spectrum of Fraction 1 from chromatographic separation of Ac_3Cy_2DETA.

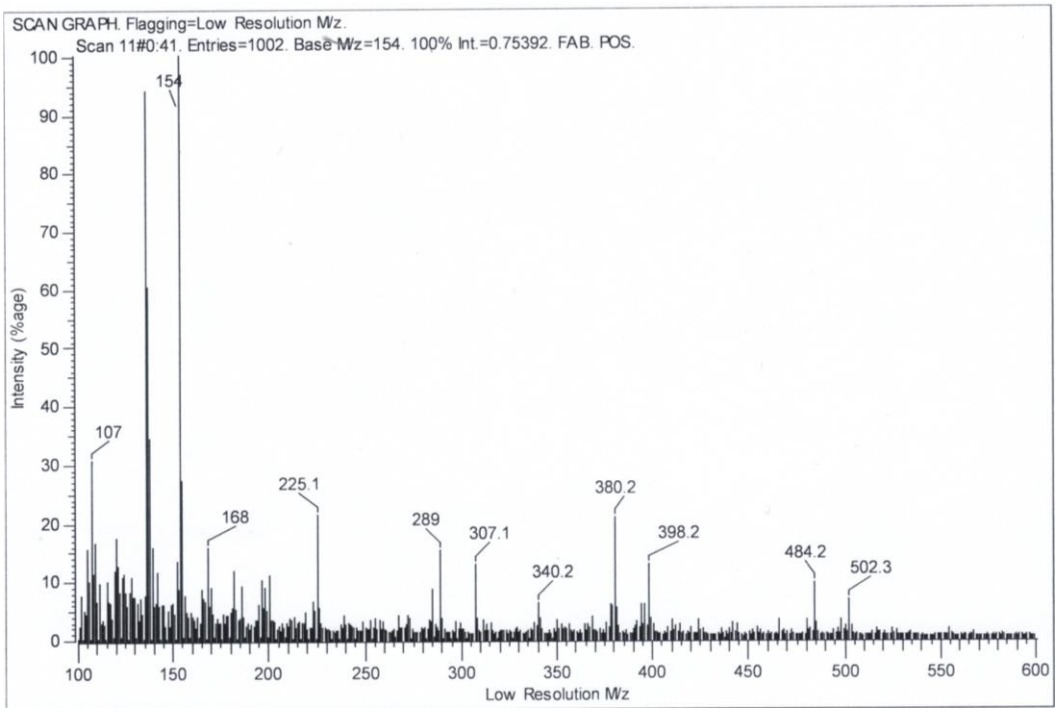


Figure A.5: FAB-MS spectrum of Fractions 2 - 4 from chromatographic separation of Ac_3Cy_2DETA.

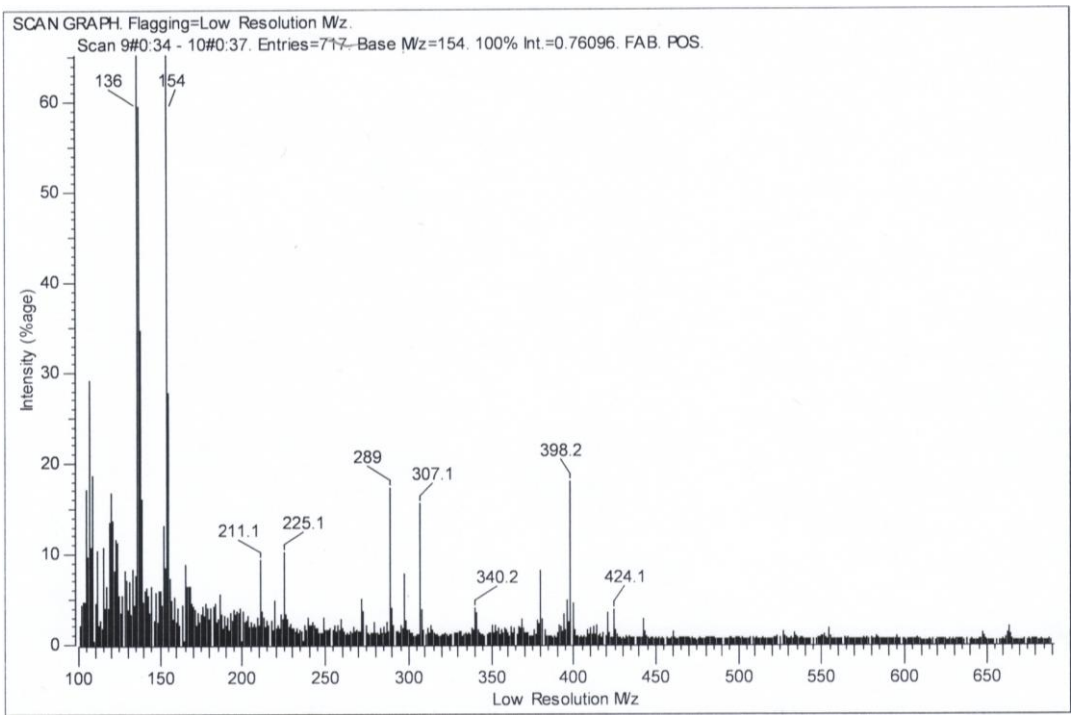


Figure A.6: FAB-MS spectrum of Fractions 5 - 14 from chromatographic separation of Ac_3Cy_2DETA.

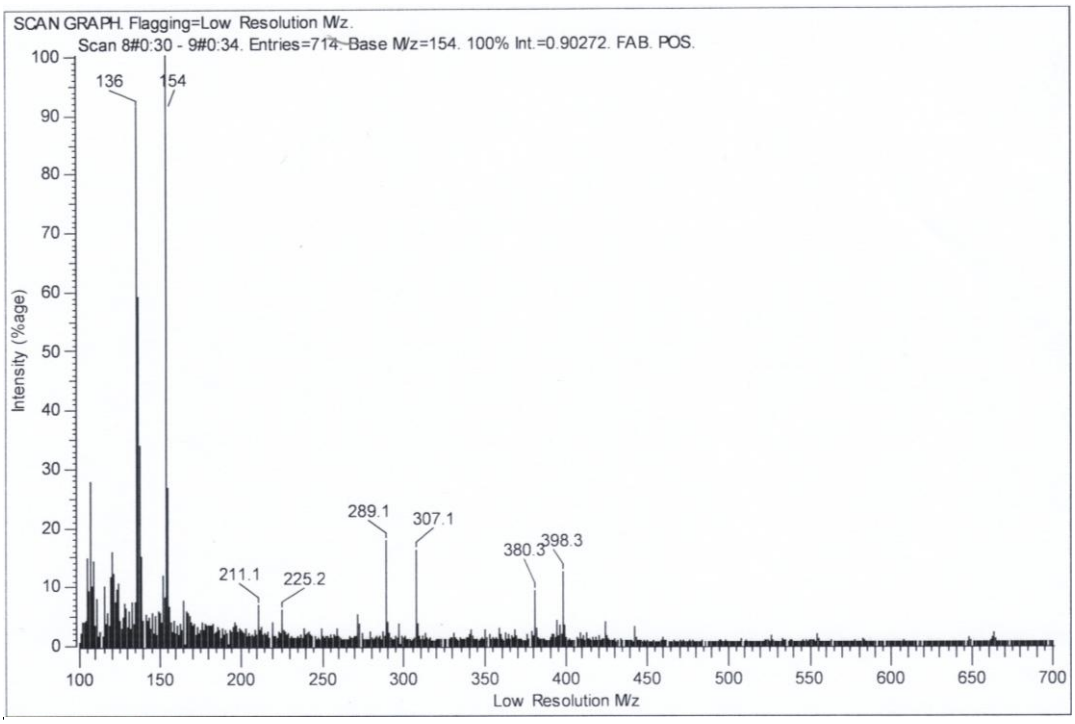


Figure A.7: FAB-MS spectrum of Fractions 15 - 17 from chromatographic separation of Ac_3Cy_2DETA.

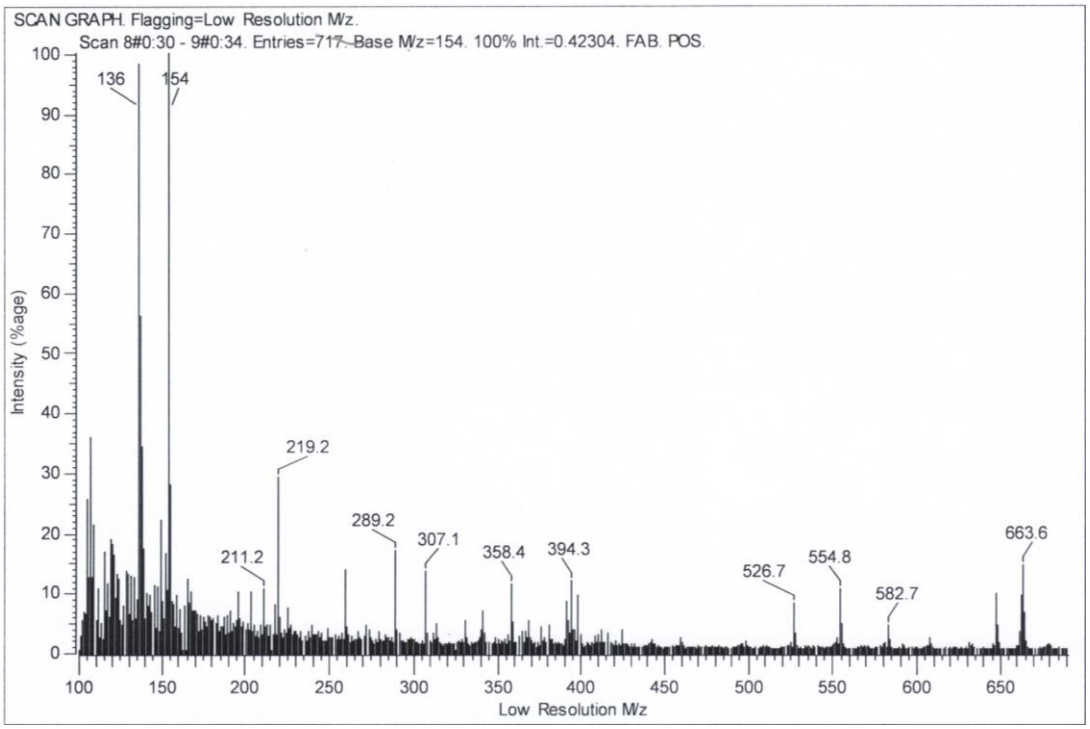


Figure A.8: FAB-MS spectrum of Fractions 18 - 21 from chromatographic separation of Ac_3Cy_2DETA.

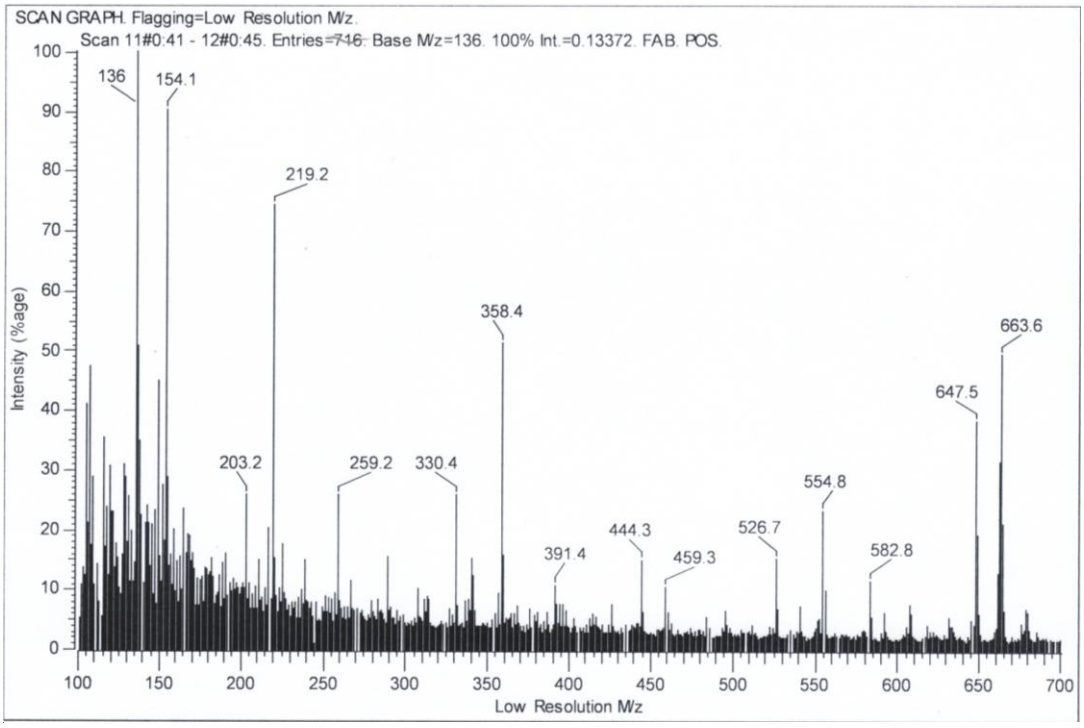


Figure A.9: FAB-MS spectrum of Fractions 22 - 62 from chromatographic separation of Ac_3Cy_2DETA.

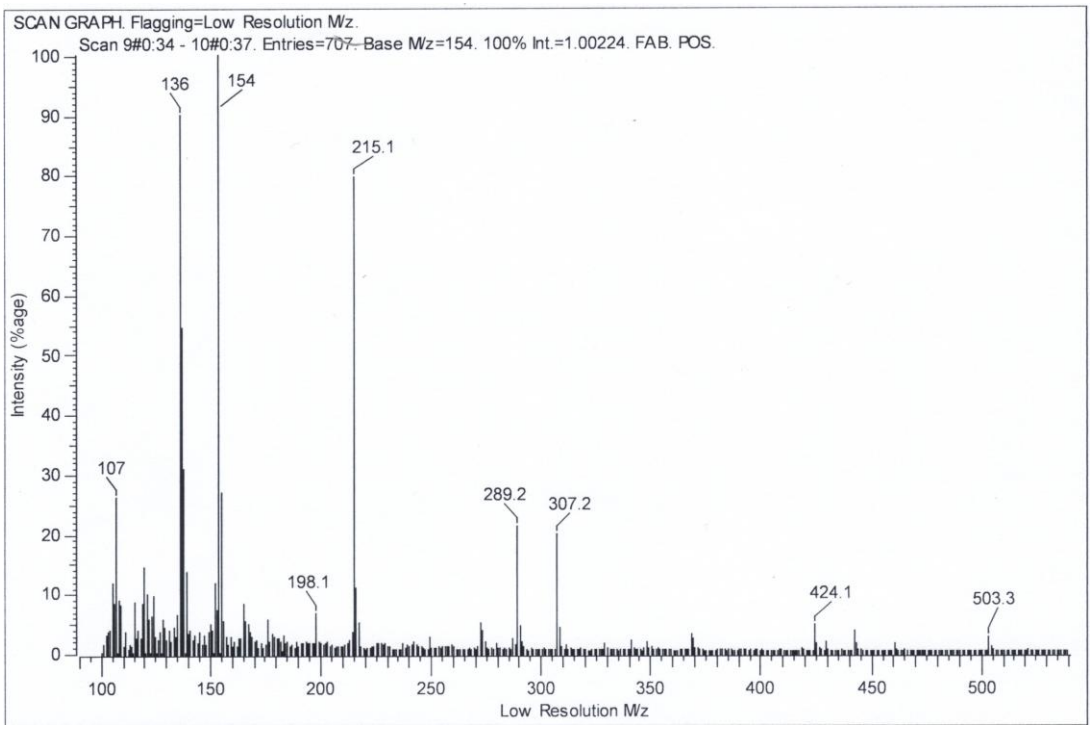


Figure A.10: FAB-MS spectrum of TsEDA.

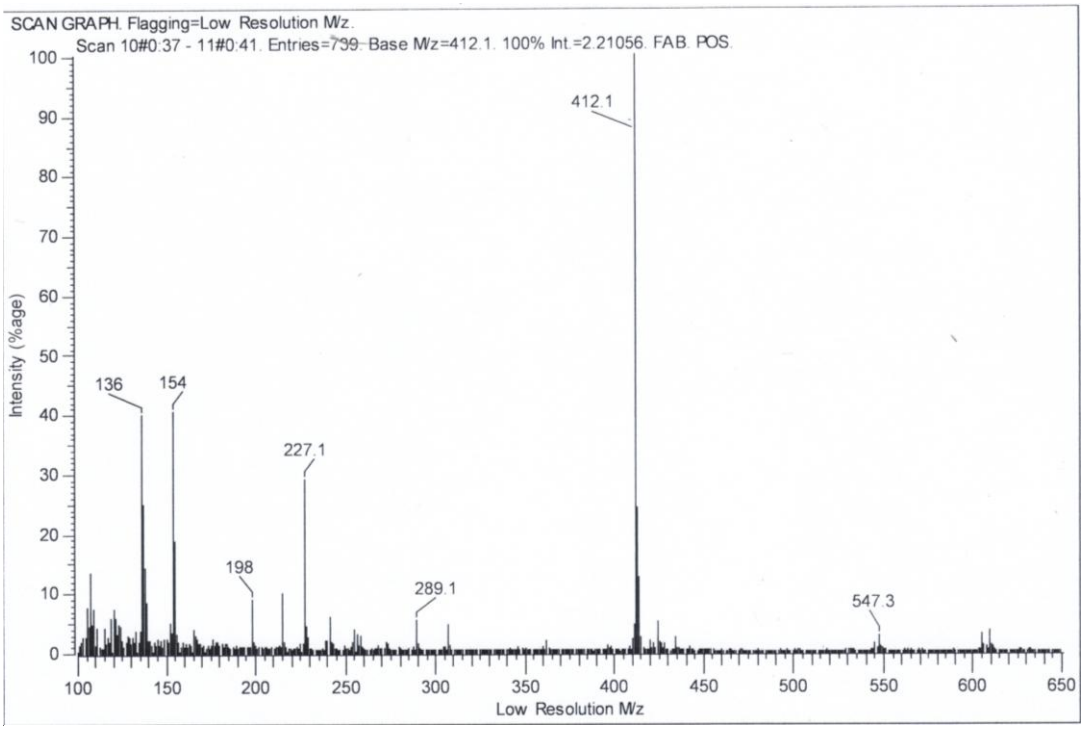


Figure A.11: FAB-MS spectrum of Ts_2DETA.

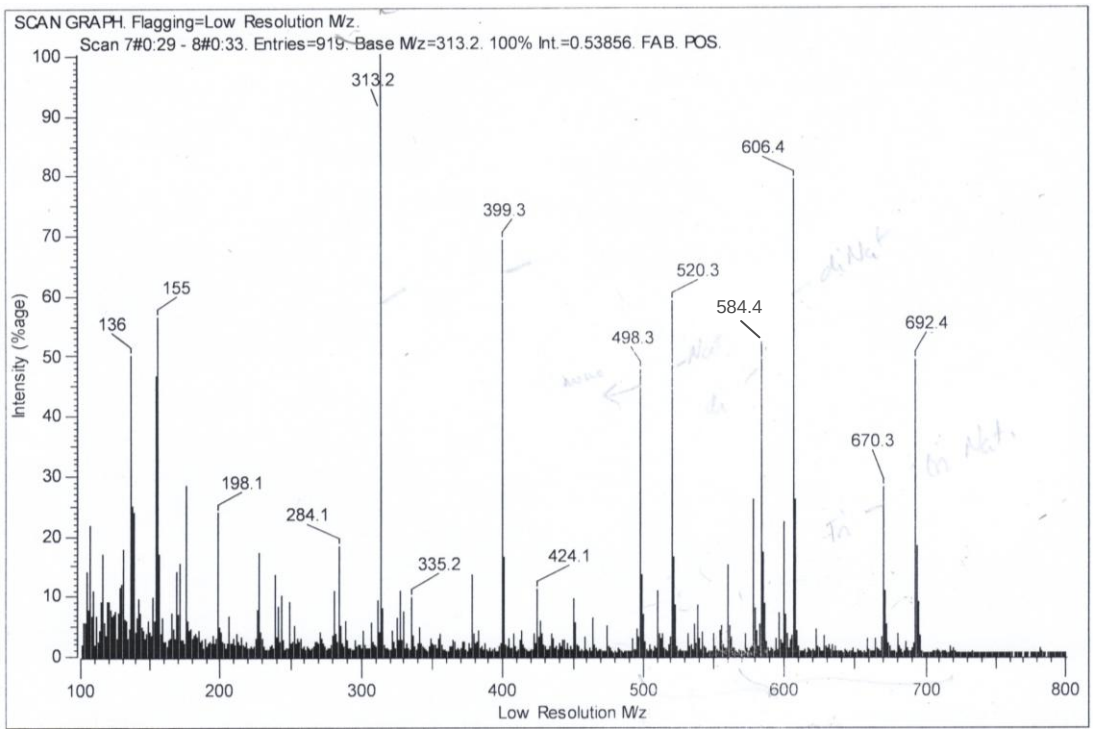


Figure A.12: FAB-MS spectrum of Ts_2DETA.3E.

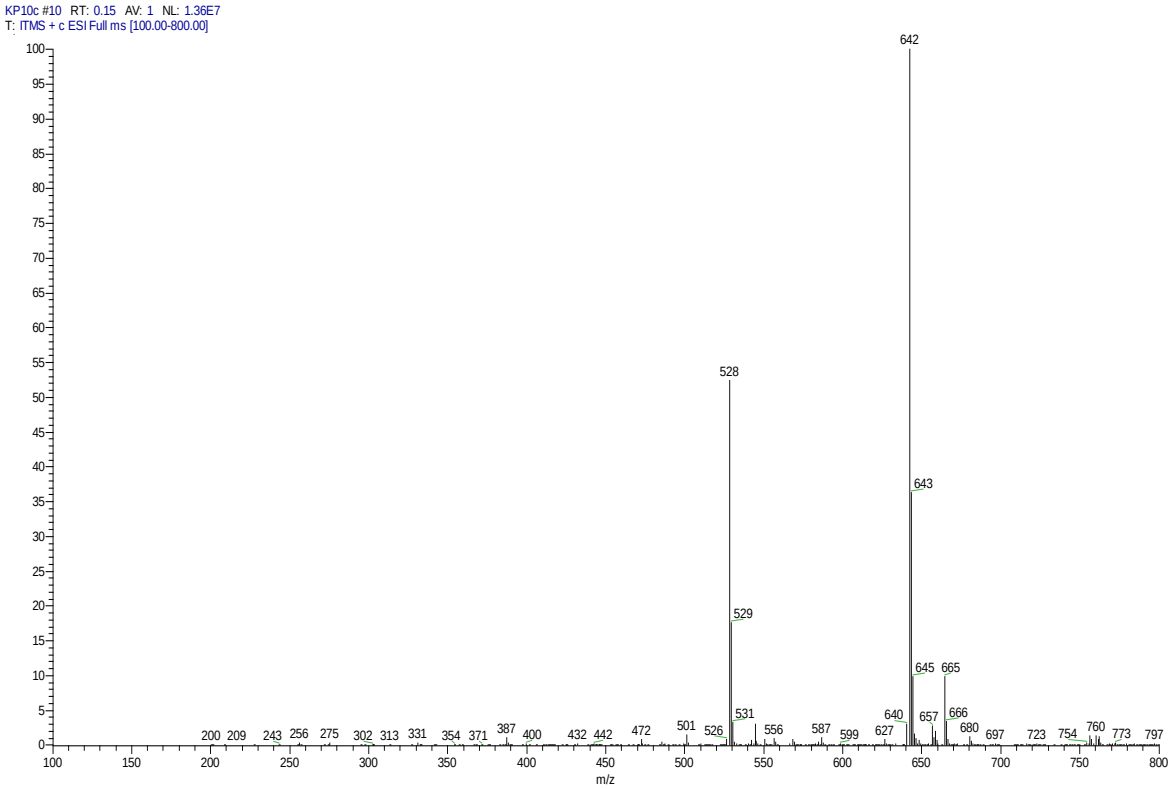


Figure A.13: ESI-MS spectrum of Cy_2DETA.3E, attempted synthesis in DCM.

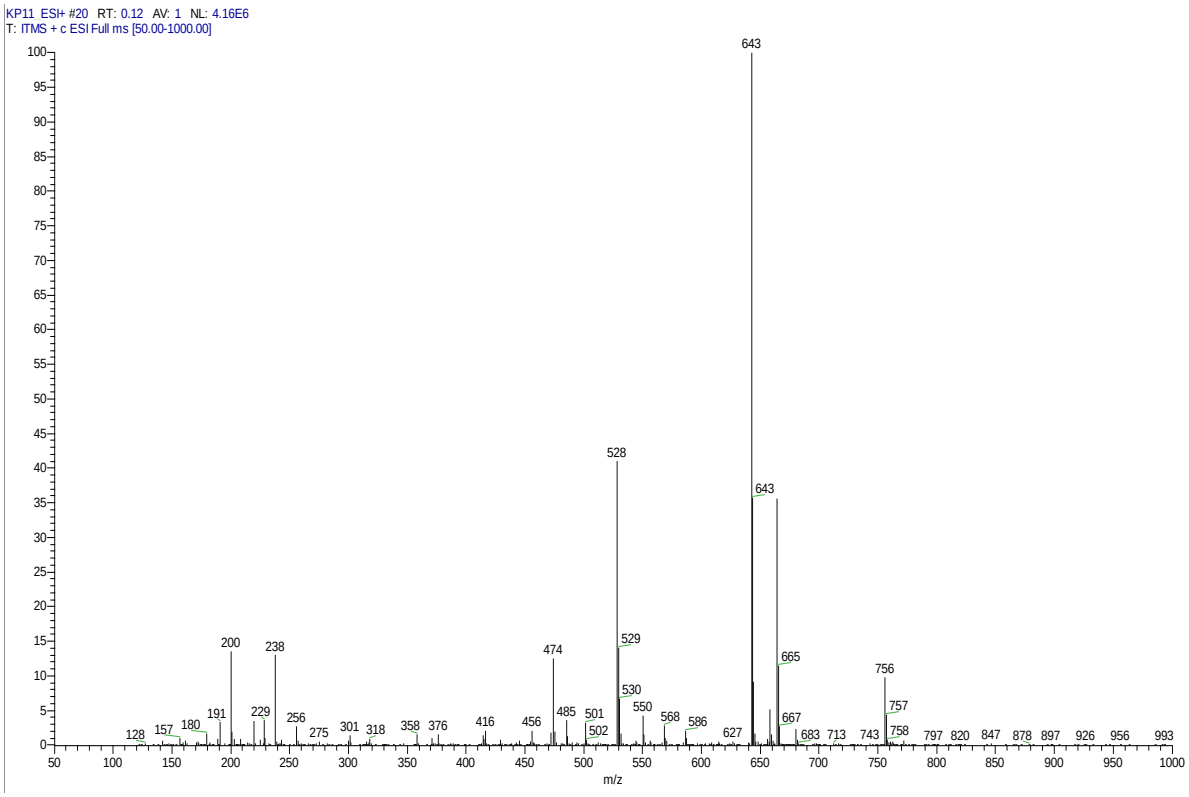


Figure A.14: ESI-MS spectrum of Cy_2DETA.3E, attempted synthesis in THF.

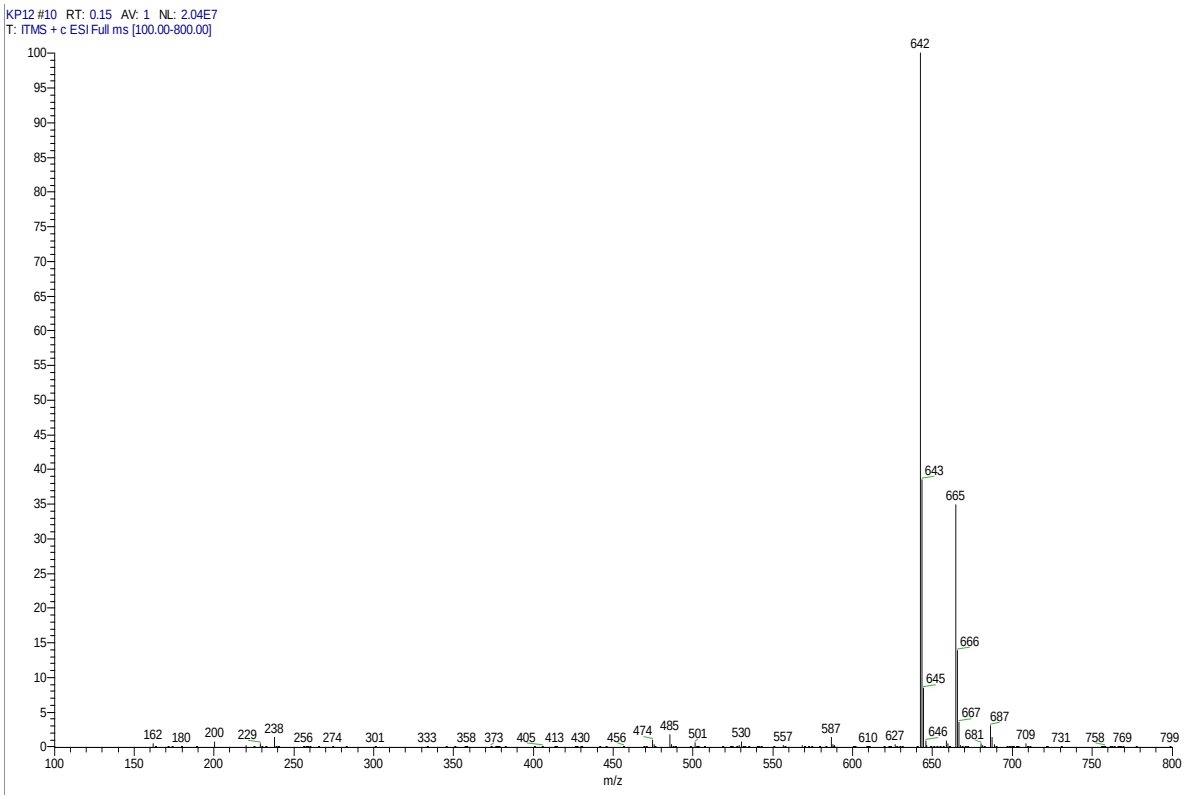


Figure A.15: ESI-MS spectrum of Cy_2DETA.3E, attempted synthesis in DMF.

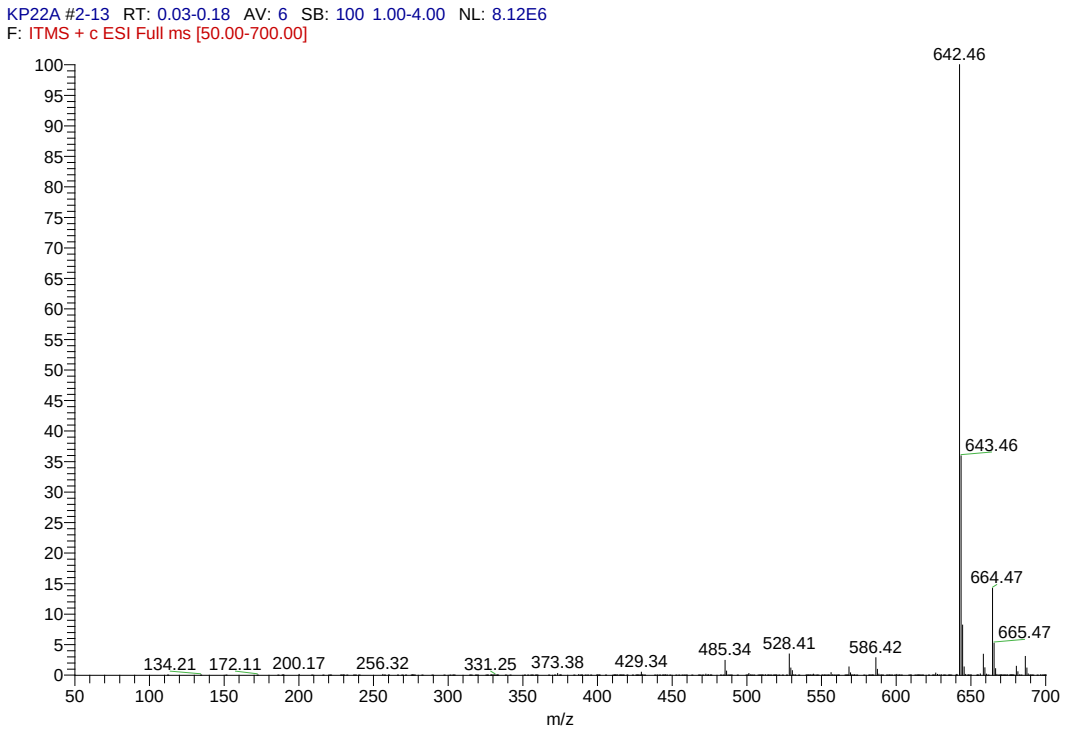


Figure A.16: ESI-MS spectrum of Cy_2DETA.3E.

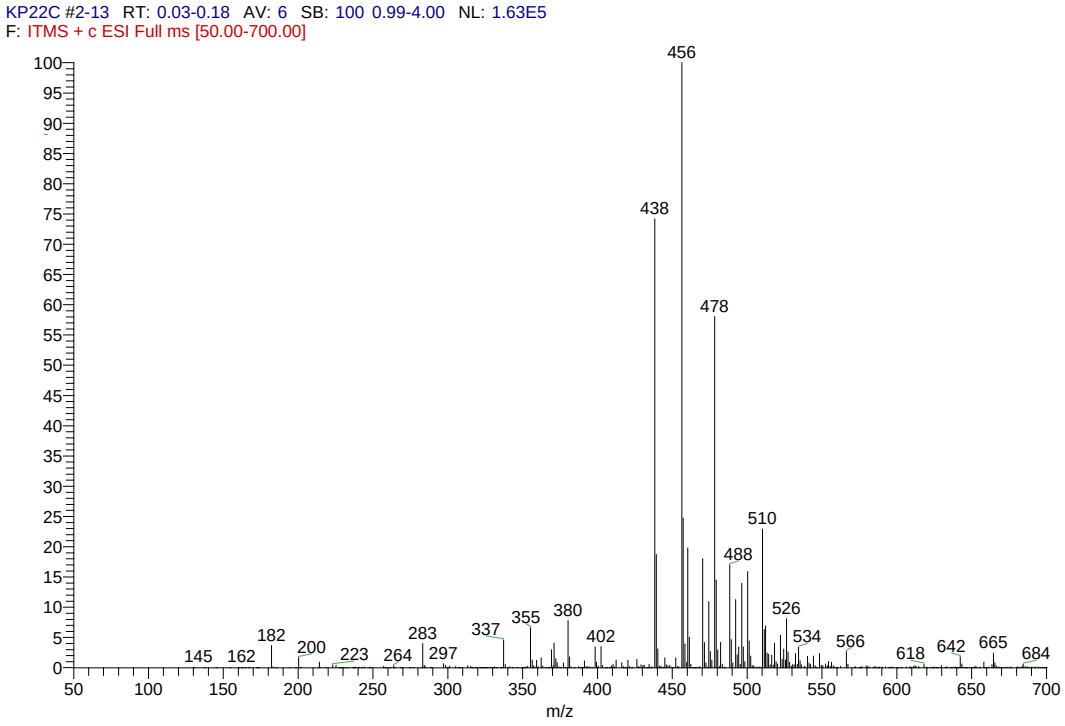


Figure A.17: ESI-MS spectrum of Cy_2DETA.3E after TFA hydrolysis.

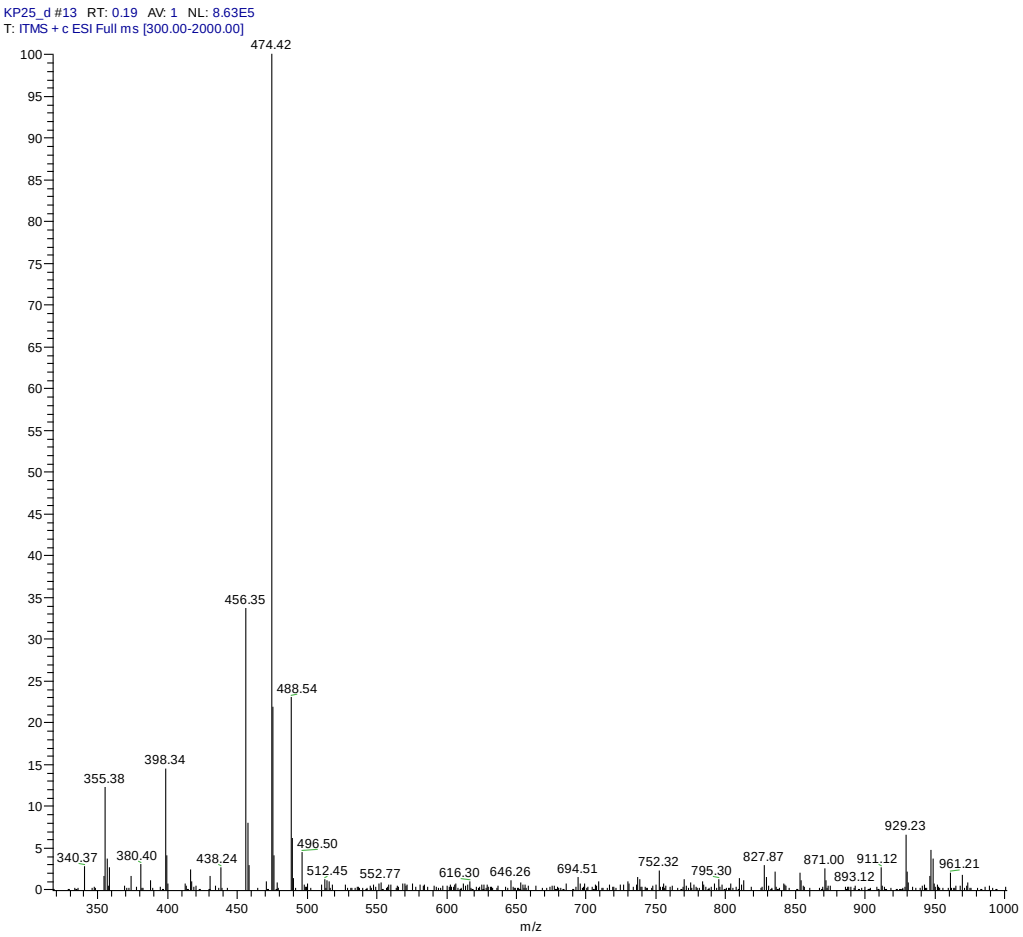


Figure A.18: ESI-MS spectrum of the TFA hydrolysis product of Cy_2DETA.3E, refluxed in H_2O for 7 days.

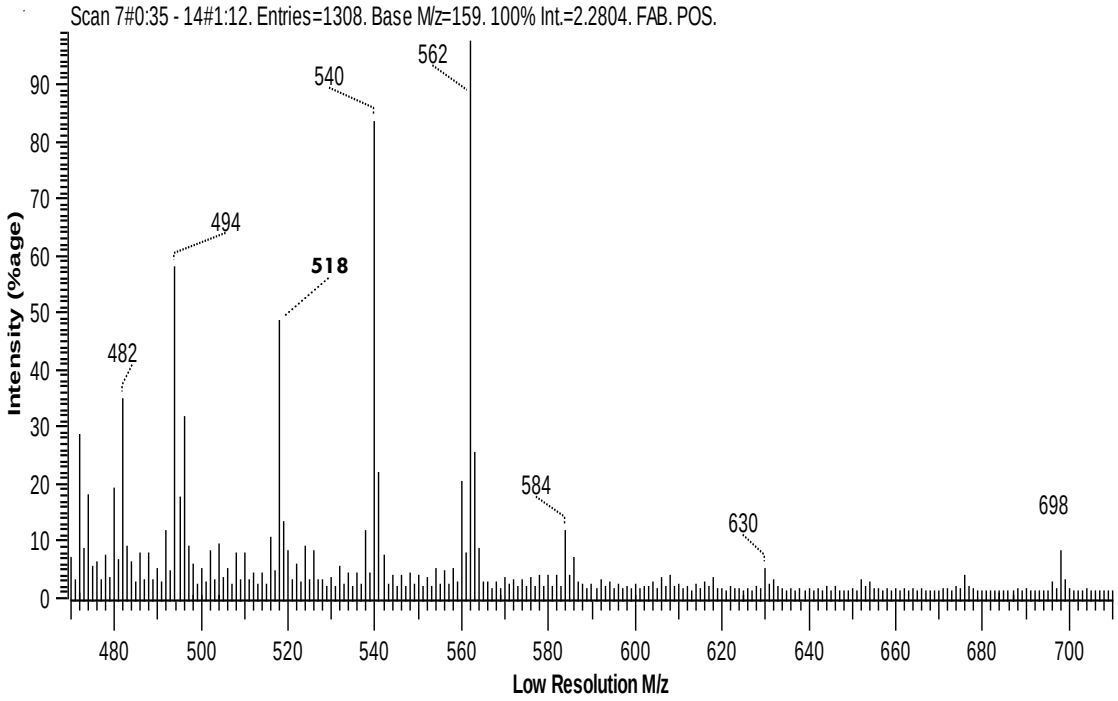


Figure A.19: FAB-MS spectrum of Na_3Cy_2DETA.3A.

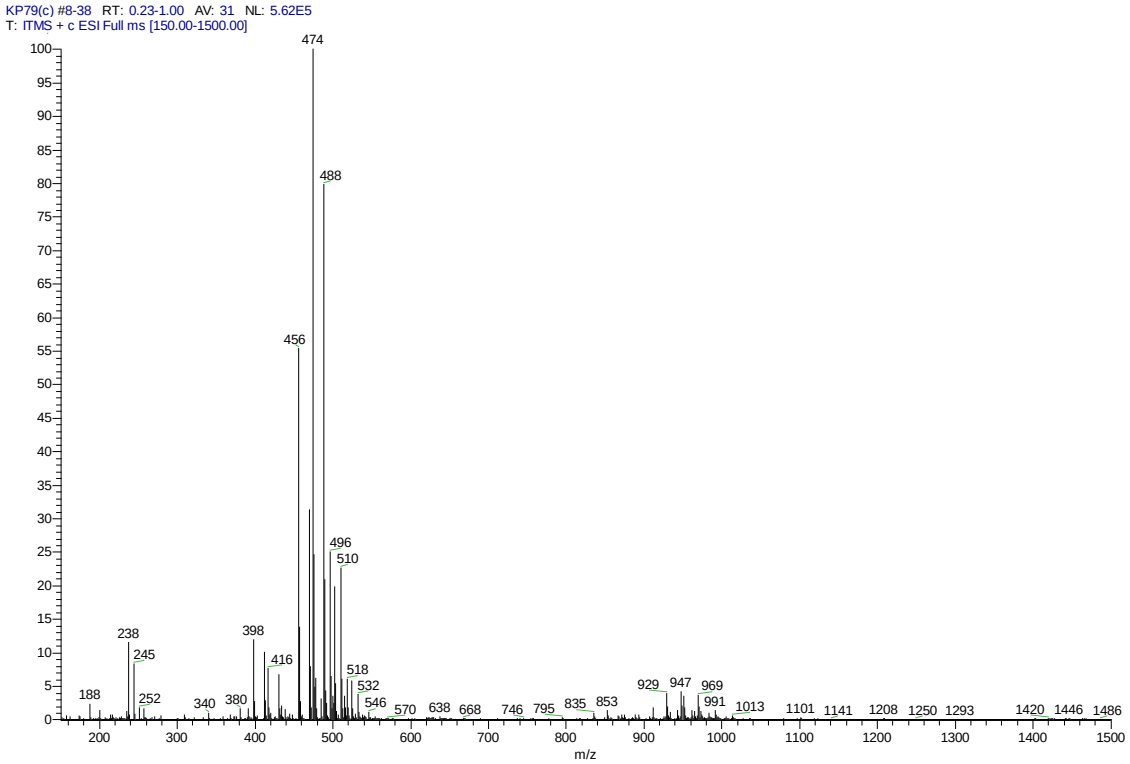


Figure A.20: ESI-MS spectrum of Cy_2DETA.3E after HCl hydrolysis.

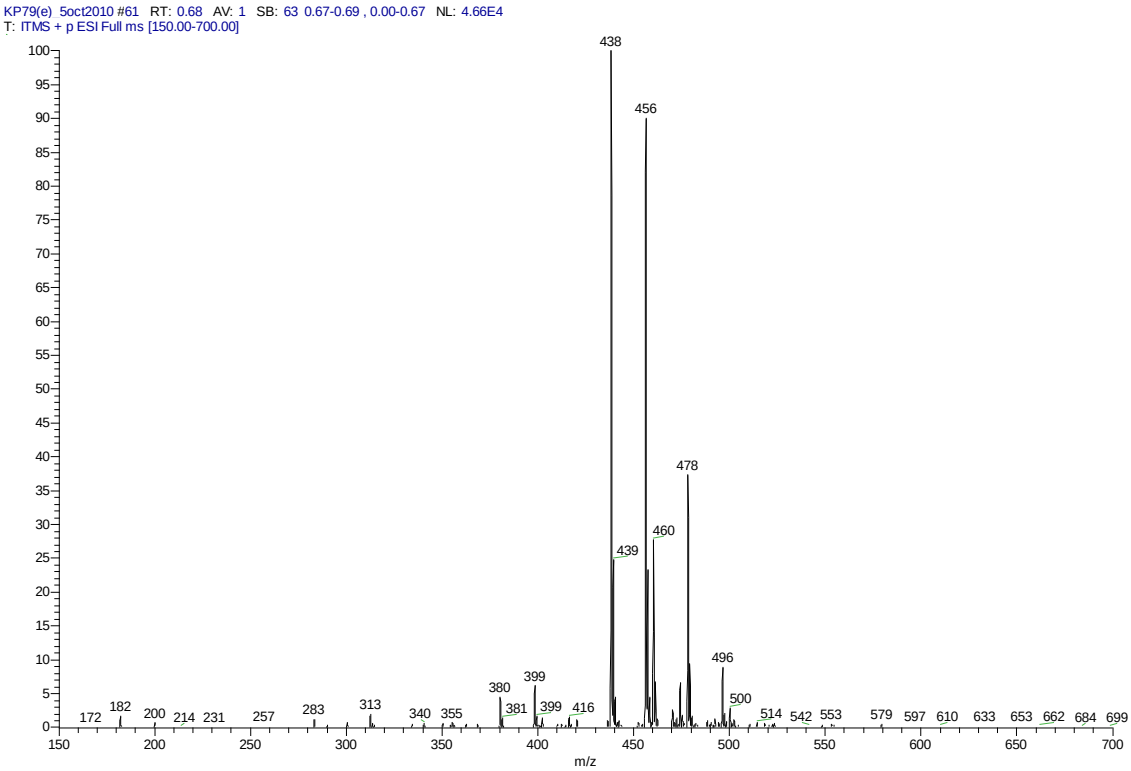


Figure A.21: ESI-MS spectrum of the HCl hydrolysis product of Cy_2DETA.3E, after continuous extraction for 10 days and lyophilization.

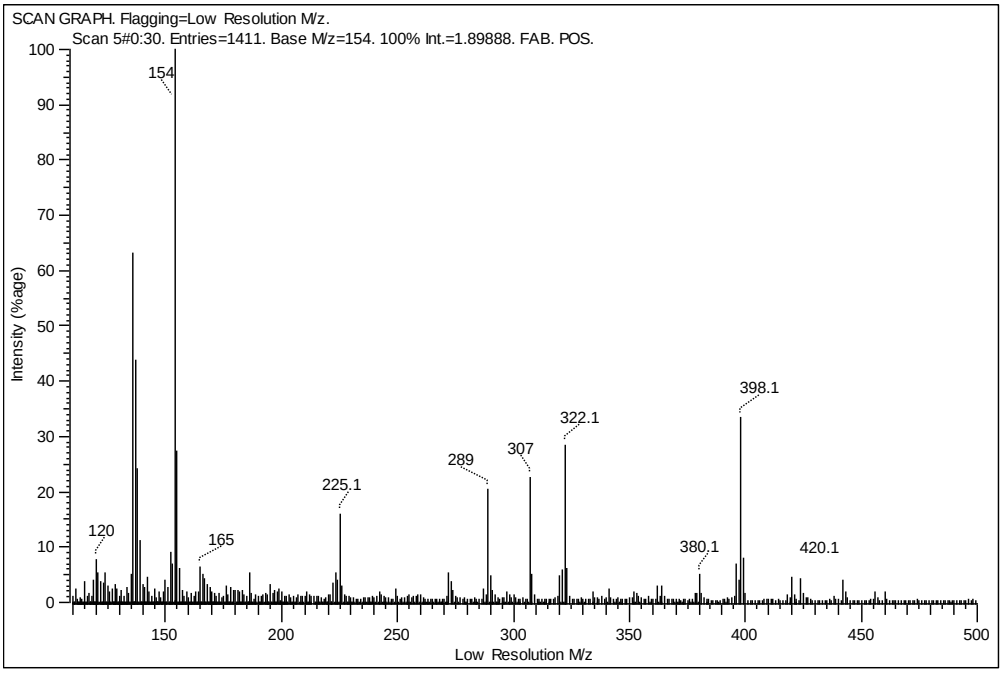


Figure A.22: FAB-MS spectrum of the crude product obtained from the reaction of glyoxal with Cy_2DETA.

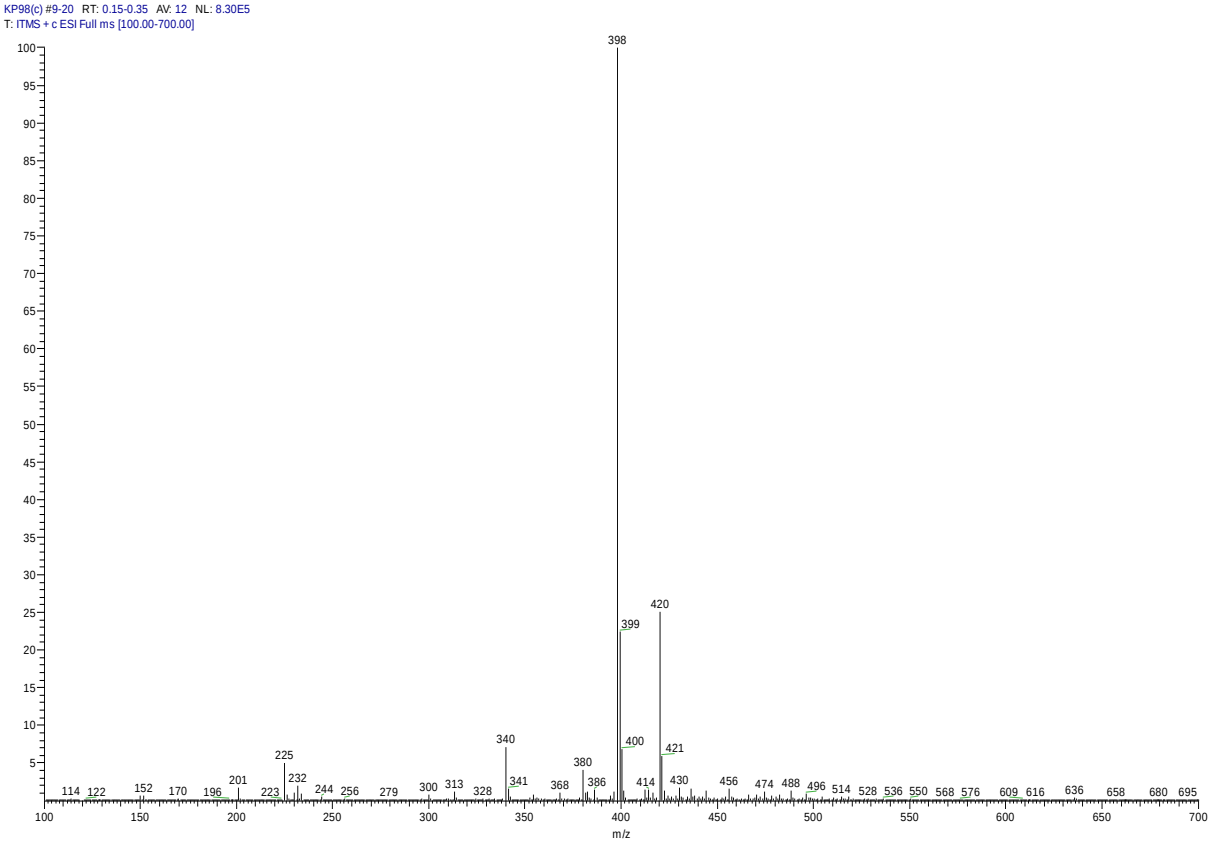


Figure A.23: ESI-MS spectrum of Cy_2DETA.2A.3HCl.

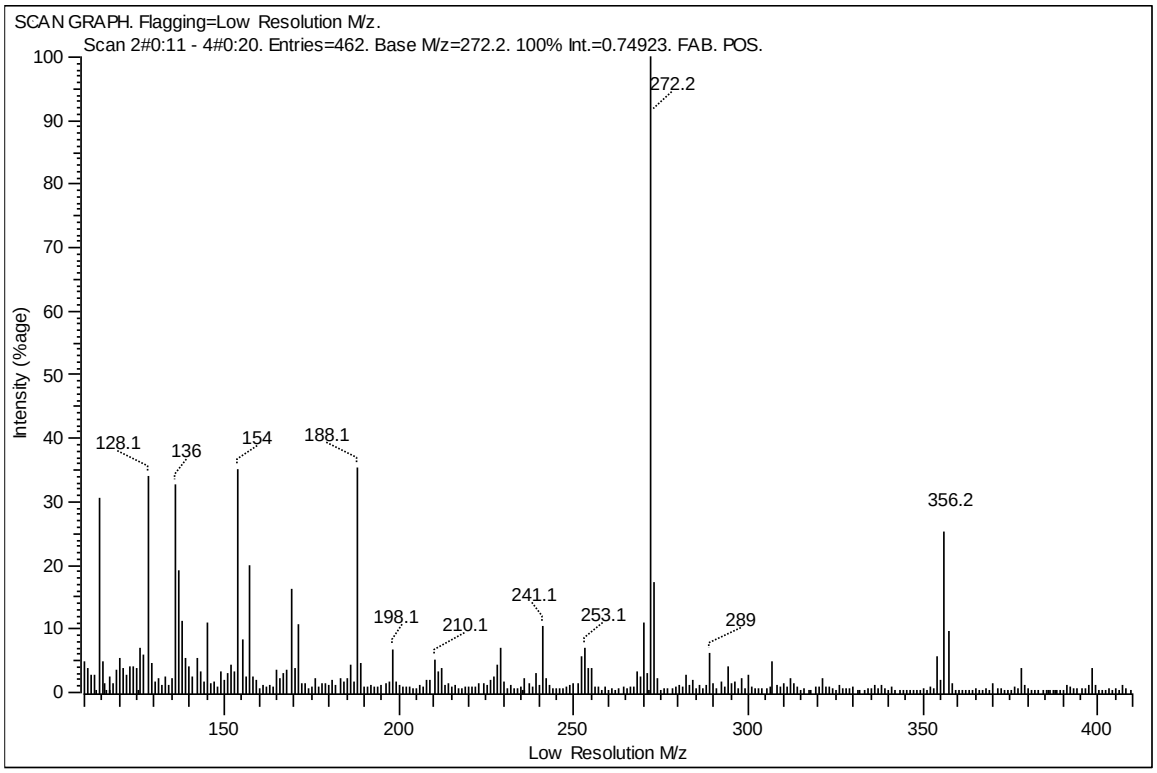


Figure A.24: FAB-MS spectrum of Cyp_2DETA.

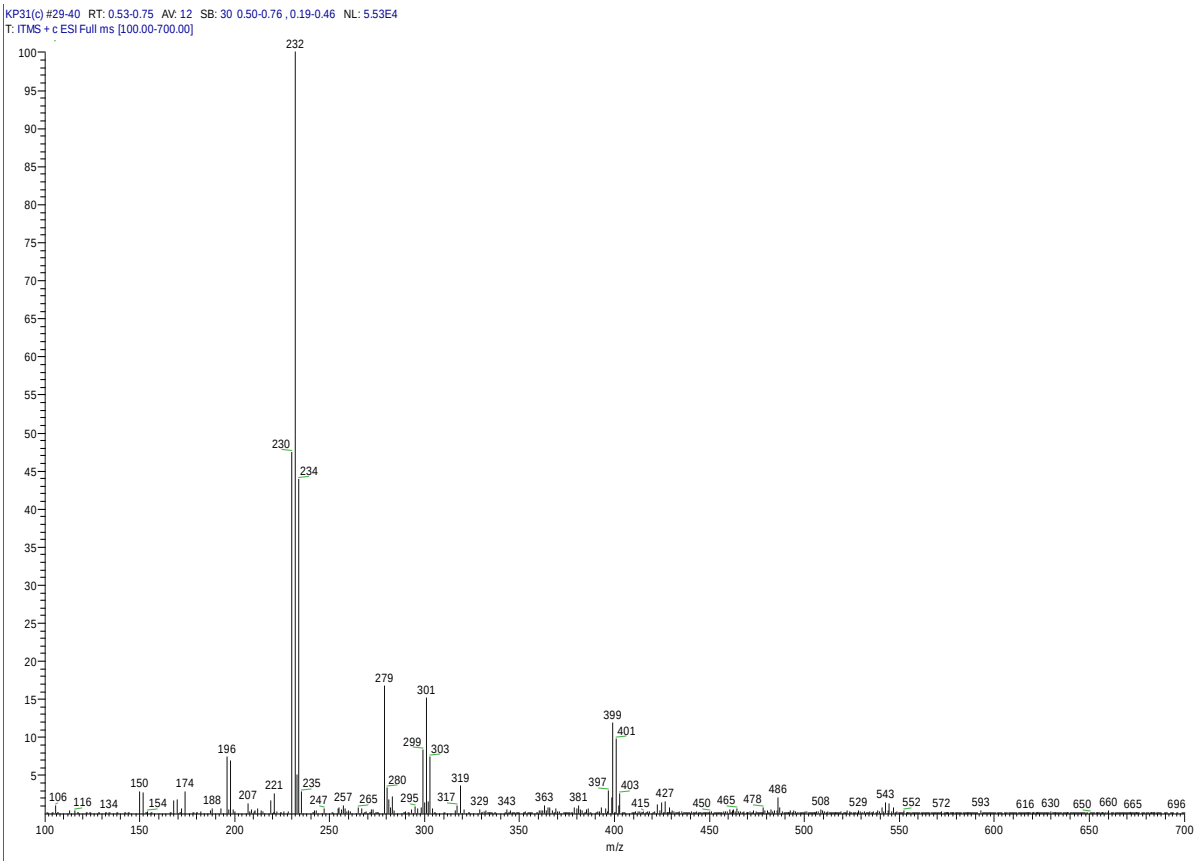


Figure A.25: ESI-MS spectrum of bis(2-bromoethyl)ammonium bromide.

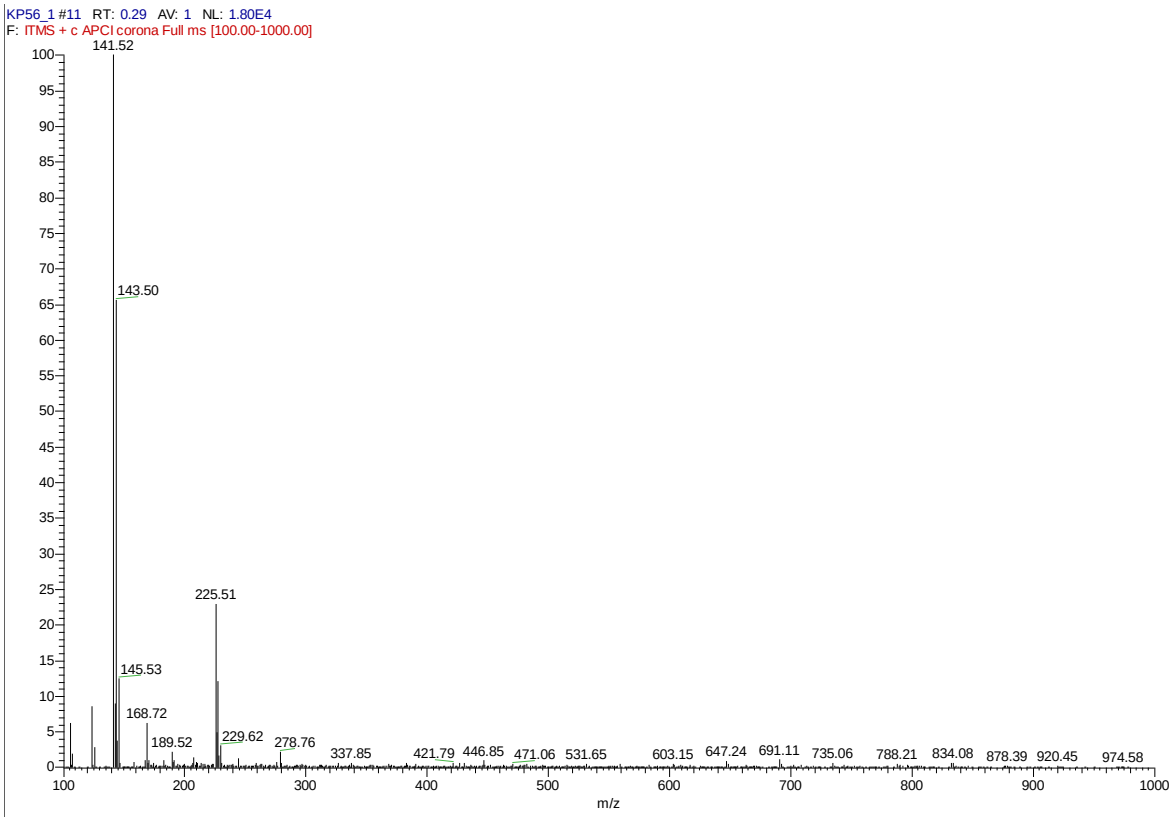


Figure A.26: ESI-MS spectrum of bis(2-chloroethyl)ammonium chloride.

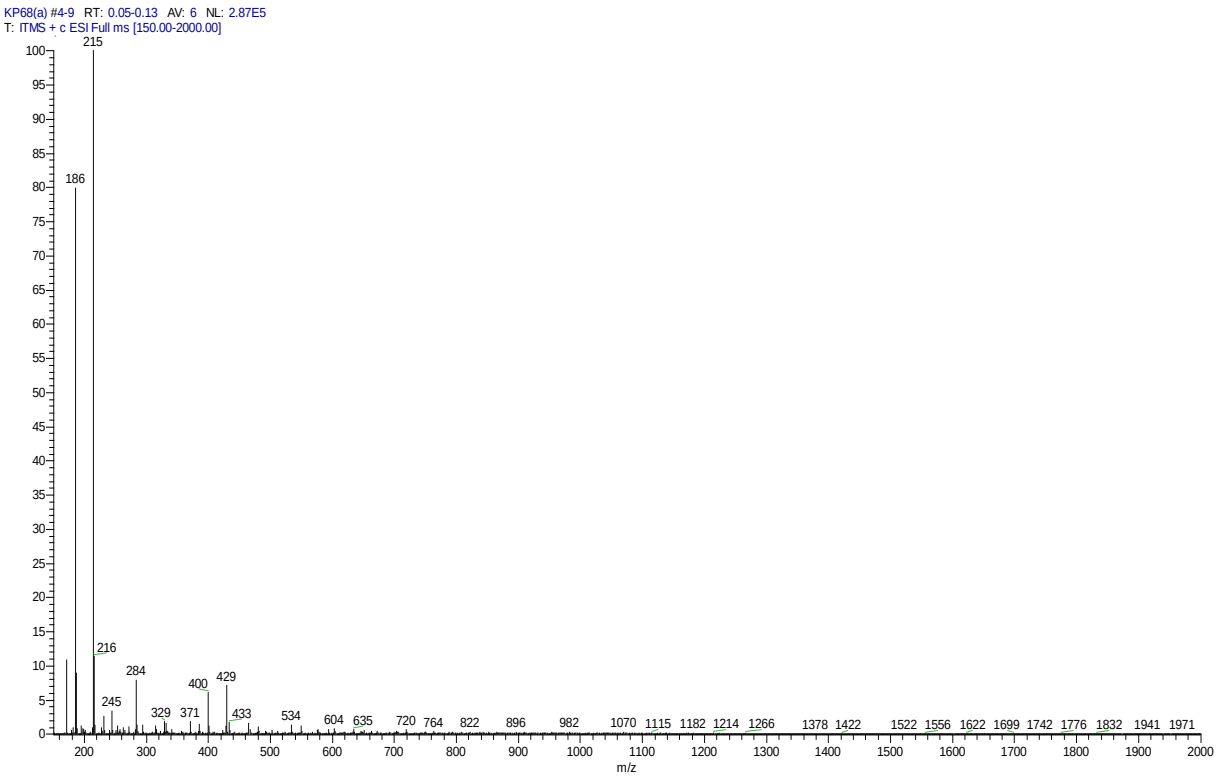


Figure A.27: ESI-MS spectrum of the crude product from the two-step synthesis of Cyp_2DETA.

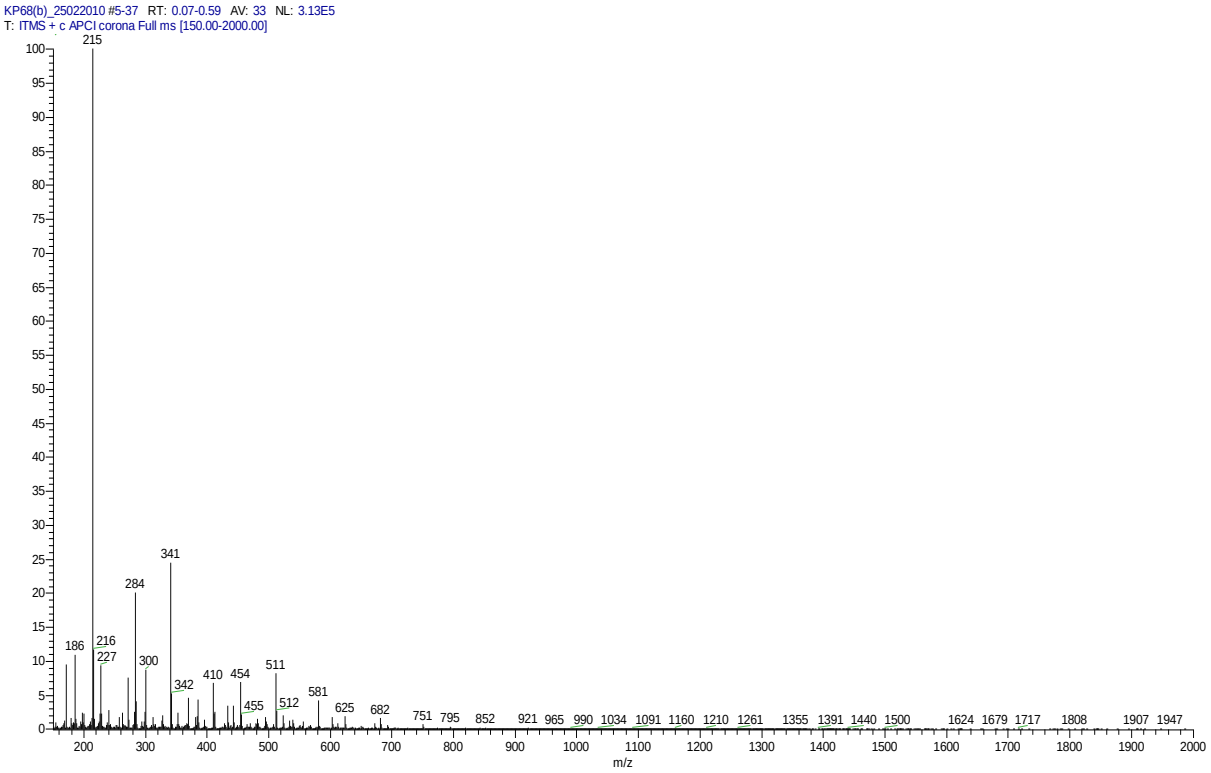


Figure A.28: ESI-MS spectrum of the aqueous extract from the two-step synthesis of Cyp_2DETA.

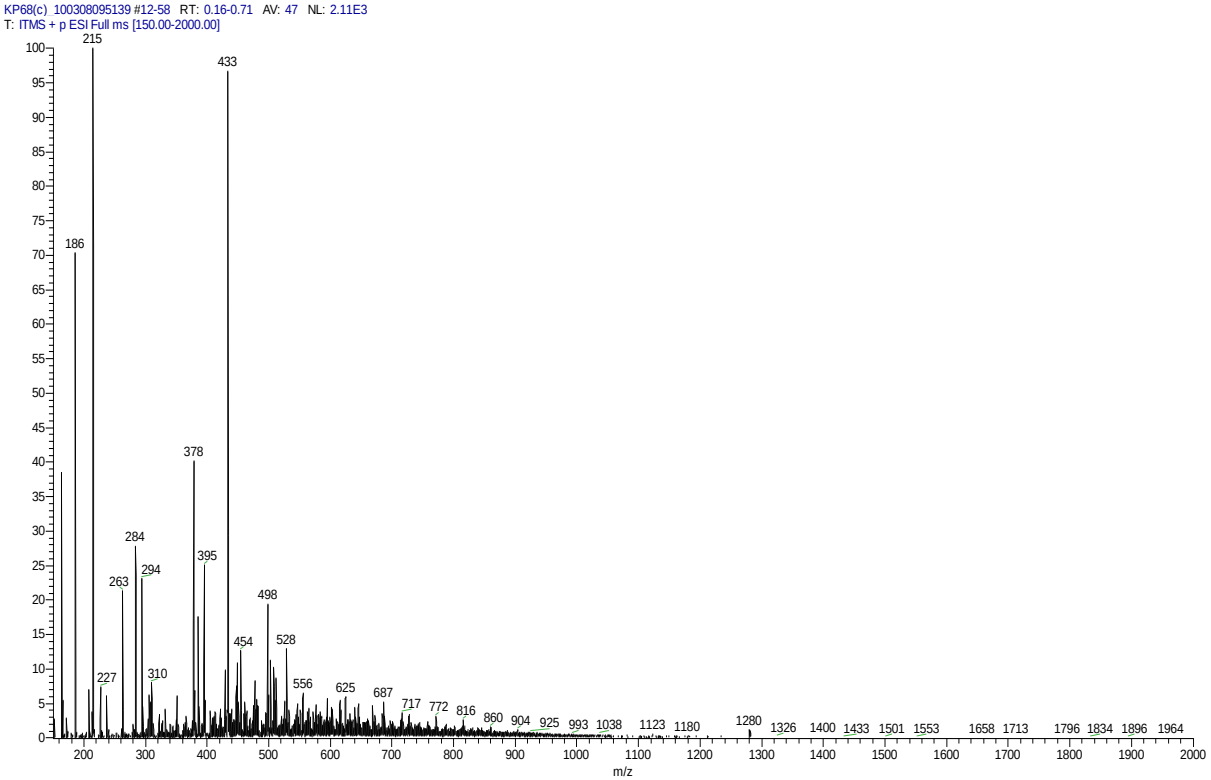


Figure A.29: ESI-MS spectrum of the organic extract from the two-step synthesis of Cyp_2DETA.

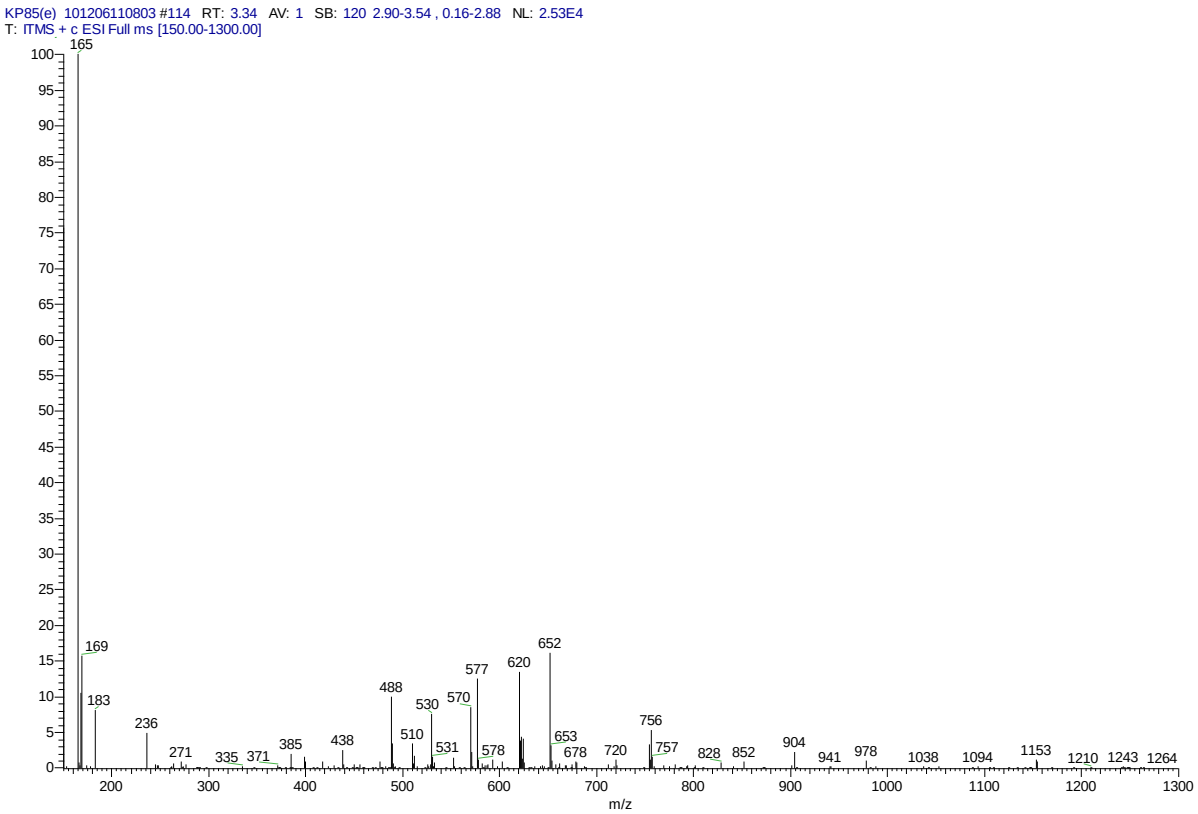


Figure A.30: ESI-MS spectrum of the [Eu(Cy_2DETA.3A)] synthesis in acetonitrile.

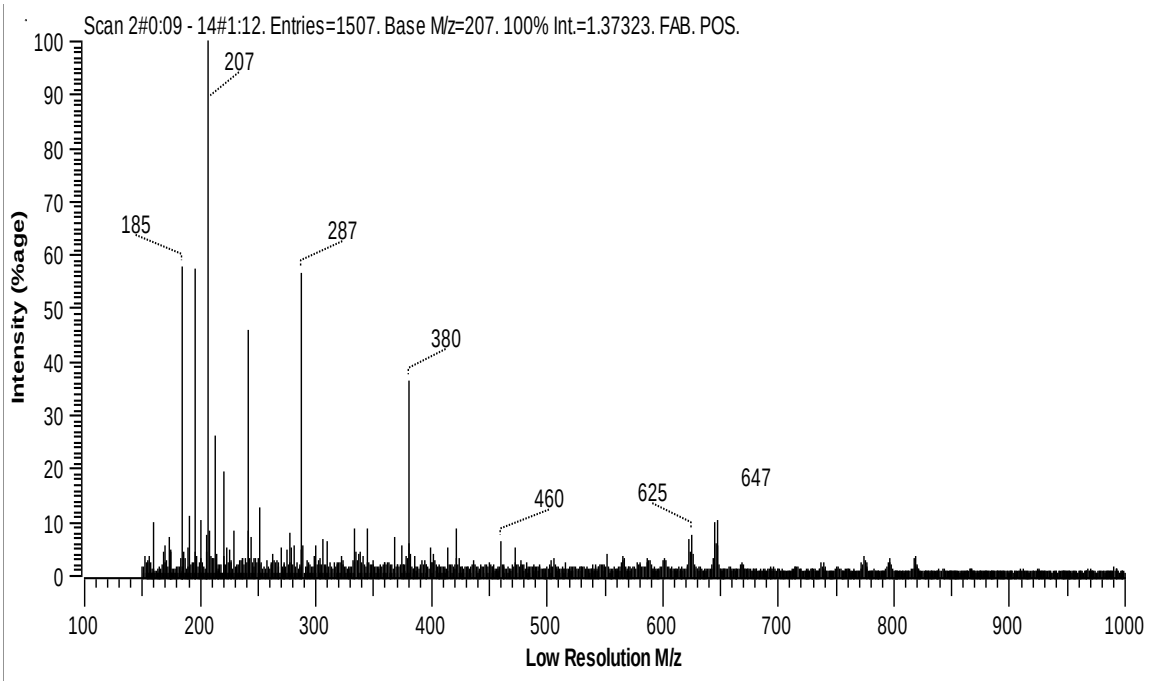


Figure A.31: FAB-MS spectrum of the [Eu(Cy_2DETA.3A)] synthesis in deionised water.

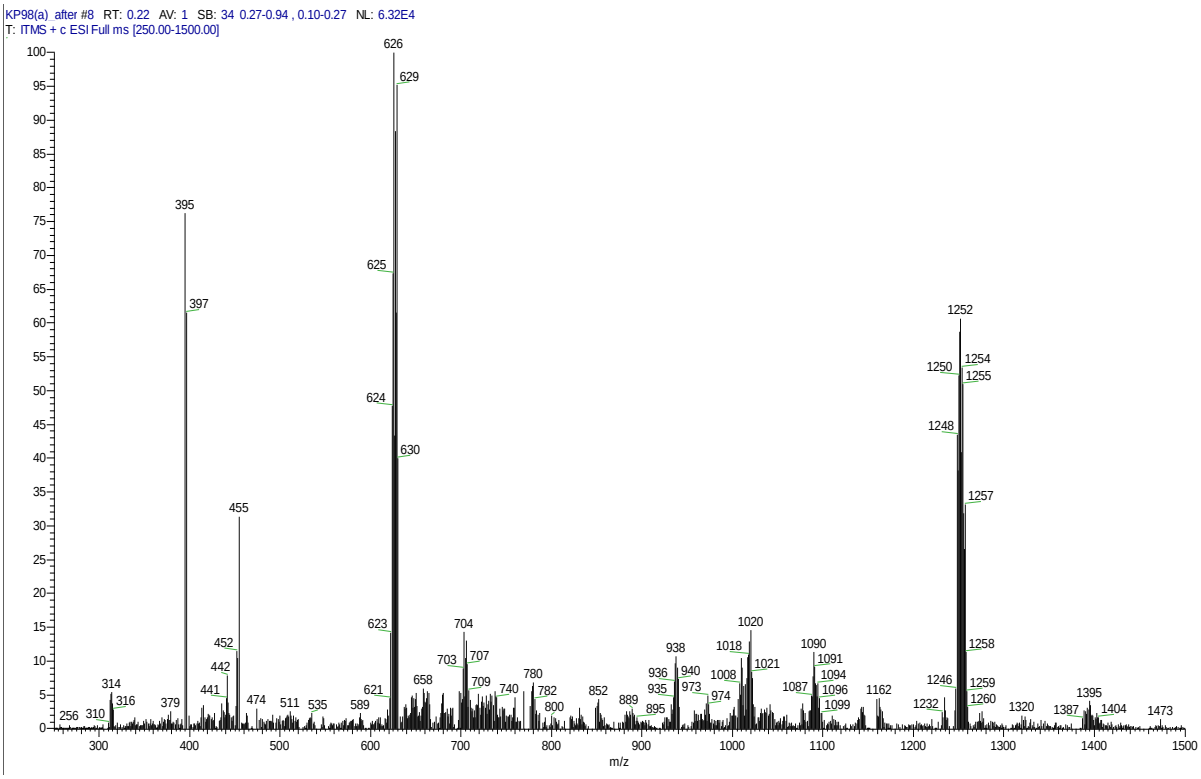


Figure A.32: ESI-MS spectrum of the [Gd(Cy_2DETA.3A)] synthesis in acetonitrile.

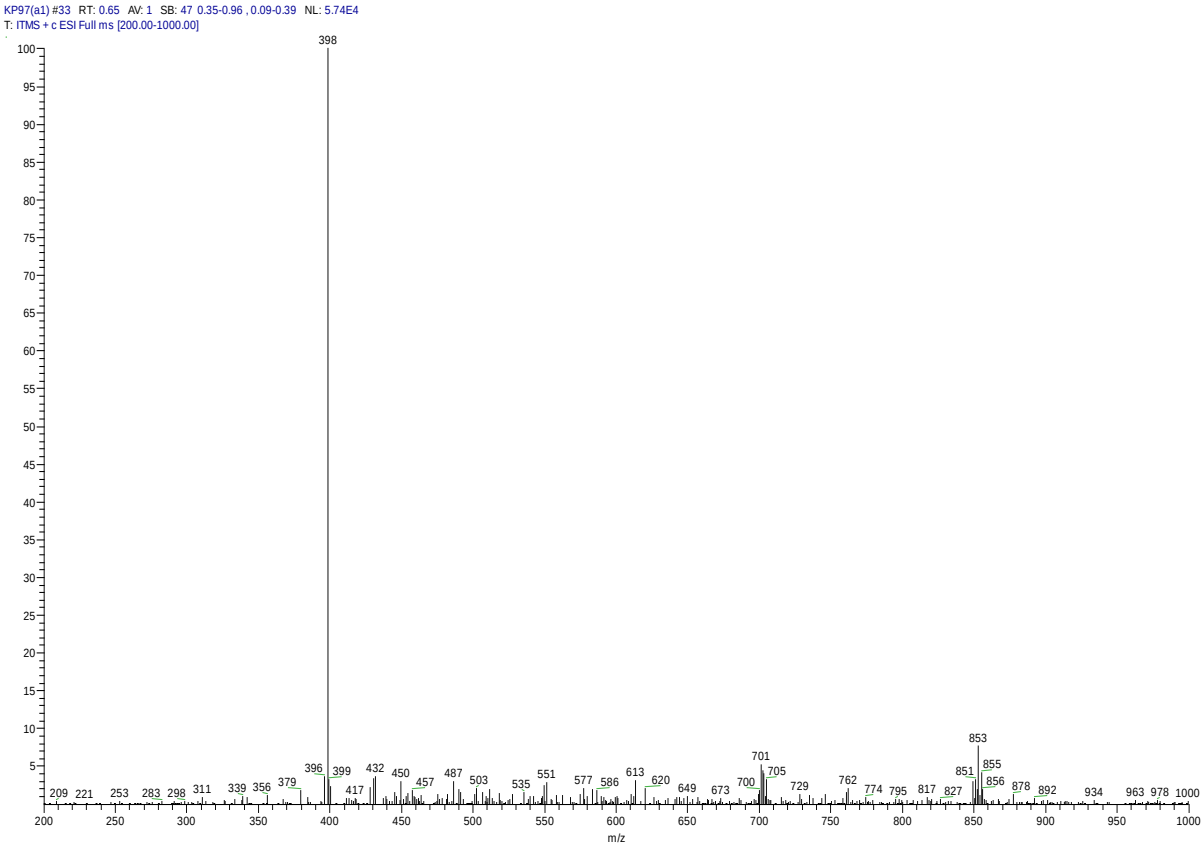


Figure A.33: ESI-MS spectrum of the [Gd(Cy_2DETA.2A)] synthesis in acetonitrile.

Appendix B – NMR Data

All NMR data was generated in the manner described in Chapter 2.

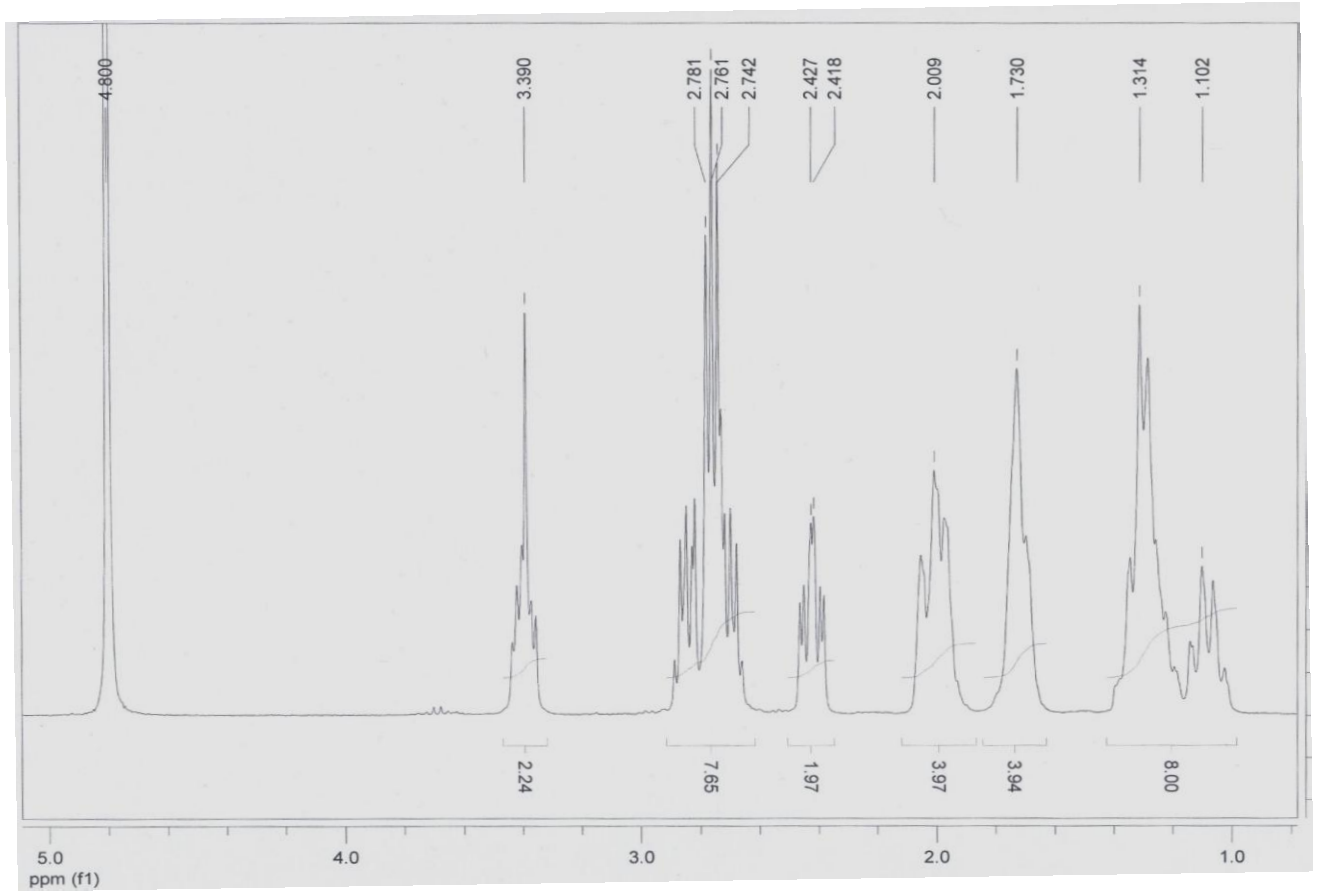


Figure B.1: ^{1}H-NMR spectrum of Cy_2DETA.

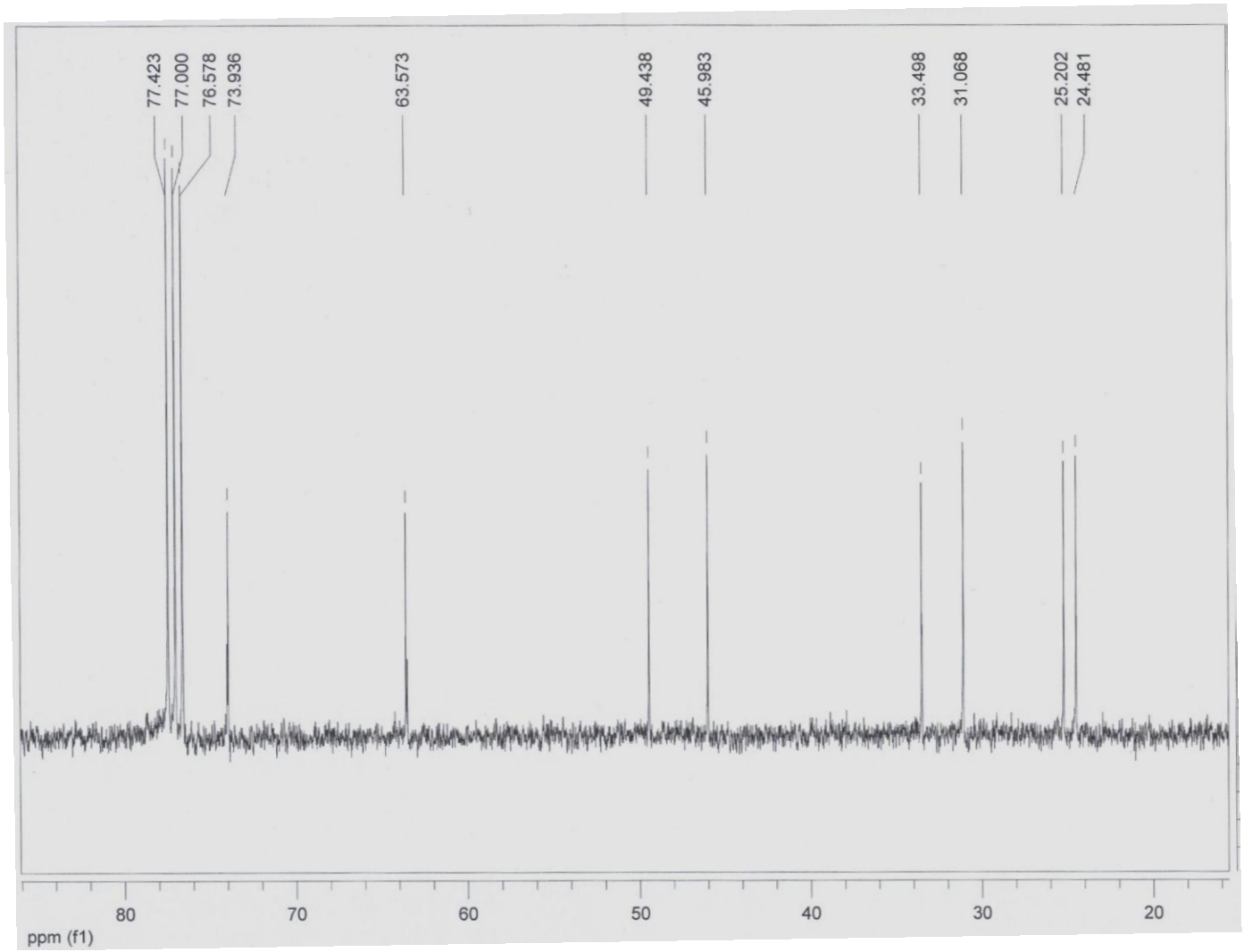


Figure B.2: ^{13}C-NMR spectrum of Cy_2DETA.

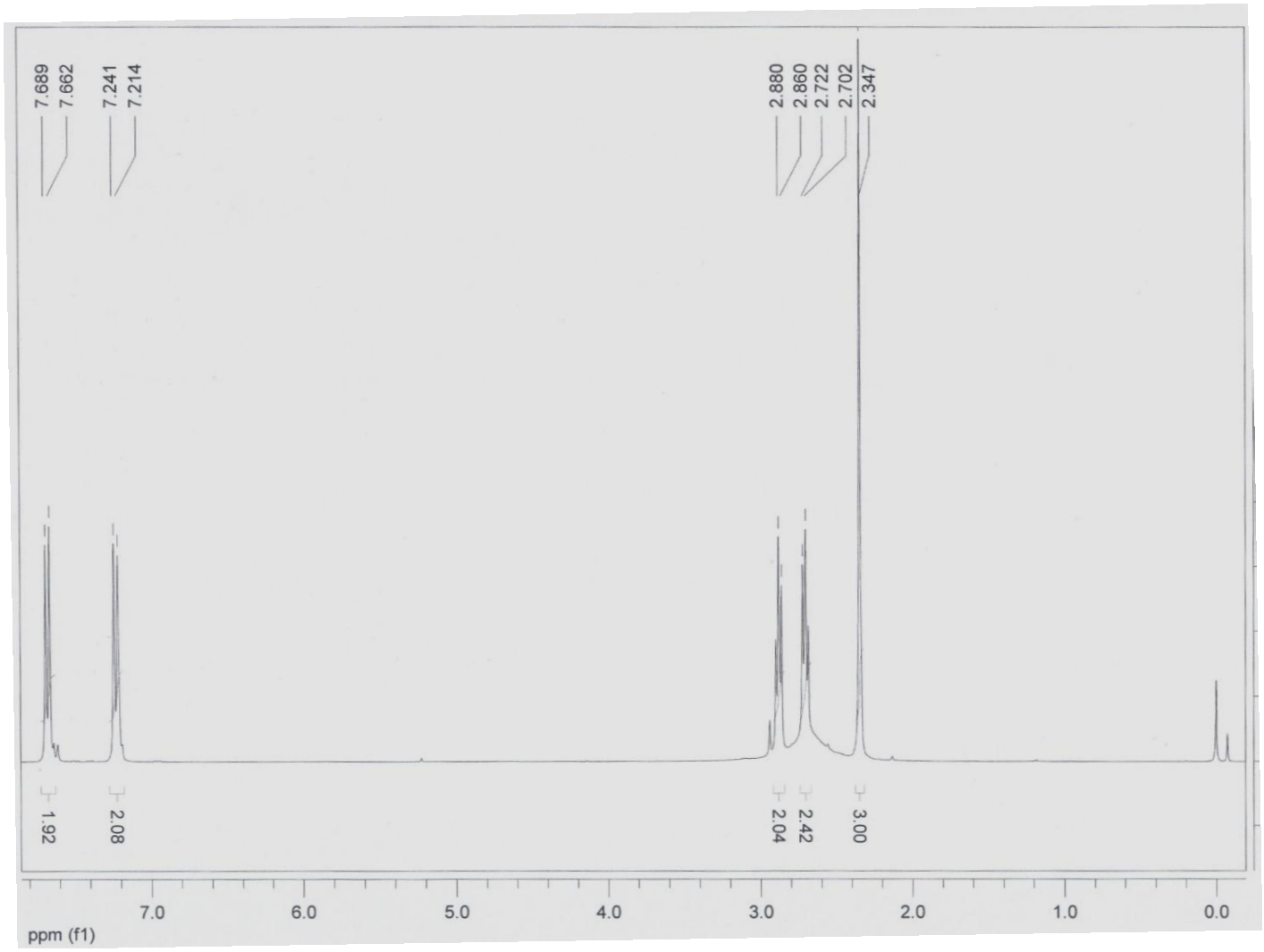


Figure B.3: ^{1}H-NMR spectrum of TsEDA.

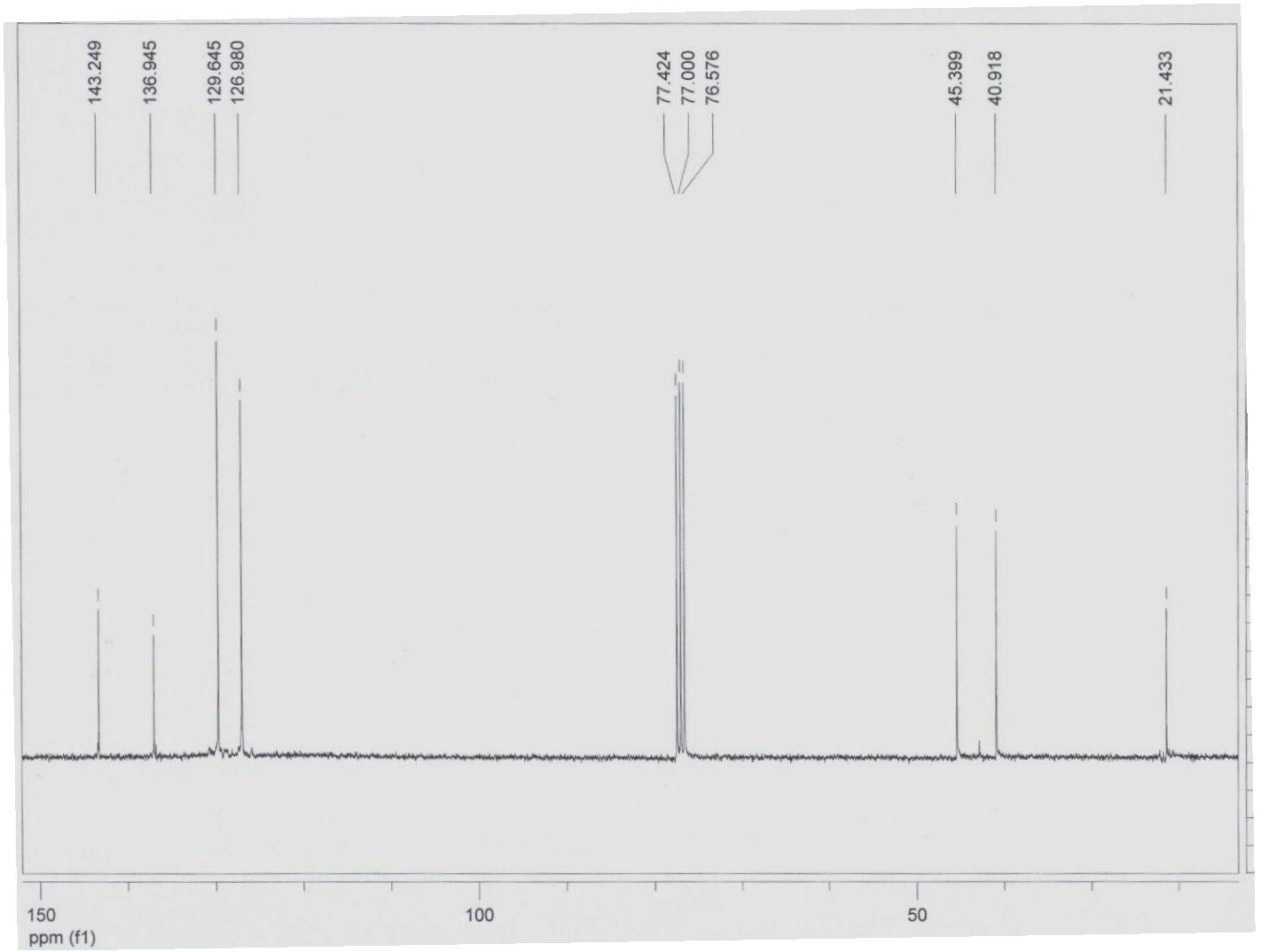


Figure B.4: ^{13}C-NMR spectrum of TsEDA.

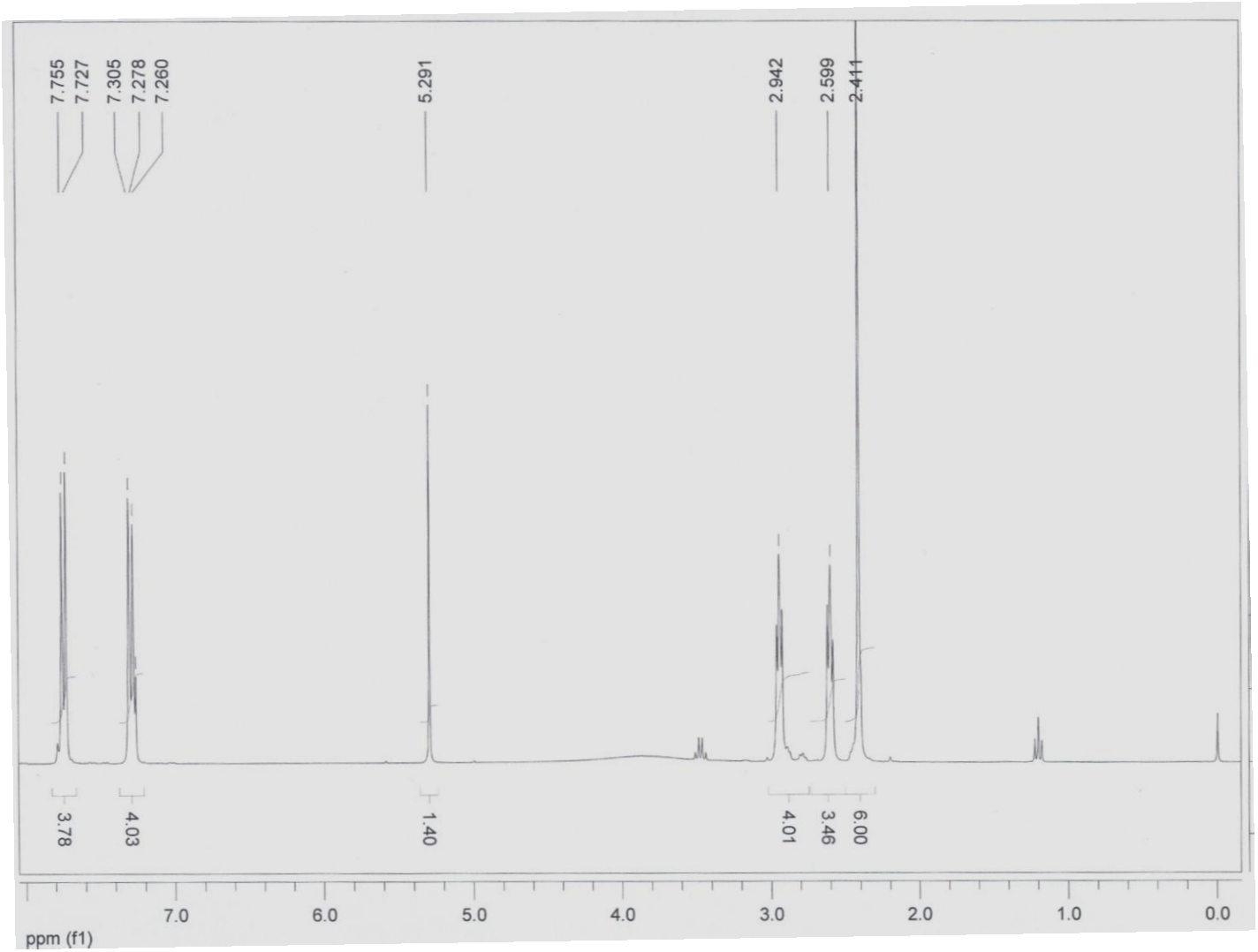


Figure B.5: ^{1}H-NMR spectrum of Ts_2DETA.

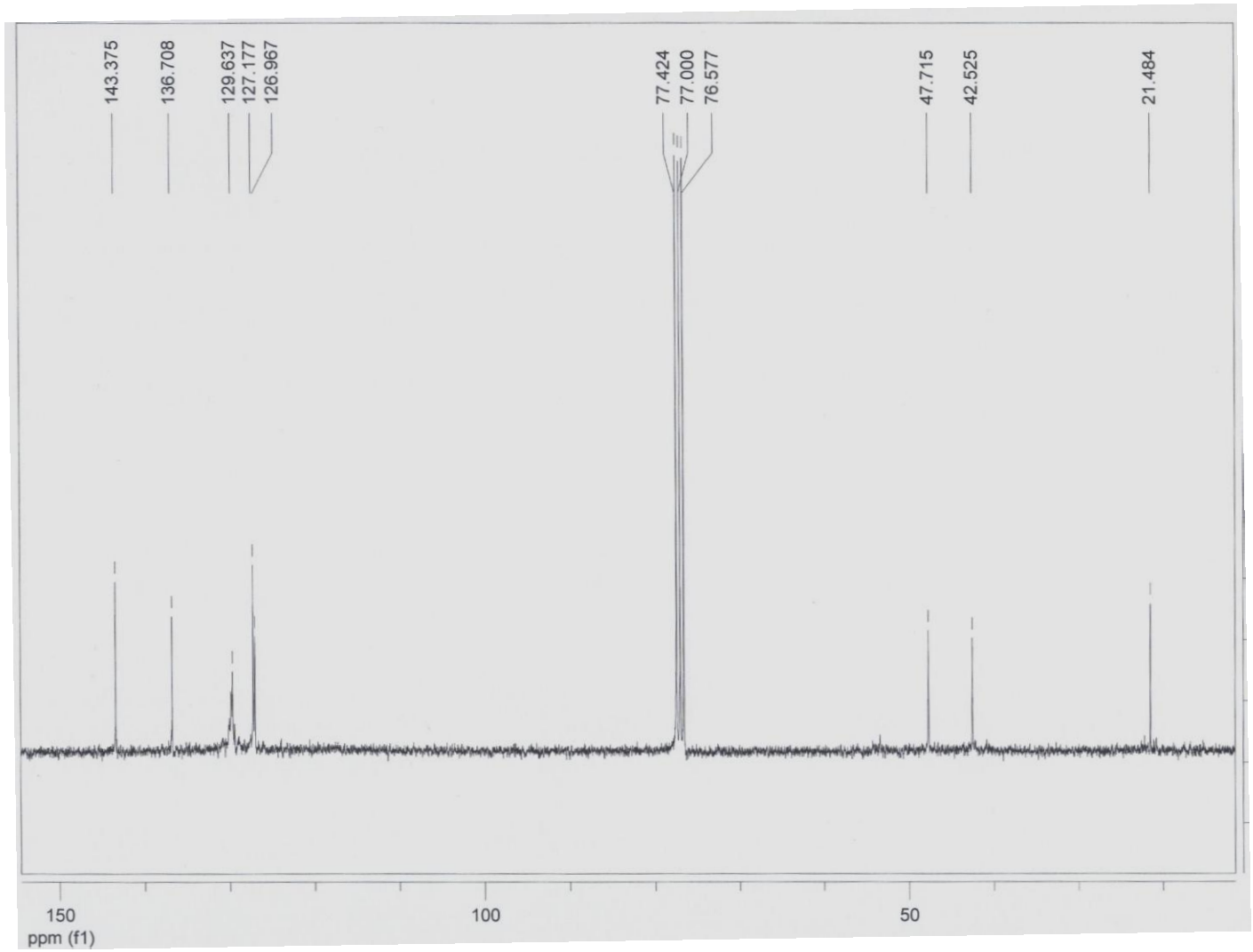


Figure B.6: ^{13}C-NMR spectrum of Ts_2DETA.

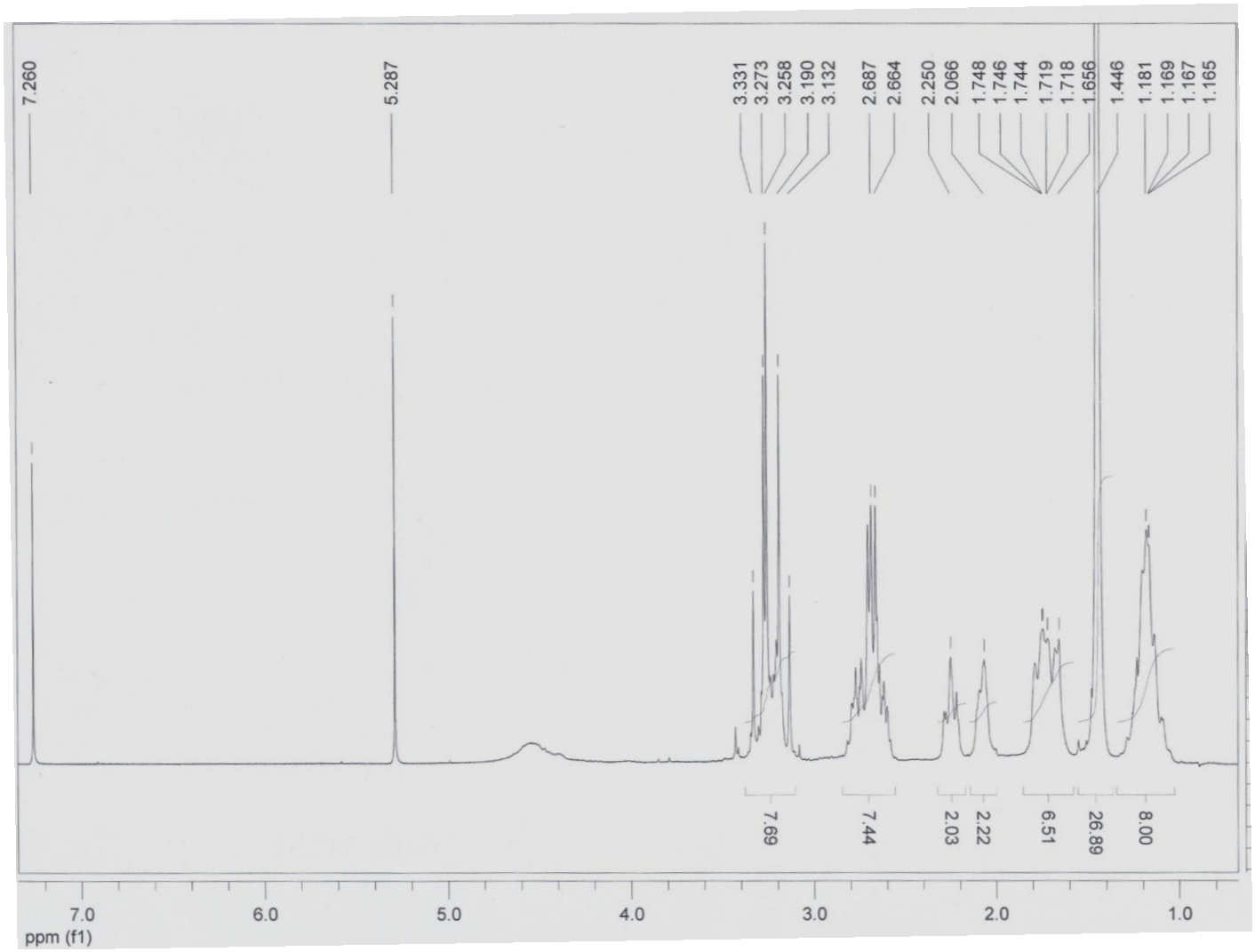


Figure B.7: ^{1}H-NMR spectrum of Cy_2DETA.3E.

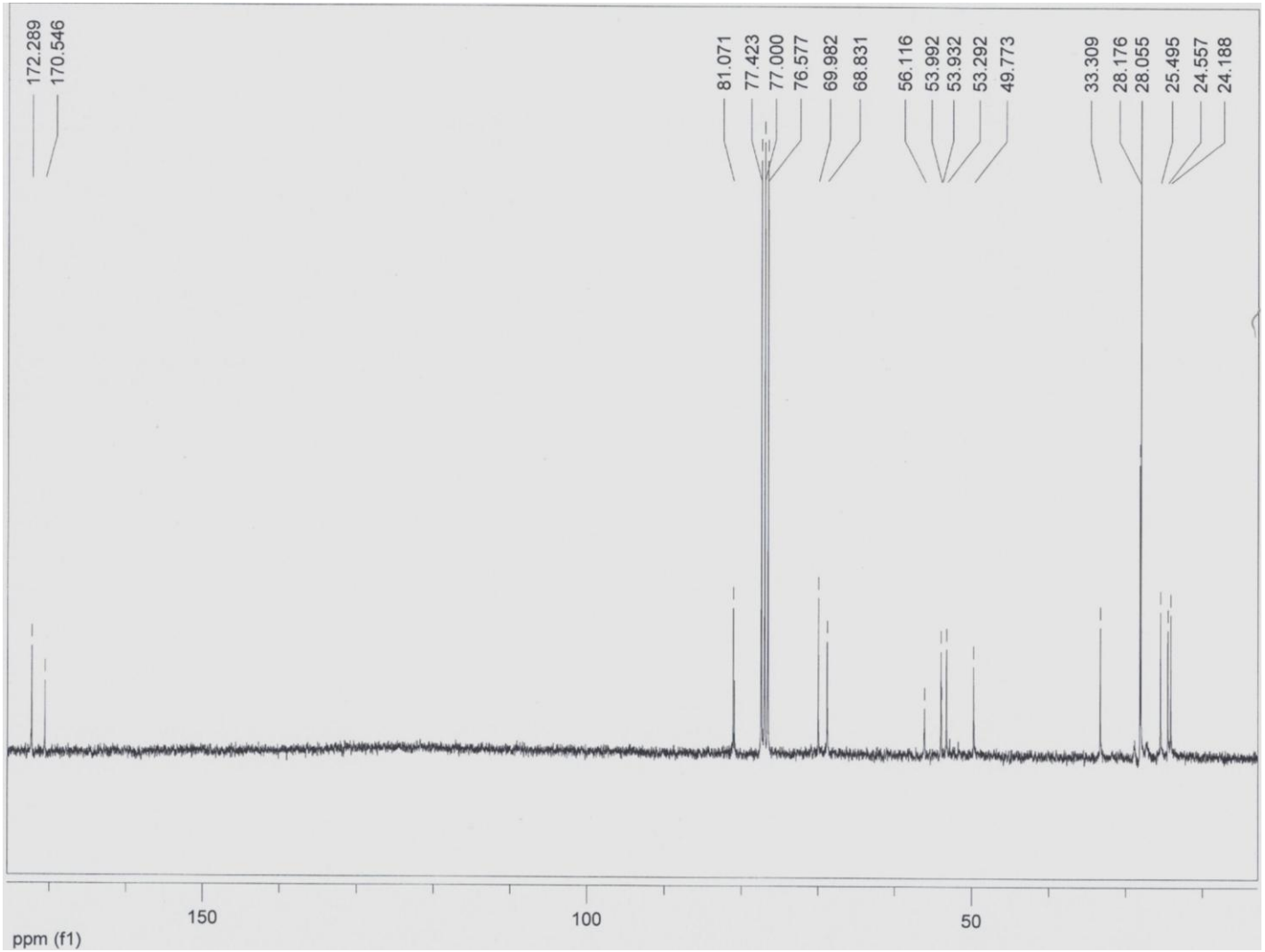


Figure B.8: ^{13}C-NMR spectrum of Cy_2DETA.3E.

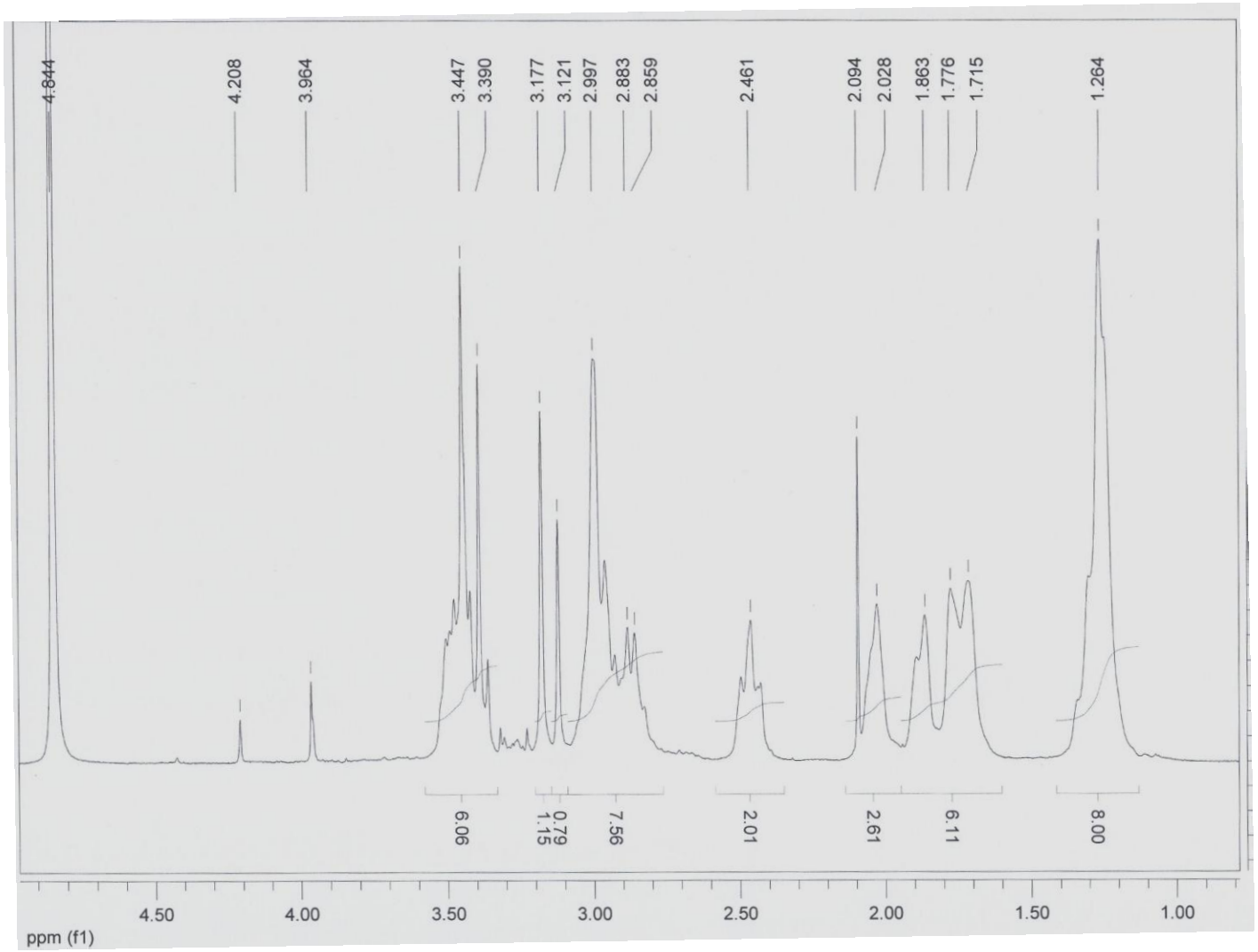


Figure B.9: ^{1}H-NMR spectrum of $Na_3Cy_2DETA.3A$.

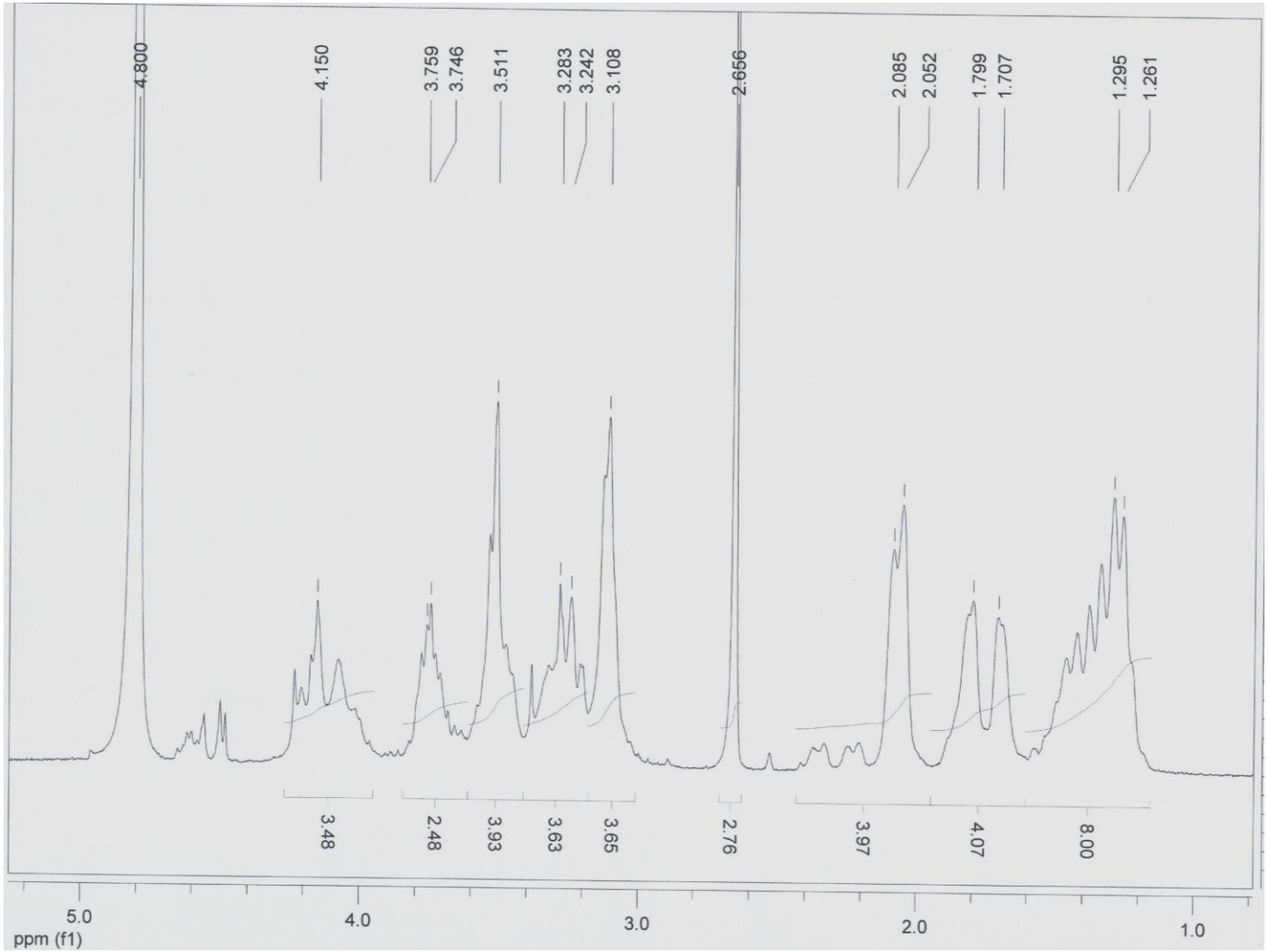


Figure B.10: ^{1}H-NMR spectrum of Cy_2DETA.3A.3HCl.

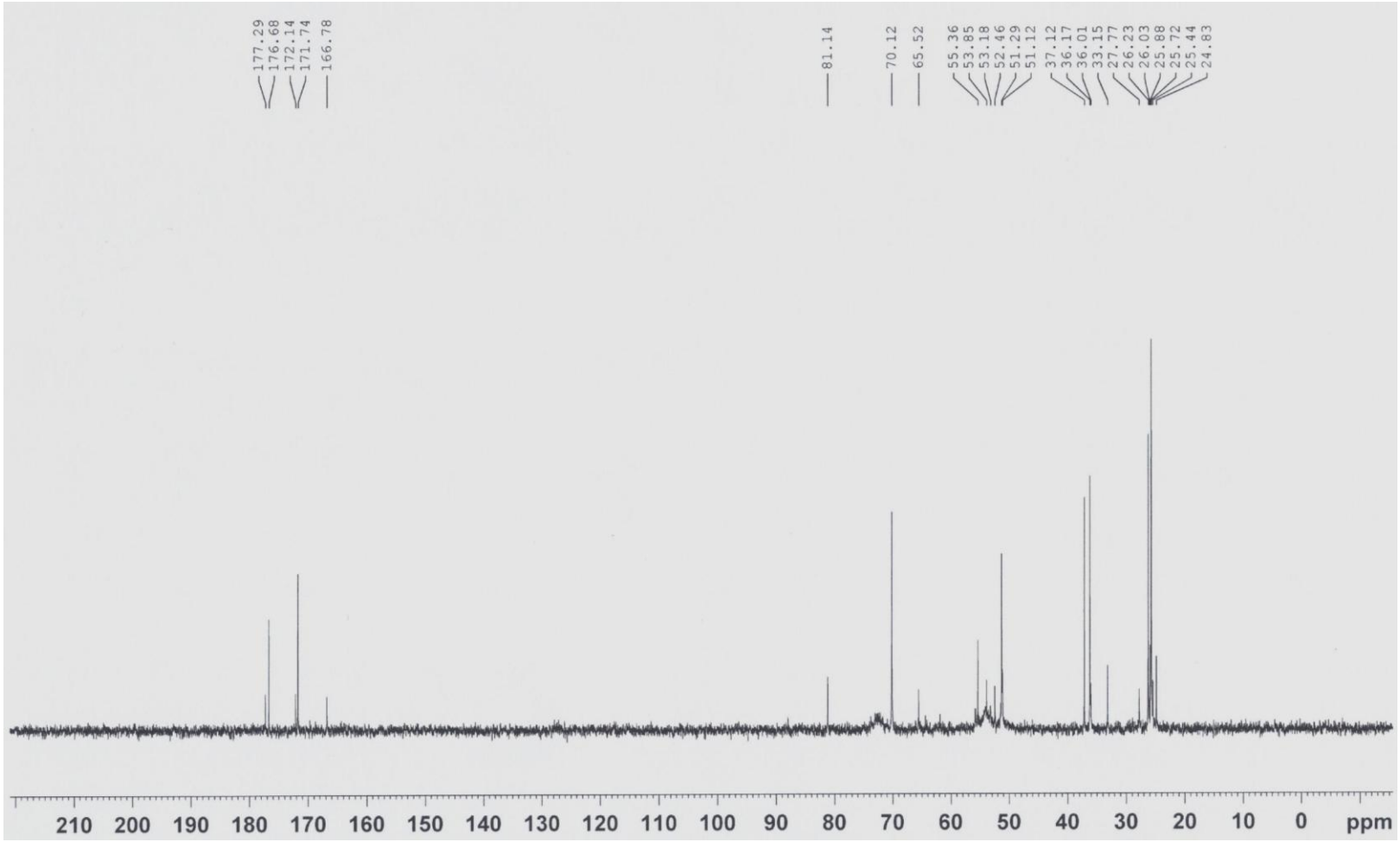


Figure B.11: ^{13}C-NMR spectrum of Cy_2DETA.3A.3HCl.

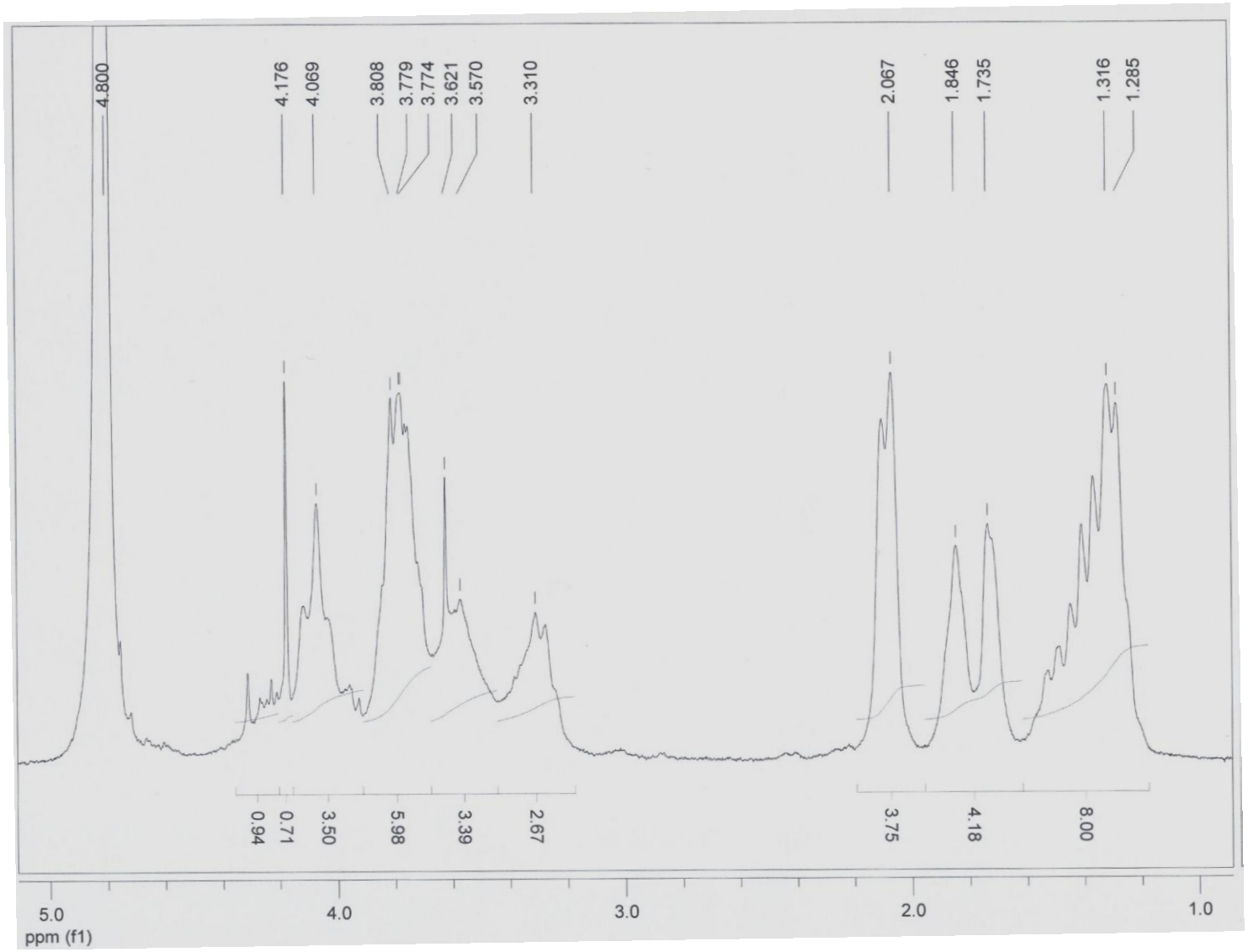


Figure B.12: ^{1}H-NMR spectrum of Cy_2DETA.2A.3HCl.

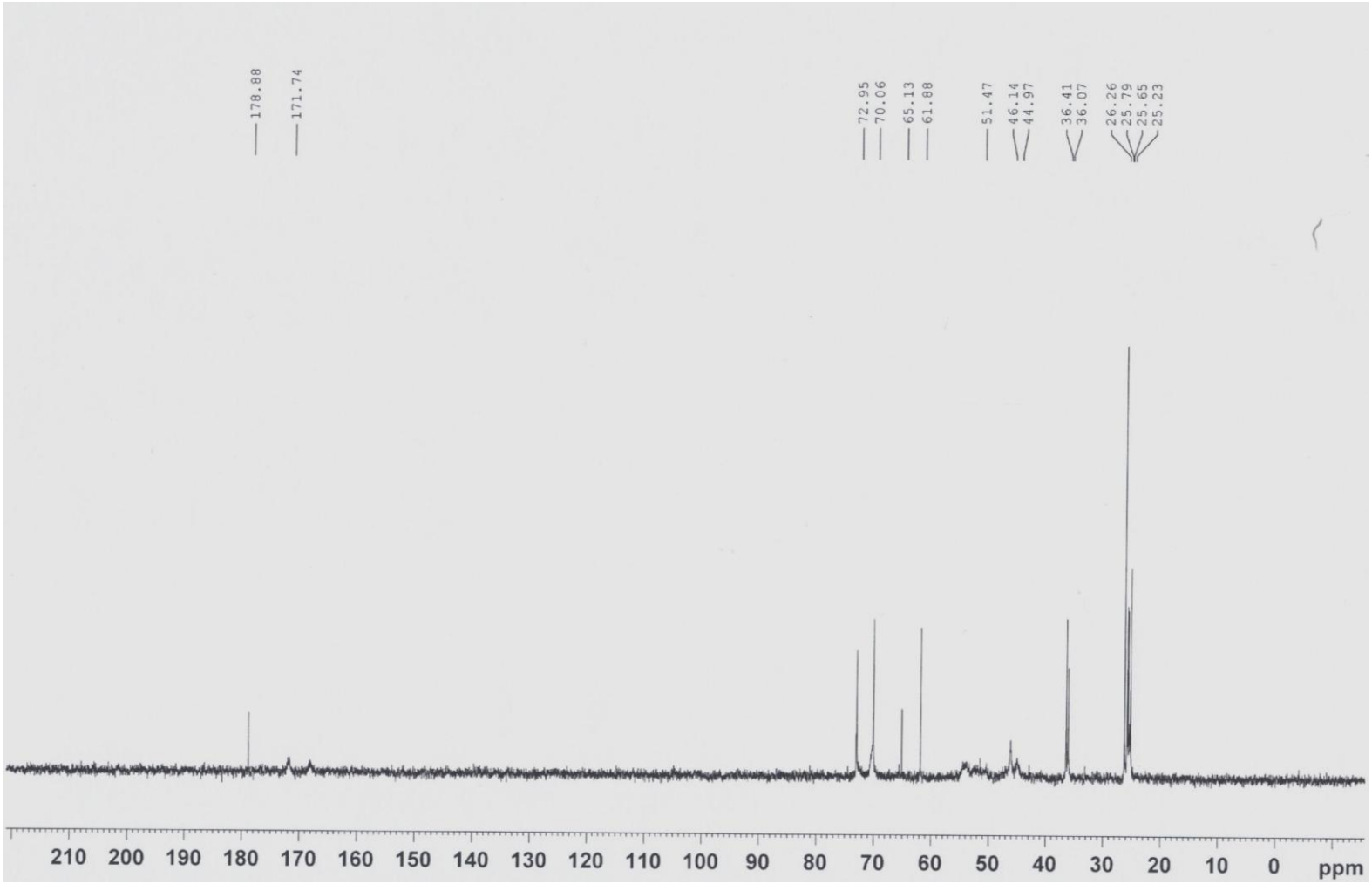


Figure B.13: ^{13}C-NMR spectrum of Cy_2DETA.2A.3HCl.

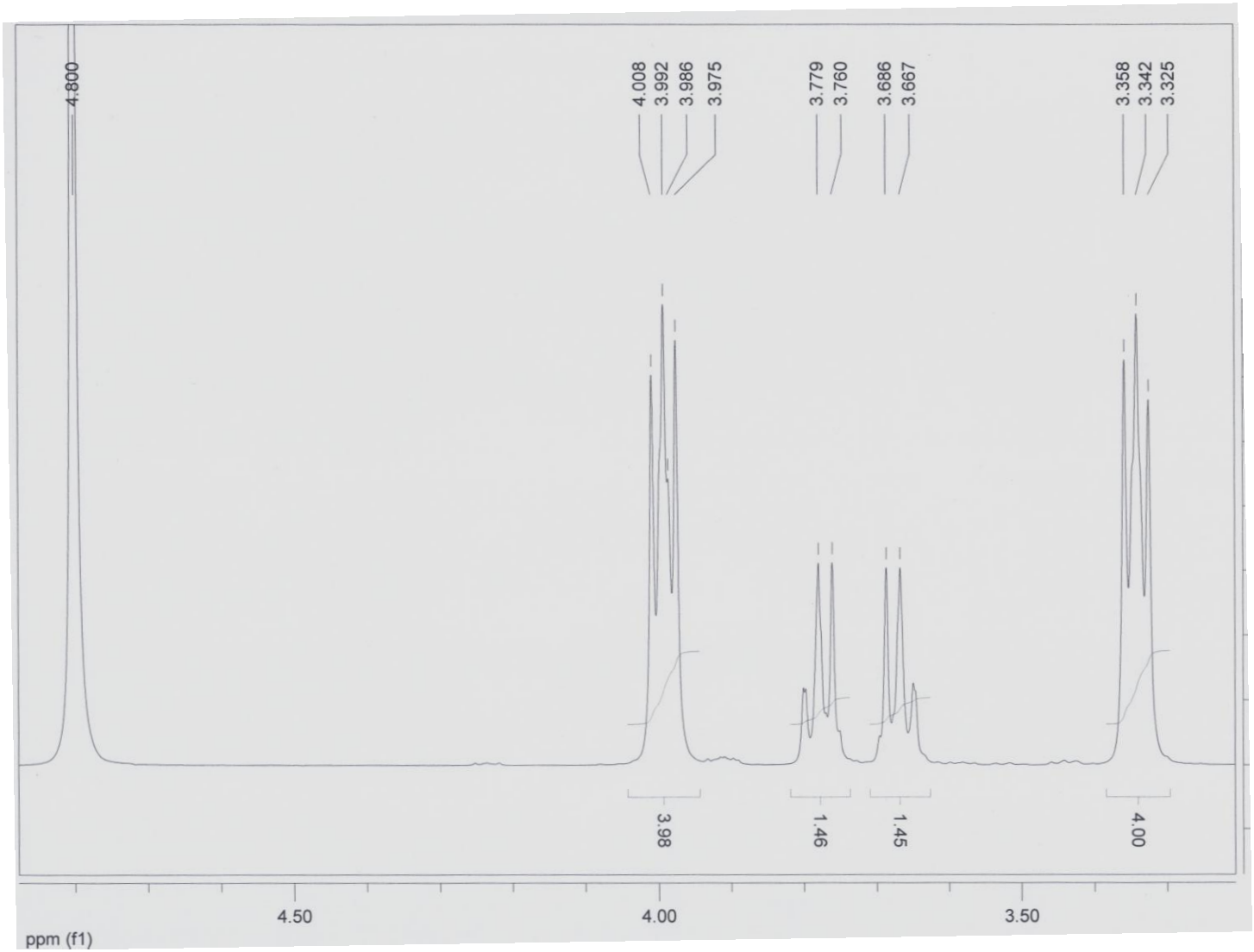


Figure B.14: ^{1}H-NMR spectrum of bis(2-bromoethyl)ammonium bromide and morpholinium bromide.

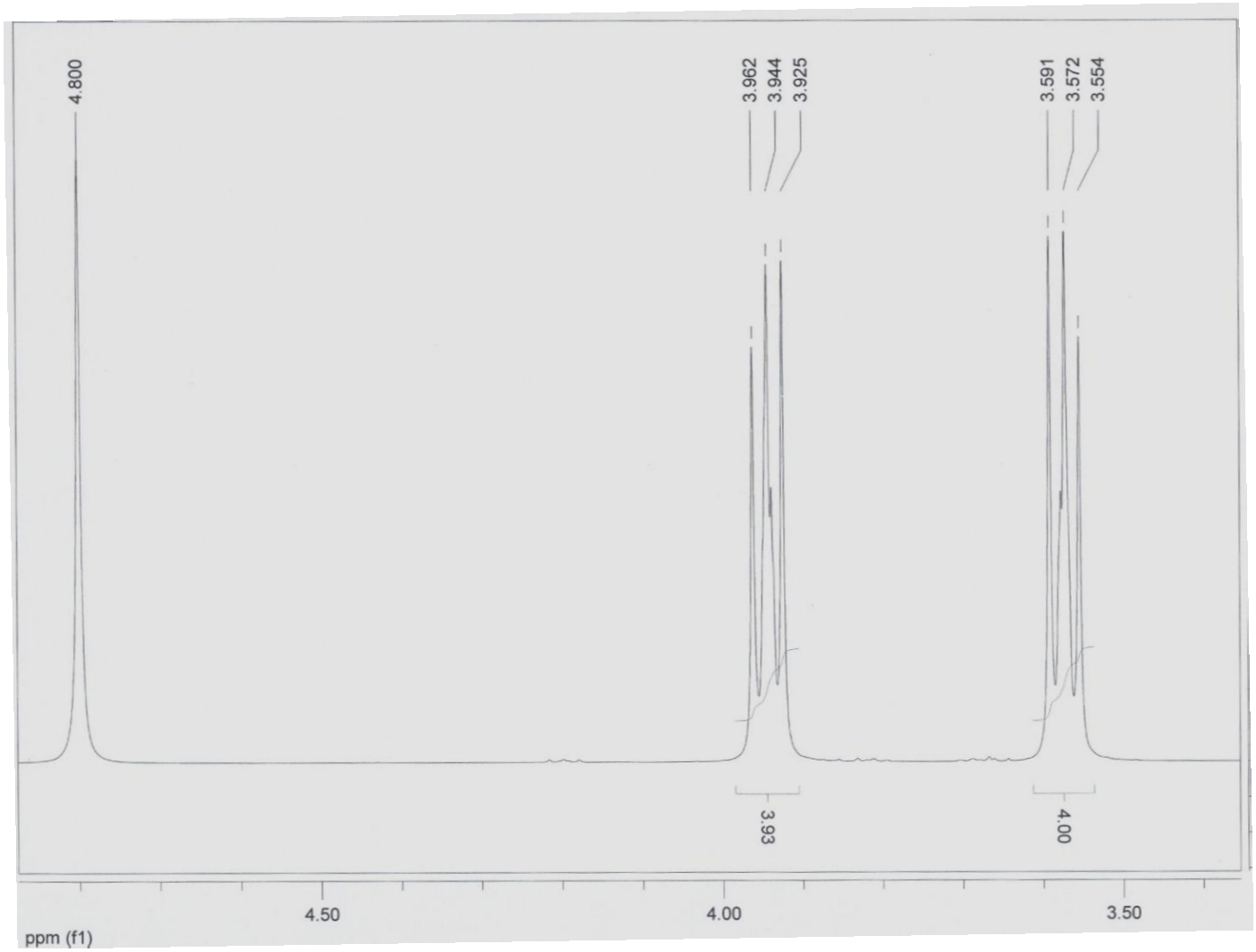


Figure B.15: ^{1}H-NMR spectrum of bis(2-chloroethyl)ammonium chloride.

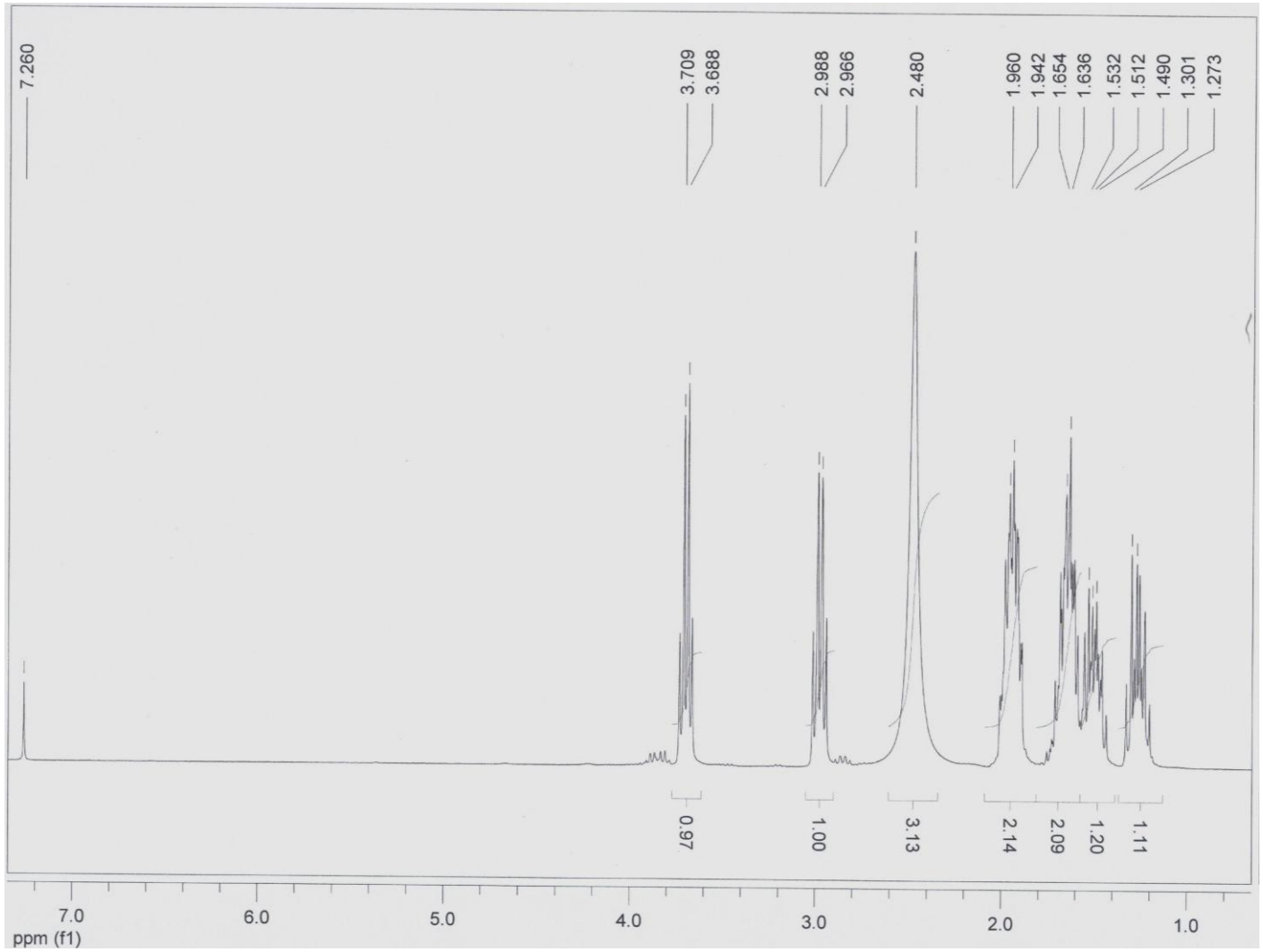


Figure B.16: ^{1}H-NMR spectrum of 2-Aminocyclopentanol.

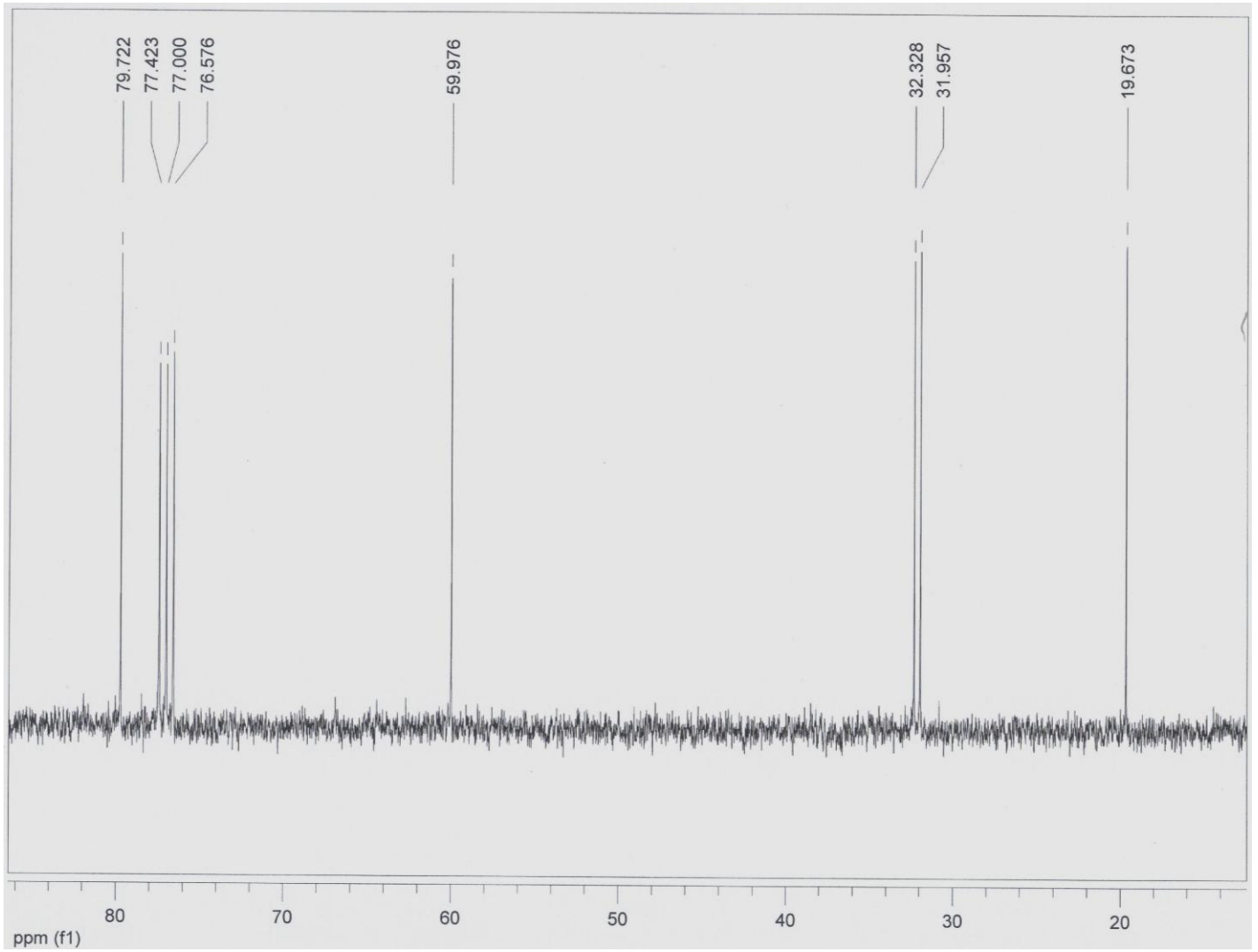


Figure B.17: ^{13}C-NMR spectrum of 2-Aminocyclopentanol.

Appendix C – IR Data

All IR data was generated in the manner described in Chapter 2.

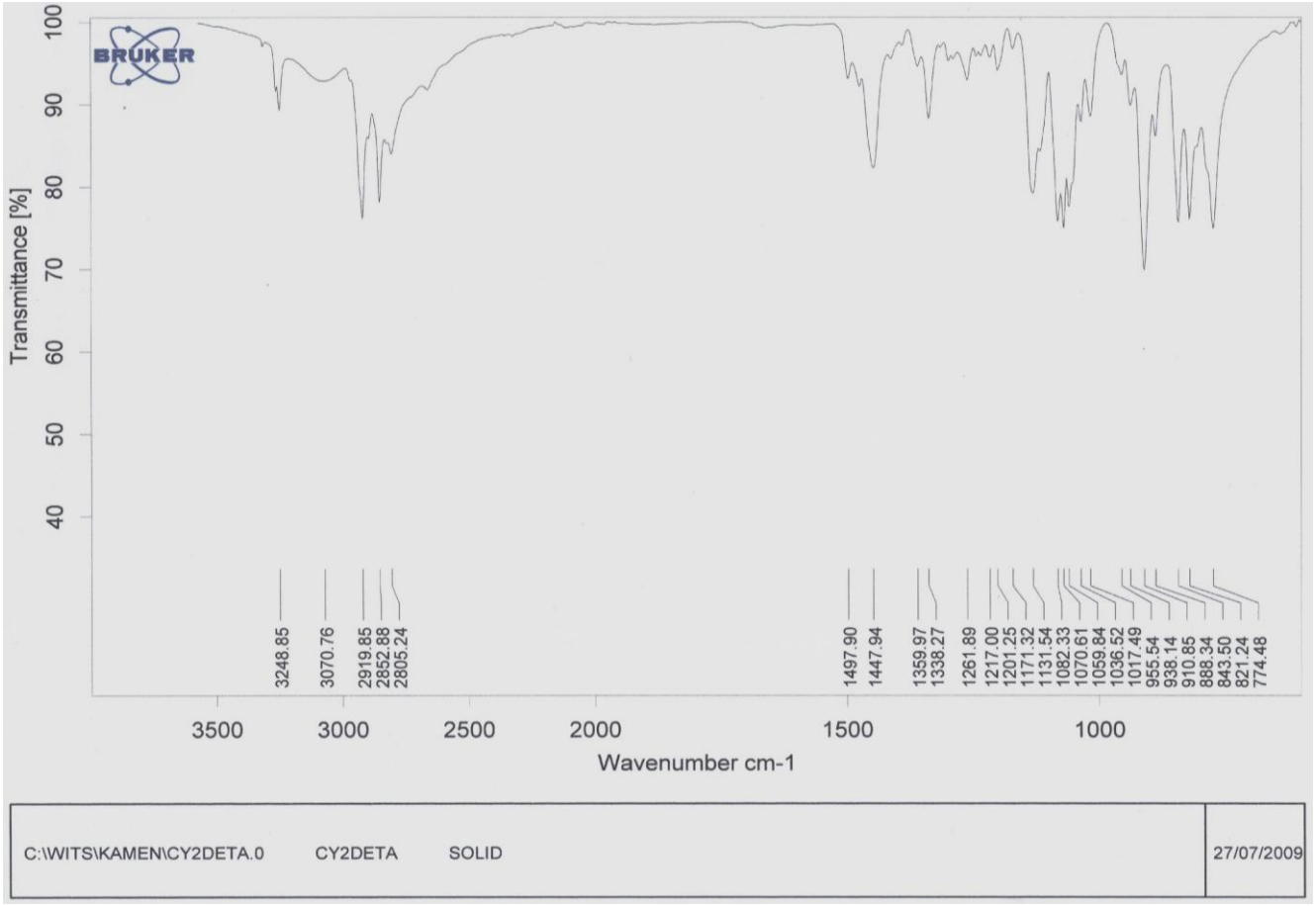


Figure C.1: IR spectrum of Cy_2DETA.

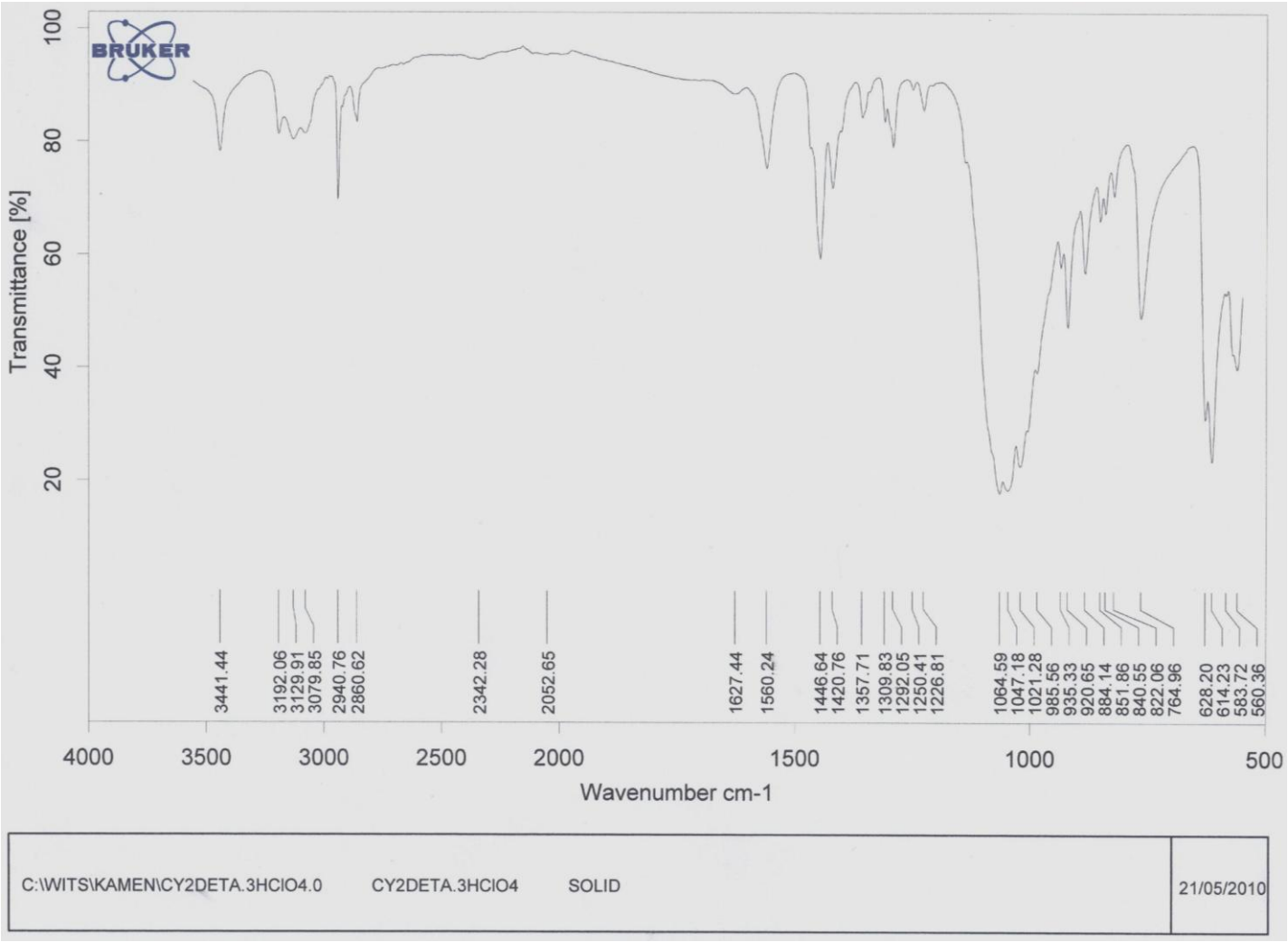


Figure C.2: IR spectrum of $Cy_2DETA.3HClO_4$.

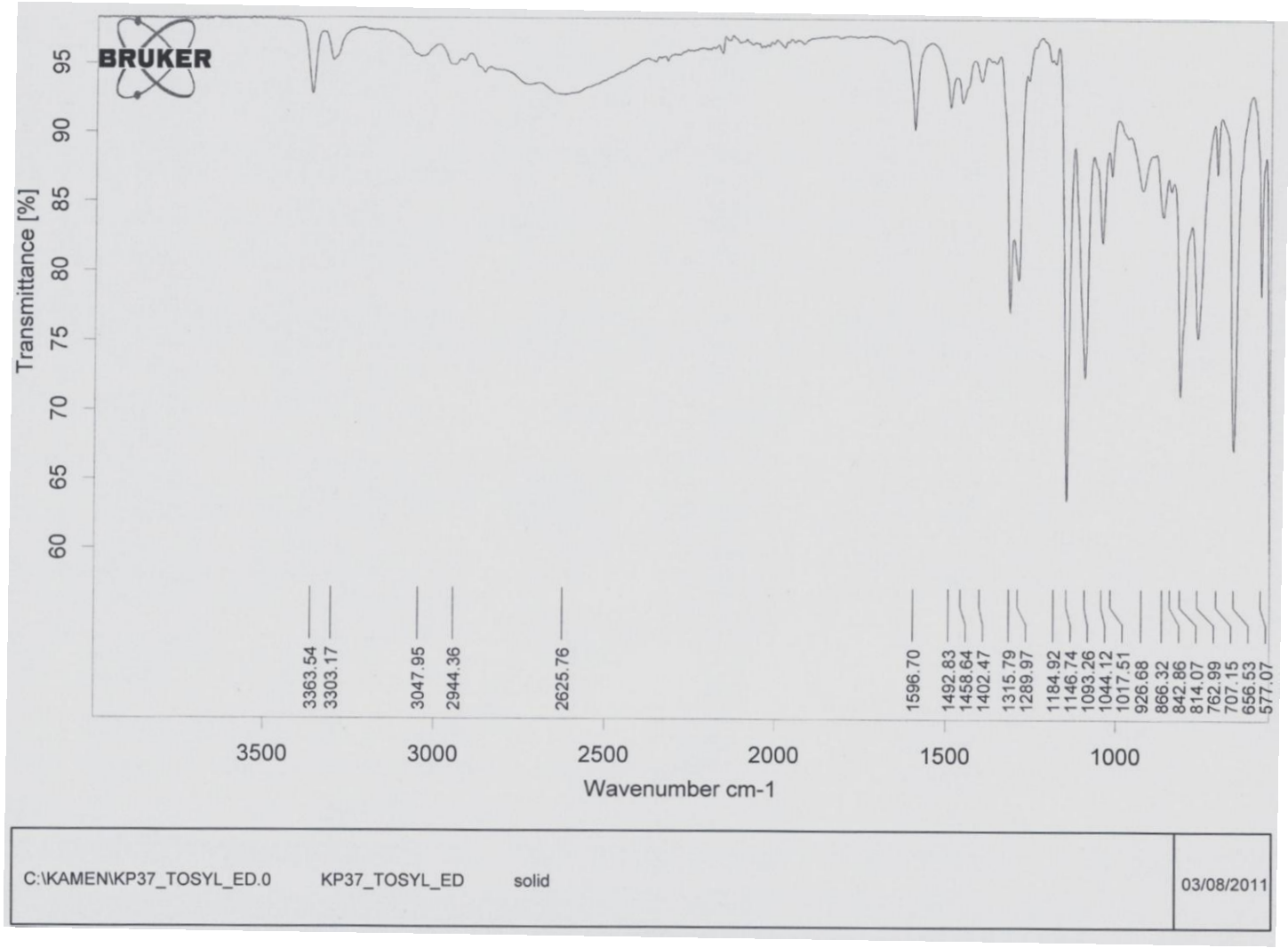


Figure C.3: IR spectrum of TsEDA.

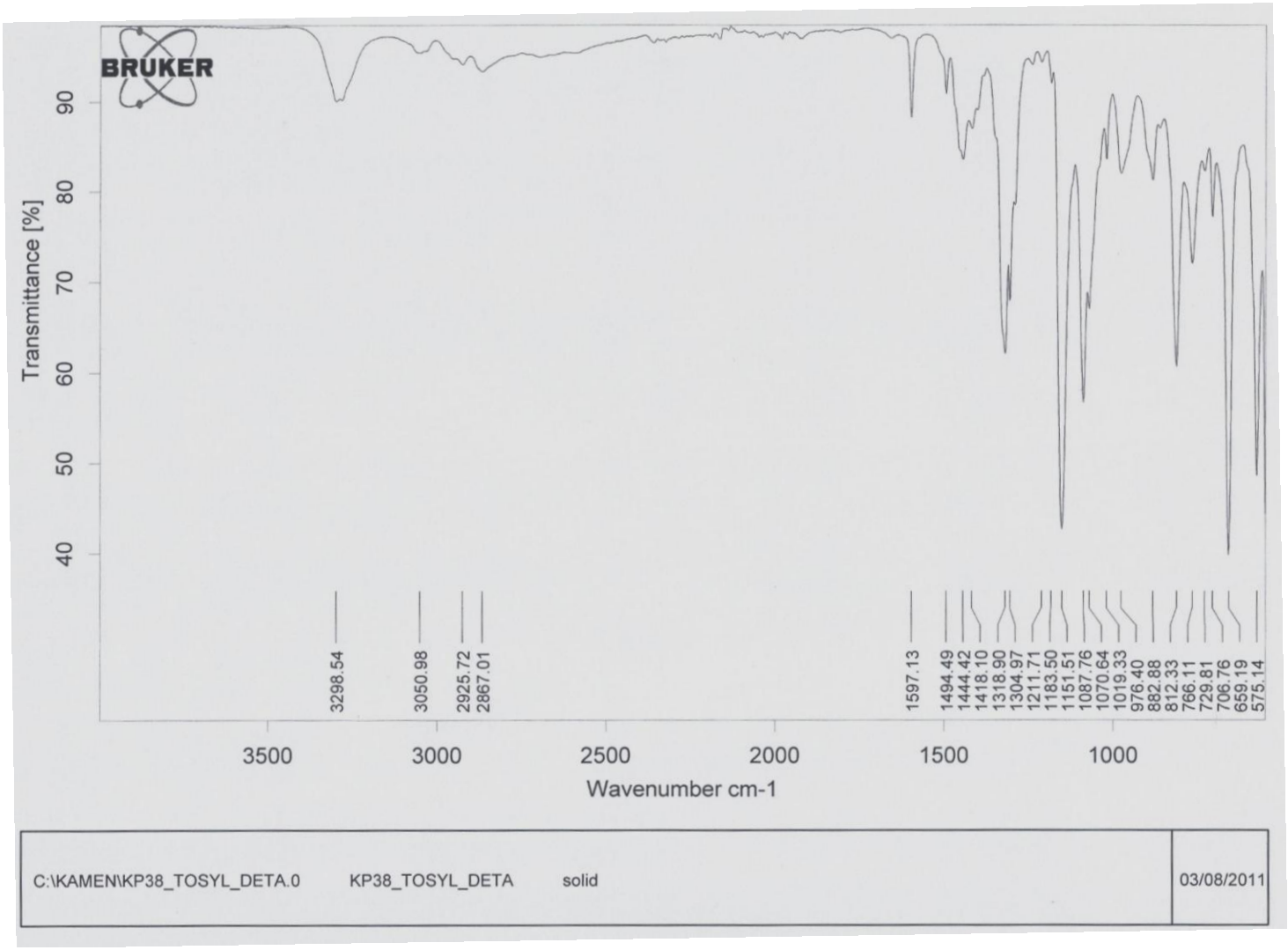


Figure C.4: IR spectrum of Ts_2DETA.

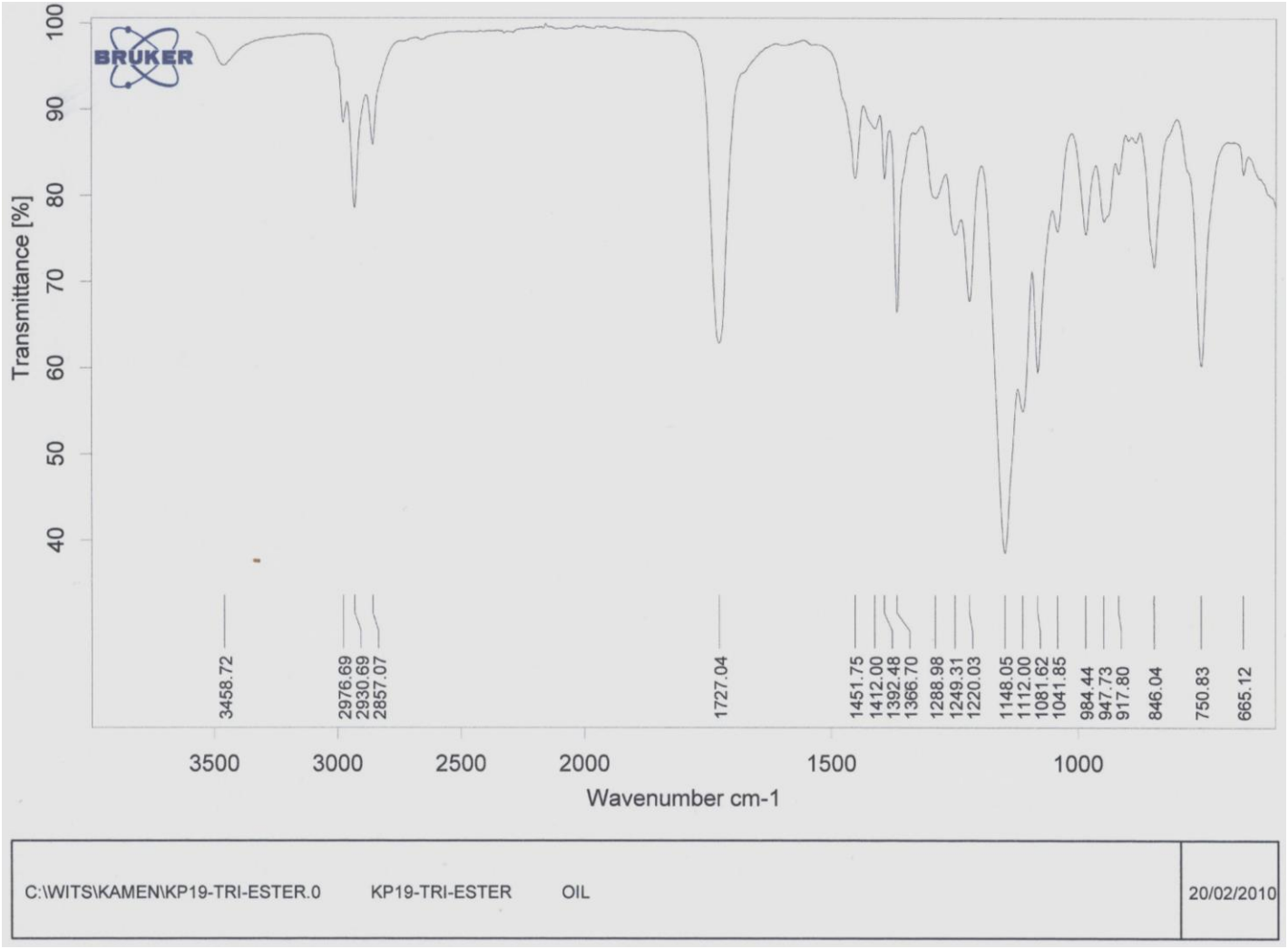


Figure C.5: IR spectrum of Cy_2DETA.3E.

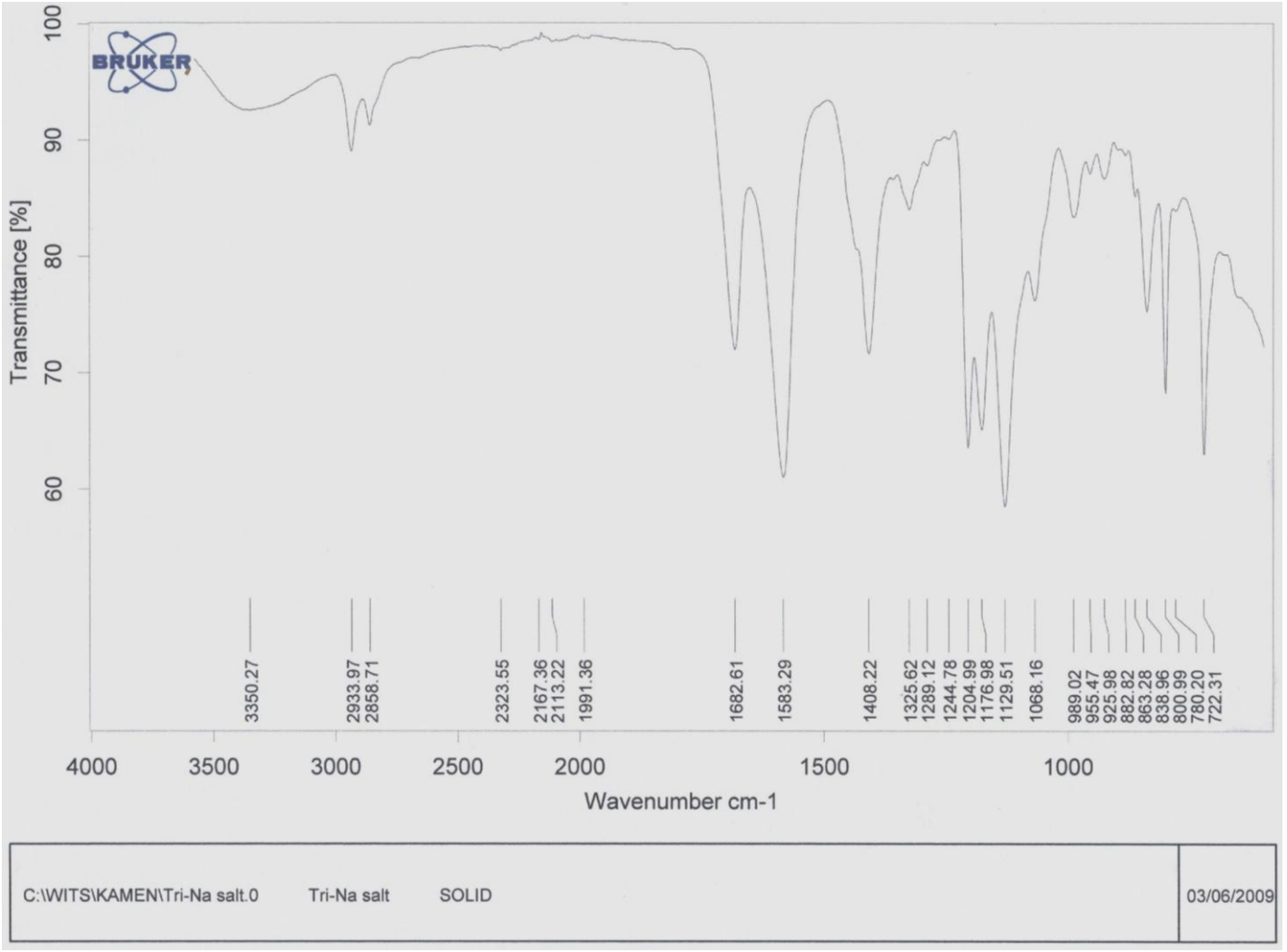


Figure C.6: IR spectrum of $Na_3Cy_2DETA.3A$.

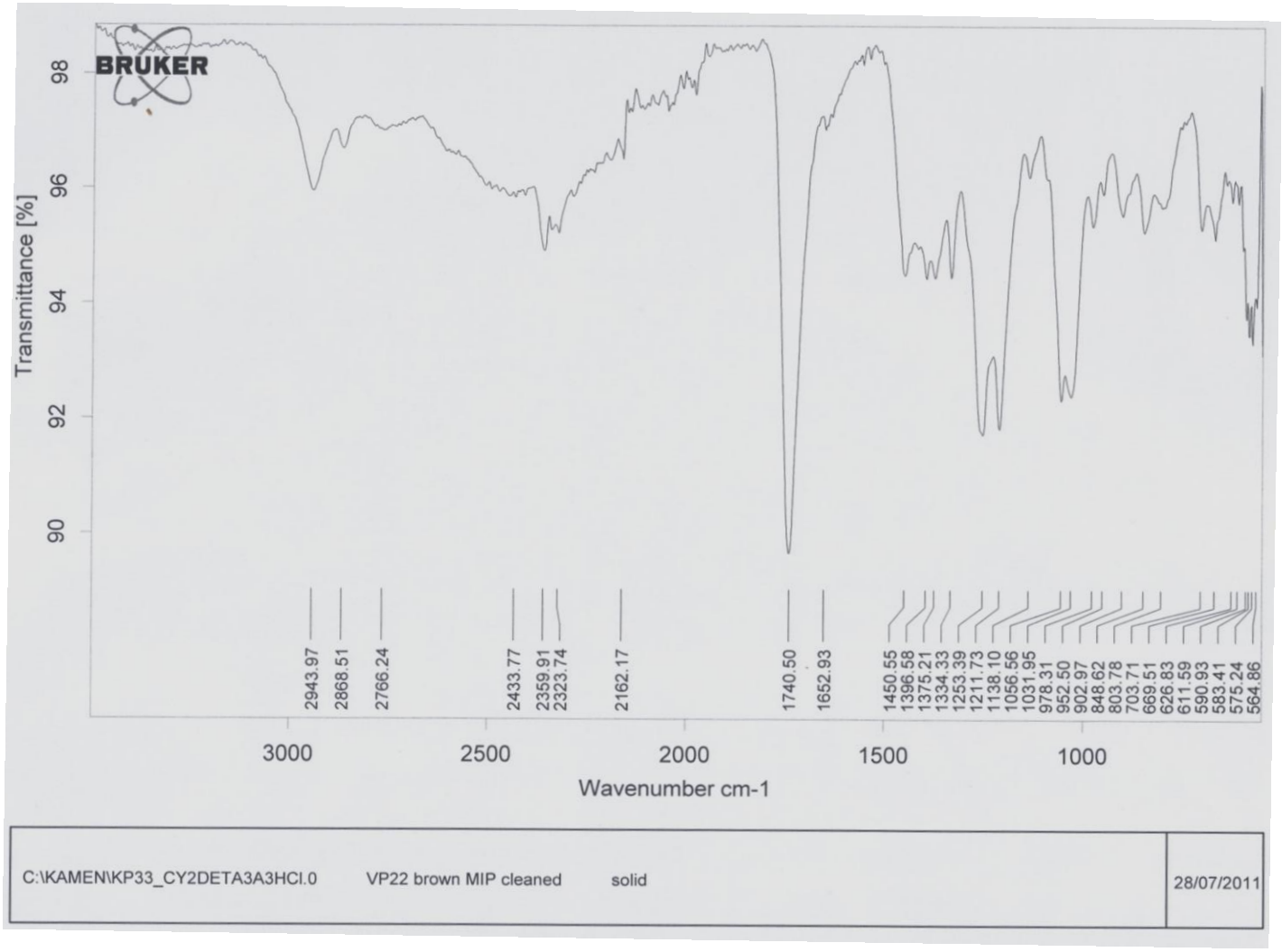


Figure C.7: IR spectrum of Cy_2DETA.3A.3HCl.

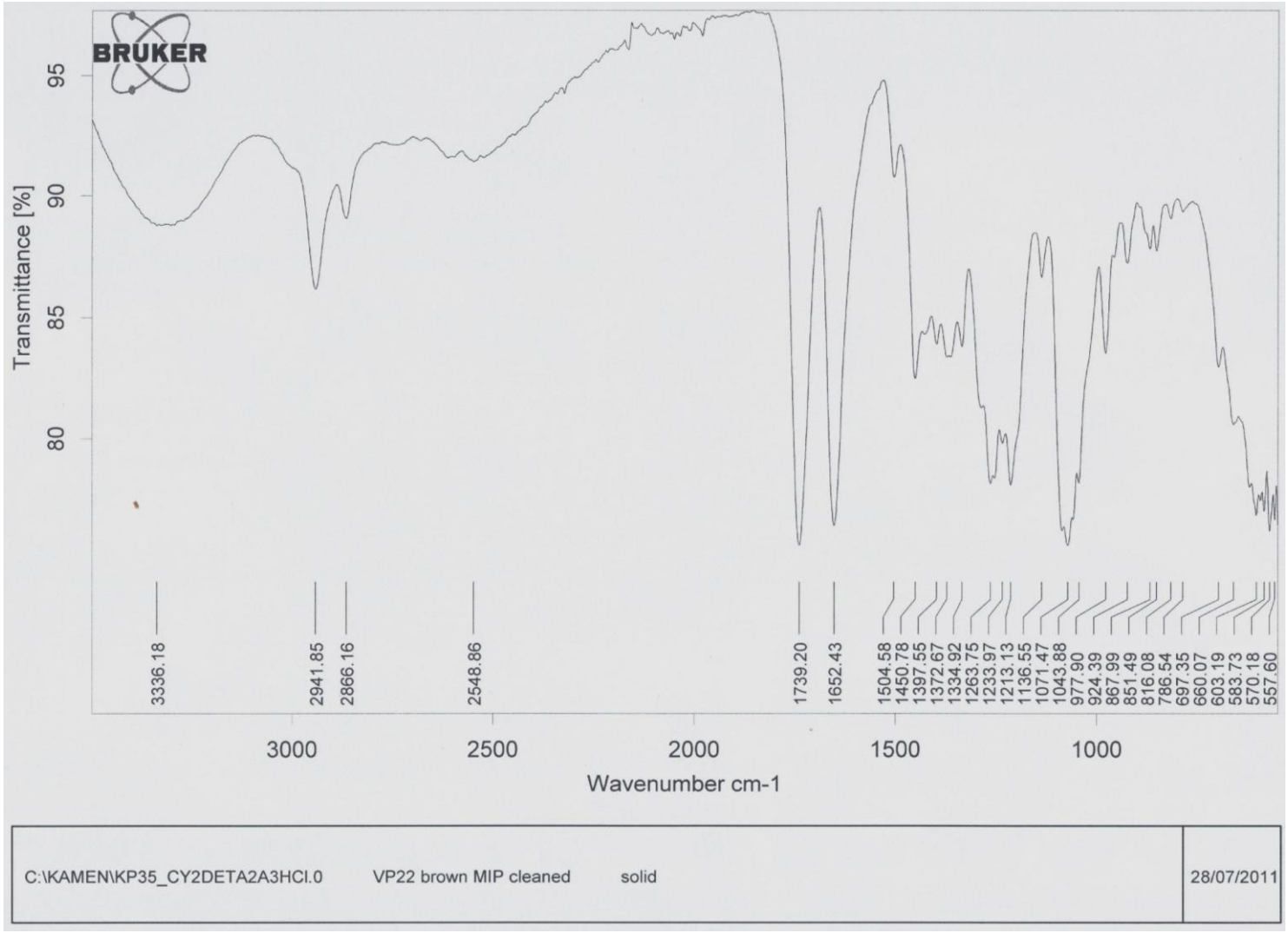


Figure C.8: IR spectrum of Cy_2DETA.2A.3HCl.

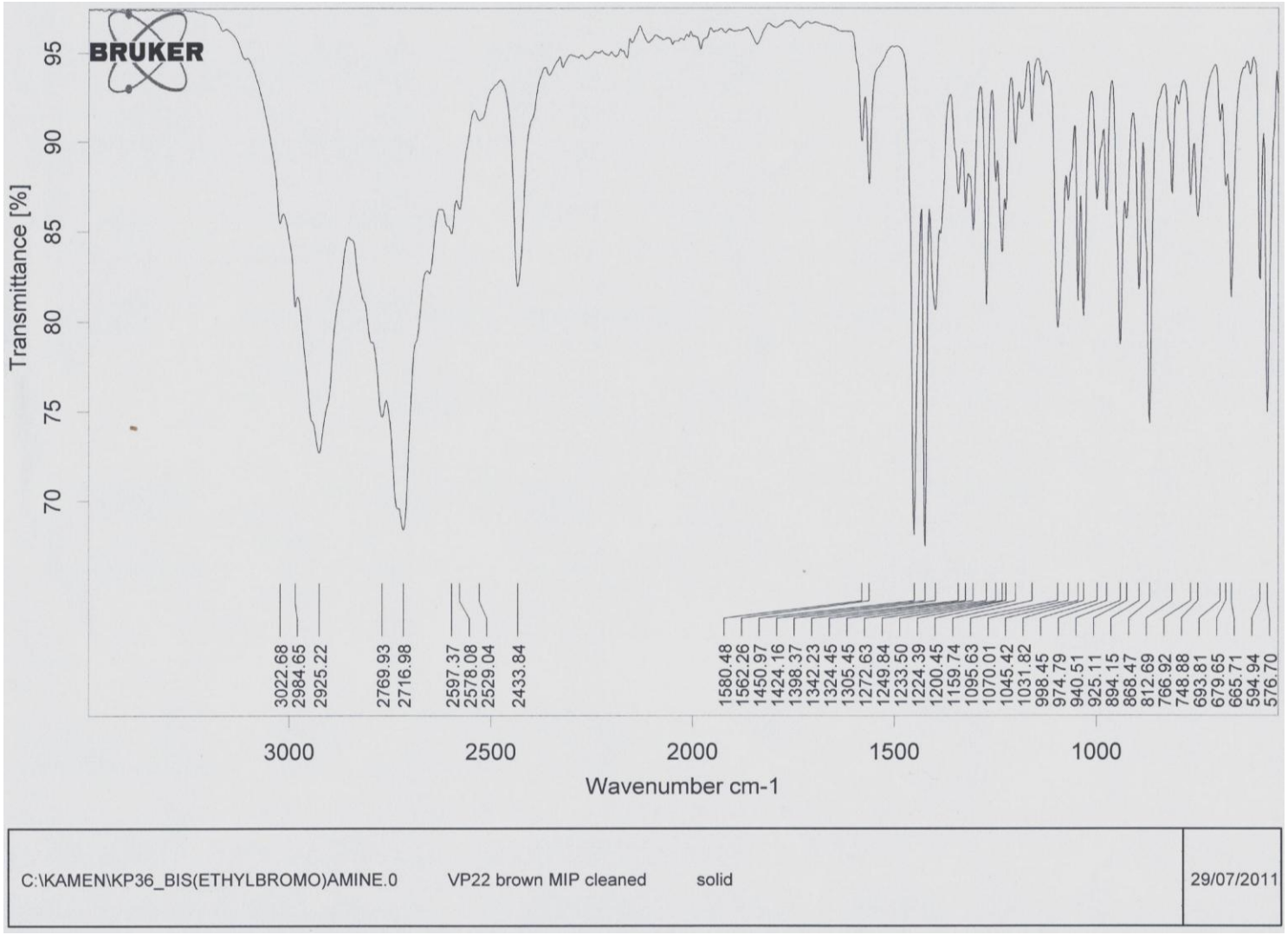


Figure C.9: IR spectrum of bis(2-bromoethyl)ammonium bromide.

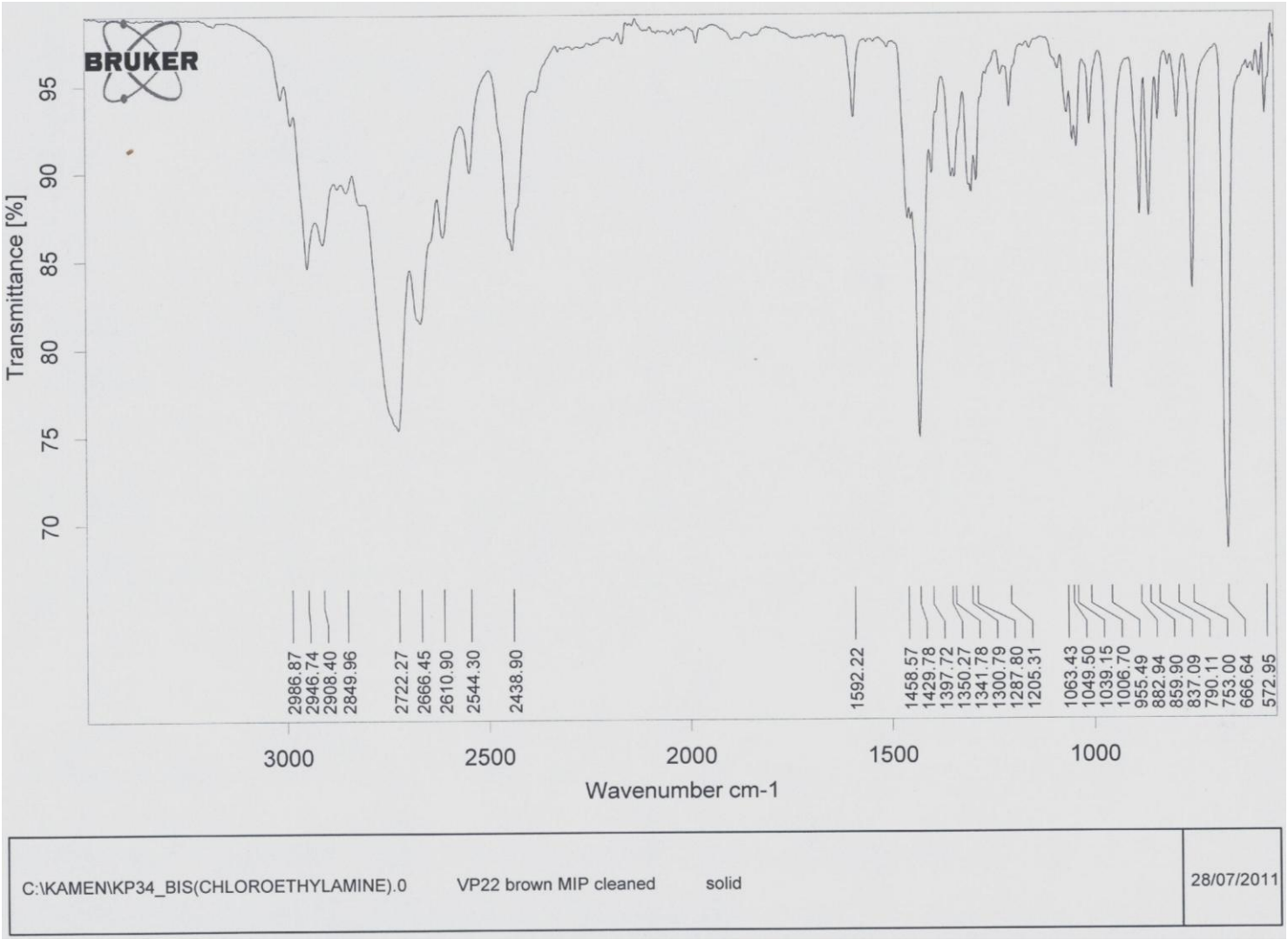


Figure C.10: IR spectrum of bis(2-chloroethyl)ammonium chloride.

Appendix D – Single Crystal X-Ray Diffraction Data

All single crystal x-ray diffraction data was generated in the manner described in Chapter 2.

D.1 Cy_2DETA

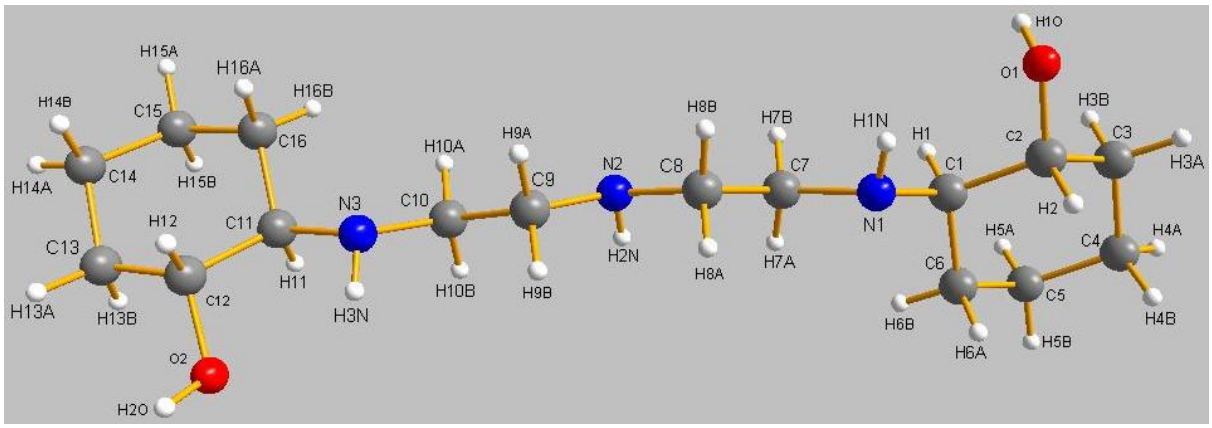


Figure D.1: XRD structure of Cy_2DETA.

Table D.1: Crystal data and structure refinement for Cy_2DETA.

Identification code	6m_al3_0s
Empirical formula	C16 H33 N3 O2
Formula weight	299.45
Temperature	173 K
Wavelength	0.71073 Å
Crystal system	Triclinic
Space group	P-1
Unit cell dimensions	a = 5.5150(1) Å α = 82.471(1)° b = 12.2025(3) Å β = 79.769(1)° c = 12.9514(3) Å γ = 84.284(1)°
Volume	847.50(3) $Å^3$
Z	2
Density (calculated)	1.173 $g.cm^{-3}$
Absorption coefficient	0.077 mm^{-1}

F(000)	332
Crystal size	0.05 × 0.18 × 0.38 mm^3
Theta range for data collection	1.6 to 27.0°
Index ranges	-7<=h<=7, -15<=k<=15, -16<=l<=16
Reflections collected	30177
Independent reflections	3684 [R(int) = 0.050]
Absorption correction	None
Refinement method	Full-matrix least-squares on F2
Data / restraints / parameters	3684 / 0 / 210
Goodness-of-fit on F^2	0.99
R indices (all data)	R1 = 0.0477, wR2 = 0.1404
Largest diff. peak and hole	-0.16 and 0.31 e.$Å^{-3}$

Table D.2: Atomic coordinates (× 10^4) and equivalent isotropic displacement parameters ($Å^2$ × 10^3) for Cy_2DETA. U(eq) is defined as one third of the trace of the orthogonalized U^{ij} tensor.

Atom	x	y	z	U(eq)
O1	1.05271(18)	0.59914(8)	-0.12190(8)	0.0299(3)
O2	-0.06783(19)	-0.22597(8)	0.16841(8)	0.0312(3)
N1	0.7726(2)	0.42043(9)	-0.13544(9)	0.0238(3)
N2	0.2845(2)	0.24590(9)	0.02333(9)	0.0228(3)
N3	0.0449(2)	-0.01122(9)	0.17945(9)	0.0254(3)
C1	0.7711(2)	0.52021(10)	-0.21236(10)	0.0244(4)
C2	1.0100(2)	0.57642(11)	-0.22152(11)	0.0274(4)
C3	1.0112(3)	0.67952(12)	-0.30180(12)	0.0330(4)
C4	0.9785(3)	0.65288(13)	-0.41002(12)	0.0404(5)
C5	0.7450(3)	0.59349(13)	-0.40158(12)	0.0379(5)
C6	0.7425(3)	0.49140(12)	-0.32062(11)	0.0310(4)
C7	0.5234(2)	0.38631(10)	-0.09250(10)	0.0240(4)
C8	0.5322(2)	0.28315(11)	-0.01420(11)	0.0258(4)
C9	0.2906(2)	0.13654(11)	0.08485(10)	0.0251(4)
C10	0.0345(2)	0.09619(11)	0.11586(11)	0.0258(4)
C11	-0.1947(2)	-0.05125(10)	0.22792(10)	0.0223(4)
C12	-0.1588(2)	-0.17504(10)	0.26213(10)	0.0229(4)

C13	-0.3973(3)	-0.22133(12)	0.32037(12)	0.0340(4)
C14	-0.5152(3)	-0.15805(13)	0.41271(12)	0.0376(5)
C15	-0.5564(3)	-0.03581(12)	0.37536(11)	0.0320(4)
C16	-0.3139(3)	0.01084(11)	0.32114(11)	0.0280(4)

Table D.3: Bond lengths (Å) for Cy_2DETA.

O1-C2	1.4187(17)	**C2-H2**	1.0000
O2-C12	1.4243(16)	**C3-H3A**	0.9900
O1-H1O	0.901(19)	**C3-H3B**	0.9900
O2-H2O	0.93(2)	**C4-H4A**	0.9900
N1-C7	1.4666(16)	**C4-H4B**	0.9900
N1-C1	1.4690(17)	**C5-H5A**	0.9900
N2-C8	1.4618(16)	**C5-H5B**	0.9900
N2-C9	1.4625(17)	**C6-H6A**	0.9900
N3-C10	1.4555(18)	**C6-H6B**	0.9900
N3-C11	1.4594(16)	**C7-H7A**	0.9900
N1-H1N	0.840(17)	**C7-H7B**	0.9900
N2-H2N	0.852(16)	**C8-H8A**	0.9900
N3-H3N	0.855(16)	**C8-H8B**	0.9900
C1-C2	1.5242(17)	**C9-H9A**	0.9900
C1-C6	1.5277(19)	**C9-H9B**	0.9900
C2-C3	1.523(2)	**C10-H10A**	0.9900
C3-C4	1.525(2)	**C10-H10B**	0.9900
C4-C5	1.520(2)	**C11-H11**	1.0000
C5-C6	1.519(2)	**C12-H12**	1.0000
C7-C8	1.5121(18)	**C13-H13A**	0.9900
C9-C10	1.5106(17)	**C13-H13B**	0.9900
C11-C12	1.5211(17)	**C14-H14A**	0.9900
C11-C16	1.5231(19)	**C14-H14B**	0.9900
C12-C13	1.516(2)	**C15-H15A**	0.9900
C13-C14	1.521(2)	**C15-H15B**	0.9900
C14-C15	1.514(2)	**C16-H16A**	0.9900

C15-C16	1.522(2)	**C16-H16B**	0.9900
C1-H1	1.0000		

Table D.4: Bond angles (°) for Cy_2DETA.

C2-O1-H1O	110.2(12)	**O2-C12-C13**	111.43(10)
C12-O2-H2O	109.6(12)	**C11-C12-C13**	111.73(10)
C1-N1-C7	112.61(10)	**O2-C12-C11**	106.45(10)
C8-N2-C9	112.07(10)	**C12-C13-C14**	112.29(12)
C10-N3-C11	115.13(10)	**C13-C14-C15**	110.31(12)
C1-N1-H1N	106.5(12)	**C14-C15-C16**	110.58(13)
C7-N1-H1N	109.5(11)	**C11-C16-C15**	111.24(11)
C9-N2-H2N	109.4(10)	**N1-C1-H1**	109.00
C8-N2-H2N	104.5(11)	**C2-C1-H1**	109.00
C10-N3-H3N	110.4 (11)	**C6-C1-H1**	109.00
C11-N3-H3N	104.1(11)	**O1-C2-H2**	107.00
N1-C1-C6	110.98(10)	**C1-C2-H2**	107.00
C2-C1-C6	109.77(11)	**C3-C2-H2**	107.00
N1-C1-C2	109.79(10)	**C2-C3-H3A**	109.00
O1-C2-C3	112.56(11)	**C2-C3-H3B**	109.00
C1-C2-C3	110.21(11)	**C4-C3-H3A**	109.00
O1-C2-C1	112.03(11)	**C4-C3-H3B**	109.00
C2-C3-C4	111.99(12)	**H3A-C3-H3B**	108.00
C3-C4-C5	110.66(13)	**C3-C4-H4A**	110.00
C4-C5-C6	111.24(13)	**C3-C4-H4B**	109.00
C1-C6-C5	111.64(12)	**C5-C4-H4A**	109.00
N1-C7-C8	111.14(10)	**C5-C4-H4B**	110.00
N2-C8-C7	110.76(10)	**H4A-C4-H4B**	108.00
N2-C9-C10	111.09(10)	**C4-C5-H5A**	109.00
N3-C10-C9	109.95(10)	**C4-C5-H5B**	109.00
N3-C11-C12	108.61(10)	**C6-C5-H5A**	109.00
N3-C11-C16	111.48(11)	**C6-C5-H5B**	109.00
C12-C11-C16	111.00(10)	**H5A-C5-H5B**	108.00

C1-C6-H6A	109.00	**C12-C11-H11**	109.00
C1-C6-H6B	109.00	**C16-C11-H11**	109.00
C5-C6-H6A	109.00	**O2-C12-H12**	109.00
C5-C6-H6B	109.00	**C11-C12-H12**	109.00
H6A-C6-H6B	108.00	**C13-C12-H12**	109.00
N1-C7-H7A	109.00	**C12-C13-H13A**	109.00
N1-C7-H7B	109.00	**C12-C13-H13B**	109.00
C8-C7-H7A	109.00	**C14-C13-H13A**	109.00
C8-C7-H7B	109.00	**C14-C13-H13B**	109.00
H7A-C7-H7B	108.00	**H13A-C13-H13B**	108.00
N2-C8-H8A	109.00	**C13-C14-H14A**	110.00
N2-C8-H8B	109.00	**C13-C14-H14B**	110.00
C7-C8-H8A	109.00	**C15-C14-H14A**	110.00
C7-C8-H8B	110.00	**C15-C14-H14B**	110.00
H8A-C8-H8B	108.00	**H14A-C14-H14B**	108.00
N2-C9-H9A	109.00	**C14-C15-H15A**	110.00
N2-C9-H9B	109.00	**C14-C15-H15B**	110.00
C10-C9-H9A	109.00	**C16-C15-H15A**	110.00
C10-C9-H9B	109.00	**C16-C15-H15B**	110.00
H9A-C9-H9B	108.00	**H15A-C15-H15B**	108.00
N3-C10-H10A	110.00	**C11-C16-H16A**	109.00
N3-C10-H10B	110.00	**C11-C16-H16B**	109.00
C9-C10-H10A	110.00	**C15-C16-H16A**	109.00
C9-C10-H10B	110.00	**C15-C16-H16B**	109.00
H10A-C10-H10B	108.00	**H16A-C16-H16B**	108.00
N3-C11-H11	109.00		

Table D.5: Anisotropic displacement parameters ($Å^2 \times 10^3$) for Cy_2DETA. Anisotropic displacement factor exponent: $-2p^2[h^2a^{*2}U^{11} + ... + 2\ h\ k\ a^*\ b^*\ U^{12}]$.

Atom	U^{11}	U^{22}	U^{33}	U^{23}	U^{13}	U^{12}
O1	0.0284(5)	0.0237(5)	0.0385(6)	-0.0075(4)	-0.0063(4)	-0.0002(4)
O2	0.0420(6)	0.0226(5)	0.0274(5)	-0.0045(4)	-0.0040(4)	0.0039(4)
N1	0.0254(6)	0.0172(6)	0.0276(6)	-0.0011(5)	-0.0007(5)	-0.0040(4)
N2	0.0249(6)	0.0192(6)	0.0228(6)	0.0012(5)	-0.0014(5)	-0.0037(4)
N3	0.0259(6)	0.0190(6)	0.0278(6)	0.0023(5)	0.0013(5)	-0.0026(4)
C1	0.0254(7)	0.0180(6)	0.0277(7)	-0.0004(5)	0.0007(5)	-0.0032(5)
C2	0.0249(7)	0.0216(7)	0.0338(8)	-0.0057(6)	0.0020(6)	-0.0025(5)
C3	0.0331(8)	0.0235(7)	0.0396(8)	-0.0013(6)	0.0041(6)	-0.0101(6)
C4	0.0458(9)	0.0357(9)	0.0342(8)	0.0046(7)	0.0063(7)	-0.0110(7)
C5	0.0464(9)	0.0386(9)	0.0275(8)	0.0029(7)	-0.0032(6)	-0.0115(7)
C6	0.0348(8)	0.0289(7)	0.0292(7)	-0.0035(6)	-0.0005(6)	-0.0104(6)
C7	0.0239(7)	0.0189(6)	0.0273(7)	-0.0012(5)	-0.0002(5)	-0.0025(5)
C8	0.0230(7)	0.0222(7)	0.0288(7)	0.0015(6)	0.0013(5)	-0.0019(5)
C9	0.0271(7)	0.0196(7)	0.0254(7)	0.0024(5)	0.0009(5)	-0.0023(5)
C10	0.0278(7)	0.0216(7)	0.0265(7)	0.0020(6)	-0.0031(5)	-0.0040(5)
C11	0.0236(7)	0.0207(7)	0.0218(6)	-0.0015(5)	-0.0009(5)	-0.0047(5)
C12	0.0270(7)	0.0211(7)	0.0205(6)	-0.0010(5)	-0.0040(5)	-0.0033(5)
C13	0.0402(8)	0.0269(7)	0.0345(8)	-0.0009(6)	-0.0005(6)	-0.0143(6)
C14	0.0376(8)	0.0426(9)	0.0296(8)	0.0001(7)	0.0057(6)	-0.0149(7)
C15	0.0284(7)	0.0403(8)	0.0261(7)	-0.0077(6)	0.0011(6)	-0.0027(6)
C16	0.0323(7)	0.0255(7)	0.0257(7)	-0.0053(6)	-0.0006(6)	-0.0040(6)

Table D.6: Torsion angles (°) for Cy_2DETA.

C7-N1-C1-C2	158.21(10)
C7-N1-C1-C6	-80.25(13)
C1-N1-C7-C8	179.68(10)
C8-N2-C9-C10	-175.80(11)
C9-N2-C8-C7	170.26(10)
C10-N3-C11-C12	162.96(11)
C11-N3-C10-C9	170.97(11)
C10-N3-C11-C16	-74.43(14)
C2-C1-C6-C5	-57.48(15)
N1-C1-C2-O1	-54.31(14)
N1-C1-C6-C5	-179.03(12)
N1-C1-C2-C3	179.54(11)
C6-C1-C2-O1	-176.58(11)
C6-C1-C2-C3	57.28(14)
C1-C2-C3-C4	-57.12(16)
O1-C2-C3-C4	177.03(12)
C2-C3-C4-C5	55.26(17)
C3-C4-C5-C6	-54.19(17)
C4-C5-C6-C1	56.18(17)
N1-C7-C8-N2	-176.56(10)
N2-C9-C10-N3	-178.39(10)
N3-C11-C12-O2	-62.19(12)
N3-C11-C12-C13	175.95(11)
C16-C11-C12-O2	174.91(10)
C16-C11-C12-C13	53.06(14)
N3-C11-C16-C15	-176.64(11)
C12-C11-C16-C15	-55.42(14)
O2-C12-C13-C14	172.60(11)
C11-C12-C13-C14	-53.66(16)
C12-C13-C14-C15	55.55(17)
C13-C14-C15-C16	-57.23(17)

C14-C15-C16-C11	57.88(15)

Table D.7: Hydrogen bonds for Cy_2DETA (Å and °).

D-H···A	d(D-H)	d(H···A)	d(D···A)	<(DHA)
N1-H1N···O1	0.840(17)	2.365(17)	2.8357(15)	116.1(14)
O1-H1O···N2[a]	0.901(19)	1.888(19)	2.7830(15)	171.8(16)
N2-H2N···O2[b]	0.852(16)	2.138(16)	2.9889(15)	176.6(16)
O2-H2O···N1[c]	0.93(2)	1.95(2)	2.7768(15)	147.8(18)
N3-H3N···O2	0.855(16)	2.288(16)	2.7800(15)	116.8(13)
C8-H8A···O2[c]	0.9900	2.5800	3.3230(16)	131.00
C15-H15B···N3[d]	0.9900	2.6200	3.6099(19)	174.00

Symmetry transformations used to generate equivalent atoms:

a = 1-x, 1-y, -z b = -x, -y, -z c = 1-x, -y, -z

d = -1+x, y, z

D.2 $Cy_2DETA.3HClO_4$

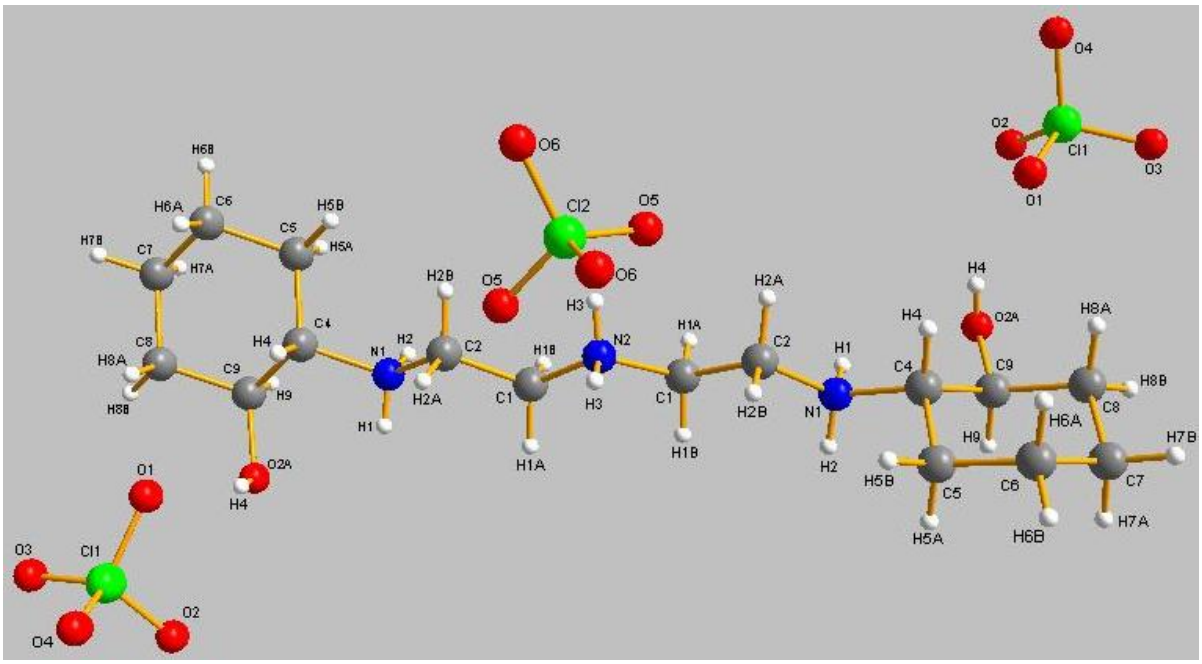


Figure D.2: XRD structure of $Cy_2DETA.3HClO_4$.

Table D.8: Crystal data and structure refinement for $Cy_2DETA.3HClO_4$.

Identification code	6m_kp1b_0s
Empirical formula	C16 H36 N3 O2, 3(Cl O4)
Formula weight	600.83
Temperature	173 K
Wavelength	0.71073 Å
Crystal system	Monoclinic
Space group	C2/c
Unit cell dimensions	a = 30.0985(5) Å α = 90° b = 8.4256(1) Å β = 99.798(1)° c = 9.6679(2) Å γ = 90°
Volume	2416.00(7) $Å^3$
Z	4
Density (calculated)	1.652 $g.cm^{-3}$
Absorption coefficient	0.456 mm^{-1}
F(000)	1264

Crystal size	0.06 × 0.39 × 0.49 mm^3
Theta range for data collection	1.4 to 28.0°
Index ranges	-39<=h<=37, -11<=k<=11, -12<=l<=12
Reflections collected	15245
Independent reflections	2914 [R(int) = 0.051]
Absorption correction	None
Refinement method	Full-matrix least-squares on F2
Data / restraints / parameters	2914 / 0 / 180
Goodness-of-fit on F^2	1.04
R indices (all data)	R1 = 0.0317, wR2 = 0.0897
Largest diff. peak and hole	-0.38 and 0.47 e.$Å^{-3}$

Table D.9: Atomic coordinates (× 10^4) and equivalent isotropic displacement parameters ($Å^2$ × 10^3) for $Cy_2DETA.3HClO_4$. U(eq) is defined as one third of the trace of the orthogonalized U^{ij} tensor.

Atom	x	y	z	U(eq)
O2A	0.87468(4)	0.92715(13)	-0.81291(11)	0.0215(3)
N1	0.90079(4)	0.84352(15)	-0.52538(13)	0.0174(3)
N2	1	0.7265(2)	-1/4	0.0155(4)
C1	0.96950(5)	0.82799(16)	-0.35217(15)	0.0171(4)
C2	0.93293(4)	0.73083(16)	-0.44205(14)	0.0157(3)
C4	0.86123(5)	0.76406(17)	-0.61674(15)	0.0180(4)
C5	0.82652(5)	0.71355(19)	-0.52796(17)	0.0224(4)
C6	0.78611(5)	0.6367(2)	-0.6200(2)	0.0324(5)
C7	0.76549(5)	0.7478(3)	-0.7372(2)	0.0356(5)
C8	0.80078(5)	0.7997(2)	-0.82513(17)	0.0283(5)
C9	0.84112(5)	0.87817(18)	-0.73318(15)	0.0202(4)
Cl1	0.89538(1)	0.30840(4)	-0.59285(3)	0.0181(1)
O1	0.88504(4)	0.36688(14)	-0.46237(12)	0.0264(3)
O2	0.92258(4)	0.16633(13)	-0.56755(12)	0.0266(3)
O3	0.85463(4)	0.27309(17)	-0.68744(15)	0.0390(4)
O4	0.92081(4)	0.42629(12)	-0.65410(11)	0.0246(3)
Cl2	1	0.29686(5)	-1/4	0.0165(1)
O5	0.98699(4)	0.39550(13)	-0.37122(11)	0.0249(3)

O6	1.03708(4)	-0.19632(13)	-0.27193(12)	0.0257(3)

Table D.10: Bond lengths (Å) for $Cy_2DETA.3HClO_4$.

Cl1-O1	1.4368(12)	**C4-C5**	1.521(2)
Cl1-O2	1.4474(12)	**C5-C6**	1.524(2)
Cl1-O3	1.4308(14)	**C6-C7**	1.519(3)
Cl1-O4	1.4414(11)	**C7-C8**	1.533(2)
Cl2-O5	1.4357(11)	**C8-C9**	1.528(2)
Cl2-O6	1.4452(12)	**C1-H1A**	0.9900
Cl2-O5_a	1.4357(11)	**C1-H1B**	0.9900
Cl2-O6_a	1.4452(12)	**C2-H2A**	0.9900
O2A-C9	1.4317(19)	**C2-H2B**	0.9900
O2A-H4	0.76(2)	**C4-H4**	1.0000
N1-C4	1.5127(19)	**C5-H5A**	0.9900
N1-C2	1.4903(18)	**C5-H5B**	0.9900
N2-C1_b	1.4970(17)	**C6-H6B**	0.9900
N2-C1	1.4970(17)	**C6-H6A**	0.9900
N1-H2	0.865(18)	**C7-H7A**	0.9900
N1-H1	0.86(2)	**C7-H7B**	0.9900
N2-H3	0.861(18)	**C8-H8B**	0.9900
N2-H3_b	0.861(18)	**C8-H8A**	0.9900
C1-C2	1.5203(19)	**C9-H9**	1.0000
C4-C9	1.525(2)		

Table D.11: Bond angles (°) for $Cy_2DETA.3HClO_4$.

O1-Cl1-O4	109.50(7)	**C5-C4-C9**	111.62(13)
O2-Cl1-O3	109.56(8)	**N1-C4-C9**	109.03(12)
O2-Cl1-O4	108.34(7)	**C4-C5-C6**	110.24(13)
O3-Cl1-O4	109.76(7)	**C5-C6-C7**	110.98(14)
O1-Cl1-O2	109.63(7)	**C6-C7-C8**	110.85 (13)
O1-Cl1-O3	110.02(8)	**C7-C8-C9**	110.97(13)
O5-Cl2-O6	109.25(6)	**C4-C9-C8**	109.45(12)

O5_a-Cl2-O6	110.42(7)	**O2A-C9-C8**	112.03(12)
O5-Cl2-O5_a	109.26(7)	**O2A-C9-C4**	110.57(12)
O5-Cl2-O6_a	110.42(7)	**C2-C1-H1A**	109.00
O5_a-Cl2-O6_a	109.25(6)	**C2-C1-H1B**	109.00
O6-Cl2-O6_a	108.23(7)	**H1A-C1-H1B**	108.00
C9-O2A-H4	106.2(18)	**N2-C1-H1A**	109.00
C2-N1-C4	114.06(11)	**N2-C1-H1B**	109.00
C1-N2-C1_b	110.33(13)	**C1-C2-H2B**	110.00
H1-N1-H2	109(2)	**H2A-C2-H2B**	108.00
C4-N1-H2	108.0(12)	**N1-C2-H2B**	110.00
C2-N1-H2	110.7(12)	**C1-C2-H2A**	110.00
C4-N1-H1	104.5(14)	**N1-C2-H2A**	110.00
C2-N1-H1	110.7(15)	**N1-C4-H4**	109.00
C1-N2-H3	110.1(12)	**C5-C4-H4**	109.00
C1-N2-H3_b	110.1(13)	**C9-C4-H4**	109.00
C1_b-N2-H3	110.1(12)	**H5A-C5-H5B**	108.00
C1_b-N2-H3_b	110.1(12)	**C4-C5-H5A**	110.00
H3-N2-H3_b	106.0(17)	**C4-C5-H5B**	110.00
N2-C1-C2	111.88(11)	**C6-C5-H5B**	110.00
N1-C2-C1	107.83(11)	**C6-C5-H5A**	110.00
N1-C4-C5	110.02(12)	**C5-C6-H6B**	109.00
C7-C6-H6A	109.00	**H8A-C8-H8B**	108.00
C5-C6-H6A	109.00	**C7-C8-H8B**	109.00
C7-C6-H6B	109.00	**C9-C8-H8A**	109.00
H6A-C6-H6B	108.00	**C7-C8-H8A**	109.00
H7A-C7-H7B	108.00	**C9-C8-H8B**	109.00
C8-C7-H7A	110.00	**C4-C9-H9**	108.00
C8-C7-H7B	109.00	**C8-C9-H9**	108.00
C6-C7-H7A	110.00	**O2A-C9-H9**	108.00
C6-C7-H7B	109.00		

Table D.12: Anisotropic displacement parameters ($Å^2 \times 10^3$) for $Cy_2DETA.3HClO_4$.

Anisotropic displacement factor exponent: $-2p^2[h^2a^{*2}U^{11} + ... + 2\ h\ k\ a^*\ b^*\ U^{12}]$.

Atom	U^{11}	U^{22}	U^{33}	U^{23}	U^{13}	U^{12}
O2A	0.0271(5)	0.0184(5)	0.0202(5)	0.0007(4)	0.0075(4)	0.0035(4)
N1	0.0188(6)	0.0148(5)	0.0172(6)	0.0011(5)	-0.0007(5)	-0.0022(4)
N2	0.0158(7)	0.0114(7)	0.0190(8)	0	0.0023(6)	0
C1	0.0180(6)	0.0126(6)	0.0192(7)	0.0008(5)	-0.0012(5)	-0.0002(5)
C2	0.0186(6)	0.0126(6)	0.0154(6)	0.0004(5)	0.0015(5)	-0.0010(5)
C4	0.0170(6)	0.0165(6)	0.0192(7)	-0.0021(5)	-0.0008(5)	-0.0012(5)
C5	0.0197(7)	0.0233(7)	0.0244(7)	0.0016(6)	0.0041(6)	-0.0025(5)
C6	0.0211(7)	0.0344(9)	0.0411(10)	-0.0018(8)	0.0038(7)	-0.0086(6)
C7	0.0179(7)	0.0463(10)	0.0400(10)	-0.0019(8)	-0.0026(7)	-0.0004(7)
C8	0.0222(7)	0.0356(9)	0.0238(8)	-0.0026(7)	-0.0056(6)	0.0028(6)
C9	0.0202(6)	0.0208(7)	0.0194(7)	-0.0003(6)	0.0025(5)	0.0040(5)
Cl1	0.0231(2)	0.0142(2)	0.0170(2)	-0.0008(1)	0.0035(1)	-0.0021(1)
O1	0.0354(6)	0.0241(6)	0.0232(6)	-0.0025(4)	0.0148(5)	-0.0005(5)
O2	0.0368(6)	0.0132(5)	0.0303(6)	-0.0011(4)	0.0070(5)	0.0028(4)
O3	0.0327(7)	0.0398(7)	0.0385(7)	-0.0031(6)	-0.0112(5)	-0.0073(6)
O4	0.0372(6)	0.0158(5)	0.0236(5)	0.0008(4)	0.0135(5)	-0.0035(4)
Cl2	0.0170(2)	0.0131(2)	0.0196(2)	0	0.0042(2)	0
O5	0.0254(5)	0.0217(5)	0.0262(6)	0.0073(4)	0.0001(4)	0.0006(4)
O6	0.0281(6)	0.0230(6)	0.0282(6)	0.0026(4)	0.0115(5)	0.0102(4)

Table D.13: Torsion angles (°) for $Cy_2DETA.3HClO_4$.

C2-N1-C4-C5	78.04(14)
C2-N1-C4-C9	-159.25(11)
C4-N1-C2-C1	-177.84(11)
C1_b-N2-C1-C2	-170.53(10)
N2-C1-C2-N1	172.21(10)
N1-C4-C5-C6	178.75(12)
C9-C4-C5-C6	57.58(16)
N1-C4-C9-O2A	56.76(15)

N1-C4-C9-C8	-179.36(12)
C5-C4-C9-O2A	178.50(12)
C5-C4-C9-C8	-57.62(16)
C4-C5-C6-C7	-56.42(17)
C5-C6-C7-C8	56.3(2)
C6-C7-C8-C9	-56.8(2)
C7-C8-C9-O2A	179.75(14)
C7-C8-C9-C4	56.74(18)

Table D.14: Hydrogen bonds for $Cy_2DETA.3HClO_4$ (Å and °).

D-H···A	**d(D-H)**	**d(H···A)**	**d(D···A)**	**<(DHA)**
N1-H1···O2[a]	0.86(2)	2.30(3)	2.8434(17)	122.0(19)
N1-H1···O2A	0.86(2)	2.346(19)	2.8457(16)	117.6(17)
N1-H1···O6[b]	0.86(2)	2.34(2)	2.9490(17)	129(2)
O2A-H4···O6[b]	0.76(2)	2.45(2)	2.8403(17)	113.5(19)
O2A-H4···O1[c]	0.76(2)	2.20(2)	2.9113(16)	156(2)
N1-H2···O2A[d]	0.865(18)	2.164(18)	3.0199(17)	170.7(16)
N2-H3···O5[e]	0.861(18)	2.498(17)	3.0246(19)	120.3(15)
N2-H3···O4[f]	0.861(18)	2.196(18)	2.9917(14)	153.6(17)
C1-H1B···O6[g]	0.9900	2.5200	3.3453(18)	141.00
C2-H2A···O4	0.9900	2.4800	3.2658(17)	136.00
C2-H2A···O5[b]	0.9900	2.5400	3.4180(17)	147.00
C2-H2A···O6[b]	0.9900	2.5900	3.1125(18)	113.00
C2-H2B···O4[f]	0.9900	2.3100	3.1593(17)	143.00
C4-H4···O4	1.0000	2.5000	3.4155(18)	153.00
C8-H8A···O1[c]	0.9900	2.5900	3.363(2)	134.00

Symmetry transformations used to generate equivalent atoms:

a = x, 1+y, z b = 2-x, 1-y, -1-z c = x, 1-y, $-^1/_2$+z

d = x, 2-y, $^1/_2$+z e = 2-x, y, $-^1/_2$-z f = x, 1-y, $^1/_2$+z

g = 2-x, 1+y, $-^1/_2$-z

D.3 Ts_2DETA

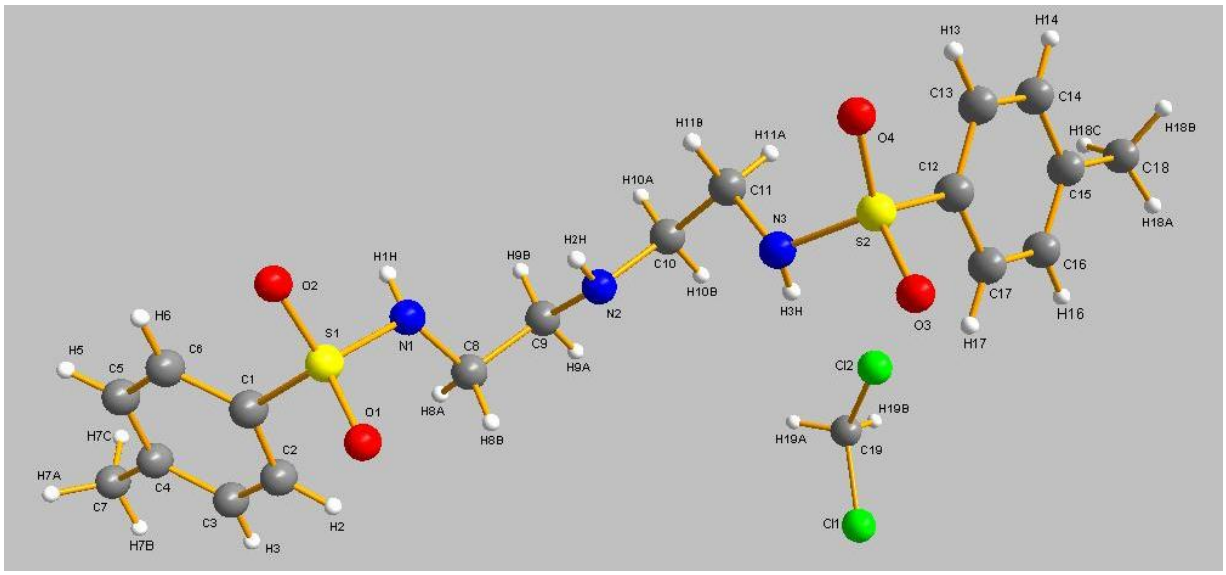


Figure D.3: XRD structure of Ts_2DETA.

Table D.15: Crystal data and structure refinement for Ts_2DETA.

Identification code	6m_kp2_0a
Empirical formula	C18 H25 N3 O4 S2, C H2 Cl2
Formula weight	496.46
Temperature	173 K
Wavelength	0.71073 Å
Crystal system	Orthorhombic
Space group	$Pca2_1$
Unit cell dimensions	a = 25.4644(4) Å α = 90° b = 11.2639(2) Å β = 90° c = 8.10410(1) Å γ = 90°
Volume	2324.49(6) $Å^3$
Z	4
Density (calculated)	1.419 $g.cm^{-3}$
Absorption coefficient	0.489 mm^{-1}
F(000)	1040
Crystal size	0.25 × 0.37 × 0.50 mm^3
Theta range for data collection	1.6 to 28.0°

Index ranges	-33<=h<=31, -14<=k<=14, -9<=l<=10
Reflections collected	23941
Independent reflections	5474 [R(int) = 0.031]
Absorption correction	None
Refinement method	Full-matrix least-squares on F2
Data / restraints / parameters	5474 / 0 / 285
Goodness-of-fit on F^2	1.06
R indices (all data)	R1 = 0.0471, wR2 = 0.1232
Largest diff. peak and hole	-0.38 and 0.39 e.$Å^{-3}$

Table D.16: Atomic coordinates ($\times 10^4$) and equivalent isotropic displacement parameters ($Å^2 \times 10^3$) for Ts_2DETA. U(eq) is defined as one third of the trace of the orthogonalized U^{ij} tensor.

Atom	x	y	z	U(eq)
S1	0.66110(3)	0.57342(6)	0.74060(9)	0.0297(2)
S2	0.82625(3)	0.14230(6)	0.14847(9)	0.0331(2)
O1	0.66543(9)	0.6305(2)	0.5837(3)	0.0385(7)
O2	0.61841(8)	0.4928(2)	0.7707(3)	0.0438(7)
O3	0.82054(12)	0.2144(2)	0.0055(3)	0.0517(9)
O4	0.78991(8)	0.0481(2)	0.1796(3)	0.0434(7)
N1	0.71369(9)	0.4981(2)	0.7733(3)	0.0272(7)
N2	0.79647(10)	0.3703(2)	0.5956(3)	0.0289(7)
N3	0.82322(11)	0.2317(2)	0.3039(3)	0.0346(8)
C1	0.65878(10)	0.6844(2)	0.8936(3)	0.0244(7)
C2	0.69572(11)	0.7750(2)	0.8917(3)	0.0272(7)
C3	0.69868(12)	0.8532(2)	1.0217(4)	0.0324(8)
C4	0.66447(11)	0.8436(3)	1.1552(4)	0.0358(9)
C5	0.62656(12)	0.7554(3)	1.1513(4)	0.0410(9)
C6	0.62356(11)	0.6758(3)	1.0233(4)	0.0352(9)
C7	0.66945(16)	0.9255(4)	1.3010(5)	0.0530(12)
C8	0.76574(10)	0.5491(2)	0.7401(4)	0.0266(7)
C9	0.80594(11)	0.4506(2)	0.7340(4)	0.0300(7)
C10	0.83673(13)	0.2763(3)	0.5953(4)	0.0367(9)
C11	0.82446(13)	0.1814(3)	0.4694(4)	0.0347(9)

C12	0.88991(10)	0.0798(2)	0.1447(4)	0.0293(8)
C13	0.89704(12)	-0.0376(3)	0.1842(4)	0.0373(9)
C14	0.94683(13)	-0.0868(3)	0.1753(5)	0.0459(10)
C15	0.98998(12)	-0.0179(3)	0.1274(5)	0.0459(11)
C16	0.98105(15)	0.1002(3)	0.0913(6)	0.0571(14)
C17	0.93178(14)	0.1494(3)	0.1001(5)	0.0484(10)
C18	1.04369(15)	-0.0725(5)	0.1145(7)	0.0706(18)
Cl1	1.03759(7)	0.59464(13)	0.3206(2)	0.0976(6)
Cl2	1.00459(5)	0.35245(10)	0.3756(2)	0.0769(4)
C19	1.0405(2)	0.4723(5)	0.4491(6)	0.086(2)

Table D.17: Bond lengths (Å) for Ts_2DETA.

Cl1-C19	1.729(6)	**C13-C14**	1.386(5)
Cl2-C19	1.736(6)	**C14-C15**	1.400(5)
S1-N1	1.607(2)	**C15-C18**	1.503(5)
S1-C1	1.762(2)	**C15-C16**	1.381(5)
S1-O1	1.429(3)	**C16-C17**	1.373(5)
S1-O2	1.437(2)	**C2-H2**	0.9500
S2-N3	1.615(2)	**C3-H3**	0.9500
S2-O3	1.422(2)	**C5-H5**	0.9500
S2-O4	1.430(2)	**C6-H6**	0.9500
S2-C12	1.768(3)	**C7-H7C**	0.9800
N1-C8	1.469(3)	**C7-H7A**	0.9800
N2-C10	1.474(4)	**C7-H7B**	0.9800
N2-C9	1.461(4)	**C8-H8B**	0.9900
N3-C11	1.456(4)	**C8-H8A**	0.9900
N1-H1H	0.81(2)	**C9-H9B**	0.9900
N2-H2H	0.80(2)	**C9-H9A**	0.9900
N3-H3H	0.79(3)	**C10-H10A**	0.9900
C1-C2	1.388(3)	**C10-H10B**	0.9900
C1-C6	1.385(4)	**C11-H11B**	0.9900
C2-C3	1.375(4)	**C11-H11A**	0.9900

C3-C4	1.393(4)	**C13-H13**	0.9500
C4-C5	1.386(4)	**C14-H14**	0.9500
C4-C7	1.504(5)	**C16-H16**	0.9500
C5-C6	1.373(5)	**C17-H17**	0.9500
C8-C9	1.510(3)	**C18-H18C**	0.9800
C10-C11	1.510(5)	**C18-H18A**	0.9800
C12-C13	1.373(4)	**C18-H18B**	0.9800
C12-C17	1.372(4)	**C19-H19A**	0.9900
C19-H19B	0.9900		

Table D.18: Bond angles (°) for Ts_2DETA.

O1-S1-O2	119.58(14)	**C3-C4-C7**	120.6(3)
O1-S1-N1	108.66(13)	**C4-C5-C6**	121.6(3)
O1-S1-C1	108.03(13)	**C1-C6-C5**	119.4(3)
O2-S1-N1	105.59(13)	**N1-C8-C9**	109.28(19)
O2-S1-C1	107.67(13)	**N2-C9-C8**	111.6(2)
N1-S1-C1	106.65(12)	**N2-C10-C11**	111.5(3)
O3-S2-O4	120.07(16)	**N3-C11-C10**	110.6(3)
O3-S2-N3	105.93(13)	**C13-C12-C17**	120.6(3)
O3-S2-C12	107.88(16)	**S2-C12-C17**	119.3(2)
O4-S2-N3	107.11(14)	**S2-C12-C13**	120.1(2)
O4-S2-C12	107.51(12)	**C12-C13-C14**	119.6(3)
N3-S2-C12	107.80(14)	**C13-C14-C15**	120.7(3)
S1-N1-C8	121.00(18)	**C14-C15-C16**	117.6(3)
C9-N2-C10	109.3(2)	**C14-C15-C18**	120.4(3)
S2-N3-C11	118.4(2)	**C16-C15-C18**	122.0(3)
C8-N1-H1H	118(2)	**C15-C16-C17**	121.9(3)
S1-N1-H1H	108(2)	**C12-C17-C16**	119.5(3)
C9-N2-H2H	116(2)	**C1-C2-H2**	120.00
C10-N2-H2H	111(2)	**C3-C2-H2**	120.00
C11-N3-H3H	108(2)	**C2-C3-H3**	120.00
S2-N3-H3H	107(2)	**C4-C3-H3**	120.00

S1-C1-C6	120.4(2)	**C4-C5-H5**	119.00
S1-C1-C2	119.42(19)	**C6-C5-H5**	119.00
C2-C1-C6	119.9(2)	**C1-C6-H6**	120.00
C1-C2-C3	120.0(2)	**C5-C6-H6**	120.00
C2-C3-C4	120.7(3)	**C4-C7-H7A**	109.00
C5-C4-C7	121.1(3)	**C4-C7-H7B**	109.00
C3-C4-C5	118.3(3)	**C4-C7-H7C**	109.00
H7A-C7-H7B	109.00	**H11A-C11-H11B**	108.00
H7A-C7-H7C	110.00	**C12-C13-H13**	120.00
H7B-C7-H7C	109.00	**C14-C13-H13**	120.00
N1-C8-H8A	110.00	**C13-C14-H14**	120.00
N1-C8-H8B	110.00	**C15-C14-H14**	120.00
C9-C8-H8A	110.00	**C15-C16-H16**	119.00
C9-C8-H8B	110.00	**C17-C16-H16**	119.00
H8A-C8-H8B	108.00	**C12-C17-H17**	120.00
N2-C9-H9A	109.00	**C16-C17-H17**	120.00
N2-C9-H9B	109.00	**C15-C18-H18A**	109.00
C8-C9-H9A	109.00	**C15-C18-H18B**	109.00
C8-C9-H9B	109.00	**C15-C18-H18C**	109.00
H9A-C9-H9B	108.00	**H18A-C18-H18B**	109.00
N2-C10-H10A	109.00	**H18A-C18-H18C**	109.00
N2-C10-H10B	109.00	**H18B-C18-H18C**	110.00
C11-C10-H10A	109.00	**Cl1-C19-Cl2**	113.0(3)
C11-C10-H10B	109.00	**Cl1-C19-H19A**	109.00
H10A-C10-H10B	108.00	**Cl1-C19-H19B**	109.00
N3-C11-H11A	110.00	**Cl2-C19-H19A**	109.00
N3-C11-H11B	110.00	**Cl2-C19-H19B**	109.00
C10-C11-H11A	110.00	**H19A-C19-H19B**	108.00
C10-C11-H11B	110.00		

Table D.19: Anisotropic displacement parameters ($Å^2 \times 10^3$) for Ts_2DETA. Anisotropic displacement factor exponent: $-2p^2[h^2a^{*2}U^{11} + ... + 2\ h\ k\ a^*\ b^*\ U^{12}]$.

Atom	U^{11}	U^{22}	U^{33}	U^{23}	U^{13}	U^{12}
S1	0.0336(3)	0.0297(3)	0.0257(3)	-0.0045(3)	-0.0048(3)	-0.0027(3)
S2	0.0419(4)	0.0308(3)	0.0265(4)	-0.0039(3)	-0.0037(3)	0.0084(3)
O1	0.0468(12)	0.0390(11)	0.0296(11)	-0.0005(9)	-0.0090(9)	0.0038(10)
O2	0.0407(11)	0.0435(12)	0.0473(15)	-0.0090(11)	-0.0064(10)	-0.0112(9)
O3	0.0801(18)	0.0439(13)	0.0310(13)	-0.0012(11)	-0.0077(12)	0.0157(13)
O4	0.0353(10)	0.0432(12)	0.0517(15)	-0.0093(11)	-0.0038(9)	0.0002(9)
N1	0.0389(12)	0.0192(10)	0.0236(13)	-0.0006(9)	0.0011(9)	-0.0010(9)
N2	0.0320(12)	0.0261(11)	0.0287(12)	-0.0024(9)	0.0015(9)	0.0044(9)
N3	0.0482(16)	0.0270(13)	0.0286(13)	-0.0057(10)	0.0009(11)	0.0070(11)
C1	0.0299(13)	0.0212(11)	0.0220(12)	0.0002(10)	-0.0025(10)	0.0071(10)
C2	0.0317(13)	0.0251(12)	0.0247(13)	0.0004(11)	0.0024(11)	0.0037(10)
C3	0.0373(15)	0.0249(13)	0.0351(16)	-0.0023(11)	-0.0024(12)	0.0041(11)
C4	0.0405(15)	0.0340(15)	0.0329(15)	-0.0046(13)	-0.0013(15)	0.0134(11)
C5	0.0405(15)	0.0477(17)	0.0348(16)	0.0001(15)	0.0107(15)	0.0107(13)
C6	0.0312(14)	0.0355(14)	0.0390(17)	0.0049(13)	0.0052(12)	0.0019(11)
C7	0.063(2)	0.056(2)	0.040(2)	-0.0153(17)	0.0002(16)	0.0164(18)
C8	0.0357(12)	0.0226(11)	0.0216(12)	-0.0020(11)	0.0014(12)	-0.0013(9)
C9	0.0386(13)	0.0263(12)	0.0252(13)	0.0010(12)	-0.0011(13)	0.0035(10)
C10	0.0457(17)	0.0387(15)	0.0258(14)	-0.0021(12)	-0.0025(12)	0.0123(13)
C11	0.0462(17)	0.0267(14)	0.0312(16)	-0.0009(12)	0.0052(13)	0.0097(12)
C12	0.0359(13)	0.0296(13)	0.0225(13)	-0.0072(12)	0.0015(11)	0.0011(10)
C13	0.0390(15)	0.0291(13)	0.0437(19)	0.0046(12)	0.0062(13)	-0.0004(11)
C14	0.0424(16)	0.0384(17)	0.057(2)	0.0051(15)	0.0044(16)	0.0087(13)
C15	0.0326(14)	0.064(2)	0.041(2)	-0.0082(17)	0.0025(14)	0.0024(14)
C16	0.0444(19)	0.050(2)	0.077(3)	-0.007(2)	0.0198(18)	0.0175(16)
C17	0.0528(19)	0.0303(15)	0.062(2)	-0.0020(15)	0.0082(16)	0.0040(13)
C18	0.0388(18)	0.083(3)	0.090(4)	-0.006(3)	0.007(2)	0.0104(19)
Cl1	0.1209(12)	0.0807(8)	0.0912(10)	0.0111(8)	-0.0223(8)	-0.0328(8)
Cl2	0.0724(7)	0.0634(7)	0.0948(9)	-0.0068(7)	-0.0032(6)	0.0021(5)

C19	0.109(4)	0.099(4)	0.050(3)	-0.005(3)	-0.020(3)	0.009(3)

Table D.20: Torsion angles (°) for Ts_2DETA.

O1-S1-N1-C8	45.1(3)
O2-S1-N1-C8	174.5(2)
C1-S1-N1-C8	-71.1(2)
O2-S1-C1-C6	6.6(3)
N1-S1-C1-C6	-106.3(2)
N1-S1-C1-C2	67.8(2)
O1-S1-C1-C2	-48.9(2)
O2-S1-C1-C2	-179.3(2)
O1-S1-C1-C6	137.0(2)
C12-S2-N3-C11	-68.7(3)
O3-S2-N3-C11	176.0(2)
O4-S2-N3-C11	46.7(3)
N3-S2-C12-C13	109.3(3)
O3-S2-C12-C13	-136.7(3)
O4-S2-C12-C13	-5.9(3)
N3-S2-C12-C17	-71.5(3)
O3-S2-C12-C17	42.5(3)
O4-S2-C12-C17	173.3(3)
S1-N1-C8-C9	-163.8(2)
C10-N2-C9-C8	179.9(2)
C9-N2-C10-C11	172.1(2)
S2-N3-C11-C10	163.9(2)
S1-C1-C2-C3	-171.6(2)
C2-C1-C6-C5	-1.8(4)
C6-C1-C2-C3	2.6(4)
S1-C1-C6-C5	172.3(2)
C1-C2-C3-C4	-0.8(4)
C2-C3-C4-C7	177.0(3)
C2-C3-C4-C5	-1.7(4)

C7-C4-C5-C6	-176.2(3)
C3-C4-C5-C6	2.6(5)
C4-C5-C6-C1	-0.8(5)
N1-C8-C9-N2	64.9(3)
N2-C10-C11-N3	61.1(3)
S2-C12-C13-C14	177.8(3)
C17-C12-C13-C14	-1.5(5)
S2-C12-C17-C16	-177.7(3)
C13-C12-C17-C16	1.5(6)
C12-C13-C14-C15	0.4(6)
C13-C14-C15-C16	0.6(6)
C13-C14-C15-C18	-178.7(4)
C14-C15-C16-C17	-0.6(7)
C18-C15-C16-C17	178.7(4)
C15-C16-C17-C12	-0.5(7)

Table D.21: Hydrogen bonds for Ts_2DETA (Å and °).

D-H···A	**d(D-H)**	**d(H···A)**	**d(D···A)**	**<(DHA)**
N1-H1H···N2[a]	0.81(2)	2.19(2)	2.994(3)	175(2)
C3-H3···O4[b]	0.9500	2.5900	3.443(4)	149.00
C6-H6···O2	0.9500	2.5300	2.908(4)	104.00
C8-H8A···O1[a]	0.9900	2.5800	3.416(4)	142.00
C9-H9B···O3[c]	0.9900	2.5700	3.472(4)	151.00
C10-H10A···O3[c]	0.9900	2.4900	3.422(4)	158.00
C13-H13···O4	0.9500	2.5100	2.894(4)	104.00
C19-H19B···O1[d]	0.9900	2.6000	3.557(6)	163.00

Symmetry transformations used to generate equivalent atoms:

a = $^3/_2$-x, y, $^1/_2$+z b = x, 1+y, 1+z c = x, y, 1+z

d = $^1/_2$+x, 1-y, z

D.4 [NaCy$_2$DETA.3E]Br

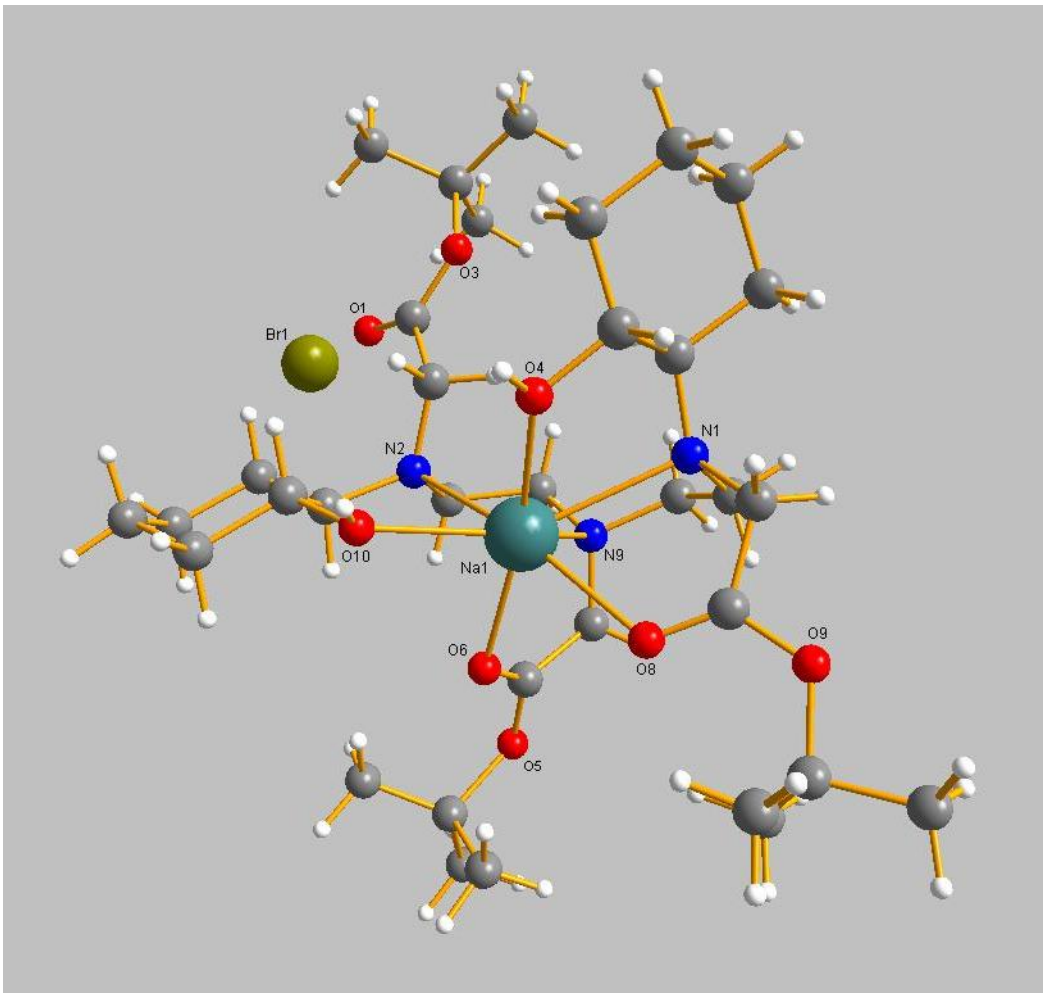


Figure D.4: XRD structure of [NaCy$_2$DETA.3E]Br.

Table D.22: Crystal data and structure refinement for [NaCy$_2$DETA.3E]Br.

Identification code	9m_alv4_0a
Empirical formula	C34 H63 N3 Na O8, Br
Formula weight	744.76
Temperature	173 K
Wavelength	0.71073 Å
Crystal system	Triclinic
Space group	P-1

Unit cell dimensions	a = 10.7723(2) Å α = 79.0030(10)° b = 10.7883(2) Å β = 80.1240(10)° c = 19.5647(4) Å γ = 66.0520(10)°
Volume	2028.57(7) $Å^3$
Z	2
Density (calculated)	1.219 $g.cm^{-3}$
Absorption coefficient	1.071 mm^{-1}
F(000)	796
Crystal size	0.21 × 0.28 × 0.37 mm^3
Theta range for data collection	1.1 to 25.0°
Index ranges	-11<=h<=12, -11<=k<=12, -22<=l<=23
Reflections collected	22699
Independent reflections	7139 [R(int) = 0.038]
Absorption correction	None
Refinement method	Full-matrix least-squares on F2
Data / restraints / parameters	7139 / 0 / 427
Goodness-of-fit on F^2	1.11
R indices (all data)	R1 = 0.0780, wR2 = 0.2566
Largest diff. peak and hole	-0.85 and 2.00 $e.Å^{-3}$

Table D.23: Atomic coordinates (× 10^4) and equivalent isotropic displacement parameters ($Å^2$ × 10^3) for [$NaCy_2$DETA.3E]Br. U(eq) is defined as one third of the trace of the orthogonalized U^{ij} tensor.

Atom	x	Y	Z	U(eq)
Na1	0.36339(15)	0.15102(16)	0.2654499)	0.0430(5)
O1	0.6044(7)	-0.3119(5)	0.1446(3)	0.116(2)
O3	0.5492(4)	-0.3648(3)	0.25729(19)	0.0649(13)
O4	0.4622(3)	0.0167(4)	0.36496(19)	0.0613(13)
O5	0.1567(5)	0.3941(6)	0.0782(3)	0.0112(2)
O6	0.3008(3)	0.3043(4)	0.16084(19)	0.0610(11)
O8	0.1897(4)	0.3434(5)	0.3170(2)	0.0894(17)
O9	0.0155(6)	0.4201(6)	0.3958(4)	0.178(3)
O10	0.5923(4)	0.1282(4)	0.2272(2)	0.0498(11)
N1	0.1917(5)	0.0809(6)	0.3634(2)	0.078(2)

N2	0.4880(4)	-0.0228(4)	0.1705(2)	0.0494(12)
N9	0.1854(4)	0.1016(6)	0.2093(2)	0.0679(18)
C1	0.5966(5)	0.0193(5)	0.1308(3)	0.0572(17)
C2	0.6799(5)	0.0430(5)	0.1768(3)	0.0562(16)
C12	0.2754(6)	-0.0502(6)	0.3991(3)	0.064(2)
C13	0.5653(6)	-0.2823(5)	0.2022(3)	0.0595(17)
C15	0.3994(5)	-0.0486(5)	0.4220(2)	0.0583(16)
C16	0.5235(5)	-0.1398(5)	0.2233(3)	0.0548(17)
C17	0.7750(6)	0.1097(7)	0.1338(3)	0.072(2)
C18	0.6910(6)	-0.0704(6)	0.0765(3)	0.071(2)
C20	0.3871(6)	-0.0131(6)	0.1264(3)	0.0628(19)
C24	0.2032(5)	0.3104(6)	0.1355(3)	0.071(2)
C25	0.5739(7)	-0.5121(5)	0.2544(3)	0.078(2)
C27	0.7869(8)	-0.0068(9)	0.0329(4)	0.098(3)
C29	0.0889(7)	0.0658(11)	0.2682(4)	0.121(4)
C30	0.1177(6)	0.2290(8)	0.1634(4)	0.089(3)
C32	0.1322(7)	0.1876(8)	0.4086(4)	0.114(3)
C33	0.8674(8)	0.0225(10)	0.0779(4)	0.109(3)
C34	0.1165(6)	0.3247(8)	0.3675(4)	0.101(2)
C37	0.4946(9)	-0.1924(7)	0.4460(3)	0.122(3)
C38	0.4869(8)	-0.5168(6)	0.2039(4)	0.093(3)
C39	0.7228(8)	-0.5850(8)	0.2329(6)	0.136(5)
C40	0.4204(16)	-0.2639(12)	0.5023(7)	0.215(6)
C41	0.3665(10)	0.4219(12)	0.0182(5)	0.135(5)
C42	0.2006(9)	-0.1171(7)	0.4593(3)	0.095(3)
C43	0.5309(14)	-0.5589(8)	0.3277(5)	0.153(6)
C45	0.2208(11)	0.4922(10)	0.0411(6)	0.127(4)
C46	0.2995(19)	-0.2591(10)	0.4861(7)	0.208(8)
C47	-0.0584(13)	0.5978(10)	0.2972(8)	0.193(7)
C49	0.0763(15)	0.6057(10)	0.3773(6)	0.161(5)
C51	0.0669(10)	0.1133(11)	0.3311(5)	0.124(3)
C52	0.1311(15)	0.5648(16)	-0.0190(7)	0.224(8)

C53	0.2544(6)	-0.0113(7)	0.1686(3)	0.075(2)
C54	-0.0307(9)	0.5651(10)	0.3668(7)	0.138(4)
C55	-0.1503(18)	0.6301(13)	0.4211(11)	0.360(9)
C57	0.1898(11)	0.5941(10)	0.0906(7)	0.152(5)
Br1	0.77232(5)	0.00524(7)	0.35646(4)	0.0801(3)

Table D.24: Bond lengths (Å) for [$NaCy_2$DETA.3E]Br.

Na1-O4	2.325(4)	**N9-C29**	1.518(9)
Na1-O6	2.378(4)	**C1-C2**	1.494(8)
Na1-O8	2.413(5)	**C1-C18**	1.524(8)
Na1-O10	2.376(5)	**C2-C17**	1.532(9)
Na1-N1	2.652(5)	**C12-C15**	1.487(9)
Na1-N2	2.683(4)	**C12-C42**	1.543(10)
Na1-N9	2.635(5)	**C13-C16**	1.534(7)
O1-C13	1.189(8)	**C15-C37**	1.508(9)
O3-C13	1.296(7)	**C17-C33**	1.527(11)
O3-C25	1.512(6)	**C18-C27**	1.522(11)
O4-C15	1.424(6)	**C20-C53**	1.518(10)
O5-C24	1.328(8)	**C24-C30**	1.490(10)
O5-C45	1.501(13)	**C25-C43**	1.487(12)
O6-C24	1.211(7)	**C25-C39**	1.496(12)
O8-C34	1.194(9)	**C25-C38**	1.494(11)
O9-C34	1.305(10)	**C27-C33**	1.489(13)
O9-C54	1.466(12)	**C29-C51**	1.369(13)
O10-C2	1.425(7)	**C32-C34**	1.501(11)
O4-H2O	0.86(9)	**C37-C40**	1.524(17)
O10-H1O	0.64(7)	**C40-C46**	1.37(3)
N1-C12	1.451(8)	**C41-C45**	1.470(17)
N1-C32	1.454(9)	**C42-C46**	1.522(14)
N1-C51	1.468(13)	**C45-C57**	1.502(16)
N2-C1	1.471(7)	**C45-C52**	1.534(19)
N2-C20	1.460(8)	**C47-C54**	1.39(2)

N2-C16	1.433(7)	**C49-C54**	1.45(2)
N9-C53	1.450(9)	**C54-C55**	1.54(2)
N9-C30	1.472(9)	**C1-H1**	1.0000
C2-H2	1.0000	**C39-H39C**	0.9800
C12-H12	1.0000	**C40-H40A**	0.9900
C15-H15	1.0000	**C40-H40B**	0.9900
C16-H16A	0.9900	**C41-H41A**	0.9800
C16-H16B	0.9900	**C41-H41B**	0.9800
C17-H17A	0.9900	**C41-H41C**	0.9800
C17-H17B	0.9900	**C42-H42A**	0.9900
C18-H18A	0.9900	**C42-H42B**	0.9900
C18-H18B	0.9900	**C43-H43A**	0.9800
C20-H20A	0.9900	**C43-H43B**	0.9800
C20-H20B	0.9900	**C43-H43C**	0.9800
C27-H27A	0.9900	**C46-H46A**	0.9900
C27-H27B	0.9900	**C46-H46B**	0.9900
C29-H29A	0.9900	**C47-H47A**	0.9800
C29-H29B	0.9900	**C47-H47B**	0.9800
C30-H30A	0.9900	**C47-H47C**	0.9800
C30-H30B	0.9900	**C49-H49A**	0.9800
C32-H32A	0.9900	**C49-H49B**	0.9800
C32-H32B	0.9900	**C49-H49C**	0.9800
C33-H33A	0.9900	**C51-H51A**	0.9900
C33-H33B	0.9900	**C51-H51B**	0.9900
C37-H37A	0.9900	**C52-H52A**	0.9800
C37-H37B	0.9900	**C52-H52B**	0.9800
C38-H38A	0.9800	**C52-H52C**	0.9800
C38-H38B	0.9800	**C53-H53A**	0.9900
C38-H38C	0.9800	**C53-H53B**	0.9900
C39-H39A	0.9800	**C55-H55A**	0.9800
C39-H39B	0.9800	**C55-H55B**	0.9800
C55-H55C	0.9800	**C57-H57B**	0.9800

C57-H57A	0.9800	**C57-H57C**	0.9800

Table D.25: Bond angles (°) for [$NaCy_2$DETA.3E]Br.

O4-Na1-O6	167.92(16)	**C15-O4-H2O**	98(5)
O4-Na1-O8	100.12(15)	**Na1-O4-H2O**	133(5)
O4-Na1-O10	81.99(14)	**Na1-O10-H1O**	116(5)
O4-Na1-N1	65.66(15)	**C2-O10-H1O**	104(5)
O4-Na1-N2	100.57(14)	**Na1-N1-C12**	104.8(4)
O4-Na1-N9	121.98(16)	**Na1-N1-C32**	107.3(4)
O6-Na1-O8	81.45(14)	**Na1-N1-C51**	107.0(4)
O6-Na1-O10	87.31(14)	**C12-N1-C32**	113.0(5)
O6-Na1-N1	125.18(16)	**C12-N1-C51**	127.3(7)
O6-Na1-N2	80.08(14)	**C32-N1-C51**	96.1(6)
O6-Na1-N9	69.64(15)	**Na1-N2-C16**	92.6(3)
O8-Na1-O10	125.03(17)	**Na1-N2-C20**	108.6(3)
O8-Na1-N1	66.83(17)	**Na1-N2-C1**	105.9(3)
O8-Na1-N2	157.68(16)	**C16-N2-C20**	115.1(4)
O8-Na1-N9	93.19(17)	**C1-N2-C20**	112.5(4)
O10-Na1-N1	147.51(17)	**C1-N2-C16**	119.1(4)
O10-Na1-N2	66.45(15)	**C29-N9-C30**	113.5(6)
O10-Na1-N9	132.23(15)	**Na1-N9-C53**	110.6(4)
N1-Na1-N2	115.08(16)	**Na1-N9-C30**	104.6(4)
N1-Na1-N9	68.90(15)	**C29-N9-C53**	109.7(6)
N2-Na1-N9	68.64(16)	**C30-N9-C53**	110.3(5)
C13-O3-C25	122.7(4)	**Na1-N9-C29**	108.1(4)
Na1-O4-C15	126.6(3)	**N2-C1-C2**	112.9(5)
C24-O5-C45	121.5(7)	**N2-C1-C18**	116.7(5)
Na1-O6-C24	118.0(4)	**C2-C1-C18**	109.6(5)
Na1-O8-C34	120.0(5)	**O10-C2-C1**	109.9(5)
C34-O9-C54	122.3(8)	**C1-C2-C17**	111.2(5)
Na1-O10-C2	124.5(3)	**O10-C2-C17**	109.6(4)
N1-C12-C15	113.0(5)	**O8-C34-C32**	125.1(7)

N1-C12-C42	116.2(6)	**O9-C34-C32**	109.6(7)
C15-C12-C42	110.6(5)	**C15-C37-C40**	110.7(8)
O3-C13-C16	108.8(5)	**C37-C40-C46**	115.5(11)
O1-C13-O3	125.6(5)	**C12-C42-C46**	109.4(9)
O1-C13-C16	125.7(5)	**C41-C45-C57**	115.1(10)
O4-C15-C37	112.0(5)	**C52-C45-C57**	107.4(10)
C12-C15-C37	110.2(5)	**O5-C45-C52**	101.4(10)
O4-C15-C12	108.0(4)	**O5-C45-C57**	105.3(9)
N2-C16-C13	119.0(5)	**O5-C45-C41**	112.2(8)
C2-C17-C33	110.7(6)	**C41-C45-C52**	114.3(10)
C1-C18-C27	111.6(5)	**C40-C46-C42**	114.9(11)
N2-C20-C53	112.4(5)	**N1-C51-C29**	114.4(9)
O5-C24-C30	110.4(6)	**N9-C53-C20**	114.9(6)
O6-C24-C30	126.0(6)	**C47-C54-C55**	116.3(12)
O5-C24-O6	123.6(6)	**C49-C54-C55**	105.1(11)
O3-C25-C38	109.4(5)	**C47-C54-C49**	111.5(11)
C39-C25-C43	113.2(8)	**O9-C54-C47**	116.1(9)
C38-C25-C43	111.8(8)	**O9-C54-C49**	105.9(9)
O3-C25-C39	107.6(6)	**O9-C54-C55**	100.7(10)
O3-C25-C43	102.4(5)	**N2-C1-H1**	106.00
C38-C25-C39	111.9(6)	**C2-C1-H1**	106.00
C18-C27-C33	111.5(6)	**C18-C1-H1**	106.00
N9-C29-C51	120.1(8)	**O10-C2-H2**	109.00
N9-C30-C24	114.6(6)	**C1-C2-H2**	109.00
N1-C32-C34	110.7(6)	**C17-C2-H2**	109.00
C17-C33-C27	111.6(7)	**N1-C12-H12**	105.00
O8-C34-O9	125.3(8)	**C15-C12-H12**	105.00
C42-C12-H12	105.00	**H27A-C27-H27B**	108.00
O4-C15-H15	109.00	**N9-C29-H29A**	107.00
C12-C15-H15	109.00	**N9-C29-H29B**	107.00
C37-C15-H15	109.00	**C51-C29-H29A**	107.00
N2-C16-H16A	108.00	**C51-C29-H29B**	107.00

N2-C16-H16B	108.00	**H29A-C29-H29B**	107.00
C13-C16-H16A	108.00	**N9-C30-H30A**	109.00
C13-C16-H16B	108.00	**N9-C30-H30B**	109.00
H16A-C16-H16B	107.00	**C24-C30-H30A**	109.00
C2-C17-H17A	109.00	**C24-C30-H30B**	109.00
C2-C17-H17B	109.00	**H30A-C30-H30B**	108.00
C33-C17-H17A	110.00	**N1-C32-H32A**	109.00
C33-C17-H17B	110.00	**N1-C32-H32B**	110.00
H17A-C17-H17B	108.00	**C34-C32-H32A**	109.00
C1-C18-H18A	109.00	**C34-C32-H32B**	110.00
C1-C18-H18B	109.00	**H32A-C32-H32B**	108.00
C27-C18-H18A	109.00	**C17-C33-H33A**	109.00
C27-C18-H18B	109.00	**C17-C33-H33B**	109.00
H18A-C18-H18B	108.00	**C27-C33-H33A**	109.00
N2-C20-H20A	109.00	**C27-C33-H33B**	109.00
N2-C20-H20B	109.00	**H33A-C33-H33B**	108.00
C53-C20-H20A	109.00	**C15-C37-H37A**	110.00
C53-C20-H20B	109.00	**C15-C37-H37B**	109.00
H20A-C20-H20B	108.00	**C40-C37-H37A**	110.00
C18-C27-H27A	109.00	**C40-C37-H37B**	109.00
C18-C27-H27B	109.00	**H37A-C37-H37B**	108.00
C33-C27-H27A	109.00	**C25-C38-H38A**	110.00
C33-C27-H27B	109.00	**C25-C38-H38B**	109.00
C25-C38-H38C	109.00	**C25-C43-H43C**	110.00
H38A-C38-H38B	109.00	**H43A-C43-H43B**	109.00
H38A-C38-H38C	110.00	**H43A-C43-H43C**	109.00
H38B-C38-H38C	109.00	**H43B-C43-H43C**	110.00
C25-C39-H39A	109.00	**C40-C46-H46A**	109.00
C25-C39-H39B	109.00	**C40-C46-H46B**	109.00
C25-C39-H39C	109.00	**C42-C46-H46A**	109.00
H39A-C39-H39B	110.00	**C42-C46-H46B**	109.00
H39A-C39-H39C	110.00	**H46A-C46-H46B**	108.00

H39B-C39-H39C	109.00	**C54-C47-H47A**	110.00
C37-C40-H40A	108.00	**C54-C47-H47B**	110.00
C37-C40-H40B	108.00	**C54-C47-H47C**	110.00
C46-C40-H40A	108.00	**H47A-C47-H47B**	109.00
C46-C40-H40B	108.00	**H47A-C47-H47C**	109.00
H40A-C40-H40B	107.00	**H47B-C47-H47C**	109.00
C45-C41-H41A	110.00	**C54-C49-H49A**	109.00
C45-C41-H41B	109.00	**C54-C49-H49B**	110.00
C45-C41-H41C	110.00	**C54-C49-H49C**	110.00
H41A-C41-H41B	109.00	**H49A-C49-H49B**	109.00
H41A-C41-H41C	110.00	**H49A-C49-H49C**	109.00
H41B-C41-H41C	110.00	**H49B-C49-H49C**	110.00
C12-C42-H42A	110.00	**N1-C51-H51A**	109.00
C12-C42-H42B	110.00	**N1-C51-H51B**	109.00
C46-C42-H42A	110.00	**C29-C51-H51A**	109.00
C46-C42-H42B	110.00	**C29-C51-H51B**	109.00
H42A-C42-H42B	108.00	**H51A-C51-H51B**	108.00
C25-C43-H43A	109.00	**C45-C52-H52A**	110.00
C25-C43-H43B	110.00	**C45-C52-H52B**	109.00
C45-C52-H52C	110.00	**C54-C55-H55C**	109.00
H52A-C52-H52B	109.00	**H55A-C55-H55B**	109.00
H52A-C52-H52C	109.00	**H55A-C55-H55C**	109.00
H52B-C52-H52C	109.00	**H55B-C55-H55C**	109.00
N9-C53-H53A	109.00	**C45-C57-H57A**	109.00
N9-C53-H53B	109.00	**C45-C57-H57B**	110.00
C20-C53-H53A	109.00	**C45-C57-H57C**	109.00
C20-C53-H53B	109.00	**H57A-C57-H57B**	109.00
H53A-C53-H53B	108.00	**H57A-C57-H57C**	110.00
C54-C55-H55A	110.00	**H57B-C57-H57C**	109.00
C54-C55-H55B	110.00		

Table D.26: Anisotropic displacement parameters ($Å^2 \times 10^3$) for [$NaCy_2DETA.3E$]Br.

Anisotropic displacement factor exponent: $-2p^2[h^2a^{*2}U^{11} + ... + 2\ h\ k\ a^*\ b^*\ U^{12}]$.

Atom	U^{11}	U^{22}	U^{33}	U^{23}	U^{13}	U^{12}
Na1	0.0298(8)	0.0398(9)	0.0561(10)	-0.0082(7)	-0.0020(7)	-0.0104(7)
O1	0.198(6)	0.073(3)	0.088(3)	-0.050(3)	0.050(3)	-0.073(4)
O3	0.089(3)	0.0361(18)	0.068(2)	-0.0129(17)	-0.0201(19)	-0.0152(18)
O4	0.0393(18)	0.081(3)	0.066(2)	-0.0078(18)	-0.0150(16)	-0.0228(18)
O5	0.085(3)	0.135(4)	0.126(4)	0.035(3)	-0.065(3)	-0.056(3)
O6	0.0449(18)	0.066(2)	0.070(2)	-0.0070(17)	-0.0167(16)	-0.0161(16)
O8	0.072(3)	0.087(3)	0.082(3)	-0.005(2)	0.025(2)	-0.019(2)
O9	0.095(4)	0.112(4)	0.159(5)	0.058(4)	0.076(4)	0.062(3)
O10	0.0369(17)	0.054(2)	0.064(2)	-0.0277(17)	0.0064(17)	-0.0192(15)
N1	0.048(2)	0.134(5)	0.057(3)	0.029(3)	-0.018(2)	-0.053(3)
N2	0.054(2)	0.049(2)	0.054(2)	-0.0170(18)	0.0056(18)	-0.0288(19)
N9	0.048(2)	0.111(4)	0.062(3)	-0.021(3)	0.004(2)	-0.048(3)
C1	0.056(3)	0.062(3)	0.065(3)	-0.028(2)	0.017(2)	-0.035(3)
C2	0.044(2)	0.062(3)	0.066(3)	-0.026(2)	0.011(2)	-0.023(2)
C12	0.095(4)	0.075(4)	0.041(3)	-0.009(2)	0.006(3)	-0.056(3)
C13	0.070(3)	0.051(3)	0.067(3)	-0.025(3)	0.004(3)	-0.030(3)
C15	0.063(3)	0.053(3)	0.043(2)	-0.006(2)	-0.009(2)	-0.005(2)
C16	0.064(3)	0.046(3)	0.062(3)	-0.027(2)	0.008(2)	-0.026(2)
C17	0.053(3)	0.093(4)	0.084(4)	-0.037(3)	0.020(3)	-0.043(3)
C18	0.076(4)	0.083(4)	0.063(3)	-0.035(3)	0.022(3)	-0.039(3)
C20	0.073(3)	0.075(4)	0.057(3)	-0.021(3)	0.003(2)	-0.044(3)
C24	0.046(3)	0.083(4)	0.076(4)	-0.006(3)	-0.020(3)	-0.015(3)
C25	0.107(5)	0.031(3)	0.089(4)	-0.010(3)	-0.028(4)	-0.013(3)
C27	0.091(5)	0.151(7)	0.080(4)	-0.059(4)	0.044(4)	-0.077(5)
C29	0.073(4)	0.212(9)	0.138(6)	-0.107(7)	0.054(4)	-0.106(6)
C30	0.046(3)	0.136(6)	0.092(4)	-0.021(4)	-0.011(3)	-0.038(4)
C32	0.054(3)	0.119(6)	0.083(4)	0.021(4)	0.035(3)	0.022(4)
C33	0.079(4)	0.169(8)	0.109(5)	-0.077(5)	0.052(4)	-0.077(5)
C34	0.047(3)	0.105(5)	0.084(4)	0.025(4)	0.016(3)	0.012(3)

C37	0.123(6)	0.083(5)	0.063(4)	0.013(3)	0.018(4)	0.038(4)
C38	0.109(5)	0.056(4)	0.131(6)	-0.018(4)	-0.036(5)	-0.037(4)
C39	0.092(6)	0.063(4)	0.255(12)	-0.071(6)	-0.063(7)	0.008(4)
C40	0.250(16)	0.089(7)	0.101(7)	0.051(6)	0.085(10)	0.075(10)
C41	0.124(7)	0.204(11)	0.110(6)	0.043(7)	-0.050(6)	-0.110(8)
C42	0.139(7)	0.096(5)	0.063(4)	-0.022(3)	0.038(4)	-0.072(5)
C43	0.271(15)	0.056(4)	0.107(6)	0.009(4)	-0.013(8)	-0.049(6)
C45	0.136(8)	0.115(7)	0.155(8)	0.052(6)	-0.099(7)	-0.073(6)
C46	0.34(2)	0.052(6)	0.145(11)	-0.016(6)	0.150(15)	-0.056(10)
C47	0.181(11)	0.111(7)	0.296(16)	0.111(10)	-0.163(12)	-0.073(8)
C49	0.185(12)	0.107(7)	0.128(8)	-0.051(6)	-0.056(8)	0.038(8)
C52	0.230(14)	0.274(16)	0.220(13)	0.160(13)	-0.179(12)	-0.173(14)
C53	0.077(4)	0.114(5)	0.068(3)	-0.022(3)	-0.003(3)	-0.068(4)
C54	0.070(5)	0.103(7)	0.156(9)	0.018(6)	0.030(6)	0.021(5)
C55	0.248(17)	0.117(9)	0.39(2)	0.072(12)	0.222(18)	0.111(11)
C57	0.124(8)	0.080(6)	0.238(13)	0.028(7)	-0.082(8)	-0.021(5)
Br1	0.0400(3)	0.1037(5)	0.1027(5)	-0.0308(4)	-0.0141(3)	-0.0240(3)

Table D.27: Torsion angles (°) for [$NaCy_2$DETA.3E]Br.

O8-Na1-O4-C15	66.4(4)
O10-Na1-O4-C15	-169.3(4)
N1-Na1-O4-C15	7.7(4)
N2-Na1-O4-C15	-105.2(4)
N9-Na1-O4-C15	-33.8(4)
O8-Na1-O6-C24	-84.2(4)
O10-Na1-O6-C24	149.8(4)
N1-Na1-O6-C24	-30.6(5)
N2-Na1-O6-C24	83.2(4)
N9-Na1-O6-C24	12.4(4)
O4-Na1-O8-C34	-48.5(5)
O6-Na1-O8-C34	143.6(5)
O10-Na1-O8-C34	-135.8(5)

N1-Na1-O8-C34	9.3(5)
N2-Na1-O8-C34	109.2 (6)
N9-Na1-O8-C34	74.8(5)
O4-Na1-O10-C2	105.7(4)
O6-Na1-O10-C2	-79.9(4)
O8-Na1-O10-C2	-157.5(4)
N1-Na1-O10-C2	100.6(5)
N2-Na1-O10-C2	0.4(4)
N9-Na1-O10-C2	-20.8(5)
O4-Na1-N1-C12	-29.6(3)
O4-Na1-N1-C32	90.7(4)
O4-Na1-N1-C51	-167.0(6)
O6-Na1-N1-C12	156.5(3)
O6-Na1-N1-C32	-83.1(4)
O6-Na1-N1-C51	19.2(6)
O8-Na1-N1-C12	-143.4(4)
O8-Na1-N1-C32	-23.1(4)
O8-Na1-N1-C51	79.2(5)
O10-Na1-N1-C12	-24.1(5)
O10-Na1-N1-C32	96.3(5)
O10-Na1-N1-C51	-161.5(5)
N2-Na1-N1-C12	61.0(4)
N2-Na1-N1-C32	-178.7(4)
N2-Na1-N1-C51	-76.4(5)
N9-Na1-N1-C12	113.3(4)
N9-Na1-N1-C32	-126.4(5)
N9-Na1-N1-C51	-24.1(5)
O4-Na1-N2-C1	-100.9(3)
O4-Na1-N2-C16	20.4(3)
O4-Na1-N2-C20	138.0(3)
O6-Na1-N2-C1	66.8(3)
O6-Na1-N2-C16	-171.9(3)

O6-Na1-N2-C20	-54.3(3)
O8-Na1-N2-C1	101.4(5)
O8-Na1-N2-C16	-137.3(4)
O8-Na1-N2-C20	-19.8(6)
O10-Na1-N2-C1	-24.6(3)
O10-Na1-N2-C16	96.7(3)
O10-Na1-N2-C20	-145.7(4)
N1-Na1-N2-C1	-168.9(3)
N1-Na1-N2-C16	-47.6(4)
N1-Na1-N2-C20	70.0(4)
N9-Na1-N2-C1	138.7(3)
N9-Na1-N2-C16	-100.0(3)
N9-Na1-N2-C20	17.6(3)
O4-Na1-N9-C29	41.8(6)
O4-Na1-N9-C30	162.9(4)
O4-Na1-N9-C53	-78.3(4)
O6-Na1-N9-C29	-141.9(5)
O6-Na1-N9-C30	-20.8(4)
O6-Na1-N9-C53	98.0(4)
O8-Na1-N9-C29	-62.3(5)
O8-Na1-N9-C30	58.9(4)
O8-Na1-N9-C53	177.6(4)
O10-Na1-N9-C29	152.0(5)
O10-Na1-N9-C30	-86.9(4)
O10-Na1-N9-C53	31.8(5)
N1-Na1-N9-C29	1.4(5)
N1-Na1-N9-C30	122.5(4)
N1-Na1-N9-C53	-118.7(4)
N2-Na1-N9-C29	131.1(5)
N2-Na1-N9-C30	-107.8(4)
N2-Na1-N9-C53	11.0(3)
C25-O3-C13-O1	-2.5(11)

C25-O3-C13-C16	176.7(5)
C13-O3-C25-C38	-56.5(8)
C13-O3-C25-C39	65.2(8)
C13-O3-C25-C43	-175.3(8)
Na1-O4-C15-C12	15.8(5)
Na1-O4-C15-C37	137.3(4)
C45-O4-C24-O6	-1.8(10)
C45-O5-C24-C30	177.4(7)
C24-O5-C45-C41	58.6(11)
C24-O5-C45-C52	-179.1(8)
C24-O5-C45-C57	-67.3(10)
Na1-O6-C24-O5	178.5(5)
Na1-O6-C24-C30	-0.7(8)
Na1-O8-C34-O9	-173.2(6)
Na1-O8-C34-C32	7.4(10)
C54-O9-C34-O8	1.2(13)
C54-O9-C34-C32	-179.3(8)
C34-O9-C54-C47	56.5(13)
C34-O9-C54-C49	-67.8(12)
C34-O9-C54-C55	-177.1(10)
Na1-O10-C2-C1	24.0(6)
Na1-O10-C2-C17	146.4(4)
Na1-N1-C12-C15	51.1(5)
Na1-N1-C12-C42	-179.5(4)
C32-N1-C12-C15	-65.3(7)
C32-N1-C12-C42	64.1(8)
C51-N1-C12-C15	176.7(6)
C51-N1-C12-C42	-53.9(9)
Na1-N1-C32-C34	33.4(7)
C12-N1-C32-C34	148.4(6)
C51-N1-C32-C34	-76.6(7)
Na1-N1-C51-C29	48.9(9)

C12-N1-C51-C29	-75.7(10)
C32-N1-C51-C29	159.1(9)
Na1-N2-C1-C2	47.3(4)
Na1-N2-C1-C18	175.5(4)
C16-N2-C1-C2	-55.1(6)
C16-N2-C1-C18	73.2(6)
C20-N2-C1-C2	165.8(4)
C20-N2-C1-C18	-65.9(6)
Na1-N2-C16-C13	162.9(5)
C1-N2-C16-C13	-87.2(6)
C20-N2-C16-C13	50.9(7)
Na1-N2-C20-C53	-44.6(5)
C1-N2-C20-C53	-161.5(5)
C16-N2-C20-C53	57.6(6)
Na1-N9-C29-C51	25.8(10)
C30-N9-C29-C51	-89.7(10)
C53-N9-C29-C51	146.4(9)
Na1-N9-C30-C24	28.0(6)
C29-N9-C30-C24	145.5(6)
C53-N9-C30-C24	-91.0(7)
Na1-N9-C53-C20	-39.6(6)
C29-N9-C53-C20	-158.7(6)
C30-N9-C53-C20	75.6(7)
N2-C1-C2-O10	-48.9(6)
N2-C1-C2-C17	-170.3(4)
C18-C1-C2-O10	179.3(4)
C18-C1-C2-C17	57.8(6)
N2-C1-C18-C27	172.9(5)
C2-C1-C18-C27	-57.3(7)
O10-C2-C17-C33	-178.4(5)
C1-C2-C17-C33	-56.7(7)
N1-C12-C15-O4	-46.6(6)

N1-C12-C15-C37	-169.2(4)
C42-C12-C15-O4	-178.8(5)
C42-C12-C15-C37	58.6(6)
N1-C12-C42-C46	174.5(8)
C15-C12-C42-C46	-55.0(9)
O1-C13-C16-N2	20.0(10)
O3-C13-C16-N2	-159.1(5)
O4-C15-C37-C40	-174.7(7)
C12-C15-C37-C40	-54.4(8)
C2-C17-C33-C27	54.3(8)
C1-C18-C27-C33	55.8(9)
N2-C20-C53-N9	60.2(7)
O5-C24-C30-N9	158.7(6)
O6-C24-C30-N9	-22.1(10)
C18-C27-C33-C17	-54.0(9)
N9-C29-C51-N1	-54.0(12)
N1-C32-C34-O8	-31.0(11)
N1-C32-C34-O9	149.6(7)
C15-C37-C40-C46	51.0(2)
C37-C40-C46-C42	-50.0(14)
C12-C42-C46-C40	51.2(12)

Table D.28: Hydrogen bonds for [$NaCy_2$DETA.3E]Br (Å and °).

D-H···A	d(D-H)	d(H···A)	d(D···A)	<(DHA)
O10-H1O···Br1	0.64(7)	2.59(6)	3.198(4)	162(7)
O4-H2O···Br1	0.86(9)	2.55(9)	3.269(4)	143(6)
C18-H18A···O1	0.9900	2.5900	3.107(9)	113.00
C20-H20A···O1	0.9900	2.4900	3.118(8)	121.00
C38-H38A···O1	0.9800	2.3700	2.937(10)	116.00
C38-H38C···O10[a]	0.9800	2.5500	3.485(7)	160.00
C39-H39B···O1	0.9800	2.4000	3.009(11)	120.00
C41-H41B···O6	0.9800	2.3200	2.932(11)	120.00
C47-H47B···O8	0.9800	2.3700	2.970(13)	119.00
C49-H49C···O8	0.9800	2.3700	2.977(11)	120.00
C55-H55B···Br1[b]	0.9800	2.8300	3.787(14)	166.00
C57-H57C···O6	0.9800	2.4000	2.997(11)	119.00

Symmetry transformations used to generate equivalent atoms:

a = x, -1+y, z b = -1+x, 1+y, z

D.5 Bis(2-bromoethyl)ammonium bromide

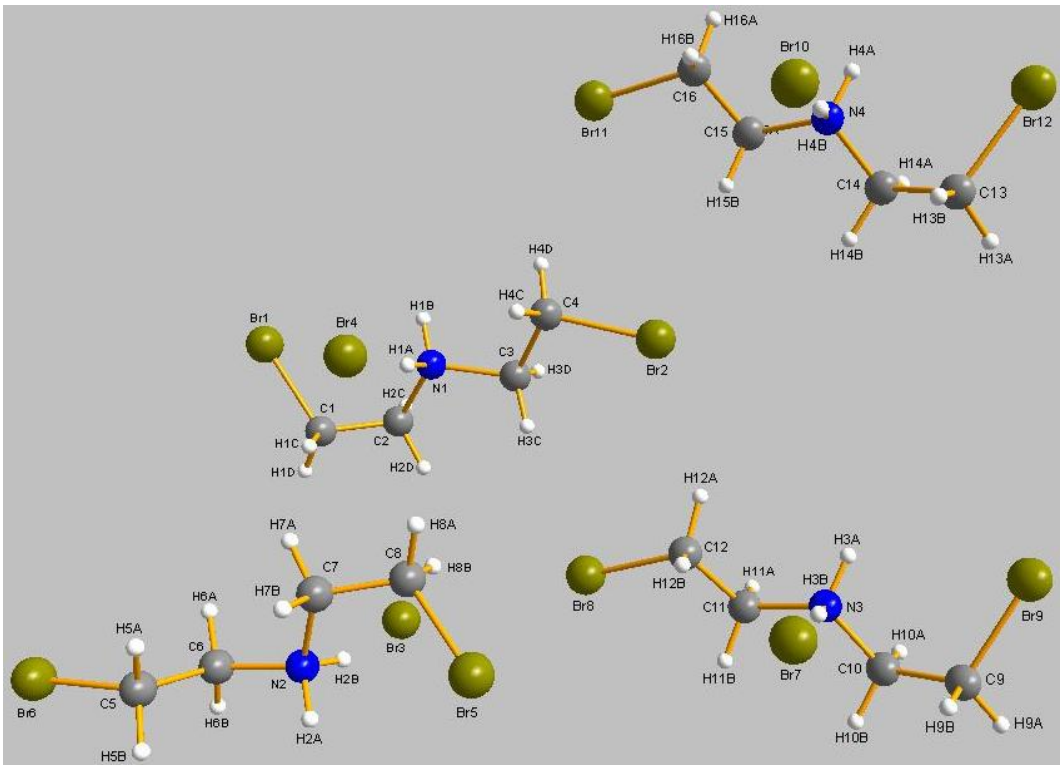


Figure D.5: XRD structure of bis(2-bromoethyl)ammonium bromide.

Table D.29: Crystal data and structure refinement for bis(2-bromoethyl)ammonium bromide.

Identification code	8m_alv31_0c
Empirical formula	C4 H10 Br2 N, Br
Formula weight	311.86
Temperature	173 K
Wavelength	0.71073 Å
Crystal system	Monoclinic
Space group	$P2_1$
Unit cell dimensions	a = 15.8861(13) Å α = 90° b = 7.4891(6) Å β = 117.450(5)° c = 17.1018(18) Å γ = 90°
Volume	1805.6(3) $Å^3$
Z	8
Density (calculated)	2.294 $g.cm^{-3}$

Absorption coefficient	13.324 mm^{-1}
F(000)	1168
Crystal size	0.02 × 0.08 × 0.59 mm^3
Theta range for data collection	1.3 to 27.0°
Index ranges	-19<=h<=20, -9<=k<=9, -21<=l<=8
Reflections collected	10233
Independent reflections	6819 [R(int) = 0.143]
Absorption correction	None
Refinement method	Full-matrix least-squares on F2
Data / restraints / parameters	6819 / 0 / 290
Goodness-of-fit on F^2	0.98
R indices (all data)	R1 = 0.1073, wR2 = 0.2846
Largest diff. peak and hole	-2.01 and 2.13 e.$Å^{-3}$

Table D.30: Atomic coordinates (× 10^4) and equivalent isotropic displacement parameters ($Å^2$ × 10^3) for bis(2-bromoethyl)ammonium bromide. U(eq) is defined as one third of the trace of the orthogonalized U^{ij} tensor.

Atom	x	y	z	U(eq)
Br1	1.0262(4)	0.5657(7)	0.6975(3)	0.0566(18)
Br2	0.7909(3)	0.6111(6)	0.2100(2)	0.0344(11)
N1	0.8992(19)	0.607(4)	0.4843(16)	0.024(8)
C1	0.890(2)	0.595(5)	0.623(2)	0.032(5)
C2	0.868(2)	0.699(5)	0.5452(19)	0.023(5)
C3	0.842(3)	0.666(5)	0.388(2)	0.032(5)
C4	0.877(3)	0.559(5)	0.334(2)	0.038(6)
Br5	0.4962(3)	0.1204(6)	0.3201(2)	0.0410(12)
Br6	0.7005(3)	0.0235(6)	0.7903(2)	0.0347(11)
N2	0.5926(19)	0.211(4)	0.5289(15)	0.027(8)
C5	0.635(2)	0.016(4)	0.6613(18)	0.024(5)
C6	0.636(2)	0.202(4)	0.6290(19)	0.024(5)
C7	0.649(3)	0.109(6)	0.492(2)	0.041(6)
C8	0.623(2)	0.165(4)	0.4031(18)	0.027(5)
Br8	0.5708(3)	0.6336(6)	0.2858(2)	0.0333(11)

Br9	0.3459(3)	0.5968(8)	-0.1998(3)	0.0545(16)
N3	0.4142(18)	0.629(4)	0.0114(15)	0.023(4)
C9	0.273(2)	0.611(5)	-0.1351(19)	0.029(5)
C10	0.321(2)	0.710(5)	-0.048(2)	0.041(11)
C11	0.455(3)	0.690(5)	0.106(2)	0.032(13)
C12	0.538(3)	0.574(6)	0.163(2)	0.045(7)
Br11	1.0931(3)	0.5783(5)	0.2892(2)	0.0325(11)
Br12	0.8319(3)	0.5275(7)	-0.1957(3)	0.0485(16)
N4	0.9227(19)	0.561(4)	0.0182(16)	0.026(8)
C13	0.769(3)	0.542(5)	-0.121(2)	0.037(6)
C14	0.830(2)	0.647(5)	-0.037(2)	0.031(10)
C15	0.966(3)	0.625(5)	0.111(2)	0.035(5)
C16	1.051(3)	0.525(5)	0.165(2)	0.038(6)
Br3	0.6231(2)	0.6258(6)	0.5118(2)	0.0284(10)
Br4	0.8830(2)	0.1738(4)	0.4877(2)	0.0284(11)
Br7	0.3904(2)	0.1919(5)	0.0112(2)	0.0290(11)
Br10	0.8945(2)	0.1288(5)	0.0195(2)	0.0284(11)

Table D.31: Bond lengths (Å) for bis(2-bromoethyl)ammonium bromide.

Br1-C1	1.95(3)	**C2-H2C**	0.9900
Br2-C4	1.96(3)	**C2-H2D**	0.9900
Br5-C8	1.88(3)	**C3-H3C**	0.9800
Br6-C5	1.96(3)	**C3-H3D**	0.9900
Br8-C12	1.97(3)	**C4-H4D**	0.9900
Br9-C9	1.94(3)	**C4-H4C**	0.9900
Br11-C16	1.95(3)	**C5-C6**	1.50(4)
Br12-C13	1.95(4)	**C7-C8**	1.44(4)
N1-C3	1.53(4)	**C5-H5B**	0.9900
N1-C2	1.51(4)	**C5-H5A**	0.9900
N1-H1B	0.9200	**C6-H6B**	0.9900
N1-H1A	0.9200	**C6-H5A**	1.0000
N2-C6	1.52(4)	**C7-H7A**	0.9900

N2-C7	1.52(6)	**C7-H7B**	0.9900
N2-H2B	0.9200	**C8-H8A**	0.9900
N2-H2A	0.9200	**C8-H8B**	0.9900
N3-C10	1.49(4)	**C9-C10**	1.52(4)
N3-C11	1.51(4)	**C11-C12**	1.50(6)
N3-H3B	0.9200	**C9-H9B**	0.9900
N3-H3A	0.9200	**C9-H9A**	0.9900
N4-C15	1.49(4)	**C10-H10A**	0.9900
N4-C14	1.48(5)	**C10-H10B**	0.9900
N4-H4B	0.9200	**C11-H11B**	0.9800
N4-H4A	0.9200	**C11-H11A**	0.9900
C1-C2	1.44(5)	**C12-H12A**	1.0000
C3-C4	1.51(6)	**C12-H12B**	0.9900
C1-H1D	1.0000	**C13-C14**	1.53(5)
C1-H1C	0.9900	**C15-C16**	1.45(6)
C13-H13A	0.9900	**C15-H15A**	0.9900
C13-H13B	0.9900	**C15-H15B**	0.9900
C14-H14A	0.9900	**C16-H16A**	0.9900
C14-H14B	0.9900	**C16-H16B**	0.9900

Table D.32: Bond angles (°) for bis(2-bromoethyl)ammonium bromide.

C2-N1-C3	113(3)	**C2-C1-H1C**	110.00
C3-N1-H1B	109.00	**C2-C1-H1D**	109.00
H1A-N1-H1B	108.00	**H1C-C1-H1D**	107.00
C2-N1-H1B	109.00	**Br1-C1-H1C**	109.00
C3-N1-H1A	109.00	**Br1-C1-H1D**	109.00
C2-N1-H1A	109.00	**N1-C2-H2D**	109.00
C6-N2-C7	113(3)	**H2C-C2-H2D**	108.00
H2A-N2-H2B	108.00	**C1-C2-H2D**	109.00
C6-N2-H2A	109.00	**N1-C2-H2C**	109.00
C7-N2-H2B	109.00	**C1-C2-H2C**	109.00
C6-N2-H2B	109.00	**C4-C3-H3C**	110.00
C7-N2-H2A	109.00	**H3C-C3-H3D**	109.00
C10-N3-C11	114(3)	**C4-C3-H3D**	110.00
C10-N3-H3B	109.00	**N1-C3-H3D**	110.00
C11-N3-H3A	109.00	**N1-C3-H3C**	110.00
H3A-N3-H3B	107.00	**H4C-C4-H4D**	109.00
C10-N3-H3A	109.00	**C3-C4-H4D**	110.00
C11-N3-H3B	108.00	**C3-C4-H4C**	110.00
C14-N4-C15	112(3)	**Br2-C4-H4C**	110.00
C15-N4-H4A	109.00	**Br2-C4-H4D**	111.00
C15-N4-H4B	109.00	**Br6-C5-C6**	107.3(19)
C14-N4-H4B	109.00	**N2-C6-C5**	112(2)
C14-N4-H4A	109.00	**N2-C7-C8**	111(3)
H4A-N4-H4B	108.00	**Br5-C8-C7**	116(3)
Br1-C1-C2	113(2)	**Br6-C5-H5B**	110.00
N1-C2-C1	112(3)	**C6-C5-H5A**	110.00
N1-C3-C4	108(3)	**Br6-C5-H5A**	110.00
Br2-C4-C3	107(3)	**C6-C5-H5B**	110.00
H5A-C5-H5B	109.00	**C9-C10-H10A**	109.00
C5-C6-H6B	110.00	**N3-C10-H10A**	110.00
C5-C6-H6A	109.00	**H11A-C11-H11B**	109.00

H6A-C6-H6B	108.00	**N3-C11-H11B**	110.00
N2-C6-H6A	109.00	**N3-C11-H11A**	109.00
N2-C6-H6B	109.00	**C12-C11-H11B**	110.00
H7A-C7-H7B	108.00	**C12-C11-H11A**	109.00
C8-C7-H7B	109.00	**Br8-C12-H12B**	111.00
N2-C7-H7A	109.00	**C11-C12-H12A**	110.00
C8-C7-H7A	110.00	**Br8-C12-H12A**	111.00
N2-C7-H7B	109.00	**H12A-C12-H12B**	108.00
Br5-C8-H8B	108.00	**C11-C12-H12B**	110.00
C7-C8-H8A	108.00	**Br12-C13-C14**	110(3)
Br5-C8-H8A	109.00	**N4-C14-C13**	113(3)
C7-C8-H8B	108.00	**N4-C15-C16**	111(3)
H8A-C8-H8B	107.00	**Br11-C16-C15**	110(3)
Br9-C9-C10	115(2)	**Br12-C13-H13A**	109.00
N3-C10-C9	111(3)	**Br12-C13-H13B**	109.00
N3-C11-C12	110(3)	**C14-C13-H13A**	110.00
Br8-C12-C11	106(3)	**C14-C13-H13B**	110.00
Br9-C9-H9B	108.00	**H13A-C13-H13B**	109.00
C10-C9-H9A	109.00	**N4-C14-H14A**	109.00
Br9-C9-H9A	108.00	**N4-C14-H14B**	109.00
H9A-C9-H9B	108.00	**C13-C14-H14A**	109.00
C10-C9-H9B	108.00	**C13-C14-H14B**	108.00
C9-C10-H10B	109.00	**H14A-C14-H14B**	108.00
H10A-C10-H10B	108.00	**N4-C15-H15A**	110.00
N3-C10-H10B	110.00	**N4-C15-H15B**	109.00
C16-C15-H15A	110.00	**Br11-C16-H16B**	110.00
C16-C15-H15B	110.00	**C15-C16-H16A**	110.00
H15A-C15-H15B	108.00	**C15-C16-H16B**	110.00
Br11-C16-H16A	110.00	**H16A-C16-H16B**	109.00

Table D.33: Anisotropic displacement parameters ($Å^2 \times 10^3$) for bis(2-bromoethyl)ammonium bromide. Anisotropic displacement factor exponent: $-2p^2[h^2a^{*2}U^{11} + ... + 2\ h\ k\ a^*\ b^*\ U^{12}]$.

Atom	U^{11}	U^{22}	U^{33}	U^{23}	U^{13}	U^{12}
Br1	0.042(3)	0.070(4)	0.044(2)	0.005(2)	0.008(2)	-0.009(2)
Br2	0.0287(19)	0.041(2)	0.0319(18)	0.005(2)	0.0127(16)	0.000(2)
N1	0.032(15)	0.014(13)	0.034(13)	-0.002(13)	0.022(13)	-0.009(12)
C1	0.033(9)	0.032(9)	0.032(9)	-0.001(5)	0.017(6)	0.000(5)
C2	0.024(8)	0.021(8)	0.023(8)	-0.002(5)	0.009(5)	0.003(5)
C3	0.030(9)	0.033(10)	0.033(9)	0.000(5)	0.015(6)	0.000(5)
C4	0.039(11)	0.038(11)	0.036(10)	0.000(5)	0.017(6)	0.000(5)
Br5	0.034(2)	0.037(2)	0.049(2)	-0.005(2)	0.0167(18)	0.004(2)
Br6	0.032(2)	0.040(2)	0.0327(19)	0.0036(17)	0.0154(17)	0.0076(17)
N2	0.032(17)	0.012(12)	0.019(12)	-0.003(11)	-0.003(12)	-0.006(12)
C5	0.025(8)	0.026(8)	0.022(8)	0.001(5)	0.013(5)	0.000(5)
C6	0.024(8)	0.025(8)	0.026(8)	0.001(5)	0.013(5)	0.001(5)
C7	0.042(10)	0.040(10)	0.041(10)	-0.002(5)	0.020(6)	0.001(5)
C8	0.025(8)	0.029(9)	0.028(8)	0.000(5)	0.013(5)	-0.001(5)
Br8	0.0307(19)	0.037(2)	0.0353(18)	-0.0001(19)	0.0178(16)	-0.0017(19)
Br9	0.055(3)	0.070(3)	0.039(2)	-0.006(2)	0.022(2)	-0.010(3)
N3	0.023(7)	0.022(7)	0.024(7)	-0.002(5)	0.011(5)	-0.001(5)
C9	0.026(8)	0.027(8)	0.031(8)	-0.001(5)	0.011(5)	-0.001(5)
C10	0.012(17)	0.04(2)	0.06(2)	-0.005(19)	0.008(17)	0.003(16)
C11	0.05(3)	0.017(15)	0.05(2)	0.001(16)	0.04(2)	-0.006(16)
C12	0.045(11)	0.047(12)	0.045(11)	-0.002(5)	0.022(7)	0.002(5)
Br11	0.026(2)	0.041(2)	0.0324(19)	0.0005(16)	0.0152(17)	-0.0030(17)
Br12	0.054(3)	0.054(3)	0.041(2)	-0.009(2)	0.025(2)	-0.018(2)
N4	0.023(14)	0.032(16)	0.019(12)	-0.005(11)	0.007(12)	-0.017(12)
C13	0.037(10)	0.037(10)	0.037(10)	0.003(5)	0.016(6)	0.000(5)
C14	0.027(18)	0.022(18)	0.032(17)	-0.011(15)	0.003(15)	0.002(15)
C15	0.034(9)	0.034(9)	0.035(9)	-0.002(5)	0.014(6)	0.003(5)
C16	0.036(10)	0.038(10)	0.038(10)	-0.003(5)	0.016(6)	0.004(5)

Br3	0.0292(18)	0.0185(18)	0.0437(18)	-0.0011(17)	0.0221(15)	-0.0031(16)
Br4	0.0198(17)	0.023(2)	0.047(2)	0.0033(15)	0.0193(16)	0.0011(13)
Br7	0.0259(19)	0.0210(19)	0.046(2)	-0.0019(15)	0.0216(17)	-0.0032(14)
Br10	0.0318(19)	0.0171(17)	0.0480(19)	0.0005(17)	0.0284(17)	-0.0017(16)

Table D.34: Torsion angles (°) for bis(2-bromoethyl)ammonium bromide.

C3-N1-C2-C1	155(3)
C2-N1-C3-C4	-178(3)
C6-N2-C7-C8	-162(3)
C7-N2-C6-C5	-65(4)
C10-N3-C11-C12	169(3)
C11-N3-C10-C9	-166(3)
C15-N4-C14-C13	-160(3)
C14-N4-C15-C16	174(3)
Br1-C1-C2-N1	65(3)
N1-C3-C4-Br2	172(3)
Br6-C5-C6-N2	176(2)
N2-C7-C8-Br5	-63(4)
Br9-C9-C10-N3	-57(3)
N3-C11-C12-Br8	-170(3)
Br12-C13-C14-N4	-62(3)
N4-C15-C16-Br11	-169(3)

Table D.35: Hydrogen bonds for bis(2-bromoethyl)ammonium bromide (Å and °).

D-H···A	d(D-H)	d(H···A)	d(D···A)	<(DHA)
N1-H1A···Br4	0.9200	2.3400	3.26(3)	174.00
N1-H1B···Br4[a]	0.9200	2.4100	3.31(3)	165.00
N2-H2A···Br3[b]	0.9200	2.3700	3.23(3)	156.00
N2-H2B···Br3	0.9200	2.3000	3.18(3)	161.00
N3-H3A···Br9	0.9200	2.9300	3.27(2)	104.00
N3-H3A···Br7[c]	0.9200	2.4600	3.33(3)	159.00
N3-H3B···Br7	0.9200	2.3700	3.30(3)	178.00
N4-H4B···Br10	0.9200	2.3500	3.27(3)	178.00
C1-H1D···Br12[d]	1.0000	2.9200	3.66(3)	131.00
C2-H2C···Br4[e]	0.9900	2.9300	3.73(4)	138.00
C2-H2D···Br3	0.9900	2.8700	3.70(4)	143.00
C3-H3C···Br8	0.9800	2.8700	3.84(5)	170.00
C7-H7B···Br3[f]	0.9900	2.6900	3.68(5)	173.00
C9-H9A···Br1[g]	0.9900	2.8700	3.65(3)	137.00
C10-H10A···Br7[e]	0.9900	2.9000	3.77(4)	148.00
C10-H10B···Br10[c]	0.9900	2.8200	3.72(4)	153.00
C12-H12A···Br2	1.0000	2.8300	3.73(5)	150.00
C14-H14B···Br7[c]	0.9900	2.8800	3.74(4)	145.00
C15-H15B···Br2	0.9900	2.8800	3.87(5)	173.00
C16-H16A···Br6[a]	0.9900	2.8300	3.66(5)	141.00

Symmetry transformations used to generate equivalent atoms:

a = 2-x, $^1/_2$+y, 1-z b = 1-x, -$^1/_2$+y, 1-z c = 1-x, $^1/_2$+y, -z

d = x, y, 1+z e = x, 1+y, z f = x, -1+y, z

g = -1+x, y, -1+z

D.6 Morpholinium bromide

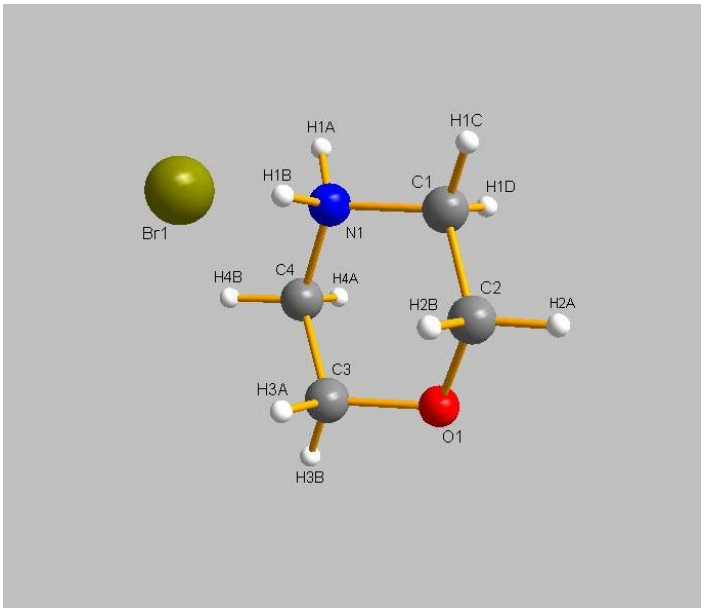


Figure D.6: XRD structure of morpholinium bromide.

Table D.36: Crystal data and structure refinement for morpholinium bromide.

Identification code	8m_alv14_0s
Empirical formula	C4 H10 N O, Br
Formula weight	168.04
Temperature	173 K
Wavelength	0.71073 Å
Crystal system	Monoclinic
Space group	P21/c
Unit cell dimensions	a = 6.1247(2) Å α = 90° b = 10.3063(3) Å β = 100.312(2)° c = 10.1141(3) Å γ = 90°
Volume	628.12(3) $Å^3$
Z	4
Density (calculated)	1.777 $g.cm^{-3}$
Absorption coefficient	6.435 mm^{-1}
F(000)	336
Crystal size	0.09 × 0.20 × 0.40 mm^3

Theta range for data collection	2.8 to 28.0°
Index ranges	-8<=h<=8, -13<=k<=13, -13<=l<=13
Reflections collected	11662
Independent reflections	1516 [R(int) = 0.210]
Absorption correction	None
Refinement method	Full-matrix least-squares on F2
Data / restraints / parameters	1516 / 0 / 64
Goodness-of-fit on F^2	1.03
R indices (all data)	R1 = 0.0388, wR2 = 0.0995
Largest diff. peak and hole	-1.38 and 1.07 e.$Å^{-3}$

Table D.37: Atomic coordinates ($\times 10^4$) and equivalent isotropic displacement parameters ($Å^2 \times 10^3$) for morpholinium bromide. U(eq) is defined as one third of the trace of the orthogonalized U^{ij} tensor.

Atom	x	y	z	U(eq)
O1	0.2489(4)	0.10940(17)	0.4694(3)	0.0264(7)
N1	0.2813(4)	0.0830(2)	0.1937(2)	0.0199(6)
C1	0.3228(5)	0.2082(3)	0.2657(3)	0.0243(8)
C2	0.1926(5)	0.2149(3)	0.3781(3)	0.0273(9)
C3	0.1915(5)	-0.0094(3)	0.4004(3)	0.0271(8)
C4	0.3199(5)	-0.0280(3)	0.2893(3)	0.0245(8)
Br1	0.74904(4)	0.11971(3)	0.07284(3)	0.0245(1)

Table D.38: Bond lengths (Å) for morpholinium bromide.

O1-C2	1.428(4)	**C1-H1C**	0.9900
O1-C3	1.422(4)	**C1-H1D**	0.9900
N1-C1	1.481(4)	**C2-H2A**	0.9900
N1-C4	1.489(4)	**C2-H2B**	0.9900
N1-H1B	0.9200	**C3-H3A**	0.9900
N1-H1A	0.9200	**C3-H3B**	0.9900
C1-C2	1.503(4)	**C4-H4A**	0.9900
C3-C4	1.495(4)	**C4-H4B**	0.9900

Table D.39: Bond angles (°) for morpholinium bromide.

C2-O1-C3	109.2(3)	**O1-C2-H2A**	110.00
C1-N1-C4	110.9(2)	**O1-C2-H2B**	109.00
C4-N1-H1B	109.00	**C1-C2-H2A**	109.00
H1A-N1-H1B	108.00	**C1-C2-H2B**	109.00
C1-N1-H1B	109.00	**H2A-C2-H2B**	108.00
C4-N1-H1A	110.00	**O1-C3-H3A**	109.00
C1-N1-H1A	109.00	**O1-C3-H3B**	109.00
N1-C1-C2	110.2(2)	**C4-C3-H3A**	109.00
O1-C2-C1	110.8(3)	**C4-C3-H3B**	109.00
O1-C3-C4	111.2(3)	**H3A-C3-H3B**	108.00
N1-C4-C3	110.2(2)	**N1-C4-H4A**	110.00
N1-C1-H1C	110.00	**N1-C4-H4B**	110.00
N1-C1-H1D	110.00	**C3-C4-H4A**	110.00
C2-C1-H1C	110.00	**C3-C4-H4B**	110.00
C2-C1-H1D	110.00	**H4A-C4-H4B**	108.00
H1C-C1-H1D	108.00		

Table D.40: Anisotropic displacement parameters ($Å^2 \times 10^3$) for morpholinium bromide.

Anisotropic displacement factor exponent: $-2p^2[h^2a^{*2}U^{11} + ... + 2\ h\ k\ a^*\ b^*\ U^{12}]$.

Atom	$\mathbf{U^{11}}$	$\mathbf{U^{22}}$	$\mathbf{U^{33}}$	$\mathbf{U^{23}}$	$\mathbf{U^{13}}$	$\mathbf{U^{12}}$
O1	0.0358(13)	0.0301(11)	0.0127(10)	0.0004(7)	0.0031(9)	0.0010(8)
N1	0.0159(11)	0.0289(11)	0.0147(11)	-0.0013(8)	0.0021(9)	0.0018(8)
C1	0.0259(14)	0.0220(13)	0.0238(14)	0.0010(10)	0.0014(11)	-0.0055(10)
C2	0.0336(16)	0.0246(14)	0.0225(15)	-0.0047(11)	0.0018(13)	0.0050(11)
C3	0.0340(15)	0.0245(14)	0.0230(14)	0.0037(11)	0.0053(12)	-0.0033(11)
C4	0.0274(14)	0.0238(14)	0.0213(14)	-0.0004(10)	0.0014(11)	0.0042(10)
Br1	0.0153(2)	0.0332(2)	0.0242(2)	-0.0076(1)	0.0012(1)	-0.0011(1)

Table D.41: Torsion angles (°) for morpholinium bromide.

C3-O1-C2-C1	-62.4(3)
C2-O1-C3-C4	62.3(3)
C4-N1-C1-C2	-52.4(3)
C1-N1-C4-C3	52.2(3)
N1-C1-C2-O1	57.8(3)
O1-C3-C4-N1	-57.4(3)

Table D.42: Hydrogen bonds for morpholinium bromide (Å and °).

D-H···A	**d(D-H)**	**d(H···A)**	**d(D···A)**	**<(DHA)**
N1-H1A···Br1	0.9200	2.5200	3.331(2)	148.00
N1-H1A···Br1[a]	0.9200	2.8900	3.389(2)	115.00
N1-H1B···Br1[b]	0.9200	2.4000	3.292(2)	164.00
C1-H1C···O1[c]	0.9900	2.5900	3.498(4)	152.00
C4-H4A···O1[d]	0.9900	2.5200	3.366(4)	143.00

Symmetry transformations used to generate equivalent atoms:

a = 1-x, -y, -z b = -1+x, y, z c = x, $^{1}/_{2}$-y, -$^{1}/_{2}$+z

d = 1-x, -y, 1-z

Appendix E – Potentiometry Data

All potentiometry data was determined in the manner described in Chapter 2.

E.1 Preparation of the Standard Solutions

0.0100 M KHP standard solution:

m_{KHP} required	=	CVM
	=	0.0100 mol/L × 0.250 L × 204.2231 g/mol
	=	0.5106 g
m_{KHP} measured	=	0.5109 g
C_{KHP}	=	(0.5109 g) ÷ (204.2231 g/mol × 0.250 L)
	=	0.0100 mol/L

0.100 M $NaNO_3$ standard solution:

m_{NaNO_3} required	=	CVM
	=	0.100 mol/L × 0.250 L × 84.9949 g/mol
	=	2.1249 g
m_{NaNO_3} measured	=	2.1250 g
C_{NaNO_3}	=	(2.1250 g) ÷ (84.9949 g/mol × 0.250 L)
	=	0.100 mol/L

0.0500 M NaOH / 0.0500 M $NaNO_3$ standard solution:

V_{NaOH} of 0.1 M HNO_3 used	=	0.500 L
m_{NaNO_3} required	=	CVM
	=	0.0500 mol/L × 1.0 L × 84.9949 g/mol
	=	4.2497 g
m_{NaNO_3} measured	=	4.2497 g
C_{NaNO_3}	=	(4.2497 g) ÷ (84.9949 g/mol × 1.0 L)

= 0.0500 mol/L

Titration with 0.0100 M KHP

V_{KHP} used = 5.00 mL

n_{KHP} = 0.0100 mol/L × 0.00500 L

= 5.00×10^{-5} mol

Table E.1: Results from titration of 0.0100 M KHP with 0.0500 M NaOH / 0.0500 M $NaNO_3$.

Titration	V_{ini} (mL)	V_{fin} (mL)	V_{Total} (mL)
1	0.00	1.04	1.04
2	1.04	2.06	1.02*
3	2.06	3.07	1.01*
4	3.07	4.11	1.04
5	4.11	5.13	1.02*

Average volume used (*) = 1.02 mL

Since KHP reacts with NaOH in a 1:1 ratio,

C_{NaOH} = 5.00×10^{-5} mol ÷ 0.00102 L

= 0.0492 mol/L

Thus, the actual concentration of 0.0500 M NaOH / 0.0500 M $NaNO_3$ solution is 0.0492 M NaOH / 0.0500 M $NaNO_3$.

0.0100 M NaOH / 0.0900 M $NaNO_3$ standard solution:

V_{NaOH} of 0.1 M HNO_3 used = 0.100 L

m_{NaNO_3} required = CVM

= 0.0900 mol/L × 1.00 L × 84.9949 g/mol

= 7.6495 g

m_{NaNO_3} measured = 7.6496 g

C_{NaNO_3} = (7.6496 g) ÷ (84.9949 g/mol × 1.00 L)

= 0.0900 mol/L

Titration with 0.0100 M KHP

V_{KHP} used = 5.00 mL

n_{KHP} = 0.0100 mol/L × 0.00500 L

= 5.00×10^{-5} mol

Table E.2: Results from titration of 0.0100 M KHP with 0.0100 M NaOH / 0.0900 M $NaNO_3$.

Titration	V_{ini} (mL)	V_{fin} (mL)	V_{Total} (mL)
1	1.66	6.73	5.07
2	2.35	7.47	5.12
3	2.87	8.04	5.17*
4	1.95	7.12	5.17*
5	2.62	7.82	5.20*

Average volume used (*) = 5.18 mL

Since KHP reacts with NaOH in a 1:1 ratio,

C_{NaOH} = 5.00×10^{-5} mol ÷ 0.00518 L

= 0.00966 mol/L

Thus, the actual concentration of 0.0100 M NaOH / 0.0900 M $NaNO_3$ solution is 0.00966 M NaOH / 0.0900 M $NaNO_3$.

0.0500 M HNO_3 / 0.0500 M $NaNO_3$ standard solution:

V_{HNO_3} of 0.1 M HNO_3 used = 0.500 L

m_{NaNO_3} required = CVM

= 0.0500 mol/L × 1.00 L × 84.9949 g/mol

= 4.2497 g

m_{NaNO_3} measured = 4.2500 g

C_{NaNO_3} = (4.2500 g) ÷ (84.9949 g/mol × 1.00 L)

= 0.0500 mol/L

Titration with 0.0495 M NaOH / 0.0500 M $NaNO_3$

V_{NaOH} used = 5.00 mL

n_{NaOH} = 0.0495 mol/L × 0.00500 L

= 2.48×10^{-4} mol

Table E.3: Results from titration of 0.0500 M HNO_3 / 0.0500 M $NaNO_3$ with 0.0495 M NaOH / 0.0500 M $NaNO_3$.

Titration	V_{ini} (mL)	V_{fin} (mL)	V_{Total} (mL)
1	1.51	6.54	5.03*
2	3.34	8.38	5.04*
3	1.30	6.35	5.05*
4	1.43	6.45	5.02

Average volume used (*) = 5.04 mL

Since HNO_3 reacts with NaOH in a 1:1 ratio,

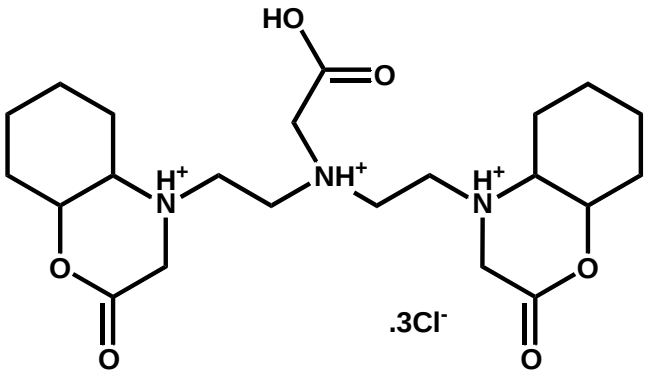
C_{HNO_3} = 2.48×10^{-4} mol ÷ 0.00504 L

= 0.0491 mol/L

Thus, the actual concentration of 0.0500 M HNO_3 / 0.0500 M $NaNO_3$ solution is 0.0491 M HNO_3 / 0.0500 M $NaNO_3$.

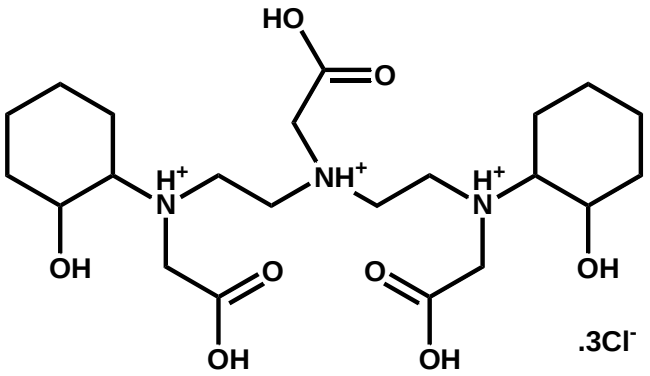
Cy$_2$DETA.3A.3HCl standard solution:

The solution to be prepared was to have an ionic strength of the solution is 0.1 M. The ligand structure as determined by mass spectrometry is shown to be:



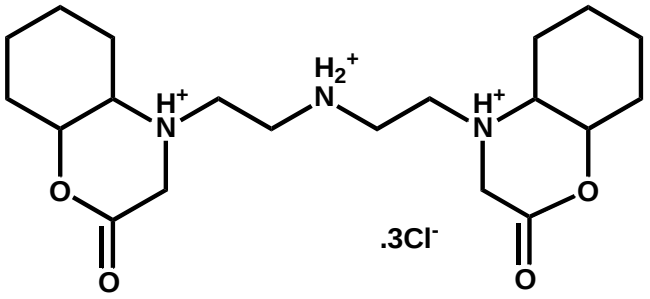
Ionic strength:	0.1	=	$\frac{1}{2} \sum C_i z_i^2$
		=	$\frac{1}{2} [(C \times (+3)^2) + (3C \times (-1)^2)]$
		=	$\frac{1}{2} [(9C) + (3C)]$
		=	6C
	C	=	0.1 ÷ 6
		=	0.0167 mol/L
Mass of ligand required		=	0.0167 mol/L × 0.100 L × 546.9177 g/mol
		=	0.9134 g
Mass measured		=	0.9118 g
$C_{Cy_2DETA.3A.3HCl}$		=	(0.9118 g) ÷ (0.100 L × 546.9177 g/mol)
		=	0.0166 mol/L
Ionic strength		=	$6 \times C_{Cy_2DETA.3A.3HCl}$
		=	0.100 mol/L

The morpholone moieties undergo hydrolysis in aqueous solution (with no change in ligand concentration), affording the tricarboxylate structure:



Cy_2DETA.2A.3HCl standard solution:

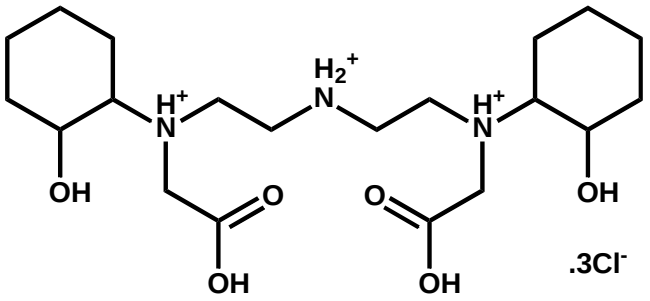
The solution to be prepared was to have an ionic strength of the solution is 0.1 M. The ligand structure as determined by mass spectrometry is shown to be:



Ionic strength:	0.1	=	$\frac{1}{2} \sum C_i z_i^2$
		=	$\frac{1}{2} [(C \times (+3)^2) + (3C \times (-1)^2)]$
		=	$\frac{1}{2} [(9C) + (3C)]$
		=	6C
	C	=	0.1 ÷ 6
		=	0.0167 mol/L
Mass of ligand required		=	0.0167 mol/L × 0.100 L × 488.8811 g/mol
		=	0.8164 g
Mass measured		=	0.8154 g
$C_{Cy_2DETA.2A.3HCl}$		=	(0.8154 g) ÷ (0.100 L × 488.8811 g/mol)
		=	0.0166 mol/L
Ionic strength		=	$6 \times C_{Cy_2DETA.3A.3HCl}$

= 0.0100 mol/L

The morpholone moieties undergo hydrolysis in aqueous solution (with no change in ligand concentration), affording the dicarboxylate structure:



E.2 Determination of pK_a Constants

E.2.1 Cy_2DETA.3A.3HCl pK_a Determination

Electrode Standardization:

The electrode standardization was performed on a solution consisting of 5.00 mL of the 0.0491 M HNO_3 / 0.0500 M $NaNO_3$ standard solution and 15.00 mL of the 0.100 M $NaNO_3$ standard solution. This 20 mL solution was titrated with 10.00 mL of the 0.0492 M NaOH / 0.0500 M $NaNO_3$ standard solution, which was dispensed in 0.50 mL increments. Potential readings were measured upon each increment addition via the glass electrode over a 3 minute period, with a 0.1 mV drift constraint allowed for each reading. The data obtained from this titration are tabulated below.

Table E.4: Electrode standardization raw data.

V_{NaOH} added (mL)	E (mV)	V_{NaOH} added (mL)	E (mV)
0.00	302.9	5.50	-211.8
0.50	300.0	6.00	-232.6
1.00	296.2	6.50	-243.2
1.50	292.6	7.00	-250.3
2.00	287.8	7.50	-256.0
2.50	283.0	8.00	-259.8
3.00	276.6	8.50	-263.6
3.50	268.7	9.00	-266.2
4.00	258.2	9.50	-269.1
4.50	240.2	10.00	-271.3
5.00	155.0		

pK_a determination:

The pK_a determination was performed on a solution consisting of 5.00 mL of the 0.0167 mol/L Cy_2DETA.3A.3HCl standard solution and 15.00 mL of the 0.1 M $NaNO_3$ standard solution. This 20 mL solution was titrated with the 0.00966 M NaOH / 0.0900 M $NaNO_3$, which was dispensed in 0.10 mL increments. Potential readings were measured upon each

increment addition via the glass electrode over a 3 minute period, with a 0.1 mV drift constraint allowed for each reading. The data obtained from this titration are tabulated below.

Table E.5: Cy_2DETA.3A.3HCl pK_a determination raw data.

V_{NaOH} added (mL)	E (mV)	V_{NaOH} added (mL)	E (mV)	V_{NaOH} added (mL)	E (mV)	V_{NaOH} added (mL)	E (mV)
0.00	294.6	15.10	251.6	30.20	-42.6	45.30	-186.6
0.10	294.3	15.20	251.2	30.30	-45.1	45.40	-187.2
0.20	294.1	15.30	250.7	30.40	-47.7	45.50	-187.3
0.30	293.5	15.40	250.5	30.50	-50.1	45.60	-187.9
0.40	293.4	15.50	250.1	30.60	-52.3	45.70	-188.5
0.50	293.2	15.60	249.5	30.70	-54.3	45.80	-188.6
0.60	292.9	15.70	249.2	30.80	-56.3	45.90	-189.0
0.70	292.5	15.80	249.1	30.90	-58.0	46.00	-189.4
0.80	292.5	15.90	248.4	31.00	-60.0	46.10	-189.7
0.90	292.0	16.00	247.9	31.10	-61.8	46.20	-190.1
1.00	291.8	16.10	247.7	31.20	-63.5	46.30	-190.6
1.10	291.7	16.20	247.2	31.30	-65.2	46.40	-190.7
1.20	291.4	16.30	247.0	31.40	-66.7	46.50	-191.4
1.30	291.1	16.40	246.4	31.50	-68.2	46.60	-191.8
1.40	291.0	16.50	246.1	31.60	-69.9	46.70	-192.0
1.50	290.3	16.60	245.7	31.70	-71.2	46.80	-192.2
1.60	290.1	16.70	244.8	31.80	-72.6	46.90	-192.5
1.70	290.0	16.80	244.8	31.90	-73.8	47.00	-193.1
1.80	289.8	16.90	244.2	32.00	-75.2	47.10	-193.1
1.90	289.6	17.00	243.7	32.10	-76.7	47.20	-193.8
2.00	289.2	17.10	243.0	32.20	-78.0	47.30	-194.2
2.10	289.0	17.20	242.6	32.30	-79.3	47.40	-194.1
2.20	288.6	17.30	242.2	32.40	-80.5	47.50	-194.8
2.30	288.4	17.40	241.7	32.50	-81.9	47.60	-194.9
2.40	288.1	17.50	241.4	32.60	-83.0	47.70	-195.1
2.50	287.9	17.60	240.7	32.70	-84.1	47.80	-195.5
2.60	287.6	17.70	240.5	32.80	-85.6	47.90	-196.2
2.70	287.5	17.80	239.7	32.90	-86.9	48.00	-196.3
2.80	287.5	17.90	239.3	33.00	-87.9	48.10	-196.6
2.90	287.1	18.00	238.7	33.10	-89.3	48.20	-196.8
3.00	286.7	18.10	238.3	33.20	-90.4	48.30	-197.2
3.10	286.6	18.20	237.9	33.30	-91.2	48.40	-197.4
3.20	286.4	18.30	237.4	33.40	-92.6	48.50	-197.6
3.30	286.2	18.40	236.8	33.50	-93.9	48.60	-198.1
3.40	285.8	18.50	236.5	33.60	-94.8	48.70	-198.6

3.50	285.4	18.60	235.9	33.70	-95.8	48.80	-198.7
3.60	285.2	18.70	235.4	33.80	-96.9	48.90	-199.1
3.70	284.9	18.80	234.8	33.90	-98.0	49.00	-199.4
3.80	284.6	18.90	234.2	34.00	-99.5	49.10	-199.6
3.90	284.6	19.00	233.5	34.10	-100.2	49.20	-199.9
4.00	284.3	19.10	233.0	34.20	-101.6	49.30	-200.4
4.10	283.9	19.20	232.7	34.30	-102.4	49.40	-200.4
4.20	283.9	19.30	231.7	34.40	-103.9	49.50	-200.8
4.30	283.7	19.40	231.2	34.50	-104.8	49.60	-201.0
4.40	283.5	19.50	230.7	34.60	-105.6	49.70	-201.4
4.50	283.2	19.60	230.1	34.70	-106.7	49.80	-201.4
4.60	282.6	19.70	229.6	34.80	-108.2	49.90	-201.7
4.70	282.6	19.80	229.0	34.90	-109.2	50.00	-202.2
4.80	282.4	19.90	228.1	35.00	-110.1	50.10	-202.5
4.90	282.2	20.00	227.7	35.10	-111.4	50.20	-202.8
5.00	281.8	20.10	226.9	35.20	-112.5	50.30	-203.1
5.10	281.5	20.20	226.2	35.30	-113.4	50.40	-203.2
5.20	281.4	20.30	225.9	35.40	-114.5	50.50	-203.3
5.30	281.2	20.40	225.4	35.50	-115.4	50.60	-203.5
5.40	280.9	20.50	224.3	35.60	-116.6	50.70	-204.2
5.50	280.6	20.60	223.7	35.70	-117.7	50.80	-204.1
5.60	280.3	20.70	223.2	35.80	-118.8	50.90	-204.4
5.70	279.9	20.80	222.5	35.90	-119.8	51.00	-204.9
5.80	279.9	20.90	221.8	36.00	-120.8	51.10	-204.9
5.90	279.3	21.00	220.9	36.10	-121.9	51.20	-205.0
6.00	279.4	21.10	220.6	36.20	-123.1	51.30	-205.3
6.10	279.1	21.20	219.7	36.30	-124.1	51.40	-205.8
6.20	279.0	21.30	218.9	36.40	-125.3	51.50	-206.0
6.30	278.4	21.40	218.5	36.50	-126.3	51.60	-206.3
6.40	278.1	21.50	217.7	36.60	-127.2	51.70	-206.4
6.50	277.9	21.60	216.7	36.70	-128.0	51.80	-206.5
6.60	277.9	21.70	216.1	36.80	-129.6	51.90	-206.8
6.70	277.5	21.80	215.4	36.90	-130.2	52.00	-207.0
6.80	277.4	21.90	214.9	37.00	-131.5	52.10	-207.4
6.90	277.1	22.00	213.7	37.10	-132.3	52.20	-207.9
7.00	276.7	22.10	213.0	37.20	-133.5	52.30	-207.9
7.10	276.3	22.20	212.6	37.30	-134.7	52.40	-208.0
7.20	276.0	22.30	211.5	37.40	-135.4	52.50	-208.4
7.30	275.9	22.40	210.8	37.50	-136.2	52.60	-208.7
7.40	275.6	22.50	210.0	37.60	-137.7	52.70	-208.7
7.50	275.3	22.60	209.1	37.70	-138.2	52.80	-209.0
7.60	275.0	22.70	208.3	37.80	-139.3	52.90	-209.2
7.70	275.1	22.80	207.4	37.90	-140.3	53.00	-209.4

7.80	274.8	22.90	206.6	38.00	-141.2	53.10	-209.8
7.90	274.1	23.00	205.9	38.10	-142.4	53.20	-210.0
8.00	274.2	23.10	205.2	38.20	-143.1	53.30	-209.9
8.10	273.6	23.20	204.3	38.30	-144.3	53.40	-210.2
8.20	273.7	23.30	203.3	38.40	-145.1	53.50	-210.8
8.30	273.2	23.40	202.4	38.50	-145.8	53.60	-210.7
8.40	272.9	23.50	201.8	38.60	-146.5	53.70	-211.2
8.50	272.6	23.60	200.8	38.70	-147.9	53.80	-211.1
8.60	272.5	23.70	199.9	38.80	-148.3	53.90	-211.2
8.70	272.2	23.80	198.8	38.90	-149.4	54.00	-211.5
8.80	271.9	23.90	198.0	39.00	-150.3	54.10	-212.0
8.90	271.6	24.00	196.9	39.10	-151.3	54.20	-212.2
9.00	271.4	24.10	196.1	39.20	-152.1	54.30	-212.4
9.10	271.1	24.20	195.0	39.30	-152.9	54.40	-212.5
9.20	270.7	24.30	193.9	39.40	-153.5	54.50	-212.5
9.30	270.7	24.40	193.3	39.50	-154.2	54.60	-212.7
9.40	270.2	24.50	192.1	39.60	-155.0	54.70	-213.0
9.50	269.9	24.60	191.2	39.70	-155.7	54.80	-213.4
9.60	269.5	24.70	189.9	39.80	-156.4	54.90	-213.2
9.70	269.4	24.80	189.2	39.90	-157.4	55.00	-213.7
9.80	269.1	24.90	188.0	40.00	-158.1	55.10	-123.8
9.90	268.8	25.00	186.9	40.10	-159.1	55.20	-214.2
10.00	268.6	25.10	185.6	40.20	-159.5	55.30	-214.0
10.10	268.2	25.20	184.9	40.30	-160.1	55.40	-214.2
10.20	268.0	25.30	183.3	40.40	-160.8	55.50	-214.4
10.30	267.8	25.40	182.2	40.50	-161.5	55.60	-215.0
10.40	267.2	25.50	181.1	40.60	-162.1	55.70	-214.8
10.50	267.0	25.60	179.9	40.70	-163.0	55.80	-215.3
10.60	267.0	25.70	178.6	40.80	-163.8	55.90	-215.5
10.70	266.5	25.80	177.6	40.90	-164.1	56.00	-215.7
10.80	266.0	25.90	176.4	41.00	-165.1	56.10	-216.0
10.90	265.8	26.00	174.8	41.10	-165.7	56.20	-216.0
11.00	265.4	26.10	173.4	41.20	-166.5	56.30	-216.0
11.10	265.2	26.20	172.2	41.30	-166.8	56.40	-216.4
11.20	265.0	26.30	170.5	41.40	-167.3	56.50	-216.6
11.30	264.6	26.40	168.9	41.50	-168.0	56.60	-216.6
11.40	264.6	26.50	167.7	41.60	-168.8	56.70	-216.7
11.50	264.1	26.60	166.2	41.70	-169.5	56.80	-217.2
11.60	264.0	26.70	164.4	41.80	-169.8	56.90	-217.3
11.70	263.3	26.80	162.6	41.90	-170.2	57.00	-217.4
11.80	263.2	26.90	160.9	42.00	-171.2	57.10	-217.6
11.90	263.1	27.00	158.8	42.10	-171.3	57.20	-217.7
12.00	262.6	27.10	156.9	42.20	-172.0	57.30	-218.0

12.10	262.4	27.20	154.7	42.30	-172.4	57.40	-218.2
12.20	262.1	27.30	152.5	42.40	-173.0	57.50	-218.3
12.30	261.4	27.40	150.3	42.50	-173.6	57.60	-218.3
12.40	261.2	27.50	147.5	42.60	-174.4	57.70	-218.7
12.50	261.1	27.60	144.8	42.70	-174.6	57.80	-219.0
12.60	260.4	27.70	142.2	42.80	-175.3	57.90	-219.1
12.70	260.1	27.80	138.8	42.90	-176.1	58.00	-219.1
12.80	259.9	27.90	135.6	43.00	-176.5	58.10	-219.7
12.90	259.5	28.00	131.6	43.10	-176.6	58.20	-219.8
13.00	259.1	28.10	127.1	43.20	-177.3	58.30	-219.9
13.10	259.1	28.20	122.3	43.30	-177.8	58.40	-219.8
13.20	258.7	28.30	116.5	43.40	-178.4	58.50	-220.0
13.30	258.3	28.40	109.8	43.50	-178.9	58.60	-220.2
13.40	258.1	28.50	101.9	43.60	-179.2	58.70	-220.3
13.50	257.8	28.60	92.5	43.70	-179.6	58.80	-220.7
13.60	257.4	28.70	81.0	43.80	-180.3	58.90	-220.8
13.70	256.7	28.80	67.5	43.90	-180.6	59.00	-221.0
13.80	256.5	28.90	52.4	44.00	-181.1	59.10	-221.2
13.90	256.0	29.00	35.9	44.10	-181.5	59.20	-221.4
14.00	255.7	29.10	21.5	44.20	-181.9	59.30	-221.3
14.10	255.4	29.20	8.9	44.30	-182.5	59.40	-221.5
14.20	255.2	29.30	-1.0	44.40	-183.1	59.50	-221.7
14.30	254.7	29.40	-8.8	44.50	-183.1	59.60	-221.9
14.40	254.2	29.50	-15.4	44.60	-183.6	59.70	-222.3
14.50	254.2	29.60	-20.6	44.70	-184.3	59.80	-222.1
14.60	253.8	29.70	-25.3	44.80	-184.8	59.90	-222.7
14.70	253.4	29.80	-29.9	44.90	-184.9	60.00	-222.6
14.80	252.8	29.90	-33.2	45.00	-185.4		
14.90	252.3	30.00	-36.6	45.10	-186.0		
15.00	252.1	30.10	-39.9	45.20	-186.2		

E.2.2 Cy_2DETA.2A.3HCl pK_a Determination

Electrode Standardization:

The electrode standardization was performed on a solution consisting of 5.00 mL of the 0.0494 M HNO_3 / 0.0500 M $NaNO_3$ standard solution and 15.00 mL of the 0.100 M $NaNO_3$ standard solution. This 20.00 mL solution was titrated with 10.00 mL of the 0.0481 M NaOH / 0.0500 M $NaNO_3$ standard solution, which was dispensed in 0.5.0 mL increments. Potential readings were measured upon each increment addition via the glass electrode over a 3 minute

period, with a 0.1 mV drift constraint allowed for each reading. The data obtained from this titration are tabulated below.

Table E.6: Electrode standardization raw data.

V_{NaOH} added (mL)	E (mV)	V_{NaOH} added (mL)	E (mV)
0.00	301.5	5.50	-213.7
0.50	298.1	6.00	-235.0
1.00	294.5	6.50	-245.6
1.50	290.8	7.00	-252.8
2.00	286.1	7.50	-258.0
2.50	280.9	8.00	-262.2
3.00	274.7	8.50	-265.7
3.50	267.0	9.00	-268.3
4.00	256.2	9.50	-271.0
4.50	238.3	10.00	-273.1
5.00	152.1		

pK_a determination:

The pK_a determination was performed on a solution consisting of 5.00 mL of the 0.0167 mol/L Cy_2DETA.2A.3HCl standard solution and 15.00 mL of the 0.100 M $NaNO_3$ standard solution. This 20.00 mL solution was titrated with the 0.00959 M NaOH / 0.0900 M $NaNO_3$, which was dispensed in 0.100 mL increments. Potential readings were measured upon each increment addition via the glass electrode over a 3 minute period, with a 0.1 mV drift constraint allowed for each reading. The data obtained from this titration are tabulated below.

Table E.7: Cy_2DETA.2A.3HCl pK_a determination raw data.

V_{NaOH} added (mL)	E (mV)	V_{NaOH} added (mL)	E (mV)	V_{NaOH} added (mL)	E (mV)	V_{NaOH} added (mL)	E (mV)
0.00	272.8	12.60	174.7	25.20	-69.1	37.80	-213.2
0.10	272.5	12.70	172.9	25.30	-70.6	37.90	-213.6
0.20	271.9	12.80	171.6	25.40	-71.7	38.00	-213.8
0.30	271.5	12.90	169.8	25.50	-73.1	38.10	-213.9
0.40	271.2	13.00	168.5	25.60	-74.1	38.20	-214.2
0.50	270.6	13.10	166.8	25.70	-75.3	38.30	-214.7
0.60	270.4	13.20	164.9	25.80	-76.8	38.40	-214.7

0.70	269.9	13.30	163.3	25.90	-77.9	38.50	-215.1
0.80	269.5	13.40	161.7	26.00	-79.2	38.60	-215.8
0.90	269.1	13.50	159.6	26.10	-80.6	38.70	-215.9
1.00	268.5	13.60	158.0	26.20	-81.5	38.80	-216.2
1.10	268.1	13.70	156.1	26.30	-82.8	38.90	-216.5
1.20	267.6	13.80	154.4	26.40	-84.0	39.00	-216.5
1.30	267.5	13.90	152.4	26.50	-85.4	39.10	-216.9
1.40	266.7	14.00	150.9	26.60	-86.8	39.20	-217.4
1.50	266.4	14.10	148.7	26.70	-87.7	39.30	-217.6
1.60	266.0	14.20	146.9	26.80	-89.0	39.40	-217.7
1.70	265.5	14.30	145.1	26.90	-90.6	39.50	-218.1
1.80	265.1	14.40	143.5	27.00	-91.8	39.60	-218.1
1.90	264.5	14.50	141.6	27.10	-92.9	39.70	-218.6
2.00	264.0	14.60	139.6	27.20	-94.3	39.80	-218.9
2.10	263.6	14.70	137.9	27.30	-95.7	39.90	-219.1
2.20	263.4	14.80	135.9	27.40	-97.0	40.00	-219.4
2.30	262.7	14.90	134.1	27.50	-98.0	40.10	-219.4
2.40	262.3	15.00	132.3	27.60	-99.4	40.20	-219.8
2.50	262.0	15.10	130.6	27.70	-101.1	40.30	-219.8
2.60	261.5	15.20	129.2	27.80	-102.4	40.40	-220.0
2.70	260.9	15.30	127.5	27.90	-103.7	40.50	-220.4
2.80	260.5	15.40	125.6	28.00	-105.1	40.60	-220.4
2.90	260.1	15.50	124.0	28.10	-106.5	40.70	-220.9
3.00	259.4	15.60	122.4	28.20	-108.1	40.80	-221.0
3.10	259.0	15.70	120.7	28.30	-109.7	40.90	-221.2
3.20	258.4	15.80	119.3	28.40	-111.1	41.00	-221.3
3.30	258.0	15.90	117.6	28.50	-112.8	41.10	-221.9
3.40	257.4	16.00	116.4	28.60	-114.0	41.20	-222.1
3.50	256.8	16.10	114.8	28.70	-115.6	41.30	-222.2
3.60	256.3	16.20	113.1	28.80	-117.4	41.40	-222.4
3.70	255.7	16.30	111.9	28.90	-119.2	41.50	-222.6
3.80	255.3	16.40	110.4	29.00	-120.8	41.60	-222.7
3.90	254.6	16.50	108.7	29.10	-122.4	41.70	-222.8
4.00	254.4	16.60	107.5	29.20	-124.1	41.80	-223.2
4.10	253.7	16.70	106.2	29.30	-126.2	41.90	-223.1
4.20	253.1	16.80	104.7	29.40	-127.7	42.00	-223.6
4.30	252.8	16.90	103.1	29.50	-129.6	42.10	-223.8
4.40	252.0	17.00	101.8	29.60	-131.3	42.20	-224.0
4.50	251.4	17.10	100.3	29.70	-133.4	42.30	-224.0
4.60	250.9	17.20	99.1	29.80	-135.3	42.40	-224.0
4.70	250.3	17.30	97.7	29.90	-137.2	42.50	-224.5
4.80	249.6	17.40	96.3	30.00	-139.1	42.60	-224.5
4.90	249.1	17.50	95.1	30.10	-141.1	42.70	-224.9

5.00	248.4	17.60	93.6	30.20	-143.0	42.80	-224.7
5.10	248.0	17.70	92.2	30.30	-144.5	42.90	-225.3
5.20	247.2	17.80	90.9	30.40	-146.5	43.00	-225.4
5.30	246.7	17.90	89.5	30.50	-148.4	43.10	-225.2
5.40	242.2	18.00	88.1	30.60	-150.4	43.20	-225.5
5.50	245.4	18.10	86.7	30.70	-152.0	43.30	-225.7
5.60	244.7	18.20	85.3	30.80	-154.0	43.40	-225.6
5.70	244.1	18.30	83.9	30.90	-155.9	43.50	-225.9
5.80	243.7	18.40	82.5	31.00	-157.3	43.60	-226.0
5.90	242.9	18.50	80.9	31.10	-159.3	43.70	-226.2
6.00	242.3	18.60	79.7	31.20	-160.7	43.80	-226.5
6.10	241.6	18.70	77.9	31.30	-162.8	43.90	-226.8
6.20	240.8	18.80	76.4	31.40	-164.3	44.00	-227.0
6.30	240.0	18.90	75.1	31.50	-165.6	44.10	-226.9
6.40	239.3	19.00	73.4	31.60	-167.4	44.20	-226.9
6.50	238.7	19.10	71.9	31.70	-168.7	44.30	-227.3
6.60	237.9	19.20	70.1	31.80	-170.0	44.40	-227.2
6.70	237.3	19.30	68.7	31.90	-171.4	44.50	-227.6
6.80	236.4	19.40	66.7	32.00	-172.8	44.60	-227.8
6.90	235.9	19.50	65.1	32.10	-174.3	44.70	-227.6
7.00	234.9	19.60	63.4	32.20	-175.5	44.80	-227.9
7.10	234.4	19.70	61.4	32.30	-176.5	44.90	-228.0
7.20	233.5	19.80	59.7	32.40	-178.1	45.00	-228.0
7.30	232.5	19.90	57.7	32.50	-179.1	45.10	-228.1
7.40	232.0	20.00	55.4	32.60	-180.0	45.20	-228.5
7.50	231.3	20.10	53.1	32.70	-181.6	45.30	-228.5
7.60	230.2	20.20	51.2	32.80	-182.6	45.40	-228.8
7.70	229.3	20.30	48.6	32.90	-183.4	45.50	-228.7
7.80	228.6	20.40	46.5	33.00	-184.5	45.60	-228.8
7.90	227.9	20.50	43.5	33.10	-185.3	45.70	-229.0
8.00	226.7	20.60	41.1	33.20	-186.6	45.80	-229.3
8.10	226.0	20.70	38.3	33.30	-187.6	45.90	-229.1
8.20	225.0	20.80	35.4	33.40	-188.2	46.00	-229.5
8.30	224.3	20.90	31.7	33.50	-189.3	46.10	-229.6
8.40	223.3	21.00	28.7	33.60	-189.8	46.20	-229.6
8.50	222.6	21.10	25.0	33.70	-190.9	46.30	-229.9
8.60	221.7	21.20	21.3	33.80	-192.0	46.40	-229.6
8.70	220.4	21.30	17.7	33.90	-192.4	46.50	-229.7
8.80	219.6	21.40	13.9	34.00	-193.3	46.60	-230.3
8.90	218.5	21.50	9.6	34.10	-194.1	46.70	-230.0
9.00	217.6	21.60	5.7	34.20	-194.9	46.80	-230.0
9.10	216.7	21.70	1.8	34.30	-195.7	46.90	-230.6
9.20	216.0	21.80	-1.8	34.40	-196.3	47.00	-230.6

9.30	214.8	21.90	-5.5	34.50	-197.0	47.10	-230.5
9.40	213.9	22.00	-9.1	34.60	-197.6	47.20	-230.5
9.50	212.7	22.10	-12.2	34.70	-198.5	47.30	-231.0
9.60	211.9	22.20	-15.7	34.80	-199.1	47.40	-230.9
9.70	210.8	22.30	-18.5	34.90	-199.5	47.50	-230.8
9.80	209.8	22.40	-21.5	35.00	-200.4	47.60	-231.3
9.90	208.8	22.50	-24.1	35.10	-200.6	47.70	-231.4
10.00	207.7	22.60	-26.7	35.20	-201.3	47.80	-231.1
10.10	206.4	22.70	-29.0	35.30	-202.2	47.90	-231.6
10.20	205.3	22.80	-31.1	35.40	-202.7	48.00	-231.3
10.30	204.1	22.90	-33.6	35.50	-203.0	48.10	-231.8
10.40	203.2	23.00	-35.4	35.60	-203.7	48.20	-231.5
10.50	201.9	23.10	-37.5	35.70	-204.2	48.30	-231.7
10.60	200.7	23.20	-39.4	35.80	-204.5	48.40	-232.1
10.70	199.9	23.30	-41.2	35.90	-205.0	48.50	-232.1
10.80	198.5	23.40	-43.1	36.00	-205.6	48.60	-231.9
10.90	197.3	23.50	-44.9	36.10	-206.1	48.70	-232.2
11.00	196.3	23.60	-46.7	36.20	-206.8	48.80	-232.2
11.10	195.1	23.70	-48.2	36.30	-207.3	48.90	-232.5
11.20	194.0	23.80	-50.0	36.40	-207.5	49.00	-232.4
11.30	192.6	23.90	-51.5	36.50	-207.8	49.10	-232.5
11.40	191.3	24.00	-53.1	36.60	-208.2	49.20	-232.5
11.50	189.9	24.10	-54.4	36.70	-209.0	49.30	-232.5
11.60	188.6	24.20	-56.1	36.80	-209.2	49.40	-232.7
11.70	187.3	24.30	-57.4	36.90	-209.8	49.50	-233.0
11.80	186.1	24.40	-58.7	37.00	-210.1	49.60	-232.8
11.90	184.7	24.50	-60.1	37.10	-210.4	49.70	-232.8
12.00	183.2	24.60	-61.6	37.20	-211.0	49.80	-232.9
12.10	181.9	24.70	-62.8	37.30	-211.4	49.90	-233.0
12.20	180.5	24.80	-64.2	37.40	-211.6	50.00	-233.0
12.30	179.2	24.90	-65.4	37.50	-211.7		
12.40	177.8	25.00	-66.9	37.60	-212.1		
12.50	176.2	25.10	-67.8	37.70	-212.9		

Appendix F – Luminescence Data

F.1 Cy_2DETA.3A.3HCl / Eu(III)

The luminescence properties of the Cy_2DETA.3A.3HCl / Eu(III) system were investigated as a function of pH.

F.1.1 Cy_2DETA.3A.3HCl / Eu(III), aqueous solution

Cy_2DETA.3A.3HCl (0.0423 g, 7.73×10^{-5} mol) and $Eu(CF_3SO_3)_3$ (0.0467 g, 7.79×10^{-5} mol) were dissolved in deionised water, in a 250 mL volumetric flask. The solution was placed in a jacketed-cell (25 °C). An in-cell titration was performed using concentrated acid (HCl) and concentrated base (NaOH) solutions. Upon each addition of acid or base, the pH of the solution was allowed to stabilize and the pH value recorded. A small quantity of the pH-adjusted solution was decanted and sealed in a marked vial prior to each subsequent pH adjustment, to obtain a series of solutions between pH 2.1 and pH 10.7, in intervals of approximately 0.2 pH units. The solutions were allowed to reach equilibrium over 24 hours.

The absorbance of the Cy_2DETA.3A.3HCl / Eu(III) stock solution was measured in order to determine the wavelength to be used for excitation in the luminescence study (Figure F.1).

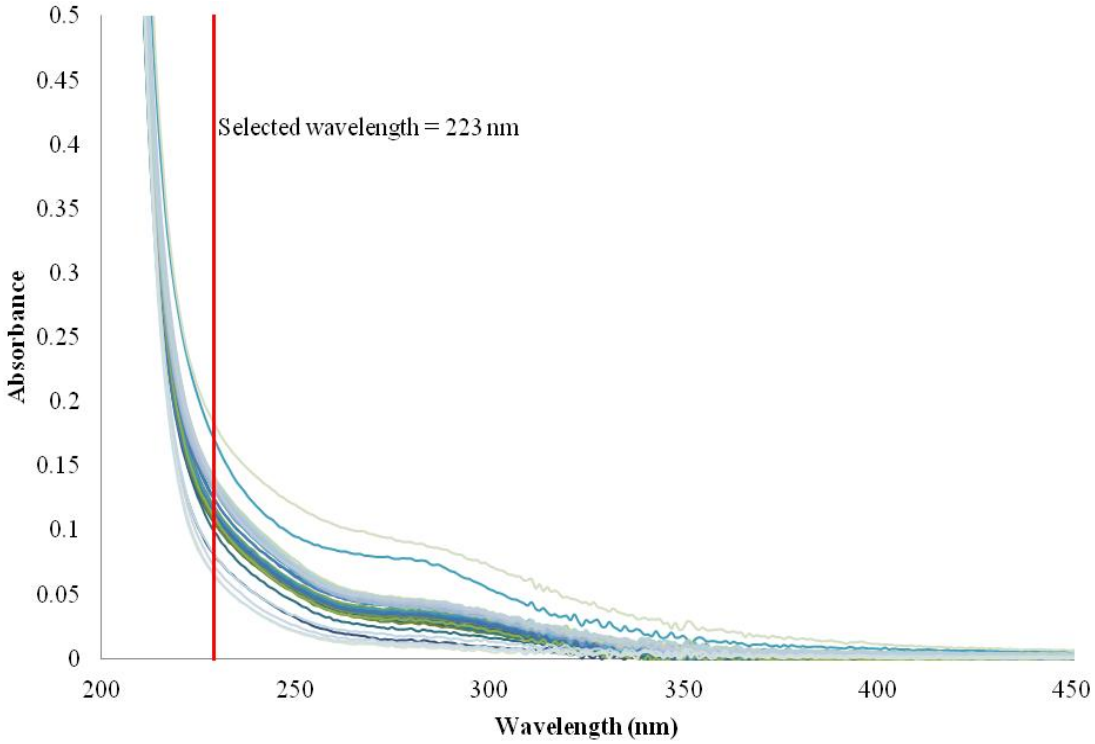


Figure F.1: Absorbance spectrum of europium(III)-1,7-bis(2-hydroxycyclohexyl)-1,4,7-tris(carboxymethyl)-1,4,7 triazaheptane, as a function of pH.

Solution pH was measured after 24 hours, prior to each absorbance and luminescence measurement. The absorbance was measured over a range of 200 nm and 800 nm.

Phosphorescence emission spectra were recorded by exciting each sample at a wavelength of 223 nm. The spectrum was recorded in the high sensitivity mode, over a range of 550 nm to 750 nm. Each measurement was recorded after a 0.100 ms time delay, with both the excitation and emission slit widths set at 10 nm.

The following table consists of peak maxima intensity values for each observable emission band as a function of pH.

Table F.1: Cy_2DETA.3A.3HCl / Eu(III) phosphorescence emission raw data, λ_{ex} = 223 nm.

Sample	pH (before equilibration)	pH (after 24 hours equilibration)	Emission Intensity (592 nm)	Emission Intensity (617 nm)	Emission Intensity (693 nm)
1	2.948	3.012	99.92763519	193.5462952	81.52636719
2	3.103	3.194	123.1015015	237.8143768	103.6033707
3	3.303	3.381	134.5740204	263.5475159	117.4717789
4	3.514	3.715	151.3382568	319.1391296	130.3235931
5	3.706	3.948	162.851532	335.619812	139.6173706
6	3.908	4.137	179.0344086	328.9893494	141.3311615
7	4.105	4.559	170.2513733	333.6289368	142.9643707
8	4.320	4.857	180.2544556	336.7661133	143.0785675
9	4.521	5.196	170.4214783	333.5965576	144.6949921
10	4.721	5.509	169.9094696	339.7315063	136.6000824
11	4.909	5.528	179.0996704	333.6923828	138.5876617
12	5.130	5.664	175.4572754	336.2967529	141.1024628
13	5.358	5.893	177.9445496	338.2461243	138.4495087
14	5.658	5.851	179.2754059	335.0730591	133.6493835
15	5.939	6.418	174.8527527	334.5765991	141.9940491
16	6.098	6.053	176.595459	339.833313	143.7406616
17	6.267	6.044	170.4083557	338.7950745	144.8253479
18	6.460	6.076	181.4172668	333.5600281	145.1815338
19	6.671	6.182	170.3503265	348.4901733	143.9003601
20	6.832	6.133	172.8847198	336.2259827	142.6092072
21	6.997	6.854	175.3621521	344.0865173	146.6138
22	7.192	6.956	174.5863037	337.502533	139.7497406
23	7.352	6.711	176.9084473	337.8465881	143.9317932
24	7.519	6.895	174.4372406	347.6579895	141.4434967
25	7.747	7.089	181.5839233	345.5848999	142.6226959
26	7.959	7.017	174.1999207	341.0187073	143.25383
27	8.165	7.057	170.3141632	346.6674194	140.0263519
28	8.360	7.180	167.1680908	336.6755676	134.5274811
29	8.515	7.243	176.0109863	334.0911865	139.0685577
30	8.664	6.580	187.8310394	358.5149841	152.3211823
31	8.808	7.149	168.6457825	337.8223267	134.9651489
32	8.935	7.074	169.5627747	347.5139465	141.5399017
33	9.040	7.225	162.8784637	352.1890564	141.6610107
34	9.175	7.250	167.9205933	344.286377	143.0201111
35	9.305	7.316	160.9845581	331.3921204	134.8436279
36	9.426	7.434	176.8371735	338.1531677	137.6282654
37	9.547	7.150	167.9003448	347.1465454	141.2612762
38	9.693	7.354	175.8196411	348.3270569	139.4285889
39	9.810	7.513	170.9747009	344.1121826	136.7444916
40	9.926	8.800	177.0696106	339.2236023	134.9824829
41	10.110	8.691	172.4522858	344.2175293	136.0027161

42	10.314	9.584	167.9490356	349.2673035	136.7655945
43	10.522	10.138	170.4555664	375.7345581	133.9903259
44	10.741	10.772	173.063858	424.3929138	122.6833038
45	2.782	2.836	67.17861176	126.4140244	58.34745407
46	2.552	2.587	25.91554451	46.45936966	21.90435982
47	2.387	2.420	18.43094826	26.36117744	13.6344347
48	2.189	2.203	13.63684082	16.8491993	5.804768562

F.1.2 Cy_2DETA.3A.3HCl / Eu(III), multi-component buffered system, no equilibration

Cy_2DETA.3A.3HCl (0.0206 g, 3.77×10^{-5} mol) and $Eu(CF_3SO_3)_3$ (0.0231 g, 3.86×10^{-5} mol) were dissolved in deionised water, in a 250 mL volumetric flask. To this flask, 37.5 μL of a 0.1 mol/L solution consisting of the buffers KHP, MES, CHES, MOPS, and Tris was added and the contents diluted to the mark. This solution was placed in a jacketed-cell (25 °C). An in-cell titration was performed on the solution using concentrated HCl and NaOH solutions. Upon each addition of acid or base, the pH of the solution was allowed to stabilize and the pH value recorded. A small volume of the adjusted solution was decanted into a marked vial before the next pH adjustment was made. The procedure was repeated to obtain a series of solutions between pH 2.0 and pH 12.1, in intervals of 0.2 pH units. The absorbance and luminescence of these solutions were immediately measured.

The absorbance of the Cy_2DETA.3A.3HCl / Eu(III) stock solution was measured in order to determine the excitation wavelengths for the luminescence study. The absorbance was measured over a range of 200 nm and 800 nm.

The phosphorescence emission spectrum was measured by exciting each sample at a wavelength of 229 nm and 279 nm (Figure F.2). The spectrum was recorded in the high sensitivity mode, over a range of 550 nm to 750 nm. Each measurement was recorded after a 0.100 ms time delay, with both the excitation and emission slit widths set at 10 nm.

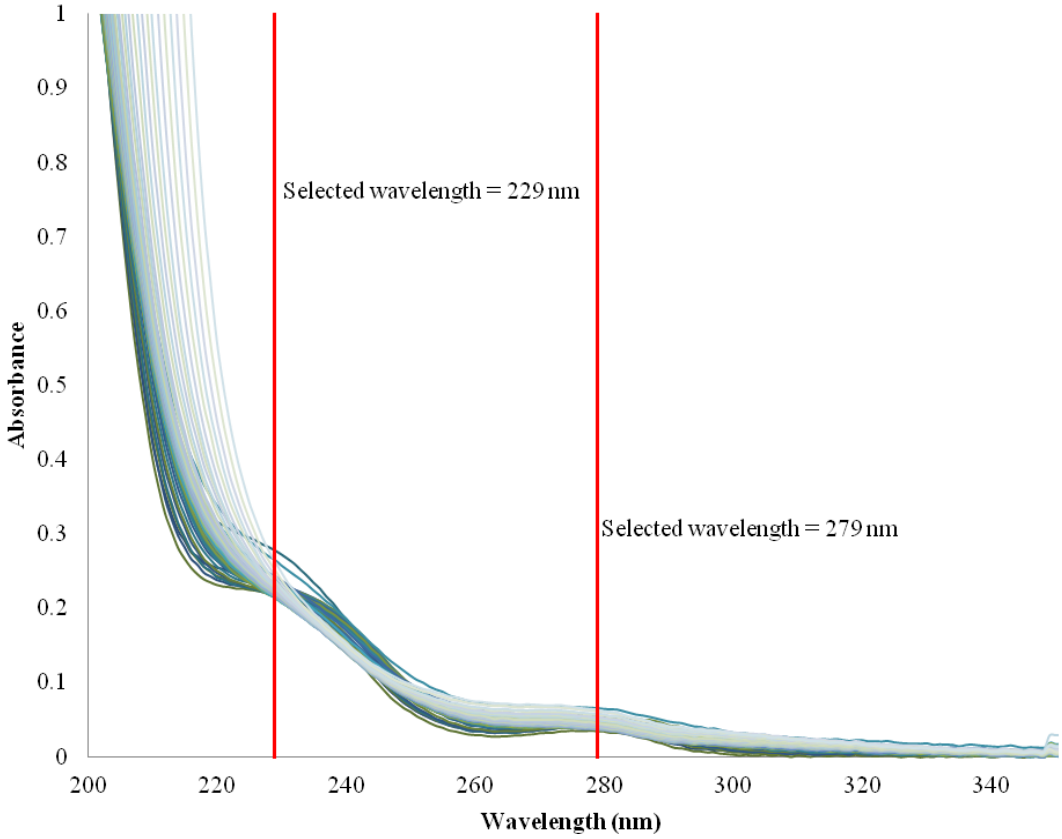


Figure F.2: Absorbance spectrum of europium(III)-1,7-bis(2-hydroxycyclohexyl)-1,4,7-tris(carboxymethyl)-1,4,7 triazaheptane, in a buffered solution, as a function of pH.

The following tables consist of peak maxima intensity values for each observable emission band as a function of pH.

Table F.2: $Cy_2DETA.3A.3HCl$ / Eu(III) phosphorescence emission raw data, λ_{ex} = 279 nm (multi-component buffered system, no equilibration).

Sample	pH	Emission Intensity (592nm)	Emission Intensity (617nm)	Emission Intensity (697nm)
1	2.007	4.345597744	2.488910913	2.012583733
2	2.133	5.562414646	3.037495136	2.819995165
3	2.264	7.304688931	3.613711596	3.345346451
4	2.392	7.973195553	4.742871284	4.23304081
5	2.523	10.72001648	6.366619587	6.076082706
6	2.654	13.76766872	9.596113205	7.276258469
7	2.783	16.2179203	14.8301363	9.175670624
8	2.912	19.22141457	21.2084198	11.54678249
9	3.045	22.44145203	28.71180534	14.00368786
10	3.172	24.851717	34.26426315	15.53194904
11	3.304	26.49123573	39.20600128	16.97757339
12	3.437	28.17985916	43.42562103	17.99956703

13	3.564	30.14788246	47.22248459	20.09839058
14	3.691	30.09975815	49.79901505	20.01900482
15	3.824	31.76021194	51.41076279	20.76934242
16	3.957	33.22105789	55.54843903	22.4538517
17	4.084	31.99722672	56.92246246	22.23800087
18	4.212	32.64025879	56.02349091	23.02714729
19	4.347	34.64782333	59.21998215	22.8061676
20	4.471	35.33437729	61.00243759	24.12589836
21	4.608	37.80475235	62.54385757	25.55380821
22	4.731	38.08469009	63.46619797	24.47980309
23	4.872	38.36476898	62.89335251	25.03877449
24	5.006	40.78576279	67.82043457	26.82912445
25	5.127	42.67896652	68.75527954	26.21702957
26	5.267	41.97287369	70.24847412	26.96119881
27	5.393	42.60488129	69.91070557	28.43270874
28	5.527	43.0799408	72.10771179	27.67629051
29	5.660	43.44350052	74.07112885	27.74229431
30	5.794	44.45366287	73.73880005	28.65775681
31	5.934	43.7229805	75.23035431	29.22486687
32	6.061	43.23042297	73.83956909	27.74004745
33	6.202	43.629776	74.98071289	27.13162231
34	6.338	43.01525116	73.32308197	28.28024101
35	6.462	42.72449493	73.47512054	27.67119026
36	6.583	40.80134201	73.91508484	28.28884125
37	6.720	41.12762451	74.50099182	27.77641869
38	6.859	40.35508347	74.16786194	26.52946091
39	6.975	39.91860199	73.83478546	26.72374344
40	7.111	43.42757797	82.20703888	28.97228432
41	7.244	40.46611786	80.23033905	26.97558975
42	7.370	37.96995926	77.0504303	25.94872093
43	7.501	36.64840317	75.62962341	25.71439362
44	7.621	35.40363693	70.74970245	24.76756668
45	7.753	31.50629616	66.14655304	22.04857635
46	7.886	31.55540848	64.3500061	22.49168205
47	8.019	29.41214371	63.10870361	22.28083801
48	8.145	28.56422615	60.00759888	21.64977646
49	8.280	28.80638695	61.03319168	21.63468552
50	8.413	29.0040226	60.24184036	20.63168526
51	8.546	28.60115242	60.73344421	21.02709579
52	8.673	28.36203766	61.25415421	20.87670517
53	8.805	28.56165123	60.63360214	21.85882568
54	8.942	28.46078873	61.66411972	20.76583481
55	9.072	30.06471825	62.74814224	22.44129181
56	9.210	29.40449715	63.45282364	21.48060417

57	9.344	29.76455498	63.30151749	21.76354027
58	9.472	29.24953079	65.5386734	21.33381462
59	9.601	29.55286789	65.3950119	21.69050217
60	9.730	31.28565979	67.8695755	22.2555542
61	9.866	30.74120522	69.76120758	23.06269264
62	9.992	32.95788193	75.56105042	24.38328362
63	10.116	33.49944687	75.86682892	25.04069519
64	10.241	32.83420181	82.2576828	23.95147133
65	10.372	34.89374924	87.77390289	24.60607338
66	10.510	37.90845871	95.78879547	26.52713013
67	10.649	40.05186844	105.6449738	26.86811829
68	10.776	40.50695801	118.1030884	28.25723457
69	10.909	44.6324501	130.2585907	29.99370384
70	11.041	46.06766129	143.1494598	31.21467972
71	11.183	49.57761765	160.5751648	31.50450134
72	11.310	52.05046844	172.8575897	32.79081726
73	11.452	54.17264557	185.6888885	34.21978378
74	11.589	56.60914612	202.9112854	35.73062897
75	11.717	59.48548126	212.9468994	36.43432617
76	11.846	62.21366882	230.8772583	38.38352966
77	11.980	68.00889587	248.5286407	39.95904541
78	12.117	70.91064453	261.461792	41.56760025

Table F.3: Cy_2DETA.3A.3HCl / Eu(III) phosphorescence emission raw data, λ_{ex} = 229 nm (multi-component buffered system, no equilibration).

Sample	pH	Emission Intensity (592nm)	Emission Intensity (617nm)	Emission Intensity (697nm)
1	2.007	23.01084137	11.62648582	11.70064735
2	2.133	32.20597839	12.91130924	14.46488953
3	2.264	37.20442963	19.26540756	18.42865944
4	2.392	45.33967209	23.2719593	24.23696899
5	2.523	59.59435272	32.0573082	27.19913864
6	2.654	67.11949158	38.95730972	32.78789139
7	2.783	76.5800705	52.17634583	40.92052078
8	2.912	88.73445129	66.8733902	47.23802185
9	3.045	94.40692139	81.09998322	50.97158051
10	3.172	92.48802948	95.50751495	53.34418106
11	3.304	94.68405914	106.8585129	55.73247528
12	3.437	96.07444763	111.3255692	58.89331436
13	3.564	96.46993256	118.7666626	60.28771973
14	3.691	95.58436584	128.1241608	60.47904968
15	3.824	98.4944458	135.2328339	60.37420654
16	3.957	94.93468475	136.0986023	61.50259399
17	4.084	101.4381943	143.2704163	64.44828033

18	4.212	106.8206711	148.7398376	65.78049469
19	4.347	112.5329208	146.7619019	69.90543365
20	4.471	115.1312027	162.7106476	69.29416656
21	4.608	126.553688	175.8606567	78.6466217
22	4.731	131.736145	181.3335876	78.88824463
23	4.872	136.7239685	187.6353912	84.82826996
24	5.006	154.447525	203.3182678	92.99160767
25	5.127	159.3886719	218.0335846	90.63839722
26	5.267	161.1305084	224.9938965	94.34503174
27	5.393	167.7830353	233.928299	99.80773926
28	5.527	174.5948944	238.7350159	104.0283127
29	5.660	172.089798	244.3929596	101.352684
30	5.794	173.7679138	248.9232178	101.317543
31	5.934	169.7963257	248.664566	104.7086258
32	6.061	167.6292419	244.1430969	96.36953735
33	6.202	175.0522003	253.0983582	103.484581
34	6.338	164.3218842	251.3357239	101.9059753
35	6.462	157.4497681	245.7583618	96.64796448
36	6.583	158.0951843	247.1690063	95.61217499
37	6.720	159.5740814	249.8291779	95.99701691
38	6.859	144.9713287	243.3291168	93.8234024
39	6.975	144.2891541	250.3418427	89.70589447
40	7.111	179.12117	318.194397	109.3444366
41	7.244	162.5804901	302.7229004	99.75463867
42	7.370	143.4286194	278.1760254	90.6629715
43	7.501	132.2813873	257.4967041	84.06571198
44	7.621	114.5056	240.1596527	76.58634949
45	7.753	96.05434418	205.4185944	65.2103653
46	7.886	85.23012543	179.3406067	58.45064545
47	8.019	79.77130127	172.149231	56.64856339
48	8.145	79.51756287	166.3219452	56.3633194
49	8.280	73.89183044	157.348053	53.85697937
50	8.413	71.77445984	150.7038116	51.89923096
51	8.546	72.69481659	148.8853302	51.39819717
52	8.673	68.4154892	146.4091644	53.31642532
53	8.805	71.31824493	146.9250183	48.83106232
54	8.942	68.09590149	149.3967285	48.98661423
55	9.072	68.01043701	150.5115967	49.62687683
56	9.210	64.98326111	149.286377	51.28241348
57	9.344	68.56778717	147.6309357	49.4016571
58	9.472	72.03481293	150.3626862	49.22079849
59	9.601	67.96044159	148.1985626	48.71830368
60	9.730	69.26620483	153.4021454	46.18186569
61	9.866	65.20488739	149.713623	47.79517746

62	9.992	65.93828583	154.161087	48.22670364
63	10.116	65.193367	165.2165222	46.71997833
64	10.241	68.67395782	166.1343384	46.31039047
65	10.372	70.02468872	173.1422577	50.04899979
66	10.510	70.04072571	174.2855682	50.50244141
67	10.649	67.74416351	178.9308472	45.27362061
68	10.776	63.36948013	190.5589294	49.38149261
69	10.909	67.04550171	195.8506165	44.90299225
70	11.041	65.41589355	210.7341461	44.17622375
71	11.183	71.05886078	210.7961273	46.12888336
72	11.310	64.7688446	223.0033569	44.08667755
73	11.452	63.75249863	230.443924	39.99315643
74	11.589	69.23842621	239.9216309	40.9834938
75	11.717	65.35795593	245.3348083	37.11253357
76	11.846	67.24237823	253.9049377	41.44821167
77	11.980	68.44406891	267.2654114	42.79914474
78	12.117	74.90124512	274.170166	44.51581192

F.1.3 Cy_2DETA.3A.3HCl / Eu(III), multi-component buffered system, upon reaching equilibrium

Cy_2DETA.3A.3HCl (0.0207 g, 3.78×10^{-5} mol) and $Eu(CF_3SO_3)_3$ (0.0242 g, 4.03×10^{-5} mol) were dissolved in deionised water, in a 250 mL volumetric flask. To this flask, 37.5 µL of a 0.1 mol/L solution consisting of KHP, MES, CHES, MOPS, and Tris was added and the contents diluted to the mark. The solution was placed in a jacketed-cell (25 °C). An in-cell titration was performed on the solution using the concentrated HCL and NaOH solutions. Upon each addition of acid or base, the pH of the solution was allowed to stabilize and the pH value recorded. A small volume of the adjusted solution was decanted and sealed in a marked vial prior to subsequent pH adjustment. The procedure yielded a series of solutions between pH 1.9 and pH 12.0, in intervals of 0.2 pH units.

These solutions were allowed to reach equilibrium (25 °C). The pH, absorbance and luminescence of each sample were recorded after 3 days and after 14 days.

The absorbance of the Cy_2DETA.3A.3HCl / Eu(III) stock solution was measured in order to determine the wavelength to be used for excitation in the luminescence study. The absorbance was measured over a range of 200 nm and 800 nm.

The phosphorescence emission spectrum was measured by exciting each sample at a wavelength of 266 nm and 240 nm (Figure F.3). The spectrum was recorded in the high sensitivity mode, over a range of 550 nm to 750 nm. Each measurement was recorded after a 0.100 ms time delay, with both the excitation and emission slit widths set at 10 nm.

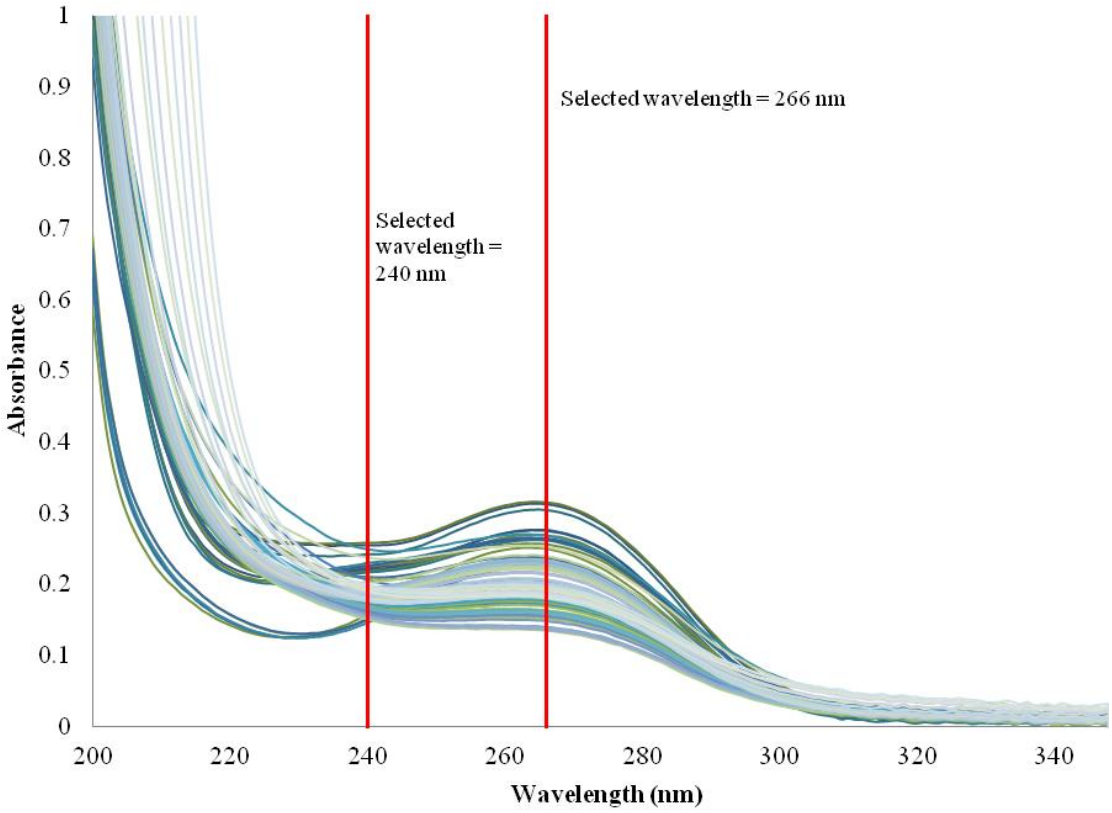


Figure F.3: Absorbance spectrum of europium(III)-1,7-bis(2-hydroxycyclohexyl)-1,4,7-tris(carboxymethyl)-1,4,7 triazaheptane, in a buffered solution, as a function of pH.

The following tables consist of peak maxima intensity values for each observable emission band as a function of pH.

Table F.4: Cy_2DETA.3A.3HCl / Eu(III) phosphorescence emission raw data, λ_{ex} = 240 nm (multi-component buffered system, upon reaching equilibrium).

Sample	Initial pH	pH (3 days)	pH (14 days)	Emission Intensity (592nm) (3 days)	Emission Intensity (617nm) (3 days)	Emission Intensity (694nm) (3 days)	Emission Intensity (592nm) (14 days)	Emission Intensity (617nm) (14 days)	Emission Intensity (694nm) (14 days)
1	1.999	2.050	2.032	25.731348	12.0116015	11.4914751	25.1931324	12.8988752	12.4822817
2	2.111	2.145	2.160	32.2915802	14.5134449	14.7068205	34.1400223	16.0576687	15.2711973
3	2.231	2.272	2.311	38.3185234	19.711338	17.3036213	39.9911118	19.5165939	16.9789295
4	2.352	2.384	2.427	47.7192078	24.8721809	19.4633389	49.4386673	26.0909004	21.9914055
5	2.476	2.512	2.560	57.0845146	32.5384445	26.852026	63.5474587	33.222477	29.3810177
6	2.603	2.648	2.715	70.1079178	42.1704063	31.5096588	78.1131668	51.1030846	36.2794647
7	2.724	2.774	2.840	83.0758514	55.2703209	39.612236	91.048439	65.3286743	43.8684692
8	2.844	2.926	3.025	89.9632797	71.7466126	46.3826447	94.8286743	83.0136643	51.1539688
9	2.961	3.070	3.202	96.4363098	87.6031342	51.9832459	100.318657	103.658325	57.7634659
10	3.081	3.228	3.463	100.558281	102.790527	59.1173515	50.945015	99.006012	44.3962746
11	3.202	3.368	3.669	98.3214569	102.735916	57.2941399	56.2628937	110.261948	46.9453278
12	3.334	3.451	4.066	99.3997421	115.838066	59.0185623	62.642334	122.178062	50.3805389
13	3.465	3.803	6.376	65.6315994	115.847885	52.8730431	61.1578102	130.301605	52.6830483
14	3.589	4.379	7.090	60.7645073	125.713951	52.3265724	67.8944016	139.047257	55.811924
15	3.713	4.568	7.075	63.0492744	130.214752	51.4449997	68.5764847	139.738617	55.0221176
16	3.831	5.442	7.067	67.7590408	131.972672	52.6618042	66.9171982	135.016846	56.4889031
17	3.959	6.056	7.240	65.9161606	136.817123	54.0351868	70.6779099	144.089493	55.7275581
18	4.073	6.143	7.243	65.6838989	133.484619	54.7977905	67.2327805	143.33638	56.9331169
19	4.193	6.358	7.349	101.943596	187.188049	70.2405167	68.8285141	147.068955	57.0095367
20	4.325	6.432	7.386	93.6682434	167.530457	67.7135773	69.0248261	141.132568	55.3499451
21	4.436	6.844	7.432	83.5257187	165.800507	61.2482147	67.1533814	147.438568	58.4683914
22	4.551	6.911	7.306	81.9713211	161.300873	64.5048523	71.38694	147.898697	56.1402855
23	4.671	7.281	7.447	66.4366226	138.20343	54.1001396	65.3435898	136.609512	53.6478691
24	4.802	6.784	7.335	86.0081253	164.411621	63.5029793	70.9397202	147.521103	55.2512207
25	4.928	7.225	7.458	68.751442	142.992615	55.6146278	70.4908905	140.861862	55.1675606
26	5.044	6.884	7.307	86.0307236	161.650833	62.1225815	67.726532	142.65242	57.3023605
27	5.168	7.188	7.375	71.0775147	146.464661	56.6436501	70.1283646	141.366882	56.3106194
28	5.289	6.982	7.377	81.2562485	163.761581	61.7818909	69.9778519	145.772385	56.3936234
29	5.412	7.104	7.441	76.0910034	156.673569	59.4535942	69.3006439	142.961319	54.7914543
30	5.547	7.232	7.531	68.0823669	142.827393	56.28088	70.4794083	140.589462	55.7122803
31	5.670	7.130	7.466	75.6047516	155.119644	58.1793442	68.9186707	144.688934	55.1458931
32	5.792	7.232	7.503	69.4553375	144.633301	54.8189125	70.8591843	143.490006	56.3536072
33	5.920	7.153	7.497	78.3552551	153.579208	59.2879372	66.9734345	143.153229	55.7216377
34	6.042	7.314	7.552	70.174324	141.623581	54.5454979	70.6922836	141.25528	56.138752
35	6.160	7.322	7.605	67.8153229	143.87027	56.2943726	70.3886414	141.982819	56.2330589
36	6.291	7.216	7.466	75.7255325	150.608017	56.0622597	69.9920807	144.722107	55.7083664
37	6.414	7.266	7.505	73.6614914	147.07048	57.3370171	68.8197556	141.810806	56.2111969
38	6.531	7.300	7.546	72.5902481	147.205292	55.5595856	69.1137543	140.928879	55.4770126
39	6.642	7.265	7.534	74.311348	152.476044	57.5808601	67.9240494	143.122269	55.9465179

40	6.753	7.519	7.694	69.4083481	141.291031	56.8811226	69.1565628	138.77153	56.5697746
41	6.875	7.411	7.635	68.0847855	145.293671	56.0965614	69.008049	141.761963	56.3056946
42	7.001	7.34	7.515	72.377655	150.65361	58.1762962	67.530983	147.467636	57.8307686
43	7.124	7.461	7.587	71.396698	144.859238	56.0396614	71.6770783	145.955032	54.5816345
44	7.246	7.495	7.625	70.6356583	145.157623	54.8872147	68.5803986	142.179428	55.1079598
45	7.361	7.496	7.654	69.577858	144.010254	54.9228401	68.598114	141.889282	56.5973969
46	7.481	7.765	7.768	68.9456558	139.228149	56.9783859	65.9468079	140.318848	55.3459358
47	7.602	7.770	7.855	67.8389511	145.002487	56.5262184	68.3682632	145.759415	56.244442
48	7.739	7.651	7.758	68.3649902	145.898377	55.9596787	69.1865311	139.896408	55.7562981
49	7.857	7.731	7.738	66.6255493	142.320282	54.0286179	69.8157044	146.21138	55.685154
50	8.006	7.899	7.867	71.2858353	144.807755	55.4863739	70.2518616	146.10379	57.5150642
51	8.131	8.134	8.032	69.6734161	141.72786	54.0661507	65.9693756	139.825317	55.3913879
52	8.262	8.130	8.089	69.7809906	143.335358	56.2629013	69.4289322	144.115143	55.4002495
53	8.395	8.011	7.902	64.7722931	137.255264	52.6185303	67.2245865	141.928452	54.9799576
54	8.522	8.320	8.176	62.9993668	133.937271	54.3081627	65.5568466	138.062988	53.1928711
55	8.650	8.295	8.165	62.5630341	131.916977	52.3985329	67.2828522	135.339569	52.5894508
56	8.783	8.202	7.988	64.8698807	135.553894	52.8716202	67.5670776	137.410965	53.6238403
57	8.911	8.705	8.393	63.2908135	132.724869	52.6756058	64.1149521	132.717712	51.7636757
58	9.042	8.752	8.502	64.0535584	137.051148	51.9274826	65.2780991	137.872009	54.1685638
59	9.173	8.986	8.816	62.417984	133.943787	51.6824722	65.2817612	141.136017	54.3674164
60	9.301	9.113	8.935	64.8254547	136.719132	53.1503143	66.3525391	137.795288	53.023922
61	9.439	9.211	9.036	64.5427475	138.008865	51.5860558	66.1791916	134.988525	53.7079468
62	9.564	9.326	9.094	63.2570496	140.255295	50.7204285	64.240036	138.613556	51.3121529
63	9.693	9.395	9.214	66.5778503	141.045395	52.4228745	65.3751526	141.454285	51.1482773
64	9.839	9.511	9.312	62.8244858	141.581467	50.657711	64.2536697	138.09613	52.4690323
65	9.962	9.517	9.294	65.2982864	145.077148	53.4822846	66.9860535	140.531265	52.4091568
66	10.093	9.589	9.393	64.9387741	139.19783	49.4184723	64.1925049	141.171051	53.5162849
67	10.228	9.475	8.751	67.6995773	142.989868	52.1398392	64.9402313	142.861816	51.2228394
68	10.351	10.013	9.640	63.082489	143.22551	50.8883972	65.6509018	139.682938	49.2678185
69	10.483	9.743	8.922	64.9370346	144.360046	50.6560898	66.2152252	142.20018	53.9282494
70	10.611	10.008	9.198	60.6432304	142.740265	51.3825378	65.1717758	143.853272	53.3501053
71	10.743	10.324	9.854	60.3226128	148.556168	48.4892883	65.3657227	147.315399	50.6774826
72	10.887	10.332	9.899	61.0353584	144.743225	47.8946877	63.849823	149.279587	52.0203552
73	11.010	10.712	9.757	58.5716591	155.352554	43.9595642	64.0879746	146.865265	51.9561997
74	11.141	11.022	10.583	52.1114388	154.996307	39.7867813	54.35606	139.130707	42.0895805
75	11.272	11.108	10.808	55.5046196	168.110336	39.4394951	53.949482	150.41359	39.9672127
76	11.400	11.291	10.912	51.0583077	167.432922	34.3097153	50.2282753	140.692169	37.1835022
77	11.533	11.446	11.007	51.0789528	172.951447	34.4209366	49.8581009	132.637283	37.0537415
78	11.664	11.630	11.530	49.7993622	177.713074	30.4661598	40.5345306	136.049835	28.3097801
79	11.796	11.766	11.683	51.0193939	188.024735	29.5318642	38.6710777	137.793625	24.6188583
80	11.927	11.894	11.847	52.0340958	197.296127	26.6647434	35.678154	129.681458	21.0725994
81	12.056	12.024	12.046	53.9635506	197.504837	26.5558472	34.7262001	128.350555	19.4648533

Table F.5: Cy_2DETA.3A.3HCl / Eu(III) phosphorescence emission raw data, λ_{ex} = 266 nm (multi-component buffered system, upon reaching equilibrium).

Sample	Initial pH	pH (3 days)	pH (14 days)	Emission Intensity (592nm) (3 days)	Emission Intensity (617nm) (3 days)	Emission Intensity (694nm) (3 days)	Emission Intensity (592nm) (14 days)	Emission Intensity (617nm) (14 days)	Emission Intensity (694nm) (14 days)
1	1.999	2.050	2.032	8.4606514	4.29349327	3.25286818	8.66672802	4.11120939	4.01063633
2	2.111	2.145	2.160	10.0295134	5.34862614	4.44371462	11.0624514	5.24263001	5.07213736
3	2.231	2.272	2.311	12.6078186	6.77933884	5.37981129	12.4664784	6.67990875	5.65656424
4	2.352	2.384	2.427	15.3289776	8.46252823	7.11613274	15.8759775	9.22645664	6.87577725
5	2.476	2.512	2.560	19.4373283	10.8609619	8.73543549	19.3560638	11.9467974	8.77681065
6	2.603	2.648	2.715	23.1603241	15.1568079	10.7466602	24.7680893	18.5976372	12.949481
7	2.724	2.774	2.84	27.3326435	20.5137825	14.4048166	29.0725632	25.4449768	15.0368481
8	2.844	2.926	3.025	29.9029789	29.9201412	16.4699554	32.2475433	34.4856224	19.4599743
9	2.961	3.070	3.202	33.2772408	37.7767487	20.3610382	36.0841713	44.9043922	22.2199612
10	3.081	3.228	3.463	35.6765747	44.2235146	23.2727261	24.8043308	47.5037613	19.9261551
11	3.202	3.368	3.669	35.6700783	47.1982842	23.6933117	27.1648693	53.0978928	22.820343
12	3.334	3.451	4.066	35.3675461	50.6728973	24.9690723	30.982193	59.0822067	24.9782219
13	3.465	3.803	6.376	29.7540779	53.3574371	23.3070965	31.3600063	64.0972214	25.9589653
14	3.589	4.379	7.090	31.4164066	60.4059677	23.8460598	34.3684197	70.0736313	27.6684456
15	3.713	4.568	7.075	29.4888439	62.0214157	24.7188854	32.122921	68.5822601	25.5131455
16	3.831	5.442	7.067	31.7634983	64.4072495	25.0814419	33.1453247	69.663681	26.4484234
17	3.959	6.056	7.240	30.9608917	64.6879654	25.4817944	33.4451103	69.8698578	27.7651291
18	4.073	6.143	7.243	31.8635216	66.2639465	25.3591614	34.5102081	69.5004349	28.3418446
19	4.193	6.358	7.349	41.0307388	79.3417511	30.6911793	33.8085785	72.1313858	27.7073364
20	4.325	6.432	7.386	38.2557259	75.651413	28.0908222	33.3532867	71.5784836	28.4386349
21	4.436	6.844	7.432	35.7433968	73.586937	29.5098095	33.8162994	72.1021652	28.1164494
22	4.551	6.911	7.306	35.0308075	74.3195648	29.2165775	35.3879433	71.7586365	28.046833
23	4.671	7.281	7.447	33.6322403	68.4583359	26.6622963	34.4832459	73.6109085	27.167141
24	4.802	6.784	7.335	36.8014221	75.4296341	29.6381664	34.1045532	72.9790573	28.9162216
25	4.928	7.225	7.458	33.1786118	70.3433228	27.3199062	32.8431015	68.1688843	27.3627739
26	5.044	6.884	7.307	34.7610741	74.0259247	29.2639599	33.6902771	69.4773941	27.6739693
27	5.168	7.188	7.375	34.2976761	71.3761978	27.9001045	33.155983	72.5067444	28.961956
28	5.289	6.982	7.377	36.1929703	73.6328659	28.7412167	35.1269341	74.3486023	27.3946304
29	5.412	7.104	7.441	34.591301	74.7486038	28.8235931	34.5238304	70.5662918	27.827404
30	5.547	7.232	7.531	33.5029106	69.6648941	27.6919689	33.5511246	72.5226288	27.7987576
31	5.670	7.130	7.466	36.029377	72.6815567	27.9402199	33.4510651	71.8380966	28.6871758
32	5.792	7.232	7.503	33.1598778	70.2838974	27.4415627	35.3823967	70.7669601	27.9272652
33	5.920	7.153	7.497	35.8186302	72.7176437	28.2960281	34.6300888	72.0545807	27.9427929
34	6.042	7.314	7.552	34.171032	71.4986954	28.2817116	34.8446388	71.5587158	29.3020649
35	6.160	7.322	7.605	34.1990967	73.1754303	28.2032433	34.6146545	71.4340973	28.501894
36	6.291	7.216	7.466	34.0914726	72.2619782	27.5479412	35.3342552	71.5497284	28.1599541
37	6.414	7.266	7.505	34.8960037	72.1789017	27.4576817	34.6212006	72.7126389	28.763279
38	6.531	7.003	7.546	33.6268959	72.3256836	27.626894	35.2367096	73.2405319	27.7754574
39	6.642	7.265	7.534	35.3734436	73.7305908	28.6908226	35.8089523	72.2479401	28.2569065

40	6.753	7.519	7.694	32.9875946	69.8659897	27.7769032	34.6128044	72.4657364	28.8405266
41	6.875	7.411	7.635	35.1588097	71.38134	27.6088181	33.9859314	73.2481461	28.1669121
42	7.001	7.340	7.515	34.6794891	73.8688965	28.4420319	35.6547051	75.510582	29.6230469
43	7.124	7.461	7.587	35.2069626	72.73526	28.8571568	34.3160324	73.0843277	28.3779659
44	7.246	7.495	7.625	35.3474846	71.3778229	28.1429367	35.3177834	73.6542816	28.8122311
45	7.361	7.496	7.654	34.6135902	72.1503983	29.0237656	35.0149384	74.8194504	29.6672363
46	7.481	7.765	7.768	35.3210945	72.3744965	29.1987343	35.7098579	70.8778839	29.272152
47	7.602	7.770	7.855	33.9228249	70.7917862	27.7299194	34.812294	73.4688187	28.1444321
48	7.739	7.651	7.758	34.7794495	74.5705414	28.7777576	35.0209885	74.4236221	29.6176796
49	7.857	7.731	7.738	35.5220528	75.0198135	28.9389324	34.4990082	75.0016937	28.4451122
50	8.006	7.899	7.867	34.3396454	72.8254242	27.3900089	35.1838112	75.5991287	29.6464024
51	8.131	8.134	8.032	34.5460625	72.8149185	28.4713669	35.122757	72.2041931	27.1677074
52	8.262	8.130	8.089	34.8846588	74.9534988	29.567255	36.712059	75.9269409	29.4527454
53	8.395	8.011	7.902	31.2774048	68.0732803	26.5494995	32.8333588	69.5376968	26.8278446
54	8.522	8.320	8.176	30.3996792	64.8322144	24.9459801	31.2873764	67.2349625	26.6737442
55	8.650	8.295	8.165	30.8310165	65.8128738	25.6158199	31.2719975	66.8566284	26.0443554
56	8.783	8.202	7.988	32.3963127	66.0428619	25.2456284	32.1683197	69.6843109	26.6009579
57	8.911	8.705	8.393	31.1594181	66.1429367	25.4584808	32.0435829	68.3978653	26.1945763
58	9.042	8.752	8.502	31.7336979	69.07267	25.9563694	32.6253357	68.9070053	27.5887833
59	9.173	8.986	8.816	31.5496693	67.6220093	26.5100994	31.8034496	69.0544128	27.3849049
60	9.301	9.113	8.935	31.2443352	68.2943115	26.1898403	33.1991043	70.1356506	26.2007828
61	9.439	9.211	9.036	32.2660866	71.3347855	26.9128323	33.0344162	71.170372	27.0480442
62	9.564	9.326	9.094	32.5490341	72.9306564	27.2440834	33.2561798	73.4532929	26.7505055
63	9.693	9.395	9.214	32.0859871	70.7504044	26.3375073	32.7088242	72.3244705	26.7855988
64	9.839	9.511	9.312	32.7377052	73.4962921	27.2153664	33.5204468	73.0139542	27.4379101
65	9.962	9.517	9.294	33.2509689	75.4095917	28.5914726	32.9027824	73.671669	27.4322529
66	10.093	9.589	9.393	34.1085129	76.4484863	28.4506569	33.2954483	74.6885452	27.7522774
67	10.228	9.475	8.751	33.5142021	76.4428482	28.0017109	34.1979942	76.3586044	28.6743031
68	10.351	10.013	9.640	36.3738403	83.0579987	27.0989513	35.0390816	76.8444595	28.3395577
69	10.483	9.743	8.922	34.0071716	78.0091171	28.2772389	34.2970696	74.3017197	28.3039875
70	10.611	10.008	9.198	34.4747391	81.082016	27.3729801	33.7680893	75.8707199	28.4248028
71	10.743	10.324	9.854	35.7476921	89.5012817	28.4262447	34.6965714	81.1219864	27.1177254
72	10.887	10.332	9.899	34.8641205	87.7655258	28.6975746	35.236908	80.9131012	28.3920879
73	11.010	10.712	9.757	40.8202629	113.255058	30.9272232	35.5820847	82.4332504	28.6242142
74	11.141	11.022	10.583	40.6352234	130.57251	30.296133	35.365284	95.0133743	27.8549233
75	11.272	11.108	10.808	44.0963173	150.060394	32.0657654	39.6805115	110.485069	28.9178925
76	11.400	11.291	10.912	48.6552849	161.735184	31.5936718	38.5582199	111.347	29.3174801
77	11.533	11.446	11.007	49.5571556	175.69809	31.2643871	37.1462631	100.713921	27.1583233
78	11.664	11.630	11.530	52.0936699	186.77858	31.043932	40.9440498	145.435867	26.2718315
79	11.796	11.766	11.683	56.8301544	201.931503	32.3782158	42.2067833	153.602249	26.2167416
80	11.927	11.894	11.847	59.5416145	219.516525	31.6816139	41.4044342	146.103821	24.0005531
81	12.056	12.024	12.046	59.454525	228.070511	30.5721149	42.0302506	151.948608	21.6642342

F.2 Cy_2DETA.2A.3HCl / Eu(III)

The luminescence properties of the Cy_2DETA.2A.3HCl / Eu(III) system was investigated as a function of pH.

F.2.1 Cy_2DETA.2A.3HCl / Eu(III), aqueous solution

Cy_2DETA.2A.3HCl (0.0376 g, 7.69×10^{-5} mol) and $Eu(CF_3SO_3)_3$ (0.0470 g, 7.84×10^{-5} mol) were dissolved in deionised water, in a 250 mL volumetric flask. This solution was placed in a jacketed-cell (25 °C). An in-cell titration was performed on the solution using the concentrated HCL and NaOH solutions. Upon each addition of acid or base, the pH of the solution was allowed to stabilize and the pH value recorded. A small volume of the adjusted solution was decanted and sealed in a marked vial prior to subsequent pH adjustment. The procedure was repeated to obtain a series of solutions between pH 1.8 and pH 9.0, in intervals of 0.2 pH units. These solutions were allowed to reach equilibrium over 48 hours.

The absorbance of the Cy_2DETA.2A.3HCl / Eu(III) stock solution was measured to determine the excitation wavelength for the corresponding luminescence study (Figure F.4).

The pH of each solution was measured after 48 hours, prior to each absorbance and luminescence measurement. The absorbance was measured over a range of 200 nm and 800 nm.

The phosphorescence emission spectrum was measured by exciting each sample at a wavelength of 252 nm. The spectrum was recorded in the high sensitivity mode, over a range of 550 nm to 750 nm. Each measurement was recorded after a 0.100 ms time delay, with both the excitation and emission slit widths set at 10 nm.

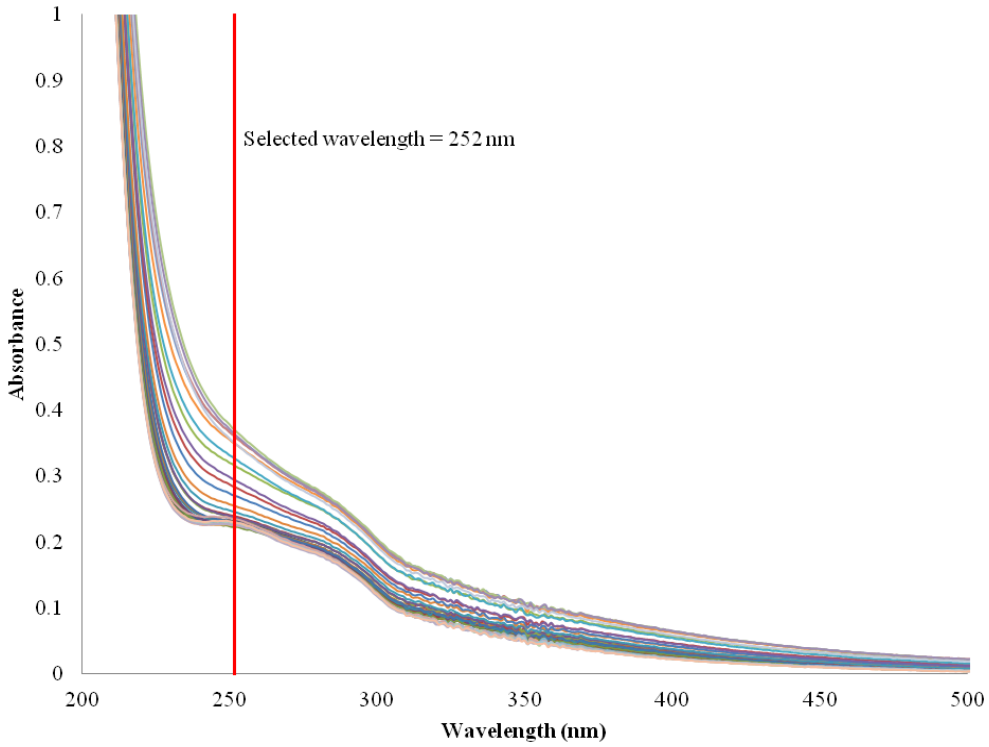


Figure F.4: Absorbance spectrum of europium(III)-1,7-bis(2-hydroxycyclohexyl)-1,7-bis(carboxymethyl)-1,4,7 triazaheptane, as a function of pH.

The following table consists of peak maxima intensity values for each observable emission band as a function of pH.

Table F.6: $Cy_2DETA.2A.3HCl$ / Eu(III) phosphorescence emission raw data, λ_{ex} = 252 nm.

Sample	pH (before equilibration)	pH (after 48 hours equilibration)	Emission Intensity (592 nm)	Emission Intensity (616 nm)	Emission Intensity (697 nm)
1	3.448	3.552	42.93080521	43.25053787	22.76435089
2	3.621	3.801	43.38515854	47.42635727	23.24345016
3	3.830	4.183	51.40377045	61.00457001	27.58598137
4	4.019	4.390	52.60830688	68.39697266	28.37495422
5	4.223	4.525	53.25760269	70.37687683	30.2851181
6	4.406	4.712	58.62576294	82.21697235	32.18595123
7	4.649	4.918	61.6415062	94.4643631	34.66175461
8	4.840	5.039	63.63729858	96.15225983	35.38137436
9	5.017	5.139	64.23397064	103.2273407	37.72711182
10	5.269	5.369	69.91288757	120.6920624	39.86144257
11	5.458	5.471	71.85903168	124.8697357	43.95445251
12	5.634	5.629	78.70262909	144.2013702	47.66046143
13	5.872	5.776	81.35881042	158.8413849	50.73130417
14	6.062	5.924	83.93402863	167.8403625	54.69465637
15	6.270	6.038	87.77313232	176.1568909	56.41465759

16	6.448	6.164	78.13336945	164.1775055	51.73294067
17	6.636	6.335	72.26226044	148.3858795	47.55564499
18	6.835	6.317	60.32130432	121.3539658	37.65353775
19	7.021	6.350	43.60978317	86.67669678	27.18471909
20	7.203	6.366	33.84265137	68.56639862	22.13843536
21	7.427	6.405	23.82795715	46.57314682	15.15705872
22	7.626	6.417	20.95366669	41.8146019	13.32491875
23	7.834	6.709	12.67601204	29.11811066	7.957433224
24	8.051	7.056	7.418306828	18.3100853	4.111913204
25	8.239	7.254	4.680511475	13.85658455	3.625882149
26	8.612	7.503	3.770884752	11.2277317	2.343324661
27	8.858	7.884	2.41496563	8.71277523	1.235779643
28	9.093	7.863	3.547502995	9.316235542	1.971533775
29	3.216	3.433	38.69892502	36.74764633	19.48169708
30	3.073	3.207	37.33812714	31.62100792	18.40790749
31	2.885	2.999	33.2942276	26.8066349	16.78497505
32	2.680	2.736	30.82821846	21.02019501	14.69099426
33	2.469	2.514	26.39553642	18.28488922	12.45153332
34	2.264	2.306	24.72664261	15.18919086	10.98508072
35	2.058	2.077	20.37124825	12.03298569	9.611775398
36	1.881	1.897	17.07165527	10.93277836	8.876339912
37	8.440	7.382	1.89324522	8.040884972	2.035526514

F.2.2 Cy_2DETA.2A.3HCl / Eu(III), multi-component buffered system, no equilibration

Cy_2DETA.2A.3HCl (0.0186 g, 3.81×10^{-5} mol) and $Eu(CF_3SO_3)_3$ (0.0236 g, 3.94×10^{-5} mol) were dissolved in deionised water, in a 250 mL volumetric flask. To this flask, 37.5 μL of a 0.1 mol/L solution consisting of KHP, MES, CHES, MOPS, and Tris was added and the contents diluted to the mark. This solution was placed in a jacketed-cell (25 °C). An in-cell titration was performed on this solution using the concentrated HCl and NaOH solutions. Upon each addition of acid or base, the pH of the solution was allowed to stabilize and the pH value recorded. A small volume of the adjusted solution was decanted into a marked vial prior to subsequent pH adjustment. The procedure was repeated to obtain a series of solutions between pH 1.8 and pH 9.5, in intervals of 0.2 pH units. The absorbance and luminescence of the solutions were immediately measured.

The absorbance of the Cy_2DETA.2A.3HCl / Eu(III) stock solution was measured to determine the luminescence excitation wavelength. The absorbance was measured over a range of 200 nm and 800 nm (Figure F.5).

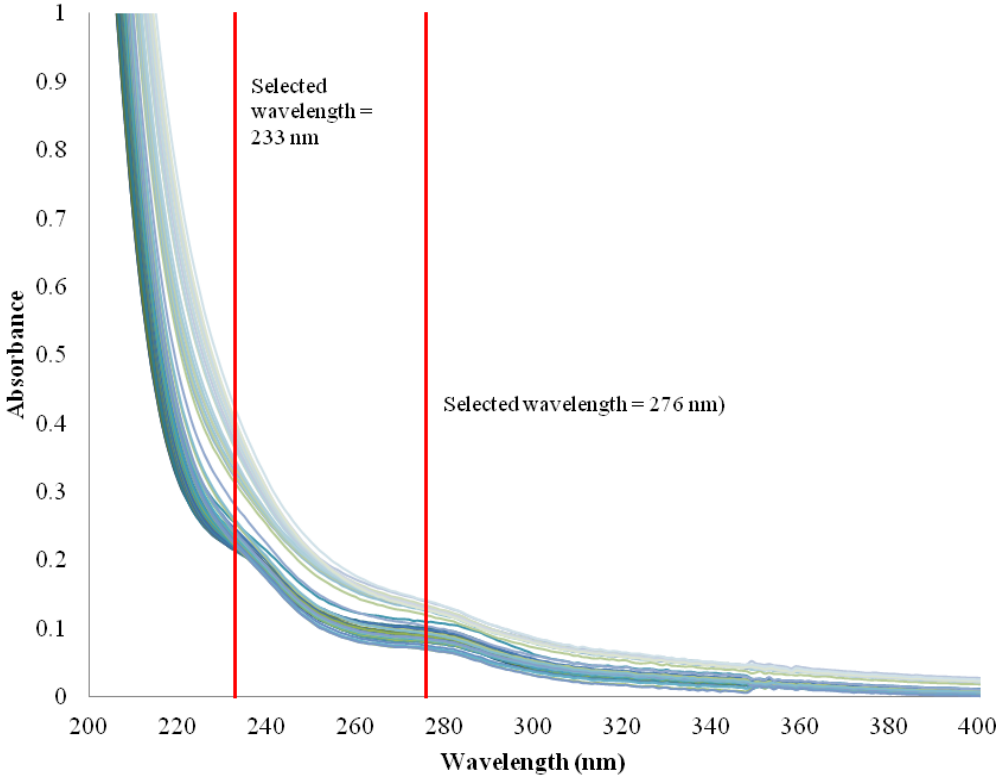


Figure F.5: Absorbance spectrum of europium(III)-1,7-bis(2-hydroxycyclohexyl)-1,7-bis(carboxymethyl)-1,4,7 triazaheptane, in a buffered solution, as a function of pH.

The phosphorescence emission spectrum was measured by exciting each sample at wavelengths of 233 nm and 276 nm. The spectrum was recorded in the high sensitivity mode, over a range of 550 nm to 750 nm. Each measurement was recorded after a 0.100 ms time delay, with both the excitation and emission slit widths set at 10 nm.

The following tables consist of peak maxima intensity values for each observable emission band as a function of pH.

Table F.7: $Cy_2DETA.2A.3HCl$ / Eu(III) phosphorescence emission raw data, λ_{ex} = 276 nm (multi-component buffered system, no equilibration).

Sample	pH	Emission Intensity (592 nm)	Emission Intensity (616 nm)	Emission Intensity (697 nm)
1	1.821	7.814621449	4.807792187	4.624673843
2	1.929	8.758323669	5.017690182	4.43969202
3	2.039	10.66525459	5.333123207	4.610454559
4	2.149	11.97679806	6.346595764	5.616354465
5	2.260	13.45780945	6.649782181	6.400961399
6	2.372	14.46082973	7.847005844	7.665996075
7	2.481	17.71564484	9.117301941	8.389397621
8	2.594	19.59659195	9.803450584	9.241473198
9	2.702	21.4228096	10.80742741	9.969649315
10	2.830	25.23252869	12.94622231	11.52189732
11	2.945	27.72511101	13.69927406	12.98871422
12	3.057	29.31557083	14.74013042	13.6369772
13	3.169	29.94154739	15.92446518	14.02406979
14	3.278	33.29376984	17.32754135	16.61161804
15	3.383	34.05158615	19.54265594	18.06489372
16	3.495	36.7530365	20.89182854	18.47802925
17	3.600	37.81851578	21.85855865	19.48721504
18	3.717	41.92352295	23.83507729	21.36373138
19	3.828	43.85614777	24.55565453	21.13145828
20	3.933	46.3263092	28.06816101	23.67712593
21	4.065	50.24572372	31.21367073	25.00640678
22	4.172	54.94150925	34.66669846	26.21079636
23	4.288	57.56103516	38.78707504	28.89224434
24	4.398	62.03171539	41.46094513	30.50843239
25	4.510	66.97280884	44.19525146	33.10625839
26	4.622	72.14802551	49.65290833	37.23417664
27	4.727	74.56231689	51.38412094	37.50894165
28	4.846	79.72375488	57.16812134	40.59814453
29	4.959	84.1991272	59.92744446	42.02235031
30	5.068	85.50177002	62.57131195	43.50736237
31	5.195	88.73097229	65.70414734	44.96834564
32	5.306	89.89060211	68.2312088	46.27281952
33	5.436	94.01967621	71.53417206	46.11478806
34	5.553	94.99580383	72.08236694	47.87189484
35	5.671	95.2322464	73.83358002	48.87511063
36	5.790	95.92689514	74.22052765	49.8032074
37	5.914	96.30413055	76.53079987	49.22870255
38	6.018	95.2461319	76.70669556	49.44694901
39	6.144	98.87258148	80.3126297	49.68060684

40	6.242	96.53569794	82.15896606	50.98404312
41	6.357	96.63265228	84.24301147	50.60038757
42	6.461	97.85651398	86.64820099	51.41771698
43	6.568	97.70493317	91.09775543	50.00495529
44	6.677	95.75215912	93.56739044	51.15594101
45	6.780	95.40727234	96.31655884	49.38502121
46	6.876	92.67470551	97.89413452	46.8549881
47	6.990	86.1247406	97.57066345	46.89836121
48	7.094	75.95001221	87.36820984	38.48823547
49	7.203	61.81266785	72.43412781	32.99816895
50	7.314	44.57408905	58.38670731	24.34742928
51	7.424	30.01371384	47.66504288	16.54802895
52	7.542	18.29223633	34.0994606	11.18401909
53	7.655	12.05433846	25.78352928	6.987697124
54	7.762	8.393678665	20.74028397	4.773160934
55	7.872	6.745064735	17.57155228	5.183382034
56	7.981	5.968804359	14.81519413	4.049934864
57	8.082	4.765892029	13.85979843	3.356540203
58	8.158	3.488528967	10.00986576	2.757013798
59	8.240	3.240872145	9.726230621	2.440250635
60	8.337	3.518944025	10.34944344	2.761593103
61	8.447	3.482762814	10.21502113	2.297191858
62	8.558	3.317880869	9.82105732	2.188625097
63	8.682	3.508411884	11.1798563	2.049291134
64	8.778	3.359441042	10.99246883	2.4326334
65	8.890	3.567781687	10.58485985	2.446130037
66	9.000	3.284593821	10.12457275	2.062712193
67	9.130	3.19876647	11.21827984	2.138687849
68	9.256	3.354375124	11.10833549	2.125937223
69	9.379	3.069160223	11.04604626	2.672266722
70	9.500	3.016864777	10.82899284	2.521372557

Table F.8: Cy_2DETA.2A.3HCl / Eu(III) phosphorescence emission raw data, λ_{ex} = 233 nm (multi-component buffered system, no equilibration).

Sample	pH	Emission Intensity (592 nm)	Emission Intensity (616 nm)	Emission Intensity (697 nm)
1	1.821	28.80597496	14.05441761	15.16164207
2	1.929	33.14177322	15.69245625	16.15571785
3	2.039	40.3662529	17.36598969	19.2711277
4	2.149	47.67998123	22.67241478	22.95213699
5	2.26	55.64881897	24.52057457	25.95183563
6	2.372	69.97412109	30.2763958	35.90758896
7	2.481	74.86149597	34.90010071	37.84495544
8	2.594	89.1513443	40.42513657	40.9011879
9	2.702	99.69168091	47.07707977	48.52353287
10	2.83	111.4419556	51.67032623	53.88419342
11	2.945	126.5483856	61.79269409	63.77908325
12	3.057	138.5809326	65.90402222	69.31389618
13	3.169	152.3823395	73.0974884	76.48388672
14	3.278	166.5324097	81.43154144	81.76787567
15	3.383	171.2176819	91.55612946	86.61286926
16	3.495	192.321991	93.70293427	94.86766052
17	3.6	204.5217438	101.2626266	98.9319458
18	3.717	217.9154053	111.4922104	102.7761841
19	3.828	234.6093292	123.6957397	116.2856979
20	3.933	244.8434906	134.0330505	125.4416122
21	4.065	277.5351563	152.4590302	135.939743
22	4.172	296.1378479	161.5241394	144.7181396
23	4.288	329.175415	185.8832397	155.9932556
24	4.398	351.4886169	202.6849365	169.5284424
25	4.51	370.9349365	221.6637573	191.6605682
26	4.622	403.896759	240.4217072	198.0724487
27	4.727	423.5360107	259.8536682	212.7320404
28	4.846	457.3185425	286.8272705	227.2323608
29	4.959	475.648407	300.3562622	236.5384064
30	5.068	502.4088745	323.7179565	247.4396362
31	5.195	514.7789917	337.3430481	259.5351563
32	5.306	522.0582275	345.3034973	255.8647766
33	5.436	534.8867188	355.36203	266.1302185
34	5.553	540.8477173	361.5657349	271.9726868
35	5.671	544.9892578	364.3277588	271.4217224
36	5.79	543.1848145	370.6407471	276.5044556
37	5.914	549.8568726	379.2029419	278.2951965
38	6.018	551.1279297	376.592865	274.7319031
39	6.144	545.328125	387.9200439	278.7792358
40	6.242	551.1759644	389.1517334	275.0906372

41	6.357	544.4343872	396.1683655	269.2937927
42	6.461	530.2497559	400.487854	269.39328
43	6.568	534.6073608	411.8097229	271.8993225
44	6.677	533.5966797	431.6028442	270.1070251
45	6.78	510.8588867	440.7201538	262.8186951
46	6.876	486.8019714	451.0989075	257.6362
47	6.99	472.7924194	456.5289307	244.6389465
48	7.094	414.9644165	416.4238892	215.1771545
49	7.203	332.967041	363.9856567	176.895813
50	7.314	249.0409851	300.2058105	132.7922516
51	7.424	163.9296417	232.4351501	84.26143646
52	7.542	96.38639832	160.2418823	54.82554245
53	7.655	58.58047867	112.848381	33.01540375
54	7.762	37.37350464	78.50048065	20.76759338
55	7.872	26.31199455	61.8841629	19.26977539
56	7.981	22.55978584	49.61784744	13.78368855
57	8.082	17.23645782	42.18837357	10.91244698
58	8.158	10.41022396	30.3991394	6.763785362
59	8.24	9.23193264	23.90489578	5.805333614
60	8.337	9.010306358	24.09025192	6.312778473
61	8.447	7.31170702	23.831213	4.49470377
62	8.558	7.740402222	20.76484871	5.401459217
63	8.682	6.282621861	22.54300117	4.375964165
64	8.778	6.824911118	21.70372963	5.257473469
65	8.89	6.407401562	20.62024498	4.590091228
66	9	7.837794781	20.26502419	5.637992859
67	9.13	6.358133793	20.38901138	4.341631889
68	9.256	6.231439114	16.45710945	2.959235191
69	9.379	5.632583618	18.19210052	5.645633221
70	9.5	6.537756443	17.26384163	3.602227211

Appendix G – Determination of q

G.1 Determination of the solution hydration state of $[Eu(Cy_2DETA.3A)]^{3+}$

The hydration state of the Cy_2DETA.3A.3HCl / Eu(III) system was determined as a function of pH.

G.1.1 Cy_2DETA.3A.3HCl / Eu(III), H_2O, aqueous solution

Cy_2DETA.3A.3HCl (0.0043 g, 7.86×10^{-6} mol) and $Eu(CF_3SO_3)_3$ (0.0049 g, 8.12×10^{-6} mol) were dissolved in deionised water, in a 50 mL volumetric flask. This solution was placed in a jacketed-cell (25 °C). An in-cell titration was performed on the solution using concentrated acid (HCl) and concentrated base (NaOH) solutions. Upon each addition of acid or base, the pH of the solution was allowed to stabilize and the pH value recorded. A small volume of the adjusted solution was decanted and sealed in a marked vial prior to subsequent pH adjustment. Solutions were prepared at pH 3.38 (stock solution), pH 4.05 (sample 1) and pH 7.75 (sample 2), as per the observed pK_a values from the corresponding luminescence study.

The absorbance of the stock solution was measured in order to determine the excitation wavelength for the luminescence study (Figure G.1).

The pH of each solution was measured upon initial preparation (0 hours), after 24 hours, and after 6 days, prior to each absorbance and luminescence measurement. The absorbance was measured over a range of 200 nm and 800 nm.

The phosphorescence emission spectrum was measured by exciting each sample at a wavelength of 223 nm. The spectrum was recorded in the high sensitivity mode, over a range of 550 nm to 750 nm. Each measurement was recorded after a 0.100 ms time delay, with both the excitation and emission slit widths set at 10 nm.

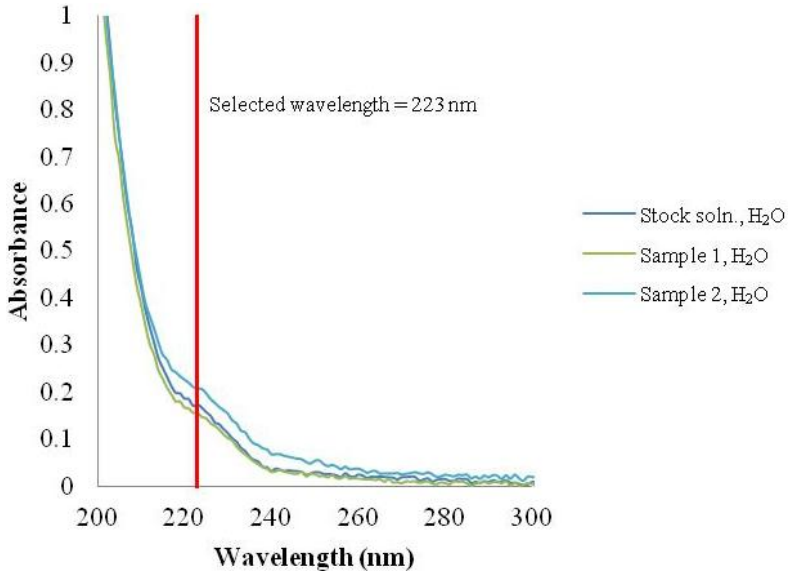


Figure G.1: Absorbance spectrum of europium(III)-1,7-bis(2-hydroxycyclohexyl)-1,4,7-tris(carboxymethyl)-1,4,7 triazaheptane in H_2O, as a function of pH, upon initial preparation.

The phosphorescence emission decay spectrum was measured by exciting each sample at a wavelength of 223 nm. The J = 1 (591 nm), J = 2 (616 nm), and J = 4 (696 nm) emission wavelengths were observed and the decay recorded over a period of 100 ms. Each measurement was recorded after a 0.200 ms time delay, at a gate time of 0.500 ms, with an excitation slit width of 20 nm and an emission slit width of 10 nm. The data set is an average of a 50 cycle run. A non-linear least squares fit was generated for each run.

The following table consists of the data obtained from the fits for each emission decay spectrum, as a function of pH.

Table G.1: Cy_2DETA.3A.3HCl / Eu(III) phosphorescence emission decay data (in H_2O, aqueous solution, λ_{ex} = 223 nm).

Sample	Time	pH	Emission Wavelength (nm)	Detector Voltage	k1	A1	C	Standard Deviation
Stock Solution	0 hours	3.377	591	high	3.528±0.2	109.3674±8.7	0.1492±0.0	0.1685
	24 hours	3.425	591	high	2.559±0.0	225.8802±2.5	0.1399±0.0	0.1203
	6 days	3.481	591	high	2.530±0.0	242.8775±2.7	0.0613±0.0	0.1361
	0 hours	3.377	616	high	2.917±0.1	128.1415±3.9	0.1054±0.0	0.1332
	24 hours	3.425	616	high	2.505±0.0	427.0151±2.8	0.0704±0.0	0.1446
	6 days	3.481	616	high	2.440±0.0	462.6205±2.9	0.0467±0.0	0.1574
	0 hours	3.377	696	high	3.451±0.2	71.4480±6.9	0.0993±0.0	0.1442
	24 hours	3.425	696	high	2.612±0.0	187.6844±2.8	0.1646±0.0	0.1303

	6 days	3.481	696	high	2.647±0.0	208.3199±3.3	0.1101±0.0	0.1476
Sample 1	0 hours	4.047	591	high	3.240±0.1	239.8819±7.0	0.1042±0.0	0.1777
	24 hours	3.863	591	high	2.506±0.0	255.4369±2.6	0.1156±0.0	0.1322
	6 days	4.035	591	high	2.490±0.0	277.8528±3.3	0.0495±0.0	0.1727
	0 hours	4.047	616	high	2.944±0.0	376.4782±6.6	0.1151±0.0	0.2234
	24 hours	3.863	616	high	2.513±0.0	518.9810±3.9	0.0220±0.0	0.1962
	6 days	4.035	616	high	2.462±0.0	553.8118±3.6	0.0622±0.0	0.1925
	0 hours	4.047	696	high	3.239±0.1	184.8662±6.3	0.2072±0.0	0.1611
	24 hours	3.863	696	high	2.600±0.0	211.1280±3.6	0.1104±0.0	0.1676
	6 days	4.035	696	high	2.434±0.0	212.3735±3.1	0.0644±0.0	0.1719
Sample 2	0 hours	7.754	591	high	2.618±0.0	225.5331±3.8	0.1412±0.0	0.1742
	24 hours	7.076	591	high	2.420±0.0	272.6394±3.2	0.1213±0.0	0.1787
	6 days	7.101	591	high	2.401±0.0	269.6860±2.9	0.1806±0.0	0.1616
	0 hours	7.754	616	high	2.668±0.0	479.4288±4.8	0.0821±0.0	0.2122
	24 hours	7.076	616	high	2.473±0.0	562.7735±3.8	0.1076±0.0	0.2011
	6 days	7.101	616	high	2.442±0.0	569.0682±3.2	0.0466±0.0	0.1759
	0 hours	7.754	696	high	2.658±0.0	186.3183±4.1	0.1352±0.0	0.1833
	24 hours	7.076	696	high	2.700±0.0	261.6119±4.0	0.0105±0.0	0.1715
	6 days	7.101	696	high	2.454±0.0	219.9439±2.9	0.00464±0.0	0.1555

G.1.2 Cy_2DETA.3A.3HCl / Eu(III), D_2O, aqueous solution

Cy_2DETA.3A.3HCl (0.0019 g, 3.47×10^{-6} mol) and $Eu(CF_3SO_3)_3$ (0.0025 g, 4.17×10^{-6} mol) were dissolved in D_2O, in a 25 mL volumetric flask. This solution was placed in a jacketed-cell (25 °C). An in-cell titration was performed on the solution using concentrated acid (DCl) and concentrated base (NaOD) solutions. Upon each addition of acid or base, the pD of the solution was allowed to stabilize and the pD value recorded. A small volume of the adjusted solution was decanted and sealed in a marked vial prior to subsequent pD adjustment. Solutions were prepared at pD 3.77 (stock solution), pD 4.09 (sample 1) and pD 7.73 (sample 2), as per the observed pK_a values from the corresponding luminescence study.

The absorbance of the stock solution was measured in order to determine the wavelength to be used for excitation in the luminescence study (Figure G.2).

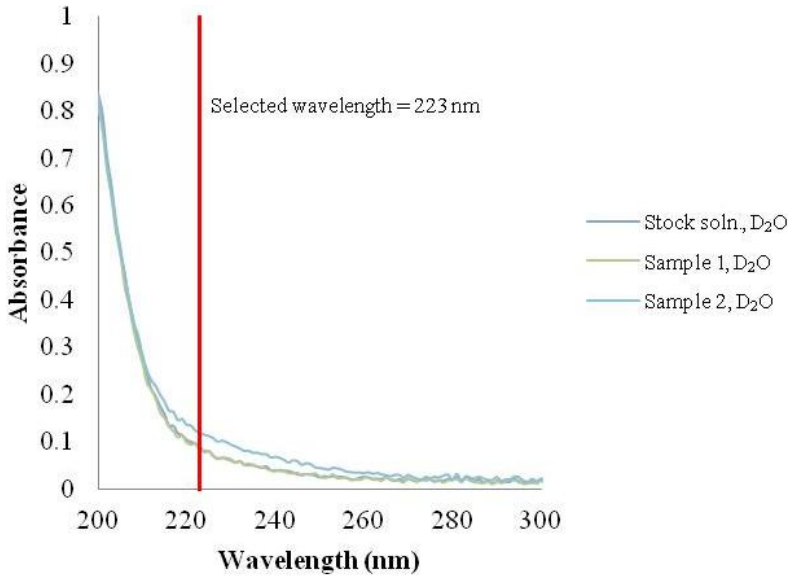


Figure G.2: Absorbance spectrum of europium(III)-1,7-bis(2-hydroxycyclohexyl)-1,4,7-tris(carboxymethyl)-1,4,7 triazaheptane in D_2O, as a function of pD, measured upon initial preparation.

The pD of each solution was measured upon initial preparation (0 hours), after 24 hours, and after 6 days, prior to each absorbance and luminescence measurement. The absorbance was measured over a range of 200 nm and 800 nm.

The phosphorescence emission spectrum was measured by exciting each sample at a wavelength of 223 nm. The spectrum was recorded in the high sensitivity mode, over a range of 550 nm to 750 nm. Each measurement was recorded after a 0.100 ms time delay, with both the excitation and emission slit widths set at 10 nm.

The phosphorescence emission decay spectrum was measured by exciting each sample at a wavelength of 223 nm. The J = 1 (591 nm), J = 2 (616 nm), and J = 4 (696 nm) emission wavelengths were observed and the decay recorded over a period of 100 ms. Each measurement was recorded after a 0.200 ms time delay, at a gate time of 0.500 ms, with an excitation slit width of 20 nm and an emission slit width of 10 nm. The data set is an average of a 50 cycle run. A non-linear least squares fit was generated for each run.

The following table consists of the data obtained from the fits for each emission decay spectrum, as a function of pD.

Table G.2: Cy_2DETA.3A.3HCl / Eu(III) phosphorescence emission decay data (in D_2O, aqueous solution, λ_{ex} = 223 nm).

Sample	Time	pD	Emission Wavelength (nm)	Detector Voltage	k1	A1	C	Standard Deviation
Stock Solution	0 hours	3.770	591	high	0.343±0.2	292.3967±0.9	0.1336±0.1	0.4888
	24 hours	3.589	591	high	0.398±0.0	307.5389±0.6	0.1827±0.0	0.4263
	6 days	3.461	591	high	0.425±0.0	321.7266±0.8	0.1143±0.1	0.3528
	0 hours	3.770	616	high	0.374±0.0	178.1617±0.9	0.1277±0.1	0.4460
	24 hours	3.589	616	high	0.412±0.0	317.2874±0.8	0.1412±0.1	0.3576
	6 days	3.461	616	high	0.450±0.0	464.8063±0.7	0.1205±0.0	0.3247
	0 hours	3.770	696	high	0.345±0.0	148.7991±0.8	0.0317±0.1	0.4399
	24 hours	3.589	696	high	0.386±0.0	189.4754±0.6	0.1324±0.0	0.3978
	6 days	3.461	696	high	0.434±0.0	217.9484±0.7	0.1072±0.0	0.3058
Sample 1	0 hours	4.087	591	high	0.397±0.1	516.2090±1.4	0.1822±0.1	0.6630
	24 hours	3.818	591	high	0.424±0.0	504.0843±0.6	0.0989±0.0	0.4253
	6 days	3.602	591	high	0.441±0.0	344.9927±0.9	0.0586±0.1	0.3921
	0 hours	4.087	616	high	0.431±0.0	359.0365±1.5	0.2618±0.1	0.6764
	24 hours	3.818	616	high	0.445±0.0	437.9845±0.2	0.1253±0.1	0.4197
	6 days	3.602	616	high	0.461±0.0	508.8354±0.8	0.1297±0.0	0.3407
	0 hours	4.087	696	high	0.402±0.0	272.4297±0.8	0.1299±0.1	0.3615
	24 hours	3.818	696	high	0.426±0.0	259.8373±1.6	0.1534±0.1	0.4398
	6 days	3.602	696	high	0.452±0.0	237.2722±1.1	0.1259±0.1	0.4680
Sample 2	0 hours	7.734	591	high	0.514±0.0	173.4727±1.6	0.1790±0.1	0.6547
	24 hours	7.103	591	high	0.511±0.0	246.7489±1.3	0.1236±0.0	0.5132
	6 days	6.881	591	high	0.511±0.0	276.1261±1.4	0.1418±0.1	0.5409
	0 hours	7.734	616	high	0.529±0.0	366.3680±3.5	0.2547±0.2	1.3677
	24 hours	7.103	616	high	0.516±0.0	437.0983±1.7	0.1721±0.1	0.4956
	6 days	6.881	616	high	0.498±0.0	554.7637±1.4	0.1083±0.1	0.5628
	0 hours	7.734	696	high	0.527±0.0	139.1424±1.3	0.1492±0.1	0.5209
	24 hours	7.103	696	high	0.519±0.0	185.2005±0.4	0.1123±0.1	0.4260
	6 days	6.881	696	high	0.510±0.0	216.3400±0.8	0.1019±0.0	0.3270

G.1.3 Cy_2DETA.3A.3HCl / Eu(III), H_2O, multi-component buffered system

Cy_2DETA.3A.3HCl (0.0041 g, 7.50×10^{-6} mol) and $Eu(CF_3SO_3)_3$ (0.0048 g, 8.01×10^{-6} mol) were dissolved in deionised water, in a 50 mL volumetric flask. To this flask, 3.75 µL of a 0.2 mol/L solution consisting of the buffers KHP, MES, CHES, MOPS, and Tris was added and the contents diluted to the mark. This solution was placed in a jacketed-cell (25 °C). An in-cell titration was performed on this solution using concentrated acid (HCl) and concentrated base (NaOH) solutions. Upon each addition of acid or base, the pH of the

solution was allowed to stabilize and the pH value recorded. A small volume of the adjusted solution was decanted and sealed in a marked vial prior to subsequent pH adjustment. Solutions were prepared at pH 3.45 (stock solution), pH 3.07 (sample 1), pH 5.42 (sample 2), pH 7.59 (sample 3) and pH 11.28 (sample 4) as per the observed pK_a values from the corresponding luminescence study.

The absorbance of the stock solution was measured in order to determine the wavelength to be used for excitation in the luminescence study (Figure G.3).

The pH of each solution was measured upon initial preparation (0 hours), after 24 hours, and after 3, 7, and 14 days, prior to each absorbance and luminescence measurement. The absorbance was measured over a range of 200 nm and 800 nm.

The phosphorescence emission spectrum was measured by exciting each sample at wavelengths of 276 nm and 227 nm. The spectrum was recorded in the high sensitivity mode, over a range of 550 nm to 750 nm. Each measurement was recorded after a 0.100 ms time delay, with both the excitation and emission slit widths set at 10 nm.

The phosphorescence emission decay spectrum was measured by exciting each sample at wavelengths of 276 nm and 227 nm. The J = 1 (592 nm), J = 2 (617 nm), and J = 4 (696 nm) emission wavelengths were observed and the decay recorded over a period of 100 ms. Each measurement was recorded after a 0.200 ms time delay, at a gate time of 0.500 ms, with an excitation slit width of 20 nm and an emission slit width of 10 nm. The data set is an average of a 50 cycle run. A non-linear least squares fit was generated for each run.

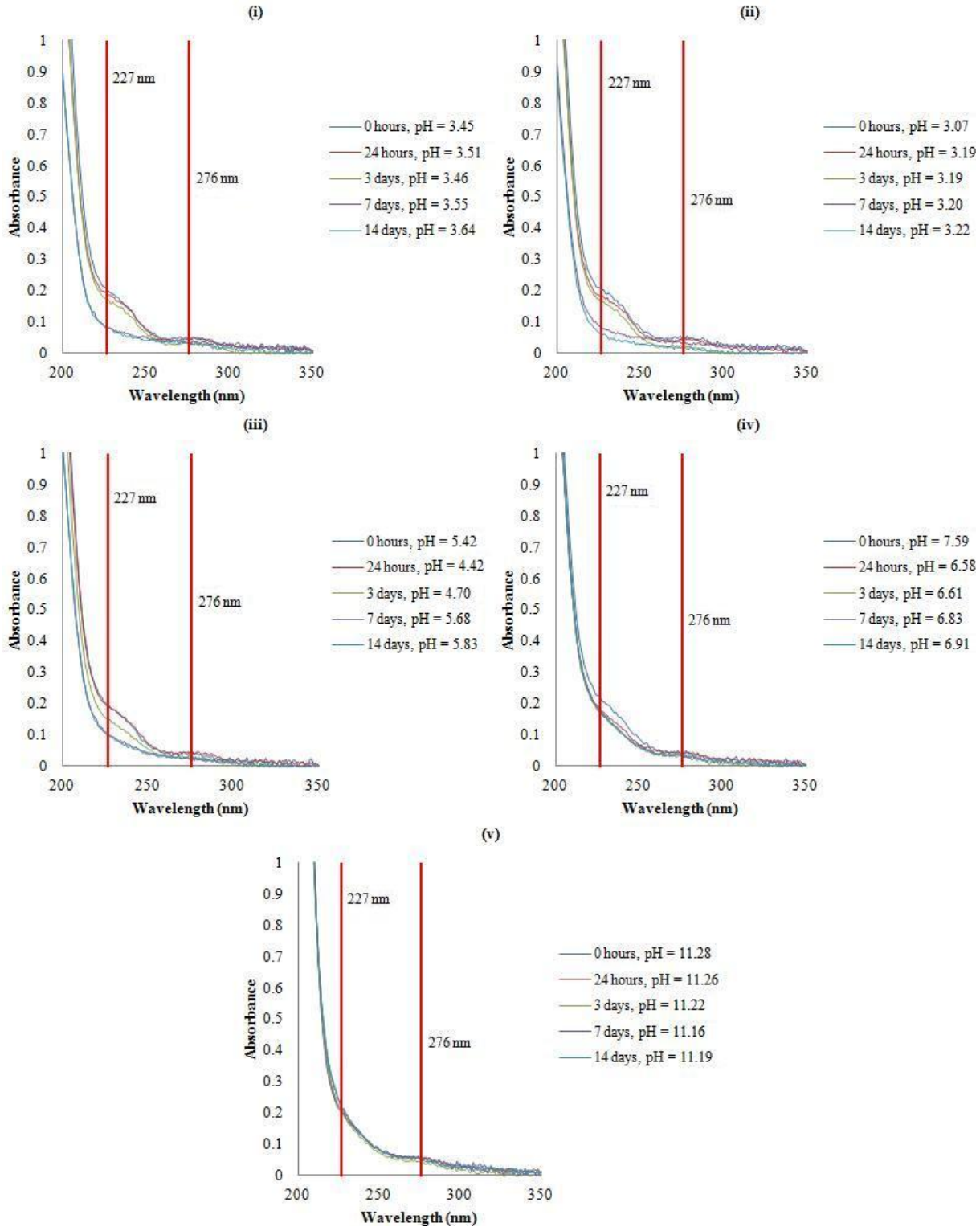


Figure G.3: Absorbance spectrum of europium(III)-1,7-bis(2-hydroxycyclohexyl)-1,4,7-tris(carboxymethyl)-1,4,7 triazaheptane in H_2O, as a function of pH, in a multi-component buffered system.

The following tables consist of the data obtained from the fits for each emission decay spectrum, as a function of pH.

Table G.3: $Cy_2DETA.3A.3HCl$ / Eu(III) phosphorescence emission decay data (in H_2O, multi-component buffered system, λ_{ex} = 276 nm).

Sample	Time	pH	Emission Wavelength (nm)	Detector Voltage	k1	A1	C	Standard Deviation
Stock Solution	0 hours	3.447	592	high	6.848±0.1	1028.2750±39.0	0.0171±0.0	0.0313
	24 hours	3.513	592	high	3.470±0.0	239.7721±3.2	0.0257±0.0	0.0654
	3 days	3.456	592	high	3.338±0.0	227.4347±3.3	0.0164±0.0	0.0770
	7 days	3.548	592	high	2.528±0.0	106.3596±0.4	0.0138±0.0	0.0193
	14 days	3.640	592	high	2.546±0.0	113.7379±0.4	0.0145±0.0	0.0207
	0 hours	3.447	617	high	4.799±0.1	241.5542±6.3	0.0275±0.0	0.0363
	24 hours	3.513	617	high	2.741±0.0	232.0675±1.5	0.0130±0.0	0.0602
	3 days	3.456	617	high	2.743±0.0	245.3350±1.7	0.0159±0.0	0.0676
	7 days	3.548	617	high	2.457±0.0	202.7752±0.3	0.0177±0.0	0.0182
	14 days	3.640	617	high	2.437±0.0	210.2605±0.4	0.0117±0.0	0.0210
	0 hours	3.447	696	high	5.977±0.1	348.0308±14.4	0.0239±0.0	0.0266
	24 hours	3.513	696	high	3.190±0.0	143.3094±2.1	0.0094±0.0	0.0572
	3 days	3.456	696	high	3.095±0.0	142.1773±2.1	0.0163±0.0	0.0614
	7 days	3.548	696	high	2.543±0.0	86.9565±0.4	0.0180±0.0	0.0200
	14 days	3.640	696	high	2.536±0.0	89.2586±0.4	0.0108±0.0	0.0207
Sample 1	0 hours	3.069	592	high	6.051±0.1	527.0799±19.3	0.0187±0.0	0.0332
	24 hours	3.194	592	high	3.716±0.0	213.1077±3.4	0.0326±0.0	0.0552
	3 days	3.189	592	high	3.745±0.0	216.2662±3.9	0.0060±0.0	0.0618
	7 days	3.195	592	high	2.583±0.0	75.6658±0.5	0.0097±0.0	0.0216
	14 days	3.220	592	high	2.554±0.0	76.7105±0.4	0.0181±0.0	0.0215
	0 hours	3.069	617	high	4.190±0.1	147.2833±3.8	0.0215±0.0	0.0388
	24 hours	3.194	617	high	2.826±0.0	172.2154±0.9	0.0076±0.0	0.0358
	3 days	3.189	617	high	2.853±0.0	177.1854±1.6	0.0219±0.0	0.0575
	7 days	3.195	617	high	2.417±0.0	129.9523±0.4	0.0177±0.0	0.0201
	14 days	3.220	617	high	2.522±0.0	146.5358±0.5	0.0186±0.0	0.0246
	0 hours	3.069	696	high	5.485±0.1	214.1992±10.3	0.0153±0.0	0.0305
	24 hours	3.194	696	high	3.358±0.0	116.3314±2.1	0.0141±0.0	0.0482
	3 days	3.189	696	high	3.266±0.0	112.6869±1.4	0.0138±0.0	0.0357
	7 days	3.195	696	high	2.508±0.0	57.0231±0.4	0.0135±0.0	0.0211
	14 days	3.220	696	high	2.555±0.0	61.6594±0.5	0.0128±0.0	0.0223
Sample 2	0 hours	5.415	592	high	5.466±0.1	1262.8680±31.2	0.0133±0.0	0.0942
	24 hours	4.416	592	high	4.173±0.0	574.7116±11.2	0.0115±0.0	0.1164
	3 days	4.696	592	high	3.872±0.0	453.9623±7.9	0.0225±0.0	0.1104
	7 days	5.683	592	high	2.970±0.0	186.7887±1.7	0.0151±0.0	0.0571
	14 days	5.832	592	high	2.924±0.0	186.1340±1.6	0.0216±0.0	0.0551
	0 hours	5.415	617	high	4.258±0.0	721.3007±14.1	0.0320±0.0	0.1357
	24 hours	4.416	617	high	3.221±0.0	448.9431±5.0	0.0238±0.0	0.1284
	3 days	4.696	617	high	3.118±0.0	440.2940±4.6	0.0303±0.0	0.1301
	7 days	5.683	617	high	2.705±0.0	291.6166±1.6	0.0214±0.0	0.0674

	14 days	5.832	617	high	2.756±0.0	314.8302±1.6	0.0045±0.0	0.0655
	0 hours	5.415	696	high	4.992±0.1	574.9331±13.9	0.0270±0.0	0.0662
	24 hours	4.416	696	high	3.687±0.0	283.7033±5.2	0.0210±0.0	0.0857
	3 days	4.696	696	high	3.341±0.0	224.4787±3.5	0.0109±0.0	0.0799
	7 days	5.683	696	high	2.738±0.0	124.0301±0.9	0.0202±0.0	0.0371
	14 days	5.832	696	high	2.752±0.0	126.6910±0.7	0.0092±0.0	0.0300
Sample 3	0 hours	7.585	592	high	3.522±0.0	248.3551±3.7	0.0191±0.0	0.0722
	24 hours	6.576	592	high	3.292±0.0	265.9362±3.6	0.0199±0.0	0.0872
	3 days	6.609	592	high	2.971±0.0	191.5202±2.2	0.0199±0.0	0.0718
	7 days	6.830	592	high	2.784±0.0	162.1675±1.0	0.0211±0.0	0.0401
	14 days	6.910	592	high	2.645±0.0	138.8950±0.9	0.0208±0.0	0.0395
	0 hours	7.585	617	high	3.370±0.0	417.5388±6.1	0.0250±0.0	0.1366
	24 hours	6.576	617	high	3.162±0.0	477.4207±4.8	0.0257±0.0	0.1313
	3 days	6.609	617	high	2.918±0.0	375.8624±2.4	0.0199±0.0	0.0832
	7 days	6.830	617	high	2.817±0.0	332.4015±1.9	0.0153±0.0	0.0740
	14 days	6.910	617	high	2.646±0.0	282.9486±1.3	0.0110±0.0	0.0583
	0 hours	7.585	696	high	3.326±0.0	160.8864±1.9	0.0247±0.0	0.0451
	24 hours	6.576	696	high	2.993±0.0	161.3304±1.3	0.0113±0.0	0.0414
	3 days	6.609	696	high	2.811±0.0	132.6997±0.9	0.0183±0.0	0.0354
	7 days	6.830	696	high	2.679±0.0	116.7143±0.7	0.0219±0.0	0.0320
	14 days	6.910	696	high	2.573±0.0	104.7563±0.5	0.0120±0.0	0.0233
Sample 4	0 hours	11.282	592	high	2.449±0.0	213.3535±0.6	0.0109±0.0	0.0314
	24 hours	11.259	592	high	2.476±0.0	211.8441±0.5	0.0189±0.0	0.0279
	3 days	11.217	592	high	2.475±0.0	200.5352±0.6	0.0168±0.0	0.0309
	7 days	11.163	592	high	2.473±0.0	191.6712±0.5	0.0154±0.0	0.0274
	14 days	11.191	592	high	2.459±0.0	179.2451±0.5	0.0103±0.0	0.0252
	0 hours	11.282	617	high	2.404±0.0	717.5434±0.7	0.0193±0.0	0.0410
	24 hours	11.259	617	high	2.382±0.0	681.8754±0.8	0.0229±0.0	0.0452
	3 days	11.217	617	high	2.391±0.0	645.6586±0.6	0.0050±0.0	0.0323
	7 days	11.163	617	high	2.395±0.0	606.9907±0.6	0.0226±0.0	0.0361
	14 days	11.191	617	high	2.382±0.0	549.8469±0.6	0.0370±0.0	0.0323
	0 hours	11.282	696	high	2.519±0.0	145.4893±0.6	0.0243±0.0	0.0279
	24 hours	11.259	696	high	2.534±0.0	142.0283±0.5	0.0089±0.0	0.0272
	3 days	11.217	696	high	2.508±0.0	135.5346±0.5	0.0215±0.0	0.0255
	7 days	11.163	696	high	2.521±0.0	132.0420±0.6	0.0066±0.0	0.0296
	14 days	11.191	696	high	2.496±0.0	123.3301±0.5	0.0051±0.0	0.0263

Table G.4: $Cy_2DETA.3A.3HCl$ / Eu(III) phosphorescence emission decay data (in H_2O, multi-component buffered system, λ_{ex} = 227 nm).

Sample	Time	pH	Emission Wavelength (nm)	Detector Voltage	k1	A1	C	Standard Deviation
Stock Solution	0 hours	3.447	592	high	7.748±0.1	8797.8010±349.6	0.0419±0.0	0.1183
	24 hours	3.513	592	high	4.484±0.1	1455.4720±37.5	0.0670±0.0	0.2906
	3 days	3.456	592	high	4.302±0.1	1341.9400±31.9	0.0604±0.0	0.2946
	7 days	3.548	592	high	2.533±0.0	259.6148±1.8	0.1002±0.0	0.0919
	14 days	3.640	592	high	2.572±0.0	285.6066±2.2	0.1149±0.0	0.1065
	0 hours	3.447	616	high	5.962±0.1	2016.3080±79.7	0.0232±0.0	0.1498
	24 hours	3.513	616	high	3.168±0.0	768.6201±10.8	0.0524±0.0	0.2929
	3 days	3.456	616	high	3.069±0.0	766.0609±9.4	0.1011±0.0	0.2823
	7 days	3.548	616	high	2.518±0.0	502.0524±1.7	0.0851±0.0	0.0865
	14 days	3.640	616	high	2.456±0.0	507.7221±2.0	0.0620±0.0	0.1059
	0 hours	3.447	696	high	7.201±0.1	3431.2080±216.3	0.0968±0.0	0.1237
	24 hours	3.513	696	high	3.952±0.1	672.1552±15.6	0.0314±0.0	0.2010
	3 days	3.456	696	high	3.871±0.0	649.2813±13.9	0.0581±0.0	0.1943
	7 days	3.548	696	high	2.518±0.0	202.0830±1.6	0.0884±0.0	0.0806
	14 days	3.640	696	high	2.447±0.0	204.5512±1.7	0.0422±0.0	0.0920
Sample 1	0 hours	3.069	592	high	7.174±0.1	4707.8340±221.3	0.0097±0.0	0.1299
	24 hours	3.194	592	high	4.923±0.1	1561.1430±45.4	0.0847±0.0	0.2312
	3 days	3.189	592	high	4.866±0.1	1475.4810±41.9	0.1094±0.0	0.2249
	7 days	3.195	592	high	2.633±0.0	179.5493±2.2	0.0311±0.0	0.1010
	14 days	3.220	592	high	2.666±0.0	197.1495±2.6	0.0502±0.0	0.1126
	0 hours	3.069	616	high	5.464±0.1	1185.5020±45.8	0.0698±0.0	0.1386
	24 hours	3.194	616	high	3.404±0.0	652.9030±9.4	0.0913±0.0	0.2035
	3 days	3.189	616	high	3.356±0.0	641.3417±10.4	0.1026±0.0	0.2372
	7 days	3.195	616	high	2.471±0.0	317.1583±2.0	0.0386±0.0	0.1055
	14 days	3.220	616	high	2.579±0.0	364.1633±2.6	0.0550±0.0	0.1258
	0 hours	3.069	696	high	6.858±0.2	2079.3750±153.7	0.1184±0.0	0.1222
	24 hours	3.194	696	high	4.328±0.1	675.1238±18.4	0.0883±0.0	0.1653
	3 days	3.189	696	high	4.264±0.1	634.9384±18.7	0.0369±0.0	0.1785
	7 days	3.195	696	high	2.515±0.0	132.4764±1.9	0.0690±0.0	0.0943
	14 days	3.220	696	high	2.595±0.0	144.8667±2.4	0.0699±0.0	0.1124
Sample 2	0 hours	5.415	592	high	6.710±0.0	13174.5400±277.2	0.1184±0.0	0.2540
	24 hours	4.416	592	high	5.542±0.1	5316.7470±133.8	0.0591±0.1	0.3758
	3 days	4.696	592	high	4.992±0.0	3582.6280±78.3	0.1012±0.1	0.3731
	7 days	5.683	592	high	3.443±0.0	783.2510±11.0	0.0929±0.0	0.2305
	14 days	5.832	592	high	3.520±0.0	809.7483±13.5	0.1023±0.0	0.2634
	0 hours	5.415	616	high	5.433±0.0	6195.9060±137.0	0.0992±0.1	0.4276
	24 hours	4.416	616	high	4.149±0.0	2632.3630±51.1	0.0646±0.1	0.5458
	3 days	4.696	616	high	3.931±0.0	2382.1290±46.3	0.0963±0.1	0.6094
	7 days	5.683	616	high	3.023±0.0	965.7190±8.7	0.1034±0.0	0.2714

	14 days	5.832	616	high	3.155±0.0	1109.2600±11.1	0.0897±0.0	0.3074
	0 hours	5.415	696	high	6.203±0.1	5642.3970±158.4	0.0970±0.0	0.2361
	24 hours	4.416	696	high	4.984±0.1	2275.3220±57.3	0.1684±0.0	0.2750
	3 days	4.696	696	high	4.489±0.0	1663.7190±31.3	0.1295±0.0	0.2410
	7 days	5.683	696	high	3.330±0.0	499.6107±9.1	0.0698±0.0	0.2130
	14 days	5.832	696	high	3.251±0.0	491.1623±8.0	0.0629±0.0	0.2009
Sample 3	0 hours	7.585	592	high	4.493±0.0	1631.2600±31.5	0.0745±0.0	0.2419
	24 hours	6.576	592	high	4.147±0.0	1555.0140±31.3	0.1119±0.0	0.3350
	3 days	6.609	592	high	3.585±0.0	864.5063±13.3	0.1227±0.0	0.2439
	7 days	6.830	592	high	3.219±0.0	583.8993±6.2	0.0893±0.0	0.1610
	14 days	6.910	592	high	2.927±0.0	427.3264±4.7	0.1156±0.0	0.1625
	0 hours	7.585	616	high	4.265±0.0	2461.1420±50.9	0.1420±0.1	0.4865
	24 hours	6.576	616	high	3.988±0.0	2658.9810±45.3	0.0938±0.1	0.5650
	3 days	6.609	616	high	3.643±0.0	1759.2190±29.7	0.1424±0.1	0.5149
	7 days	6.830	616	high	3.227±0.0	1170.6520±13.8	0.1350±0.1	0.3564
	14 days	6.910	616	high	2.915±0.0	866.8267±7.1	0.1022±0.0	0.2452
	0 hours	7.585	696	high	4.239±0.1	935.0468±22.5	0.0564±0.0	0.2201
	24 hours	6.576	696	high	3.853±0.0	885.6932±19.6	0.0576±0.0	0.2776
	3 days	6.609	696	high	3.336±0.0	521.5886±7.8	0.0342±0.0	0.1804
	7 days	6.830	696	high	3.073±0.0	393.0548±4.9	0.0534±0.0	0.1451
	14 days	6.910	696	high	2.781±0.0	295.5099±9.0	0.0811±0.0	0.1175
Sample 4	0 hours	11.282	592	high	2.509±0.0	264.2086±2.4	0.0714±0.0	0.1228
	24 hours	11.259	592	high	2.365±0.0	230.6418±2.4	0.0656±0.0	0.1377
	3 days	11.217	592	high	2.528±0.0	249.3860±2.7	0.0675±0.0	0.1372
	7 days	11.163	592	high	2.450±0.0	235.5095±2.1	0.1321±0.0	0.1138
	14 days	11.191	592	high	2.458±0.0	227.8646±2.2	0.0938±0.0	0.1199
	0 hours	11.282	616	high	2.403±0.0	834.8275±2.5	0.0591±0.0	0.1423
	24 hours	11.259	616	high	2.365±0.0	797.1254±2.9	0.0054±0.0	0.1720
	3 days	11.217	616	high	2.383±0.0	752.8119±2.3	0.0639±0.0	0.1293
	7 days	11.163	616	high	2.432±0.0	729.6937±3.1	0.1333±0.0	0.1712
	14 days	11.191	616	high	2.407±0.0	686.4568±2.3	0.0713±0.0	0.1311
	0 hours	11.282	696	high	2.625±0.0	184.6718±3.0	0.0150±0.0	0.1358
	24 hours	11.259	696	high	2.486±0.0	169.4153±2.6	0.0180±0.0	0.1344
	3 days	11.217	696	high	2.461±0.0	159.8941±2.3	0.0363±0.0	0.1216
	7 days	11.163	696	high	2.494±0.0	163.7882±2.3	0.0356±0.0	0.1206
	14 days	11.191	696	high	2.482±0.0	157.2949±2.2	0.0749±0.0	0.1168

G.1.4 Cy_2DETA.3A.3HCl / Eu(III), D_2O, multi-component buffered system

Cy_2DETA.3A.3HCl (0.0019 g, 3.47×10^{-6} mol) and $Eu(CF_3SO_3)_3$ (0.0025 g, 4.17×10^{-6} mol) were dissolved in D_2O, in a 25 mL volumetric flask. To this flask, 66 µL of a 5 mmol/L solution consisting of the buffers KHP, MES, CHES, MOPS, and Tris was added and the contents diluted to the mark. This solution was placed in a jacketed-cell (25 °C). An in-cell

titration was performed on the solution using concentrated acid (DCl) and concentrated base (NaOD) solutions. Upon each addition of acid or base, the pD of the solution was allowed to stabilize and the pD value was recorded. A small volume of the adjusted solution was decanted and sealed in a marked vial prior to subsequent pD adjustment. Solutions were prepared at pD 4.36 (stock solution), pD 3.06 (sample 1), pD 5.46 (sample 2), pD 7.62 (sample 3) and pD 11.28 (sample 4) as per the observed pK_a values from the corresponding luminescence study. Due to the high intensity obtained for each prepared sample, measurements were conducted on diluted samples (using 600 μL of the prepared sample and diluting to a total volume of 3000 μL).

The absorbance of the stock solution was measured in order to determine the wavelength to be used for excitation in the luminescence study (Figure G.4).

The pD of each solution was measured upon initial preparation (0 hours) and after 3, 7, and 14 days, prior to each absorbance and luminescence measurement. The absorbance was measured over a range of 200 nm and 800 nm.

The phosphorescence emission spectrum was measured by exciting each sample at wavelengths of 276 nm and 227 nm. The spectrum was recorded in the high sensitivity mode, over a range of 550 nm to 750 nm. Each measurement was recorded after a 0.100 ms time delay, with both the excitation and emission slit widths set at 10 nm.

The phosphorescence emission decay spectrum was measured by exciting each sample at wavelengths of 276 nm and 227 nm. The J = 1 (592 nm), J = 2 (616 nm), and J = 4 (696 nm) emission wavelengths were observed and the decay recorded over a period of 100 ms. Each measurement was recorded after a 0.200 ms time delay, at a gate time of 0.500 ms, with an excitation slit width of 20 nm and an emission slit width of 10 nm. The data set is an average of a 50 cycle run. A non-linear least squares fit was generated for each run.

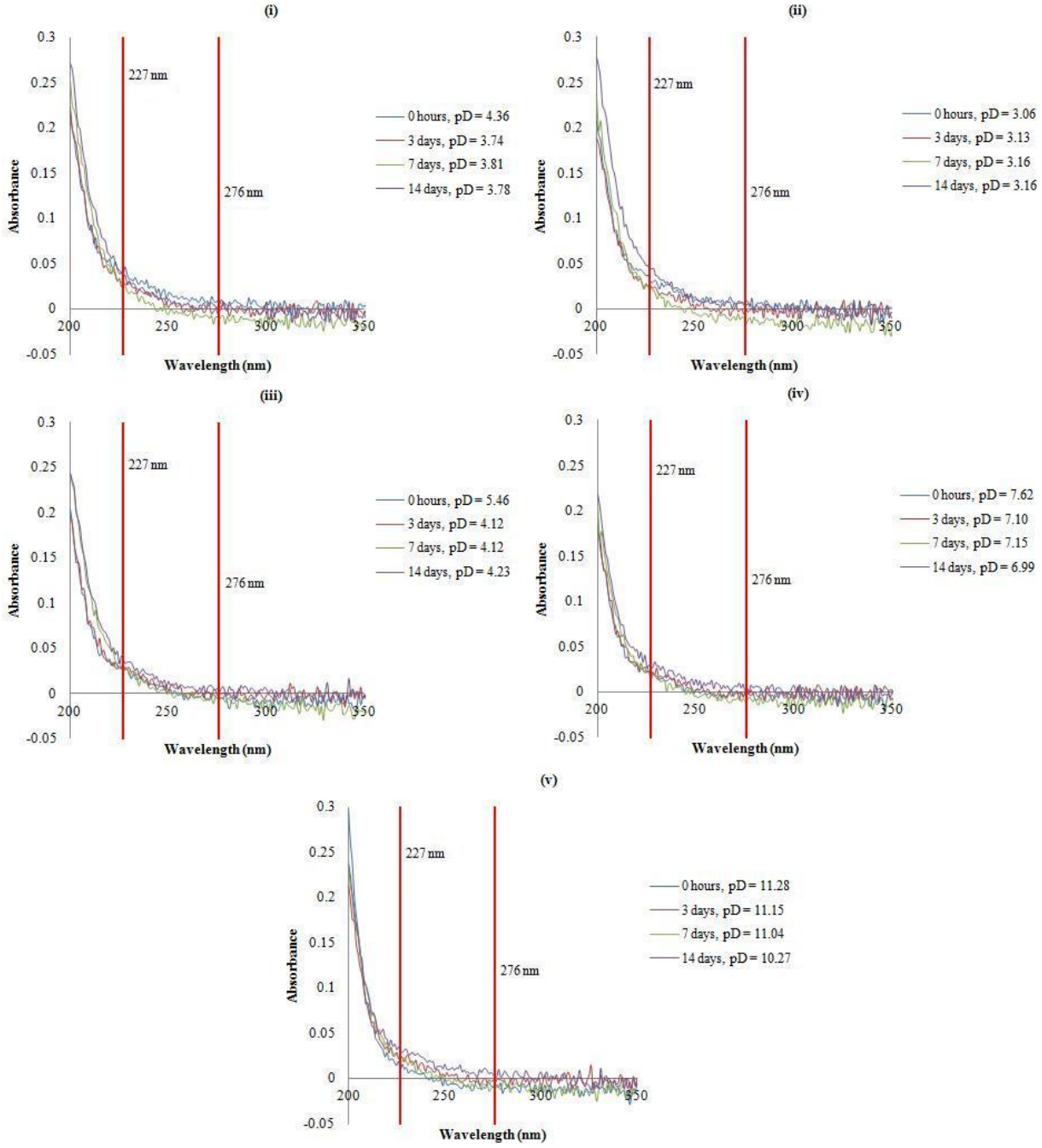


Figure G.4: Absorbance spectrum of europium(III)-1,7-bis(2-hydroxycyclohexyl)-1,4,7-tris(carboxymethyl)-1,4,7 triazaheptane in D_2O, as a function of pD, in a multi-component buffered system.

The following table consists of the data obtained from the fits for each emission decay spectrum, as a function of pD.

Table G.5: $Cy_2DETA.3A.3HCl$ / Eu(III) phosphorescence emission decay data (in D_2O, multi-component buffered system, λ_{ex} = 276 nm).

Sample	Time	pD	Emission Wavelength (nm)	Detector Voltage	k1	A1	C	Standard Deviation
Stock Solution	0 hours	4.356	592	high	0.736±0.0	15.6444±0.6	0.0296±0.0	0.1755
	3 days	3.738	592	high	0.470±0.0	19.6582±0.1	0.0062±0.0	0.0412
	7 days	3.809	592	high	0.488±0.0	19.4884±0.1	0.0216±0.0	0.0554
	14 days	3.775	592	high	0.488±0.0	19.6391±0.1	0.0166±0.0	0.0430
	0 hours	4.356	616	high	0.848±0.0	42.2872±2.0	0.0839±0.1	0.5132
	3 days	3.738	616	high	0.478±0.0	43.2191±0.2	0.0080±0.0	0.0675
	7 days	3.809	616	high	0.498±0.1	42.4573±0.2	0.0248±0.0	0.0829
	14 days	3.775	616	high	0.499±0.0	42.6273±0.2	0.0182±0.0	0.0924
	0 hours	4.356	696	high	0.724±0.0	10.6372±0.4	0.0339±0.0	0.1334
	3 days	3.738	696	high	0.479±0.0	14.5042±0.1	0.0135±0.0	0.0392
	7 days	3.809	696	high	0.481±0.0	14.5684±0.1	0.0157±0.0	0.0366
	14 days	3.775	696	high	0.483±0.0	14.3808±0.1	0.0154±0.0	0.0350
Sample 1	0 hours	3.057	592	medium	0.441±0.0	13.3864±0.1	0.0142±0.0	0.0241
	3 days	3.132	592	high	0.486±0.0	21.4341±0.2	0.0155±0.0	0.0679
	7 days	3.162	592	high	0.511±0.0	20.4704±0.1	0.0274±0.0	0.0484
	14 days	3.157	592	high	0.493±0.0	18.5759±0.1	0.0192±0.0	0.0466
	0 hours	3.057	616	medium	0.436±0.0	21.7633±0.1	0.0099±0.0	0.0224
	3 days	3.132	616	high	0.475±0.0	43.2369±0.1	0.0230±0.0	0.0598
	7 days	3.162	616	high	0.502±0.0	42.2019±0.2	0.0195±0.0	0.0740
	14 days	3.157	616	high	0.497±0.0	39.9383±0.1	0.0253±0.0	0.0560
	0 hours	3.057	696	medium	0.441±0.0	7.2693±0.0	0.0147±0.0	0.0177
	3 days	3.132	696	high	0.486±0.0	15.3377±0.1	0.0127±0.0	0.0368
	7 days	3.162	696	high	0.505±0.0	14.9561±0.1	0.0068±0.0	0.0459
	14 days	3.157	696	high	0.489±0.0	13.7550±0.1	0.0081±0.0	0.0460
Sample 2	0 hours	5.456	592	high	0.731±0.0	38.8988±1.4	0.0615±0.1	0.4047
	3 days	4.115	592	high	0.482±0.0	17.7033±0.1	0.0191±0.0	0.0494
	7 days	4.119	592	high	0.483±0.0	17.3491±0.1	0.0000±0.0	0.0388
	14 days	4.226	592	high	0.487±0.0	17.4202±0.1	0.0201±0.0	0.0433
	0 hours	5.456	616	high	0.842±0.0	90.2416±3.6	0.1540±0.1	0.9533
	3 days	4.115	616	high	0.489±0.0	38.2864±0.2	0.0235±0.0	0.0867
	7 days	4.119	616	high	0.494±0.0	37.6503±0.1	0.0152±0.0	0.0597
	14 days	4.226	616	high	0.487±0.0	36.8515±0.2	0.0181±0.0	0.0720
	0 hours	5.456	696	high	0.706±0.0	31.9133±1.1	0.0417±0.0	0.3377
	3 days	4.115	696	high	0.482±0.0	13.5079±0.1	0.0132±0.0	0.0407
	7 days	4.119	696	high	0.489±0.0	12.9997±0.1	0.0207±0.0	0.0362
	14 days	4.226	696	high	0.489±0.0	13.0304±0.1	0.0216±0.0	0.0368
Sample 3	0 hours	7.619	592	high	0.490±0.0	10.3665±0.1	0.0266±0.0	0.0436
	3 days	7.095	592	high	0.487±0.0	15.4916±0.1	0.0306±0.0	0.0504
	7 days	7.145	592	high	0.486±0.0	15.9072±0.1	0.0266±0.0	0.0439

	14 days	6.988	592	high	0.482±0.0	16.5959±0.1	0.0074±0.0	0.0492
	0 hours	7.619	616	high	0.500±0.0	21.2446±0.1	0.0001±0.0	0.0550
	3 days	7.095	616	high	0.498±0.0	32.5703±0.2	0.0201±0.0	0.0749
	7 days	7.145	616	high	0.494±0.0	34.1685±0.1	0.0242±0.0	0.0550
	14 days	6.988	616	high	0.493±0.0	35.3170±0.1	0.0198±0.0	0.0481
	0 hours	7.619	696	high	0.494±0.0	8.1721±0.1	0.0110±0.0	0.0322
	3 days	7.095	696	high	0.495±0.0	12.0714±0.1	0.0115±0.0	0.0367
	7 days	7.145	696	high	0.488±0.0	12.5710±0.1	0.0185±0.0	0.0439
	14 days	6.988	696	high	0.488±0.0	12.9035±0.1	0.0177±0.0	0.0525
Sample 4	0 hours	11.281	592	high	0.536±0.0	12.3876±0.1	0.0175±0.0	0.0406
	3 days	11.146	592	high	0.447±0.0	10.6321±0.1	0.0198±0.0	0.0434
	7 days	11.035	592	high	0.487±0.0	12.5669±0.1	0.0153±0.0	0.0392
	14 days	10.271	592	high	0.473±0.0	12.6096±0.1	0.0127±0.0	0.0352
	0 hours	11.281	616	high	0.553±0.0	31.2052±0.1	0.0268±0.0	0.0483
	3 days	11.146	616	high	0.487±0.0	21.5637±0.1	0.0229±0.0	0.0472
	7 days	11.035	616	high	0.493±0.0	25.0646±0.1	0.0225±0.0	0.0573
	14 days	10.271	616	high	0.486±0.0	25.3428±0.1	0.0236±0.0	0.0434
	0 hours	11.281	696	high	0.526±0.0	9.3743±0.1	0.0101±0.0	0.0322
	3 days	11.146	696	high	0.482±0.0	8.7065±0.1	0.0049±0.0	0.0341
	7 days	11.035	696	high	0.486±0.0	10.1552±0.1	0.0133±0.0	0.0355
	14 days	10.271	696	high	0.500±0.0	10.4837±0.1	0.0154±0.0	0.0354

Table G.6: Cy_2DETA.3A.3HCl / Eu(III) phosphorescence emission decay data (in D_2O, multi-component buffered system, λ_{ex} = 227 nm).

Sample	Time	pD	Emission Wavelength (nm)	Detector Voltage	k1	A1	C	Standard Deviation
Stock Solution	0 hours	4.356	592	high	0.922±0.1	67.6759±3.3	0.2105±0.1	0.8017
	3 days	3.738	592	medium	0.493±0.0	3.5479±0.1	0.0852±0.0	0.0560
	7 days	3.809	592	medium	0.534±0.0	3.5376±0.2	0.0457±0.0	0.0631
	14 days	3.775	592	medium	0.511±0.0	3.2371±0.1	0.1031±0.0	0.0549
	0 hours	4.356	616	high	1.117±0.1	197.7311±11.2	0.4463±0.3	2.1937
	3 days	3.738	616	medium	0.485±0.0	7.8529±0.2	0.0554±0.0	0.0673
	7 days	3.809	616	medium	0.508±0.0	7.6953±0.1	0.0679±0.0	0.0598
	14 days	3.775	616	medium	0.500±0.0	7.3013±0.2	0.1156±0.0	0.0615
	0 hours	4.356	696	high	0.858±0.0	41.8847±2.0	0.0732±0.1	0.5280
	3 days	3.738	696	medium	0.445±0.0	2.3018±0.1	0.0629±0.0	0.0542
	7 days	3.809	696	medium	0.525±0.0	2.5854±0.1	0.0402±0.0	0.0584
	14 days	3.775	696	medium	0.547±0.0	2.5558±0.1	0.1035±0.0	0.0566
Sample 1	0 hours	3.057	592	medium	0.440±0.0	92.6331±0.4	0.0672±0.0	0.1644
	3 days	3.132	592	medium	0.523±0.0	4.3227±0.2	0.1076±0.0	0.0595
	7 days	3.162	592	medium	0.530±0.0	3.9852±0.2	0.0584±0.0	0.0590
	14 days	3.157	592	medium	0.530±0.0	3.1193±0.2	0.0139±0.0	0.0638
	0 hours	3.057	616	medium	0.428±0.0	148.8967±0.2	0.0590±0.0	0.0712

	3 days	3.132	616	medium	0.503±0.0	9.5210±0.1	0.0797±0.0	0.0592
	7 days	3.162	616	medium	0.540±0.0	8.5050±0.1	0.0422±0.0	0.0533
	14 days	3.157	616	medium	0.519±0.0	6.5513±0.2	0.0337±0.0	0.0624
	0 hours	3.057	696	medium	0.438±0.0	50.2293±0.2	0.0599±0.0	0.0946
	3 days	3.132	696	medium	0.534±0.0	3.1323±0.1	0.0964±0.0	0.0575
	7 days	3.162	696	medium	0.563±0.0	2.7664±0.1	0.0457±0.0	0.0533
	14 days	3.157	696	medium	0.632±0.1	2.5208±0.2	0.0602±0.0	0.0578
Sample 2	0 hours	5.456	592	medium	1.301±0.1	15.0347±0.9	0.1248±0.0	0.1425
	3 days	4.115	592	medium	0.545±0.0	3.5253±0.2	0.0548±0.1	0.0608
	7 days	4.119	592	medium	0.530±0.0	3.2070±0.2	0.0724±0.0	0.0604
	14 days	4.226	592	medium	0.548±0.0	3.3242±0.1	0.0753±0.0	0.0562
	0 hours	5.456	616	medium	1.382±0.1	35.2573±2.0	0.1316±0.0	0.3004
	3 days	4.115	616	medium	0.522±0.0	7.7086±0.2	0.0821±0.0	0.0709
	7 days	4.119	616	medium	0.522±0.0	7.2225±0.2	0.0813±0.0	0.0685
	14 days	4.226	616	medium	0.503±0.0	6.8628±0.1	0.0234±0.0	0.0605
	0 hours	5.456	696	medium	1.187±0.1	10.9625±0.7	0.1271±0.0	0.1192
	3 days	4.115	696	medium	0.562±0.0	2.5897±0.2	0.0598±0.0	0.0643
	7 days	4.119	696	medium	0.572±0.0	2.5464±0.1	0.0705±0.0	0.0531
	14 days	4.226	696	medium	0.582±0.0	2.5445±0.2	0.0366±0.0	0.0582
Sample 3	0 hours	7.619	592	medium	0.635±0.1	2.2429±0.2	0.0755±0.0	0.0632
	3 days	7.095	592	medium	0.551±0.0	2.8269±0.2	0.0176±0.0	0.0578
	7 days	7.145	592	medium	0.540±0.0	2.9219±0.2	0.1007±0.0	0.0638
	14 days	6.988	592	medium	0.523±0.0	3.0431±0.2	0.0308±0.0	0.0595
	0 hours	7.619	616	medium	0.642±0.0	4.6448±0.2	0.0761±0.0	0.0655
	3 days	7.095	616	medium	0.503±0.0	5.9312±0.2	0.0975±0.0	0.0613
	7 days	7.145	616	medium	0.519±0.0	6.2713±0.1	0.1071±0.0	0.0592
	14 days	6.988	616	medium	0.508±0.0	6.3150±0.1	0.0232±0.0	0.0586
	0 hours	7.619	696	medium	0.766±0.1	1.9096±0.2	0.0902±0.0	0.0581
	3 days	7.095	696	medium	0.584±0.1	2.2400±0.2	0.0449±0.0	0.0598
	7 days	7.145	696	medium	0.551±0.0	2.1819±0.1	0.0992±0.0	0.0547
	14 days	6.988	696	medium	0.564±0.0	2.2358±0.2	0.0518±0.0	0.0568
Sample 4	0 hours	11.281	592	medium	0.818±0.1	2.1890±0.2	0.0605±0.0	0.0605
	3 days	11.146	592	medium	0.564±0.1	2.0181±0.2	0.0364±0.0	0.0574
	7 days	11.035	592	medium	0.544±0.0	2.2328±0.2	0.1176±0.0	0.0595
	14 days	10.271	592	medium	0.610±0.0	2.5259±0.2	0.0450±0.0	0.0568
	0 hours	11.281	616	medium	0.593±0.0	4.6752±0.2	0.0544±0.0	0.0594
	3 days	11.146	616	medium	0.509±0.0	3.7590±0.1	0.0256±0.0	0.0545
	7 days	11.035	616	medium	0.496±0.0	4.2288±0.1	0.1142±0.0	0.0605
	14 days	10.271	616	medium	0.518±0.0	4.6692±0.1	0.0392±0.0	0.0529
	0 hours	11.281	696	medium	0.807±0.1	1.5739±0.2	0.0461±0.0	0.0617
	3 days	11.146	696	medium	0.721±0.0	1.8189±0.2	0.0335±0.0	0.0568
	7 days	11.035	696	medium	0.591±0.0	1.8329±0.2	0.1242±0.0	0.0563
	14 days	10.271	696	medium	0.600±0.1	2.0083±0.2	0.0408±0.0	0.0558

G.2 Determination of the solution hydration state of $[Eu(Cy_2DETA.2A)]^{3+}$

The hydration number of the Cy_2DETA.2A.3HCl / Eu(III) system was determined as a function of pH.

G.2.1 Cy_2DETA.2A.3HCl / Eu(III), H_2O, aqueous solution

Cy_2DETA.2A.3HCl (0.0037 g, 7.57×10^{-6} mol) and $Eu(CF_3SO_3)_3$ (0.0048 g, 8.01×10^{-6} mol) were dissolved in deionised water, in a 50 mL volumetric flask. This solution was placed into a jacketed-cell (25 °C). An in-cell titration was performed on the solution using concentrated acid (HCl) and concentrated base (NaOH) solutions. Upon each addition of acid or base, the pH of the solution was allowed to stabilize and the pH value recorded. A small volume of the adjusted solution was decanted and sealed in a marked vial prior to subsequent pH adjustment. Solutions were prepared at pH 3.87 (stock solution), pH 2.89 (sample 1) and pH 5.43 (sample 2), as per the observed pK_a values from the corresponding luminescence study.

The absorbance of the stock solution was measured in order to determine the wavelength to be used for excitation in the luminescence study (Figure G.5).

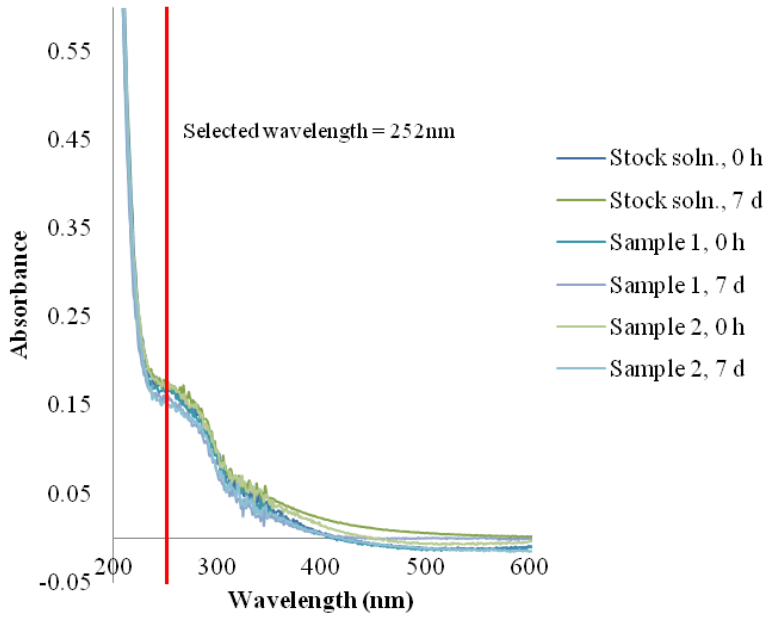


Figure G.5: Absorbance spectrum of europium(III)-1,7-bis(2-hydroxycyclohexyl)-1,7-bis(carboxymethyl)-1,4,7 triazaheptane in H_2O, as a function of pH.

The pH of each solution was measured upon initial preparation (0 hours) and after 1, 2, 3, and 7 days, prior to each absorbance and luminescence measurement. The absorbance was measured over a range of 200 nm and 800 nm.

The phosphorescence emission spectrum was measured by exciting each sample at a wavelength of 252 nm. The spectrum was recorded in the high sensitivity mode, over a range of 550 nm to 750 nm. Each measurement was recorded after a 0.100 ms time delay, with both the excitation and emission slit widths set at 10 nm.

The phosphorescence emission decay spectrum was measured by exciting each sample at a wavelength of 252 nm. The J = 1 (592 nm), J = 2 (616 nm), and J = 4 (696 nm) emission wavelengths were observed and the decay recorded over a period of 100 ms. Each measurement was recorded after a 0.200 ms time delay, at a gate time of 0.500 ms, with an excitation slit width of 20 nm and an emission slit width of 10 nm. The data set is an average of a 50 cycle run. A non-linear least squares fit was generated for each run.

The following table consists of the data obtained from the fits for each emission decay spectrum, as a function of pH.

Table G.7: Cy_2DETA.2A.3HCl / Eu(III) phosphorescence emission decay data (in H_2O, aqueous solution, λ_{ex} = 252 nm).

Sample	Time	pH	Emission Wavelength (nm)	Detector Voltage	k1	A1	C	Standard Deviation
Stock Solution	0 hours	3.870	592	high	9.087±0.9	866.3268±356.7	0.0221±0.0	0.0336
	24 hours	4.054	592	high	6.518±0.1	462.8535±27.1	0.0097±0.0	0.0298
	48 hours	4.189	592	high	6.231±0.1	450.1115±24.5	0.0161±0.0	0.0355
	3 days	4.301	592	high	6.091±0.1	492.3644±17.7	0.0161±0.0	0.0294
	7 days	5.097	592	high	5.286±0.1	492.5983±11.5	0.0257±0.0	0.0412
	0 hours	3.870	616	high	6.533±0.2	292.9601±31.5	0.0250±0.0	0.0342
	24 hours	4.054	616	high	5.206±0.1	342.2292±8.8	0.0000±0.0	0.0340
	48 hours	4.189	616	high	4.871±0.0	347.9313±7.4	0.0273±0.0	0.0396
	3 days	4.301	616	high	4.701±0.0	394.2665±7.2	0.0158±0.0	0.0445
	7 days	5.097	616	high	4.410±0.0	657.0325±7.4	0.0180±0.0	0.0612
	0 hours	3.870	696	high	11.044±4.5	1112.1750±2250.3	0.0153±0.0	0.0342
	24 hours	4.054	696	high	6.184±0.2	217.8557±18.7	0.0185±0.0	0.0284
	48 hours	4.189	696	high	5.718±0.1	218.9150±14.4	0.0210±0.0	0.0341
	3 days	4.301	696	high	5.803±0.1	254.4522±13.8	0.0206±0.0	0.0301

	7 days	5.097	696	high	4.794±0.1	254.0927±6.8	0.0031±0.0	0.0390
Sample 1	0 hours	2.886	592	high	11.128±2.9	1863.4110±2391.0	0.0185±0.0	0.0337
	24 hours	2.923	592	high	8.112±0.5	570.3460±139.2	0.0283±0.0	0.0333
	48 hours	2.945	592	high	8.675±0.7	771.3298±250.6	0.0210±0.0	0.0350
	3 days	2.935	592	high	8.888±0.5	905.0252±219.7	0.0139±0.0	0.0250
	7 days	2.980	592	high	8.324±0.6	723.8840±182.0	0.0390±0.0	0.0355
	0 hours	2.886	616	high	7.722±0.7	335.1786±99.2	0.0000±0.0	0.0345
	24 hours	2.923	616	high	6.552±0.3	250.5633±31.1	0.0213±0.0	0.0332
	48 hours	2.945	616	high	7.109±0.3	357.0540±48.6	0.0190±0.0	0.0303
	3 days	2.935	616	high	6.366±0.2	261.4104±21.3	0.0184±0.0	0.0271
	7 days	2.980	616	high	6.061±0.2	231.2239±20.7	0.0266±0.0	0.0354
	0 hours	2.886	696	high	11.434±6.7	1104.8530±3313.7	0.0153±0.0	0.0356
	24 hours	2.923	696	high	8.765±1.5	412.5208±272.6	0.0196±0.0	0.0349
	48 hours	2.945	696	high	9.986±2.6	714.0126±822.6	0.0000±0.0	0.0332
	3 days	2.935	696	high	10.203±2.4	835.9440±915.3	0.0158±0.0	0.0300
	7 days	2.980	696	high	7.871±0.9	302.2112±116.7	0.0241±0.0	0.0351
Sample 2	0 hours	5.430	592	high	5.438±0.1	353.7006±11.5	0.0320±0.0	0.0356
	24 hours	5.600	592	high	4.895±0.0	413.6159±7.5	0.0106±0.0	0.0394
	48 hours	5.652	592	high	4.916±0.0	468.1255±8.4	0.0194±0.0	0.0430
	3 days	5.909	592	high	4.760±0.0	503.9428±7.7	0.0156±0.0	0.0456
	7 days	6.066	592	high	4.511±0.0	498.5689±6.3	0.0244±0.0	0.0473
	0 hours	5.430	616	high	4.509±0.0	429.6610±6.6	0.0339±0.0	0.0501
	24 hours	5.600	616	high	4.274±0.0	666.1055±6.3	0.0128±0.0	0.0594
	48 hours	5.652	616	high	4.220±0.0	733.1074±8.1	0.0221±0.0	0.0812
	3 days	5.909	616	high	4.163±0.0	856.5704±7.1	0.0212±0.0	0.0751
	7 days	6.066	616	high	4.140±0.0	976.4167±8.6	0.0199±0.0	0.0926
	0 hours	5.430	696	high	5.096±0.1	189.8495±7.8	0.0155±0.0	0.0338
	24 hours	5.600	696	high	4.539±0.0	236.2240±5.3	0.0192±0.0	0.0391
	48 hours	5.652	696	high	4.468±0.0	263.1146±4.9	0.0233±0.0	0.0385
	3 days	5.909	696	high	4.443±0.0	305.1975±4.6	0.0192±0.0	0.0374
	7 days	6.066	696	high	4.311±0.0	316.7646±4.7	0.0089±0.0	0.0427

G.2.2 Cy_2DETA.2A.3HCl / Eu(III), D_2O, aqueous solution

Cy_2DETA.2A.3HCl (0.0019 g, 3.78×10^{-6} mol) and $Eu(CF_3SO_3)_3$ (0.0023 g, 3.84×10^{-6} mol) were dissolved in D_2O, in a 25 mL volumetric flask. This solution was placed in a jacketed-cell (25 °C). An in-cell titration was performed on the solution using concentrated acid (DCl) and concentrated base (NaOD) solutions. Upon each addition of acid or base, the pD of the solution was allowed to stabilize and the pD value recorded. A small volume of the adjusted solution was decanted and sealed in a marked vial prior to subsequent pD adjustment.

Solutions were prepared at pD 5.41 (stock solution), pD 2.56 (sample 1) and pD 4.46 (sample 2), as per the observed pK_a values from the corresponding luminescence study.

The absorbance of the stock solution was measured in order to determine the wavelength to be used for excitation in the luminescence study (Figure G.6).

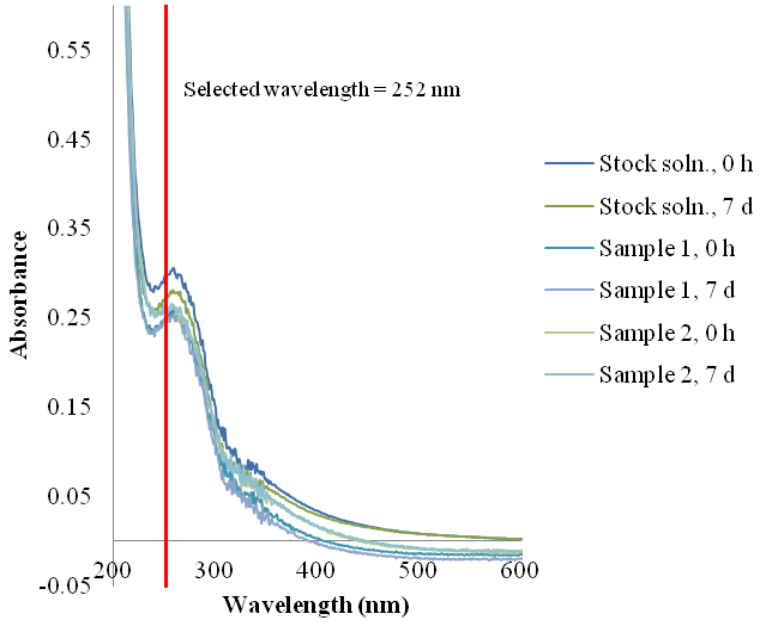


Figure G.6: Absorbance spectrum of europium(III)-1,7-bis(2-hydroxycyclohexyl)-1,7-bis(carboxymethyl)-1,4,7 triazaheptane in D_2O, as a function of pD.

The pD of each solution was measured upon initial preparation (0 hours), after 2 days, and 7 days, prior to each absorbance and luminescence measurement. The absorbance was measured over a range of 200 nm and 800 nm.

The phosphorescence emission spectrum was measured by exciting each sample at a wavelength of 252 nm. The spectrum was recorded in the high sensitivity mode, over a range of 550 nm to 750 nm. Each measurement was recorded after a 0.100 ms time delay, with both the excitation and emission slit widths set at 10 nm.

The phosphorescence emission decay spectrum was measured by exciting each sample at a wavelength of 252 nm. The J = 1 (592 nm), J = 2 (616 nm), and J = 4 (696 nm) emission wavelengths were observed and the decay recorded over a period of 100 ms. Each measurement was recorded after a 0.200 ms time delay, at a gate time of 0.500 ms, with an

excitation slit width of 20 nm and an emission slit width of 10 nm. The data set is an average of a 50 cycle run. A non-linear least squares fit was generated for each run.

The following table consists of the data obtained from the fits for each emission decay spectrum, as a function of pD.

Table G.8: Cy_2DETA.2A.3HCl / Eu(III) phosphorescence emission decay data (in D_2O, aqueous solution, λ_{ex} = 252 nm).

Sample	Time	pD	Emission Wavelength (nm)	Detector Voltage	k1	A1	C	Standard Deviation
Stock Solution	0 hours	4.691	592	high	2.275±0.1	781.7654±24.1	0.3065±0.2	1.5334
	48 hours	5.023	592	high	1.762±0.1	1020.7812±22.8	0.4586±0.0	1.2315
	7 days	4.828	592	high	1.663±0.0	1155.1510±27.3	0.5926±0.4	3.1184
	0 hours	4.691	616	high	1.526±0.1	646.4974±22.4	0.5313±0.4	2.9115
	48 hours	5.023	616	high	1.391±0.1	1098±6783±31.7	0.7637±0.1	1.4755
	7 days	4.828	616	high	1.207±0.0	1240.5310±31.8	0.9844±0.8	5.6681
	0 hours	4.691	696	high	2.049±0.1	386.5393±13.7	0.2218±0.2	1.0798
	48 hours	5.023	696	high	1.668±0.0	485.0198±12.5	0.3489±0.3	2.1592
	7 days	4.828	696	high	1.514±0.0	613.7297±16.3	0.4149±0.3	2.1481
Sample 1	0 hours	2.881	592	high	1.456±0.0	487.3390±1.7	0.0623±0.0	0.2367
	48 hours	2.887	592	high	1.397±0.0	469.7439±0.8	0.0784±0.0	0.1934
	7 days	2.955	592	high	1.320±0.0	668.4536±1.3	0.0618±1.3	0.2022
	0 hours	2.881	616	high	1.374±0.0	304.1466±3.3	0.1107±0.1	0.4933
	48 hours	2.887	616	high	1.269±0.0	417.1794±1.2	0.1205±0.0	0.3785
	7 days	2.955	616	high	1.265±0.0	434.0297±3.9	0.1344±0.1	0.6518
	0 hours	2.881	696	high	1.425±0.0	236.5111±0.8	0.0505±0.0	0.1092
	48 hours	2.887	696	high	1.401±0.0	309.8643±0.5	0.0599±0.0	0.1840
	7 days	2.955	696	high	1.325±0.0	339.3827±1.0	0.0582±0.0	0.1557
Sample 2	0 hours	5.395	592	high	1.925±0.1	790.7881±22.8	0.3938±0.3	2.0199
	48 hours	5.436	592	high	1.697±0.0	979.6167±21.4	0.5123±0.5	2.2689
	7 days	5.478	592	high	1.513±0.0	1007.5110±22.4	0.5141±0.4	2.9576
	0 hours	5.395	616	high	1.324±0.0	763.2865±22.7	0.6047±0.5	3.6073
	48 hours	5.436	616	high	1.238±0.0	1138.0653±26.5	0.7064±0.1	2.4073
	7 days	5.478	616	high	1.128±0.0	1244.9920±28.6	0.8907±0.8	5.5348
	0 hours	5.395	696	high	1.741±0.1	414.3155±13.4	0.2718±0.2	1.4150
	48 hours	5.436	696	high	1.535±0.1	509.6200±16.9	0.2518±0.8	1.7883
	7 days	5.478	696	high	1.364±0.0	552.7390±13.3	0.3705±0.3	2.0299

G.2.3 Cy_2DETA.2A.3HCl / Eu(III), H_2O, multi-component buffered system

Cy_2DETA.2A.3HCl (0.0035 g, 7.16×10^{-6} mol) and $Eu(CF_3SO_3)_3$ (0.0047 g, 7.84×10^{-6} mol) were dissolved in deionised water, in a 50 mL volumetric flask. To this flask, 3.75 mL of a 0.2 mol/L solution consisting of the buffers KHP, MES, CHES, MOPS, and Tris was added and the contents diluted to the mark. This solution was placed in a jacketed-cell (25 °C). An in-cell titration was performed on this solution using concentrated acid (HCl) and concentrated base (NaOH) solutions. Upon each addition of acid or base, the pH of the solution was allowed to stabilize and the pH value recorded. A small volume of the adjusted solution was decanted and sealed in a marked vial prior to subsequent pH adjustment. Solutions were prepared at pH 3.85 (stock solution), pH 2.58 (sample 1) and pH 4.44 (sample 2) as per the observed pK_a values from the corresponding luminescence study.

The absorbance of the stock solution was measured in order to determine the wavelength to be used for excitation in the luminescence study (Figure G.7).

The pH of each solution was measured upon initial preparation (0 hours) and after 1, 2, 3 and 7 days, prior to each absorbance and luminescence measurement. The absorbance was measured over a range of 200 nm and 800 nm.

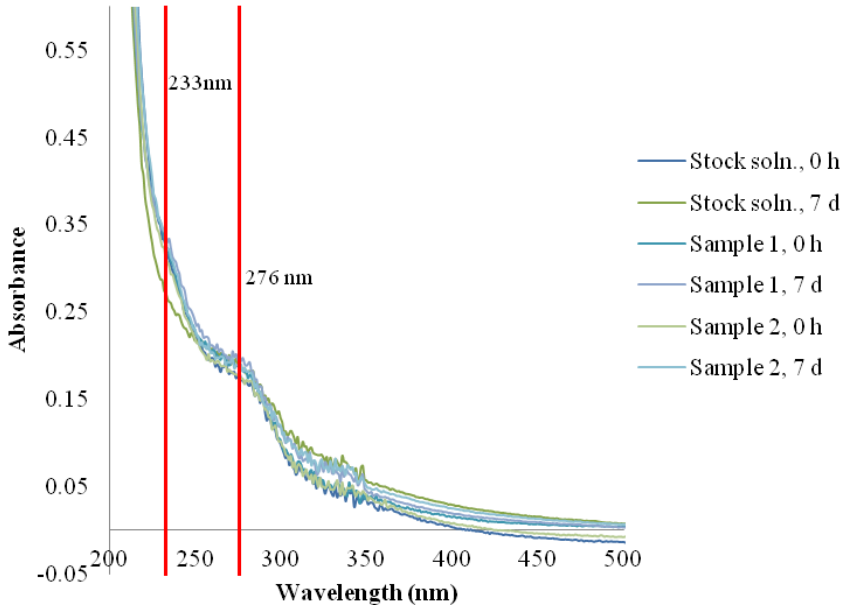


Figure G.7: Absorbance spectrum of europium(III)-1,7-bis(2-hydroxycyclohexyl)-1,7-bis(carboxymethyl)-1,4,7 triazaheptane in H_2O, as a function of pH, in a multi-component buffered system.

The phosphorescence emission spectrum was measured by exciting each sample at wavelengths of 276 nm and 233 nm. The spectrum was recorded in the high sensitivity mode, over a range of 550 nm to 750 nm. Each measurement was recorded after a 0.100 ms time delay, with both the excitation and emission slit widths set at 10 nm.

The phosphorescence emission decay spectrum was measured by exciting each sample at wavelengths of 276 nm and 233 nm. The J = 1 (591 nm), J = 2 (616 nm), and J = 4 (696 nm) emission wavelengths were observed and the decay recorded over a period of 100 ms. Each measurement was recorded after a 0.200 ms time delay, at a gate time of 0.500 ms, with an excitation slit width of 20 nm and an emission slit width of 10 nm. The data set is an average of a 50 cycle run. A non-linear least squares fit was generated for each run.

The following table consists of the data obtained from the fits for each emission decay spectrum, as a function of pH.

Table G.9: Cy_2DETA.2A.3HCl / Eu(III) phosphorescence emission decay data (in H_2O, multi-component buffered system, λ_{ex} = 276 nm).

Sample	Time	pH	Emission Wavelength (nm)	Detector Voltage	k1	A1	C	Standard Deviation
Stock Solution	0 hours	3.850	591	high	9.792±0.5	2487.9250±507.0	0.0116±0.0	0.0245
	24 hours	4.182	591	high	7.370±0.1	1253.6370±51.4	0.0043±0.0	0.0250
	48 hours	4.384	591	high	7.084±0.1	1299.2580±44.9	0.0195±0.0	0.0288
	3 days	4.667	591	high	6.517±0.1	1039.8050±23.4	0.0162±0.0	0.0258
	7 days	5.475	591	high	5.359±0.0	609.9064±10.4	0.0133±0.0	0.0350
	0 hours	3.850	616	high	7.112±0.1	663.2866±42.5	0.0206±0.0	0.0265
	24 hours	4.182	616	high	5.571±0.0	649.1077±12.5	0.0134±0.0	0.0341
	48 hours	4.384	616	high	5.332±0.0	742.1915±13.7	0.0193±0.0	0.0472
	3 days	4.667	616	high	5.057±0.0	765.7401±10.1	0.0215±0.0	0.0451
	7 days	5.475	616	high	4.498±0.0	814.2153±7.2	0.0268±0.0	0.0550
	0 hours	3.850	696	high	9.453±0.7	1088.2170±359.2	0.0118±0.0	0.0239
	24 hours	4.182	696	high	6.870±0.1	538.5388±31.6	0.0185±0.0	0.0249
	48 hours	4.384	696	high	6.439±0.1	547.2733±19.8	0.0138±0.0	0.0235
	3 days	4.667	696	high	6.155±0.1	510.8025±15.5	0.0170±0.0	0.0242
	7 days	5.475	696	high	4.971±0.0	334.8651±5.9	0.0305±0.0	0.0286
Sample 1	0 hours	2.579	591	high	8.999±0.5	1051.9930±244.2	0.0176±0.0	0.0250
	24 hours	2.670	591	high	9.646±0.7	1473.8530±465.3	0.0166±0.0	0.0258
	48 hours	2.669	591	high	9.118±0.5	1252.9280±285.4	0.0150±0.0	0.0261
	3 days	2.658	591	high	9.574±0.6	1581.6060±429.5	0.0083±0.0	0.0255

	7 days	2.670	591	high	9.087±0.5	1300.4350±284.8	0.0179±0.0	0.0268
	0 hours	2.579	616	high	7.004±0.3	288.9304±38.3	0.0126±0.0	0.0265
	24 hours	2.670	616	high	7.667±0.3	423.1418±65.7	0.0100±0.0	0.0241
	48 hours	2.669	616	high	7.398±0.3	382.3951±48.5	0.0101±0.0	0.0230
	3 days	2.658	616	high	7.286±0.3	390.4316±45.5	0.0042±0.0	0.0240
	7 days	2.670	616	high	7.029±0.2	367.2746±35.8	0.0213±0.0	0.0241
	0 hours	2.579	696	high	9.757±1.5	785.9238±512.7	0.0111±0.0	0.0256
	24 hours	2.670	696	high	9.222±1.1	626.7591±312.0	0.0137±0.0	0.0258
	48 hours	2.669	696	high	9.742±1.4	835.5657±520.6	0.0038±0.0	0.0263
	3 days	2.658	696	high	8.922±0.9	568.0026±221.7	0.0126±0.0	0.0244
	7 days	2.670	696	high	9.889±1.3	942.5724±540.7	0.0148±0.0	0.0238
Sample 2	0 hours	4.441	591	high	7.583±0.1	1320.2520±62.8	0.0195±0.0	0.0249
	24 hours	4.932	591	high	6.952±0.1	1471.1290±38.6	0.0002±0.0	0.0281
	48 hours	4.982	591	high	6.682±0.0	1428.1460±32.0	0.0137±0.0	0.0301
	3 days	5.392	591	high	6.448±0.0	1412.3270±28.9	0.0259±0.0	0.0341
	7 days	5.716	591	high	5.889±0.0	1257.3910±19.0	0.0189±0.0	0.0383
	0 hours	4.441	616	high	5.801±0.0	677.7003±14.2	0.0113±0.0	0.0312
	24 hours	4.932	616	high	6.376±0.0	972.1921±16.1	0.0238±0.0	0.0530
	48 hours	4.982	616	high	5.201±0.0	1025.2400±13.4	0.0222±0.0	0.0521
	3 days	5.392	616	high	5.145±0.0	1197.8960±13.4	0.0113±0.0	0.0648
	7 days	5.716	616	high	4.822±0.0	1298.5280±16.0	0.0146±0.0	0.0898
	0 hours	4.441	696	high	7.324±0.2	619.7024±46.3	0.0218±0.0	0.0236
	24 hours	4.932	696	high	6.318±0.1	637.3353±19.4	0.0188±0.0	0.0260
	48 hours	4.982	696	high	6.160±0.1	659.6035±18.5	0.0170±0.0	0.0288
	3 days	5.392	696	high	5.944±0.1	667.9066±15.8	0.0151±0.0	0.0303
	7 days	5.716	696	high	5.459±0.0	641.6628±10.5	0.0021±0.0	0.0319

Table G.10: Cy_2DETA.2A.3HCl / Eu(III) phosphorescence emission decay data (in H_2O, multi-component buffers present, λ_{ex} = 233 nm).

Sample	Time	pH	Emission Wavelength (nm)	Detector Voltage	k1	A1	C	Standard Deviation
Stock Solution	0 hours	3.850	591	high	10.797±0.6	14451.4600±4157.4	0.0080±0.0	0.0795
	24 hours	4.182	591	high	9.597±0.2	12601.2400±1276.5	0.0161±0.0	0.0740
	48 hours	4.384	591	high	8.925±0.1	11319.4700±684.2	0.0426±0.0	0.0752
	3 days	4.667	591	high	8.380±0.1	8464.6700±365.4	0.0465±0.0	0.0676
	7 days	5.475	591	high	7.010±0.1	2980.9570±118.5	0.0366±0.0	0.0814
	0 hours	3.850	616	high	9.123±0.4	4962.8910±819.5	0.0446±0.0	0.0746
	24 hours	4.182	616	high	7.102±0.1	3503.0200±131.1	0.0537±0.0	0.0825
	48 hours	4.384	616	high	7.099±0.1	4463.4490±132.8	0.0608±0.0	0.0838
	3 days	4.667	616	high	6.492±0.1	3526.7860±84.0	0.0237±0.0	0.0948
	7 days	5.475	616	high	5.383±0.0	1810.1150±34.4	0.0406±0.0	0.1126
	0 hours	3.850	696	high	10.670±1.1	7111.0740±3496.4	0.0327±0.0	0.0746
	24 hours	4.182	696	high	8.912±0.3	4800.1850±674.0	0.0483±0.0	0.0750

	48 hours	4.384	696	high	8.035±0.2	3987.3370±293.0	0.0352±0.0	0.0754
	3 days	4.667	696	high	7.742±0.1	3387.6930±224.9	0.0593±0.0	0.0766
	7 days	5.475	696	high	6.408±0.1	1297.0680±62.8	0.0425±0.0	0.0770
Sample 1	0 hours	2.579	591	high	9.698±0.9	3768.1380±1446.3	0.0231±0.0	0.0762
	24 hours	2.670	591	high	9.794±0.9	4247.8610±1781.2	0.0133±0.0	0.0858
	48 hours	2.669	591	high	9.349±0.6	3491.3050±1004.7	0.0333±0.0	0.0737
	3 days	2.658	591	high	10.486±1.1	5822.7520±2973.7	0.0423±0.0	0.0749
	7 days	2.670	591	high	10.147±0.9	5278.0680±2192.7	0.0333±0.0	0.0758
	0 hours	2.579	616	high	10.598±2.6	3058.8590±3521.3	0.0537±0.0	0.0800
	24 hours	2.670	616	high	8.817±1.0	1424.7950±611.0	0.0777±0.0	0.0744
	48 hours	2.669	616	high	8.314±0.7	1230.2400±412.6	0.0412±0.0	0.0812
	3 days	2.658	616	high	8.101±0.6	1108.8200±305.4	0.0094±0.0	0.0738
	7 days	2.670	616	high	8.174±0.6	1198.8600±316.5	0.0159±0.0	0.0712
	0 hours	2.579	696	high	11.583±23.0	4426.3800±8475.7	0.0703±0.0	0.0799
	24 hours	2.670	696	high	10.578±2.6	2879.1560±3354.9	0.0297±0.0	0.0776
	48 hours	2.669	696	high	11.175±3.2	4174.7990±5917.2	0.0239±0.0	0.0799
	3 days	2.658	696	high	10.803±2.2	3490.4000±3440.1	0.0334±0.0	0.0655
	7 days	2.670	696	high	10.807±2.8	3602.9690±4601.5	0.0296±0.0	0.0867
Sample 2	0 hours	4.441	591	high	9.256±0.2	10869.0800±1021.5	0.0555±0.0	0.0819
	24 hours	4.932	591	high	8.730±0.1	12524.6800±588.2	0.0241±0.0	0.0778
	48 hours	4.982	591	high	8.556±0.1	12861.5700±485.0	0.0000±0.0	0.0760
	3 days	5.392	591	high	8.370±0.1	12669.6300±459.6	0.0201±0.0	0.0858
	7 days	5.716	591	high	7.861±0.1	10684.6600±295.4	0.0427±0.0	0.0898
	0 hours	4.441	616	high	7.557±0.1	4258.2820±195.6	0.0303±0.0	0.0796
	24 hours	4.932	616	high	7.028±0.1	5621.6690±141.5	0.0380±0.0	0.0956
	48 hours	4.982	616	high	6.828±0.0	5807.8870±109.4	0.0416±0.0	0.0896
	3 days	5.392	616	high	6.763±0.0	6405.3500±125.9	0.0479±0.0	0.1096
	7 days	5.716	616	high	6.205±0.0	5657.9170±79.9	0.0796±0.0	0.1188
	0 hours	4.441	696	high	9.229±0.4	5597.0000±949.7	0.0219±0.0	0.0781
	24 hours	4.932	696	high	8.633±0.2	6325.8070±523.9	0.0413±0.0	0.0761
	48 hours	4.982	696	high	8.214±0.1	5813.6820±356.8	0.0370±0.0	0.0773
	3 days	5.392	696	high	8.010±0.1	5755.4800±296.4	0.0335±0.0	0.0781
	7 days	5.716	696	high	7.343±0.1	4612.8540±166.4	0.0547±0.0	0.0830

G.2.4 Cy_2DETA.2A.3HCl / Eu(III), D_2O, multi-component buffered system

Cy_2DETA.2A.3HCl (0.0019 g, 3.78×10^{-6} mol) and $Eu(CF_3SO_3)_3$ (0.0023 g, 3.84×10^{-6} mol) were dissolved in D_2O, in a 25 mL volumetric flask. To this flask, 66 µL of a 5 mmol/L solution consisting of the buffers KHP, MES, CHES, MOPS, and Tris was added and the contents diluted to the mark. This solution was placed in a jacketed-cell (25 °C). An in-cell titration was performed on this solution using concentrated acid (DCl) and concentrated base (NaOD) solutions. Upon each addition of acid or base, the pD of the solution was allowed to

stabilize and the pD value recorded. A small volume of the adjusted solution was decanted and sealed in a marked vial prior to subsequent pH adjustment. Solutions were prepared at pD 5.41 (stock solution), pD 2.56 (sample 1) and pD 4.46 (sample 2) as per the observed pK_a values from the corresponding luminescence study. Due to the high intensity obtained for prepared samples, measurements were made on diluted samples (using 600 µL of the prepared sample and diluting to a total volume of 3000 µL).

The absorbance of the Cy_2DETA.3A.3HCl / Eu(III) stock solution was measured in order to determine the wavelength to be used for excitation in the luminescence study (Figure G.8).

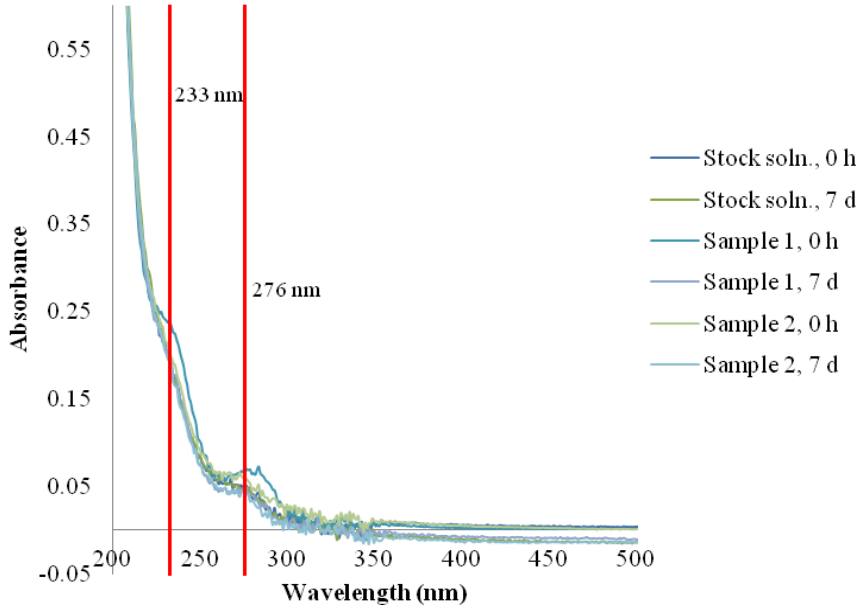


Figure G.8: Absorbance spectrum of europium(III)-1,7-bis(2-hydroxycyclohexyl)-1,7-bis(carboxymethyl)-1,4,7 triazaheptane in D_2O, as a function of pD, in a multi-component buffered system.

The pD of each solution was measured upon initial preparation (0 hours), and after 3 and 7 days, prior to each absorbance and luminescence measurement. The absorbance was measured over a range of 200 nm and 800 nm.

The phosphorescence emission spectrum was measured by exciting each sample at wavelengths of 276 nm and 233 nm. The spectrum was recorded in the high sensitivity mode, over a range of 550 nm to 750 nm. Each measurement was recorded after a 0.100 ms time delay, with both the excitation and emission slit widths set at 10 nm.

The phosphorescence emission decay spectrum was measured by exciting each sample at wavelengths of 276 nm and 233 nm. The J = 1 (592 nm), J = 2 (616 nm), and J = 4 (696 nm) emission wavelengths were observed and the decay recorded over a period of 100 ms. Each measurement was recorded after a 0.200 ms time delay, at a gate time of 0.500 ms, with an excitation slit width of 20 nm and an emission slit width of 10 nm. The data set is an average of a 50 cycle run. A non-linear least squares fit was generated for each run.

The following table consists of the data obtained from the fits for each emission decay spectrum, as a function of pD.

Table G.11: $Cy_2DETA.2A.3HCl$ / Eu(III) phosphorescence emission decay data (in D_2O, multi-component buffered system, λ_{ex} = 276 nm).

Sample	Time	pD	Emission Wavelength (nm)	Detector Voltage	k1	A1	C	Standard Deviation
Stock Solution	0 hours	5.413	592	high	0.811±0.0	195.3533±0.7	0.0366±0.0	0.1819
	3 days	5.651	592	high	0.713±0.0	43.3547±0.3	0.0304±0.0	0.0886
	7 days	5.655	592	high	0.695±0.0	35.2256±0.3	0.0245±0.0	0.0875
	0 hours	5.413	616	high	0.812±0.0	432.9576±1.4	0.0674±0.1	0.3904
	3 days	5.651	616	high	0.722±0.0	106.2051±0.8	0.0424±0.0	0.2399
	7 days	5.655	616	high	0.698±0.0	87.1969±0.6	0.0434±0.0	0.1762
	0 hours	5.413	696	high	0.801±0.0	111.9256±0.3	0.0333±0.0	0.0933
	3 days	5.651	696	high	0.684±0.0	25.7329±0.2	0.0236±0.0	0.0540
	7 days	5.655	696	high	0.687±0.0	21.5449±0.2	0.0266±0.0	0.0619
Sample 1	0 hours	2.561	592	high	0.951±0.0	714.1848±0.9	0.0397±0.0	0.2028
	3 days	2.638	592	medium	0.935±0.0	136.0501±0.2	0.0423±0.0	0.0569
	7 days	2.651	592	medium	0.943±0.0	122.6088±0.2	0.0280±0.0	0.0413
	0 hours	2.561	616	high	0.930±0.0	474.1176±1.2	0.0673±0.0	0.2844
	3 days	2.638	616	medium	0.915±0.0	190.7710±0.5	0.0411±0.0	0.1121
	7 days	2.651	616	medium	0.930±0.0	188.4915±0.3	0.0372±0.0	0.0721
	0 hours	2.561	696	high	0.947±0.0	355.6739±0.5	0.0296±0.0	0.1077
	3 days	2.638	696	medium	0.923±0.0	71.0112±0.1	0.0095±0.0	0.0330
	7 days	2.651	696	medium	0.934±0.0	64.6660±0.1	0.0210±0.0	0.0284
Sample 2	0 hours	4.463	592	high	0.855±0.5	469.3847±1.2	0.0537±0.0	0.3100
	3 days	4.838	592	high	0.756±0.0	62.8144±0.3	0.0207±0.0	0.0760
	7 days	4.928	592	high	0.745±0.0	37.1969±0.2	0.0265±0.0	0.0673
	0 hours	4.463	616	high	0.843±0.0	960.8701±1.0	0.0714±0.0	0.2505
	3 days	4.838	616	high	0.772±0.0	147.3133±0.8	0.0546±0.0	0.2184
	7 days	4.928	616	high	0.753±0.0	89.2689±0.7	0.0365±0.0	0.1913
	0 hours	4.463	696	high	0.846±0.0	264.5554±0.5	0.0405±0.0	0.1374
	3 days	4.838	696	high	0.747±0.0	38.1807±0.2	0.0220±0.0	0.0685

	7 days	4.928	696	high	0.733±0.0	23.1569±0.2	0.0080±0.0	0.0524

Table G.12: Cy_2DETA.2A.3HCl / Eu(III) phosphorescence emission decay data (in D_2O, multi-component buffered system, λ_{ex} = 233 nm).

Sample	Time	pD	Emission Wavelength (nm)	Detector Voltage	k1	A1	C	Standard Deviation
Stock Solution	0 hours	5.413	592	medium	0.833±0.0	77.3191±0.5	0.0197±0.0	0.0620
	3 days	5.651	592	medium	0.778±0.0	12.8215±0.2	0.0697±0.0	0.0440
	7 days	5.655	592	high	0.762±0.0	144.0599±0.8	0.0648±0.0	0.2315
	0 hours	5.413	616	medium	0.825±0.0	163.6444±0.3	0.0245±0.0	0.0773
	3 days	5.651	616	medium	0.767±0.0	29.9070±0.1	0.0686±0.0	0.0407
	7 days	5.655	616	high	0.775±0.0	339.5687±1.7	0.1237±0.1	0.4755
	0 hours	5.413	696	medium	0.829±0.0	43.2567±0.2	0.0114±0.0	0.0477
	3 days	5.651	696	medium	0.776±0.0	7.5875±0.1	0.0680±0.0	0.0354
	7 days	5.655	696	high	0.750±0.0	84.7135±0.5	0.0509±0.0	0.1592
Sample 1	0 hours	2.561	592	medium	0.955±0.0	275.6956±0.2	0.0567±0.0	0.0408
	3 days	2.638	592	medium	0.943±0.0	770.5117±1.0	0.0826±0.0	0.2397
	7 days	2.651	592	medium	0.953±0.0	698.4007±0.8	0.0881±0.0	0.1877
	0 hours	2.561	616	medium	0.949±0.0	178.0730±0.2	0.0702±0.0	0.0521
	3 days	2.638	616	medium	0.930±0.0	1068.3290±2.0	0.1431±0.1	0.4818
	7 days	2.651	616	medium	0.945±0.0	1070.9420±1.2	0.1135±0.0	0.2731
	0 hours	2.561	696	medium	0.954±0.0	138.0635±0.2	0.0716±0.0	0.0438
	3 days	2.638	696	medium	0.937±0.0	405.2753±0.7	0.0830±0.0	0.1544
	7 days	2.651	696	medium	0.946±0.0	369.4240±0.5	0.0583±0.0	0.1087
Sample 2	0 hours	4.463	592	medium	0.865±0.0	192.3574±0.3	0.0166±0.0	0.0835
	3 days	4.838	592	medium	0.815±0.0	21.7206±0.2	0.0324±0.0	0.4330
	7 days	4.928	592	high	0.830±0.0	159.1299±1.0	0.0903±0.0	0.2689
	0 hours	4.463	616	medium	0.855±0.0	386.3592±0.3	0.0481±0.0	0.0882
	3 days	4.838	616	medium	0.812±0.0	48.0146±0.2	0.0328±0.0	0.0470
	7 days	4.928	616	high	0.819±0.0	358.2818±1.5	0.0654±0.1	0.4073
	0 hours	4.463	696	medium	0.862±0.0	107.1916±0.3	0.0163±0.0	0.0735
	3 days	4.838	696	medium	0.831±0.0	12.9038±0.2	0.0177±0.0	0.0417
	7 days	4.928	696	high	0.790±0.0	90.6564±0.5	0.0811±0.0	0.1483

List of Publications

1. A. S. de Sousa*, M. A. Fernandes, K. Padayachy, H. M. Marques* *"Amino-alcohol ligands. Synthesis and structure of N,N'-bis(2-hydroxycyclopentyl)ethane-1,2-diamine, its salts, and an assessment of its fitness and that of related ligands for complexing metal ions",* Inorg. Chem., 2010, 49 (17), 8003-8011.

   Journal impact factor: 4.325

   Citation record: 3

2. K. Padayachy, Z. Mgcima, M. A. Fernandes, H. M. Marques A. S. de Sousa*, *"Hydrogen Interactions in Morpholinium Bromide",* Acta Cryst. E67, o2594, 2011.

   Journal impact factor: 0.413

   Citation record: --

3. K. Padayachy, M. A. Fernandes, H. M. Marques, A. Lemmerer, A. S. de Sousa *"Bis(2-hydroxyethyl)ammonium 2-bromophenolate",* Acta Cryst. E68, o2610, 2012.

   Journal impact factor: 0.413

   Citation record: --

4. K. Padayachy, M. A. Fernandes, H. M. Marques A. S. de Sousa*, *"Bis(2-bromoethyl)ammonium bromide",* Acta Cryst. E68, o2570-o2571, 2012.

   Journal impact factor: 0.413

   Citation record: --

5. K. Padayachy, M. A. Fernandes, H. M. Marques A. S. de Sousa*, *"Intramolecular Hydrogen Bonds and the Supramolecular Structure of N,N'-Bis(p-tolylsulfonyl)diethylenetriamine",* J. Chem. Cryst., 2008, 38 (8), 577-582.

   Journal impact factor: 0.413

   Citation record: --

6. S. Mathura, A. S. de Sousa, M. A. Fernandes, K. Padayachy, H. M. Marques* *"5,10,15,20-Tetra-p-phenylsulfonylporphinatocobalt(III), a water-soluble Co(III) porphyrin",* Inorg. Chim. Acta, 2012, 392 (17), 108-111.

   Journal impact factor: 1.976

   Citation record: --

7. A. S. de Sousa, K. Padayachy, M. A. Fernandes, H. M. Marques, *"Modulating Cavity Size of an Amino Alcohol Assembly",* J. Chem. Cryst. Submitted, in press.

   Journal impact factor: 0.566

   Citation record: --

TurnItIn Report

The 12% contribution towards the similarity index (15%) is a result of my own publications.

00916756 KP THESIS FIRST SUBMISSION (15-10-2013).pdf

ORIGINALITY REPORT

15 %	3 %	2 %	12 %
SIMILARITY INDEX	INTERNET SOURCES	PUBLICATIONS	STUDENT PAPERS

PRIMARY SOURCES

Submitted to University of Witwatersrand *Student Paper*	12%
www.patentstorm.us *Internet Source*	< 1%
Meyer, M.. "Conformations and coordination schemes of carboxylate and c… *Publication*	< 1%
www.internetworking.hitachi.com *Internet Source*	< 1%
www.patents.com *Internet Source*	< 1%
Éva Tóth. "Gadolinium-based linear polymer with temperature-independent … *Publication*	< 1%
Jayaraman, N.. "Molecule matters", Resonance: Journal of Science Educat… *Publication*	< 1%
www.freshpatents.com *Internet Source*	< 1%
www.crbtrader.com *Internet Source*	< 1%
www.coursehero.com *Internet Source*	< 1%
kubus.rulez.pl *Internet Source*	< 1%
www.avtechlabs.com *Internet Source*	< 1%
coaldiver.org *Internet Source*	< 1%
www.ofcom.org.uk *Internet Source*	< 1%
sfwmd.gov *Internet Source*	< 1%

Hancock, Robert D., Alvaro S. de Sousa, George B. Walton, and Joseph H. *Publication*	< 1%
etd.ohiolink.edu *Internet Source*	< 1%
Werts, Martinus H.V.. "Making sense of lanthanide luminescence.", Science… *Publication*	< 1%
asiafoundation.org *Internet Source*	< 1%
www.umweltdaten.de *Internet Source*	< 1%
mdpi.org *Internet Source*	< 1%
Leverett, Peter Williams, Peter A. Hibbs. "Ca-Mg-Fe-rich rhodonite from the… *Publication*	< 1%
znaturforsch.com *Internet Source*	< 1%
Schmitt-Willich, H. Brehm, M. Ewers, Ch.. "Synthesis and physicochemical … *Publication*	< 1%
bellota.ele.uva.es *Internet Source*	< 1%
www.tampabaymri.com *Internet Source*	< 1%
minsocam.org *Internet Source*	< 1%
203.158.6.22:8080 *Internet Source*	< 1%
Tian, X. Knapp, A.D. Gibson, L.R. Struth. "Response of eastern gamagras… *Publication*	< 1%
Mihailova, Irena Mehandjiev, Dimitar. "Catalytic activity of Co-akermanite and… *Publication*	< 1%
www.kyb.tue.mpg.de *Internet Source*	< 1%
cbm.cnrs-orleans.fr *Internet Source*	< 1%
A. A. Formanovsky. "One-Stage Monosubstitution in Cyclen - Two Novel E… *Publication*	< 1%
starbase.jpl.nasa.gov *Internet Source*	< 1%
John C. Gilbert & Stephen F. Martin. "Experimental Organic Chemistry: A M…	< 1%

Publication	
etd.wfu.edu *Internet Source*	< 1%
etd.gatech.edu *Internet Source*	< 1%
search.ohiolink.edu *Internet Source*	< 1%
Logothetis, Nikos K.. "What we can do and what we cannot do with fMRI.(fu… *Publication*	< 1%
scholar.lib.vt.edu *Internet Source*	< 1%
authors.library.caltech.edu *Internet Source*	< 1%
www.faculty.ait.ac.th *Internet Source*	< 1%
yukonflatseis.ensr.com *Internet Source*	< 1%
dspace.mit.edu *Internet Source*	< 1%
www.shrm.org *Internet Source*	< 1%
Tzu-Ming Lee. "Physicochemical characterization of the dimeric lanthanide … *Publication*	< 1%
"ebook_s250_topic3", TOPIC 3 Water and well-being: arsenic in Banglades… *Publication*	< 1%
Sonar, Swapnil Ambrose, Kenson Hendsbee,. "Synthesis and application o… *Publication*	< 1%

EXCLUDE QUOTES ON
EXCLUDE BIBLIOGRAPHY ON
EXCLUDE MATCHES < 1 WORDS